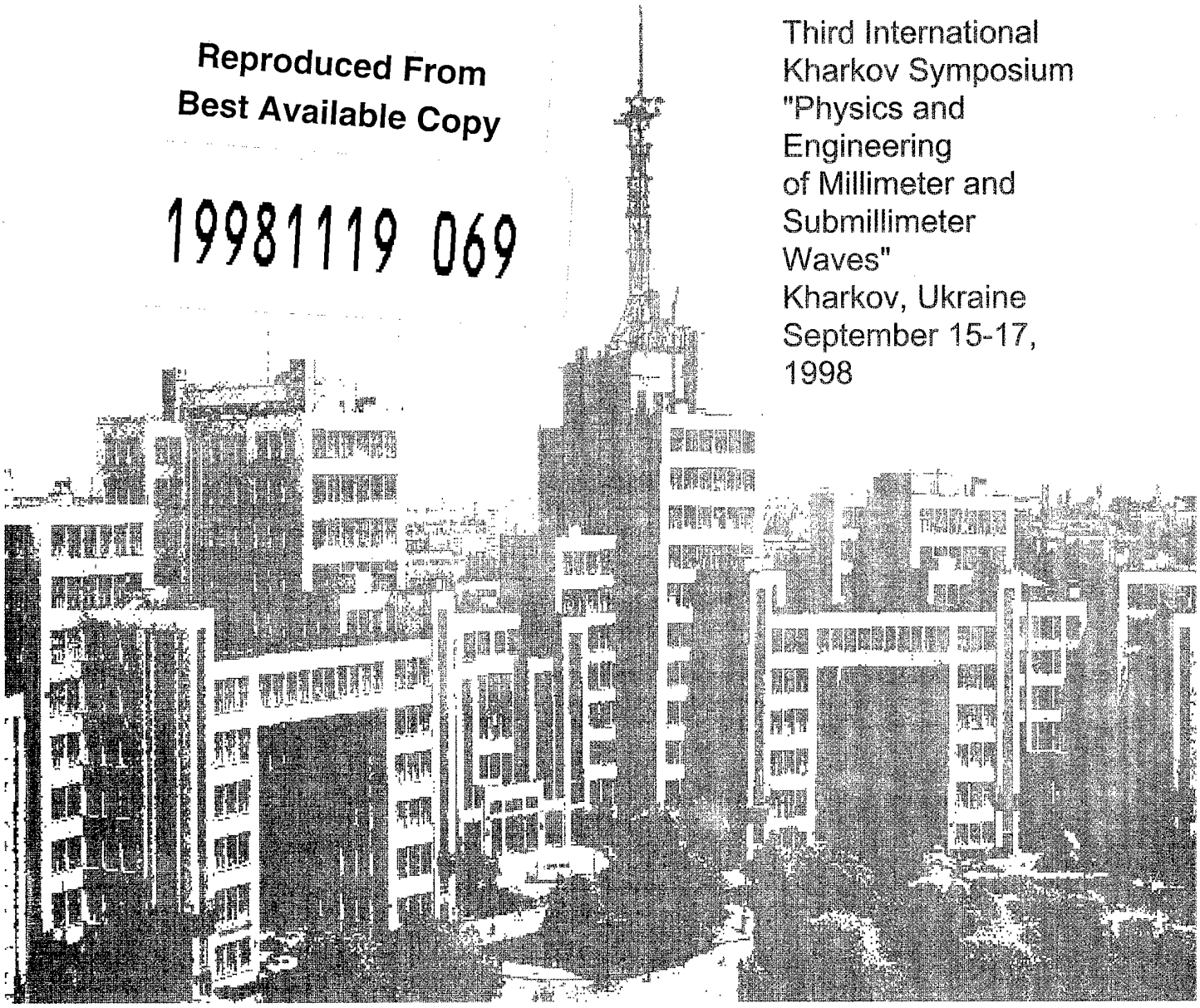
MSMW'98

SYMPOSIUM PROCEEDINGS

Reproduced From
Best Available Copy

19981119 069

Third International
Kharkov Symposium
"Physics and
Engineering
of Millimeter and
Submillimeter
Waves"
Kharkov, Ukraine
September 15-17,
1998



DTIC QUALITY INSPECTED 3

U.R.S.I.

IEEE

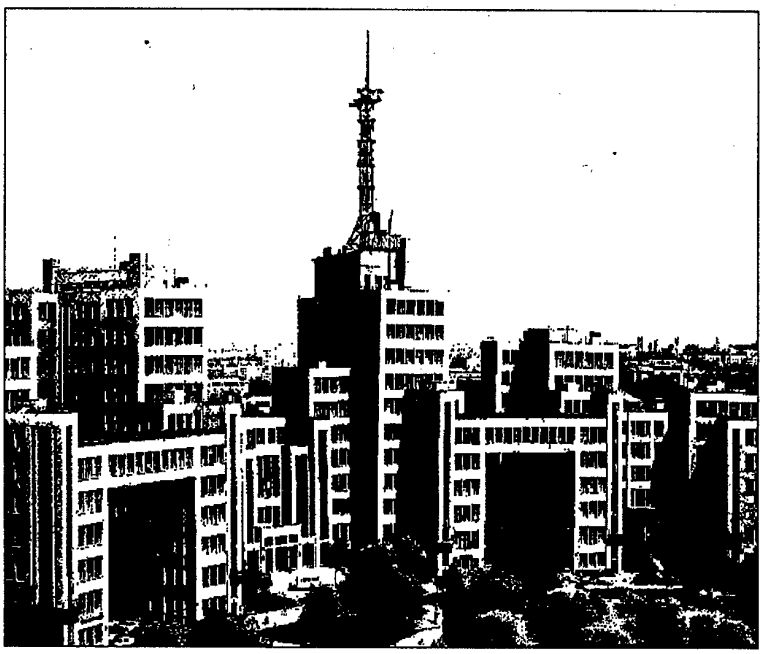
EDS

MTTS ®

EUROPEAN RESEARCH OFFICE

YHTLI
Ukrainian Engineering Research Institute
Science and Technology Center in Ukraine
STCU

THIRD INTERNATIONAL KHARKOV SYMPOSIUM
"PHYSICS AND ENGINEERING
OF MILLIMETER AND SUBMILLIMETER WAVES"



MSMW'98

Symposium Proceedings

Volume 2

Kharkov, Ukraine
September 15-17, 1998

THIRD INTERNATIONAL KHARKOV SYMPOSIUM "PHYSICS AND ENGINEERING OF MILLIMETER AND SUBMILLIMETER WAVES"

Organized by

Usikov Institute for Radiophysics and Electronics, National Academy of Sciences of Ukraine

Institute of Radio Astronomy, National Academy of Sciences of Ukraine

Kharkov State University, Ministry of Education of Ukraine

IEEE AP/ED/MTT/AES Societies Joint Chapters of Ukraine

Ukrainian URSI Committee

Sponsored/Technically Sponsored by

URSI - International Union of Radio Science

IEEE ED/MTT Societies

US Army European Research Office

UNTC - Science and Technology Center in Ukraine

Proceedings of Third International Kharkov Symposium "Physics and Engineering of Millimeter and Submillimeter Waves" (September 15-17, 1998)

IEEE Catalog Number: 98EX119
ISBN: 0-7803-4389-1 Microfiche Edition

Copyright and Repint Permission: Abstracting is permitted with credit to the source. Libraries are permitted to photocopy beyond the limit of U.S. copyright law for private use of patrons those articles in this volume that carry a code at the bottom of the first page, provided the per-copy fee indicated in the code is paid through Copyright Clearance Center, 222 Rosewood Drive, Danvers, MA 01923. For other copying, reprint or republication permission, write to IEEE Copyrights Manager, IEEE Service Center, 445 Hoes Lane, P.O. Box 1331, Piscataway, NJ 08855-1331. All rights reserved. Copyright @ 1998 by the Institute of Electrical and Electronics Engineers, Inc.

Prepared directly from the authors' camera-ready copies.
Design by a computer group of Usikov Institute for Radiophysics and Electronics,
National Academy of Sciences of Ukraine.
c/o IRE NASU, 12 Ac. Proskura St., Kharkov, 310085, Ukraine
Phone/ Fax: +380 (572) 441105 E-mail: <symposium@ire.kharkov.ua>

Printed by Business Inform Co.
Office 319, 28, Marshal Bazhanov St., Kharkov, 310002, Ukraine
Phone/ Fax: +380 (572) 142755

MSMW'98 Organizing Committee

Chairman

Prof. V.M. Yakovenko (Ukraine)

Co-Chairmen

Prof. L.N. Litvinenko (Ukraine)
Prof. V.A. Svich (Ukraine)

Co-Organizers

Dr. A.A. Kostenko (Ukraine)
Prof. A.I. Nosich (Ukraine)

Members

Prof. V.P. Churilov (Ukraine)
Prof. B.I. Makarenko (Ukraine)
Dr. P.N. Melezhik (Ukraine)
Dr. V.F. Mescheryakov (Ukraine)
Dr. V.G. Pavlovsky (Ukraine)
Dr. I.E. Pochanina (Ukraine)
Mr. A.D. Ustimenko (Ukraine)
Prof. I.I. Zalubovsky (Ukraine)

MSMW'98 International Program Committee

Dr. V.M. Chmil (Ukraine)
Prof. S.F. Dyubko (Ukraine)
Dr. O.P. Fedorov (Ukraine)
Dr. L.I. Fedoseev (Russia)
OC Special Representative in Nizny Novgorod
Prof. Dr. H.C.C. Fernandes (Brazil)
Prof. L.G. Gassanov (Ukraine)
Dr. H.F. Harmuth (USA)
Dr. M. Henini (UK)
Prof. Dr.-Ing. R.H. Jansen (Germany)
Prof. A.A. Kirilenko (Ukraine)
Prof. Dr. P. Kordos (Germany)
Prof. V.F. Kravchenko (Russia)
Dr. M.J. Lancaster (UK)
Prof. V.V. Meriakri (Russia)
OC Special Representative in Moscow
Prof. Koji Mizuno (Japan)
Prof. N.G. Nakhodkin (Ukraine)
Prof. A.P. Naumov (Russia)
Prof. G. Nusinovich (USA)
Prof. Yu.K. Požela (Lithuania)
Prof. A. Räisänen (Finland)
Prof. V.B. Razskazovsky (Ukraine)
Prof. B.A. Rozanov (Russia)
Prof. Dr.-Ing. K.Schünemann (Germany)
Prof. V.P. Shestopalov (Ukraine)
Prof. Ya.S. Shifrin (Ukraine)
Prof. V.M. Shulga (Ukraine)
Dr. K.S. Sunduchkov (Ukraine)
Prof. M. Thumm (Germany)
Prof. O.A. Tretyakov (Ukraine)
Prof. D.M. Vavriv (Ukraine)
Prof. O.G. Vendik (Russia)
Prof. A.A. Vertiy (Ukraine)
Prof. Kiyotoshi Yasumoto (Japan)

Table of MSMW'98 Geography

Country	*Papers*
Kharkov	*134*
Russia	*46*
Ukraine non-Kharkov	*22*
Germany	*7*
Ukraine + Russia	*7*
Brazil	*4*
Russia + Belarus	*3*
Ukraine +Turkey	*3*
Japan	*2*
Russia + Germany	*2*
UK	*2*
Ukraine + Mexico	*2*
Belarus	*1*
China	*1*
Finland	*1*
Germany +Switzerland	*1*
India	*1*
Italy	*1*
Switzerland	*1*
Ukraine + Finland	*1*
Ukraine + Germany	*1*
Ukraine +Italy	*1*
Ukraine + Russia + Mexiko	*1*
Ukraine + Sweden	*1*
USA	*1*
Total	***247***

Ladies and gentlemen,
Dear colleagues and friends,

I am proud to be able to welcome the MSMW'98 participants in Kharkov.

First and foremost, I should say that we highly appreciate your interest in the 3-rd International Kharkov Symposium "Physics and Engineering of Millimeter and Submillimeter Waves". We are confident that your contributions will certainly be helpful in making this meeting a real success. Your presence here will add significantly to the prestige of the MSMW'98.

MSMW symposia have been held in Kharkov since 1978 as a regular Soviet Union meeting on MM and SubMM waves and used to provide an extremely wide exchange of information, ideas, approaches, technological concepts and applications in this particular field of radiophysics and electronics.

Following the break-up of the Soviet Union a decision was made to maintain that tradition by periodically convening MSMW symposia. As a matter of fact, in 1991 the research community put forward a suggestion that it should be called as the International Kharkov Symposium "Physics and Engineering of Millimeter and Submillimeter Waves". It is owing to this decision that Kharkov had received a fairly wide recognition as one of the leading centers of fundamental and applied research on radiophysics and electronics, particularly, in the development of MM and SubMM waves.

Over a long span time the basic research of the Ukrainian radiophysicists had been carried out for the benefit of the military-industrial complex which was hugely financed by the Soviet government. As a result, we developed a great scientific potential with the aid of highly experts, engineers and technicians who were able to deal with many sophisticated problems.

Unfortunately, nowadays the close ties that had been earlier maintained broke down, and researchers found themselves isolated. Therefore, it became extremely imperative to preserve those groups of researchers who are still capable of pursuing investigations.

We are very hopeful that the present MSMW'98 Symposium will contribute towards integrating the experts in radiophysics and electronics into the world-wide research community. It will offer an ample opportunity to find new ways of resolving numerous issues.

At the same time we would be pleased to see the new ideas, all kinds of innovations and problems implemented on a large scale. We believe that in this context the borders separating our nations should never stand in the way of achieving whatever results by joint effort.

Let me express my gratitude to all those prestigious international institutions: URSI (International Union of Radio Science), IEEE (Institute of Electrical and Electronics Engineers) ED/MTT Societies, US Army European Research Office, UNTC (Science and Technology Center in Ukraine), which committed themselves to provide their share of financial support. We are grateful to all authors who have submitted their papers to MSMW'98. It was a pleasure to work with the members of Organizing and Program Committees.

We will do our best to make you feel satisfied and impressed so that you could remember it for a long time and have a strong desire to come back to the future MSMW in the next millennium.

Thank you very much for your participation.

Yours sincerely,

Prof. Vladimir M.Yakovenko
MSMW'98 Chairman

Contents

Volume 1

INV. INVITED PAPERS

INV.1. A Review of the Principles of Holographic Power Combining at Millimeter and Submillimeter-Wave Frequencies
H.-G.Unger, M.Shahabadi, and K.Schünemann 22

INV.2. InP Transferred Electron Devices for Power Generation at Frequencies above 130GHz
R.Judaschke and K.Schünemann 24

INV.3. Transition Radiation of Charged Particles and the Possibility of Submillimeter Waves Generation in the Semiconductor Structures
V.M.Yakovenko 30

INV.4. Measurements of High Gain Antennas at Millimeter Wavelength Using Hologram CATR
A.Räisänen, T.Hirvonen, J.Ala-Lauriaho, A.Lehto 35

INV.5. The Synergy of Submillimetre and Infrared Spectroscopy in Predicting Global Warming Effects of CFC Replacement Molecules
G.Duxbury, K.Smith, M.McPhail, R.McPheat, J.Ballard, and D.Newnham 40

INV.6 New Trends in GaAs-Based Devices For Generation of Millimeter and Submillimeter Waves
P.Kordoš 44

INV.7. Microwave Components and Devices Based on High Temperature Superconductors
O.G.Vendik 50

INV.8. Radar Estimations of Soil Parameters by Multichannel Methods
G.P.Kulemin 53

INV.9. State of the Art of Gyrotron Developments and Investigations
A.Goldenberg 60

INV.10. Detection System for the Measurements of Collective Thomson Scattering Spectra in Fusion Plasma
L.V.Lubyako, E.V.Suvorov, A.B.Burov, A.M.Shtanuk, Yu.A.Dryagin, L.M.Kukin, and N.K.Skalyga 64

INV.11. Hypersonic Delay Lines: Physical Base, Technology and Application in the Space Radar Engineering
V.N.Balabanov, E.M.Ganapolskii, A.V.Golik, V.B.Efimov, A.P.Korolyuk, A.C.Kurekin, A.G.Sergeev, V.V.Tarakanov, and V.N.Tcymbal 70

INV.BI. MM-Wave Transmitters Using Magnetrons with Cold Secondary-Emission Cathode
V.D.Naumenko, K.Schünemann, V.Ye.Semenuta, D.M.Vavriv, and V.A.Volkov 76

INV.C1. Superconducting Passive Microwave Components for Mobile Communications
M.J.Lancaster, J.-S.Hong, D.Jedamzik, and R.B.Greed 82

INV.E1. Value Estimations of the Third Stokes-Vector Component Both Precipitation Microwave Emission and Sun Scattered Radiation Observations
B.G.Kutuza, G.K.Zagorin, A.Hornbostel, and A.Schroth 88

INV.F1. Remote Sensing of the Atmospheric Ozone at Millimeter Waves
E.P.Kropotkina, A.N.Lukin, S.B.Rozanov, and S.V.Solomonov 91

INV.F2. Millimeter Wave Noise Radar Technology
K.A.Lukin 94

INV.G1. Millimeter and Submillimeter Wave Spectroscopy of Interstellar Medium
I.I.Zinchenko and V.M.Shulga 98

INV.G2. Low-Noise Millimeter and Submillimeter Wave Receivers
B.A.Rozanov and S.B.Rozanov 104

INV.H1. Integrated Software Package for Synthesis, Analysis and Optimization of Frequency-Selective Devices of Millimeter and Centimeter Waves
A.A.Kirilenko, L.A.Rud', V.I.Tkachenko, L.P.Mos'pan, and D.Yu.Kulik 110

INV.I1. Precise Measurements in Millimeter and Submillimeter-Wave Range Based on Phase-Locked Primary Radiation Sources
A.F.Krupnov, M.Yu. Tretyakov, V.N.Markov, E.N.Karyakin, G.Yu.Golubyatnikov, V.V.Parshin, S.A.Volokhov, A.M.Schitov, V.V.Bychkov, and I.I.Leonov 115

INV.I2. Material Properties in the Millimeter Range
V.V.Meriakri 121

INV.J1. Multifunctional Millimeter Wave Radar Sensor for Vehicle Applications
M.Wollitzer, J.Büchler, J.-F.Luy, U.Siart, and J.Detlefsen 124

INV.J2. High Temperature Processing of Materials Using Millimeter-Wave Radiation
Yu.V.Bykov, A.G.Eremeev, V.V.Holoptsev, K.I.Rybakov, and V.E.Semenov 130

INV.K1. The Elaboration Measurement Accuracy Problems of the Frequency Characteristics of the Sources of High Stability Oscillations in the Millimeter and Submillimeter Range and of the Means of Their Traceability
A.S.Kleiman 136

INV.L1. Mechanism of Interection of EHF Radiation with Biological Systems
O.V.Betskii, N.N.Lebedeva, and Yu.G.Yaremenko 139

Session A. NEW PRINCIPLES OF GENERATING AND RECEIVING MM AND SUBMM WAVES

A1. Harmonic Mode Operation of GaAs-IMPATT Devices above 200 GHz
M.Claassen and H.Böhm 142

A2. Mixing of 28 THz CO2-Laser Radiation by Nanometer Thin-film Ni-NiO-Ni Diodes with Difference Frequencies up to 176 GHz
C.Fumeaux, W.Herrmann, F.K.Kneubühl, H.Rothuizen, B.Lipphardt, and C.O.Weiss 145

A3. Infrared Raman Solitons, Self-phase Modulation and Self Focusing in CO2-Laser Pumped NH3
M.O.Baumgartner and F.K. Kneubühl 147

A4. Semiconductor Microwave Device in HSRI of China
Li Songfa 149

A5. Antenna - Coupled Schottky Diodes for Millimeter Wave Receivers
E.O.Iounevitch and V.E.Lioubtchenko 152

A6. Dynamic and Noise Parameters of the Power Adders Using the Multistructural IMPATT Diodes
A.A.Nikitin and A.S.Shapovalov 155

A7. Thesis's About Gunn Diode Work with Two Transit-Time Regions and Heterojunction Between them
I.Storozhenko 157

A8. Power and Frequency Characteristics of Gunn GaAs-Diodes with Tunnel Injection of Cold Electrons
Yu.V.Arkusha, E.D.Prokhorov, and I.P.Storozhenko 159

A9. Compensented GaAs Diodes Oscillator
O.V.Botsula and E.D.Prokhorov 161

A10. Frequency Dependence of MM-Wave GaAs Gunn Diode Oscillators Efficiency Operated on 2-nd or 3-rd Harmonic
A.V.Dyadchenko, A.A.Mishnjov, and E.D.Prokhorov 163

A11. Efficiency Possibilities of the RTD Generators
E.D.Prokhorov, V.V.Medvedev 166

A12. Whispering Gallery Oscillations in an Anisotropy Ball
Yu.F.Filipov and Z.E.Eremenko 168

A13. Exact Simulation Method for Analysis of Open Resonators with Step-Like Deformation of Mirrors
O.I.Belous, AI.Fisun, A.A.Kirilenko and V.I.Tkachenko 170

A14. Millimeter Wave Signals Detection by Means of Monocrystal Hexagonal Ferrite Ellipsoid
M.Yu.Koledintseva, A.A.Kitaytsev 173

A15. Gunn Diode Cathode Contacts Part in the Increase of the Oscillation Efficiency
Yu.V.Arkusha **176**

A16. MESFET VCO for Use in MM-Wave Communications
S.S.Slesarenko **178**

A17. Basic Principles of Elaborated of Solid-State Millimeter Wave Sources with Dispersive Open Oscillating Systems
O.I.Belous, B.M.Bulgakov, and A.I.Fisun **181**

A18. Efficiensy of the Aperture of the Reconstructive Interferometer
V.N.Uvarov **183**

Session B. ELECTRONICS OF MM AND SUBMM WAVES, INCLUDING QUANTUM AND RELATIVISTIC ELECTRONICS

B1. Gyrotron as a Source of Probing Radiation for Collective Thomson Scattering Experiments
E.V.Suvorov, W.Kasparek, L.V.Lubyako, N.K.Skalyga, V.Erckmann, and T.H.Laqua **188**

B2. Relativistic Gyrotron at the 5th Cyclotron Harmonic
V.L.Bratman, Yu.D.Grom, Yu.K.Kalynov, V.N.Manuilov, M.M.Ofitserov, and S.V.Samsonov **191**

B3. Simulation of the Excitation Mechanisms of Oscillation in Diffraction Electronics Devices on Coupled Open Resonators
G.S.Vorobjov and A.I.Ruban, and A.I.Tsvyk **194**

B4. Simulation of the Excitation Processes of Diffraction-Cerenkov Radiation by the Electron Beam Space Charge Waves on Metal-Dielectric Periodic Structures
G.S.Vorobjov, K.A.Pushkaryov, A.I.Ruban and A.I.Tsvyk **196**

B5. Installation for Investigation of Electron Beams of Vacuum Electronic Devices of Millimeter Wave Band
G.S.Vorobjov, D.A.Nagornyi, K.A.Pushkaryov, Ye.V.Belousov, and V.G.Korzh **198**

B6. Investigation of Phase-Locked Diffraction Radiation Generator
M.Yu.Demchenko, G.P.Ermak, and I.D.Revin **200**

B7. On Mechanism for Oscillation Excitation by Electron Beam in Cavity
V.A.Buts and I.K.Kovalchuk **203**

B8. The Peniomagnetron with Barrel-Shaped Resonator
V.D.Yeremka and O.P.Kulagin **206**

B9. Autosoliton Mode of the Oscillations in the Smooth Anode Magnetron
O.P.Kulagin **209**

B10. Effect of Load on Characteristics of a Magnetron Cavity
A.E.Serebryannikov and A.V.Sova **212**

B11. HCN-Laser with Combined Pumping of Active Medium
Yu.E.Kamenev **215**

B12. Submillimetre Discharge HCN Laser with the Inside Film Electrodes
N.F.Dachov, Yu.E.Kamenev, V.K.Kiseliov, E.M.Kuleshov, and V.P.Radionov **216**

B13. Quantum Chaos in the 3D Electrodynamic Systems of Millimeter Wave Range
E.M.Ganapolskii **218**

B14. Investigation of Critical Regimes in Periodical Structure of FEL, Formed by Coupled Grooved Waveguides
V.S.Miroshnichenko **221**

B15. "Buch" Oscillations in Diffraction Radiation Oscllator
I.K.Kuz'michev and B.K.Skrynnik **224**

B16. Experimental Detection and Analysis of the Morse Critical Point of Open Electrodynamical Structure Involved in Diffraction Radiation Oscillator
I.K.Kuz'michev **227**

B17. Analysis of the Steady-State Mode of the Ormotron
G.A.Alexeev **230**

B18. Analysis of Electpon-Wave Interaction in Cathode Driven Crossed-Field Amplifiers by Coupled-Mode Method
G.I.Churyumov and T.I.Frolova **233**

B19. Simulation of an Inverted Cold Secondary Emission Magnetron Gun invited design
D.B.Eremeev, G.I.Churyumov, N.I.Ayzatskiy, A.N.Dovbnya, V.V.Zakutin **236**

B20. The MM-Wave Cold Cathode Peniomagnetron
V.D.Yeremka **239**

B21. Slow-Wave Structure High-Power MM Band TWT
V.D.Yeremka, M.O.Khorunzhiy, and V.N.Koshparenok **242**

B22. Millimeter Band Magnetron Triodes with Lens Optics
V.D.Yeremka, G.Ya.Levin, S.N.Teryokhin, and O.P.Kulagin **245**

B23. Diffraction Radiation Generator with Local Inhomogeneity of Magnetostatical Field in the Interaction Space
A.I.Tsvyk, A.V.Nesterenko, and V.N.Zheltov **248**

B24. Low-Noise MM Traveling-Wave Maser with Instantaneous Bandwidth of 470 MHz
N.T.Cherpak, A.A.Lavrinovich, T.A.Smirnova **251**

Session C. WAVE PROCESSES IN FINITE-SIZE SEMICONDUCTORS, SOLID-STATE STRUCTURES AND HTSC MATERIALS

C1. Connection of Residual Losses of a Microwave Energy in Superconductive State of $YBa_2Cu_3O_{7-8}$ Films on Saphire Substrates with Their Resistance in a Normal State
O.D. Poustylnik **254**

C2. Phenomenological Approach to Radiofrequency Response of HTS Thin Samples to Microwave Irradiation
N.T.Cherpak, E.V.Izhyk, A.Ya.Kirichenko, and A.V.Velichko **257**

C3. Interaction of Magnetostatic Surface Waves with Film Granular HTSC Structure
V.A.Krakovskiy **260**

C4. Evolution of Oscillations of Semibounded Electron Plasma
V.L.Falko, S.I.Khankina, and V.M.Yakovenko **263**

C5. Semiquantal Dynamics of the Electrons in a Periodic Potential Under the Microwave Excitation
L.V.Yurchenko and V.B.Yurchenko **266**

C6. Influence of Microcorrugated Surface on Electron States in 2D Quantum Well
V.A.Pogrebnyak **269**

C7. Resonant Field Emission in Multilayer Cathods with Quantum Well
N.M.Goncharuk, V.E.Chayka, V.G.Litovchenko, A.A.Evtukh, and Yu.M.Litvin **272**

C8 Negative Dynamic Conductivity in Diode Structure with the Cone Cathode
V.E.Chayka, N.M.Goncharuk, and D.V.Mironov **275**

C9. Losses in Diamonds at Millimeter Range
B.M.Garin, A.N.Kopnin, M.P.Parkhomenko, E.E.Chigryai, Y.V.Parshin, A.B.Mazur, V.G.Ralchenko, and V.I.Konov **278**

C10. Polariton Excitations in Two-Dimensional Electron Magnetoplasma
V.V.Popov, T.V.Teperik, and G.M.Tcymbalov **281**

C11. Perturbation of Quasioptical Dielectric Resonator by a Radial Slot with Anisotropic Substrate
N.T.Cherpak, E.V.Izhyk, A.Ya.Kirichenko, A.Ya.Dan'ko, A.T.Budnikov, and V.G.Pedyash **284**

C12. On Collisionless Damping of Surface Plasmons
V.M.Yakovenko and I.V.Yakovenko 286

C13. Quantizing of Transition Radiation of the Surface Polaritons by the Charge, Intersecting Two-Layer Two-Dimensional Electron System, Placed Into Strong Magnetic Field
Yu.O.Averkov, N.N.Beletskii, and V.M.Yakovenko 289

C14. Non-Radiative Polaritons in a GaAs/AlGaAs Heterostructures Under Quantum Hall Effect Conditions
N.N.Beletskii and S.A.Borisenko 292

C15. Features of a Spectrum of Magneto-Plasma Waves in Periodic Semiconducting Lattice
A.A.Bulgakov, O.V.Shramkova 295

C16. Surface Polaritons in the Finite Superlattice Placed Into the Quantizing Magnetic Field
J.V.Bludov 298

C17. Non-Linear Magnetoplasma Excitations in Compensated Metals: Periodic and Solitary Waves
N.M.Makarov, G.B.Tkachev, and V.E.Vekslerchik 301

C18. Acoustic Wave Resonances in a Solid Layer with Periodically Irregular Boundary
A.S.Bugaev and V.V.Pogrebnyak 304

C19. Optical Surface Modes in a Random System of Small Metallic Particles
A.Ya.Blank, L.V.Garanina, L.G.Grechko 307

C20. Interaction of Submillimeter Electromagnetic Waves with Ferroelastic Solid-State Structures
Ya.O.Shablovsky 310

C21. Peculiarities of Electron-Wave Interactions in the Resonance System with a Semiconductor
V.A.Abdulkadyrov 313

C22. The Theory of an Electromagnetic Radiation by a Semiconducting Heterostructure with Periodic Screens
V.A.Abdulkadyrov 316

Session D. PROBLEMS OF THE THEORY OF WAVE DIFFRACTION

D1. A Regularization Method for a Class of Dual Series Equations in Diffraction Theory
A.V.Brovenko and A.Ye.Poyedinchuk 320

D2. Harmonic Filters on Ridger Waveguides
A.A.Kirilenko, L.A.Rud', and V.I.Tkachenko 323

D3. Waveguide Band Pass Filters with Increased Stop Band Attenuation
M.E.Ilchenko, A.A.Kirilenko, A.G.Yushchenko, L.A.Rud', and V.I.Tkachenko 326

D4. Investigation of Different Non-Uniform Grids in Waveletbased Planar Circuit Analysis
K.Bubke, G.Oberschmidt and A.F.Jacob 329

D5. Fundamental and Applied Synthesis Problems for Periodic Structures
L.G.Velychko 332

D6. An Efficient Educational Program for a Fin Line Coupler on Semiconductor
H.C.C.Fernandes 334

D7. Microstrip Line with Superconductivity in Multilayer Semiconductor
H.C.C.Fernandes, G.A.de B.Lima, and W.P.Pereira 337

D8. Project and Analysis of Unilateral Fin Line Power Dividers
H.C.C.Fernandes, R.L.M.Lima, and E.L.Freitas 340

D9. HTc Superconducting Planar Antennas Design Using the TTL Method in the Fourier Transform Domain
H.C.C.Fernandes 343

D10. Analysis of Wave Diffraction on the Systems of Screens by the Method of the Product of Parabolic Regions
I.V.Petrusenko 346

D11. Method of Analysis of the Thin-Film Dielectric Parameters
V.N.Derkach, A.E.Pojedinchuk, A.V.Brovenko, and A.A.Vertij 349

D12. Bandpass and Bandstop Multiaperture Irises for Millimeter and Centimeter Wave Range
A.A.Kirilenko and L.P.Mos'pan 352

D13. The Analytical and Numerical Solution Method of the Wave Diffraction Problem for a One-Dimensional Periodic Grating with Chiral Medium
S.B.Panin and A.Ye.Poyedinchuk 354

D14. Fractal Electrical and Magnetical Radiators
E.I.Veliev and V.M.Onufrienko 357

D15. The Morse Critical Points and Problems of Synthesis and Analysis Dielectric Layer
V.V.Yatsik 360

D16. Scalar Wave Diffraction by Axially Symmetrical Flat System of Infinitely Thin Perfectly Conducting Circular Rings
Y.A.Tuchkin, E.Karacuha, and F.Dikmen 363

D17. A Rigorous Approach to the Analysis of Transients in Complete-Parametric Periodic Structures
A.O.Perov 366

D18. Resonance Effects in Electromagnetic Wave Diffraction by a Thin Strip with Anisotropic Conductivity
A.D.Shatrov and P.A.Malyshkin 370

D19. Proper and Improper Waves of Strip with Anisotropic Conductivity
E.N.Korshunova, I.P. Korshunov, A.N.Sivov, and A.D.Shatrov 373

D20. The Diffraction of Nonsinusoidal Radio Waves on Natural Media
S.O.Masalov, O.O.Puzanov, and A.I.Timchenko 376

D21. Excitation of Electromagnetic Waves in Space with Spherical-Layerd Structure
Yu.M.Penkin 379

D22. Coherent Backscattering by a Medium of Randomly Oriented Multiple-Sphere Clusters
V.P.Tishkovets and P.V.Litvinov 382

D23. Modelling and Visualisation of the Electromagnetic Fields in Channel Waveguides
G.F.Zargano, K.V.Vdovenko, and G.P.Sinyavskij 385

D24. Analysis of Line Current Wave Diffraction from Metal-Backed Dielectric Strip by Extended PO Method
A.S. Andrenko and Makoto Ando 387

D25. The Effective Mathematical Model of Microstrip Frequency Selective Surfaces
A.O.Kasyanov, V.A.Obukhoveths 390

Subsession ATOMIC FUNCTION

D26. Atomic Functions and Wavelet Matrix Transform Approach for Efficient Solution of Electromagnetic Integral Equations in the Boundary Value Problems of Millimeter Wave Diffraction
V.F.Kravchenko and A.A.Zamyatin 393

D27. Optimization of the Profile of the Electrodynamic System of a Powerful Gyro-Traveling-Wave-Tube (Gyro-TWT)
V.F.Kravchenko, A.A. Kuraev, and S.V.Kolosov 396

D28. Applications of Atomic Functions to the Boundary Value Problems and Signal Processing Millimeter Band
V.F.Kravchenko, V.L.Rvachev, and V.A.Rvachev 399

D29. Relativistic Travelling-Wave-Tube-O (TWT-O) with an Irregular Moderating System
V.F.Kravchenko, A.A.Kuraev, and A.B.Zakalyukin 402

D30. Optimization of the Variation of a Phase Velocity Wave in an Orotron of Millimeter Band Based on Atomic Functions
V.F.Kravchenko, A.A.Kuraev, A.K.Sinitsyn, and A.I.Shakirin 405

D31. Computation of Electrodynamical Characteristics of Arbitrarily Shaped Domains Based on R-functions Method
V.F.Kravchenko, V.L.Rvachev, and V.V.Torchinov 407

D32. Calculation of a Millimeter Wave Electrooptical Modulator of Laser Bundles by a Method of R-functions
V.F.Kravchenko, N.I.Kravchenko, and N.D.Sizova 410

D33. An effective Solution of Electromagnetic Integral Equations in the boundary Value Problems of Millimeter Wave Diffraction Based on Atomic Functions
V.F.Kravchenko and A.A.Zamyatin 413

D34. Application of R-functions Method to the Calculation of Microstrip Element of Pentagonal Shape
V.F.Kravchenko, V.L.Rvachev, and V.V.Torchinov 416

D35. Analytical and Numerical Methods in the Boundary Value Problems of Superconducting Electrodynamics of Structures in the Millimeter Band
V.F.Kravchenko 418

Authors Index 421

Volume 2

Session E. MM AND SUBMM WAVE PROPAGATION

E1. Research of the Propagation of Broadband Signals of Millimetre Range in the Near-Earth Layer of an Atmosphere
L.F.Chornaya, S.V.Titov, and G.K.Zagorin 450

E2. Monitoring Spatially - Temporary Distributions of Fields of Harmful Impurities in Atmosphere by Methods of Microwave Sounding it from a Surface of the Earth and from Space
S.D.Dubko, L.V.Kostenko, L.N.Litvinenko, B.I.Makarenko, and E.I.Solokha 453

E3. Attenuation Factor of X-and Ka-Band Field Near Sea Surface
V.B.Razskazovsky, Yu.A.Pedenko, and Yu.F.Logvinov 455

E4. Spectral and Correlation Characteristics of Fluctuations of a Point Radiation Source Bearing Under Strong Effect of a Sea Surface in W-Range
N.V.Gorbach, L.I.Sharapov, and N.V.Ryazantseva 458

E5. Prediction of Millimeter Wave Attenuation in Indian Continent
T.K.Bandopadhyaya and P.Saxena 460

E6. Theory of Waveguide Propagation in Randomly Corrugated Channels
N.M.Makarov and A.V.Moroz 463

E7. Localization of Waves in a Single-Mode Waveguide with Statistically Identical Rough Boundaries
N.M.Makarov and Yu.V.Tarasov 466

E8. Estimation of Electrical Path Delay Fluctuations in the Atmosphere by Microwave Radiometry
B.G.Kutuza 469

E9. Quasi-Synchronous Measurements of Radiowave Attenuation by Falling Snow at 138 and 247 GHz
N.I.Furashov and B.A.Sverdlov 472

E10. Computer Simulation of Radiowave Attenuation in Snowfalls at 138 and 247 GHz
A.M.Osharin 474

E11. Some Peculiarities of Vegetation Doppler Spectra and Estimation of Their Influence on the Selection Performance of the 2mm Wavelength Radar
N.V.Gorbach, V.G.Gutnic, and L.I.Sharapov 476

E12. On the Influence of an Ionised Above-Surface Layer on Wave Propagation
G.A. Alexeev 478

Session F. COMMUNICATIONS AND RADARS; REMOTE SENSING

F1. Application of Millimeter Radio Waves in Radio Engineering Systems (Review)
V.N.Antifeev, A.B.Borsov, R.P.Bystrov, E.V.Vashenko, and A.V.Sokolov **482**

F2. Experimental Research on Detection and Recognition of Ground Objects on the Basis of Polarization Parameters
N.S.Akinshin, V.N.Antifeev, A.B.Borsov, R.P.Bystrov, V.A.Nikolaev, A.V.Sokolov, I.A.Panin, and D.A.Nosdrachev **485**

F3. Radar-Tracking Converters in Alarm Systems
R.P.Bystrov, E.V.Vashenko, and A.V.Sokolov **492**

F4. Alarm Complex for Detection and Recognition of Ground Objects
R.P.Bystrov, E.V.Vashenko, and A.V.Sokolov **493**

F5. Digital Computer Simulation of Radar Scattering Fields for Complex Shape Objects
V.N.Antifeev, A.B.Borzov, R.P.Bystrov, D.A.Nosdrachev, G.L.Pavlov, and A.V.Sokolov **494**

F6. The Analysis of Radar-Tracking Scenes VIA Mathematical Simulation Method
V.N.Antipeev, A.B.Borzov, R.P.Bystrov, D.A.Nosdrachev, A.V.Sokolov, V.B.Suchkov **496**

F7. Methodology of Multichannel Radar Image Processing and Interpretation
G.P.Kulemin,A.A.Zelensky, V.V.Lukin, A.A.Kurekin, and K.P.Saarinen **497**

F8. The Influence of Phase and Amplitude Fluctuations of Microwaves in Troposphere on Sar Operation
G.P.Kulemin, V.V.Lukin, and A.A.Zelensky **500**

F9. Use of Homomorphic Transforms for Low Contrast Edge/Detail Detection and Filtering of MM-Band Images
V.I.Chemerovsky, A.N.Dolia, A.A.Kurekin, V.V.Lukin, and A.A.Zelensky **503**

F10. Remote Sensing of the Minor Gas Constituents of the Lower and Middle Atmosphere
Sh.D.Kitaj, A.P.Naumov, N.N.Osharina, and A.V.Troitskij **506**

F11. The Influence of Air-Water Interface Boundary Conditions on Thermal Radio Emission at 2, 5 and 8 mm
K.P.Gaikovich and R.V.Troitsky **509**

F12. Detection of Small Scale Structures in Ozone Layer by Microwave Sounding
A.A.Krasilnikov, Y.Y.Kulikov, V.G.Ryskin, and L.I.Fedoseev **512**

F13. Polarization of Atmospheric Millimeter-Wave Radiation from Scattering Particles Cloud, and Remote Sensing of Volcanic Eruption Column
A.A.Shvetsov **515**

F14. Frequency-Temporal Distributions of Radar-Returns from Sea Surface in X- and Ka-Band
V.A.Kirichenko, G.P.Kulemin, and V.G.Sugak **517**

F15. Polarization Selection of Non-Doppler Ground Objects in MM-Wave Range
A.N.Zubkov, N.S.Akinshin, and B.V.Sukhinin **520**

F16. Clutter Rejection in Short-Range Radar with Uncoded and Wideband Pulsed Signals
G.P.Kulemin **523**

F17. Rough Sea Surface Observation Scheme Optimization at Microwave Radiometric Sensing
V.A.Komyak, S.A.Shilo, and Ya.I.Stephanishin **526**

F18. Millimeter Band Scanning Multi-Beam Radiometer
S.A.Shilo and V.A.Komyak **529**

F19. Methods of Remote Sensing of Stratified Mediums and Their Applications
V.M.Velasco Hererra, V.K.Volosyuk, S.E.Falkovich, O.A.Gorbunenko, and A.V.Sokolnikov **532**

F20. Optimized Complex Signal Processing in Multichannel Synthesized Aperture Radar
V.K.Volosyuk, V.F.Kravchenko, A.V.Sokolnikov, O.A.Gorbunenko, V.A.Onishchuk, and V.M.Velasco Hererra **535**

F21. To the Accuracy of Small Slope Approximation of Kirchhoff Technique
D.V.Mikhailova and L.V.Stulova 538

F22. Millimeter Wave Null-Modem Radio Communication
N.M.Zaitsev and V.E.Lioubtchenko 541

F23. On Energy Potential of a Millimeter-Wave Radar
B.A.Rozanov and G.V.Cheslavsky 543

F24. Optimum Synthesis of Transmitting-Receiving Sections of an Underground Radar
A.A.Orlenko and P.V.Kholod 546

F25. The Problems of the Possible Non-Linear Radiolocation on the Objects of Low Perception
S.A.Gayvoronskaja and V.I.Sergeev 549

F26. Brightness Variations Resistant Algorithms of Object Location on Radiometric Images
V.I.Antyufeev, V.N.Bykov, B.I.Makarenko, and A.M.Grichaniuk 552

F27. Reconstruction of the Continuum Object from the Sampled Radio Image
A.S.Viltchinsky, B.I.Makarenko, E.D.Prilepsky, and M.G.Shokin 555

F28. Influence of the Oil Film on Spectral and Polarization Features of S- , KA- and V-Band Water Surface Back Scattering
V.I.Lutsenko, S.I.Homenko, A.A.Uzlenkov, and V.A.Kirichenko 558

F29. Two-Parametric Representation of Nonstationary Random Signals in Millimeter Wave Radar
K.A.Lukin and A.A.Mogila 561

F30. Mathematical Models and Spatial Characteristics of Coherent and Incoherent Imaging Systems
I.Prudyus, S.Voloshynovskiy, andT.Holotyak 562

Session G. MM AND SUBMM WAVE RADIO ASTRONOMY

G1. Observations of Total Solar Eclipses at Short Millimeter Waves
B.A.Rozanov, N.A.Zharkova, and V.G.Nagnibeda 566

G2. The Interferometric Method of Image Formation and Associated Mathematical Problems
Yu.V.Kornienko 569

G3. Optimization of Non-redundant Apertures on Integer Grids
L.E.Kopilovich 572

G4. A Calculated Choice in the Problem on the Input Aperture of an Optical Multibeam Interferometer
L.V.Stulova 575

G5. Construction on Nonredundant Apertures for Interferometric Radiotelescope by Method on Random Search
Yu.V.Kornienko 578

G6. Immunity of the Interferometric Method for Image Formation to Phase Distortion of the Wave Front
Yu.V.Kornienko 581

Session H. MM AND SUBMM DEVICES BASED ON THE PLANAR AND QUASI-OPTICAL TRANSMISSION LINES (PASSIVE AND ACTIVE COMPONENTS, ANTENNAS)

H1. A New De-embedding Method for Microstriplines with Coaxial Adapters
J.Marquardt and J.Passoke 586

H2. Coupled-Mode Formulation for Double-Strip NRD Waveguides Based on Singular Perturbation Technique
K. Watanabe and K. Yasumoto 589

H3. A Microstrip Array Fed by a Non-Homogeneous Stripline Feeding Network
N.I.Herscovici, N.K.Das, and J.Klugman 592

H4. Properties of Oversized Corrugated Waveguides at Moderate Diameter-Wavelength Ratio
D.A.Lukovnikov, A.A.Bogdashov, and G.G.Denisov 595

H5. Integrated P-I-N-Structures Designed for MM and SubMM Wave Quasi-Optical Modulators
V.V.Grimalsky, Ya.I.Kishenko, I.P.Moroz, and S.V.Koshevaya **598**

H6. Wide-Range System of Turning Mirrors for the Waveguide Laser Resonator
V.A.Svich, V.M.Tkachenko, A.N.Topkov, V.A.Maslov, and I.M.Militinskiy **601**

H7. Short Pulse Generation in a Cavity with an Active Layer and a Dielectric Mirror
L.V.Yurchenko and V.B.Yurchenko **604**

H8. Resonant Reflection of Electromagmetic Wave from Thin Strip Grating
I.K.Kuzmichev, S.N.Vorobiov **607**

H9. On the Diffraction Coupling Organisation in Open Resonators
D.G.Afonin and A.K.Malyshkin **610**

H10. Computer Analysis of Side Radiation of Narrow-Beam Antenna Array
N.N.Gorobets, Yu.N.Gorobets, and V.I.Kiyko **611**

H11. Influence of Side Radiation on One-Reflector Antenna Parameters
N.N.Gorobets and S.S.Vyazmitinova **615**

H12. Millimetre-Range Multi-Channel Two Polarization Horn Antenna
N.N.Gorobets, V.M.Dakhov, and I.V.Cherny **618**

H13. The Principles of Electrodynamics of Planar Periodic Structures
V.V.Khoroshun **620**

H14. Optimization of the Eigenmodes Spectrum of Parallel-Plate Waveguide with Knifelike Diaphragm
V.V.Khoroshun, I.E.Pedchenko, and N.A.Syvozalizov **623**

H15. Super Narrow-Band Low-Dimentional Ultra-High Frequency Filter on the Basis of Waveguide-Dielectric Resonator
A.A.Zvyagintsev, A.V.Strizhachenko, V.V.Chizhov, and V.V.Popov **624**

H16. Surface Wave HTS Resonators
G.A.Melkov, Y.V.Yegorov, A.N.Ivanyuta, and V.Y.Malyshev **625**

H17. The Phased Array Antenna for the Radar of a Millimetric and Centrimetric Range
B.N.Bakhvalov, A.V.Gomozov, and L.V.Kostenko **628**

H18. Ring Antenna Array of Millimeter Wavelength Band
V.N.Rudenko, E.I.Solokha, V.I.Gomozov, and L.V.Kostenko **631**

H19. Electromagnetic Modelling of Microwave High Power Multiplexers
B.I.Makarenko, A.S.Soroka, and I.S.Tsakanyan **633**

H20. Simulation of Multichannel Waveguide Power Dividers
A.S.Soroka, A.O.Silin, V.I. Tkachenko, and I.S.Tsakanyan **634**

H21. On Application of Multicomponent Copper Alloys for Making Microstrip Line Conductors of EHF Microcircuits
V.A. Bessonov, S.A.Barantsev, and I.I.Uliyanova **636**

H22. Waves in Irregular Rectangular Waveguide with Inhomogeneous Anisotropic Impedance of Wall
V.F.Borulko **638**

H23. Two-Dimensional Bragg Resonator with Nonperiodic Radial Perturbation of Parameters
V.F.Borulko and V.E.Ivanilov **641**

H24. Polarizable-Spectral Characteristics of Revolving Linear Polarizer
V.N.Polupanov, Y.M.Kuleshov, B.N.Knyaz'kov, and M.S.Yanovsky **644**

H25. Consideration of Optimum Sectional Waveguide Tapers for Quasi-Optical Transmission Lines
V.K.Kiseliov **647**

H26. Stochastical Resonator for the Accumulation of Millimeter Wave Range Electromagnetic Field Energy
E.M.Ganapolskii **650**

H27. Open Hemispherical Imagine Dielectric Resonator with Whispering Gallery Modes
Z.E.Eremenko, Yu.F.Filipov, and S.N.Kharkovsky **653**

H28. Three-Mirror Open Resonator with a Saturating Paramagnetic
I.Gudim and N. Popenko 655

H29. Diffraction Radiation Oscillator with the Long-Focus Small-Aperture Open Resonator
M.Demchenko, I.Ivanchenko, and V.Korneyenkov 658

H30. Millimeter Wave Linear Antenna Arrays Based on Ridge Dielectric and Groove Waveguides
A.P.Yevdokimov and V.V.Krizhanovsky 661

H31. Millimeter Wave Planar Cosecant Antenna Array for Airborne Radar for the Ukrainian Ministry of Extreme Situations
A.P.Yevdokimov and V.V.Krizhanovsky 663

H32. Automobile Radars for Collision Avoidance
A.P.Yevdokimov and V.V.Krizhanovsky 666

H33. Airborne Radiometer Broadband Quasi-Optical Scanning Antenna System
G.I.Khlopov, V.A.Komyak, A.A.Kostenko, and S.P.Martynuk 667

H34. Excitation of the Whispering-Gallery-Modes at the Shielded Hemispherical Dielectric Resonator
S.N.Kharkovsky, V.V.Kutuzov, A.E.Kogut, and V.A.Solodovnik 669

H35. Open Radiating Systems for Microwaves and Millimeter Waves
V.K.Korneenkov, V.I.Lutsenko, V.S.Miroshnichenko, and V.I.Uzlenkov 671

H36. The Main Type of Oscillations in Waveguide Branching of Three Orthogonal Below Cutoff Waveguides
Yu.G.Makeev 674

H37. Charactors of Waveguide-Dielectric Resonator
Yu.G.Makeev and A.P.Motornenko 677

Session I. MM AND SUBMM WAVE SPECTROSCOPY

I1. Wide-Range Millimeter-Wave Spectrometer for High-Resolution Investigation of Molecular Rotational Spectra
E.A.Alekseev, V.V.Ilyushin, and S.F.Dyubko 682

I2. Millimeter Wave Spectrometer and Its Application
A.N.Kopnin and V.V.Meriakri 685

I3. The Registration of Distortions by Microwave Components of Measurements of the Multifrequency Radiointerferometer of Millimeter Waves
M.V.Andreev 687

I4. Time Spectroscopy of a Film Bolometric Response to MM-Waves Power as a Method of the Thermodynamic Coefficients Diagnostics in a Film Structures
A.M.Grishin, Yu.V.Medvedev, and Yu.M.Nicolaenko 690

Session J. MM AND SUBMM WAVELENGTH INSTRUMENT-MAKING FOR SCIENTIFIC RESEARCH (HOT-PLASMA DIAGNOSTICS, CONTROL OF TECHNOLOGICAL PROCESSES)

J1. Heterodyne Spectrometer for Remote Sensing of the Atmospheric Ozone
V.A.Gusev, E.P.Kropotkina, S.V.Logvinenko, A.N.Lukin, P.L.Nikiforov, S.B.Rozanov, A.M.Shtanjuk and S.V.Solomonov 694

J2. Optimisation of UHF Reflectometer Device for Study of Plasma Density Profile and Fluctuation in Magnetically Confined Plasmas
A.I.Skibenko, L.V.Berezhnyj, O.S.Pavlichenko, V.L.Ocheretenko, I.B.Pinos and I.P.Fomin 697

J3. Graphite-Made UHF Resonator of Fabry-Perot Type for Investigation of the Plasma Divertor Flow in Fusion Devices and the Small-Scale Particles of a Substance
V.L.Bereshnyj, V.S.Voitsenya, V.L.Ocheretenko, A.I.Skibenko, and I.P.Fomin 700

J4. Extension of Functional Possibilities of MM-Range Modulation Radiometers
Yu.A.Skripnik and A.F.Yanenko 703

J5. Investigation of a New Quasi-Optical Waveguide Modeling Method for Backward and Forward Scattering Study in Millimeter and Submillimeter Wave Bands
V.K.Kiseliov, T.M.Kushta, and P.K.Nesterov 706

J6. About Digital Processing Signals of the Dynamic Spectrum Fourie
V.K.Lapty 709

J7. Profound Spectral-Frequency Analysis of the Cardiograms
V.K.Lapty 712

Session K. ELECTROMAGNETIC METROLOGY

K1. Electromagnetic Metrology of Millimeter and Submillimeter Wavelength Bands at Last Years in Ukraine
B.I.Makarenko 716

K2. Thin-wire Bolometers of Intensive Electromagnetic Radiation
V.M. Kuzmichov 719

K3. Measurement of the Generalized Laser Beam Cross Section Area
V.M. Kuzmichov, S.N.Pokhil'ko 722

K4. Intensive Laser Radiation Elleptical Polarization Measurement by Thin-wire Bolometers
V.M.Kuzmichov and E.V.Kuzmichova 725

K5. Nonlinearity of the Characteristic of Transformation Thin-wire Bolometer of Focused Laser Radiation
V.M. Kuzmichov and S.V.Pogorelov 728

K6. Microwave Diagnosis of Protective Coatings Quality
O.B.Ljashchuk and Z.T.Nazarchuk 731

K7. The Error's Influence on the Accuracy of Inverse Problems Solution for the Microwave Electromagnetic Diagnosis of Multilayer Materials
O.B.Ljashchuk 734

K8. Measurement of a Dielectric Permeability of Solutions by a Resonator Aperture Method
A.V.Koberidze 737

K9. Realization of Principle of Fourier Holographic Processing in Multifrequency Measurements in Range 126.6-145.4 GHz
O.O.Drobakhin, D.Yu.Saltykov, and A.Yu.Velikiy 739

K10. Vibratory String as a Perturbation Body in Order to Measurement Electromagnetic Field of Microwave Radiators
A.Ya.Kirichenko and O.A.Suvorova 742

Session L. BIOMEDICAL APPLICATIONS OF MM AND SUBMM WAVES

L1. Radiothermograph Millimeters of a Range for Medical Diagnostics
B.I.Makarenko, V.E.Kudryashov, E.V.Khomenko, and D.V.Martinenko 746

L2. Using of the EHF Method for Investigation of Radiation-Induced Changes in DNA Hydration Shell
O.V.Dubovitskaya, V.A.Kashpur, A.A.Krasnitskaya, and V.Ya.Maleev 748

L3. The Physical Evidence of the Weak Electromagnetic Field Action in the 30-300 GHz Region upon Biological System
L.I.Berezhinsky and G.I.Dovbeshko 751

L4. Dynamics of Indexes Water-Electrolitic Composition of the Blood for Patients with Alcoholic Psichosis under EHF-Therapy
M.Yu.Ignatov, A.V.Malihin, V.N.Derkach, and L.I.Zolotuhina 754

L5. Effects of Low Power Microwave Electromagnetic Fields on Brain Neurodynamics
T.N.Sulima and A.I.Fisun 757

L6. Research of Controlling Connection Systems of Cell Macromolecul Mechanisms by Method Dielectrometry in MM Range of Radiowaves
T.Yu.Shchegoleva and V.G.Kolesnikov 760

L7. About Possible Low-Intensive Combined Fields of Various Physical Nature Mechanisms of Interaction with Bioobjects
Yu.V.Chovnjuk 763

L8. EHF Radiation Impact on Drosophila Melanogaster Viability
V.G. Shachbazov, B.M.Bulgakov, S.P.Sirenko, L.M. Chepel', A.I.Fisun, O.I.Belous 766

L9. Using of EHF and IR Methods for Studying Hydration of Polycytidylic Acid
V.A.Kashpur, M.A.Semenov, and N.N.Sagaidakova 768

L10. Study of the Weak Electromagnetic Field Action upon the Biological Molecules and Tissues by Holographic Interferometer
L.I.Berezhinsky, G.I.Dovbeshko, and N.Ya.Gridina 771

L11. Method of EHF-Therapy at Treatment of Endogene Mental Diseases
A.N.Bacherikov and V.N.Derkach 774

L12. The Research of Molecular Mechanisms of Sperm Control Systems Functioning
M.V.Zubez, V.G.Kolesnikov, and T.Yu.Shchegoleva 776

L13. Application of Method of EHF-Dielectrometry in Analysis of Mechanisms, Stipulating Individual Lever of Coronary Risk
L.N.Gridasova, T.Yu.Shchegoleva, V.G.Kolesnikov, and U.J.Nicolenko 779

L14. EHF-Dielectrometry Method in Investigation Molecular Mechanisms of Stress Realization
O.Kovaljova, D.Sidorov, V.Smirnova, T.Ju.Shchegoleva, and E.A.Lepeeva 782

L15. Application of Dielectrometry in MM Range of Radiowaves for Research of Molecular Mechanisms of Pharmacological Preparations Action
N.E.Kiselova, T.Yu.Shchegoleva, and V.G.Kolesnikov 785

L16. Research of a Singularities of Drugs Toxycological Action on the Pregnant Women Blood by Method EHF-Dielectrometry
N.E.Kiselova, T.Yu.Shchegoleva, V.G.Kolesnikov, and N.S.Nikitina 788

L17. The Methodology of the Analysis of Molecular Mechanisms of Antrogeneous Influence by Method of HF-Dielectrometr
T.Yu.Shchegoleva, V.G.Kolesnikov, L.A.Begma, A.A.Begma, and N.E.Kiselova 791

Authors Index 794

Volume 2

E 

MM AND SUBMM WAVE PROPAGATION

F 

COMMUNICATIONS AND RADARS; REMOTE SENSING

G 

MM AND SUBMM WAVE RADIO ASTRONOMY

H 

MM AND SUBMM DEVICES BASED ON THE PLANAR AND QUASI-OPTICAL TRANSMISSION LINES (Passive and Active Components, Antennas)

I 

MM AND SUBMM WAVE SPECTROSCOPY

J 

MM AND SUBMM WAVELENGTH INSTRUMENT-MAKING FOR SCIENTIFIC RESEARCH (Hot-Plasma Diagnostics, Control of Technological Processes)

K 

ELECTROMAGNETIC METROLGY

L 

BIOMEDICAL APPLICATIONS OF MM AND SUBMM WAVES



MM AND SUBMM WAVE PROPAGATION

Preceding Page Blank

RESEARCH OF THE PROPAGATION OF BROADBAND SIGNALS OF MILLIMETRE RANGE IN THE NEAR-EARTH LAYER OF AN ATMOSPHERE

L.F.Chornaya, S.V.Titov, G.K.Zagorin
Institute of Radioengeneering & Electronics
1, Vvedensky sq., Fryazino, Moscow region, 141120,
Russia
(095)526-91-94, 401-98-18, lfc245@ire216.msk.su

The purpose of this work is the estimation of the influence of the turbulence, deposits and the dispersion of the complex index of refraction of the atmosphere to the propagation of broadband signals of MM range on the near-earth paths of the length more than 10 km.

1. The influence of the **turbulence** on a broadband signal is characterized by the two-frequency function of coherence $\Gamma(k_1, k_2)$, which is analogue of the frequency characteristic of a channel ($k_{1,2}$ is wave vectors appropriate to the frequencies $\omega_{1,2}$). With the help of this function it is possible to estimate an influence of troposphere turbulence inhomogeneities on propagation a pulse with arbitrary envelop.

The following task was solved. The initial field on the transmitting antenna was represented by the one-mode Gaussian collimated beam with an effective radius of ρ_e. The turbulence was assumed statistically homogeneous and isotropic with Karman spectrum $G_n(\kappa)$. of turbulent fluctuations of a refractive index n In the MM range of waves the approach of the smooth perturbations method (SPM) was used for the description of a field on the paths of direct visibility (up to 30 km) [1].

By expressing the field in any point $\boldsymbol{r} = \{L, \boldsymbol{r}\}$ through a complex phase $\Phi(\boldsymbol{r}, k, t)$ the following expression is received for two-frequency coherence function in SPM approximation:

$$\Gamma(L, \rho, k_1, k_2) = \exp\{ 2\pi^2 \int_0^L dx \int_0^\infty d\kappa\, \kappa\, G_n(\kappa) [k_1^2 H^2(P_{1*}, \kappa) + k_2^2 H^{*2}(P_{2*}, \kappa) +$$

$$+ 2k_1 k_2 H(P_{1*}, \kappa) H^*(P_{2*}, \kappa) I_0(2\kappa\rho(P_{1*} - P_{2*}^*))] \}, \quad (1)$$

where $H(P_*, \kappa)$ depends on effective radius of a beam and length of a path L.

The calculation was carried out on formula (1) for paths of length L = 15 and 30 km, frequencies f_1 = 34,9 GHz and 136,4 GHz and effective radius ρ_e = 30 cm. It is shown, that if the frequency difference achieves of the order to 10 GHz the absolute value of coherence function decreases down on 2 - 6 %. The speed of dropping of coherence function can essentially increase, if the frequency f_1 does not correspond to the windows of a transparency of MM range, but it is situated on a slope of the absorption path (for example f = 54 GHz).

When Gaussian pulse $A(t)=\exp(-t^2/\tau_0^2)$ with carrier frequency on MMW and with half-width of τ_0 = 0,1 ns propagates through the turbulent environment, the Gaussian form is practically kept, the effective duration is insignificantly increased and relative broadening does not surpass 1 -2 %. The calculations of a root-mean-square phase difference were also carried out to determinate the degree of influence of various natural factors on pulse propagation in atmosphere with the difference between frequencies up to 2 GHz. The results of calculations of the phase difference in turbulent atmosphere are given in Table 1.

2. Two components have the essential influence on propagation of very short pulses in the earth **clean atmosphere**: water pairs and oxygen. The theoretical investigation of this influence is based on the models of molecular absorption in these gases (see, for example [2]). The influence of an atmosphere is displayed not only in strong attenuation of a signal, which is investigated enough well nowadays. The pulse distortion can also appear due to dispersion.

The effect of dispersion is caused by the difference group velocity of pulse frequency components and it is displayed in broadening (compression) of pulses, in disintegration of one pulse to some pulses. A size and a sign of the effect of broadening (compression) depend on carrier frequency of a pulse. In this work the propagation of Gaussian pulses with duration from 0.1 up to 2 ns on near-earth atmospheric paths of length from 1 up to 50 km with carrier frequencies ranging between 1 — 200 GHz is investigated.

The effect of the **dispersion and absorption** on a broadband signal is convenient to characterize by factor of compression (broadening) $\Delta T/T$, where T is a width of a pulse; ΔT is a width change of a pulse in a near-earth layer. To estimate the broadening or compression of a pulse the task was solved analytically with the help of the method of slowly varying amplitudes [3]. The expression for factor $\Delta T/T$ has a form:

$$\Delta T/T = \sqrt{\frac{\left(1+2\alpha''\ L/T^2\right)^2 + \left(2\beta''L/T^2\right)^2}{\left(1+2\alpha''L/T^2\right)}} - 1 \qquad (2)$$

where L – the length of path, $\alpha''(\omega_0), \beta''(\omega_0)$ - the second derivatives of absorption coefficient and phase delay coefficient respectively with respect to frequency, ω_0 - the carrier frequency of a pulse. The program for calculation of the pulse envelope is made using the computing program Mathematica. It allows to carry out as a numerical calculations of the pulse envelope and compression factor due to pulse propagation through the atmosphere. It was used the program model of an atmosphere described in [2].

The calculations were executed for absorption paths of atmospheric oxygen, located on frequencies near 60 GHz. The estimations have shown that the pulse can both be compressed and broadened. The compression of a pulse is observed in those spectral areas, in which second derivative of absorption factor has a negative sign (area near the maximum of absorption).

The compression is observed near the maximum of absorption. It achieves up to 5% for the pulse of duration 0,5 ns. The expansion is observed on a slope of a strip and can achieve 10 % for ns pulses, sharply decreasing in a wing of a strip up to the 0,1%. Calculations also show that in the maximum of absorption the pulse breaks up to two and more pulses under some conditions.

Thus, the theoretical researches show that on paths of direct visibility short pulse envelope are not practically deformed in windows of transparency of MM range. But on slopes of paths of absorption the changes of the pulse envelope are possible.

3. Despite of long-term researches of **propagation of MMW in deposits**, it is impossible to think that the study of mechanisms of distortion of pulses in rains is finished. The distortion of the form of pulses in a rain is theoretically investigated in [4], but the influence of rain on the form of frequency dependencies of factors of relaxation and phase displacement in CM range of waves is considered only.

In this work Crain method [4] is extended. It is utilized for the analyses of effect of frequency dispersion and phases transference in the rain on distortion of envelope of coherent pulse in MMW. A propagation of coherent Gaussian pulse with initial truncated spectrum $a(\sigma,0)$ in homogeneous **layer of rain** on a horizontal path is discussed. This spectrum is given by following formula

$$\bar{a}(\sigma,0) = \begin{cases} \exp\left[-\pi\left(\dfrac{\sigma}{\sigma_0}\right)^2\right], |\sigma| < |\sigma_m| = 2.5\,\Gamma\Gamma\text{ц}, \sigma_0 = 2\,\Gamma\Gamma\text{ц} \\ 0 \qquad\qquad |\sigma| > |\sigma_m|, \end{cases} \qquad (3)$$

where $\sigma = f - f_0$ - frequency difference. The envelope *of* pulse $a(t, z)$, which is passed through rain layer of thickness z with complex index of refraction m, was received with the help of Fourier transformation

$$a(t,z) = \int_{-\infty}^{\infty} \bar{a}(\sigma,0) e^{-i2\pi\sigma t - ikm(\sigma)z} d\sigma \qquad (4)$$

Instead of Crane method we approximated the frequency dependence of complex index of refraction of rain volume element $m = m_r + i\, m_i$ in a simple analytical form. The results of numerical calculation under the Mie theory were used. It was assumed that the rain drop sizes were distributed on according to the Laws-Parsons law and the temperature of water was 20 C. The results are shown below.

$$\begin{cases} m_r = 1 + 47{,}746 \times 10^{-6} f^{-1} (0{,}0642 \ln f - 0{,}1515) R^{1{,}62 - 0{,}25 \ln f}, 30 < f < 40 ГГц \\ m_i = 6{,}58 \times 10^{-10} f^{1.15} R^{2 - 0{,}29 \ln f}, \end{cases}$$

$$\begin{cases} m_r = 1 + 47{,}746 \times 10^{-6} f^{-1} (0{,}376 - 0{,}0647 \ln f) R^{1{,}16 - 0{,}138 \ln f}, 85 < f < 95 ГГц \\ m_i = 5{,}05 \times 10^{-7} f^{-0{,}46} R^{1{,}2 - 0{,}098 \ln f}, \end{cases} \quad (5)$$

where R is rain rate intensity

The meanings of the difference of phases $\Delta\varphi$ are given between the waves which frequency difference Δf = 1 GHz (see. Tab. 1). Intensity of the rain is 12,5 mm / hour

Table 1. The difference of phases in the turbulent atmosphere and in the rain

Central frequency f_0, GHz	Length of a path L, km	Difference of frequencies Δf, GHz	Phases difference $\Delta\varphi$, Deg.	
			Turbulence	rain
34,9	10	1	0,8	1,5
34,9	30	1	2	4,5
90,9	10	1	0,4	2,3
90,9	30	1	1,5	6,9

The rain layer transfer function $H(\sigma)$ expressed by formula

$$H(\sigma) = exp[-km_i(\sigma)z] \times exp[ikm_r(\sigma)z] \quad (6)$$

It is easy to see the frequency dependencies of the phase function $\varphi(\sigma) = 2\pi\sigma t - km_r(\sigma)z$ within transparency windows 30-40 GHz and 85-95 GHz are different. At frequency range 30-40 GHz the points of stationary phase σ_s are located within interval $(-\sigma_m, \sigma_m)$. This fact allows to use the stationary phase technique for analytical presentation of pulse envelope. The numerical calculation of Fourier integral is used for obtaining pulse envelope in the frequency range 85-90 GHz.

References

1. A. Isimaru, "Propagation and dispersion of waves in random non-uniform environments", p. 2, "World", Moscow, 1981.
2. Yu.P. Kalmykov, S.V. Titov, "Advances in Chemical Physics", Ed. W.T.Coffey, New York, Vol. 87, pp. 31-123, 1994.
3. G.J.Gibbins, "Propagation of very short pulses trough the absorptive and dispersive atmosphere", IEEE Proceedings, V. 137, No. 5. pp. 304 – 310, 1990.
4. R.K. Crane, "Coherent Pulse Transmission Through Rain", Trans. AP-15, № 2, pp. 252-256, 1967.

Monitoring spatially - temporary distributions of fields of harmful impurities in atmosphere by methods of microwave sounding it from a surface of the Earth and from space

S.D.Dubko, L.V.Kostenko, L.N.Litvinenko,
B.I.Makarenko, E.I.Solokha
Joint-stock company Research institute of radio engineering measurements
310054, Ukraine, Kharkov, street. The academician Pavlov, 271
Ph. (0572) 26-52-00, fax (0572) 26-41-12
E-mail: niiri@ cnti.uanet.kharkov.ua

The importance of a problem of monitoring of concentration of harmful scanty gas components (SGC) of atmosphere of the Earth and the stratum of ozone is well-known. There is a lot of appropriate techniques permitting to decide the given problem. All of them have the dignities and defects.

It is offered to use stationary space vehicles for monitoring of atmosphere of the Earth with the help of microwave radiometry and microwave radio spectroscopy.

The radiometric methods are based on a reception of own heat radiation of molecules of SGC and suppose development and creation of highly sensitive multichannel radiometers located both on the Earth, and on flight vehicles, including satellites, for realization of limb sounding.

The entries, obtained with the help of such radiometers, of radio brightness temperature from frequency in windows of a transparency of atmosphere in ranges of lengths of waves of 4-1,5 mm contain an authentic information for determination in atmosphere of the following SGC:

O_3, SO_2, H_2O_2, HCN, ClO, BrO, CH_3Cl, HOCl, CH_3OH and others, all up to 30 types of molecules.

From the entries structures of concentration of an ozone and temperature of atmosphere at heights up to 120 km also can be obtained.

The method of microwave radio spectroscopy is based on radioscopying throughout all atmosphere by a coherent radiation of a source of a microwave radiation with high stability of frequency 10^{-10} from the satellite located on geostationary orbit. For this must be:

the frequency of a source with a small pitch of a discretization is rebuilt in a broad band;

the antenna of an emitter has the narrow directional diagram and supposes scanning of an irradiated surface of the Earth;

the rough level of a potency of an emitter when using for sounding windows of a transparency of atmosphere does not exceed 100 mW.

The high sensitivity of a method is achieved due to use in a ground equipment of receivers with a narrow band, which heterodynes are rebuilt strictly synchronously with a modification of frequency of a spacecraft emitter.

The lines of an absorption of rotary transitions of SGC are registered, as characteristics on a unresonance pedestal of an absorption of atmosphere.

Information about concentration of an ozone and other SGC, and also the structures of their high-altitude distribution are obtained by accounts from entries of spectral lines

The method of microwave spectroscopy is connected to the certain technical difficulties for the realization.

The development of following items is necessary for realization of the method of microwave spectroscopy:

highly sensitive multichannel radiometric complexes of ground basing in a range of lengths of waves of 4-1,5 mm;

onboard radiometric complexes of the same range which are capable to be placed as on airplanes and on the satellites;

controlled scanning antennas of radiometric complexes with a high exactitude of the space sanction;

onboard microwave emitter with high stability and exactitude of installation of frequency of a radiation with the appropriate software;

a highly sensitive heterodyne receiving complex of a microwave range with an antenna and computer complex realizing management of the heterodyne and realizing the collection and information processing with the appropriate software;

technique of account of high-altitude structures of concentration of an ozone and SGC along a line the transmitter - receiver.

At the same time, the dignities of active coherent spectroscopic methods such as sensitivity and resolving power are inherent in an offered method.

Large dignity of radiometric methods is the absence in measuring complexes of active sounding emitters. However use of a weak non-coherent radiation of atmospheric molecules entails known problems with sensitivity, resolving power and dynamics of updating of a received information.

For modelling of conditions of distribution of radiowaves in altitude range of 0-100 kms the stend was developed.

With the help of given stend the model experiments were conducted and the possibility of synonemous solution of a problem of a determination of a high-altitude structure of concentration of molecules SGC is confirmed, having for primary datas of entries jf lines of an absorption on a long line in conditions, when the pressure of gas varies depending on height from 1 up to 0,001 atm.

The conducted accounts, prototyping and experimental researches testify to marketability of a combined method of monitoring of atmosphere of the Earth, giving a possibility to inspect spatially - temporary distribution of fields of harmful impurities in atmosphere, and allow to formulate specifications to onboard and ground means of a complex ensuring realization of a method.

There is a basis for development of a technique of account of high-altitude structures of concentration SGC along a line the transmitter - receiver.

On our sight, the transition to new methods of monitoring will be a large pitch forwards in a solution of ecological problems in global scale.

ATTENUATION FACTOR FOR X- AND Ka-BAND NEAR SEA SURFACE

V.B.Razskazovsky, Yu.A.Pedenko, Yu.F.Logvinov
National Academy of Sciences of Ukraine, Usikov Institute for Radiophysics and Electronics
Adress: 12 Proskura St., Kharkov, 310085, Ukraine
Tel. (0572)44-83-33, Fax (0572)44-11-05, E-mail: sugak@ire.kharkov.ua

The results of the experimental investigations concerning the attenuation factor of the electromagnetic field in X- and Ka radiowave band for it's propagation at grazing angles nearby sea surface have been analyzed in the report. Attention is devoted basically to the statistical parameters of the field in the space area that corresponds the penumbra in the standard refraction conditions. The phenomena in illuminated zone have been investigated well enough for now and the applicability of the interference field description for practical calculations is proved. At the same time the radar monitoring realized by ship and coastal radar and focused on sea waves and objects elevated slightly above the water surface, such as floating ice, logs or reefs has to be realized in the conditions of operating in the penumbra. As the experimental researches and the theoretical analyses results show [1-5], both interference model and the diffraction phenomenon on the Earth spherical surface can not be used for the description of the millimeter and centimeter waves in this zone. It was presented in our papers [1,2], that a series of the phenomena discovered in the penumbra experimentally, in particular, signal fluctuations spectra features, one can explain presenting the field at low height above the surface as a result of a diffraction on the wave crests, that are simulated as opaque half-planes in the calculation. In the submitted paper the characteristics of the attenuation factor are discussed, that are needed for the radar set power computing: its mean values, distribution laws as the functions of the range and the elevation of the observation point above the sea surface.

The conditions and the measurement technique were as following. The receiving unit was placed at the steep coast, its antennas elevation above the sea level was about 12 m, and beam widths were 150 mrad in X-band and 35 mrad in Ka-band. With such antennas parameters the boundary of the illuminated area was not less than 750 m off the coast, where sea depth was more than 25 m. The transmitter units was mobile one and at measurements was located on the shoreline at distances 7.8 km or 14.5 km, its antenna height was altered from 0.1 m to 1.5 m over sea level. The range 14.5 km corresponds to radio horizon in the case of the minimum elevation of the transmitting antenna and the standard refraction. The beam width of the transmitting antennas was about 0.2 rad in both planes, so the boundary of the illuminated sea surface was close enough to antennas. The experiments were produced at June, the sea state was 1...3. During an experiment the signal amplitude had being recorded at the receiving point for each range and transmitter unit elevation; the interval of the recordings was about 100 sec, that allowed through the following statistical processing to derive the fluctuations characteristics known usually as fast fading. The experiments in X- and Ka-bands realized by turns, after all of the elevations varying was finished. The determination of the methodical (measurer's) constants that were need for the attenuation factor calculation, were provided by the calibration procedure on the short path with exact known length under the propagation conditions met the free space requirements. Taking into account the calibration errors and the inaccuracy in the mutual antennas orientation, the error for determination of the attenuation factor absolute value was not more than 3 dB; within one record realization the relative values of the random errors were less 0.2 dB. By the statistical processing of the experimental data it was obtained the attenuation factor mean values for each 100-sec record, the second direct and central moments, skewness and kurtosis coefficients of the amplitude fluctuation distribution, as well as the fluctuations power spectra. The peculiarities of the last and the explanation of these features appearance were analyzed in our papers [1,2] in detail and are not discussed here.

The most interesting results are ones detected for 14.5 km range. It has been presented (Fig.1) the height dependencies of the attenuation factor mean values for X- and Ka-bands. The solid and dashed curves show the computed values for the standard refraction case (solid line) and for critical refraction, i.e. for the «flat» Earth (dashed line). One can see from the figure, first, that the attenuation factor does not depend from the wave polarization, second, that it's values were higher during the probing than it has to be for the standard refraction; on the average it was close to the values calculated for the «flat» Earth, i.e. for the critical refraction in the boundary layer. It is noticeable, too, there is more slow decreasing of the attenuation factor causing by the transmitted antenna lowering, than it has been predicted by the interference model. This phenomena manifests stronger in Ka-band. This peculiarity was observed by authors of the paper [3], too, where in the purpose of the matching of the computed and measured values they used to assume the mean square height of the sea waves was

about 3 times more than was provided by the sea waves heights data. At the ranges 14.5 km and 7.8 km and during the transmitted antenna elevation varying from 0.2 to 1.5 m the value of the attenuation factor in Ka-band is higher up to 10 dB in average than one in X-band, that could be shown at Fig.2. At this figure the measurement results in these two bands are presented, that were obtained during the same probation, i.e. with the time difference less than 1.5...2 hours. During this period the conditions of the radio refraction can not change significantly on the path. The solid line in this figure is the regression line, that characterize the statistic dependence of the attenuation factors in X- and Ka-bands. This result agrees with the experimental work [5] conclusions, where it was established that the X- band field amplitude is higher than calculated predictions in the penumbra , while at the 3 GHz and 1 GHz frequencies the measured fields are close to calculated ones.

The distribution of the attenuation factor fluctuations had been investigated, first, from the point of view of their influence on the parameters of the backscattering by sea surface and by objects located there, second, focusing on the corrections of the field forming physics in the penumbra above real sea surface. As a theoretical probability distribution needed to compare with the experimental data, the m-distribution (Nakagami distribution) were chosen, that has more power than the Rice distribution. Its dimensionless parameter is

$$m = \left(\overline{A^2}\right)^2 \Big/ \left(A^2 - \overline{A^2}\right)^2 \geq 0.5 \ ,$$

where A - the signal amplitude. For $m = 1$ the Nakagami distribution coincides with the Rayleigh law, and for $m > 1$ – with the Rice law, the parameter of the last is connected with the m by the dependence

$$\eta = \frac{A_0}{\sqrt{\left(A - A_0\right)^2}} = \left(\frac{\sqrt{m^2 - m}}{m - \sqrt{m^2 - m}}\right)^{\frac{1}{2}} ,$$

where A_0 - the amplitude of the signal stable component. The m calculation results on the experimental data base shown, that with the very rare exceptions its values in the penumbra are $m \geq 2$, and with the 50 % probability $m > 10$ in both wave bands under investigation. In the case of the transmitters elevation varying from 0.25 m to 1.5 m it accompanies with the growing of the high values m appearance probability. The statement can be confirmed by Fig.3, where the empirical cumulative distribution functions are shown for the m parameter in X- and Ka-bands for the 14.5 km range and 0.25 m and 0.5 m elevations. One can see that the wavelength shortening and the lowering of the transmitter antenna lead to probability increasing of less values of m parameter, i.e. to the raising of the attenuation factor fluctuation depth, that were noticed in paper [5], too, and could be seen from the figures in the paper [3].

The results of the skewness and kurtosis coefficients of the attenuation factor fluctuations for the 7.8 km and 14.5 km ranges and for transmitter heights from 0.2 m to 0.6 m are presented in Fig.4 and Fig.5; its marked by various signs the combinations of the different ranges, elevations and polarizations, while corresponding m values are on the vertical axes. The solid line shows the calculated values for the Nakagami distribution in these figures. Its clear from the figures, that the experimental values of the skewness coefficients are drifted into the negative area, while the kurtosis coefficients into the positive area relatively to the curves of the m-distribution. As the comparison with the data of 0.6...1.5 m transmitter heights shows, the differences with the m-distribution appear less in the last case.

The realized investigations allow to make the next conclusions, that is useful for the practice:

1. For the case of the radio path geometry, that corresponds to the sea surface monitoring by the ship and coast radar in the penumbra, the using of the Ka-band provides for the heights above the surface less than 1 m the increasing of the attenuation coefficient up to about 10 dB in comparison with the X-band.

2. Within the time periods comparable with one hundred seconds the attenuation factor fluctuations can be described with the accuracy, that is good enough for the practice, by the Nakagami distribution (m-distribution) or by the Rice distribution. The relation of the mean power square of the field to the mean square of their fluctuation component (parameter m) even at tens centimeters height above the surface is more than $m \geq 10$ in the Ka-band; the relation increases with the height above the surface and the wave length increasing.

The work was realized with the support of the Science and Technology Center in Ukraine, project No.145.

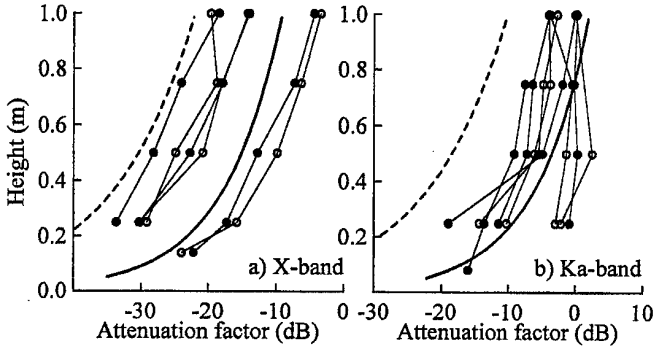


Figure 1. Field attenuation factor versus height:
o - horizontal polarization; • - vertical polarization.

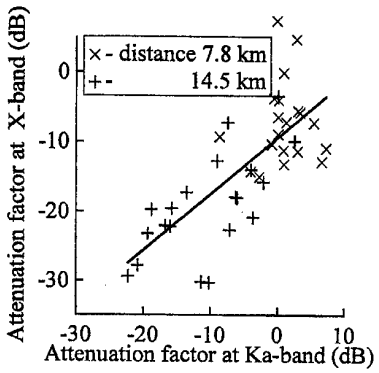


Figure 2. Correlation between attenuation factors at X- and Ka-band

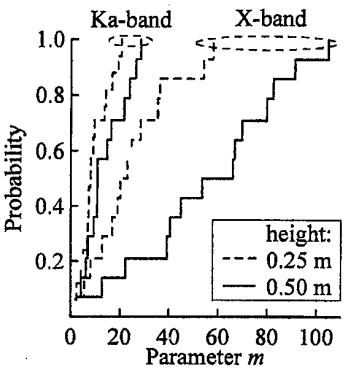


Figure 3. Empirical cumulative distribution functions for parameter m

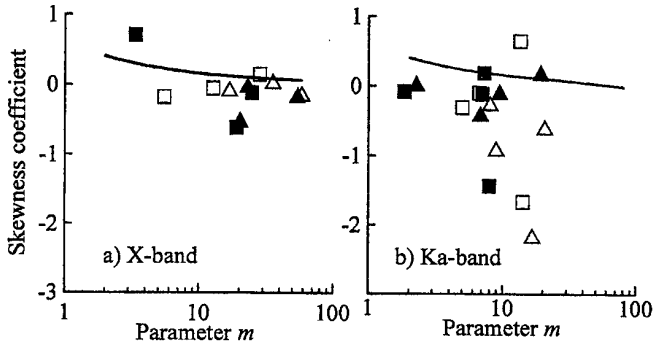


Figure 4. Skewness coefficient versus parameter m*

*Conventional signs for Fig.4 and Fig.5

□ ■ - height 0.25 m;
△ ▲ - height 0.5 m;
■ ▲ - vertical polarization;
□ △ - horizontal polarization.

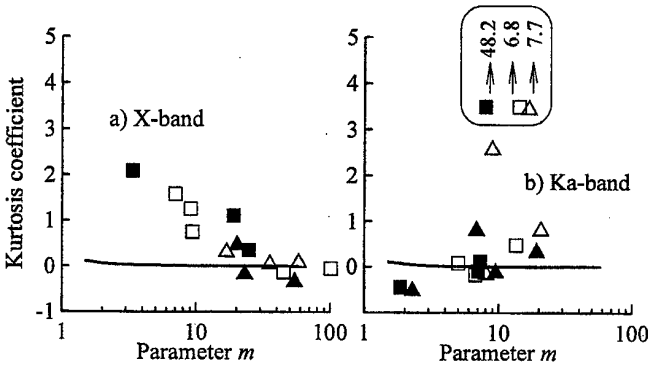


Figure 5. Kurtosis coefficients versus parameter m*

References

1. V.B.Razskazovsky, Yu.A.Pedenko, "Multipath propagation over the sea", Zarubezhnaya radioelekrtonika, No.7, pp.23-39, 1996, (in Russian).
2. Yu.F.Logvinov, Yu.A.Pedenko, V.B.Razskazovsky, "Influence of shadowing on spectra of millimeter waves fluctuations under multipath propagation over the sea", Radiotekhnika i elektronika, Vol.43, No.7, pp. 1-6, 1998, (in Russian).
3. S.P.Zehner, W.M.O'Dowd, Jr, F.B.Dyer, "Forward-scatter of microwaves near the surface of the ocean", "Int.IEEE/AP-S Symp.Program and Dig., Atlanta, Ga, 1974", New York, N.Y., pp.8-10, 1974,.
4. P.D.L.Williams, "Change of the fading characteristics of reputed steady targets as a function of sea state in a marine-radar environment", Electronics Letters, Vol.6, No.26, pp.853-855, 1970.
5. R.E.H.Berry, "Radar propagation at very low altitude over the sea", "Int. Conf. on Radar-Present and Future, 23-25 Oct. 1973", London, pp.140-145, 1973.

SPECTRAL AND CORRELATION CHARACTERISTICS OF FLUCTUATIONS OF A POINT RADIATION SOURCE BEARING UNDER STRONG EFFECT OF A SEA SURFACE IN W-RANGE

N.V.Gorbach, L.I.Sharapov and N.V. Ryazantseva
Wave Propagation Laboratory, Department of Space Radiophysics,
Institute of Radio Astronomy of the National Academy of Sciencies,
4, Krasnoznamennaya St., Kharkov, 310002, Ukraine
Tel. 0572 44 85 81, Fax 0572 47 65 06, E-mail sharapov@rian.kharkov.ua

Results of experimental investigation of amplitude interference-fading and angular fluctuation of a point source near a sea surface are discussed. The analysis enables one to make conclusion that on sliding propagation along the line-of-sight sea path, even in case of a strongly rough surface, there is a rather high probability of existence of the limited number of quasi-mirror reflections. In this paper the main results of experimental investigation of statistic characteristics of amplitude and arrival angle fluctuation of detecting and direct 3mm-band signals are reported, related to the case of over sea propagation with sliding angles from 1 to 10mrad (distances from 300m to 5000m).

The investigations fulfilled of the mutual correlation function of signals in the amplitude and angular direction finder channels have shown that the distance dependence of correlation coefficient ($R_{A\varepsilon}(0)$) have a sufficiently well pronounced extreme (such dependence type will be subsequently referred to as ''resonance type''). Such a ''resonance type'' dependence was observed during the investigation of radio wave propagation in the surface troposphere layer [1].

As an argument of the functional dependence $R_{A\varepsilon}=f(\tau_*)$ in these papers the parameter $\tau_*=l/\sqrt{(\lambda D)}$ as used which represents the ratio of troposphere inhomogeneity dimensions (l) to the Fresnel first zone dimensions (λD). The correlation maxima were observed at $\tau_*=1$. As stated above, in the case under consideration, the increasing of correlation may be produced by the existence of the limited number of reflectors on the interface, their dimensions being considerable with the first Fresnel zone dimensions.

We have established that the ''resonance''- dependence extreme position on the distance axis is connected with the sea-way period value (the dispersion relation for gravitational waves is $\Lambda=1.5T^2$, the Λ(meters) and T(sec) being the dimensional and time period of the sea-way respectively).The smaller was the period the smaller were the distances at which the maximum values of the mutual correlation coefficient module ($|R_{A\varepsilon}(0)|$) were registered. In case of the emission source being at the bore sight, basically the negative correlation was observed.. In some experiments it was discovered that angle and amplitude spectra-width (ΔF) distance dependence have the ''resonance'' form.

We have established that when the sea-way period decreasing the effect of fadings, which show up in reducing of quasi-mirror reflection intensity manifests itself at lesser distances. In such a manner one would explain a faster drop in the correlation level with an increasing distance when the sea-way period decreases and therefore the shifting of the extremum toward the lesser distances. The similar results that enter into the treatment of fading effects were obtained in [2].

For systematizing of results we have used a wave parameter $D_\xi=\Lambda(h_1+h_2)/(2D\sqrt{D\lambda})$ having the meaning of unevenness correlation radius (in our case it is $\Lambda/2$, one-half of the sea wave length) to the first Fresnel zone longitudinal dimension ratio [3]. The use of D_ξ in the distance distributions $R_{A\varepsilon}(0)$ has led to ''resonance'' dependence coincidence along the abscissa axis and allowed to construct empirical curves limiting the region in which all the experimental $R_{A\varepsilon}(0)$ values obtained for various sea surface states. The resulting dependence and experimental $R_{A\varepsilon}(0)$ values, taken by absolute value and normalized to $|R_{A\varepsilon}(0)_{max}|$ separately for each experiment series with various sea-way, are presented in Fig.1. The character of the dependence resembles the behaviour of amplitude and phase correlation coefficient theoretical

dependence of D_ξ shown in [3]. However, it is necessary to stress some distinctions. Firstly, where the theoretical dependence have an increasing section and plateau beginning from values $D_\xi > 1$, the experimental curves have a rather well pronounced resonance character. The existence of a descending section that in our case corresponds to small distances may be explained by the directional diagram influence, because the diagrams reject at short distances a significant part of the power reflected by the interface. Secondly, D_ξ values corresponding to maximum values of correlation coefficients in experimental dependence differ more than by order of magnitude from the D_ξ values corresponding to transition into plateau of the theoretical dependence [3]. Consequently, while in the physical model adopted in [3] the correlation between amplitude and phase fluctuation tends to limiting values if the correlation radii of unevenness are comparable with or exceed the first Fresnel zone dimensions $D_\xi \geq 1$, in our case the $\left| R_{A\varepsilon}(0)_{max} \right|$ are noted if the number of unevenness periods within the first Fresnel zone makes several tens (Fig.1).

The suggestion can be made that such a behavior of experimental dependence is connected with the sea-way structure periodicity, if the sea surface is regarded as some diffraction grating. as noted above, a significant influence on the rereflected field characteristics must exert shadowings. To check the suggestions the development of theoretical models and carrying out of further experimental investigation is needed.

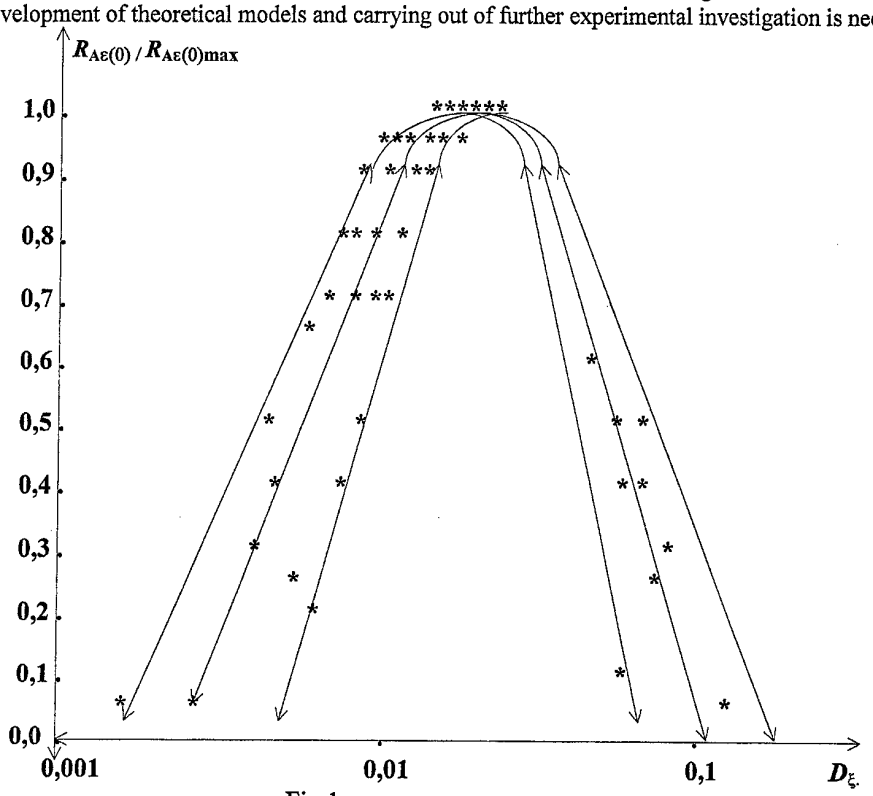


Fig.1.

References

1. A.S. Zakharov, V.A. Timofiejv, "Cross-correlation of the fluctuation of level and arrival angle of millimeter waves in a turbulent boundary layers", Vsessojus. konf. po rasprostr. radiovoln (Kharkov, Oct., Tez. dokl. p. 6, 1990).

2. N.V. Gorbach, A.I. Mikhailovskij, I.M. Fuks, L.I. Sharapov, " Spectrum of interference noise over a rough surface at small sliding angles", Iv. Vusor., Radiofizika, Vol. 36, ¹ 11, ðð. 1294-1302,1994.

3.F.G. Bass, I.M. Fuks, " Scattering of waves by a statistically uneven surface", Nauka, M., 424 p., 1972.

PREDICTION OF MILLIMETER WAVE ATTENUATION IN INDIAN CONTINENT

Bandopadhyaya T. K. & Poonam Saxena

Deptt. of Electronics & Computer Engineering
Maulana Azad College of Technology
(Regional Engineering College)
Bhopal - 462 007 (INDIA)

Introduction

With the advent of Satellite communication, the propagation of electromagnetic wave through atmosphere has created some interest in recent years. In India, in the recent years, Microwave and also Millimeter wave have been extensively used for voice and data communications. However the Millimeter wave propagation is very much affected by the atmospheric constituents namely : rain, fog, sand dust storms and different participants present in the atmosphere. The phase and amplitude of the signal changes considerably due to several phenomena like reflection, refraction, scattering, absorption or depolarisation of Millimeter Wave passing through Atmosphere.[2]

Analytical Treatment of Attenuation

The attenuation caused by such particles is one of the major problems in the utilization of Millimeter Wave bands for terrestrial and space communication. When these waves pass through the medium containing participation like sand and dust storms or through rainy area three phenomena occurs :
Reflection of wave;
Absorption of energy by these particles; and
Scattering of energy out of the beam by these particles.

As the wave incident dust particles oscillate and radiate energy in all directions, resulting in an appreciable amount of attenuation which is a function of size and the concentration of these particles. In general, these particles are never uniformly distributed over an extended region of storm. Therefore, concentration of particles as well as attenuation are the function of distance along the path. The total Volume of particles in unit volume of the storm is defined by the following relation [3] :

$$\text{Total Volume of particles in unit volume of the storm} = \frac{9.43 \times 10^{-9}}{V^{\gamma} \times (4\pi/3)a^3} \qquad \ldots\ldots 1$$

where V = Visibility in Km ;
a = radius of the particles ; and
γ = a constant = 1.07.
and the attenuation due to these particles can be obtained in Db/Km as [1]

$$\text{Attenuation in Db/Km} = \frac{434 \times 9.43 \times 10^{-9} \lambda^2 X^3}{V^{\gamma} \times (4\pi/3)a^3 \times 2\pi} (C_1 + C_2X^2 + C_3X^3) \qquad \ldots\ldots 2$$

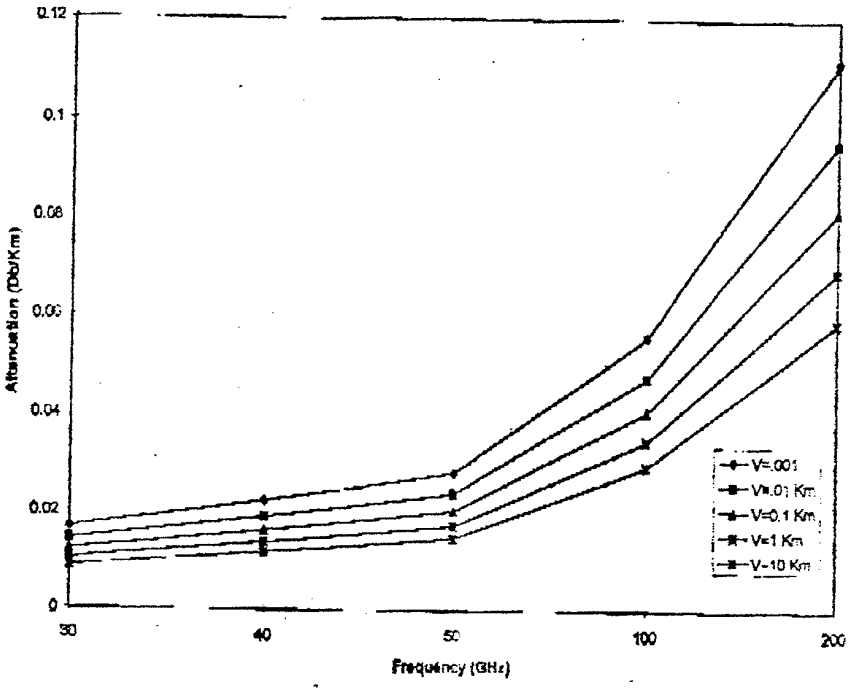
where $X = 2\pi/\lambda$ and C_1, C_2, C_3 are the constants.

A record of all sand and dust storm and long-term mateorological data have been collected from Indian meteorological department for different stations of India and several calculations have been carried out relating attenuation due to adverse atmospheric conditions.

Since particle size is statistical in nature hence on an average radius of particle size is assumed to be constant = 0.155 mm for all over the country. In order to find the variation in attenuation with frequency, visibility, and particle size some calculations have been carried out . Attenuation with frequency curve has been plotted as a function of visibility (Fig. 1).

The size of the particles (sand and dust) are very small in comparison to wavelength at such high frequencies, the attenuation is directly proportional to concentration . Hence The attenuation almost linearly with frequency for the given value of visibility. *Visibility* is nothing but "Concentration of Particles " . Since visibility is not constant in nature , calculations have been carried out for different values of visibility. [3]

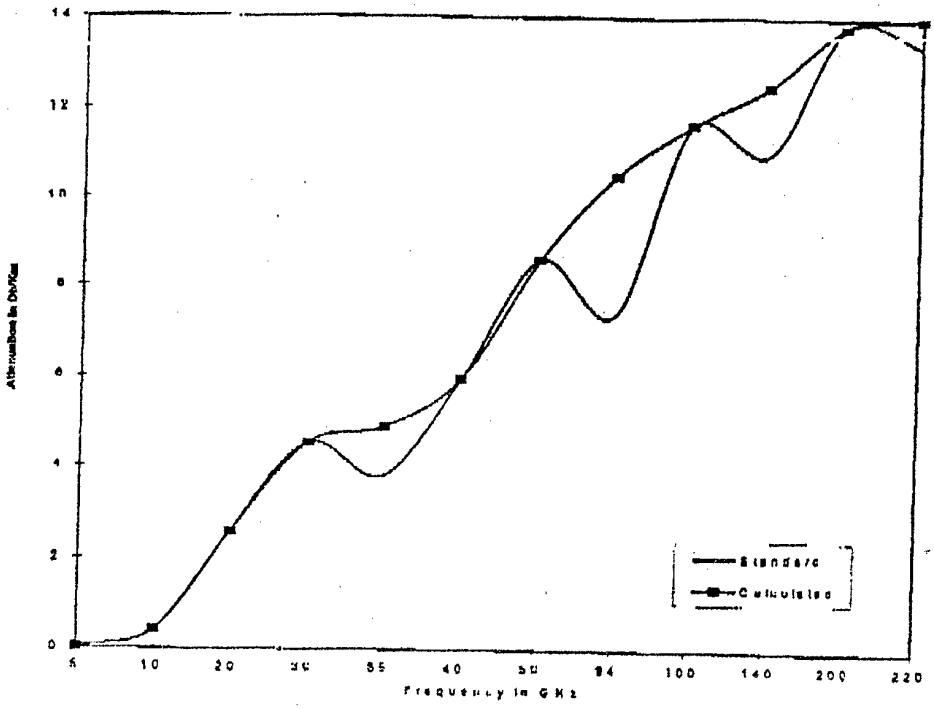
Fig. 1 Variation of Attenuation with frequency for different Visibilities



It may, therefore, be concluded that the attenuation due to sand and dust particle depends heavily on the frequency, visibility (Concentration of particles) , Maximum particle radius, and complex dielectric constant of the particle. The concept of Raleigh scattering is used to predict the losses due to attenuation at such high frequencies.

In the case of raintall, attenuation is a function of rain rate, intensity and drop-size distribution. The results are presented in the form of curves (fig. 2) relating attenuation as a function of rainrate & frequencies. The calculations have been carried out using long-term meteorological data for indian condition. However our results are not strictly match with those reported elsewhere for western country because their weather climete are entirely different from Indian weather condition. [4-5]

Fig.-2 Attenuation Vs. Frequency Curve



Conclusion

It may, therefore, be concluded that the attenuation in the propagating electromagnetic wave in adverse atmospheric condition strongly depends on the operating frequencies , visibility and rainrate. The loss is significantly high at higher frequencies and at low visibility due to higher reflection and low transmission at low visibility. The result are presented in the form of curves considering Indian atmospheric conditions and compare with western results as their weather climate are different.

References

1. B.R. Vishwakarma et. al. " Transmission Line Model for Loss Evaluation in Sand and Dust storms" Indian Journal of Radio & Space Physics Vol. 23, June 1994, pp.205-212.
2. C.S. Rai et. al. "Depolarisation of Millimeter Wave Back Scattered by Sand and Dust Storms " IE(I) Journal-ET, February 1993, pp. 111-116.
3. Dr. C.S. Rai et. al. "Prediction of mmw Attenuation in Dust Storms Under Rayleigh Approximation "IE(I) Journal-ET, Vol 77, September 1996, pp. 11-16.
4. Saxena Poonam & T.K. Bandopadhyaya "Rain Rate Statistics and Fade Distribution of Millimeter Wave Radio Link in Indian Continents" International Journal of Infrared and Millimeter waves, Vol. 19, March 1998.
5. Sharma " Significance of Rain Induced Attenuation and multipath in the Design of Digital Microwave Links", IETE Technical Review Vol 12 Nos5&6 September-December 1995,pp359-373.

THEORY OF WAVEGUIDE PROPAGATION IN RANDOMLY CORRUGATED CHANNELS

N. M. Makarov, A. V. Moroz
Institute for Radiophysics and Electronics of National Academy of Sciences of Ukraine
12 Academician Proskura St., Kharkov, 310085, Ukraine
Tel. (380)572-448331, Fax (380)572-441105, E-mail: mak@ire.kharkov.ua

Evolution of an emitted signal in a waveguide line is known to be highly sensitive to perturbations of lateral boundaries. Mainly depending on the size of the perturbations, there exist different evolutional scenarios for the signal. Evidently, in extremely imperfect systems, where the typical height ζ of the surface corrugations is comparable with the average channel thickness d, the wave field is expected to be locked by a few adjacent high elevations. In this case a long-distance propagation of the signal through the waveguide is certainly out of the question. However, for telecommunication applications, the most favourable regime is exactly that when the primary wave packet passes sufficiently long distances from a source owing to *multiple* re-reflections from the opposite walls. In what follows such regime will be referred to as a *waveguide propagation.*

The process of multiple re-reflections is seriously obstructed by a non-coherent surface scattering that always accompanies wave propagation in rough-bounded systems. As a result of the multiple successive scattering events, the spectrum of normal waves in an imperfect channel differs from that peculiar to the flat-walled situation. If a waveguide type of propagation is the case, then that spectrum difference can be attributed to the complex deviation $\delta k_n = \gamma_n + i(2L_n)^{-1}$ of the longitudinal wavenumber of an n-th natural mode from its unperturbed value k_n. The real part γ_n of δk_n is responsible for *dephasing*, or a modification of the phase velocity, for the n-th mode. The value of L_n, which specifies the imaginary part of δk_n, has the meaning of the *attenuation length* for the given mode. In order that the rough-bounded system retains the waveguide properties, the complex dephasing associated with δk_n must remain small within a scale of the *cycle length* Λ_n, i.e. within the distance passed by the n-th mode between two successive reflections from the rough surface, $|\delta k_n|\Lambda_n \ll 1$. This criterion automatically ensures a large number $L_n/\Lambda_n \gg 1$ of the wave re-reflections within the attenuation length L_n. Note that the inequality $|\delta k_n|\Lambda_n \ll 1$ also implies the small deviation δk_n in comparison with the unperturbed wavenumber k_n, since always $k_n\Lambda_n > 1$.

Usually it seems more reasonable (from both theoretical and practical standpoints) to calculate the wave field averaged over some ensemble of the random reflecting surfaces rather than the exact field itself for a given (experimentally irreproducible) relief. If relief of lateral walls in realistic waveguides is believed to be *ergodic*, then an average over the ensemble of all realizations of the random surface is equivalent (in a sense of convergence in probability) to an average over coordinates for a certain realization (see, e.g., Refs. [1,2]). This statement is based on a definition that an ergodic random surface has the minimal fragment (region) which is statistically equivalent to a surface realization. Obviously, the effective linear dimension of the realization is of the order of the variation scale $\widetilde{R}_c$ (correlation radius) of the surface scattering potential. Therefore, statistical averaging is guaranteed correct if the complex deviation δk_n evokes merely weak complex dephasing within the realization length $\widetilde{R}_c$, $|\delta k_n|\widetilde{R}_c \ll 1$.

Thus, the *statistical investigation* of the *waveguide propagation* in a channel with randomly rough walls implies two conditions to hold,

$$|\delta k_n|\Lambda_n \ll 1, \qquad |\delta k_n|\widetilde{R}_c \ll 1, \tag{1}$$

$$\delta k_n = \gamma_n + i(2L_n)^{-1}. \tag{2}$$

Note that these inequalities are basically equivalent to the general criteria for weak surface wave scattering in finite systems.

We have calculated the average field of a point source (average Green's function) in a planar hollow waveguide with absolutely soft lateral walls, one of which is smooth and the other contains random roughness with the Gaussian probability distribution. We consider the stationary regime of propagation, when the temporal dependence of the wave field is governed by a factor $\exp(-i\omega t)$ with the frequency ω related to the wavenumber k as $k = \omega/c$. Our result is proven to be valid in the framework of Eqs. (1). From the formulae obtained we derived the most general by now explicit expressions for the shift γ_n of the eigen-wavenumber and the attenuation length L_n of an n-th waveguide mode.

To compare our results with those of the predecessors [1,3], we considered a 2D cylindrical model for roughness of an imperfect waveguide boundary (extremely anisotropic relief function, "wash-board" model). Within such assumption, the attenuation length L_n is given by

$$L_n^{-1} = \zeta^2 \frac{(\pi n/d)^2}{k_n d} \sum_{n'=1}^{n_d} \frac{(\pi n'/d)^2}{k_{n'} d} \left[\widetilde{W}_C(k_n, k_{n'}) + \widetilde{W}_C(k_n, -k_{n'}) \right]. \tag{3}$$

Here ζ is the r.m.s. height of surface asperities, $n_d = [kd/\pi]$ a number of the propagating natural modes, and $k_n = \sqrt{k^2 - (\pi n/d)^2}$ a longitudinal component of the wavenumber.

The value of L_n can be interpreted as "outgoing" (from a given n-th mode to all the n_d propagating modes) *surface scattering length*. Length L_n (3) is formed by probabilities of incoherent scattering of the natural mode in both forward and backward directions. The forward scattering is governed by the terms proportional to $\widetilde{W}_C(k_n, k_{n'})$, whereas the backward scattering (backscattering) is determined by those with $\widetilde{W}_C(k_n, -k_{n'})$.

In a widely used and simple limiting case of *small surface perturbations*, when

$$k\zeta \ll 1, \tag{4}$$

the probability kernel $\widetilde{W}_C(k_n, \pm k_{n'})$ is reduced to the spatial spectrum $W(k_n \mp k_{n'})$ of boundary irregularities, thereby transforming our expression (3) for L_n to that from the earlier papers [1,3]. Analysis shows that the inverse attenuation length L_n^{-1} is quadratic in the roughness height ζ as ζ falls into interval (4), $L_n^{-1} \propto \zeta^2$.

The expression for the real spectrum shift γ_n within the anisotropic, "wash-board", geometry was found to be too cumbersome and therefore it seems not worth citing. However, a principal point is that γ_n, as opposed to L_n (3), is formed by scattering of the travelling wave into *all* normal waves, both propagating with $n' \leq n_d$ and evanescent with $n' > n_d$. As $k\zeta \ll 1$, among the evanescent modes there always exists a group of modes, whose normal component $(\pi n'/d)^{-1}$ of the wavelength is comparable to ζ for any, however small, heights of surface perturbations. That group of modes can be shown to interact with the rough surface most efficiently (in comparison with other groups), thereby demonstrating a resonant type of scattering, in some way. Within limit (4), each of the "resonant" waves gives a contribution to γ_n proportional to ζ^2. Because the "resonant" modes are singled out by the requirement $(\pi n'/d)^{-1} \sim \zeta$, their total number is inversely proportional to ζ. Hence the value of the real spectrum shift γ_n turns out to be *linear* in ζ,

$$\gamma_n \sim \zeta \frac{(\pi n/d)^2}{k_n d} \qquad \text{at} \qquad k\zeta \ll 1. \tag{5}$$

This fact seems especially surprising from a standpoint of an asymptotic accordance with the earlier theory [1,3], where γ_n was found to be quadratic in ζ, $\gamma_n \propto \zeta^2$. The solution to the contradiction can be immediately understood if we point out that the theory [1,3] was actually built under assumption of small (perturbative) magnitude of the roughness height ζ as compared to any other typical lengths of the problem. In particular, the value of ζ was apriori believed to be smaller than normal wavelengths for all significant scattered modes (both propagating and evanescent). Obviously, this approach could not yield the correct answer for γ_n, which is mainly formed by the "resonant" waves with wavelengths comparable with or shorter than ζ.

Linear law $\gamma_n \propto \zeta$ (5) has a very important consequence. Actually, since $L_n^{-1} \propto \zeta^2$ at $k\zeta \ll 1$, the value of the spectrum shift γ_n becomes dominating over the inverse attenuation length L_n^{-1} as ζ tends to zero. In other words, the imaginary part $(2L_n)^{-1}$ of complex spectrum dephasing δk_n (2) appears to be negligible in comparison with its real part γ_n. This means that a signal propagating through a nearly perfect (weakly rough) waveguide is expected to be dephased (chaotized) much earlier (along much shorter distances) than its initial amplitude would be considerably damped.

We remind that our theory of waveguide propagation has been constructed within the framework of requirements (1). Those requirements are formulated in terms of the complex spectrum deviation δk_n which needs to be calculated itself for any specific set of external parameters d, ζ, R_c, and n. So, inequalities (1) are actually equations themselves with respect to the external parameters. Every time as new asymptotics for L_n and γ_n have been derived, they should be verified to satisfy defining requirements (1). Such verification gives actual intervals for the external parameters, where the obtained asymptotics are applicable.

In particular, in case (4) with small boundary perturbations, when $\delta k_n \simeq \gamma_n$, the verification of formula (5) generates different results depending on the ratio of the cycle length Λ_n to the mean asperity length R_c. So, if $R_c \ll \Lambda_n$, then Eqs. (1) are reduced to the restriction $k_\perp \zeta \ll 1$ on a normal (transversal) component $k_\perp$ of the wavenumber, which is evidently fulfilled in the framework of approximation (4). This physical situation is known as a regime of *weak correlations* between neighbouring reflections of the travelling wave from the randomly rough boundary (see, e.g., Refs. [1,2]). On the contrary, when $\Lambda_n \ll R_c$, the wave experiences multiple (of the order R_c/Λ_n) "impacts" with a same surface elevation and the neighbouring reflections are therefore *strongly correlated.* In this case the role of a single elevation in forming the spectrum deviation δk_n can be thought of as increased by a large factor of R_c/Λ_n. As a consequence, conditions (1) give an additional restriction $k_\perp \zeta \ll \Lambda_n/R_c \ll 1$ to guarantee a weak-scattering regime (and, hence, applicability of our theory) in waveguides with small surface perturbations (4) and strong correlations ($\Lambda_n \ll R_c$).

One important thing should be noted. Along with relatively simple perturbative case (4), our theory allows analyzing a much more complicated and practically important situation with *large boundary defects*, when

$$k\zeta \gg 1. \tag{6}$$

This situation can be hardly treated analytically in full and numerical computations work as a powerful additional tool. Both methods combined reveal a lot of interesting features in behaviour of L_n and, especially, of γ_n when the asperity height ζ is large enough. So, e.g., the real spectrum shift γ_n as a function of the parameter $k\zeta$ keeps positive and increases linearly with ζ while $k\zeta$ does not exceed unity in the order of magnitude (see asymptotic (5)). However, as soon as $k\zeta$ crosses over the unity, γ_n reaches its maximum and the increase gives place to a rather rapid decrease. This decrease changes the sign of γ_n from positive to negative shortly and further growth of $k\zeta$ is accompanied by a slowed (roughly square-root) increase of the absolute value of the negative shift γ_n. This type of behaviour can be observed numerically up to those large values of $k\zeta$ (about some tens) when weak-scattering requirements (1) fail. In other words, the surface defects can, under definite conditions, not only decrease (positive γ_n) but also increase (negative γ_n) the phase velocity of the propagating wave. This effect has certainly nothing to do with absorption of additional energy from outside, but is originated, most probably, from "pumping-over" of the energy from slower into faster modes as a result of non-coherent surface scattering.

As an important application of our theory, we passed to a limit of the infinitely large waveguide thickness d, $d \to \infty$. In this case the finite waveguide is virtually transformed into a randomly rough half-space. The spectrum of normal waves in such infinite system becomes continuous and the complex dephasing $\delta k_n \simeq \delta k_\parallel$ can be related to the average reflectance $V(k_\parallel)$ of a plane wave with a longitudinal wavenumber $k_\parallel$ scattered from the half-space,

$$\delta k_\parallel = i\frac{1+V(k_\parallel)}{\Lambda(k_\parallel)}. \tag{7}$$

This relation allows to apply many of results of the analysis of $\delta k_\parallel$ to ascertain properties of the reflectance $V(k_\parallel)$, which is an extensively used characteristic of rough surfaces in various branches of radio-location and remote sensing. So, e.g., we can infer that scattering of a wave from slightly irregular half-space (4) leads mainly to the shift of its phase velocity with the amplitude attenuation being relatively weak.

Defining weak-scattering conditions (1) can be reformulated in terms of the reflectance $V(k_\parallel)$ as the single requirement

$$\left|1+V(k_\parallel)\right| \ll 1. \tag{8}$$

This inequality certainly implies a nearly specular reflection of waves from a rough boundary.

References

1. F. G. Bass, I. M. Fuks, "Wave Scattering from Statistically Rough Surfaces", Pergamon, New York, 1979.

2. S. M. Rytov, Yu. A. Kravtsov, V. I. Tatarskii, "Principles of Statistical Radiophysics", Springer, Berlin, 1989.

3. F. G. Bass, V. D. Freylikher, I. M. Fuks, "The average field of a point source in a waveguide with rough walls", Izv. Vuzov: Radiofizika, Vol. XII, No. 10, pp. 1521 – 1531, 1969.

Localization of Waves in a Single-mode Waveguide with Statistically Identical Rough Boundaries

N. M. Makarov and Yu. V. Tarasov

Institute for Radiophysics & Electronics, National Academy of Sciences of Ukraine, 12 Academician Proskura St., Kharkov 310085, Ukraine
E-mail: mak@ire.kharkov.ua, yutarasov@ire.kharkov.ua

We analyze wave propagation in a narrow 2D waveguide which properties are substantially controlled by scattering of wave at random rough boundaries. Usually the opposite side boundaries of the waveguides are considered to have exactly the same or sufficiently close statistical properties. Among all the models of such statistically identical rough boundaries two substantially different are distinguished. One of them includes the waveguides with no correlation between the asperities of the opposite edges. Within the other model, correlation between the asperities of the opposite boundaries is exactly the same as the correlation at any waveguide edge. We refer boundaries of the latter type as completely correlated (CCB). The majority of current investigations deal with the former (not intercorrelated) kind of boundaries (e.g. [1]). At the same time, the CCB waveguides have not received due attention so far. Recently this problem was analyzed in our paper [2].

Let a two-dimensional waveguide of the length L and the average width d occupy the region of (x, z) plane specified by the inequalities

$$-L/2 \le x \le L/2, \qquad \xi_1(x) - d/2 \le z \le \xi_2(x) + d/2. \tag{1}$$

The random functions $\xi_{1,2}(x)$ with zero mean values describe asperities of the edges of the 'strip'. The inhomogeneities $\xi_{1,2}(x)$ of such a waveguide lead to randomness of its local width $d(x)$ and to fluctuations of its symmetry axis $z = \xi(x)$,

$$d(x) = d + [\xi_2(x) - \xi_1(x)], \qquad \xi(x) = [\xi_1(x) + \xi_2(x)]/2. \tag{2}$$

For stating the CCB model of $2D$ waveguide we assume the correlation equalities to be held,

$$\langle \xi_i(x) \rangle = 0; \qquad \langle \xi_i(x)\xi_k(x') \rangle = \sigma^2 \mathcal{W}(x - x'), \qquad i, k = 1, 2. \tag{3}$$

Here $\mathcal{W}(x)$ is the correlation coefficient specified by the unity amplitude and the correlation radius R_c. As a consequence of Eq. (3), it follows immediately that $\langle d(x)d(x') \rangle = d^2$ and $\langle \xi(x)\xi(x') \rangle = \sigma^2 \mathcal{W}(x - x')$. Thus the model under consideration is physically equivalent to that with the waveguide width kept constant along the whole length, despite inhomogeneities of the waveguide edges. In this case the wave scattering results from the fluctuations of the symmetry axis $z = \xi(x)$ only. For simplicity we suggest the asperities mildly sloping and neglect the shadowing effect,

$$|\xi'(x)|^2 \sim (\sigma/R_c)^2 \ll 1, \qquad \sigma^2/R_c d \ll 1. \tag{4}$$

Since the local mode structure of the waveguide remains undisturbed within the CCB model, it is convenient to use for the Green function, which specifies the transmittance, the mode representation that is valid under the Dirichlet boundary conditions at the 'strip' edges $z = \xi(x) \pm d/2$,

$$\mathcal{G}(x,x';z,z') = \frac{2}{d}\sum_{n,n'=1}^{\infty} G_{nn'}(x,x')\sin\left[\left(\frac{z-\xi(x)}{d}+\frac{1}{2}\right)\pi n\right]\sin\left[\left(\frac{z'-\xi(x')}{d}+\frac{1}{2}\right)\pi n'\right]. \tag{5}$$

In this research we address to the narrow, namely single-mode, waveguides which transmittance $T(L)$ is provided by the Fourier transform $G_{11}(x,x')$ only,

$$T(L) = -\frac{4}{L^2}\iint_{-L/2}^{L/2} dx dx' \frac{\partial G_{11}(x,x')}{\partial x}\frac{\partial G_{11}^{*}(x,x')}{\partial x'}. \tag{6}$$

We argue that under the conditions (4) the retarded mode Green function $G_{11}(x,x')$ obeys the following differential-integral equation,

$$\left(\frac{\partial^2}{\partial x^2}+k_1^2+i0-\hat{\mathcal{V}}(x)\right)G_{11}(x,x') - \int_{-L/2}^{L/2} dx_1\,\hat{K}(x,x_1)G_{11}(x_1,x') = \delta(x-x'). \tag{7}$$

Here $k_1 = [k^2-(\pi/d)^2]^{1/2}$ is the longitudinal wavenumber ($k=\omega/c$ the total wavenumber). The wave-surface scattering operators $\hat{\mathcal{V}}$ and $\hat{K}$ in Eq. (7) have different physical origins. The operator $\hat{\mathcal{V}}$,

$$\hat{\mathcal{V}}(x) = (\pi/d)^2\left[\xi'^2(x) - \langle\xi'^2(x)\rangle\right], \tag{8}$$

describes the direct intramode wave scattering. In contrast to that, the operator $\hat{K}$ governs intramode scattering of the single propagating mode with $n=1$, but through intermode transitions into the virtual evanescent modes with $n\geq 2$. Its kernel reads

$$\hat{K}(x,x') = -\left(\frac{4}{d}\right)^2\sum_{m=2}^{\infty} A_m^2\left[\hat{\mathcal{U}}(x)G_m^{(0)}(|x-x'|)\hat{\mathcal{U}}(x') - \langle\hat{\mathcal{U}}(x)G_m^{(0)}(|x-x'|)\hat{\mathcal{U}}(x')\rangle\right], \tag{9}$$

$$\hat{\mathcal{U}}(x) = \xi'(x)\frac{\partial}{\partial x}+\frac{\partial}{\partial x}\xi'(x), \qquad A_m = \frac{m}{m^2-1}\sin^2\left[\frac{\pi}{2}(m-1)\right]. \tag{10}$$

The unperturbed Green functions $G_m^{(0)}(|x-x'|)$ of the modes with $m\geq 2$ attenuate exponentially along the 'strip' over the wavelengths $|k_m|^{-1}$. In accordance with Eqs. (8) – (10) both the scattering operators $\hat{\mathcal{V}}$ and $\hat{K}$ are quadratic functionals of the derivative $\xi'(x)$. They contribute equally (in order of magnitude) to the wave-surface interaction, so taking into account the evanescent modes in solving the problem is certainly imperative.

The equation (7) for the Green function $G_{11}(x,x')$ is strictly one-dimensional and, consequently, makes it possible to analyze in detail the effects of coherent multiple scattering of waves. Inequalities (4) provide the existence of two groups of substantially different spatial scales in our problem. On the one hand, there is a group of 'macroscopic' lengths, the backscattering length L_{bs} and waveguide length L, and on the other a pair of the 'microscopic' lengths, k_1^{-1} and R_c. This makes it reasonable to apply for calculating the Green function G_{11} the two-scale model of oscillations. As the outcome, we arrive at the expression for the averaged transmittance,

$$\langle T(L)\rangle = \frac{4}{\sqrt{\pi}}\left(\frac{L_{bs}}{L}\right)^{3/2}\exp\left(-\frac{L}{4L_{bs}}\right)\int_0^{\infty}\frac{z^2dz}{\cosh z}\exp\left(-z^2\frac{L_{bs}}{L}\right). \tag{11}$$

The result (11) matches absolutely the concepts of the localization theory for one-dimensional disordered systems. It shows perfect transparency for the short enough waveguides ($\langle T(L)\rangle \approx 1 - L/L_{bs}$ at $L \ll L_{bs}$). At the same time, for the 'strips' longer than the localization length $L_{loc} = 4L_{bs}$ the transmittance (11) falls exponentially with the length L. The method used in this work enabled us to obtain the expression for the localization length $L_{loc} = 4L_{bs}$ despite complexity of Eq. (7). Here we do not write down the exact formula for the backscattering length L_{bs} giving its asymptotic estimates only,

$$\begin{aligned} L_{bs}^{-1} &\sim (\sigma/R_c)^4 \left(R_c/d^2\right) \qquad \text{if} \qquad R_c/d \ll 1 \ (k_1 R_c \ll 1), \\ L_{bs}^{-1} &\sim (\sigma/d)^4 \left(R_c/d^2\right) \exp\left(-k_1^2 R_c^2\right) \qquad \text{if} \qquad R_c/d \gg 1 \ (k_1 R_c \gg 1). \end{aligned} \tag{12}$$

In Eq. (12) we assume the correlation function $\mathcal{W}(x)$ of the asperities $\xi(x)$ gaussian, $\mathcal{W}(x) = \exp(-x^2/2R_c^2)$.

The main feature of our result is the unexpected dependence of the length L_{bs} on the asperity r.m.s. height σ. Indeed, though habitually L_{bs}^{-1} is obtained proportional to σ^2 [1], in the CCB case $L_{bs}^{-1} \propto \sigma^4$. At first glance it should give rise to an increase of the localization length as compared to that usually obtained. However, it is not the case as a rule. In a single-mode CCB waveguide even with mildly sloping boundary asperities (4) the wave localization length at certain, easily reachable, conditions appears to be much less than that in Ref. [1].

The fact that localization lengths in single-mode strips with different interboundary statistics of the inhomogeneities could deviate significantly from one another can be explained, in our opinion, in a following way. The localization length from Ref. [1] corresponds to the wave scattering by the effective potential

$$U = 2(\pi/d)^2 \xi(x)/d, \tag{13}$$

which depends on the asperity height $\xi(x)$ only. In the CCB case, all the scattering potentials $\hat{\mathcal{V}}$ and $\hat{K}$ in Eq. (7) contain the gradient $\xi'(x)$ instead of the function $\xi(x)$. Scattering by the potential (13) can be regarded as scattering by the asperity heights (or, what is more precisely, by the waveguide width fluctuations). At the same time, scattering by the potentials from Eq. (7) can be interpreted as caused by the asperity slope fluctuations (or by the waveguide bends). The strength of the by-height and by-slope scattering depends on different parameters. Whereas the scattering from the potential (13) is governed by the Rayleigh parameter $(\sigma/d)^2$, the by-slope scattering depends on the slope parameter $(\sigma/R_c)^2$. Besides, not the least of the factors is the functional dependence of the potentials on the random function $\xi(x)$. Indeed, the potential (13) is linear in $\xi(x)$ whereas the potentials from Eq. (7) are quadratic in $\xi'(x)$. Thus, the distinction between the scattering mechanisms in the waveguide with independent rough boundaries and in the CCB 'strip' brings about the difference of the corresponding localization lengths.

[1] Freylikher V D, Makarov N M, Yurkevich I V 1990 Phys. Rev. B **41** 8033.
[2] Makarov N M and Tarasov Yu V 1998 J. Phys.: Condens. Matter **10** 1523.

ESTIMATION OF ELECTRICAL PATH DELAY FLUCTUATIONS IN THE ATMOSPHERE BY MICROWAVE RADIOMETRY

B.G.Kutuza
Institute of Radio Engineering & Electronics
11, Mokhovaya st., Moscow, 103907, Russia
Tel: (7095) 203-4793, Fax: (7095) 203-8414, e-mail: kutuza@mail.cplire.ru

At the solution of tasks related to radiowave propagation through the atmosphere, it is necessary frequently to know not only average phase delay, but also its fluctuation component. Spatial - temporal variations of phase delay of millimeter waves in the troposphere depend on meteorological conditions and create significant restrictions on work of large antennas, long base inteferometer systems, space communication etc. In this paper the influence of short time (with a period less than 10 minutes) variations of water vapor and liquid water in clouds on phase delay is considered. The estimations of variations of phase delay are obtained by means of microwave radiometric measurements of the atmosphere.

The wet component of the real part of refraction index of a cloudless atmosphere in accordance with [1] is directly proportional to absolute humidity ρ $[g/m^3]$ and at the same time it is inversely proportional to temperature $T[K]$

$$n_\rho 10^6 = N_\rho = \frac{1720\rho}{T} . \qquad (1)$$

The contribution of humidity to phase delay will make

$$\varphi_\rho = \frac{2\pi}{\lambda}\int_0^\infty n_\rho(l)dl . \qquad (2)$$

The integration of expression (2) provided that the high-altitude profiles of temperature and humidity are close to the standard atmosphere, we shall obtain

$$\varphi_\rho[rad] = \frac{1{,}124\cdot 10^{-4} R}{\lambda T(0)}\sec z , \qquad (3)$$

where $R[g/cm^2]$ is total water vapor mass in the atmosphere , λ $[cm]$ is wavelength, z is zenith angle.

For a description of temporal fluctuation phase delay intensity can be taken a root square of the structural function

$$\Delta\varphi_\rho = \sqrt{\overline{[\varphi_\rho(t)-\varphi_\rho(t+\tau)]^2}} , \qquad (4)$$

where τ is temporal interval.

The connection between fluctuation intensities of phase delay and total water vapor mass can be expressed by a ratio

$$\Delta\varphi_\rho = \frac{38.9\sqrt{\sec z}}{\lambda}\frac{293}{T(0)}\Delta R. \qquad (5)$$

Total water vapor mass fluctuation were investigated in [2,3] by results of microwave radiometry of a cloudless atmosphere at wavelengths of 8 and 13.5 mm. According to this data for angle close to zenith, the relative variations of total water vapor mass change from 0.4% to 1.5 % for time intervals from 12 up to 150 sec. In the assumption, that the relative variations R do not depend on a meteorological conditions and the horizontal component of the wind velocity in troposphere is equal 10 m/sec, estimations of temporal structural functions of phase delay were obtained. The dependences $\Delta\varphi_\rho$ as function of temporal interval at the wavelength of 10 mm are shown in Fig.1. The following models of a cloudless atmosphere are presented: tropics a), standard atmosphere c), middle latitudes - summer b) and winter d). The phase delay at millimeter waves can appreciablly will change during several tens seconds at large humidity for tropics and summer atmosphere. The dependence of variations of phase delay is represented by power function

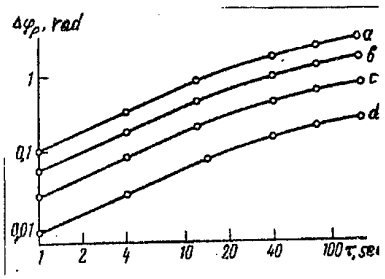


Fig.1

$\Delta\varphi_\rho(\tau) = A\tau^{5/6}$ at time intervals up to 36 sec. The phase delay variations monotonous grow with temporal interval.

An electromagnetic wave propagation in clouds and fogs results in change of its phase speed because of scattering by small drops. This effect causes increase of length of a way in the atmosphere and accordingly additional phase delay. It is assumed that the Rayleigh scattering condition is fulfilled for small drops in clouds and permitivity of liquid water is defined by the Debye formula. Let's consider the representation [5] for the formal refraction index , which for medium consisting of identical particles is written as

$$\hat{m} = 1 - iS(0)2\pi N k^{-3}, \qquad (6)$$

where $S(0)$ is amplitude function of scattering particle in a direction of wave propagation; $k = \frac{2\pi}{\lambda}$ - wave parameter; N is number of particles in unit of volume.

Real part of the expression (6) is

$$m_1 = 1 + 2\pi k^{-3} N \ \mathrm{Im}\{S(0)\} \qquad (7)$$

describes of a phase delay of an electromagnetic wave which is taking place in medium. If the size of a particle it is a lot of less than wavelength, the amplitude function of scattering $S(0)$ is defined by a ratio [5]

$$S(0) = ik^{-3}\alpha, \qquad (8)$$

where α is polarization of a particle. The drops in clouds and fogs, as is known, have the form of a sphere. The polarization of a sphere is isotrope, its value is established by the Lorentz formula

$$\alpha = \frac{\varepsilon_c - 1}{\varepsilon_c + 2} a^3, \qquad (9)$$

where ε_c is the complex permitivity of water; a is radius of a drop. Substituting (8), (9) in expression (7) we shall receive a ratio for phase delay on unit of length

$$\varphi_n = \frac{2\pi(m_1 - 1)}{\lambda} = 2\pi N k a^3 \ \mathrm{Re}\left(\frac{\varepsilon_c - 1}{\varepsilon_c + 2}\right) \qquad (10)$$

For a cloud containing small drops of the various size, the phase delay on unit of length can be written down in the following form:

$$\varphi_w = \frac{3\pi}{\lambda} \mathrm{Re}\left(\frac{\varepsilon_c - 1}{\varepsilon_c + 2}\right) w, \qquad (11)$$

The coefficient $\mathrm{Re}\left(\frac{\varepsilon_c - 1}{\varepsilon_c + 2}\right)$ determines character of temperature and spectral dependences of phase delay. The estimations show, that for wavelengths longer than 3 cm temperature of a cloud

practically does not render appreciable influence on size of phase delay. There are appreciable temperature changes of phase delay at the millimeter waves. So for example, at the wavelength of 0.4 cm the phase delay varies approximately on 7 % at change of temperature on 20 C. If the expression (11) is integrated along propagation ray with ignoring of the temperature dependence, we shall obtain phase delay at passage of a radiowave through a cloudy layer

$$\varphi_W = \frac{3\pi}{\lambda} \frac{(\varepsilon_1 - 1)(\varepsilon_1 + 2) + \varepsilon_2^2}{(\varepsilon_1 + 2)^2 + \varepsilon_2^2} W , \qquad \text{[rad]} \qquad (12)$$

where W is total liquid water content in cloud, in g/cm2; ε_1 and ε_2 real and image parts of complex permitivity of water accordingly.

In the table the average and maximal values of phase delay in cumuli form clouds Cu cong, Cu med and strati form clouds Sc are given

.Table

λ [cm]	Cu cong		Cu med		Sc	
	$\overline{\varphi_W}$	φ_W^{max}	$\overline{\varphi_W}$	φ_W^{max}	$\overline{\varphi_W}$	φ_W^{max}
0.4 cm	3.3	10	1.3	6.1	0.46	1.2
0.8 cm	1.8	5.5	0.64	3.3	0.25	0.64
3.0 cm	0.5	1.5	0.18	0.91	0.07	0.18

The table is constructed at total liquid water content in clouds, which were determined by results of multi-years microwave radiometer measurements of an atmosphere in the Moscow region. The data concern to zenith angle equals 60 degree and temperature of a cloud equals 0 C.

The temporal variations of phase delay depend on a cloudy form and volume total water content. According to the data of measurements [3,6] at strati clouds the root-mean-square variations of the brightness temperature of a cloudy atmosphere make 3.5-6 K. At cumuli clouds the root-mean-square variations of emission increase up to 15-25 K. These values are correspond to the phase delay on a wave 0.8 cm accordingly 0.1-0.2 rad and 0.3-0.6 rad.

References

1. Kerr D.E. Propagation of short radio waves, 1951, M.I.T., v. 13, New York (Me Graw-Hill).
2. Kutuza, B.G., 1974, Izv. Acad. Nauk USSR, Fiz. Atm. i Okeana, vol. 10, no 11, pp.1148-1156.
3. Gagarin , S.P. and B.G.Kutuza, 1976, Izv. VUZov, Radiofiz., vol. 9, no 11, pp. 1636-1643.
4. Gagarin, S.P. and B.G.Kutuza, 1983, IEEE J. Ocean. Eng., vol. OE-8, no 2, pp. 62-70.
5. Van de Hulst, H.C., 1957, Light Scattering by Small Particles. Willey, New York.
6. Gagarin, S.P. and B.G.Kutuza, 1977, Izv. Acad. Nauk, Fiz. Atm. i Okeana, vol. 13, no 12, pp. 1307-1311

QUASI-SYNCHRONOUS MEASUREMENTS OF RADIOWAVE ATTENUATION BY FALLING SNOW AT 138 AND 247 GHZ

N.I.Furashov, B.A.Sverdlov
Radiophysical Research Institute
Bolshaya Pecherskaya st., 25, N.Novgorod, 603600, Russia
phone : (8312) 366751, fax : (8312) 369902, e-mail : osh@nirfi.nnov.su

Introduction

Attenuation of millimeter waves by falling snow in comparison with attenuation of these waves by other hydrometeors is least studied for the present. This is explained on the one hand by known difficulties of constructing the adequate snowfall model and calculating the absorption and scattering characteristics of snow particles and on the other hand by experimental difficulties connected with obtaining data on parameters of separate snowflakes and a snowfall as a whole. Recently the investigations in the field of computer modeling of the millimeter wave attenuation by snowfalls taking into account the complicated shapes of the flakes led to first practically significant results[1-3]. As for the experimental data on snow attenuation of millimeter waves, they are rather scanty (see combined data in Ref.[4]), so that for the exposure of regularities of the attenuation and for estimate of possibilities of the theoretical models the further accumulation of such data is necessary. This paper presents the results of the comparative quasi-synchronous measurements of radiowave attenuation by falling snow at frequencies 138 and 247 GHz.

Apparatus and measurement procedure

The measurements were conducted on the territory of the out-of-town NIRFI laboratory using an almost horizontal 1-km path run at the height of 2.5-5 m above an even underlying surface. The antenna of the transmitter consisted of an elliptic primary radiator and a parabolic mirror with a diameter of 920 mm. The same parabolic mirror antenna with a detector placed at its focus was used in the receiver. The radiation was brought to the transmitting antenna from one of the two backward-wave tubes simultaneously operating in different frequency bands. The transverse size of the radiation beam (at 0.5 intensity level) at the receiver site was less then 3 m for both operating frequencies. As detectors of radiated and received power we used OAP-5M and OAP-7 thermal optical- acoustic receivers. The detector sensitivity was checked by calibration signals from near infrared radiation from incandescent lamps. The linearity of the energy scale of the receiving-registering devices was tested by special measurements. The signal recording from output of the receiver was realized both in the receiving and transmitting points.

The measuring procedure was as follows. Before each measuring seance we aimed the transmitting and receiving antennas for the maximum received signal. This was made always at 247 GHz. Then we registered the signal levels of the detectors of the radiated and received power in turn at 138 and 247 GHz and periodically calibrated of their sensitivity. The duration of signal recording at both frequencies depending on the rate of change of the received signal level was from 5-7 s to several minutes. Signal registrations were accompanied by measurements of the atmospheric pressure, temperature and the partial pressure of water vapor. According to experimental estimates the error of the measured snow attenuation coefficients was ±0.07 and ±0.1 dB/km at most at the frequencies 138 and 247 GHz respectively.

Results

Six snowfall events lasted from 2 to 6 hrs were observed. Maximum water-equivalent snowfall rate was equal to 2.7 mm/h, air temperature during the snowfall events was -7 - +0.5 C. The measurements gave the following results.

1.At distinct stages of a snowfall event the relationship between the attenuation coefficients Γ(138 GHz) and Γ(247 GHz) was found to be stable, nearly functional, and mainly nonlinear, rather well approximable by exponential function of the form $\Gamma(247\ \text{GHz}) = a\Gamma^{b}(138\ \text{GHz})$. The duration of the stage, where a=const and b=const, varied within wide limits - from 15 minutes to 2 hrs and more. For two snowfall events (out of six) such stable relationship was kept during all the time of precipitation falling(about 2 and 3 hrs). The values of the approximation parameters a and b, obtained for different stages of snowfall events, lie in the intervals:

a=2.8-4.6, b=0.6-1.3. The correlation coefficient between lg Γ(138 GHz) and lg Γ(247 GHz) (or between Γ(138 GHz) and Γ(247 GHz) in case of the linear relationship of their magnitudes) was equal to 0.97-0.99. Example of the highly correlated relationship between Γ(138 GHz) and Γ(247 GHz) given in Fig.1.

2.The relationship between the attenuation coefficients of a snowfall at some stages may have "hysteresis" character. We registered four cases, when the graphical dependence Γ(247 GHz) on Γ(138 GHz) formed a loop. In all cases the ascending branch of the loop was disposed below the descending one. Note that similar hysteresis effects were also observed by measurements of the microwave attenuation by rains[5,6].

3.Analysis of all the obtained data as a whole showed existence of the linear correlative relation between Γ(138 GHz) and Γ(247 GHz) with the correlation coefficient about 0.97; in this case the average value of the ratio Γ(247 GHz)/Γ(138 GHz), characterizing frequency dependence of the snow attenuation, turned out to be equal to 3.8 (at the interval of the observed values ranging from 1.6 to 6.2).

According to the measurements [7] of the attenuation coefficients Γ(138 GHz) and Γ(247 GHz) depending on snowfall rate the ratio Γ(247 GHz)/Γ(138 GHz) is on the average equal to 4.3. The approximation of the frequency dependence of the snow attenuation, offered on the basis of the generalization of experimental data in Ref.[4], leads to the value of this ratio equal to 3.5. Taking into account of the possible difference (on the average) of the microphysical snowfall parameters, which were not controlled in experiments, we suppose that the adduced above values of Γ(247 GHz)/Γ(138 GHz) are found in the fairly good consent with each other.

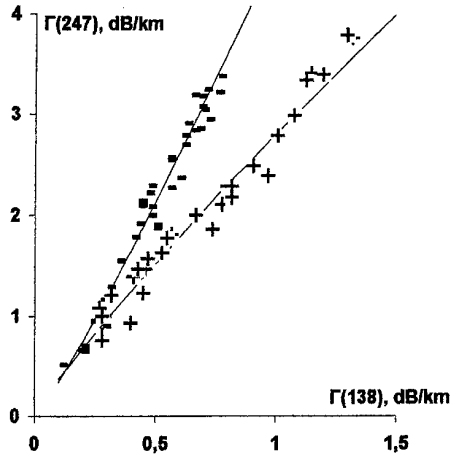


Fig.1. Relationships between Γ(247 GHz) and Γ(138 GHz) at two adjacent stages of the snowfall event. The curves-the regression lines.

References

1.P. Chylek, J.Zhan, R.G. Pinnich, «Absorption and scattering of microwaves by falling snow», Int. J. Infrared and Millimeter Waves, Vol.14, No.11, pp. 2295-2310, 1993.

2.A.M. Osharin, «Modeling of electromagnetic millimeter wave extinction by dry snowfalls», Izv. Vyssh. Uchebn. Zaved., Radiophys., Vol.41, No.4, pp.446-455, 1998.

3. A.M. Osharin, «Computer simulation of radiowave attenuation in snowfalls at 138 and 247 GHz», (see Proceedings of the present conference).

4.V.N. Pozhidaev, «Calculation of probability distributions of CM and MM radiowave attenuation on communication links taking into account of different atmospheric phenomenons», Radiotekh. Electron., Vol.37, No. 10, pp. 1764-1772, 1992.

5.D.G Sweeney, T.Pratt, C.W. Bostian, «Hysteresis effects in instantaneous frequency scaling of attenuation on 20 and 30 GHz satellite links», Electron. Letters, Vol.28, No.1, pp.76-78, 1992.

6.V.Yu. Katkov, B.A. Sverdlov, N.I, Furashov, «On the relationship between rain intensity and attenuation of short millimeter waves», Izv. Vyssh. Uchebn. Zaved., Radiophys., Vol. 40, No.5, pp.626-632, 1997.

7.N.I.Furashov, V.Yu. Katkov, B.A. Sverdlov, «Attenuation of short millimeter waves by falling snow», Abstracts of the 25-th General Assambly of URSI, Lille, France, p.266, 1996.

COMPUTER SIMULATION OF RADIOWAVE ATTENUATION IN SNOWFALLS AT 138 AND 247 GHz

A.M. Osharin
Radiophysical Research Institute
B. Pecherskaya st., 25, N.Novgorod, 603600, Russia
phone : (8312) 366751, fax : (8312) 369902, e-mail : osh@nirfi.nnov.su

In the present submission the computer simulation of the radiowave attenuation featuring in snowfalls at frequencies 138 and 247 GHz, previously investigated experimentally by our colleagues [1], is carried out. The coupled dipole method [2,3] is used as a working tool to treat the problem of the plane electromagnetic wave scattering by an arbitrary geometry particles. In this method the particle of an arbitrary shape is replaced by an array of polarizable units or cells, interacting with each other through rescattering of the incident radiation. Each cell size is supposed to be small compared to the wavelength of the incident field and to any structural lengths of the particle. In original formulation of the coupled dipole method the Clausius-Mossotty polarizability (CMP) is used to express the cell polarizability. One of the main drawbacks of CMP is the discrepancy with optical theorem arising in calculation of the particle cross sections. To avoid this we choose the cell polarizability to be the single sphere polarizability ensuing from the low frequency limit to Mie theory[3]:

$$\alpha = \frac{3}{2}\frac{\rho}{k^3}, \qquad (1)$$

where k is the wave number of the incident plane wave, $\rho = \sin(\delta)\exp(i\delta)$, $\delta = \frac{2}{3}(kR)^3\frac{\varepsilon - 1}{\varepsilon + 2}$, R-radius of the spherical cell having the same volume as cubical cell, ε-complex ice permittivity at appropriate frequency. This way chosen polarizability in contrast to the CMP permits to exactly preserve the optical theorem in calculation of the particle cross sections. Snowfall flakes were represented as a collection of dendrite-like ice crystals, intersected with each other. In present paper we used the set of dendrites containing different number of dipole cells to model the flakes. The minimum number of dipole cells in dendrite was 133 and maximum was 635. The gexagonal diameter and thickness of the dendrites were chosen to fit the empirically obtained relation between these two parameters [4]. The density of the flakes generally decrease as their characteristic size increase[5] and strongly depends upon the wetness of the flake. Considering only dry snowflakes, this property was also taken into account in computer construction of the model aggregates. The description of the flake building algorithm is described in [3]. Assuming the absence of the prevalent flake orientation in space, averaged over 27 orientations the extinction cross sections of the model aggregates were calculated. So obtained cross sections were evaluated as a function of the equivalent drop diameter size, the equivalent drop being defined as the spherical water drop, remaining after the flake complete melting. The plane wave attenuation coefficient K in snowfall was then obtained by integrating these cross sections with snowflake distribution function $n(D)dD$ also expressed in terms of equivalent drop diameter size D:

$$K = \int_{D_{min}}^{D_{max}} n(D)\, C_{ext}(D)\, dD, \qquad (2)$$

where $C_{ext}(D)$ is the averaged over orientations the value of the flake extinction cross section, D_{min}-minimum and D_{max}-maximum diameter values of the equivalent spherical drop in snowfall. We used gamma-type distribution function as a snowfall particle size distribution[5]:

$$n(D)dD = \frac{N D^{\alpha} e^{-D/\beta}}{\Gamma(\alpha + 1)\,\beta^{\alpha+1}} dD, \qquad (3)$$

where N is the concentration of the flakes, Γ- gamma-function, α and β-parameters. The specific values of these parameters can be found in[5]. All calculations were conducted at t= -5 ^{0}C for which in accordance with [6] the ice permittivity ε =3.15+i 0.01189 at 137 GHz and ε =3.15+i 0.02128 at 247 GHz. For small and medium sized snowflakes, producing drops lesser then approximately 2 mm in diameter, the average flake cross section values turn out to be well approximated by the exponential function up to the frequencies ~ 225 GHz. If a specific snow event contains flakes with equivalent drop diameter values less then ~2 mm, then in such a case the radiowave attenuation coefficient calculation can be reduced to incomplete gamma-function evaluation[7]. This approach was used previously to calculate attenuation of the plane electromagnetic wave by dry snowfalls of moderate intensities at frequencies 30, 96 and 225 GHz[7]. For bigger snowflakes having greater equivalent drop size values this approximation has lesser precision, especially at higher frequencies, and numerical integration in (2) to get the attenuation coefficient should be performed. Using gamma-type distribution (3) parameters from [5], we calculated attenuation values as a function of snowfall intensity at frequencies 138 and 247 GHz. Seven snowfall events observed in [5] at negative temperatures were used to this end. In fig.1 the results of the computed ratio K(247 GHz)/ K(138 GHz) are shown. The curve is the exponential approximation of the calculated values having the form K(247 GHz)=3.49 $K^{0.997}$(138 GHz), which is very close to linear dependency. The average value of this ratio turns out to be ~3.5 with minimum 3.2 and maximum 4.05 and gets into the range of observed in [1] values, deviated from 1.6 up to 6.2 with average value 3.8, demonstrating rather good agreement with experiment.

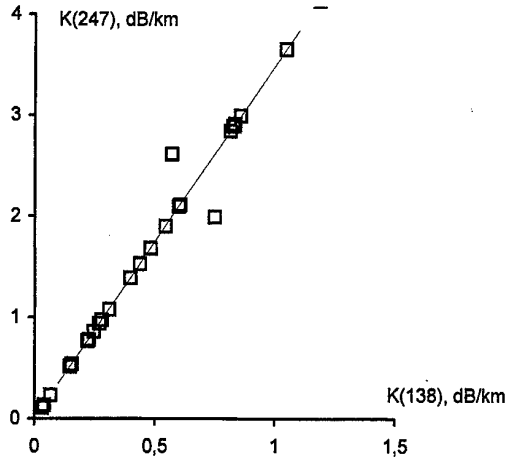


Fig.1. Calculated relationships between K(247 GHz) and K(138 GHz) for seven snowfall events.

References

1. N.I.Furashov, B.A.Sverdlov, «Quasi -synchronous measurements of radiowave attenuation by falling snow at 138 and 247 GHz», (see Proceedings of the present conference).
2. E. Purcell, C.Pennypacker, «Scattering and absorption of light by nonspherical dielectric grains», Astrophys. J., Vol. 186, No.2(1), p.705, 1977.
3 A.M. Osharin, «Scattering of millimeter radiowaves by dry snowflakes», Digest of IGARSS'94, Pasadena, USA, August 8-12, Vol.1, pp.82-83, 1994.
4. I.V. Litvinov, «Structure of the atmospheric precipitation», Leningrad, 1974.
5 I.V.Litvinov I.V. "The experience of the snowfall particle size distribution investigation», Izvestiya of the Academy of Sciences of the USSR, ser. geophysika, No.10, pp.1473-1480, 1959.
6.G.A.Hufford «A model for the permittivity of ice from 0 to 1000 GHz», URSI Nat.Radio Sci.Meet.Digest, p.14, 1989.
7. A.M. Osharin, «Modeling of electromagnetic millimeter wave extinction by dry snowfalls», Izv. Vyssh. Uchebn. Zaved., Radiophysika, Vol.41, No.4, pp.446-455, 1998.

SOME PECULIARITIES OF VEGETATION DOPPLER SPECTRA AND ESTIMATION OF THEIR INFLUENCE ON THE SELECTION PERFORMANCE OF THE 2MM WAVELENGTH RADAR

N.V.Gorbach, V.G.Gutnic and L.I.Sharapov
Wave Propagation Laboratory, Department of Space Radiophysics,
Institute of Radio Astronomy of the National Academy of Sciencies,
4, Krasnoznamennaya St., Kharkov, 310002, Ukraine
Tel. 0572 44 85 81, Fax 0572 47 65 06, E-mail sharapov@rian.kharkov.ua

In this paper spectral characteristics of passive clutter when reflected from vegetati on at the wind velosity (**V**) from 0 to 10 m/sec are discussed and the estimation of operating of doppler selection standard system (with a filter and interperiod compensation) is presented.

The measurement were performed using a pulse radar with internal cocherent wich was devised in the Institute of Radio Astronomy of NASU.

The distinguishing features of the millimeter wavelength radar`s are:
- the moderate range of detection;
- high linear and angular coordinates resolution.

This defines a small size of the reflecting ground and its commensurability with spatial sizes of reflectors at interface, in its turn, resulting in millimeter wavelength doppler spectra variation from spectra for longer wavelengths.

Using the mock-up of a coherent radar with continuous radiation, echo signals from trees, shrubbery and grass were obtained at various velocity of wind. The main feature of these spectra, which were obtained for a short time period (of order 10mcsec), is clearly defined nonstationary nature, i.e. temporal variation of main spectra parameters, such as intensity, the form and the band. Moreover, these parameters depend on vegetation type, velocity of wind and its fluctuations.

At increasing observation period (to tens of seconds) spectra become more stable and their parameters practically do not change in time.

Approximation for the averaged spectra is suggested. To levels of -8...-10dB they are adequately described by the function $\exp(-a\tilde{F}^2)$, where $\tilde{F} = F_d / F$, F_d is the doppler frequency, F is the work frequency and a is a parameter, which depends on the vegetation type and the wind velocity.

The second feature is that at levels lower than -10dB the averaged spectra slope down slowly than spectra obtained at more long wavelengths. Approximation for these portions is adequately described by the function $\exp(-b\tilde{F})$, where b is a parameter, which depends on the wind velocity and vegetation type. Similar results were obtained by authors in previous papers, for example, in [1].
The examples of spectra are shown in Fig 1. and Fig. 2.

For the averaged spectra from vegetation estimations for suppression coefficient (K_s) were obtained for traditional systems of doppler selection:
- with a filter;
- with single interperiod compensation;
- with double interperiod compensation.

According to the rejection band and repetition frequency the value K_s was:
- -3...-25dB for filter mobile target selection;
- -3...-15dB for single interperiod compensation;
- -5...-25dB for double interperiod compensation.

By this means for discussed conditions of the experiment it can be said that in 2-mm wavelength range effective systems of doppler selection can be devised.

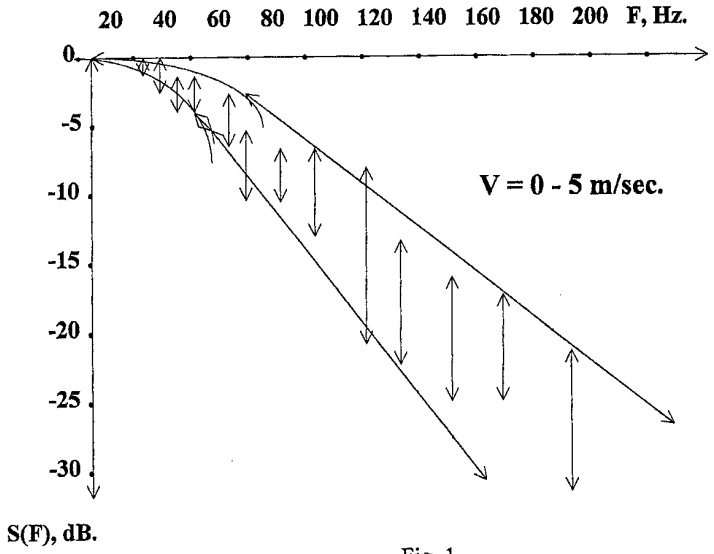


Fig. 1.

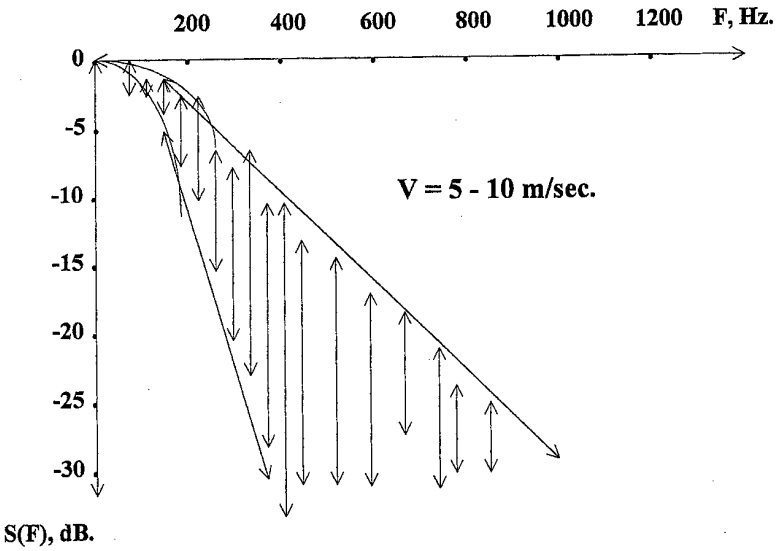


Fig. 2.

References

1. V.G. Gytnik, N.V. Gorbach, L.I. Sharapov, "Doppler Spectrum Characteristics of Radar Signals Reflected From Sea Surface and Vegetation", Turkish Journal of Physics, Vol. 19, № 8, pp. 943-945, 1995.

ON THE INFLUENCE OF AN IONIZED ABOVE-SURFACE LAYER ON WAVE PROPAGATION

G. A. Alexeev
Institute of Radiophysics and Electronics of NAS of Ukraine
12 Acad. Proscura str., Kharkov,310085,Ukraine
Tel: 380 572 448 340; Fax 380 572 441 105; E-mail: homenko@ire.kharkov.ua

The information about the new mechanisms of the beyond-the-horizon wave propagation, realized in a boundary atmospheric layer [1], gives rise to the need to analyse of the influence on the radio-wave propagation of the above-surface ionized layer, whose appearance may result in the radioactive surface, radiation, the presence of radioactive impurities in the air, penetrating cosmic radiation, an external photoeffect, evaporation of hydrated sodium ions, etc.

The importance of electron conductivity in the lower atmospheric layers is insignificant since the electrons tend to recombine with the neutral molecules for a period of 10^{-4} to 10^{-7} sec., thereby forming the negative ions. However, the mass and mobility of the lightest atmospheric ions exceed the electron parameters by an order of four, which dictates the conditions of appearance of high-frequency conductivity. The total ion static electrical conductivity of the lower atmospheric layers, which is determined by the volume aeroion concentration,is usually approximated by the exponential dependence with a positive gradient $\beta(h)$, decreasing with height, and $\beta=\beta_0 \approx 1{,}25$/km at $0 < h < 3{,}6$ km. The ionic addition to the high-frequency permittivity may have an influence upon the latter only on relatively long radiowaves $\lambda \approx 10^{3} \div 10^{4}$ m (which,in particular,are utilized by the exact time services) and this leads to an additional decrease with height:

$$\varepsilon(h)=1+2(n_0-1)\exp[-bh/(n_0-1)]-4\pi e^2 N_0 \exp[\beta(h)h]/m\omega^2,$$

where $m \approx m_+ \approx m_-$ is the mass of positive and negative aeroions, N_0 is the near-the-Earth value of their total concentration, n_0 and $b=4\cdot10^{-5}$ /km are the near-the-Earth values of standard atmosphere refraction index and its gradient. That is, in the "best"case (when the neutral atmospheric composition is neglected) the critical (which is equal to plasma) frequency of the electromagnetic wave will be less by an order of two than that corresponding to the reflection from regular ionospheric layers. The monotonous character of the height ionic addition dependence with the small gradient makes the existence of the wavequide decameter wave channel impossible.

Yet, the presence of the atmospheric static electrical field,being sustained by the thunderstorm activity,may bring about the redistribution of the above-surface layer ions, due to the so-called "electrode" effect [2], and the formation of the relatively thin (< 4 m) ionized layer with a noncompensated positive charge. The physical mechanism, which leads to the formation of the this layer, is an ambipolar diffusion of ionized atoms and molecules. The typical curves describing the height dependencies of the volume concentrations n_+, n_- of positive and negative aeroions above the earth's surface are shown in Fig. for the cases of the vertically uniform (solid lines) and non-uniform exponentially-decreasing (dotted lines) ionization sources. They were obtained as a result of the solution of the self-consistent system of equations of ambipolar current continuity and the Poisson equation [3]. These equations have the form :

$$\frac{d}{dh}\left[n_+ b\left(E_0+E_x\right)\right]=\nu-\alpha n_+ n_-; \tag{1}$$

$$-\frac{d}{dh}\left[n_- b\left(E_0+E_x\right)\right]=\nu-\alpha n_+ n_-; \tag{2}$$

$$\frac{d}{dh}E_x=4\pi|e|(n_+-n_-); \tag{3}$$

where $E_x(x) = -dU/dh$ - is vertical the component of the Poisson field, α and b are the recombination coefficient and aeroion mobility, V (h) is the ion formation intensity, E_0 is the electrical field in absence of the ionization sources, e is the charge of the electron.

From Fig. one can see that the near-the Earth volume density of the noncompensated charge N_0 is congruous with the electron concentration in D-ionospheric layer (in the day-time) and E, F_1 - ionospheric layers (in the night). The "electrode" effect is accompanied by a considerable (by an order of two) increase of the ionic addition gradient $4\pi e^2 N_0 \beta_0 / m\omega^2$ in an electrode layer, since the gradient β_0 of the total ionic concentration N= $n_+ + n_-$ may be equal to ≈ 0,5/m.

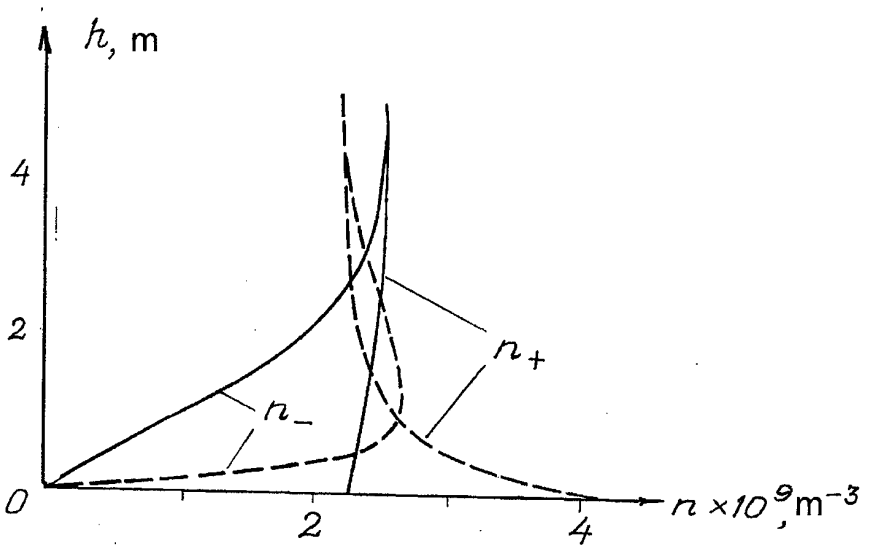


Fig. The height dependencies of the volume concentrations of the positive and negative aeroions

Unfortunately, the thickness (≈ 4 m) of the "high-gradient" electrode layer is too small for it to have an influence on the long decameter-wave propagation (the critical wavelegth of the waveguide propagation of the horizontally-polarized radiowave is ≈ 8 m), and with shorter wavelengths, as it was earlier noted, the ionic addition to ε is much lesser than the tropospheric addition.

Thus, the analysis does not permit of identifying the influence of the ionic "electrode" layer on the propagation of waves of any frequency band. However, it is possible that such an influence might be appreciable above the powerful radioactive surface-localized spots.

References

1. ''The Financial Times'' (U.K.), No.29921, p.16, 6.05.1986.
2. ''Atmosphere. Handbook'', Gidrometeoizdat. Leningrad. 510 p, 1991.
3. W.A Hoppel ''Theory of the electrode effect'', J.Atm. Terrest. Phys., Vol. 29, No.6, pp.709-721, 1967.

F



COMMUNICATIONS AND RADARS; REMOTE SENSING

F COMMUNICATIONS AND RADARS; REMOTE SENSING



Preceding Page Blank

APPLICATION OF MILLIMETER RADIOWAVES IN RADIO ENGINEERING SYSTEMS (REVIEW)

V.N.Antifeev, À.B.Borsov, R.P.Bystrov, E.V.Vashenko, A.V.Sokolov

During the last twenty years the fundamental and applied research is being conducted on effective tools for generation, reception and transformation of electromagnetic radiation in a range from 1 sm up to 0,1 mm, as well as on the analysis of practical application areas of such tools. As a result, the new principles of generation, amplification and transformation of a microwave oscillations were offered, and also the new receiving-transmitting radio engineering complexes [1-3] were developed. It has put a beginning to wide use of millimeter and shorter radio-waves in radio engineering systems of various purposes.

In works [4-7] the outcomes of the analysis of millimeter and shorter radio-waves applications are given. The block diagrams and basic parameters of priority radio engineering tools for military and civil purposes were offered. The most broad practical use belongs to active and passive radar-tracking systems for automatic detection and recognition of ground and air objects, monitoring systems for agricultural fields, cartography of terrestrial covers along with communication and information transmission systems.

The radar-tracking systems of military usage.

The analysis of Russian and foreign publications allows to make a conclusion, that the main developmental trends of military radar-tracking systems have very much in common.

Let us consider the examples of prime foreign millimeter-range radar-tracking systems which relate to an extensive class of tools for target detection and controlled weapon aiming.

In paper [4] the basic parameters of military radio engineering systems of the following classes are given:

1. Target detection and weapon control radars.

– Mono-pulse radar for antitank missile gun control with the increased reserve by means of an optimal selection of parameters of a signal and its polarization. Operational frequencies 94 and 140 GHz, firm "Sperroy", USA.

– Tank radar "Startle" for detection of the ground objects and target destination with compression of pulses and line-frequency modulation (LFM). Operational frequencies 94 and 230 GHz, distance of operation on the tank of 3-5 km., number of simultaneously tracked objects is up to 20. Firm "Rockwell", USA.

– The radar-tracking system for radiovision in complicated meteorological conditions (rain, fog). Operational frequencies 300-400 GHz, operation distance is 1-2 km. A linear resolution of 0,5 m. The research is being carried out in USA.

– Shooting artillery radar (aiming). Operational frequency 94 GHz. Firm "Standard Elektronic Lorens", FRG.

2. Flight vehicles radar.

– Onboard radar for detection and tracking of the ground objects and cartography of district, "WX-50". Operational frequency 35 GHz, impulse radiation power of 100 kW, pulse duration 200 nñ, frequency of repetition 2 êHz. Firm "Westinghaus", USA.

– Helicopter radar for collision warning with wires of electric high-voltage transmission lines. Operational frequency 94 GHz. Firm "Telefunken", FRG.

– Helicopter solid-state radar weapon aiming. Operational frequency 94 GHz, radiation power of the transmitter on the impulse diode Impatt of 5 W, pulse duration 100 ns. Firm " Lincoln Lab. Massachusets Inst. of Tech ", USA.

– Helicopter digital solid-state radar with a complicated signal. Operational frequency 35 GHz. Pulse radiation power of the faze-manipulated signal - 10 mW, pulse duration 10-15 ms, distance of operation is to 100 km. Firms of USA.

3. Passive radar.

– Radar for detection of the ground objects "Sadarm". Operational frequency 94 GHz. Firms of USA.

– Aircraft system for detection of the objects and surface cartography (radiometers). Operational frequencies 120 and 220 GHz. Firms of USA.

– Aircraft radiometer for detection of the ground objects . Operational frequencies 83,9-85,1 and 90-92,1 GHz, passband on intermediate frequency 2,9-4,1 GHz, fluctuation sensitivity 0,46 Ê. Firm "DEVIR", FRG and "EMIE", Great Britain.

4. Passive - active radar for detection of the ground objects combines modulating super-heterodyne radiometer

Dicke and frequency modulated locator. Operational frequency 94 GHz. Firms of USA.

Aircraft radar for battle-field observation . Operational frequency 35 GHz. Firms of USA.

Weather-protected active - passive system for battle-field observation. Operational frequency 220 GHz. Firms of USA.

5. Homing weapon-heads are used on rockets of "air - ground" class and on antitank rockets. Operational frequency 90-100 GHz. Firms "Hughes" and "Rockwell", USA.

6. Radar of other purposes.

– Systems for antimissile defense. Operational frequencies 35 and 95 Ghz. Firms " Lincoln Lab. Massachusets Inst. ", USA.

– Measuring radar: coherent - impulse for search of possible application areas for a short part of millimeter range (parameters of a signal: frequency of repetition, polarization, pulse duration etc.). A range of tuning of frequency 144 MHz, impulse potency 500 mW, noise factor of the receiver 11,5 dB. Firm "Texas Instrument", USA;

– Radar for investigation of ground objects reflective properties and conditions of radio-waves propagation. Operational frequencies 140 and 225 GHz. Firms of USA.

– Radio station - binocular. Operational frequency 70 GHz. Firm "TRW", USA.

– Radio-frequency voice communication station. Operational frequency 60 GHz, secure communications distance is 1,5 km. Firm "AEG-Telefunken", FRG.

In papers [4-7] the civil radio engineering systems are considered.

1. *System for marine and river navigation* in coastal zones, at pass of ships, at a lack of visibility, guiding of ice breakers and ships through northern marine path. It is shown, that for increasing of ships navigation safety the application of 8 mm and 3,3 mm radar is planned, though within the small distances for in-ports navigation of ships the application of a mm range can be extended by 1.64, 2.5 and 5 mm waves.

2. *Microcellular and picocellular communication lines* in cities with mobile and stationary objects and communication lines with re-translators along the streets with antenna systems elevated on a height 5-10 m and is almost omni-directional in difference from cellular systems. Besides, the possibilities of mm waves application for picocellular communication lines inside industrial buildings are considered. The length of such lines makes 0,4-1 and 0,1-0,4 km correspondingly. It is offered to use maximal absorption range of 5 mm, that allows to supply repeated re-translation of signals and suppression of mutual noises. Use of mm waves allows to increase transmission band-width approximately by an order and to reduce intensity of radiation operators are faced.

3. *Measuring complexes for* self-heat radiation - heat radiation of troposphere, stratosphere and mesosphere. These measurements are conducted on water vapour and oxygen absorption lines from artificial satellites of the Earth, flying vehicles, ground installations and radio telescopes. Basic directions of these investigations - definition of concentration of water vapour, its full mass, water volume in clouds and atmosphere and also recovery of temperature profiles, air density, humidity and pressure in troposphere and stratosphere [4].

4. *Application in medicine and biology* of millimeter and shorter radio-waves radiation of low (not-thermal) intensity on biological objects, including animals and men. It is shown, that the streams of continuous radiation with densities to 10-15 mW/cm^2 do not render harmful influence on health of men and biological objects. It is discovered, that the low-intensity radiation renders medical action on men in various aspects of diseases [5-7].

Inference.

Basic directions of research for the nearest years are:

– research on influence of atmosphere on accuracy of objects coordinate determination;

– study of effects of short millimeter waves propagation for rather long non-homogeneous lines;

– theoretical and experimental research of a problem of discernment of objects;

– use of polarizing matrixes for objects recognition;

– the development of passive - active radar-tracking systems for detection of the disguised and hidden objects;

– development of communication systems and radar-tracking systems on water vapour and oxygen absorption lines for security and noise-protection;

– development of high-precision radar-tracking systems for observation in space;

– development of radar-tracking systems for river and marine navigation;

– development of picocellular and microcellular systems for communication with mobile and stationary objects in urban conditions.

There is no doubt that in the future the millimeter and shorter radio-waves will discover new

applications in various areas of national economy and in military systems.

1. R.P.Bystrov, A.A.Potapov, A.V.Sokolov, L.V.Fedorova, R.N.Chekanov. - Foreign radio electronics (in Russian), 1997, N 1, pp 4-19.

2. R.P.Bystrov, A.N.Vystavkin, M.B.Golant, V.V.Meriakry, V.P.Koshelets, N.I.Sinitsyn, A.V.Sokolov, M.A.Tarasov. - Foreign radio electronics (in Russian), 1997, N 11, pp 3-31.

3. R.P.Bystrov, A.A.Merkin, A.A.Potapov, A.V.Sokolov, L.V.Fedorova. - Electromagnetic waves and electronic systems (in Russian), 1997, N 1, v.2, pp 47-53.

4. R.P.Bystrov, A.V.Sokolov. Transactions IY All-Union School on propagation of mm and sbmm of waves in atmosphere.3-10 Sept.1991 -(in Russian), N.Novgorod: AS USSR, 1991, pp 229-235.

5. N.D.Deviatkov, O.V.Betsky. - Application of mm of a radiation of low intensity in a biology and medicine. (in Russian) -M.: 1989, pp 5-20.

6. M.B.Golant . Application of mm of radiation of low intensity in a biology and medicine. (in Russian) -M.: 1989, pp 21-34.

7. A.S.Dmitriev, V.Ya.Kislov, A.I.Panas, S.O.Starkov. A device of a radiation low of intensity electromagnetic waves of mm range, MM waves in medicine. (in Russian) -M.: 1991, v.2, pp.562-564.

EXPERIMENTAL RESEARCH ON DETECTION AND RECOGNITION OF GROUND OBJECTS ON THE BASIS OF POLARIZATION PARAMETERS

N.S.Akinshin, V.N.Antifeev, A.B.Borsov, R.P.Bystrov., V.A. Nikolaev, A.V.Sokolov, I.A.Panin, D.A.Nosdrachev

It is known that one of the most complicated problem in a radar direction finding is a problem of an effective detection and recognition of objects, especially fixed ones [1,3]. In the paper it is shown that one of the promising approaches for solution of the problem lies in use of polarization parameters of radar-tracking signals.

The results of analysis of radiation scattering by objects confirm, that the polarisation characteristics can bear an extensive information both about object parameters and about its operation. It is established, that the polarization characteristics of objects at the specific frequency of exploration and fixed direction of observation can be given by five material parameters (Hujnen's descriptors) [2,4-6]:

"Noticability or size of an object" (m) - maximum amplitude of a polarized signal is a measure of a size or effective scattering surface (ESS) of object;

"Object orientation angle" (φ) - is defined as an angle between a large axe of an ellipse and axe of an object's symmetry (measure of orientation concerning a line-of-sight);

" Angle of an ellipticity " (τ) - (measure of object's symmetry to right-hand and left-hand circular polarisation);

"Slide angle" (ν), describing a multiplicity of signal from object reflections;

" Polarization angle, characteristic angle " (γ), (measure the ability of object to polarize an incident non-polarized radiation).

When studying different options of radar-tracking systems construction the specified parameters contain full information about polarization structure of a signal. These parameters are also invariant to object's velocity, power of the reflected signals and polarizing base of the radar-tracking system.

In the paper the expressions for calculation of five descriptors are derived and the theoretical investigation on evaluation of possibility of small-size ground objects detection based on polarization properties using polarization parameters vector was carried out.

Basic outcomes of experimental research of descriptors for objects in millimeter range are given below which rather well confirm theoretical conclusions about the possibility of such objects detection using polarization parameters vector

Fig. 1-3 shows the variants of experimental histograms of m,ν and γ descriptors approximation for wheel and caterpillar-based (tankemode) vehicles (fixed) and underlying earth surface (equal district with a grass and rare bush of less than 1m height) are submitted. The following designations are used: number 1- curve for an light armoured drive truck (EADT), number 2 - for ZIL-131 truck and number 3 - for a underlying earth surface.

The experiments shown that the probability of correct detection of objects is 0,87 and 0,81 correspondingly.

On the fig. 4 the two-dimensional image for the same objects and similar conditions is given in the space of parameters z and m. Here z is magnitude of a ratio component cross-sectional and basic polarizations expressed in decibels. The Δ numeral designates magnitude z for a underlying earth surface, $\square$- the same for ZIL-131 and O- the same for EADT . From the fig.4 it is clear, that the classes of areas " a underlying surface" and "object " can be easily separated.

On fig. 5 and fig. 6 the three-dimensional map of classes of ground objects in space of parameters z, ν and m is shown. Here as on fig. 4 classes can be easily separated. Obviously, that with increase of control features number the reliability of detection and recognition increases, but computing procedure becomes more complex.

Nowadays, it is known, that the simple methods of separate objects recognition brings significant error because of some simplifications and non-optimality of classification procedures[5,6]. In the paper a simpler and rather effective discriminatory analysis technique is offered. On fig. 7 the block diagram of the recognition procedure based on multiple etalons principle is given.

On fig.8 the training algorithm of recognition system is submitted. The training of a system was completed using the following input data:

Initial number of standards $n_{e1}=n_{e2}=2$; Initial number of features used $n_{in}=2$;

The generation of objects from training and testing sets was done by generating corresponding scattering matrices to be saved in the computer memory.

Number of selective measurements of the elements of scattering matrix is N=500.

The problem of development of the most rational structure of the recognition system was reduced to the investigation of influence of the number of standards, number of features and their structure on a criterion of effectiveness. As a result of the experiment the probabilities of correct recognition P_{ri}, for possible organisations of feature vector and for various number of the standards were obtained.

The outcomes of experiment is presented as curves plotted on Fig.9-11.

Fig.9 , 10 - the dependence P_{ri} on the number of used standards and indications,

Fig.11 - P_{ri} depedence on signal-to-noise ratio and number of the standards used. Modification of n_{el} from 5 to 15 leads to 20% increase of correct recognition probability. Obviously, that there is some optimum number n_{el}, which maximizes P_{ri}. It is clear that increase of the standards number to more than 10 does lead to increase of P_{ri} . The dependence of number of indications has a smooth character, however influence of their number is less noticeable. So, at increase of number of indications from 2 up to 6 P_{ri} increases less, than by 8%.

Dependence of P_{ri} from signal-to-noise ratio has a smooth character, as can be seen from Fig.11. And, if q<10 dB, at any number of the standards and indications P_{ri} <0,7. However, the increase from 25 up to 35 dB practically does not lead to growth of P_{ri}.

Thus, the model and technique for detection of the ground objects on the basis of their scattering polarization matrixes and polarization parameters were developed. Block diagrams of such a system and recognition algorithm are given. The outcomes of theoretical and experimental research of a detection (recognition) of small size ground objects on the basis of independent polarization parameters in millimeter range prove effectivity of the offered method on detection and recognition of ground objects. It is shown, that the probability of correct detection with use of descriptors can reach values 0,85-0,89.

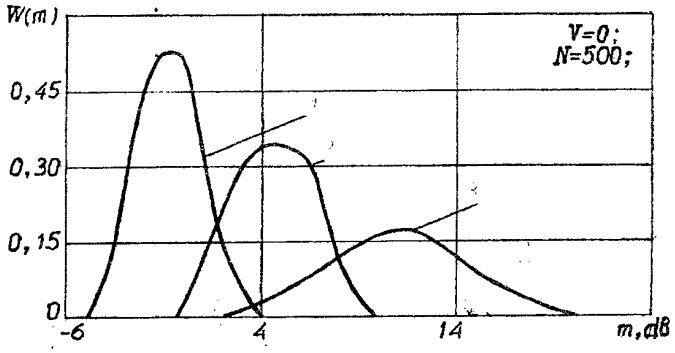


Figure 1.

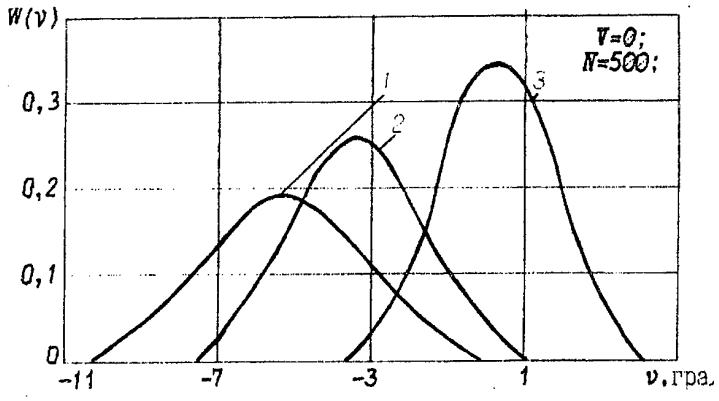


Figure 2.

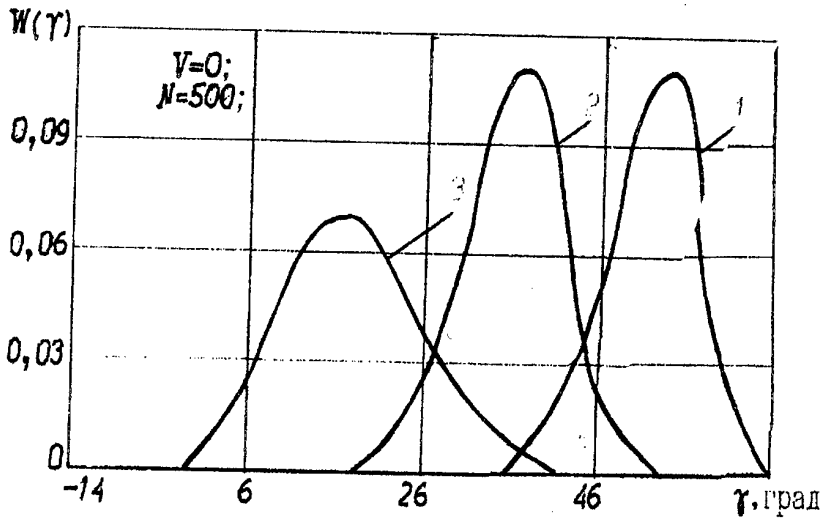


Figure 3. Approximation γ parameter experimental histogramm

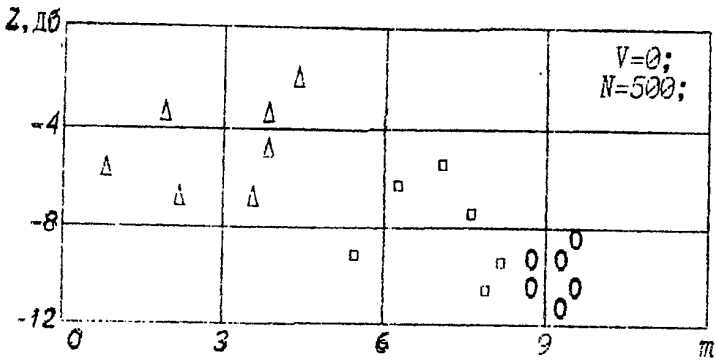
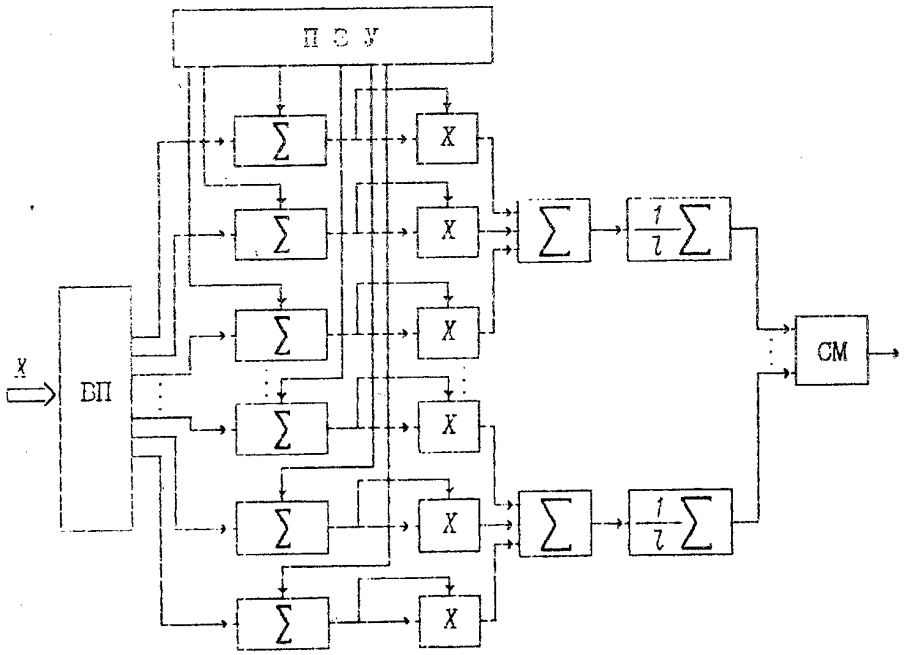


Figure 4. 2D image target class and underlying earth surface in Z and m space parameters


П У
X
ВП
X
X
X

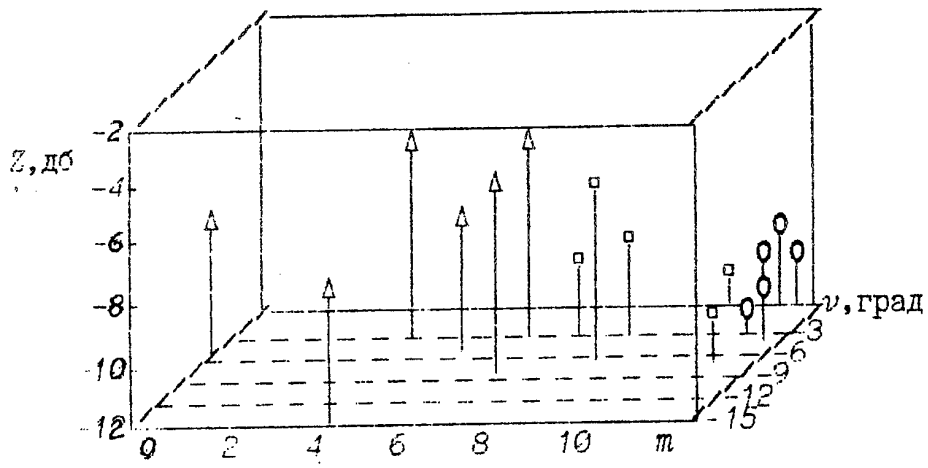


Figure 5. 3D image target class and underlying earth surface in Z, m and ν space parameters

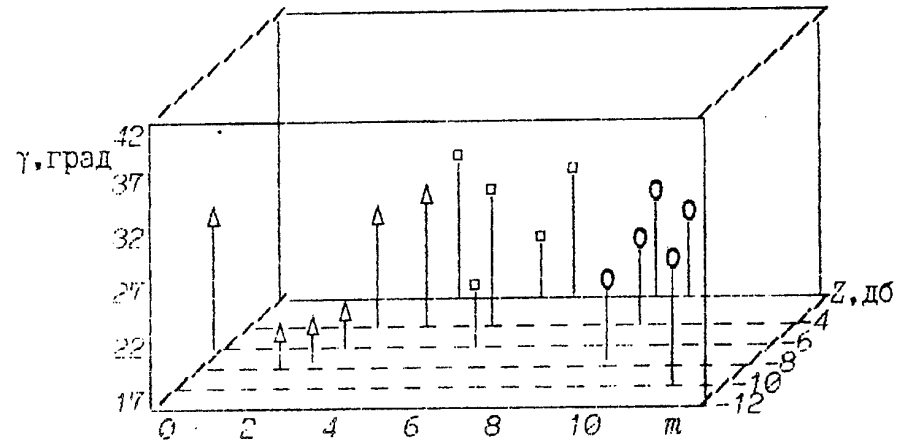


Figure 6. 3D image target class and underlying earth surface in γ,Z and m space parameters

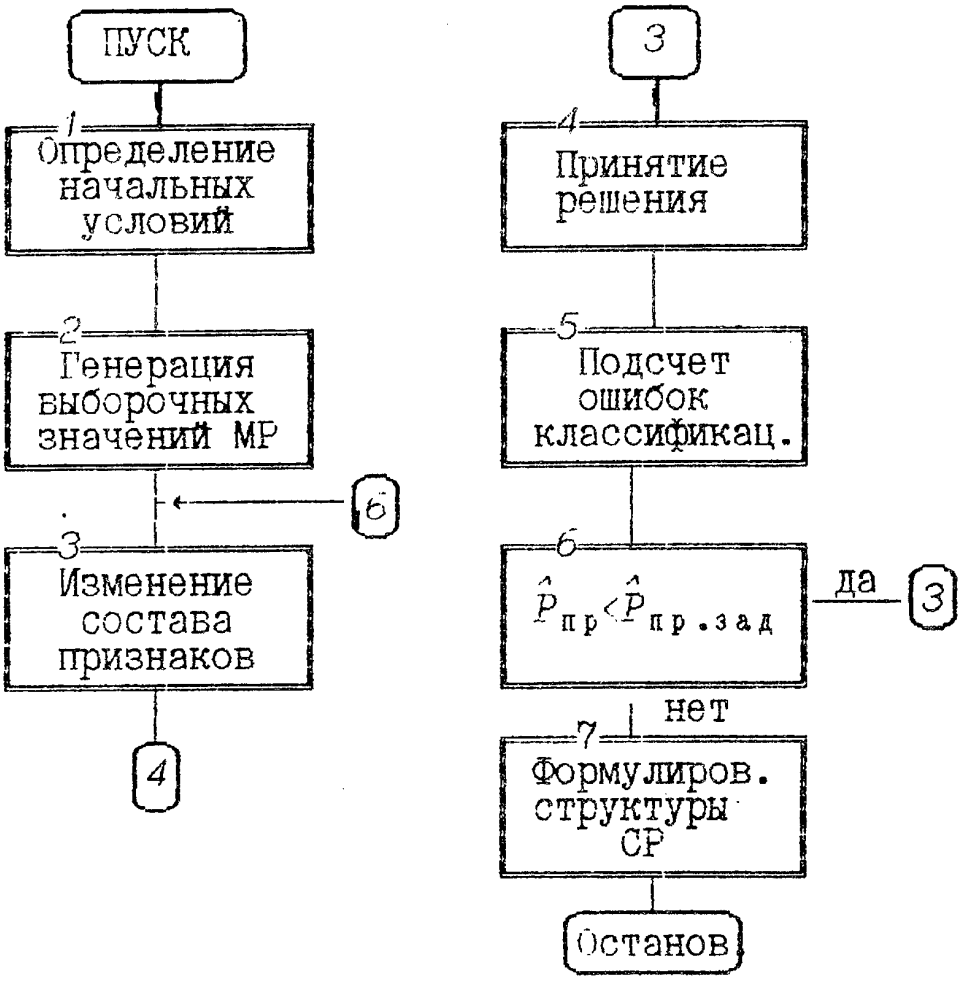


Figure 8. Training algorithm of recognition system.

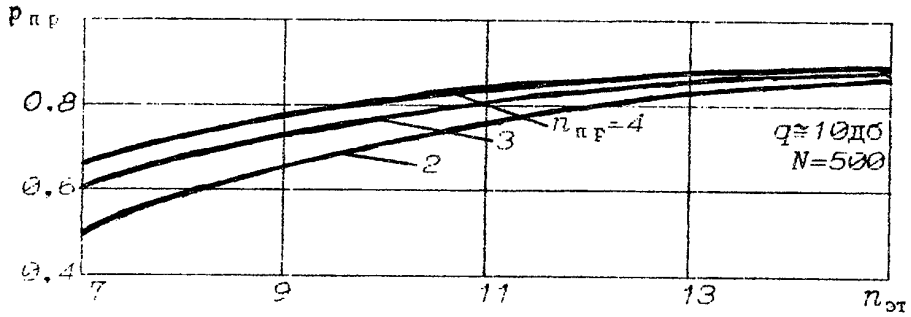


Figure 9. The dependence P_{ri} on the number of used standards.

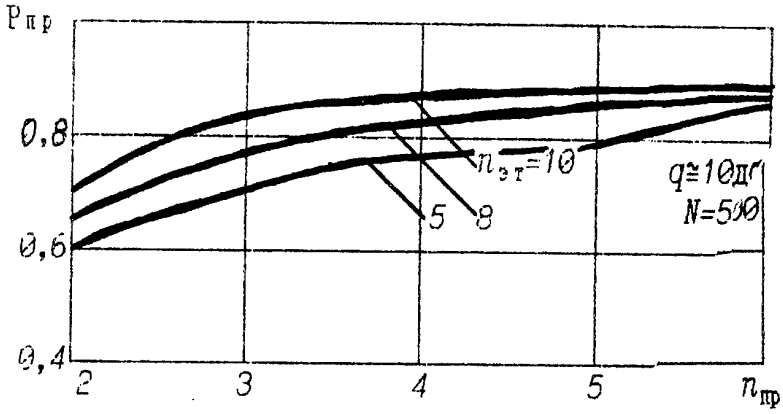


Figure 10. The dependence P_{ri} on the number of used indications.

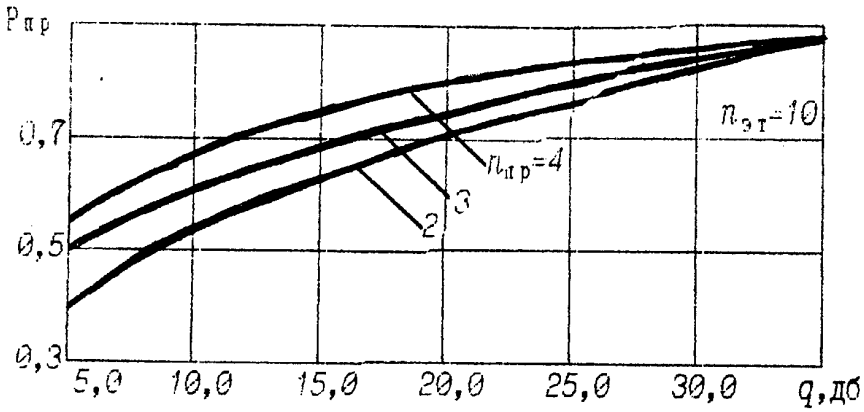


Figure 11. P_{ri} depedence on signal-to-noise ratio on fixed n_{et} and n_{pr}

1. R.P.Bystrov, A.V.Sokolov .Proceedings of the 1V-th All-Union School on propagation of MM and SBMM radiowaves in atmosphere (in Russian). Application of millimetr and submillimeter waves, - N.Novgorod: AS USSR, 1991, pp.229-235.
2. Hujnen J.R. Phenomelogical theory of radar targets.-In:Electromagnetic scattering. New. York, 1988, pp.653-712.
3. G.P Kulemin, V.B.Razskasovsky. Scattering of millimeter radiowaves by a surface of ground under small angles. - Kiev.:Naukova dumka.-1987.-231 p.
4. N.S.Akinshin , V.A.Nikolaev , V.L.Rumyancev. An adaptive detection of the fixed purposes on correlation OPK the reflected radar-tracking signal./Defensive engineering (in Russian), -1995.-N 2.-pp.57-61.
5. V.L.Rumyancev . An adaptive detection of the radar-tracking purposes on polarizing parameters reflected signal./Defensive technik (in Russian).-1995. N 8.-pp ,35-38.
6.V.A.Nikolaev Â.À., V.L.Rumyancev. An experimental research of polarizing performances of some terrestrial coversat expansion of a matrix of scattering. - Scientific and Technical collection (in Russian), N11.-Tula: TVAIU.-1994.-pp.9-16.

RADAR-TRACKING CONVERTERS IN ALARM SYSTEMS

R.P.Bystrov, E.V.Vashenko, A.V.Sokolov

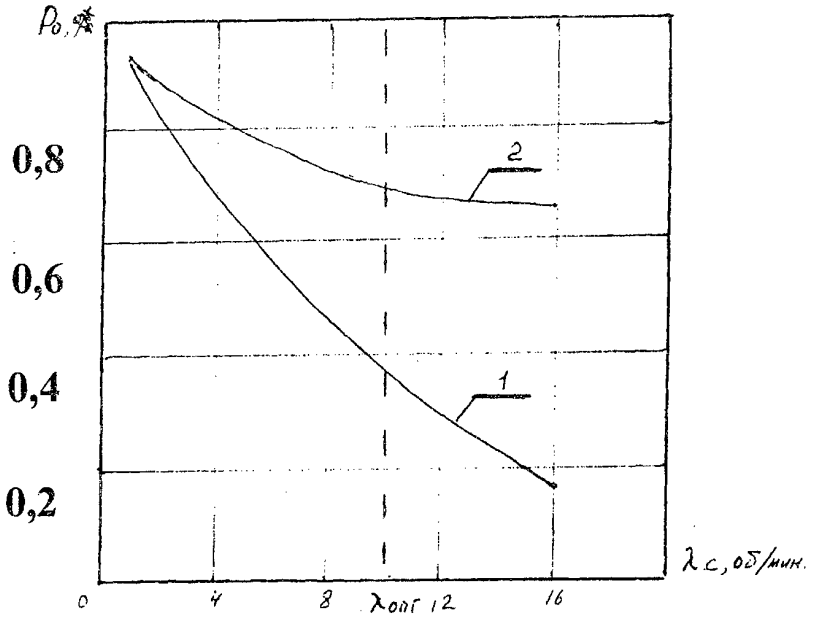
The basic task of an alarm complex is detection and recognition (classification) of moving objects (group or single) along with information processing and transmission. Such complexes are also used to determine coordinates and the number of objects.

Now it is known, that the existing complexes with acoustic and seismic transducers can not solve appointed problems effectively.

It is offered to supplement the existing complexes with radar-tracking transducers, which would provide determination of parameters of the moving objects in a group.

The modelling (simulation) of this problem shows, that use of additional RTC (transducer) operating in a longer part of sub-millimiter and a shoter part of millimiter ranges as a part of the complex increases correct detection and recognition probability. Fig. illustrates the way correct detection probability P_0 depends on the number of objects per time unit. Detection zone is 300 m. It can be seen, that in case of RTC (curve 2) probabilities of correct detection increases at c = 10-12 objects / minute (optimum case) by 2-2,5 times if to compare with curve 1. It is also necessary to note, that RTC has a higher resolution accuracy on distance to the moving objects in a group. So within 200-300 m distance and antenna aperture of 10 cm the average distance resolution error did not exceed 7 m.

Effectiveness evaluation which was carried out within this work, when using the complex as an alarm system for artillery, has shown that use of RTC as a part of a complex increases effectiveness of shooting by 3-5 times.



1. R.P.Bystrov, A.V.Sokolov and oth. - Electromagnetic waves and electronic systems (in Russia), v.2, N 1,-1997- pp.47-53.
2. R.P.Bystrov, A.V.Sokolov. and oth. - Foreign radio electronics (in Russia), N 1,-1997- pp.4-20.

ALARM COMPLEX FOR DETECTION AND RECOGNITION OF GROUND OBJECTS

R.P.Bystrov, E.V.Vashenko, A.V.Sokolov.

In present time the alarm complex with highly sensitive seismic, acoustic, magnetic, radio, optical and other transducers operating on the basis of different physical principles for a detection and recognition of ground and air (low flying) objects is developed. If needed it can also be used for aiming and firing at these objects.

For this purpose the complex should incorporate receiving equipment and tools for information processing.

The paper investigates the structure of such complex and substantiate the parameters of radio, seismic, thermal and acoustic tools for detection and recognition.

The important requirement to the alarm (signalling) complex is determination of both group of objects content and objects' coordinates. These requirements are not sufficiently fulfilled by existing and widely used complexes based on seismic and acoustic transducers. This shortage can be compensated by introducing the radar-tracking alarm(signalling) system with highly directed beamform to provide resolution of the separate closely located objects (1-2 m) in a group within small distances to the latter (hundred meters). Radar tracking system can be activated by a signal from passive standby acoustic system.

The basic parameters of transducers for perspective alarm (signalling) can be the following:

The radio can be represented by either passive or active radar-tracking transducer

Performances of a passive transducer:

- distance of operation up to 150-200 m;
- range of waves of 0,88-1,25 mm;
- sensitivity in a band 1 Hz - 0,1 K;
- diameter of an antenna no more than 100 mm;
- linear resolution on an azimuth on the distance of object up to 200 m not more than 3 m
- the probability of a detection of object is not lower 0,8.

Performances of an active transducer:

- distance of operation up to 500 m;
- a range of lengths of waves of 1,25-2,2 mm;
- average power of a generator up to 30 mW;
- sensitivity of the receiver in a band ~ 300 MHz - 10^{-11} W;
- diameter of antenna no more than 100 mm;
- linear resolution on an azimuth on a distance of object 300 m no more than 3-4 m;
- resolution on distance up to 5 m; the probability of a detection of object is not lower 0,8 [1].

Acoustic channel. The research of acoustic fields of the sources with use of microphone array have allowed to reveal reliable information features of objects within distances up to 5 km. Thus, power spectral density of separate sources and their mutual coherence functions represented in Karunena-Loeva basis[2] were defined. The experiments on determination of mortar calibre were carried out which have confirmed a possibility of recognition of acoustic sources with probability 0,7-0,8.

The thermal channel is characterized by high temporal and spatial resolution, that ensures necessary conditions for recognition of artillery and rocket systems types with probability up to 0,8.

The seismic channel of the complex ensures remote detection and recognition of object types. The effective algorithm for recognition of moving single and group objects was developed. It provides correct recognition probability not less than 0,9.

1. R.P.Bystrov, A.V.Sokolov and oth. - Foreign radio electronics (in Russia), N 1-1997, pp.4-20.
2. V.A.Omelchenko - Radio Engineering (in Russia), N12-1980, pp.11-17.

DIGITAL COMPUTER SIMULATION OF RADAR SCATTERING FIELDS FOR COMPLEX SHAPE OBJECTS

V.N.Antifeev, A.B.Borsov, R.P.Bystrov, D.A.Nosdrachev, G.L.Pavlov, A.V.Sokolov

The modern level of development of computers systems opens a possibility of application of universal methods of the physical theory of diffraction to calculation of effective surfaces of scattering of objects of the various form (configuration). In this case surface of object is represented in an analytical aspect, and the radar-tracking performances of complicated form of objects are calculated with use of numerical methods. Most known now is the technique N.Yusefa and its realization as the program "Recota", which uses triangulated model of complicated object. However this model is intended only for calculations in far zone of monostatic radar-tracking performances of aerodynamic objects. Besides this technique does not allow to organize adaptive procedures and requires significant expenditures of machine time.

In the present work the mathematical model of fields of scattering (FS) of millimeter radiowaves on objects of the complicated spatial form is offered. Singularities of the model are:

Piece-analytical model of object of the complicated spatial form;

The form of components FS and their integrated form of representation is adaptive - coherent;

Possibility of an evaluation of the contribution any element of object in common FS;

Possibility of coherent and non-coherent summation of signals from the elements of a model in the aperture of a receiving antenna;

Possibility of synthesis of signals of onboard radar systems from objects in case of bistatic and semi-active radar, and also location of extended objects with application of complicated signals, etc.;

Possibility of synthesis of a multipoint model of object .

With the help of current method the effect of scattering of radiowaves is represented as a composition spatially - distributed radiants. It allows to present coherent FS in the aperture of a receiving antenna as vectorial (in view of a phase) sum of four integrated components:

$A_s = A_1 + A_2 + A_3 + A_4$

Here first component A_1 corresponds the contribution from the smooth elements of a surface in a common field of scattering. Second -A_2 determines the contribution of boundary waves, i.e. surfaces of scattering on acute edges of object of location. The component A_3 takes into account appearances of repeated interaction (rereflections) of the elements of objects, and fourth -A_4 corresponds to a vectorial sum of surfaces of scattering of configuration items of object, which performances are determined with the help of natural modelling.

Common singularity of first three components of waves is them the additive - integrated form of the representation. Each term of a sum is an integral from oscillating radiants of the surfaces, distributed on regular sites of object, limited by a piecewise smooth contour. Such representation of components has allowed to apply to their evaluations only adaptive algorithms based on the definition of coordinates of critical points of oscillating integrals and on selection of areas of heavily scattering. It allows to reduce considerably the time of an evaluation at a simultaneous raise of accuracy of components estimations.

The analytical model of object is formed of the base spatial elements of three types of a various configuration oriented in space and joining to each other with the help of of algorithms. So the closed piecewise smooth model of object is formed. The first type of the elements represents sites of planes of a convex polygon with number of tops no more to than five, and second type the same polygon, but one from legs which includes a curve of the second order. The third type are surfaces of the second order or their sites.

In fig. 1 the summarized diagram of an inverse of scattering (DIS) (curve 1) and DIS of three separate components of standard object an armoured equipment is reduced which are obtained with the help of offered technique on a wavelength of 8 mm and vertical polarization. The analysis of performances has shown, that all components have the strong oscillating character. The contribution of a component of scattering on a smooth part object (curve 2) in summarized effective surface of scattering (ESS) has made 33 %, the contribution of boundary waves (curve 3) and rereflection (curve 4) have made accordingly 2 and 64 %.

The verification of algorithms and outcomes of digital simulation was carried out on identification of performances of reference reflectors and objects of the various complicated form obtained with the help of of asymptotic methods and with take into account of outcomes of measurements. The comparison of an evaluation average ESS of complicated aerodynamic object on

offered method with experimental outcomes have shown their good coincidence. The magnitude of an error did not exceed - 3,6 dB, and the magnitude of a dispertion made 6 dB .

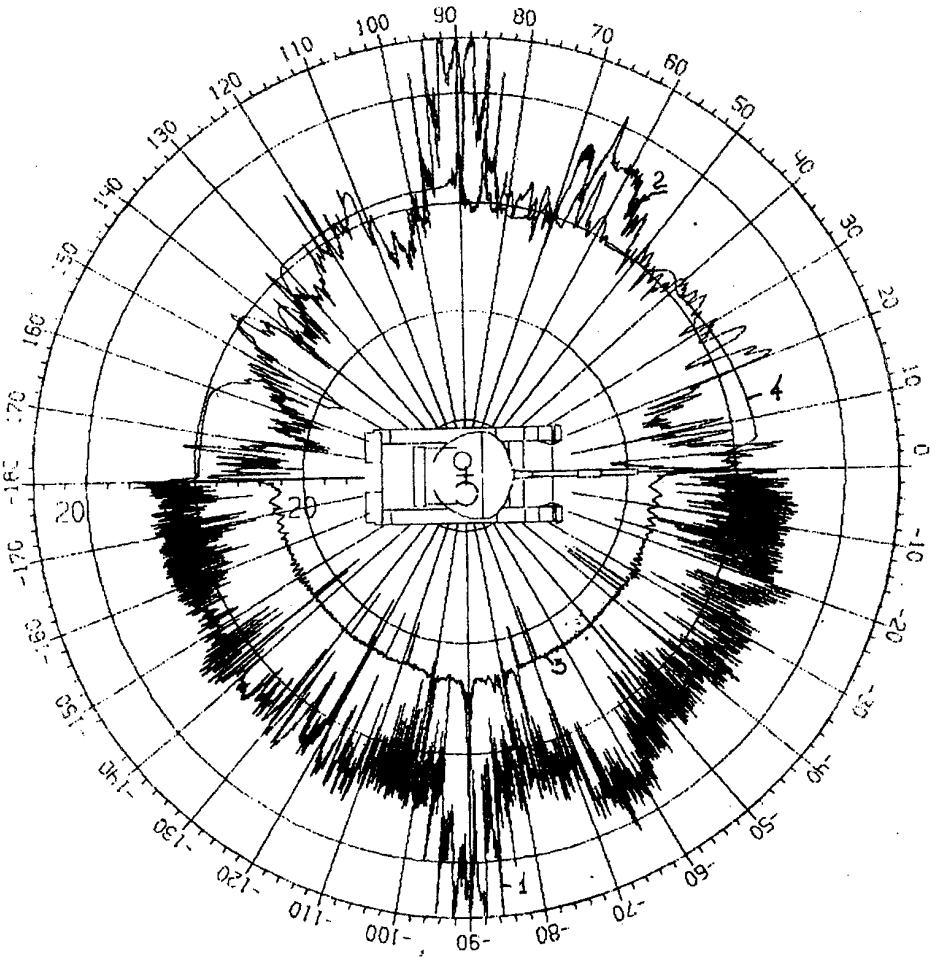


Figure 1. Summarized DIS (curve 1) and DIS of three separate components of standard object.

1. A.V.Borsov. The analysis of radar-tracking performances of objects of the complicated form by a method mathematical simulation // Boepripasy (in Russia).-1994, N 3-4.-pp.32-38.

2. Keller J.B., Lewis R.M., Sekler B.D. Asymtotic solution of some difraction problems. // Comm. Pure and Appl. Math.,-1956.-v.9, N 2.-pp. 207- 265.

THE ANALYSIS OF RADAR-TRACKING SCENES VIA MATHEMATICAL SIMULATION METHOD

V.N.Antifeev, A.B.Borsov , R.P.Bystrov, D.A.Nosdrachev, A.V.Sokolov , V.B.Suchkov

For a rational design of onboard radar systems the analysis and synthesis of radar-tracking fields of scattering from objects of the complicated spatial form in view of noises of a underlying surface are necessary. A totality of sites of a natural and antropogeneous form a radar-tracking scene, which elements have electrodynamic and statistical properties.

For description of a radar-tracking stage the method of mathematical simulation is used, in which basis the representation it as a totality of elementary reflectors with a defined of electrodynamic and statistical properties lies. The field of scattering of each reflector (object and sites of a underlying surface) at use of electrodynamic models practically is possible for to determine with any specific exactitude. The contribution which is brought in by separate types of the elements to a reflected signal, is various and depends on direction of radar-tracking observation and polarization of a radiation.

The polarizing components of a full field from an observable of a scene are as a sum of coherent fields from elementary reflectors by approximation of a scattering surface of a scene:

$$\left\|\dot{E}_s^{v(h)}\right\| = \left\|\sum_{m=1}^{M}\sum_{n=1}^{N}\dot{E}_{mn}\right\|, \dot{E}_{mn} = f_i f_s \dot{e}_{mn}^{v(h)}\left(1+\sum_{j=1}^{J}P_j\right),$$

where

M - amount of types of the elements of j- tipe a scene ;

N - amount of reflectors, approximating surface of j-tipe a scene;

$v(h)$ - indexes of polarizing basis vectors incident and reflected of waves;

E_{mn}- signal of a field of scattering of reflectors on an exit of a receiving antenna radar;

f_i, f_s - functions of a directivity of transmiting and receiving antennas accordingly;

e_{mn}- function of scattering of the reflector.

Thus the size of the elementary reflector should not exceed magnitudes

$$R < \frac{1}{2}\sqrt{\lambda \cdot r_{\min}}, r_{\min} = \min(r_i, r_s),$$

Where

λ - wave length of a higher harmonics of a spectrum of a sounding signal;

r_i , r_s - distances up to a fixed point of the elementary reflector from the transmitter and receiver, accordingly.

The scattering properties of elementary reflectors of a radar-tracking scene of observation are calculated way, or the models of the diagrams of scattering are used in view of measurements.

The effect of interaction of the elements of a scene of radar-tracking observation is estimated by function of a reaction "j" of the elementary reflector on the given element P_j. This function takes into account influences of a multiradiant character of propagation of waves near to a underlying surface and rereflections of waves on the elements of a scene.

The influence of driving of transmiting and receiving antennas were onboard a fliging vehicle can be accepted in attention in modification of phase function of the elementary reflector. This modification on a fixed wavelength corresponds spectral component of a sounding signal, which can be presented as

$$\Delta\varphi = \frac{2\pi}{\lambda}\left\{r_i\left[1+\frac{(\vec{V}_i\cdot\vec{r}_i)}{c}\right]+r_s\left[1+\frac{(\vec{V}_s\cdot\vec{r}_s)}{c}\right]\right.$$

where $\vec{V}_i, \vec{V}_s$ - vectors of velocities of transmiting and receiving antennas relativily of the elementary reflector, accordingly;

c - velosity of light. The magnitude of phase function depends on dispersing properties of a surface of the elements of a scene of radar-tracking observation, that results in a modification of tenzorial reflections coefficient of the elementary reflector.

The given technique of an evaluation of fields of scattering of scene of radar-tracking observation is realized as the applied programs and successfully was used at development of modern onboard radar-tracking systems of various assigning.

METHODOLOGY OF MULTICHANNEL RADAR IMAGE PROCESSING AND INTERPRETATION

G.P. Kulemin
Institute of Radiophysics and Electronics, Ak.Proskura 12,
310085, Kharkov, Ukraine, tel. +38 0572448508, e-mail gena@ire.as.kharkov.ua
A.A. Zelensky, V.V. Lukin, A.A. Kurekin,
Dept 507, Kharkov Aviation Institute, 17 Chkalova St.,
310070, Kharkov, Ukraine, tel. +38 0572 442352,
fax +38 0572 441186, e-mail lukin@xai.kharkov.ua
K.P. Saarinen
Visy Oy, Hermiankatu 6-8 D, FIN 33720, Tampere, Finland,
e-mail Kari.Saarinen@visy.fi

The multichannel (i.e. multifrequency or multipolarization) radar images provide an opportunity to increase the probability of correct identification of remote sensing data and to solve some practical tasks when it is difficult to retrieve information from one-channel image /1-3/. But, at the same time, many new applied problems arise dealing with necessity to process and interpret the images jointly /4-6/. They are the following: the image-to-image and/or image-to-topology map superimposing, geometric distortion correction, image filtering and information extraction.

So we analysed the main factors degrading the image quality and obstructing reliable data interpretation. It was proposed to remove them at different stages of multichannel image processing mainly by means of application of nonlinear algorithms /5-9/. First, the techniques of geometric distortion correction and superimposing execution using linear or nonlinear transformations are proposed and tested for data arrays having both relatively small and large sizes. For radar images geometric correction we used reference points by selecting them in interactive mode and marking the position of easily recognizable objects for the images that are superimposed /4, 10/ (crossroads, bridges, buildings, river twisting, borders of agriculture fields, etc.). Coordinates of reference points were used to determine unknown parameters of image geometric transformation model by means of minimization of reference point superimposing errors. For these purposes we applied the least square error method and second order nonlinear optimization methods (in particular Broyden-Fletcher-Goldfarb-Shanno algorithm was found to be efficient) /11/.

For geometric correction of images of relatively large sizes (about 3000x2000 pixels) it was recommended to use nonlinear model of geometric transformations, that provide rotation, shift and scale changes of the image coordinate system, slant range to horizontal range coordinates transformation. It is shown that introducing of nonlinear model of deterministic component geometric distortions (caused by nonlinear dependence between slant and horizontal ranges) considerably improves the accuracy of image-to-topology map superimposing. For correction of random distortions of the images of relatively small sizes (256x256 pixels) we used polynomial model that is based on the linear combination of nonlinear orthogonal basis functions of two variables. For selection of basis functions used in the polynomial model we proposed the technique based on the analysis of reference point superimposing errors. It provides minimum of total systematic and random errors for the model of geometric distortions.

It is shown that additional improvement of images superimposing accuracy can be reached by the following ways: 1) detecting and eliminating reference points that have rough errors caused by wrong visual classification; 2) optimization of reference points number and their spatial location on the images /4/. The detection of rough errors in the selected set of reference points is based on the analysis of their superimposing accuracy characterized by discrepancy. If the error value is greater than predetermined threshold, it indicates that some reference points are selected with abnormal errors. Such reference points have the greatest contribution to the superimposing error value and can be easily detected (and eliminated or reselected). Investigation of the influence of the second factor on superimposing errors shows that the optimal number of reference points lies within the range from 7 to-10. The selection of additional reference points doesn't result in considerable improvement of superimposing accuracy /4/. Recommendations concerning reference point optimal location are also got and presented in /4, 10/. For airborne multifrequency/multipolarization radar images the proposed technique provides the accuracy of superimposing characterized by rms of remained errors

approximately equal to one-two resolution elements /10, 12/.

The nonlinear vector filter can be then applied with the aim of more careful correction of remained distortions and noise removal /5/. Its operation is based on separate filtering of multichannel image components followed by vector image processing of locally active regions such as edge neighborhoods and small size objects where the influence of superimposing errors is dominant. The goal of separate filtering is the efficient multiplicative and impulse noise removal providing with simultaneous edges and details preservation. The locally adaptive nonlinear filters were designed by the authors and they are able to suppress both speckle and impulsive noises efficiently. For images formed by side-look aperture radar we proposed modified sigma filter /13/ and L_{pq} adaptive filter /8/ that are efficient for multiplicative Gaussian noise suppression. For synthetic aperture radar images corrupted by nongaussian (Raleigh, exponential) multiplicative noise we elaborated modified L_{pq} filter /8/ and iterative filtering algorithm /7/. All these filters efficiently remove impulse noise.

The second stage of image filtering is based on vector representation of pixels of superimposed radar images and the use of vector median filter for their processing /5/. The vector processing techniques use correlation between multichannel image components and outperform separate image filtering techniques /5/. Combining vector median operation with preliminary component filtering we achieved removing of harmful effects, caused by remained images superimposing errors. Besides, the proposed filter enhances edges and improves sharpness of multichannel radar images enhancing their color representation. For test and real multifrequency/multipolarization radar images vector filter has better performance in comparison to known algorithms of separate image filtering. The provided accuracy occurs to be appropriate for further interpretation of multichannel remote sensing data. Edge/detail preservation property of vector filter is better than if the separate filtering of image components is performed.

The interpretation of data includes two stages. The first one is their primary recognition to be performed by expert (or decision rule based) system. It enables to detect small size objects, edges and spikes (and to remove the latter ones), to recognize the homogeneous regions of images. The improved version of expert system uses seven information parameters calculated for every image pixel to make a decision about pixel classification. Test images with typical objects having different orientations, positions and contrast values are used for training expert system to classify them correctly in the presence of multiplicative and impulse noise of different intensity. Application of seven information parameters and the use of expert system for their analysis considerably improves image recognition accuracy compared technique /9/ where 6 parameters were used. The achieved probability of correct recognition is within the limits 0.9-0.99.

There are two ways to be followed after this. First, the neural networks (NN) can fulfill the interpretation of data being trained in the mode of supervised preliminary learning. The main advantages of NN classifier are: 1) soft and hard data classification methods can be used; 2) no restrictions on the type of information parameters are imposed and no a priori information is needed; 3) high performance in the case of hardware realization that provides the possibility of real time image classification. We considered the application of two type NNs - perceptrons and radial basis function networks. The designed NN contained one hidden layer, thus providing universal hyperspace division capabilities /14/. Besides, we used linear neurons in the output layer. It let us to apply a cascade correlation algorithm to train the network in the supervised mode /14/. As it follows from Table it is expedient to use radial basis function networks instead of perceptrons.

The other variant is the use of radiophysical models. This case demonstrated itself well for soil erosion and moisture content estimation from multipolarization Ka-band radar images. For the majority of models of surface scattering the cross-section function can be expressed as a product of dielectric function and surface roughness. The investigation of dielectric function features in Ka-band has shown its weak frequency dependence and high sensitivity to moisture content /10, 12/. By attracting multifrequency information, i.e. combined processing of two Ka-band and one X-band data the additional estimation of soil erosion degree can be provided. The method is based on obtaining the ratio of surface scattering cross-section values for different vision angles/polarizations and further reconstruction of moisture and soil erosin maps with the use of experimental radiophysical dependences. For estimation of surface roughness dealing with soil erosion state the different models of spatial spectrum and correlation function were applied /12/. The proposed approach was tested for agricultural field without vegetation in autumn 1995. In situ measurements of soil moisture and granulometric contents were done with application of traditional methodologies. The results of remote estimation of soil parameters were compared to ones evaluated by in situ measurements. They confirmed appropriate reliability of discrimination of four classes of soil erosion state.

All stages of multichannel image processing are tested for simulated and real data. The quantitative results proving the efficiency of proposed procedures are presented in Table. For the proposed methods of multichannel radar image processing the probability of correct classification is the greatest. here we mean that

1) neural network approach outperforms the parametric Bayesian classifier, 2) the proposed vector filters permit to essentially increase the probability of correct classification of multichannel remote sensing data.

The corresponding software able to perform all operations from described set has been elaborated /6/.

Table. The values of correct classification probability for test three channel radar image.

Filtering type	Classifier type				
	Bayesian classifier	perceptron		radial basis function NN	
	probability of correct classification	P_c	the optimal number of hidden neurons	P_c	the optimal number of hidden neurons
vector filtering	0.986	0.998	20	0.998	16
separate filtering	0.949	0.979	5	0.987	4
no filtering	0.956	0.971	28	0.972	13

References

1. А.И. Калмыков, И.М. Фукс, "Проблемы рассеяния радиоволн подстилающей поверхностью в задачах дистанционного зондирования", Труды Междунар. НТК "Современная радиолокация" - Киев, С.10-16, 1994.
2. A. Freeman, D. Evans, J.J. Zyl, "SAR Applications in the 21st Century", Proceed. of European Conference on SAR (EUSAR'96) - Konigswinter (Germany), pp.25-30, 1995.
3. А.И. Калмыков, В.Н. Цымбал, А.Н. Блинков и др., "Многоцелевой радиолокационный самолётный комплекс исследования земли", - Харьков (Препр./ НАН Украины. ИРЭ; 90-21), 34 с, 1990.
4. А.А. Зеленский, В.В. Лукин, "Обработка многочастотных изображений: подход, методы и алгоритмы", Труды Междунар. НТК "Современная радиолокация" - Киев, С. 70-78, 1994.
5. А.А. Курекин, В.В. Лукин, А.А. Зеленский, "Применение методов векторной медианной фильтрации при обработке многоканальных радиолокационных данных дистанционного зондирования", Космічна наука і технологія, Т. 2, № 5-6, С.53-63, 1996.
6. A.A. Zelensky, A.V. Totsky, N.N. Ponomarenko, I.P. Anukhin, V.P. Melnik, A.N. Dolia, V.V. Lukin, A.A. Kurekin, "Airborne multichannel remote sensing data processing techniques and software", Proceed. of the Second Int. Airborne Remote Sensing Conference and Exhibition ERIM. - San Francisco (California, USA), Vol. III, pp.151-159, June 1996.
7. V.V. Lukin, A.A. Kurekin, V.P. Melnik, A.A. Zelensky, "Application of Order Statistic Filtering to Multichannel Radar Image Processing", Proceed. of IS@T/SPIE Sympos. on Electronic Imaging: Science and Technology. - San Jose (USA), Vol. 2424, pp. 302-312, 1995.
8. V.V. Lukin, V.P. Melnik, A.B. Pogrebniak, A.A. Zelensky, J.T. Astola, K.P. Saarinen, "Digital adaptive robust algorithms for radar image filtering", Journal of Electronic Imaging, Vol. 5(3), pp.410-421, July 1996.
9. O. Zelensky, A. Kurekin, V. Lukin, M. Ponomarenko, "Techniques of Scene Radar Image Processing and Their Recognition by Expert System", Proceed. of The Second All-Ukrainian Int. Conf. on Signal/Image Processing and Pattern Recognition. - Kiev, pp.163-167, 1994.
10. G.P. Kulemin, A.A. Kurekin, V.V. Lukin, A.A. Zelensky, "MM-Wave Multichannel Remote Sensing Radar Systems and Algorithms of Image Processing", Digest of Intern. Confer. ICMWFST'94. - Guanzhou (China), pp. 359-362, Aug. 1994.
11. Г. Реклейтис, А. Рейвиндран, К. Рэгсдел Оптимизация в технике: В 2-х кн. Кн. 1. Пер. с англ. - М.: Мир. 349 с., 1986.
12. G.P. Kulemin, A.A. Kurekin, V.V. Lukin, A.A. Zelensky, "Soil Moisture and Erosion Degree Estimation from Multichannel Microwave Remote Sensing Data", Proceed. of Europ. Symp. SPIE on Satellite Remote Sensing II. - Paris (France), Vol. 2585, pp.144-155, Sept. 1995.
13. V.V. Lukin, N.N. Ponomarenko, P.S. Kuosmanen, J.T. Astola, "Modified Sigma Filter for Processing Images Corrupted by Multiplicative and Impulsive Noise", Proceed. of EUSIPCO'96. - Trieste (Italy), Vol. III, pp.1909-1912, Sept. 1996.
14. Zelenskyj O., Kurekin A., Lukin V. Techniques of Multichannel Radar Images Processing and Interpretation by Multilayer Neural Network// Proceed. of the Third All-Ukrainian Int. Conf. on Signal/ Image Processing and Pattern Recognition. - Kiev. - 1996. - P. 231-233.

THE INFLUENCE OF PHASE AND AMPLITUDE FLUCTUATIONS OF MICROWAVES IN TROPOSPHERE ON SAR OPERATION

G.P. Kulemin*, V.V. Lukin**, A.A. Zelensky**
Institute of Radiophysics and Electronics, National Academy of Science of Ukraine, Ac. Proskura St. 12, Kharkov 310085, Ukraine, tel. 38-0572-448508, fax 38-0572-441105,
e-mail gena@ireas.kharkov.ua
Kharkov Aviation Institute, Chkalova St. 17, Kharkov 310070 , tel./fax 38-0572-441186,
e-mail lukin@xai.kharkov.ua

An essential influence on SAR operation can be caused by both attenuation of microwaves in troposphere, clouds and precipitations and the phase and amplitude fluctuations of SAR received signal resulting from radiowave propagation through random inhomogeneous medium. In other words, there are deterministic and stochastic components of errors determining SAR calibration accuracy. Here we suppose that SAR external calibration using sample reflector is performed /1/. Besides, the considered effects influence the remote sensing data interpretation accuracy - evaluation of intensity ratios for small-size objects and even large area fragments.

Certainly, the degree of considered factor influence depends upon several factors: radar operation wavelength and principle - side-look radar or SAR, radar installation - airborne or satellite radar, observation time (is focused or non-focused procedure used), and, upon troposphere state and characteristics.

The estimations of troposphere attenuation influence for short-wave part of centimeter and millimeter bands of radiowaves are presented in our paper /2/. The attenuation in fogs and clouds is determined by their specific water content. The obtained values of error mean vary within the limits 0.1...0.2 dB for 3cm wavelength and increase to 0.1...2.0 dB for 8mm wavelength. Obviously, fogs and clouds lead not only to deterministic errors but also to random ones because the density of fogs and, especially, clouds is not uniform, this characteristic is space and time invariant. Even higher attenuation is observed for tropical regions of the Earth.. Such "Shuttle" SIR-C/X-SAR images of forestry regions of Brasil have been demonstrated at EUSAR'96 /3/ and it was well seen that clouds almost fully masked the corresponding image fragments of Earth surface. The systematic calibration errors occuring due to rain are of even higher level especially for MM waves /2/.

In troposphere the sources of amplitude and phase fluctuations are the random fluctuations of refractive index due to turbulent motion of air, the similar effects are observed due to inhomogeneity of cloud and precipitation areas. These fluctuations of the SAR signal result in errors of its output intensity and the spatial shifting of the response main maximum position, in turn leading to errors of object location estimation.

Let us discuss these effects more in details. The amplitude and phase fluctuations of SAR received signal are caused by the turbulent structure of troposphere refractive index, i.e. the fast and small-scale variations of dielectric constant. The refractive index fluctuation root mean square (rms) values averaged for altitudes from 0 to 6 km were about (0.5 - 1) N-units /4/. Only for small altitudes over sea surface the maximal values of rms reached (4,0 - 4,5)N -units. With altitude increasing up to 20 m over sea surface the rms median value diminishes and for altitudes greater than 6000 m it becomes small - about (0,01 - 0,05) N-units. In the framework of Kolmogorov - Obukhov's theory /5/ the estimations of phase and amplitude fluctuations rms, the phase fluctuation temporal correlation function are obtained. The exponential model of phase fluctuation correlation function describes their properties well enough /5,6/. The same relates to amplitude fluctuation spatial and, therefore, temporal correlation characteristics.

In practical conditions the phase fluctuations of reflected signal are determined by the medium inhomogeneity motion. The phase fluctuation temporal spectra occur to be rather low frequency, its main part is concentrated in the frequency area less then 0.1 Hz. Therefore, for time interval of SAR signal coherent processing of about 0.5 - 1.0 s these fluctuations occur to be highly correlated; so the temporal fluctuations of troposphere parameters almost do not influence the SAR output signal. But the SAR carrier movement in respect to turbulent troposphere results in phase fluctuation spectra shifting into higher frequency area, i.e. it decreases the phase correlation interval. It has been shown that for airborne SAR with mean speed 200 m s^{-1} the value of phase correlation interval is equal to 0.75s, i.e. it is comparable to signal coherent processing time. For spaceborne SAR the correlation interval of 20 ms occurs to be much less than signal coherent processing time.

The amplitude fluctuations of signal due to troposphere inhomogeneity are discussed in /7/, their values are estimated in /6/. The experiments carried out for frequencies 4 - 6 GHz have shown that the amplitude

fluctuation variances are greater than ones derived. The maximal rms values reached 1 - 1.5 dB for incidence angles more than 4°. Therefore, it is possible to expect that the amplitude fluctuation rms values for SAR signals propagating in turbulent troposphere can be of about 0.2 - 1.0 dB and they can essentially contribute the SAR calibration accuracy especially for short-wave part of CM-band and for MM-band. The other reason of SAR signal random phase fluctuations caused by troposphere is the presence of cloud cover. In comparison to the turbulent atmosphere the sufficient external turbulence scale decreasing occurs; its average values are about several meters reaching 10 m for St, Cu and Ac cloud types. Internal structure of cloud formations causes relatively great refractive index fluctuations. The refractive index fluctuation rms values reach (10 - 20) N-units. The signal phase fluctuations caused by these factors are characterized by exponential correlation function.

Another reason of SAR signal amplitude and phase fluctuations occurence are the precipitations, in particular, the signal scattering by rain drops /8/. Phase shift derivations for different frequencies and for precipitation intensity from 2.5 to 150 mm/h are presented in /6/. For turbulent motion, assuming the precipitation inhomogeneity and the exponential spatial correlation function the expression for derivation of phase fluctuation variance was obtained Phase fluctuation temporal spectrum is wide because of scattering caused by rain drops with Doppler spectrum due to mutual translation and gravitational falling. For frequencies greater than 5 GHz and for the incidence angles greater than 60^0 the maximal frequencies of phase fluctuation temporal spectra can exceed 16 Hz, i.e. they are relatively fast, at least, the correlation interval is essentially less than SAR image synthesis time. It is shown in /6/ that for clouds as well as for precipitations the variances of amplitude and phase fluctuations are mutually dependent and amplitude fluctuation variance is of the same order as its values caused by the turbulent troposphere.

Generalizing the results of analysis we can conclude the following:

1. Phase fluctuation variance lies in the typical limits from 0.01 to 1.0, the amplitude fluctuation variance is a little bit less reaching the maximal values 0.05 - 0.2 approaching from gaussian to Rayleigh-Rice distribution.
2. SAR received signal amplitude and phase fluctuations are spatially (and, thus, temporally) correlated, they can be described by the same shape function (in particular, exponential) with high correlation interval width varying from several samples to about 30 - 40 samples of the synthesized hologram.

Thus, the effects of SAR signal amplitude and phase fluctuations caused by wave propagation through the turbulent troposphere and precipitations can essentially influence on SAR operation and external calibration accuracy. Some results can be predicted from the theory of statistical analysis of antenna arrays /9/. The generalized model of SAR signal distorted by considered factors and errors is the following:

$$I_{ij} = \left| \sum_{k=-N/2}^{N/2} a_{i+k} h_{i+k,j} A_s \left(1 + \Delta A_{kj}\right) \exp\left(j \Delta \psi_{kj}\right) \right|^2 , \qquad (1)$$

where I_{ij} is the ij-th SAR image pixel value, $\{a_k\}$ denotes the array of weighting window factors (it is supposed that some weighting window is used for SAR response parameter improvement), $\{h_k\}$ defines the complex focusing function (in case when focused image formation is performed) that takes into account the carrier speed v_0, the distance to the j-th image row and the radar operation wavelength λ; A_s is the received signal mean amplitude; $\{\Delta A_{i+k,j}\}$ and $\{\Delta \psi_{i+k,j}\}$ define the amplitude and phase fluctuations of SAR signal for $i+k$-th sample of the hologram registered for the j-th distance. Just this model was used in simulations performed for wide range of conditions: focused and non-focused procedures of image formation, application and absence of weighting windows taken from the set of ones described in /10/, amplitude and phase fluctuation variances, different width of stron correlation area and number of hologram sampled used for image formation.

For non-focused image formation the results of simulations lead to the following conclusions:

1. The bias of the mean value of the image sample (pixel) can be observed even for reference points as well as its values great variations reaching several dB. The bias is caused by both uncompensated phase errors and the fluctuations. The first factor can be taken into account and then compensated if the maximal phase shift at the edges of synthesized aperture is known. The influence of the second factor is determined by many obstacles - the variances of fluctuations, the ratio of synthesized aperture length to spatial correlation function mainlobe width, time of synthesis, etc. The greater is the spatial correlation function mainlobe width, the greater is the bias, it varies within the limits of about 0.3 dB for considered variances of amplitude and phase fluctuations. The greater are the amplitude and phase fluctuation variances the larger is the bias. If the phase fluctuation rms is 1.0 radian then the bias for non-focused image formation procedure can exceed 2 dB.

2. SAR resolution and response maximum position are much less influenced by fluctuations, due to them the main lobe width increases only by 1-3% and the maximum position shifts no more than by one pixel only.
3. The use of data weighting leads to response maximum value bias depending upon window type. But it can be preestimated and compensated. The data weighting produces the reduction of the response side lobe and energy concentrated in the response side lobes but only for case of small variances of fluctuations. The effects noted in items 1 and 2 are observed in case of data weighting application as well and the described tendencies remain.
4. The severe degradation of SAR response side lobe structure takes the place resulting in additional reduction of SAR radiometrical accuracy. This also results in general reduction of the formed mage quality.

The analysis of results for focused image formation procedure leads to the following conclusions:
1. With amplitude and phase fluctuation variance growth the reduction of mean value of the response maximum also takes place and the bias reaches 1 dB for phase fluctuation rms equal to 1.0; the narrower is the high correlation area the greater is the bias, it is important for spaceborne SARs and this effect can not be avoided by increasing the synthesis time. The relative variance of response maximal value reduces with increasing of synthesis time and this obstacle is one more item in favor of focused image formation procedure application
2. As for non-focused image formation the amplitude and phase flluctuations result in resolution reduction but it is much less than in the previous case, i.e. practically negligible. The same conclusion relates to errors in response maximal side lobe position. The response maximum value has almost gaussian distribution for focused image formation procedure while for non-focused one iti tended to Raileigh-Rice distribution law.
3. The weighting window application is expedient only in case of relatively small fluctuation variances: the side lobe level can be decreased as well as the energy concentrated in response side lobes. The resolution becomes worse and, thus, only some weighting windows can be applied, in particular, the two-step one proposed in /10/.
4. The increase of amplitude and phase fluctuation variances leads to the SAR response side lobe level growth and their structure degradation, for example, for phase r.m.e equal to 1.0 the maximal side lobe mean for normalized response is within the limits 0.15-0.29, i.e. is very high. It evidences about severe degradation of the response and, thus, about very low level of SAR calibration accuracy. There exist the most unfavorable conditions destructively influencing SAR operation - when the error spatial correlation interval is of about 5...7 times less than the synthesized aperture length. However, the designer is unable to predict the properties of real troposphere turbulence and to avoid SAR operation in such unfavorable conditions.

Finally, it is worth to emphasize the following. Because the level of amplitude and phase fluctuations of SAR received signal are determinged by SAR operation wavelength and the path length in troposphere that depends upon vision (incidence) angle the available calibration accuracy can be provided only for imaging systems with operation wavelength greater than 2...10 cm and for vision angles not greater than 50...60°. The latter limitation is especially strict for spaceborne SARs with high carrier orbit because in this case the sensed terrain curvature can cause the reduing of incidence angle and the increasing of calibration errors.

References

1. Ph.Hartl, W.Keydel, H.Keetzmann, "Radar Calibration Techniques Including Propagation Effects", Adv.Space Res., V.7(11), pp. 259-268, 1987.
2. G.P.Kulemin, S.A.Velichko, "Effects of Radiowave Propagation Conditions on SAR Calibration Accuracy", Proceedings of Europ. Conf. EUSAR'96, Konigswinter, Germany, pp. 507-510, March 1996.
3. H.Runge, "The German Processing and Archiving Facility for X-SAR", Proceedings of Europ. Conf. EUSAR'96, Konigswinter, Germany, pp. 469-472, March 1996.
4. C.M.Crain, "Survey of Airborne Microwave Refraction Measurements", Proceed. IRE, V.43, pp.1405-1411, 1955.
5. V.I.Tatarsky, Wave Propagation in Turbulent Atmosphere", Nauka edit., Moscow, 548 p. (in Russian).
6. S.A.Velichko, G.P.Kulemin, V.V.Lukin, N.N.Ponomarenko, A.A.Zelensky, "Influence of Phase Fluctuations in Troposphere on SAR Calibration Accuracy", Proceedings of the Second International Airborne Remote Sensing Conference and Exhibition, San Francisco, CA, USA, pp. , July 1996.
7. A.I.Kalinin, "Radiowave Propagation through Near Earth and Space Paths", Swiaz Edit., Moscow, 263 p.
8. D.E.Setzer, "Computed Transmission through Rain at Microwave and Visible Frequencies", Bell Syst. Techn. Journal, V.49, pp. 1873-1880, 1970.
9. A.A.Zelensky, V.V.Lukin, I.P.Anukhin, "Apodized Array Pattern Analysis and Synthesis for Spatially Independent and Correlated Errors Influence under Constructive and Technological Restrictions", Proceedings of Intern. Conf. PIERS'94, Noorwijk, Netherlands, pp. 440-443, July 1994.
10. I.P.Anukhin, V.V.Lukin, A.A.Zelensky, "Fast Data Weighting Algorithms for Non-Focused SAR Image Forming", Proceed. of Intern. Symp. AeroSense'95, SPIE V.2487, Orlando, USA, pp. 404-411, April 1995.

USE OF HOMOMORPHIC TRANSFORMS FOR LOW CONTRAST EDGE/DETAIL DETECTION AND FILTERING OF MM-BAND IMAGES

Chemerovsky V.I., Dolia A.N., Kurekin A.A.,
Lukin V.V., Zelensky A.A.
Dept 507, Kharkov Aviation Institute
17 Chkalova St, 310070, Kharkov, Ukraine
tel/fax +38 0572 441186, e-mail lukin@xai.kharkov.ua

MM-band radar and radiometric images are usually corrupted by data-dependent noise (with gaussian distribution) being, for instance, the mixture of additive and multiplicative components /1/. This causes problems in direct application of many filtering algorithms specially designed for cases of dominant influence of additive or multiplicative noise, but not for intermediate situations. Moreover, many edge/detail detectors that do not take the mentioned noise peculiarities into account also fail to perform well /2/. Besides, if the multiplicative noise is a prevailing factor then the traditional detail detectors indicate the details having equal but positive or negative contrast in respect to surrounding background with different reliability. This prevents the appropriate preservation of negative contrast details when nonlinear, in particular, adaptive filters are used for image processing.

So here we consider the use of homomorphic transforms in order to avoid these problems. The transform should be selected in such a way that after its application the noise becomes additive and its variance remains constant for all regions of the image. In case of multiplicative noise prevailing influence such operation can be expressed in the following way

$$I_{ij}^{h} = k \log_r \left(I_{ij} \right)$$

where I_{ij} is the ij-th pixel value of initial noisy image, I_{ij}^{h} denotes the same image pixel value after homomorphic transform, k and r are the constant parameters. In other, more complex, situations the function for performing homomorphic transform has to take into account the additive noise variance and dependence between local mean level and signal dependent component variance /3/. Anyway, the function describing homomorphic transform is a monotonic one and an inverse function should exist.

If the root mean square of noise is essentially less than the mean value for almost all homogeneous regions of the image (this assumption is often valid in practice) then after homomorphic transform the noise distribution remains gaussian as it was for initial image. So one may directly apply the wide set of standard or adaptive filters and traditional edge/detail detectors /3/. It is worth mentioning here that the performance of adaptive nonlinear filters is determined by several characteristics: the type of noise suppressing filter and its efficiency, the type and properties of detail preserving filter applied to detected locally active areas and, finally, upon type and reliability of edge detector.

If the distribution law of multiplicative noise is gaussian then the efficiencies of noise suppressing filters applies with and without homomorphic transform (usually they are the same or have corresponding modifications for multiplicative or additive noise dominant influence cases) are almost the same. This relates to standard mean, median, Wilcoxon and many other order statistic filters. A little difference exists in performance properties of detail preserving filters like local statistic Lee, sigma, center weighted median, FIR median hybrid and some other ones but they are not too great for cases of homomorphic transform use or their direct application to initial image processing. But the results for edge detectors are rather different.

The considered approach permits to get expressions for many detectors to be directly applied to images corrupted by dominant multiplicative noise. In particular, this relates to quasirange. For edge detection in images corrupted by additive noise the quasirange is calculated as the difference between the q-th and p-th order statistics determined for current scanning window position data sample ($Q_{ij}^{a} = Q_{ij}^{h} = I_{ij}^{h(q)} - I_{ij}^{h(p)}$). This shows that if the logarithmic homomorpic transform is used to get additive noise then for initial image the quasirange should be calculated as the ratio of the q-th and p-th order statistics $Q_{ij}^{\mu} = I_{ij}^{(q)} / I_{ij}^{(p)}$ but not as

$Q_{ij}^{\mu} = \left(I_{ij}^{(q)} - I_{ij}^{(p)}\right) / \left(I_{ij}^{(q)} + I_{ij}^{(p)}\right)$. This recommendation is based on results of numerical simulation performed for test image containing small size objects with equal positive and negative 3 dB contrasts in respect to surrounding background with relative variance of multiplicative noise $\sigma_{\mu}^2 = 0.01$. Because the detection of such objects depends upon many factors, in particular, on threshold selection we have fixed the false alarm rate (i.e. the percentage of incorrectly detected image pixels in image homoheneous regions) and then compared the probabil;ity of correctly detected object pixels really belonging to small size objects. The total probability was evaluated as well as the probabilities for negative and positive contrast objects separately. It was shown that for false alarm rate of 3-7% the results for homomorphic transform case were better for total probability of correct detections and for negative contrast objects, in particular.

The local variance can be also used as edge/detail detector but there doesn't exist direct analogs for multiplicative and additive noise dominant influence cases. An interesting fact is that the use of homomorphic transform permits to detect equal positive and negative contrast objects with almost identical probability and for false alarm rate greater than 4% the total probability of correct detections is higher than for case when the homomorphic transform is not applied. Negative contrast objects are detected essentially better if the homomorphic transform is applied while for positive contrast ones the situation is the opposite. Therefore, it is expedient to us the homomorphic transform when the detection and preservation of negative contrast objects is the first priority task.

At the same time the use of homomorphic transforms results in necessity to solve some specific problems dealing with real and integer value representation of images. Processing of real valued data requires higher computational efforts. On the other hand, integer value representation of data after homomorphic transform can cause increasing influence of quantization errors. It can be minimized due to application of specified selection of the transform and methodology of its practical execution. I particular, the parameters k and r can be adjusted in such a way that for $I_{ij} = 255$ one gets $I_{ij}^{n} = 255$ for 8-bit array data representation being traditional for many practical applications.

The proposed approach was used for real images formed by 8-mm radar installed on Il-18D aircraft exploited by IRE NASU and remote sensing system of Ukrainian satellite "Sich-1". In the former case the noise was mainly multiplicative (See Fig.1,a). That is why the logarithmic transform (1) was applied to it and then the image processing using sigma filter was performed. After inverse homomorphic transform the image presented in Fig.1,b was obtained. It is seen that a good trade-off of processing algorithm properties and especially an excellent preservation of low negative contrast small elongated objects like rivers was provided.

An original image formed by "Sich-1" imaging system is presented in Fig.2,a. Besides noise with specific properties (nonlinear dependence between local varianve and squared mean level) it is strongly distorted by interlacing effects. That is why its processing included several stages. First, the interlacing effects were removed, then the obtained corrected image was processed using modified sigma filter (the modification took into account the noise peculiarities mentioned above) and, finally, the 3x3 median filter was iteratively applied to sigma filter output in order to avoid the remainder distortions. The resulting image is represented in Fig. 2,b and it is seen that its quality has been essentially enhanced.

Thus, the homomorphic transforms can be a useful tool in the following situations and applications: 1) when it is impossible to say that the influence of multiplicative or additive noise is prevailing and the filter to be applied needs the information about the noise properties (like local statistic Lee or sigma filters, for example); 2) when the first priority task is to detect and then preserve the small size or elongated objects with low negative contrasts in respect to surrounding background. Another conclusion is that there not always exist a strict correspondence between edge/detail detectors to be applied for processing the images corrupted by different kinds of noise.

References

1. A.A.Zelensky, G.P.Kulemin, V.V.Lukin and V.P.Melnik,"Locally adaptive robust algorithms of image processing"(in Russian), Institute of Radiophysics and Electronics of Ukrainian Academy of Science, Preprint '93-8, Kharkov,Ukraine (1993).
2. I.Pitas and A.N.Venetsanopoulos, Nonlinear Digital Filters: Principles and Applications, Kluwer Academic (1990).

3. R.Ding and A.N. Venetsanopoulos,"Generalized homomorphic and adaptive order statistic filters for the removal of impulsive and signal-dependent noise," IEEE Trans.Circuits and Systems CAS-34(8), 948-955 (1987)



Fig.1,a

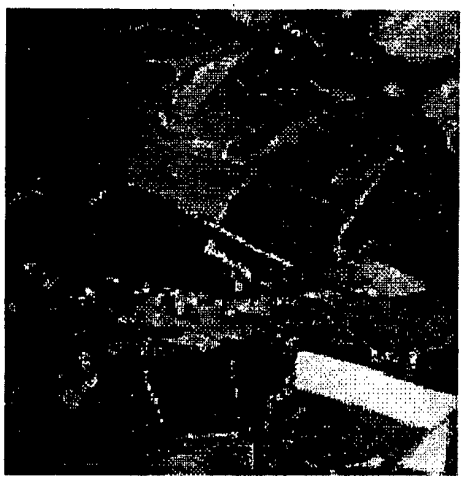


Fig.1,b

a) Initial MM-band radar image;
b) The output image processed using homomorphic transform and modified sigma filter.



Fig.2,a



Fig. 2,b

a) Initial obtain by system installed on "Sich-1"satellite;
b) Output imge after interlacing effect removal and processing by modified sigma filter.

REMOTE SENSING OF THE MINOR GAS CONSTITUENTS OF THE LOWER AND MIDDLE ATMOSPHERE

Sh.D. Kitaj., A.P. Naumov , N.N. Osharina , A.V. Troitskij
Radiophysikal Research Institute (NIRFI)
B. Pecherskaja st., 25, Nizhny Novgorod, 603600, Russia
Tel. (097) 8312 366751. Fax (097) 8312 369902, E-mail kit@nirfi.nnov.su

The principle possibility of atmosphere minor gas constituents (MGC) radiometric monitoring is based on the features of the thermal radio emission generated by atmospheric gases having magnetic and electric dipole moments. These gases according to quantum laws give radiation (absorption) maxima at the resonance frequencies of their molecules. By measuring the level of the atmosphere thermal radiation near MGC resonances one can get information on the contents of polluting gas components. The radio frequency band is accounted for rotation spectra of gas molecules. So, the radiometric monitoring deals with simpler atmospheric gas spectra as compared with IR and optics which are accounted for vibrational and electron quantum transitions, respectively. Table 1 presents the list of a number of atmospheric gas admixtures which molecules have dipole moments and in principle can be detected by their own thermal radiation.

The basic point of the MGC radiometric monitoring possibility is the fact that many spectral lines and bands of admixtures fall on atmospheric radio windows. This makes it possible to separate the MGC contribution by their spectral peculiarities from the absorption and radiation background of the main atmospheric molecular components (water vapour and oxygen). Along with all these positive moments there are some difficulties in MGC radiometric indication. They are associated first that the MGC diagnostics by their radio emission in the microwave region is rather a complicated problem of measuring weak signals on the strong background of the atmosphere radio emission. Second, in overlapping absorption bands the intensity of pure atmosphere emission (the background) is nonlinear by frequency and requires correct accounting. The calculations of the atmosphere radio emission in the overlapping bands of MGC (the calculation of kernels of remote sensing inverse problems) should be carried out taking into account the spectral line interference, however, the quantitative theory of such effects has not much been developed yet. And, finally, for a wide enough atmosphere radiation bands ($\delta\nu$ ~5 - 10 GHz) there are some technical problems in creating wide - band radiometer microwave channels providing the spectral analysis of the bands studied. Some of these problems are overcome by the measurement technique used in radioastronomical observations, the other require their own solution.

We have considered the possibilities of MGC indication in lower atmospheric layers for the ground remote sensing (RS) and in the middle atmosphere for the limb satellite RS. To analyse the radiophysical aspects of MGC diagnostics we use height profiles of impurity component background concentrations, the data on maximum permissible concentrations (MPC) including cases of MPC excess, the parameters of millimetre absorption spectra of MGC, water vapour and oxygen as well as calculation algorithms of absorption coefficients, optical thicknesses and radio brightness temperatures of the atmosphere taken from observations with different platforms. In the cases of lower layer pollutions these characteristics have been analysed for the impurities listed in Table 1. Besides these gases we considered also ozone.

The impurity gas absorption has been found less than that of the main atmospheric gases at the surface level for MGC background and even MPC. However, at some heights H_i (specific for each MGC) the contributions of impurities and main atmospheric gases become equal for a number of resonance regions, and for larger heights ($h > H_i$) the MGC contribution becomes dominating. For example, H_i values in optimal resonance regions are 13 km for O_3, lie within 16-19 km for N_2O, HNO_3, ClO, HOCl and grow up to 24-32 km for CO, H_2O_2, NO. The optimal choice of MGC remote sensing conditions includes the determination of operating frequencies and sounding angles at which radio brightness temperature contrasts $\Delta T_b = T_b - T_{ab}$ become measurable and take maximum values. Here T_b is the atmosphere brightness temperature with the gas impurity studied, T_{ab} is the atmosphere brightness temperature without the impurity (the background temperature). Table 1 gives ΔT_b values for RS zenith diretion for MGC relative concentrations $f = 10^{-5}$ in summer.

Modern microwave radiometers make it possible to register weak signals on the atmospheric background with radio brightness contrasts ~ 0.1 K. The results given show the possibility of remote radiometric indication of industrial and working zone area pollution by ammonia, sulfur dioxide and hydrogen sulfide. ΔT_b contrasts for MGC natural background concentrations are not large: $\Delta T_b \leq 0.1$- 0.3 K, however, they grow in several times (especially in winter) for RS optimal angles and of course they increase at higher MGC levels. Ozone ΔT_b contrasts at background medium concentrations ranges up to ~10 K that is widely used nowadays in O_3 radiometric monitoring. RS results for ammonia in the band ν~ 25 GHz and for hydrogen sulfide (ν ~ 131 GHz) in life-scale conditions for industrial blowouts have been given in [1,2]. Microwave measurements (ν ~ 115 and 230 GHz) of carbon monoxide content in the mesosphere have been started in [3].

A spectral radiometer for the absorption band 131 GHz has been constructed at the Institute of Space Research of the Russian Academy of Sciences to carry out radiometric indication of sulfur dioxide. The radiometer has been assembled as a superheterodyne modulation receiver with a mixer at its input. The signal frequency filtration is made by radiometer intermediate frequency.The radiometer performs the line convolution over direct and mirror channels relative the band centre of SO_2 131 GHz which coincides with the heterodyne frequency[2]. The radiometer fluctuation sensitivity is ~ 0.2 K at the time constant 1 s. Experimental studies of the atmosphere radio emission near the resonance region 131 GHz were carried out in the area of a large heat and electric power plant. The radiometer was at a distance of 2.5 km from the plant. The atmosphere radio emission was received at a scalar-horn antenna with the antenna beam width 6^o under zenith angle $\theta = 70^o$. Some cases were registered when SO_2 content in the line of sight was tens of g/m^2 (~ 25-45 g/m^2).The recalculation of sulfur dioxide content to the vertical column is usually made in plane-layer stratification approximation although it may not work due to a local character of anthropogenic blowouts. The impurity content in the vertical column is in ~ 3 times less than the values given above. The preferred wind direction during the radiometric measurements was from the observer to the atmosphere pollution source. The lee side contrast (at the same angles of antenna azimuth removal) was significantly weaker or absent that testifies to a wind transfer of sulfur dioxide from the visible contour of the smoke tongue of flame and its turbulent diffusion over a large distance. Estimations made from the scanning geometry showed that the linear dimensions of the pollution zone exceeded 7 km.

Results of considerable promise on MGC content control in the middle atmosphere can be expected using the limb satellite RS method considered in detail in [4].The spectral contrasts of practical interest in this method are $\delta T_b = T_b(\nu_0) - T_b(\nu)$, where $T_b(\nu_0)$ is the atmosphere brightness temperature near the resonance of a corresponding impurity componet, $T_b(\nu)$ is the brightness temperature at the line slope, the brightness temperatures being estimated with an account of the signal reception band $\delta\nu$. The latter was changed from a few units up to ~ 50 MHz in numerical simulation of the limb radiometric experiment.

The estimations showed that the maximum height range of ozone sounding $15 \leq h_0 \leq 60$ km is achieved in the line 110.8 GHz for all values of $\delta\nu$. Similar results are obtained in the lines with resonances $\nu_0 \approx 195.7$ GHz ($\delta\nu \leq 30$ MHz) and $\nu_0 \approx 101.7$ GHz ($\delta\nu \leq 20$ MHz). The proximity and possible impact of ozone lines should be carefully considered in the analysis of sounding conditions of other impurity components because the ozone rotational spectrum is closely disposed over the band. For this reason, for example, some serious problems arise in remote monitoring of hydroclorous acid intensive line $\nu_0 \approx$ $\approx$ 195.5 GHz which contribution to the thermal radiation is very hard to be separated on the background of closely disposed intensive ozone lines. For HOCl RS monitoring one can use the line $\nu_0 \approx$ 202.5 GHz. Corresponding contrasts of brightness temperatures for a number of tangent heights h_0 are given in Table 2.

Now, let us note here some results on nitric acid vapour monitoring. HNO_3 molecule has the most line half-width among other molecules considered in this work. HNO_3 content sounding can be done in the line $\nu_0 = 206.6$ GHz at heights h_0 ~ 15 - 35 km for $\delta\nu$ = 10 - 50 MHz. Nitrous oxide monitoring is expedient to do in the line $\nu_0 = 201.0$ GHz with measurable contrasts of ~9 -2 K at tangent heights h_0 ~ 15 - 35 km for $\delta\nu$ = 50 MHz. Chlorine oxide content can be controlled up to height h_0 ~ 30 km in the line $\nu_0 = 204.3$ GHz , $\delta\nu$ = 10 MHz with expected contrasts ~1.5 -4.5 K. ClO radio brightness temperatures measured in [5] by the limb satellite method for tangent heights h_0= 20 - 30 km are very close to our theoretical results obtained with an account of radiometer parameters realized in the experiment.

From all these results we may conclude that MGC radiometric monitoring is very promising in the microwave band.

Table 1. MGC dipole moments (in Debye units) and radio brightness contrast values ΔT_b in impurity resonance regions for pollution layers 100 ... 200 m (ΔT_{b1}) and 0 ... 500 m (ΔT_{b2}).

GAS	μ_i, D	ν, GHz	ΔT_{b1}, K	ΔT_{b2}, K
ClO	1.2974	130.0	0.9	4.5
		278.6	2.7	12.1
CO	0.112	115.3	<0.1	<0.1
		230.5	<0.1	0.1
N_2O	0.166	150.7	<0.1	0.1
		276.3	0.1	0.3
NO	0.160	150.5	<0.1	0.1
		250.5	<0.1	0.2
NO_2	0.290	98.0	<0.1	0.1
		146.2	<0.1	0.1
		277.9	0.1	0.4
COS	0.709	146.0	0.0	2.8
		279.7	1.0	5.0
H_2CO	2.310	140.8	0.9	4.6
		192.4	3.2	14.1
HNO_3	2.000	143.7	2.4	11.6
		194.3	4.6	19.2
H_2O_2	1.573	91.4	0.6	3.0
		251.9	0.5	2.5
SO_2	1.634	130.9	1.1	5.5
		282.3	1.9	8.7
HOCl	1.471	98.1	0.3	1.5
		291.3	0.6	2.6
NH_3	1.468	24.0	0.9	4.2
H_2S	1.020	168.9	0.2	1.1

Table 2. Limb sounding contrasts of the atmosphere brightness temperature in HOCl line 202.5 GHz for tangent heights h_0= 15 - 40 km.

δν, GHz h_0, km	0.05	0.03	0.02	0.01
15	5.8	6.5	6.9	7.3
20	7.2	8.0	8.5	9.0
30	5.7	7.0	7.8	8.7
40	0.8	1.2	1.7	2.4

References

1. A.P. Naumov, V.M. Plechkov, V.P. Borin et al, "On possible indication of atmosphere ammonia pollution by the radiophysical method", Izv. VUZov, Radiofizika, Vol. 23, No. 5, pp. 632-635, 1980.
2. I.A. Strukov, A.V. Troitskij, "Detection of sulphur dioxide radio line ν≈ 131 GHz in the lower troposhere", Izv. VUZov, Radiofizika, Vol. 40, No. 6, pp. 702 - 705, 1997.
3. K.F. Kunzi, E.R. Carlson, "Atmospheric CO volume mixing ratio profiles determined from ground-based measurements of the J=1→0 and J=2→1 emission lines", J. Geoph. Res., Vol. 87, No. C9, pp. 7235--7241, 1982.
4. K.P. Gaikovich, Sh.D. Kitaj, A.P. Naumov, "Determination of height distributions of ozone and other minor atmospheric components from satellite limb measurements in the microwave range", Issledovanie Zemli iz kosmosa, No. 3, pp. 73-81, 1991.
5. J.W. Waters, "Submillimeter-wavelength heterodyne spectroscopy and remote sensing of the upper atmosphere", Proc. IEEE, Vol. 80, No. 11, pp. 1679-1701, 1992.

The Influence of Air-Water Interface Boundary Conditions on Thermal Radio Emission at 2, 5 and 8 mm

K.P.Gaikovich, R.V.Troitsky

Radiophysical Research Institute, B.Pecherskaya st., 25,
Nizhny Novgorod, Russia, 603600,
Phone: 8312 367294, Fax: 8312 369902,E-mail: gai@nirfi.nnov.su

The influence of air turbulence and oil films presence on thermal radio emission of water at millimeter wavelengths has been investigated. This paper continues our radiometry investigations of water thermal regime dynamics due to air turbulence by measured dynamics of radiobrightness using the measurements method which have been worked out in laboratory conditions [2] and investigations of thermal emission of water in the presence of oil films [3]. The investigation of water near-surface thermal regime by one-wavelength radiobrightness dynamics are especially interesting because temperature gradients in thin subsurface layer and evaporation from water surface determine the heat exchange between ocean and atmosphere. The strong dependence of the radiobrightness on the oil film thickness, which is due the interference of the thermal radio emission retroreflected at the interface, can be used to determine this parameter from radiometric data.

Measurements have been carried out in the open air using the equipment which included the water pool with sizes 2, 1.5, and 0.2 m, three radiometers at wavelengths 0.23, 0.5 and 0.8 cm with horn nadir-looking antennas at 1 m above the water surface. The radiometers sensitivity was about 0.1 K. The diameter of the beam footprints on the water surface was about 10 cm.

So, firstly, the radiobrightness dynamics due the water cooling by air turbulence has been measured. For this purpose, the initial homogeneous temperature distribution in the water was obtained by means of mixing and this distribution was unchanged in the absence of air turbulence during a few minutes interval. On the basis of the solution of corresponding inverse problem [1], all the details of temperature profile dynamics in the water and of the heat flux dynamics through air-water interface have been retrieved. In Fig.1 it is possible to see the radiobrightness dynamics related with atmosphere air turbulence variations (after mixing of water to make the homogeneous initial distribution of the temperature) at wavelength 0.5 cm (solid line) and at 0.2 cm (dashed line) as well as retrieved dependencies of surface temperature T_0 (by radiobrightness T_b at 0.5 cm - solid line, by radiobrightness at 0.2 cm - dashed line) and the temperature at depth level z = - 0.1 cm (solid line - by $T_b(0.5)$ and dashed line - by $T_b(0.2)$).

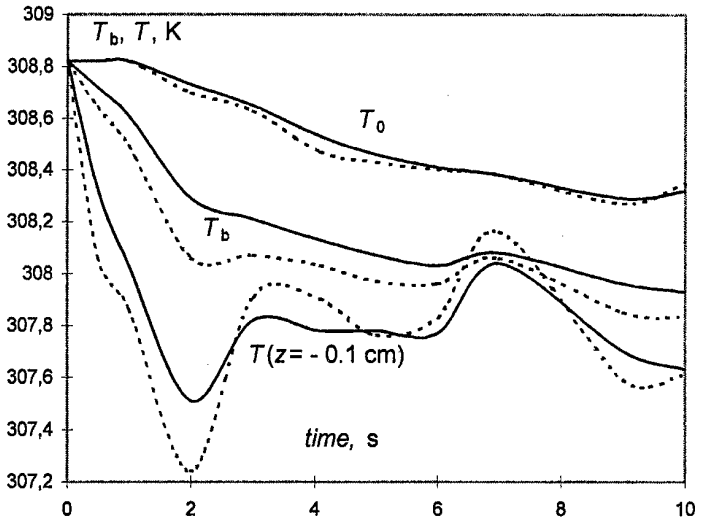


Fig1. Measurements of radiobrightness dynamics at 0.229 and 0.5 cm and retrieved temperature

In Fig.2-4 the radiobrightness dynamics and corresponding retrieval of temperature and heat flux is given at more long time interval.

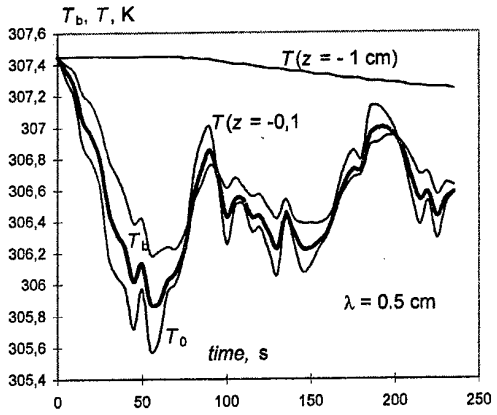


Fig.2. Radiobrightness at 0.5 cm and retrieved temperature at various depths

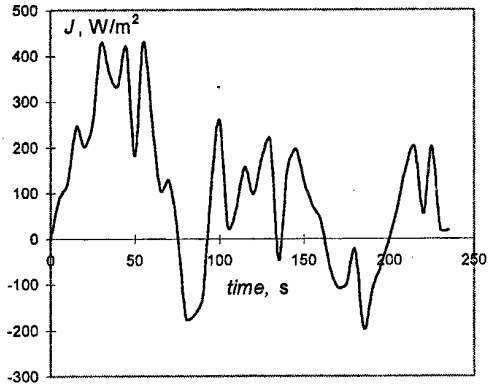


Fig.3. Retrieved heat flux dynamics through air-water interface

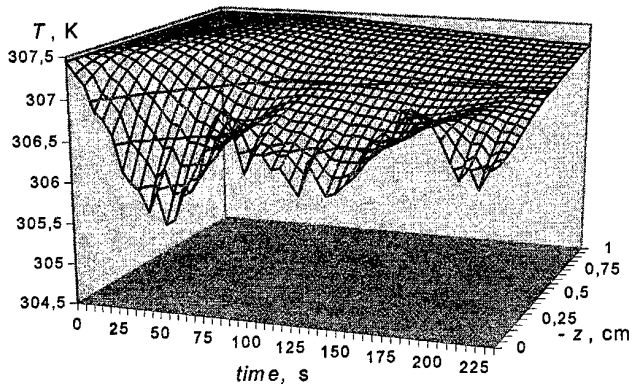


Fig.4. Retrieved temperature profile dynamics due natural air turmulence

Second, the dependence of radiobrightness on oil thickness at both wavelength has been measured. Many authors (see, e.g. [4-6]) have developed theories of thermal radio emission and experimentally investigated oil films on water surface. It has been found that the strong dependence of the radiobrightness on the oil film thickness in such two-layered medium, which is due the interference of the thermal radio emission retroreflected at the interface, can be used to determine this parameter from radiometric data. In principle, measurements at one wavelength are sufficient for film-thickness determination, but it is more reasonable to use two or three wavelengths, because the dependence on film thickness is periodic, so that the interpretation of the results becomes ambiguous in a certain stage. Of course, it is possible to choose a sufficiently large wavelength to ensure that the ambiguity domain besides outside the range of potential film thickness, but this would reduce accuracy in the measurements of thin films. Therefore, it is reasonable to make measurements at two wavelengths, using a long-wave channel to avoid ambiguity, and a short-wave channel to estimate exactly the oil-film thickness.

Experience shows, however, that, as a rule, the observed radiobrightness do not fall on the curve calculated for pure oil [4-6]. The reason of such deviation is the fact that in natural conditions the pure oil includes the water and forms oil-water emulsion. Investigations show that this effect is absent only in fresh spills. To take into account humidity, which radically changes the permittivity of oil films, the well-known Clausius-Mosotti equation is in use. This equation has been checked experimentally in laboratory conditions [5], and used

in interpretation of real experiments. To determine both thickness and water content in oil-water film it is necessary to use two-frequency measurements.

In reality, there are other factors, which influence the radio emission of oil films, for example, in [6] the authors considered the influence of film-thickness variations within the limits of the antenna pattern spot. It was found that the interference flattened with the increase of film-thickness variations, but this effect is strong enough only if the variations are about 30% of the average film thickness.

The experimental results, presented in this paper, show the influence of the new effect which leads to practical disappearance of periodical dependence of thermal radio emission on the oil thickness related with the interference. For the pure oil film on the water surface measurements results appeared in excellent agreement with the theory (see results in Fig.5).

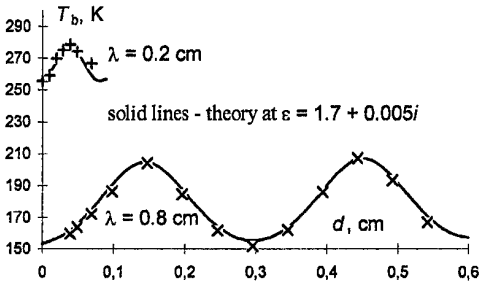


Fig.5. Measurements in pure oil films on water surface

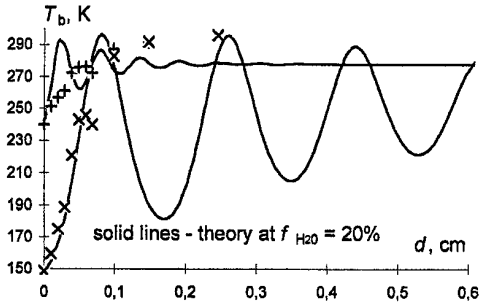


Fig.6. Measurements in oil-water emulsion films

Next, measurements have been carried out after the first summer rainfall. The results are given in Fig.6. In that case the radiobrightness dependence changes drastically - there was practically no interference features at both wavelength, and this dependence was unaccountable from the point of view of mixing theory at all possible values of water content. It is also impossible to explain observed radiobrightness dependencies on the basis of thickness variations in the pattern footprints. It should be mentioned, that the obvious interference features were not seen during our above mentioned helicopter radiometer measurements (at wavelengths 0.8 and 3 cm) of oil spills on lakes in Siberia [3], and this fact enforced us to make the present investigations. Also, the temperature dependence of oil films radio emission has been measured.

This work was supported by by RFBR under Grant 96-02-16514 and by Education Ministry of Russian Federation under Grant 95-0-8.1-71.

Refrrences

1. Gaikovich K.P. Simultaneous solution of emission transfer and thermal conductivity equations in the problems of atmosphere and subsurface radiothermometry. IEEE Trans. Geosci. Remote Sens., vol.32, pp.885-889, 1994.
2. Gaikovich K.P., Troitsky R.V. Dynamics of temperature profile, heat, and mass exchange through air-water interface by measurements of thermal radio emission evolution at 60 GHz. IEEE Trans. Geosci. Remote Sensing, 1998, vol.36, *No.*1, pp.341-344.
3. Gaikovich K.P., Troitsky A.V., Snopik L.M. Helicopter radiometry of oil pollution on lakes and soils. 24-th General Ass□mbly of U.R.S.I., Kioto, Japan, 1993, p.237.
4. Gaikovich K.P., Snopik L.M., Troitsky A.V. Helicopter radiometer measurements of thin lake ice and oil spills on lakes and soil // Radiophysics and Quantum Electronics, 1995, vol.38, *No.*11, pp.719-726.
5. Skou N. Microwave radiometry for oil pollution monitoring, measurements and systems. IEEE Trans.Geosci.Remote Sensing, v.23, 1986, *No.*3, p.360-367.
6. Laaperi A. Experimental results from oil thickness measurements with the microprocessor controlled microwave radiometer.IGARSS-83: Remote Sens.; Extend. Man's Horiz (San Francisko, Calif., 31 Aug. - 2 Sept., 1983), Digest, v.2, New York, N.Y., 1983, FA6, p.6/1-6/5.

DETECTION OF SMALL SCALE STRUCTURES IN OZONE LAYER BY MICROWAVE SOUNDING

A.A. Krasilnikov, Y.Y. Kulikov, V.G. Ryskin, L.I. Fedoseev
Institute of Applied Physics
Address: 46, Ulyanov str., N.Novgorod, 603600, Russia
Tel.: (7-8312) 384522, Fax: (7-8312) 362061, E-mail: yuyukul@appl.sci-nnov.ru

The microwave measurements here have been made at N.Novgorod (56°N, 44°E) during October-December 1994 and during January-February 1996. The first series of the observations were carried out during CRISTA/MAHRSI campaign. The Cryogenic Infrared Spectrometers and Telescopes for the Atmosphere (CRISTA) was flown on the ASTRO-SPAS satellite and operated from November 4 through November 12 1994, yielding thousands of ozone radiance profiles with excellent coverage and resolution. With this data set it will be possible to examine details of the dynamics of the nearly global ozone distribution from 59°S to 64°N latitude and from about 15 to 80 km [1]. We have measured the stratospheric ozone using original two-beam technique for a correlative measurement program was set up for validation studies. This technique allows investigating spatial-temporal variations of ozone in two regions spaced about 150-350 km along north-south directions at the altitude above 20 km. With this technique, observations do not depend on sunlight, and may be conducted through moderately thick cloud cover, and are not significantly affected by aerosols. For elaboration of the instrument a total power radiometer scheme was used [2].

The instrument consists of a millimeter wave receiver and multichannel spectrometer. The receiver converts input millimeter wave signals to lower "intermediate" frequencies by heterodyning them with a local oscillator. The intermediate frequency signals are then processed by multichannel filter spectrometer. The spectrometer's filters are followed by detectors. The detector outputs are digitized, integrated and stored in the system computer. The receiver is tuned to observe the rotational transition $6_{1,5}$-$6_{0,6}$ of ozone at 110.836 GHz. A simple conical horn is used as antenna at the microwave spectrometer input. It has an axial length of about 1 meter and an aperture 7 cm. The antenna has 2.7° beam width (full width for half maximum). Placed in front of the conical horn a system of plane mirrors made possible to receive atmospheric emissions from two different directions simultaneously and to realize spectrometer calibration by means of black bodies at ambient and at liquid nitrogen (~77K) temperatures. The uncooled receiver has a single sideband noise temperature about 2500 K. The receiver includes a filter, which suppresses mixer image sideband response by 15 dB. The filter bank of spectrometer covers 113 MHz with 21 filter channels, which corresponds to an altitude range of 20 to 60 km. The filters have several different bandwidths from 1.0 MHz to 9 MHz. The filters are spaced out unevenly because the information content of ozone lines per unit of frequency decreases rapidly away from the line center.

The altitude profiles of the ozone concentration will be computed from the microwave spectral data by a model fitting. This model considers that the brightness temperature is obtained as the result of a stratified atmospheric emission which every layer is characterized by constant pressure, temperature and constant absorbing molecule density. The pressure and temperature profiles used here were taken from middle reference model derived from satellite data [3]. Upper limit on uncertainty in the ozone altitude distribution (range 20-70 km) is about 20%.

The microwave observations started October 7, 1994 and continued almost two months. The weather conditions in this period were the satisfactory for millimeter-wave observations in N. Novgorod. At the time the zenith atmospheric opacity was varied from 0.25 to 0.4 Np.

For the comparisons, CRISTA ozone measurements were chosen from a square of 6° latitude and longitude around centered at N. Novgorod. Good agreement is found with ground based millimeter wave ozone data.

Our measurements by means of two beam technique have reveled appearance of difference in ozone content by (20-50%) in two regions spaced about 300 km in north-south direction at the height more than 40 km (marked by arrows in Fig. 1). Lifetime estimations of these spatial peculiarities are about several hours. Such peculiarities "ozone clouds" was observed at the period when gradient zone of the total ozone content passed through the observatory site, which was carried out by total ozone content measurement which has been executed by means of the spectrophotometer M-124. In order to estimate technique errors two beams measurement in the common directions have been made. This experiment has showed that type difference of ozone content is less than (5-10%) in the altitude range 40-60 km. It seems likely that ozone spatial variations revealed in the

observations have been caused by dynamic processes. The last ones also disturbed regularity of ozone diurnal variations at the height above 40 km.

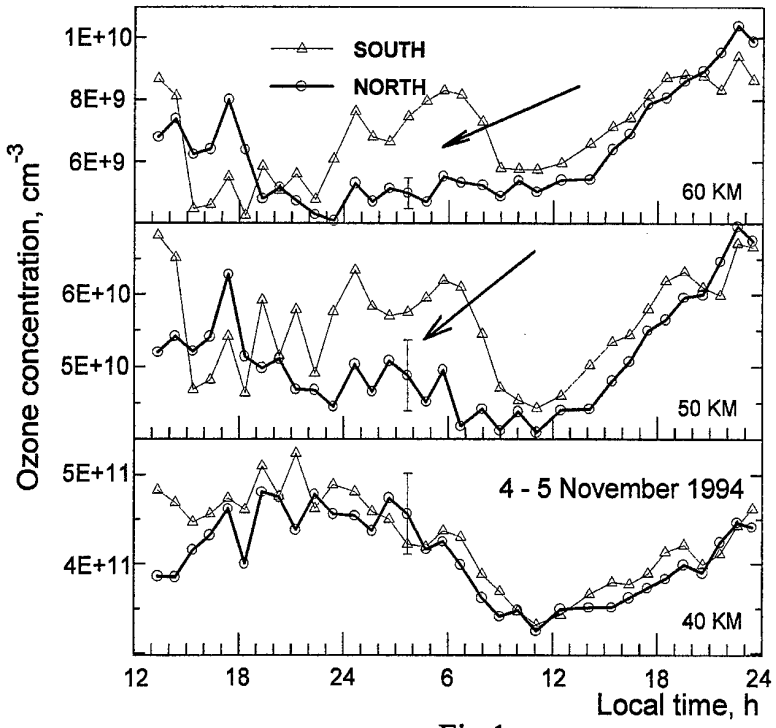


Fig.1

In consequent observations (January-February 1996) by two-beam microwave instrument we have fixed appearance of the spatial peculiarity (ozone clouds) at the bottom of the sounding layer (see Fig. 2). Besides we have found out temporal delays in variations of an ozone for different directions (south-north) on heights more 20 km.

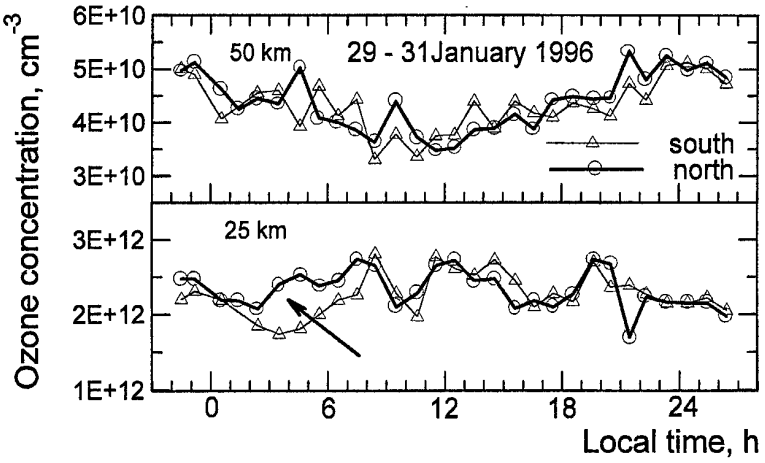


Fig.2

The results of our observations with the high spatial resolution indicate a rather complicated and variability structure of ozone layer for a middle and upper stratosphere , which is possible determined by dynamic processes.

References

1. D. Offermann, CRISTA: A Space Shuttle experiment for middle atmosphere small scale structures, in Coupling Processes in the Lower and Middle Atmosphere, edited by E.V. Thrane et al., pp. 389-401, Kluwer Academic, Hingham, Mass., 1993.
2. A.A. Krasilnikov, Total power spectral radiometer of 3 mm wavelength range, Izv.Vyssh.Ucheb.Zaved. Radiofiz., Vol. 38, No 6, pp. 608-614, 1995.
3. J.J. Barnett, M. Corney, Middle atmosphere reference model derived from satellite data, Handbook for MAP, 16, 47-85, 1985.
4. A.A. Krasilnikov, Y.Y. Kulikov, A.B. Mazur, V.G. Ryskin, N.V. Serov, L.I. Fedoseev, A.A. Shvetsov, The detection of ozone clouds in upper stratosphere Earth by the method millimeter-wave radiometry, Geomagnetism&Aeronomy, Vol. 37, No. 3, pp. 174-183, 1997.

POLARIZATION OF ATMOSPHERIC MILLIMETER-WAVE RADIATION FROM SCATTERING PARTICLES CLOUD, AND REMOTE SENSING OF VOLCANIC ERUPTION COLUMN

A. A Shvetsov
Institute of Applied Physics Russian Academy of Sciences
Address: 46, Ulyanova, N. Novgorod, 603600, Russia
tel. (7-8312)384522, fax. (7-8312)362061, E-mail: shvetsov@appl.sci-nnov.ru

Scattering of atmospheric thermal radiation from the clouds of dielectric particles is considered. It has been shown that in the case of small particles (Rayleigh scattering), radiation scattered from such clouds is partly linear-polarized if observation is made in the near horizontal direction. Difference of the brightness temperatures of optical thin clouds on vertical and horizontal ΔT is directly proportional to the column density of the particles N. It is a function of particles shape and size distribution, and its dielectric characteristics. It also depends on the atmospheric optical depth. For isothermal plane parallel atmosphere with temperature T_0 and zenith optical depth τ_0 the polarizing difference of brightness temperatures of the cloud is equal

$$\Delta T = \frac{3}{8} T_0 \tau_s [3E_4(\tau_0) - E_2(\tau_0)]$$

where $E_4(\tau_0)$ and $E_2(\tau_0)$ - exponential integral of argument τ_0 with indexes 4 and 2, respectively. Maximum polarization difference of brightness temperatures are realized under optical depth of the atmosphere approximately equals to 0.3 (other things being equal). Under standard atmospheric conditions such optical depths are realized on absorption line wings of molecular oxygen and water vapour, as well as in short-wavelength atmospheric windows of transparency. However optimum frequencies for this effect observation vary depending on the cloud altitude above sea level, season and weather conditions.

The foregoing effect can be form the basis of the remote detection method of solid particles in the earth atmosphere and estimation of its amount. In particular, it can be useful for detection an ash in eruptive columns and plumes of volcanoes in conditions of bad visibility, and at presence of steam clouds. Value of given method is independence from the thermodynamic temperature of the erupted piroclastic material, which vary strongly with space and time.

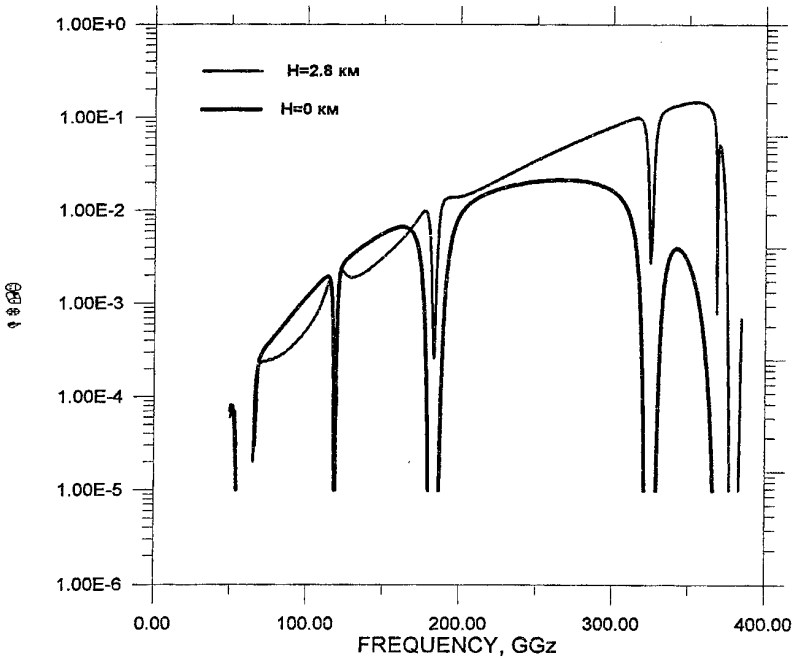
The evaluations have been executed for cloud model that consists of spherical particles of silicon dioxide having diameter of 0.2 mm with $N = 100$ cm^{-2}. Example of the frequency dependence of ΔT is shown in Figure for two cases.

Case 1: winter conditions, altitude of the vent (and of the cloud) 2.8 km above sea level, ambient temperature -25°C, absolute humidity 1 g/m^3.

Case 2: summer conditions, altitude of the vent (and of the cloud) 0 km above sea level, ambient temperature 20°C, absolute humidity 1 g/m^3.

Absorption of gases is calculated using Liebe's MPM code[1]. Maximum of polarization difference is expected in atmospheric windows centred to wavelength 1.3 mm and 0.87 mm. But the most stable polarization effect are expected in 2-mm window.

It have demonstrated, that 2-mm wave radiometric polarimeter having fluctuation sensitivity ~ 0.1 K (under time constant 1 s) makes it possible to detect the piroclasts in the typical eruption stream of volcano for a time of integration in order of several minutes during active stage. During as strong volcano eruption as the eruption of Mount Redoubt, Alaska, in January 1990 the value of N may by as much as 10^4 and polarization difference of brightness temperature be as great as several K.



Fige 1

References

. H.J. Liebe, "MPM — An Atmospheric Millimeter-Wave Propagation Model" International Journal of Millimeter Waves< Vol. 10< No 6, pp. 631–650, 1989.

FREQUENCY - TEMPORAL DISTRIBUTIONS OF RADAR-RETURNS FROM SEA SURFACE IN X- AND Ka- BAND

V.A. Kirichenko, G.P. Kulemin, V.G. Sugak
Usikov Inst. for Radiophysics & Electronics of the National Academy of Sciences of Ukraine
12 Proscura St., Kharkov, 310085, Ukraine
Tel. 0572 448333, Fax (0572) 441105, E-mail: sugak@ire.kharkov.ua

It has been analyzed one of the widely used methods of representation and research of Doppler signals reflected from a sea surface: the frequency - temporal two-dimensions distributions of ones. It obtains as a result of a sliding time window application which helps to look the researched sample with subsequent use of one of the numerous methods of transform of the obtained results in frequency area. Nowadays there is a large class of such representations (Wigner-Will, Cohen, Wavelet analysis etc.) with a not less extensive class of time windows.

It has been used the discrete Fourier transform of current sample to be seen through a used time window. In result it is obtained the two dimension transform of signals allowing to observe and to investigate the dynamics of development in time of their Doppler structure.

We applied the similar analysis to investigate the cross-polarized radar-returns signals reflected from the sea surface on the radio-wave lengths of 3.2 and 0.8 cm. For allocation of effects connected with synchronous in time and conterminous (coinciding) speeds of a scattering elements movement on the sea surface it was used the frequency-time distribution of the result of multiplication of current Doppler spectra of the cross-polarized component from an output of a rectangular time window sliding on researched samples with the subsequent weighing which is carried out by their coherent function. Such approach allows to investigate characteristic times of statistical connection of the signal cross-polarized components in their spikes and in pauses with different polarization of radiation and for different lengths of radio-waves.

The further processing of the obtained frequency - temporal distributions was carried out by calculation of their two-dimension auto-correlation function describing a measure of statistical interaction of these distributions with displacement of adjacent indications at frequency and time. By the basic motive of such transform application was rather frequently observable characteristic trajectories of distinctly selected groups of spectral lines corresponding the appropriate regularly moving and incurring the modulating influence by the part of large wind waves scattering ones on the sea surface.

Thus, the more influence of the mentioned modulating appearing in statistically greater speed of change of frequency of the appropriate spectral lines is the on the greater corner relatively of the time axis the elongated estimation (ambiguity body) of the two-dimension covariance function of frequency-time distribution of signals is deviated. On the other hand, the wider time of correlation interval of this function the more statistical time of life for the mentioned elements (which scatter the radio-waves) is. With presence of steady periodic (not less then one period) modulation of the Doppler frequency of a observable spectral line trajectory in a body of the two-dimension ambiguity function the characteristic X-figurative symmetric structure (fig.1) is allocated, the inclination of axes of which is connected to speed of frequency change of this line.

The observable two-dimension covariance function of frequency-temporal distributions at a wavelength of 3.2 cm have the essential differences from similar functions at a wave length of 0.8 cm to be appeared, first of all, for spike and pause of signals. For spike the axis of symmetry of bodies of this function have the greater inclination relatively a time axis and essentially greater correlation interval on time. The bodies of these functions have considerably greater relief at wave length of 3.2 cm (fig.1).

At wavelength of 0.8 cm the two-dimension functions near to zero of meanings of their arguments have sharper peak and much more dim pedestal , that makes less visible the effects of frequency modulations of spectral areas appropriate to groups of regularly moving scattering elements on wind waves.

Analyzing the correlation intervals of these functions both on frequency and on time and also inclinations of their bodies concerning a time axis it is possible to connect in further these parameters with parameters of sea excitement, first of all, with the characteristics of large wind waves. We hope to work out on these ideas the algorithms for detection of difference inhomogenates caused by presence on sea surface of ice blocks, oil spots and so on.

For instance, presence of periodicity in wave-wind process (under which one can observe periodic spectral line paths like length of the periodic function at fig.2a), must have a distinctive type two-dimensional auto-correlation function (like at fig.2b). Consequently, when the similar picture in real signal is found in two-dimensional auto-correlation function of spectral-temporary presentation one can allows to judge about presence of periodic structure in it and to value its feature.

The main defect of the approach considered above is a restriction on the reduction of size of elementary temporal segment on which it is produced evaluation of parameters of spectral component corresponding to moving scatters on sea surfaces. This is connected first of all with particularities of using of Fourie transformation to short lengths of temporal rows (faults of evaluations of spectrum and essential reduction of resolution ability on the frequency).

So, natural continuing a stated approach is an using of the high-resolution spectral methods on the frequency instead of the Fourie transformation in step of getting of the frequency temporal distribution. It allows to cut down a temporary window without the loss of resolution ability on the frequency and ,as an effect, to appear a possibility of more detailed study of spectral components forming for radar return samples from the sea surface. We have used the spectral method based on the decomposition of information space of selective covariance matrixes on signal and noise space. High-resolution spectral evaluation was built on the following formula:

$$Sp = \sum_{k} \frac{Sr^{\langle k \rangle}}{ev_k}, \qquad Sr^{\langle k \rangle} = F(\vec{r}(ev_k)),$$

where $F(...)$ is operator of discrete Fourie transformation;
ev_k is k-th eigenvalue of covariance matrix R corresponding to its eigenvector;

The spectral estimation is carried out in noise subspace. The process of decomposition was based on statistic eigenvalues of the covariance matrixes. We have used the averaging of the covariance matrix on all considered temporal segments to obtain more stable estimation of spectral components characteristics.

The following stage of processing, getting as a result of high-resolution spectral estimation of frequency-temporal distribution was an using the algorithms of smoothing and separations of borders of spectral line paths by methods of the scenes processing. It was used some methods of two-dimension smoothing and interpolating to get more distinguished relief of frequency-temporal distributions. It allowed to obtain a little better estimation of two-dimension auto-correlation functions of radar returns from sea surface.

Getting as a result stated above cycle of consequent steps at the radar returns study from the sea surface, the mutually three-dimensional and auto-correlation functions in coordinates a frequency-time-intensity possible to use herein for the building of completely autonomous algorithms of spectral analysis for the evaluation of parameters of wind waves on a sea surface and recognition of presence in under investigation samples of signals, reflected by scatters unconnected in immediate conjunction with the sea surface waves. As example, on fig.2 the frequency-temporal distribution of radar returns from sea surface at moment of appearance of signal spike (a) and corresponding him the three-dimensional auto-correlation function (b) with distinctive areas connected with periodicity of processes of wind waves (dribbled by circle) are brought.

Thus, the offered methods of processing of radar returns from a sea surface can be used :

1. for the estimation of parameters of wind excitement;
2. further elaboration of radar detection techniques of sea pollution and sea navigation clutter caused by shallows, separate blocks of ice, ice-block fields, etc. placed not deeply under water surface or protruding from it a little;
3. for construction of various algorithms of allocation and identification of reflections from slowly moving objects having distinct the characteristic oscillatory or regular movements from sea excitements caused by wind.

The work is executed partly at the Science and Technology Center in Ukraine (STCU) support, project No. 145.

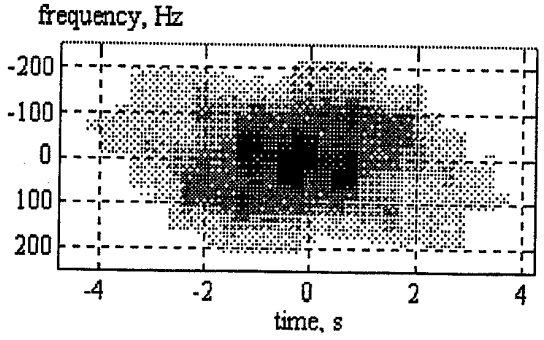


Figure1. The two-dimension auto-correlation function of radar returns from sea in X-band.

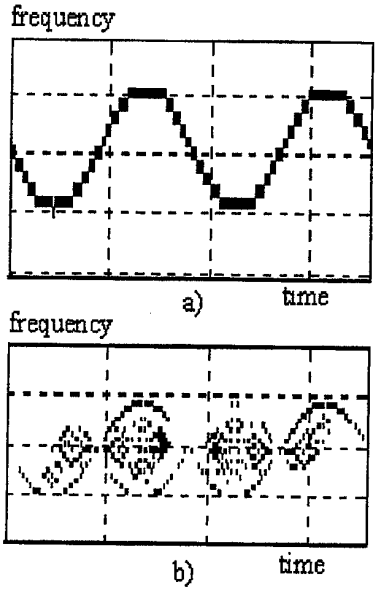


Figure 2. Two-dimension periodic function (a) and its auto-correlation function (b).

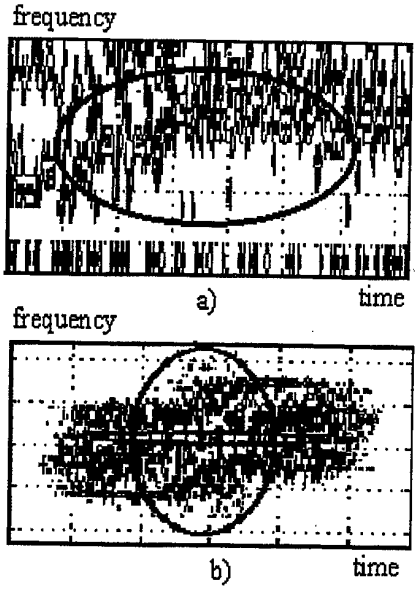


Figure 3. Two-dimension frequency temporal Distribution of radar return from sea at the radio-wave 3.2 cm (a) and its auto-correlation function (b).

References

1. V.B. Razskazovskyy, V. G. Sugak, "Features of spectra of radar-returns from wind waves with the high resolution on frequency" Radio- Engineering and Electronics, Vol. 41, No. 5, pp. 543-547, 1996.

POLARIZATION SELECTION OF NON-DOPPLER GROUND OBJECTS IN MM-WAVE RANGE

A.N. Zubkov, N.S. Akinshin, B.V. Sukhinin
TsKB Apparatostroyeniya
36, ul. Demonstratsii, Tula, 300034, Russia
Tel. 20-77-58, Fax 20-77-63

Radar methods of ground objects spectral selection against ground surface clutter, based on Doppler effect use [1], are low-effective for low-speed objects and non-applicable for motionless objects. Selection methods using coherent signature analysis [2] demand an essential complication of a radar receiver-transmitter. The use of polarization diversity methods for ground objects selection [3] is of great practical interest. The prospects of these methods in mm-wave range are caused by the presence of strong depolarizing effects when probing signals are scattered by real artificial objects, the construction of which presents a set of curvelinear and brockenlinear planes. In this circumstances areas of a ground surface in the neighbourhood of the observed object may be considered homogeneous and isotropic.

For experimental verification of the suggested selection method there was designed and manufactured the 35 GHz polarimetric solid-state radar, its block-diagram is presented in Figure 1. The radar has the following characteristics:

antenna gain	...43 dB
receiver pulse power	...0,3 W
transmitter sensitivity	... -120dBW
probing pulse width	...50...200ns

During the experiment in the interval of 1,5 ns four guadratures of the received signal were simultaneously registered from four adjacent range resolution elements. Probing signal polarization changed with radar repetition frequency, which provided mutual normalization of the orthogonal polarization receiving channels during the processing. The polarization characteristics of different ground-based eguipment and different kinds of the earth cover were studied. As an example, Figures 2, 3, 4 present the densities of the polarization features distribution for three types of the observed objects:

1 - the motionless military tracker of the MTLBU type with the shut-off engine;

2 - the motionless car ZIL-131 with the shut-off engine;

3 - the ground surface in the form of the grass cover.

Figure 2 corresponds to the anisotropy factor distribution of the object «m», Figure 3 corresponds to Huynen descriptor (γ) distribution, Figure 4 corresponds to the distribution of the ellipticity angle of the first own polarization of the object.

The analysis of the obtained results allows to state that the above - mentioned features for targets and clutter separate (have low match possibility) and may be used for selection of the ground - based equipment against the ground surface irrespective of speed. It is necessary to note, that the use of the polarization features opens up good vistas for solving the problem of the radar ground objects identification.

Figure 1. Block - diagram of the polarimetric radar.

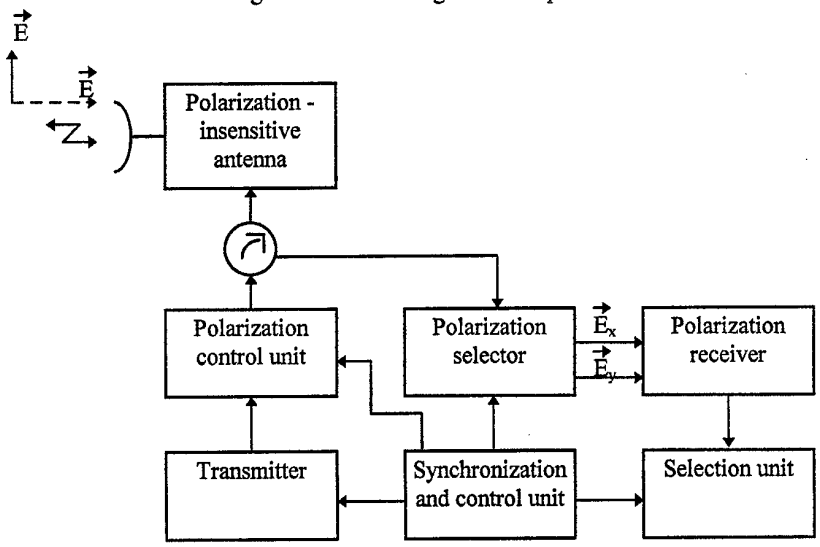


Figure 2. Density of the anisotropy factor distribution.

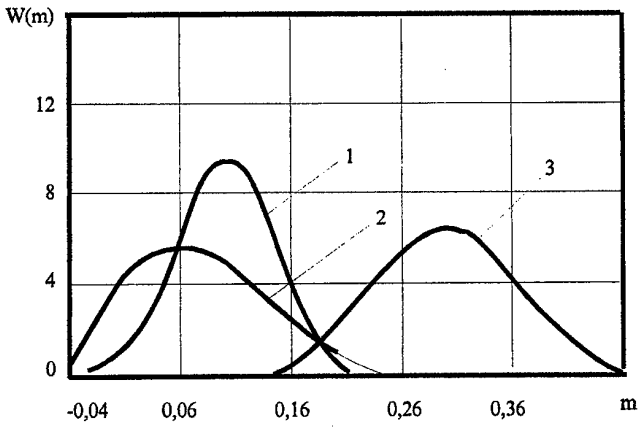


Figure 3. Density of Huynen descriptor distribution.

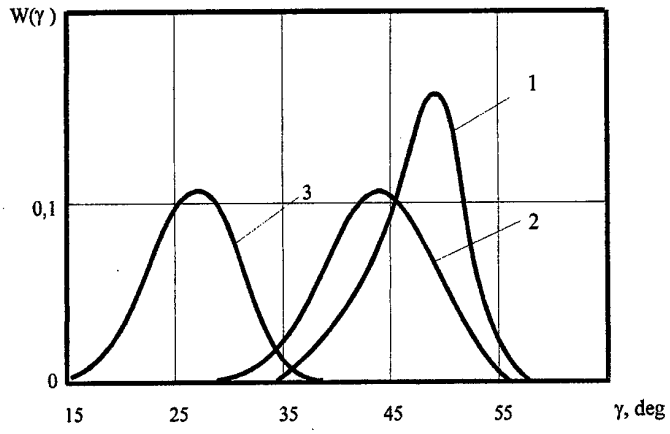
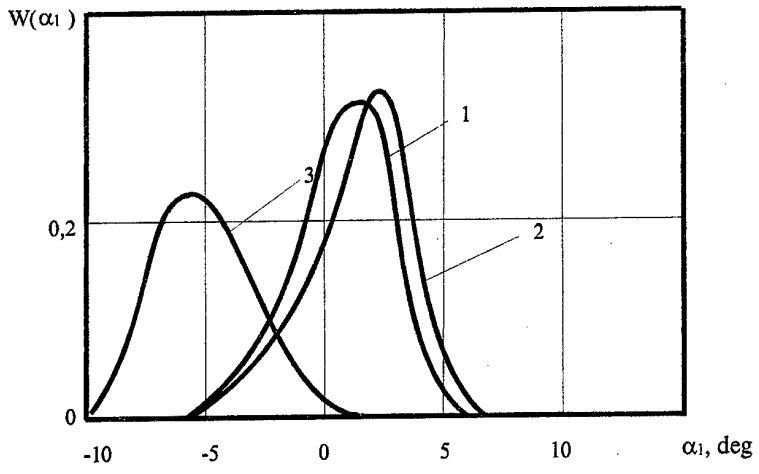


Figure 4. Density of the ellipticity angle distribution.



References

1. P.A. Bakulyev, V. M. Styepin , «Methods and Devices of the Moving Targets Selection» , Radio i svyaz , Moskow, 1986.
2. A.N. Zubkov, V.V. Alamanyuk , Yu.N. Kosovtsov, «Mm - Wave Range Radar Measuring Complex (RIK - 94)» , Proceedings of the First Ukrainian Symposium «Physics and Engineering of Millimeter and Submillimeter Waves», Kharkov, 1991.
3. D.Giuli , «Polarization Diversity in Radars», Proceedings of the IEEE , Vol. 74 , No. 2 , pp. 6 - 34 , February 1986.

CLUTTER REJECTION IN SHORT-RANGE RADAR WITH UNCODED AND WIDEBAND PULSED SIGNALS

G.P. Kulemin
Institute of Radiophysics and Electronics, National Academy of Science of Ukraine,
Proskura st. 12, Kharkov 310085, Ukraine
Tel. (380572)448-508, Fax (380572)441-105, E-mail: gena@ireas.kharkov.ua

The clutter rejection of pulsed signals is analysed for short-range radar of centimeter and millimeter bands of radiowaves. The signal to clutter ratio (SCR) for uncoded pulsed sequence and pulse-compression signals is estimated. It is shown that for radars operating over the land and sea surface the use of wideband signals does not permit to improve the clutter rejection in comparison with the uncoded pulsed sequence. This rejection gets worse when the resolution cell dimensions of pulse-compression radar are compared with the range to the target.

For majority of radars operating over the land or sea surface the main source of interference is the clutter determined by backscattering from surface because the clutter power is significantly greater than the receiver noise power. The analysis of statistical characteristics for land and sea backscattering has shown that the radar clutter from these medii possesses some features [1,2]. Among them one can note the difference of the normalized radar cross-section (RCS) distributions for land and sea backscattering from gaussian model, the spatial and temporal non-stationarity of clutter, and the specific form of backscattering signal spectra. These circumstances demand to take into consideration the real properties of clutter for estimation of clutter rejection for land and maritime radar systems with different types of transmitted signal.

In the framework of this paper we consider the clutter rejection in radar for two types of transmitted signal: a periodic uncoded pulsed sequence permitting to ensure the range resolution and the velocity indication of moving targets and pulse-compression signals (the typical examples of such signals are the pulsed signals with linear FM or phase coded pulsed sequence).

As well known, the target detection efficiency is determined by the ratio of the target signal power to the clutter power (SCR) if the clutter power is significantly greater than the receiver noise power. For periodic uncoded pulsed sequence the SCR can be presented as [3]

$$q = \frac{S}{C} = \frac{\sigma_t}{\frac{c\tau}{2}\theta_0 r \sum_{l=0}^{\infty} \frac{\sigma^o(r)}{[1-(l_0-l)cT_r/2r]}} \qquad (1)$$

where σ_t is a target RCS, τ is a transmitted pulse duration, θ_0 is an antenna pattern main lobe width, r is a range from radar to target, $\sigma^0(r)$ is the normalized RCS of clutter as a function of range, T_r is a pulsed repetition period, $l_0 = [\,2r / c\,T_r\,]$ is an integer part of the range to unambiguous interval ratio.

The contribution of backscattering from the surface cells placed more far than the target is essentially less than the backscattering from surface cell under the target and from cells at shorter ranges. For these conditions one can restrict the value of l to $l_{max} = [\,2r_{max} / c\,T_r]$.

For the unambiguous target range determination ($r_{max} \le c\,T_r / 2$ and $l_0 = 0$) the clutter power is a sum of backscattering from the surface cell under the target and from the cells situated at ranges greater than the maximum range of radar.

As well known [3], for the grazing angles the clutter power decreases with the range increasing proportionally to r^{-3} for land and to r^{-7} for sea. In these conditions the calculation of clutter from ranges of $r > r_{max}$ is usually not necessary.

The range ambiguity appears for high pulse repetition frequencies (PRF) that are necessary for the effective clutter rejection by MTI systems. In this case the clutter power is a sum of backscattering from radar cell under the target and from the cells situated at ranges nearer than the range to the target. As a result, the signal - clutter ratio changes for the worse and for ranges closed *to* $r = l\,cT_r/2$ the target observation is impossible because of transmitter leakage and receiver saturation by transmitted pulses at these ranges.

As an example, in Fig. 1 the dependences of $q = f(r)$ for the different target altitudes are presented calculated for the following conditions: $\sigma^0(r) = -35$ dB = const, $\sigma_t = 0.01$ m^2, and $\tau = 0.1$ μs. The curves 1

- 5 correspond to unambiguous range estimation and curves 6 - 7 correspond to case when the PRF exceeds the value of unambiguius range estimation by two times, i.e. $2r_{max}/c\,T_r = 2$.

Thus, the clutter rejection of uncoded pulsed sequence for sea and land clutter is ensured in the best way in the regime of unique range estimation and turns to worse for radar with high PRF.

The use of wideband signals permits to increase the clutterrejection. In particular, for pulses with linear FM or phase coded signals the gain in signal-clutter ratio in comparison with uncoded pulsed sequence equals to $K = q_W/q$ if the pulse durations are equal where $K = \tau\,\Delta f$ is the compression factor, Δf is a spectrum bandwidth, and q_W is a *S/C* ratio for wideband signal.

If the media contains a great number of scatterers with high density the resulting signal has the random noise characteristics. If, besides, the range to target is great it is possible to not take into account the dependence of the clutter level on the range. Then the resulting signal can be presented as a stationary and gaussian random process for which the results of works [4-6] can be applied practically completely. In this case the resulting clutter power density per one cell of resolution reduces when the range resolution of radar increases. But the expedient value of range resolution is limited by the target dimensions as well as the change of the clutter statistical characteristics which leads to increasing of false alarm level.

For equal range resolution of considered signals the other situation is observed. The normalized RCS of clutter is practically a constant value in the radar resolution cell for short duration uncoded pulsed signal at great ranges. For wideband signal with equal range resolution the cell sizes are determined as

$$\Delta r = Kc\tau/2 = K\Delta r. \tag{2}$$

The normalized RCS of clutter can not be considered as a constant value in the resolution cell for the great compression factors. Then the clutter power P_c at the receiver input equals to

$$P_c = P_t \frac{G^2\lambda^2\theta_0}{(4\pi)^3}\int_{r-\Delta r/2}^{r+\Delta r/2}\frac{\sigma^0(r)}{r^3}dr \tag{3}$$

here P_t is a transmitter power, G is an antenna gain.

For two dependences of σ^0 as a function of the range typical for grazing angles ($\sigma^0 \sim r^{-4}$ for sea and $\sigma^0 \sim r^{-1}$ for land) the clutter power equals

$$P_c = \begin{cases} \dfrac{16}{3}AK\dfrac{12+\beta^2}{(4-\beta^2)^3} & \text{for land} \\ 256AK\dfrac{(\frac{4}{3}+\beta^2)(12+\beta^2)}{(4+\beta^2)^6} & \text{for sea} \end{cases} \tag{4}$$

Here

$$A = P_t\frac{G^2\lambda^2\theta_0\sigma^0(r_0)\Delta r_0}{(4\pi r_0)^3} \tag{5}$$

is the clutter power from radar resolution cell at range of r_0 for uncoded pulsed signal with duration of τ, $\beta = \Delta r/r = K\Delta r_0/r_0$ is the relative gain of radar cell for wideband signal.

For "pin-like " ambiguity function with residues level δ the clutter is distributed uniformly on the "range - velocity " plane. This makes worse the signal- clutter ratio in comparison to that one for uncoded pulsed sequence. The losses for this case are equal

$$L=\frac{q_{pc}}{q}=\begin{cases}\dfrac{16}{3}AK\dfrac{12+\beta^2}{(4-\beta^2)^3} & \text{for land}\\[2ex] 256AK\dfrac{(\frac{4}{3}+\beta^2)(12+\beta^2)}{(4+\beta^2)^6} & \text{for sea}\end{cases} \qquad (6)$$

The dependence of losses in SCR for pulse-compression signal as a function of relative gain β is presented in Fig. 2. For level of residues determined as $\delta = K^{-1}$ (this is typical for noise and noise-like signals) the losses are significant when the radar cell dimensions are compared with the range to target r_0. If the level of residues is equal to $\delta = K^{-1/2}$ then the SCR is considerably worse than that one for uncoded pulsed sequence at throughout values of β.

Thus, the use of the wideband signals with pulse - compression in radars operating over the land and sea surface does not improve the clutter stability in comparison with the uncoded pulsed sequence, especially for short-range radars with the equal range resolution. This obstacle limits the use of these signals for increasing of the detection range when the transmitted power is limited.

The differences of clutter distributions from the gaussian model for high resolution radar when the clutter has the σ^0 distributions with the greater level of "tails" lead to increase of the threshold level in the receiver to maintain the same false alarm rate. As result, the SCR improve is needed for maintaining of the detection probability. This improvment compensates partially the gain obtained by the expense of use of pulse-compression signal with higher range resolution in comparison with uncoded pulsed sequence.

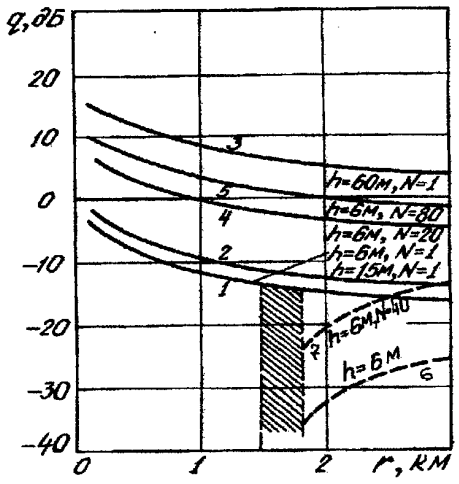


Fig. 1. SCR as function of radar range

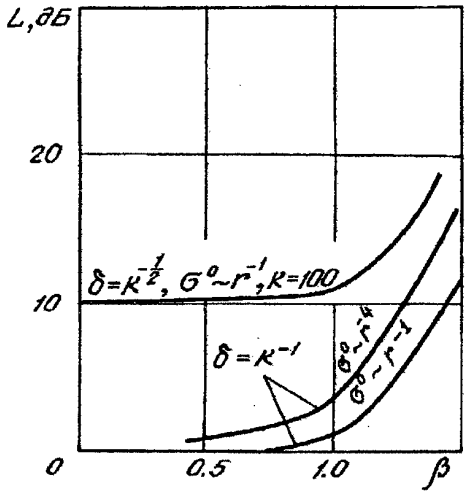


Fig. 2. SCR losses as function of relative gain

References

1.Kulemin G.P., Razskazovsky V.B., The scattering of millimeter radiowaves by Earth for low grazing angles, Kiev, Naukova Dumka, 1987 (in Russian).
2. Kulemin G.P., Razskazovsky V.B., Complex effects of clutter, weather and battlefield conditions on the target detection in millimeter radars, Proc. SPIE, 1994, v. 2222, pp. 862 - 871.
3. Cook C.E., Bernfeld M., Radar Signals, an Introduction to Theory and Application, Acad. Press, N.Y., 1967.
4. Middleton D., An Introduction to Statistical Communication Theory, McGraw - Hill Book Co., N.Y., 1960.
5. R.S. Berkowitz (edit.), Modern Radar, analysis, evolution, and system design, Wiley and Sons, N.Y., 1965.
6. Marcum J.I., A statistical theory of target detection by pulsed radar, Trans. IRE , 1960, IT-6, No 2.

ROUGH SEA SURFACE OBSERVATION SCHEME OPTIMIZATION at MICROWAVE RADIOMETRIC SENSING

V.A. Komyak*, S.A. Shilo*, Ya.I. Stephanishin**
* Institute of Radiophysics and Electronics, Ukraine National Academy of Sciences
** National Space Agensy of Ukraine
Address: Bildg. 12, Ac. Proskura Street, Kharkov, 310085, Ukraine
Tel. 38(0572) 448-446, Fax 38(0572) 441-105, E-mail shilo@ire.kharkov.ua

The scanning radiometric complexes (SRC) allocated on space satellites come broad application in practice of remote sensing of the Earth environment. Expansion of resolving tasks for these systems requires further magnification of its information density by means of increasing a set of operational bands and polarizations. More rigid becomes limitations to absolute accuracy of radiometric measurements. For example, radiometric accuracy required to reconstruction of sea surface temperature (SST) should make 0,5 K, and in any way mustn't be worse then 1 K.

At such high accuracy of measurements, the results may be affected not only by errors called through limitations of radiometric sensitivity and accuracy of calibration procedure, but also by singularities of systematical principals to be used at the measurements.

Nowadays, most perspective radiometric systems for ocean surface monitoring are satellite systems with conical scanning of antenna beam. One of their advantages is provision of broad width on the surface at constant angle of observation θ (angle between antenna beam axis and a normal to the surface). Satellite altitude and selection of this angle depends not only on the system field of view, but also, in a noticeable degree, on the list of the resolved tasks for ocean monitoring SRC.

As shown in [1], radiobrightness temperature of ocean surface can be submitted as the sum

$$T_{w\,h,v}(\theta,\lambda) = T_{0\,h,v}(\theta,\lambda) + \Delta T_{w\,h,v}(\theta,\lambda)\,,$$

where $T_{0\,h,v}(\theta,\lambda)$ - radiobrightness temperature of smooth water surface, $\Delta T_{w\,h,v}(\theta,\lambda)$ - an increment by means of rough surface (under wind); h,v - indexes of polarization, λ - radio wave length.

Relationships of increments $\Delta T_w=(T_w-T_0)$ from observation angle θ and for wind speed 7 and 15 m/s (without foam component) shown on Fig.1. and calculated for λ = 8 мм by dint of methodic [1] checked up at "Bering" experiment [2]. As we see, the increments of radio brightness temperature essentially depends from an angle of observation. For disturbed sea surface, at functional relation of radio brightness temperature from angle of observation there's "special" angle θ_o specific to each radio wave band and polarization, for which sea surface parameters (wave direction, wind speed, degree of wave magnification) poorly affect on the radiant characteristics of the surface ($\Delta T_{w\,h,v}(\theta) \approx 0$) and brightness temperature depends only upon thermodynamic temperature of the water and percentage of foam cover on the surface. At simultaneous observations on these angles at several radio frequency bands and polarizations it's possible to separate contributions of these two factors and to determine SST, and through amount of foam on the surface to estimate a module of near-surface wind speed. The relations of θ_o from λ calculated accordant to a technique [1] for values $\varepsilon'(\lambda)$ and $\varepsilon''(\lambda)$ from [3] are shown on Fig. 2. These data can be putting in the fundamentals at remote sensing of the ocean - for selection of observation angles and for arrangement of a set of irradiators at the focal zone of antenna mirror, depending from SRC tasks.

It's necessary to mark, that appropriate selection of observation angles determines, but not guarantee high accuracy to restoration procedures for geophysics parameters by means passive radio sensors. Essential influence on the accuracy of the radiometric measurements can also exert instabilities of altitude and orientation of the carrier [4]. Herewith, the errors connected to a sea surface state may lead to significant errors at SST determination (against geometric distortions, that can be comparatively easy taken into account at the processing algorithms with the actual data about satellite orbit and orientation parameters). Deviations of actual angle θ from defined θ_o can result to additional errors of SST measurements: first, the increment called by roughness has significant steepness at angular relationship; secondly, depending from mutual orientation of azimuth observation direction and of near-surface wind speed vector, extent of this increment will be essentially varied due to azimuth anisotropy of sea roughness. Experimental data demonstrated an influence of azimuth anisotropy of sea surface roughness on measured brightness temperature shown on Fig.3. The data obtained

from airplane side-looking microwave radiometer at λ= 8 mm, horizontal polarization, wind speed W ≈ 10 m/s, observation angles θ = 20°, 30° and 70°, and submitted as $\Delta T_w(\varphi) = (T_w(\varphi) - T_w(\varphi)_{min})$. As it's visible from the figure, the azimuth anisotropy at θ = 30° practically doesn't appear. Make oneself conspicuous a modification of the shapes and of maximum directions for azimuth relations on both sides from θ = 30° (pursuant to Fig.2, $\theta_o \approx 35°$ at λ=8 mm for horizontal polarization). At small observation angles $\theta \in [\ 0° - 20°\ ]$ the maximum contrasts are observed in directions, orthogonal to direction of wave motion (wind speed vector); at angles range 30° - 40° brightness temperatures are distributed rather evenly through azimuth and azimuthal contrasts practically aren't expressed, at observation angles $\theta > 50°$ the steady maximums of azimuth relationships to back sea wave direction are observed.

Thus, evidently, that from selection of observation angle (for top of a cone at scanning) and from stability of satellite parameters of orientation in considerable extent depends an accuracy of remote microwave brightness temperature measurements and, therefore, effectiveness of space multi-frequent radiometric systems with conical beam scanning.

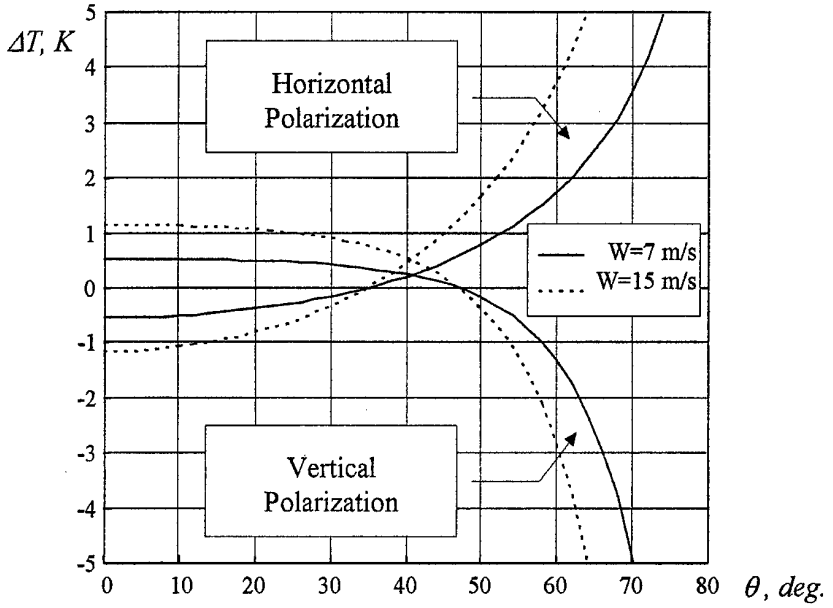


Figure 1. The results of calculations of increments $\Delta T_w = (T_w - T_0)$ from observation angle θ; Wind speed W=7, 15 m/s; λ = 0.8 cm; T_{sea}=0°C; S = 40 $^0/_{00}$; ε_r =9,15; ε_i =18,11;

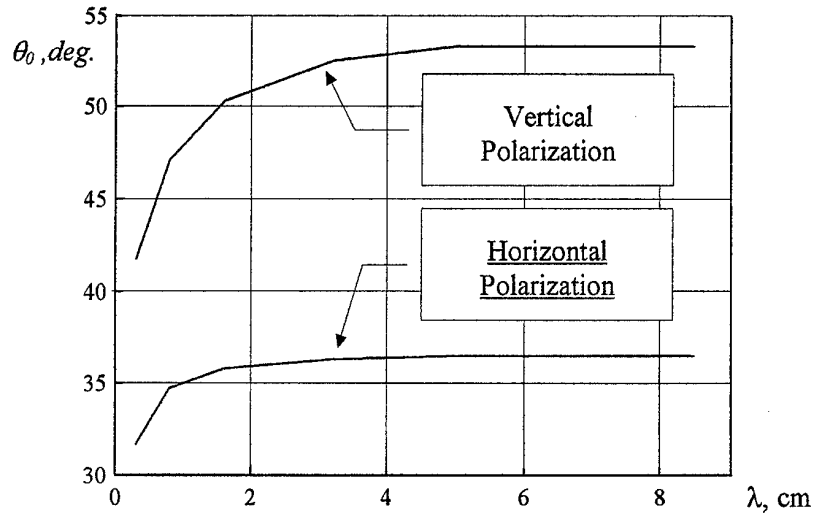


Figure 2. The results of calculations of angles θ_0 corresponding to zero increments ΔT_w; W=0÷15 m/s

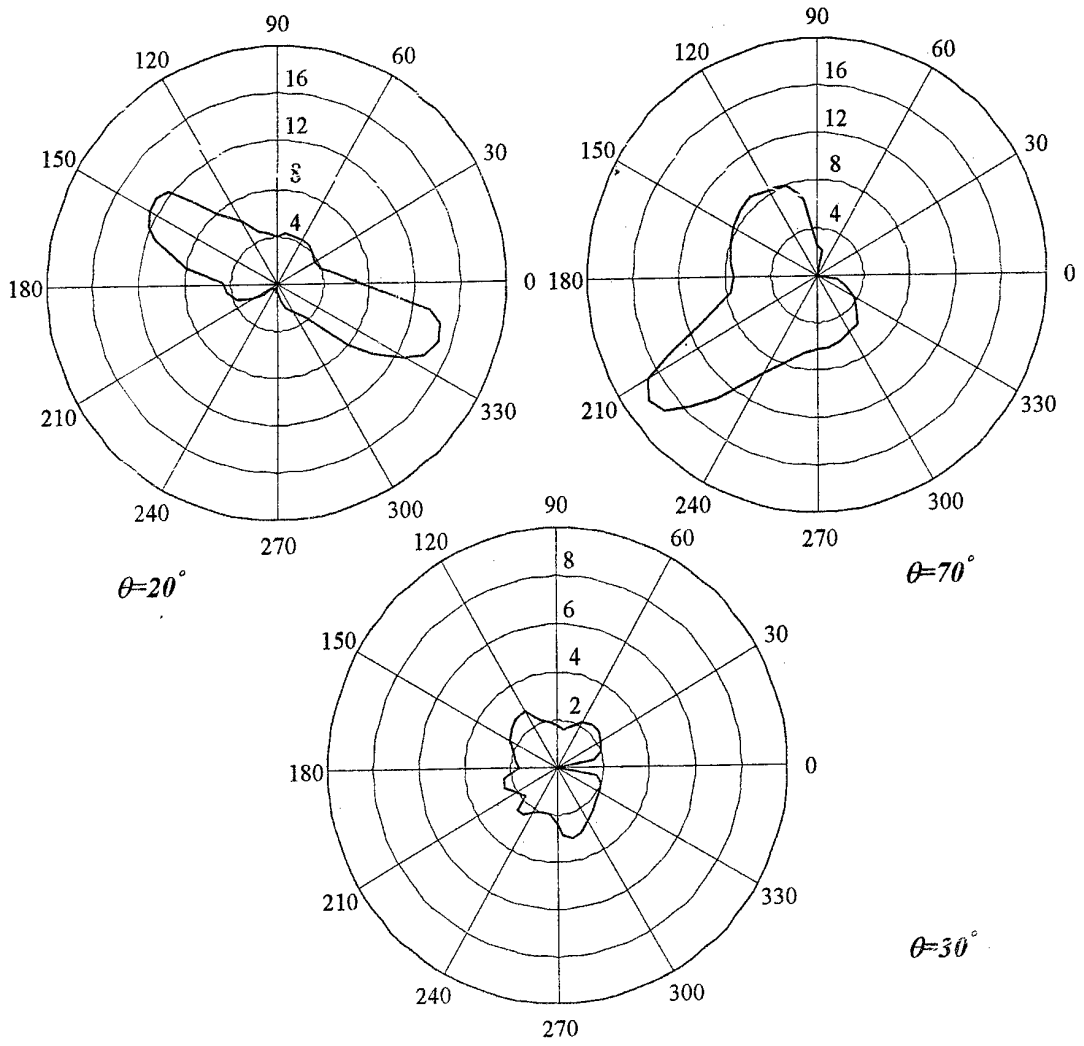


Figure 3. Experimental azimuthal relations of brightness temperature increment ΔT_w to an angle of observation θ; λ= 8 mm; $W \approx$ 10 m/s; θ= 20°, 30°, 70°, H- polarization

References

1. E.M.Shulgina, "Calculation of radiation ability of the disturb sea surface at microwave band", Izvestiya AN USSR. Physics of atmosphere and ocean, Vol. 8, № 7, pp. 773 - 776, 1972. (in Russian).
2. L.M.Marcenkevich, "The analysis of sea surface state condition characteristics influential on thermal radio emission at location of scientific ship "Priboj"", In: Soviet-American experiment "Bering", Hydrometeoizdat, Leningrad, pp. 108 - 126, 1975. (in Russian).
3. "Meteorological sensing of underlying surface from space", Under red. of K.Ya.Kondratyev, Hydrometeoizdat, Leningrad, p. 247, 1979. (in Russian).
4. V.A.Komyak, S.A.Shilo, V.M.Bykov, Ya.I.Stephanishin, "Influence of nonstable location of satellite on results of microwave radiometric remote sensing of environment", Earth Research from Space, № 5, pp. 46-53, 1997. (in Russian).

MILLIMETER BAND SCANNING MULTI-BEAM RADIOMETER

S.A. Shilo, V.A. Komyak
Institute of Radiophysics and Electronics, Ukraine National Academy of Sciences
Address: Bildg. 12, Ac. Proskura Street, Kharkov, 310085, Ukraine
Tel. 38(0572) 448-446, Fax 38(0572) 441-105, E-mail shilo@ire.kharkov.ua

At creation microwave scanning radiometric systems intended for remote sensing of environment from flight vehicles (airplane, satellite), one of the main problem is achievement a compromise between requirements of fulfilling the greatest possible spatial resolution, broad field of view and extremely accessible radiometric sensitivity and absolute accuracy for measured brightness temperature. The contradictions are provoked by time limitations imposed on measurement cycle duration for one pixel of radiometric image at high speed of the carrier, - the higher spatial resolution and wider field of view, the more amount of independent elements (points) in formed image and the less time may be appointed on data estimation for one element. Besides this, a way of scanning may impose limitations upon marginal speed of motion of the antenna beam. In the case of using antennas with full moving aperture, significant mechanical moments may appear at large rates of scanning, which make lower the greatest speed of motion of the antenna and will increase weight and power consumption of mechanical drive. These problems stimulates researches at such areas of microwave radiometric systems design as utilization non-mechanical ways of antenna beam control jointly with rising operating frequencies to short-wave part of centimeter range and to millimeter range of radio waves, - it's possible to realize high antenna directivity under rather small sizes of receiving aperture at these bands and, at the consequence of that, high speeds of spatial motion of antenna beam may be ensured. However, the contradictions related with providing the highest radiometric sensitivity in these wavebands become more significant, because of monotonous deterioration of noise parameters of active receiving modules and passive microwave elements with increasing of frequency.

To resolve considered problems possible way is application of non-traditional means of antenna beam spatial position control likewise radiothermal images formation with assistance of multi-beam systems.

As an example of mapping microwave radiometric system with non-mechanical antenna beam control, the RM-08 scanning radiometric system developed in IRE NASU for space satellites «Kosmos», «Ocean-01» series may be submitted [1]. This system has passed truth operational tests at the composition of radiophysical instrumentation complexes of more then 10 satellites, have been launched in USSR since 1983. It embodied a scanning antenna with electromechanical beam control developed on the principles of surface-to-volume conversion of electromagnetic waves at open electrodynamic structures. Antenna contained a fixed reflecting mirror of parabolic cylinder shape with dimensions 1150×580 mm^2 and linear scanning radiator borne out from the aperture bounds and executed on the basis of linear dielectric waveguide connected by means of electromagnetic field to one of diffraction grating from their set located on the rotated cylinder along its forming [2]. Antenna pattern spatial position is determined by parameters of interacting diffraction grating. When cylinder rotates about its own axis with assistance of low-power mechanical drive executed on the basis of step-by-step engine, diffraction gratings consistently interacting with electromagnetic field of dielectric waveguide and, as a consequence of that, by choosing parameters of diffraction gratings antenna pattern required spatial position, sector of elevation angles and the rule of scanning may be realized. RM-08 radiometric system main parameters represented in Table 1. It's necessary to mark comparatively low radiometric sensitivity, which has made about 3,0 K, that is caused by insufficient value of radiometric award $\sqrt{\Delta f \tau}$ under values of integration time τ = 8 ms and operational frequency band Δf = 290 MHz. Radiometric receiver frequency band Δf was terminated by means of band-pass filter with the aim to reduce undesirable affect of dispersion properties of electrodynamic system of the radiator on the resultant beam width in elevation plane. For this radiator the angle-to-frequency factor come to ~ 1° of beam revolution at the frequency augment on 1%, and the total signal losses reaches for it - 0,8 dB at the length about 950 mm.

At creation RM-08 radiometric system its parameters were optimized emanated from resolving the tasks of sea ice cover and atmospheric formations above the ocean monitoring, together with side looking radar and optical scanner included at the hardware complex of the satellite. In spite of a set of novel engineering solutions applied to this system, some factors, first of all a poor sensitivity and a limited amount of spatial positions of antenna beam, equal to a number of diffraction grating located at the radiator, constrain implantation the

systems that category to the practice of monitoring a variety of natural objects, researches of which require much higher parameters of instrumentation.

As development of engineering solutions placed at the fundamentals of RM-08 scanning radiometric system, with all its advantages utilization, the multi-beam scheme of scanning based on adaptation of dispersion properties of electrodynamic system of the scanning radiator may be offered [3]. This scheme of scanning presented on Figure 1. Radiometric image is formed by lines with scanning antenna pattern in a plane orthogonal to the speed vector of the carrier. Full sector of elevation angles $\Delta\psi$ is divided on some subsectors $\Delta\psi_i$ $(1 \le i \le N)$, amount of which N is equal to a number of diffraction grating located at the cylinder of the radiator. When cylinder rotates, the spatial position of antenna pattern is changed, according to parameters of concrete diffraction grating. One revolution of the cylinder corresponds to one cycle of scanning, thus there are no costs of time to return antenna pattern in an initial position - it discontinuously passes from the last subsector to the first at transition from last to first diffraction grating. Within the limits of everyone subsector of elevation angles antenna pattern is splitted at some friend-to-friend beams total number of M formed by means of frequent separation directions of observation. For this purpose, general frequency passband Δf of the system is divided on series of contiguous subbands Δf_i by means of the unit of bandpass filters (located, for example, at intermediate frequency part of radiometric receiver). Radiometric receiver is constructed under multichannel scheme of signal processing with common antenna and radio frequency sircuitry. Amount of frequency channels, general passband of the system and operational bandwidth for everyone receiving channel are optimized proceeding from parameters of the scanning scheme, characteristics of electrodynamic system of the radiator and from dimensions of antenna aperture (from planned beamwidth). At high scanning rate exceeded one revolution per second the channels of radiometric receiver can be constructed under full power radiometer scheme with every line calibration procedure. In this case, essentially, the scheme of signal processing with superlow frequency of modulation will be realized, that is most prospective from the point of view of radiometric system fluctuation sensitivity approach to it potentially possible limit [4].

It's necessary to mark some dignities of offered scheme of scanning, in comparison to used monobeam scheme, to number of which may be concern (i) increased in M times duration of observation for single pixel, that in $\sqrt{M}$ times increases radiometric resolution; (ii) most effective usage of radio frequency band for microwave elements of the system; (iii) mach lover mechanical moments of antenna drive and it regular unidirectional rotation, that will able to rich high rates of scanning; (iv) an absence of monotonous spatial motion of the beam at transition from one subsector $\Delta\psi_i$ to another, that reduces dynamic distortions of the image along the string (effect of shifting).

Conclusions. Radiometric systems with potentially high technical and design parameters may be realized on the basis of offered scheme of scanning. Offered principals are most prospective for construction of radiometric systems operated at the millimeter band of radio waves, in the cases when it's required to ensure broad field of view at the surface with significant dimensions of receiving aperture and with high both spatial and radiometric resolution.

Table 1. RM-08 radiometric system main parameters

Parameter	Value	Remark	Parameter	Value	Remark
Wavelength	8,2 mm	Δf = 290 MHz	**Polarization**	H	
View angles sector	20°-51°	from nadir	**Antenna beamwidth** - on azimuth (H) plane - on elevation (V) plane	 0,8° 0,5°	
Spatial resolution	10 × 15 km^2	mean value at swath width	**Sensitivity**	3.0-3,5 K	at τ=8 ms, Δf = 290 MHz
Integration time	8 ms		**Scanning rate**	1/ s	line per second
Antenna elevation angle position	45°	normal to aperture	**Output temperatures range, K**	110-330 150-250	by commands from the Earth
Altitude	650 km	mean value	**Swath width**	550 km	at mean altitude

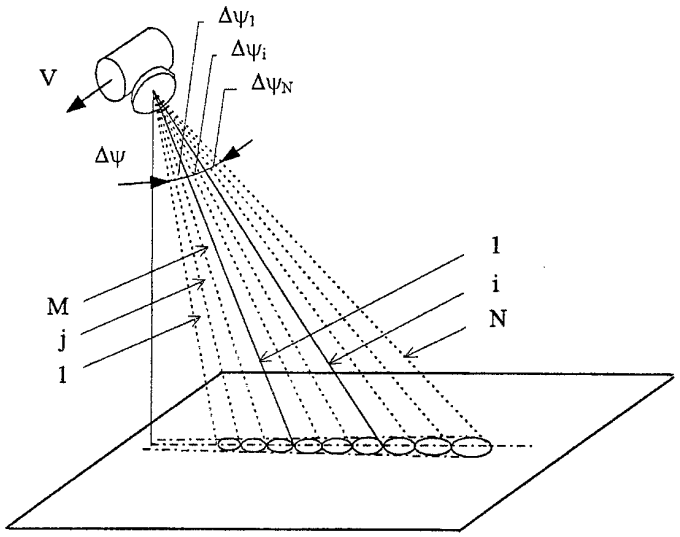


Figure 1. The scheme of scanning for multi-beam radiometric system.

References

1. A.P.Yevdokimov, V.A.Komyak, S.A.Shilo et al.," Scanning Radiometer for Remote Sensing", SU Author Certificate №1217101, G01S13/95, 1985 (in Russian).
2. A.P.Yevdokimov, V.V.Kryzhanovsky, S.A.Provalov, "Modern state of beam scanning problem at antennas of millimeter band radiometric complexes", In: Radiophysical methods and means for investigation of environment at millimeter wave band, Naukova dumka, Kiev, pp. 160-166, 1988. (in Russian).
3. V.P.Shestopalov, V.A.Komyak, S.A.Shilo et al., "Scanning Radiometer", SU Author Certificate №1384024, G01S13/95, 1987 (in Russian).
4. M.S.Hersman, G.A.Poe, "Sensitivity of total power radiometer with periodic absolute calibration", IEEE Trans. on Microwave Theory and Tech., Vol. 29, № 1, pp32-40, 1981.

METHODS OF REMOTE SENSING OF STRATIFIED MEDIUMS AND THEIR APPLICATIONS

* Velasco Hererra V.M., ** Volosyuk V.K.,
** Falkovich S. E.,** Gorbunenko O.A., ** Sokolnikov A.V.,

* Instituto de Geografia UNAM, A.P. 20-850, 01000 Mexico D.F.
Tel. (525) 622-4340, Fax: (525) 616-2145
** Kharkov Aviation Institute, kafedra 502,Chkalova str. 17, Kharkov -70,
310070 Ukraine, Tel. (0572) 44-23-52, E-mail: velasco@io.itl.net.ua

ABSTRACT

The methods and tools offered in the given paper are based on use of coherent impulse and multifrequent signals in one range of waves (not excluding basically integration's of handling of images in various ranges). Their essential distinctive singularity is the use of spatial (on an angle of a place) and temporal (on delay of signals) distinctions of signals reflected from heterogeneity's of stratified mediums.

These distinctions are realized by additional spatially-temporally handling of signals on lattices consisting from elementary (in particular, along fuselage) antennas, which phase centers are located on a line (vertical, horizontal or sloping), perpendicular to flight direction. Thus the focusing of a system on specific stratums and suppression of signals reflected from the upper stratums of mediums is carried out spatially - temporally. All necessary information about an image of heterogeneity's of stratified mediums, is received thus for one flight of the carrier. The high solution of an image is reached, as well as in usual synthesized aperture radar (SAR), at the expense of a matched filtration of signals ensuring synthesis of the aperture.

1. OPTIMAL ALGORITHMS

We use the model, consisting of set of discrete layers with discrete changes of a refraction index on depth coordinate. To find of optimal algorithms of signal processing it is possible to use two equations of possible definition of input signals;
the first model is:

$$V_m(t,r') = \mathrm{Re}\sum_{i=1}^{N}\int_{D_i} F_{im}\left[t,r',r_i,\lambda_{1i}(r_i)\right]\times S_{omi}\left[t,r',r_i,\lambda_{21}(r_i)\right]dr_i + n_m(t,r') \qquad (1)$$

and the second one is:

$$V_m(t,r') = \mathrm{Re}\sum_{i=2}^{N}\int_{D_i} F_{im}\left[t,r',r_i,\lambda_{1i}(r_i)\right]S_{omi}\left[t,r',r_i,\lambda_{21}(r_i)\right]dr_i +$$

$$+\,\mathrm{Re}\int_{D_1} F_{im}\left[r_1,\lambda_{11}(r_1)\right]S_{o\perp m}\left[r_1,\lambda_{21}(r_1)\right]dr_1 + n_m(t,r') \qquad (2)$$

$r_i = (x,y,z)\in D_i, r'\in D', t\in(0,T)$. Where $F_{im}[\cdot]$ is scatter- factor of waves connected with element dr_i of i subsurface layer. $S_{omi}[\cdot]$-is principal signal of this layer [1].

$$S_{oim}\left[t,r_i,R_{oi}(r_i)\right] = G(t-x_i/V)S_{olm}(t-2R_{oi}/c)\exp\left\{j(\omega_o t-2kR_{oi})\right\}*$$
$$*\exp\left\{jk(x_i-Vt)^2/R_{oi}\right\}\varphi(r_i)$$

Here R_{oi} is distance to i layer. Indexes "m" determine the kind of polarization of radiation, number of frequency band and etc. and function $\varphi(r_i)=\exp[jkr_i\cos\theta]$ for vertical or $\varphi(r_i)=\exp[jkr_i\sin\theta]$ for horizontal antennas. All stratified mediums images can be restored in the first model (1) and in the second one (2) the image of upper surface layer which is the most powerful is interpreted as an additional interference and have to be suppressed. Noise components n_m are modeled by white noise. The main procedures over signal receipt which is necessary to fulfill for solving the stratified mediums imaging problem can be found from the method of the maximum of likelihood function. In the case of first model this function can be represented by following expression [1,2]:

$$P[V(t,r')/\lambda(r)] = \kappa \exp\left\{-\sum_{m=1}^{M}\frac{1}{N_{om}}\int_0^T\int_{D'}\left[V_m(t,r') - \mathrm{Re}\sum_{i=1}^{N}\int_{D'} F_{im}\left[t,r',r_i,\lambda_{1i}(r_i)\right]*\right.\right.$$

$$\left.\left.*S_{oim}\left[t,r',r_i,\lambda_{2i}(r_i)\right]dr_i\right]^2 dr'dt\right\} \quad (3)$$

By differentiating the likelihood functional on functions to be found we have received the integral equation systems for stratified mediums images and other parameters $\lambda_{1i}, \lambda_{2i}$. Usually parameters λ_{1i} determine electrophisical parameters of stratified mediums layers and λ_{2i} determine the ranges to layers for angles given or angles when the ranges are given. It is necessary to use a set of signals not smaller, than set of estimated parameters. Functions Ψ_{jj}, Ψ_{ij} defined below are functions of signal ambiguity for the stratified mediums imaging problem. These functions Ψ_{ij} and Ψ_{jj} are determined by individual properties of signals reflected from given element of the layer. It is obvious, that these functions are:

$$\Psi_{jj}[\cdot] = \int_0^T\int_{D'} S^*_{ojm}\left[t,\hat{\lambda}_{2j}(r'_{j1}),r_{j1},r'\right]S_{ojm}\left[t,\hat{\lambda}_{2j}(r_j),r_j,r'\right]dtdr' \quad (4)$$

$$\Psi_{ij}[\cdot] = \int_0^T\int_{D'} S^*_{oim}\left[t,\hat{\lambda}_{2i}(r_i),r_i,r'\right]S_{ojm}\left[t,\hat{\lambda}_{2j}(r_j),r_j,r'\right]dtdr' \quad (5)$$

Functions Ψ_{jj} and Ψ_{ij} determine the resolution of the imaging system and should be narrow on coordinates. So signals should be orthogonal. Small width of functions and orthogonality of the signals could be fulfilled by choosing the form of the signals radiating by antennas systems. As well as at ranging of point sources, to obtain an sufficient resolution in the stratified mediums imaging problem it is necessary to use the complex signals multifrequecy, with into pulse modulation, and wide band of the frequencies. It is possible to simplify the system of maximum likelihood equations to such form (Ψ_{jj} and Ψ_{ij} are narrow):

$$\int_0^T\int_{D'} V_m(t,r')S_{ojm}\left[t,\hat{\lambda}_{2j}(r_j),r_j,r'\right]dr'dt =$$

$$= 1/2\int_{D_j} F^*_{jm}\left[r_j,r_{j1},\hat{\lambda}_{1j}(r_{j1})\right]\Psi_{jj}\left[r_j,r_{j1},\hat{\lambda}_{2j}(r_j),\hat{\lambda}_{2j}(r_{j1})\right]dr_{j1} \quad (6)$$

$$\frac{\partial}{\partial\lambda_{k2j}}\int_o^T\int_{D'} V_m(t,r')S_{ojm}\left[t,\hat{\lambda}_{2j}(r_j),r_j,r'\right]dr'dt = 0;\ \hat{\lambda}_{2j}(r_{j1}) = \hat{\lambda}_{2j}(j_j) \quad (7)$$

Left part of the equation (7) contains the main procedures over receipt signals S_{0jm} and determines the "focusing" of the system on necessary layer into stratified mediums. The parameters of the focusing signals are determined in result of the solution of equation (8). The parameters of the subsurface layer $\lambda_{1j}(r_1)$ or electrophysical radar-tracking image could be found from eq.(7)

2. ALGORITHMS OF PROCESSING

In the case of multifrequency signal we have such equations for the signal used

$$S(t) = \mathrm{Re}\sum_{k=1}^{N} S_{ok}\exp\{j\omega_k t\}, \quad (8)$$

where ω_k are the equidistant frequencies and N is number of frequencies used. By means of use coherent filtration and transformations of multifrequency signals it is possible to fulfill the spatial-temporal focusing on a layer given and suppress sufficiently the background reflections from upper layer. So, the algorithms have to be found in this case use the procedures which approximate the optimal ones from eq. (7). After antenna phase arrays the signal can be written in such form:

$$S_\Sigma(t,r'_i) = \mathrm{Re}\sum_{k=1}^{N} I_k(r'_i)\exp\{j\omega_k t\} = \mathrm{Re}\sum_{k=1}^{N}\exp\{j\omega_k t\}\int F_{\Sigma k}(\theta)\exp\{-j\kappa_k r'\theta\}d\theta \quad (9)$$

where, $F_{\Sigma k}(\theta) = F_{1k}(\theta)\exp\{j2\kappa_k R_1(\theta)\} + F_{2k}(\theta)\exp\{-j2\kappa_k R_2(\theta)\}$. The signal, on every output of each element of antenna arrays, should be filtered on each frequency component, and as a result we receive the set of signals filtered of a kind:

$$S_k(t,r') = \mathrm{Re}\, I_k(r')\exp\{j\omega_k t\} = \mathrm{Re}\exp\{j\omega_k t\}\int_{\Theta} F_{\Sigma k}(\theta)\exp\{-j\kappa_k r'\theta\}d\theta \qquad (10)$$

It is easy to see that $I_k(r)$ is Furrier transformation of $F_{\Sigma k}(\theta)$. The signal, each on the own frequency, passes into the antenna diagram circuit, which works as a set of beams, covering given sector of the tracking. In this circuit each element of antenna phase arrays is entered the phase shift, that provides the coherent adding in each of directions calculated for beams appropriate to a maximum.

3. CONTRAST COEFFICIENT FOR MULTIFREQUENCY SIGNAL

The power of the signals on output of the subsurface imaging system are determined:
for upper layer

$$P^{(1)} \approx \int_{\theta} \sigma_1^0(\theta)\left|g(\theta-\theta_0)\right|^2 \sin^{2(N-1)}[\Delta\kappa Hb(\theta_z-\theta_{z0})]d\theta \qquad (15)$$

and for stratified mediums reconstructed layer

$$P^{(2)} \approx \int_{\theta} \sigma_2^0(\theta)\left|g(\theta-\theta_0)\right|^2 \sin^{2(N-1)}\Delta\kappa\left[Hb(\theta_z-\theta_{z0})+d(a+b\theta_z)\right]d\theta \qquad (16)$$

The quality of the reconstruction of the subsurface layer image can be represented by means of coefficient of contrast $K_N : K_N = \dfrac{P^{(2)}}{P^{(1)}} =$

$$\frac{\int_{\Theta}\left|g(\theta-\theta_0)\right|^2 \sin^{2(N-1)}\Delta\kappa\left[Hb\times(\theta_z-\theta_{z0}+d(a+b\theta_z)\right]d\theta}{\int_{\Theta}\left|g(\theta-\theta_0)\right|^2 \sin^{"(N-1)}\Delta\kappa\left[Hb(\theta_z-\theta_{z0})\right]d\theta} \qquad (17)$$

It has been found the approximation of this coefficient for rectangular function g in area $\Delta\theta$ and small angle observation $\Delta\theta$ p 1: $K_N \approx \dfrac{(2(N-1)+1)}{(\Delta\kappa Hb\Delta\theta/2)^{2N-1}}$. It is necessary to note that on a choice of the radiation frequencies we take into account the following factors:

- the increasing of frequency (decreasing of wavelength) the resolution of system increases but the attenuation into subsurface mediums increases too;
- for more long wavelengths it is possible to have better characteristics of propagation into the subsurface mediums but the resolution characteristics become worth.

Values of normalized contrast coefficient K (in dB) are presented in the Table 1 for λ_1=0.3m, $\Delta\theta$= 0.02, θ_0 = (-15^0 , 15^0), Δk =0.01 K, $X_m = Y_m$ =15m, $\pi/2\Delta K$ =7.5m

Table 1

N/H	2	3	4	5	□	7	8	9	10	11
100 m	29.5	56	83	108	134	160	185	191	235	261
1 km	9.5	16	23	28	34	40	45	51	56	61

The normalized coefficient of contrast as a function of number of frequencies used and H for λ_2=0.3m and Δk =0.001K and for the same values for other parameters (as in previous Table) have shown in Table2.

Table 2

N/H	2	3	4	5	6	7	8	9	10	11
100 m	49.5	96	143	188	234	280	325	371	415	461
1 km	29.5	56	83	108	134	160	185	211	235	281

REFERENCES

1. FALKOVICH S.E, .PONOMARYOV V.I,.SHKVARKO YU.V.: "Optimal reception of spatial-temporal signals in dissipation medium radiochannels". (Radio and Communication, Moscow 1989).(in Russian).
2. GONCHARENKO A.A., RAVCHENCO V.F,. PONOMARYOV V.I.:" Remote sensing in inhomogeneous mediums". (Radio and Communication, Moscow, 1991) (in Russian).

OPTIMIZED COMPLEX SIGNAL PROCESSING IN MULTICHANNEL SYNTHESIZED APERTURE RADAR

* Volosyuk V.K., **Kravchenko V. F., * Sokolnikov A. V.,
* Gorbunenko O. A., * Onishchuk V.A., *** Velasco Hererra V.M.,

* Kharkov Aviation Institute, kafedra 502, Chkalova str. 17, Kharkov-70, 310070 Ukraine
Tel. +38(0572)44-23-51, E-mail: cds@lincom.kharkov.ua, victor@xai.kharkov.ua
**Institute of Radio Engineering and Electronics, Russian Academy of Sciences,
Mokhovaya str. 11, Moscow, Center, GSP-3, 103907 Russia,
Tel. +7(095)9214837, Fax +7(095)9259241, E-mail: kvf@mx.rphys.mipt.ru
*** Instituto de Geografia UNAM, A.P. 20-850, 01000 Mexico D.F.
Tel. (525) 622-4340, Fax: (525) 616-2145

ABSTRACT

The problems complexing of surfaces remote sensing by SAR, increased demands for accuracy and resolution, necessity for multiparametric measurings performing turn for necessity of different frequency bands, on different polarization, from different directions etc. These signals processing must be complexed (combined). In these systems it is worth while to use additional (surplus) information under images forming in one channel, which has the presence in other signals, received in other channels. In the proposed manuscript the algorithms of combined processing in multichannel SAR construction receiving signals in the different frequency bands, on the different types of polarization, from the different directions are examined. These algorithms were synthesized by the solving of the optimization problems. They include the classic operations of the aperture synthesis and operations of the adaptive signal whitening, operations of its power meaning in filters with non-permanent and non-linear structures of smoothing windows, operations of the Earth covers parameters and statistical characteristics calculating as well.

1. INTRODUCTION

In the proposed manuscript the optimization of the received signal processing is examined, beginning from the moment of the signal registration by the antenna and ending by the parameters and statistical characteristics of the Earth covers $\vec{\lambda}(\vec{r})$ forming. The algorithm of the specific radar (scattering) cross section (RCS), $\sigma^{\circ}(\vec{r})$, forming is viewed as particular case. Parameters $\vec{\lambda}(\vec{r})$ and $\sigma^{\circ}(\vec{r})$ are considered as functions of the surface coordinates $\vec{r} = (x, y) \in D$ (or $\vec{r} = (x, R_0(y))$, R_0 is remoteness). Such functions are the surface images (maps). The moisture content, root-mean-square of the irregularities altitude, components of the microterrain energetic spectrums, velocity field of the overwater oceanic wind etc. can be the measured parameters $\vec{\lambda}(\vec{r})$. The function RCS $\sigma^{\circ}(\vec{r})$ shows the surface image in scatterometric SAR.

The problem of parameters $\vec{\lambda}(\vec{r})$ measuring is usually the problem of the secondary data processing of SAR. In our papers the entire scope of processing is suggested by the united algorithms. However, for the conclusion the particularities of the single algorithm dividing into the stages of primary ($\sigma^{\circ}(\vec{r})$ imaging) and secondary processing (information about parameters $\vec{\lambda}(\vec{r})$ getting) are looked for.

2. THE PROBLEM

The equation of observation (signal model on the antenna output) we shall write in next form :

$$\vec{u}(t) = \mathrm{Re}\,\vec{S}(t, \vec{\lambda}(\vec{r}))\exp(j\varpi_0 t) + n(t), \vec{u}(t) = \|u_k(t)\|,$$
$$\vec{S}(t, \vec{\lambda}(\vec{r})) = \|\dot{S}_k(t, \lambda(\vec{r}))\|, \vec{n}(t) = \|n_k(t)\|, k = \overline{1, K}, t \in (0, T) \quad (1)$$

where $\dot{S}_k(t,\lambda(\vec{r}))$ is the complex amplitude of the useful signal which was reflected by the surface and received by the antenna.

The correlation matrix of the received signal has the next form :

$$\underline{R_u}(t_1,t_2)=\left\langle \vec{u}(t_1)\vec{u}^T(t_2)\right\rangle \approx \frac{1}{2}\mathrm{Re}\,\rho(t_1-t_2)\int_D \underline{\sigma^o}(\vec{r},\vec{\lambda}(\vec{r}))\times \dot{S}_o(t_1,\vec{r})\dot{S}_o^*(t_2,\vec{r})d\vec{r}+\frac{N_o}{2}\delta(t_1-t_2), \qquad (2)$$

where $\underline{\sigma^o}(\vec{r},\vec{\lambda}(\vec{r}))$ is the scattering covariation matrix which main diagonal consists of specific RCS (when the signals are received on vertical, horizontal and crossed polarization types, such matrix consists of 4x4 elements).

$$\underline{\sigma^o}(\vec{r},\vec{\lambda}(\vec{r}))\cdot\rho(t_1-t_2)=\int_D\left\langle \vec{F}(\vec{r},\lambda(\vec{r}),t_1)\vec{F}^+(\vec{r},\lambda(\vec{r}),t_2)\right\rangle\times\exp(-\vec{q}_\perp\Delta\vec{r})d\Delta\vec{r},$$

$$\rho(0)=1;\ \underline{N_o}/2=diag(N_{ok}/2); \qquad (3)$$

$\vec{q}_\perp$ is the horizontal projection of the reverse scattering vector; "T","+",< > are the signs of transpolarization, Ermit connection and statistical averaging accordingly.

To begin with we shall examine the optimization problem solution by the use of maximum Likelihood method. By calculating of the variational derivative of the likelihood functional and putting it equal to zero, $\delta P[\vec{u}(t)/\vec{\lambda}(\vec{r})]/\delta\lambda_M(\vec{r})=0$, we shall get the next set of the integral equations :

$$\frac{1}{4}\int_D \underline{\dot{\Psi}_W}(\vec{r},\vec{r}_1)\underline{\sigma^o}[\vec{r}_1,\vec{\lambda}(\vec{r}_1)\dot{\Psi}_W^*(\vec{r},\vec{r}_1)d\vec{r}_1+\frac{1}{2}\int_0^T \underline{\dot{S}_W}(t,\vec{r})\underline{N_o}\,\underline{\dot{S}_W^*}(t,\vec{r})dt=\vec{\dot{Y}}_{out}^+(\vec{r})\vec{\dot{Y}}_{out}(\vec{r}). \qquad (4)$$

In this set of equations next designations are defined :

$$\vec{\dot{Y}}_{out}=\int_0^T\int_0^T \underline{W}(t_1,t_2,\lambda(\vec{r}))\vec{u}(t_2)\dot{S}_o^*(t,\vec{r})dt_1dt_2 \qquad (5)$$

is vector, which components are the optimal output effects of the multichannel SAR;

$$\underline{\dot{S}_W}(t,\vec{r})=\int_0^T \underline{W}(t,t_1,\lambda(\vec{r}))\dot{S}_o(t_1,\vec{r})dt_1 \qquad (6)$$

is the signal of support matrix;

$$\underline{\dot{\Psi}_W}(\vec{r},\vec{r}_1)=\int_0^T\int_0^T \underline{W}(t_1,t_2,\lambda(\vec{r}))\dot{S}_o(t_1,\vec{r})\dot{S}_o^*(t_2,\vec{r})dt_1dt_2 \qquad (7)$$

is the matrix ambiguity function (Woodward function) which defines SAR's resolution.

One of the basic operations, performed in such multichannel SAR with the received signals, is the operation of the output effect $\vec{\dot{Y}}_{out}(\vec{r})$ forming.

The operation of the output effect $\vec{\dot{Y}}_{out}(\vec{r})$ forming includes adaptive whitening (decorrelation) of the received signals with the weight matrix $W(t_1,t_2,\vec{\lambda}(\vec{r}))$, which depends from the measured values of $\vec{\lambda}(\vec{r})$ and signal optimal filtration with the weight function $\dot{S}_o(t,\vec{r})$. When there is no decorrelating adaptive filter

$W(t_1,t_2,\vec{\lambda}(\vec{r}))$ the output effect $\vec{Y}_{out}(\vec{r})$ forming operation are the same as the classic operation of the aperture synthesis with the focused signal processing $\vec{Y}_{out}(\vec{r}) = \int_0^T \vec{u}(t)\dot{S}_o(t,\vec{r})dt$.

The measurement errors of the parameters $\vec{\lambda}(\vec{r})$ and also of the specific RCS $\underline{\sigma}^o(\vec{r})$ of the operator track which is inverse to the Fisher operator are the next :

$$\rho = \int_D Spur\,\underline{F}^{-1}(\vec{r}_1,\vec{r}_2)\,|_{\vec{r}=\vec{r}_1=\vec{r}_2}\,d\vec{r}\,, \text{ where}$$

$$\underline{F}^{-1} = -\left\|\frac{\delta \ln P(\vec{u}(t)/\vec{\lambda}(\vec{r}))}{\delta\lambda_\mu(\vec{r}_1)\delta\lambda_\nu(\vec{r}_2)}\right\|^{-1} \approx 4\left\|\sum_{k=1}^{K}\frac{\partial\sigma_k^o(\vec{r}_1,\lambda(\vec{r}_1))}{\partial\lambda_\mu}\frac{\partial\sigma_k^o(\vec{r}_2,\lambda(\vec{r}_2))}{\partial\lambda_\nu}\left|\Psi_{Wk}(\vec{r}_1,\vec{r}_2)\right|^2\right\|^{-1} \quad (8)$$

After examination of the matrix $\underline{F}^{-1}$ we are able to find sensing conditions (frequencies, polarization types, sensing angles) when the errors of the measurements are minimal.

However, for the sound estimates forming it is needed the characteristics averaging of the output effect $\vec{Y}_{out\Sigma}(\vec{r})$ momentary power in the limits of some temporal or spatial windows. The maximum likelihood method makes possible to define their structure.

The regularized solution of the problem can be got with the use of the APM method if, for example, the correlation matrix $\underline{R}_\lambda(\vec{r}_1,\vec{r}_2) = \left\langle\vec{\lambda}(\vec{r}_1)\vec{\lambda}^T(\vec{r}_2)\right\rangle$ or $\underline{R}_{\sigma^o}(\vec{r}_1,\vec{r}_2) = \left\langle\vec{\sigma}^o(\vec{r}_1)\vec{\sigma}^{oT}(\vec{r}_2)\right\rangle$ is known. Examining the equality $\delta P[\vec{\lambda}(\vec{r})/\vec{u}(t)]/\delta\lambda_\mu(\vec{r}) = 0$ we have got, in gaussian approximation, the algorithm for the functions $\vec{\lambda}(\vec{r})$ getting (and, in particular, functions $\underline{\sigma}^o(\vec{r})$, if consider $\partial\sigma_k^o/\partial\lambda_\mu = \partial\sigma_k^o/\partial\sigma_k^o = 1$).

In this algorithm the most complicated complexing of the processes $U_k(t)$ take place which are received in different receiving channels. This was reached not only by the mutual links of the scattered fields defined by the correlation matrix $R_{uk}[t_1,t_2,\lambda(\vec{r})]$ elements and, in particular, for the taking into account of all the covariation scattering matrix $\underline{\sigma}^o[\vec{r},\vec{\lambda}(\vec{r})]$ elements, but also by the use of the a-priori statistical links between $\lambda_\mu(\vec{r})$ parameters which are defined by the elements of the correlation functions matrix $\underline{R}_\lambda(\vec{r}_1,\vec{r}_2) = \left\langle\vec{\lambda}(\vec{r}_1)\vec{\lambda}^T(\vec{r}_2)\right\rangle$.

One of the essential operations in the equations which provides the estimates sound is the smoothing of the first component which consist of the output effects $\vec{Y}_{out\Sigma}$ by the weight functions (windows) defined by the elements of correlation functions matrix $\underline{R}_\lambda(\vec{r}_1,\vec{r}_2)$.

3. CONCLUSION

The proposed methodology of the surface imaging and parameters estimating can serve as theoretical base of the new generation of measuring multichannel scatterometric SAR construction which have high resolution and measuring accuracy. Also, such methodology is applied for the statistical synthesis of the multichannel passive systems and combined active-passive systems as well.

REFERENCES

1.Volosyuk V.K., Kravchenko V.F., Ponomaryov V.I., "Optimal evaluations of electrophysical parameters for models of scattering covers in remote sensing", *Doklady Akademii Nauk (Soviet Reports of Acad. Sci. USSR)*, vol.319, No5, pp.1120-1124, 1991.

2.Volosyuk V.K., Kravchenko V.F., Falkovich S.E., "Optimization of estimates of spatially-distributed parameters for electrodynamic models of surfaces in inverse interpretation problems of active remote sensing", *Doklady Akademii nauk SSSR (Soviet Reports of Acad. Sci. USSR)*, vol.322, No 2, p.277-280, 1992.

3.S.E. Falkovich, V.I.Ponomaryov, Yu.V.Shkvarko, *Optimal reception of space-time signals in radiochannels with dissipation*, Sovetskoe radio, Moscow, 1989.

TO THE ACCURACY OF SMALL SLOPE APPROXIMATION OF KIRCHHOFF TECHNIQUE

D.V.Mikhailova,
(4 Chervonopraporna st., Institute of Radio Astronomy, National Academy of Sciences of Ukraine, Kharkiv, 310002, Ukraine)

L.V.Stulova
(12 Proskura st., Institute of Radio Physics and Electronics, National Academy of Sciences of Ukraine, Kharkiv, 310085,Ukraine)

Abstract. - **For remote sensing data interpretation, it is necessary to take influence of the surface roughness on the brightness temperature of the surface radio thermal self-radiation into account. Of practical use is to obtain analytical equations for the brightness temperature. In this work, within the scope of Kirchhoff technique (within the geometrical optics), accuracy of the analytical equations for the surface brightness temperature, which were obtained by the authors in their previous works in the small slope approximation, is investigated. These analytical equations are numerically compared to those for Kirchhoff technique for arbitrary slopes, for which shadowings are taken into account. It is shown that the analytical equations can be used for the incident angle values far from nadir ones. This fact can be of use when interpreting actual surface remote sensing data, as it can significantly simplify calculations of the brightness temperature expected.**

Introduction

When actual surfaces are studied by means of remote radiophysical methods, it is necessary to take influence of the surface roughness on the brightness temperature T^B of surface radio thermal self-radiation (RTSR) into account. Of practical use is to obtain analytical equations for T^B.. In [1 - 3], within a small-slope approximation of Kirchoff technique (within the geometrical optics), equations are obtained for T^B both of the surface self-radiation and of the atmosphere RTSR rescattered by the surface, for two polarizations.
Here, the validity range of the analytical equations obtained in [1 -2] is studied by numerical comparison with the similar ones for arbitrary values of roughness slopes obtained in [1, 4], shadowings being taken into account. The results of numerical studies are given for two quite different dielectric constant values (corresponding to dry ground surface and to the sea surface) and for two roughness slope variance values.

Problem formulation

Assume a random rough surface described by equation $z = \varsigma(\vec{r})$ (here $\vec{r} = \{x, y\}$ is a radius-vector within the plane of z=0) to be a boundary for two homogeneous media: the upper one, in the area of $z > \varsigma(\vec{r})$, corresponds to an atmosphere, and the lower one, in the area of $z < \varsigma(\vec{r})$, does to a commonly observed medium under the Earth surface, which has a dielectric constant of $\varepsilon=\varepsilon'+i\varepsilon''$, the surface being plane in average ($<\varsigma>=0$) and having statistically homogeneous irregularities. The vector of irregularity slope is $\vec{\gamma} \equiv \nabla_{\vec{r}}\varsigma = \left\{\frac{\partial\varsigma}{\partial x}, \frac{\partial\varsigma}{\partial y}\right\} \equiv \{\gamma_x, \gamma_y\}$, and it has a probability density distribution function $w(\vec{\gamma})$. For the surface RTSR, its brightness temperature T^B is related with the surface thermodynamical one T through its emissivity function $\kappa_{\text{II},\perp}(\theta_0)$ for vertical and/or horizontal polarization, which depends on an observation angle θ_0 and the dielectric constant ε [1 - 4]:

$$T^B_{\text{II},\perp} = \langle\kappa_{\text{II},\perp}\rangle T .$$

In Kirchhoff approximation, the equation for $<\kappa_{\text{II},\perp}>$ is [1 -3]

$$(1)\ \langle\kappa_{\text{II},\perp}\rangle = 1 - \langle F_{\text{II},\perp}(\theta_0, \vec{\gamma})\rangle ,$$

with $F_{\text{II},\perp}(\theta_0,\vec{\gamma})$ being determined in[1], R_{II}, $R_\perp$ being Fresnel coefficients of the plane wave reflection by a plane surface, and θ being a 'local' observation angle (see [1] for details)

Small slope approximation

Let the surface irregularities have sufficiently small slopes: $|\vec{\gamma}| << 1$. Expanding (1) in terms of small parameters γ_x, γ_y, we can yield (omitting the II,⊥ indices wherever it would not cause misunderstanding) [1, 2]:

(2) $$\langle\kappa\rangle = \kappa_0 + \langle\gamma_x^2\rangle A_{xx} + \langle\gamma_y^2\rangle A_{yy},$$

with κ_0 being a plane surface emissivity function in the direction making an angle of θ_0 with z axis; the expressions for the former, as well as for A_{xx}, A_{yy} are given in [1].

Kirchhoff approximation, shadowings being taken into account

Now assume the Σ surface slopes γ_x, γ_y not to be small, so one has to take the ray shadowings into account. In [1, 4] it is shown that, in this case, in Kirchhoff approximation formula (1) may take a form

(3) $$\langle\kappa_{\text{II},\perp}\rangle = 1 - \iint_\Omega \frac{F_{\text{II},\perp}(\theta_0,\vec{\gamma})w(\vec{\gamma})}{1+\Lambda(\pi,\theta_0)}\mathrm{d}\gamma_x\gamma_y,$$

with Λ being a shadowing function (see [1] for its determination) and the integration area Ω being determined by

$$\Omega:\ (\gamma_x - \tan\theta_0)^2 + \gamma_y^2 \le 1/\cos^2\theta_0$$

(Here, we take only the incident ray shadowings into account but assume the rays having a negative z component of the wave vector to be entirely absorbed by the surface, i.e. we take the 'intermediate' model of account of shadowings from[1].)

Numerical results and discussion

To study the validity range of the small-slope approximation of the Kirchhoff technique, a numerical comparison was made between the values of correction terms to T^B of the plane surface self-radiation that are caused by the surface roughness with small roughness slopes, and the similar correction terms caused by the surface roughness obtained from (3), shadows being taken into account. Correction terms $\Delta\kappa = \langle\kappa\rangle - \kappa_0$ to the emissivity were normalized to slope variance $\langle\gamma^2\rangle$ of an isotropic rough surface:

(4) $$\alpha_s = \Delta\kappa \Big/ \langle\gamma^2\rangle.$$

Figs.1, 2 show plots of the correction factors α_s versus θ_0, which were calculated using (2-6) for κ, with $\varepsilon=60+30.5i$ (Fig.1) and $\varepsilon=2+0.00i$ (Fig.2 - 4). In those Figs., similar plots for which α_s was calculated according to (3), with shadowing being taken into account, are also displayed. We assumed the surface corrugated ($\gamma_y = \frac{\partial\zeta}{\partial y} = 0$ for Fig.1-2, $\gamma_x = \frac{\partial\zeta}{\partial x} = 0$ for Fig.3, and $\vec{\gamma} \equiv \vec{\gamma}_{45^\circ} = \frac{\partial\zeta}{\partial\vec{r}_{45^\circ}}$, with $\vec{r}_{45^\circ} = \{1;1\}$ for Fig.4). In the case of shadowings being taken into account, the slopes were assumed sufficiently small: $\langle\gamma^2\rangle=0.01$ and $\langle\gamma^2\rangle=0.1$, and the slope distribution function to be Gaussian: $w(\vec{\gamma}) = \exp\left(-\gamma^2/2\langle\gamma^2\rangle\right)$. From the Figs., we notice that, with $\langle\gamma^2\rangle=0.01$, the values of the correction factors for the both equations appear to match well (to within 5%) for $\theta_0 \le 60^\circ$, i.e. when the slopes are small, the formula (2) is valid even if an observation angle value is far from nadir one. However, if the irregularity slopes increase (with $\langle\gamma^2\rangle=0.1$), formula (2) is, in general, valid poorly for horizontal polarization, and they can considered to be valid to an extent for the observation angle value less than 40°, for vertical polarization.

So, for remote sensing data interpretation, when using Kirchhoff approximation with Gaussian slope distribution function, for sufficiently small roughness slopes having variance of order of 0.01, one can use the analytical expression (2) , instead of (3), for the observation angles rather far from nadir one (to within 60°), which may essentially simplify the interpretation procedure.

Acknowledgment

The authors would like to thank Prof. I.Fuks for valuable advice.

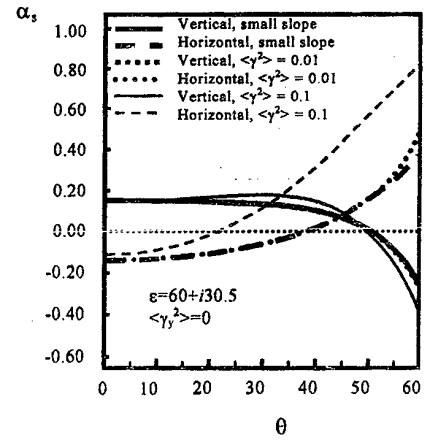


Fig. 1

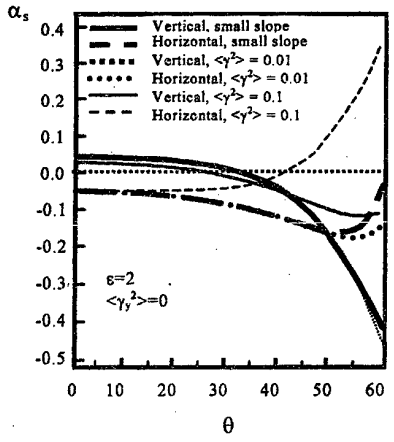


Fig.2

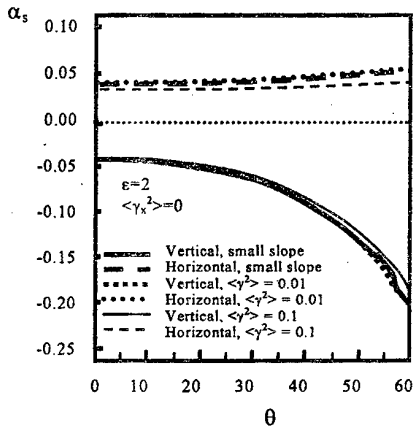


Fig. 3

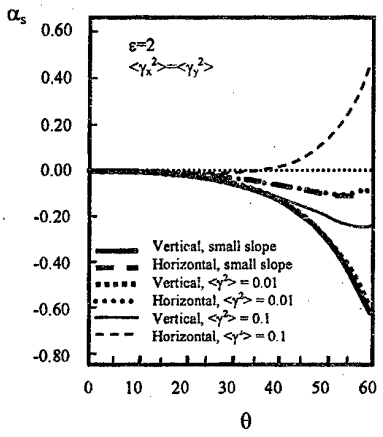


Fig. 4

References

1. Mikhailova D.V., Fuks I.M. The Emissivity of the Statistically Irregular Surface Taking Multiple Scattering into Account. Radiotekhnika i Elektronika, vol.38, No 6, Moscow, pp. 1016 -1025, 1993.
2. D.V.Mikhailova, I.M.Fuks. The thermal radio emissiom and scattering by a rough surface, Proceedings of the Progress in Electromagnetic Research Simposium (PIERS'97), July 7-11, 1997, Cambridge, Massachussets, USA, p.109
3. Bubukin I.T., Dokuchaev V.P., Krotikov V.D. Investigation of Rough Surface Brightness Temperature in Kirchhoff Approximation. Radiotekhnika i elektronika, vol.25, No 6, pp. 652-656, 1982.
4. Pavelyev A.G. Thermal Radiation of the Bodies Statistically Limited by Rough Surfaces. Radiotekhnika i elektronika, vol.12, No 7,pp.1178-1184, 1967.

MILLIMETER WAVE NULL-MODEM RADIO COMMUNICATION

N.M.Zaitsev, V.E.Lioubtchenko
Institute of Radioengineering & Electronics
Russian Academy of Sciencies
Bildg.1, Acad.Vvedenskii Sq., Fryazino, Moscow Reg., 141120, Russia
Tel.: 8 (095) 526-9217

There are several methods for computer network accomplishment: directly via COM or LPT ports, so called null-modem connection, via modems, by network adapters.

Millimeter wave radio channel (MMW-channel) embedded into any connection provides wireless communication indoors, between floors and buildings through the windows, communication between mobile objects. In conditions of line-of-sight absence the periscope antenna systems are used [1].

However, MMW channel is not universal for all computer connections. It is caused by the difference in typical technologies listed below.

1. Direct connection, COM ports.

RS-232 interface, NRZ code digital signals are on line. Input level is 15V; output level is 5V; load is 3 KOhm; DB-9, DB-25 connectors.

2. Modem technology, telephone network used

Analog signals with FSK, DPSK and QAM modulation are on line. Bandwidth is 300-3400 Hz. Input level is 0 ÷ -15 dBm, output level is 0 ÷ -43 dBm. Load is 600 Ohm, RJ11 connector. (See the example of MMB channel in [2]).

3. Network technology, 10BASE-T type.

IEEE 802.3 interface, ETHERNET topology. Data packets with Manchester code are on line. Band pass is 5-15 MHz, input level is 3V. Line unit segment loss are less than 11,5 dB, load is 100 Ohm, RJ 45 connector. (See the example of MMB channel in [3]).

Concerning the design (two twisted wire pairs and two connectors) and software (LINK protocol for IBM PC) null-modem connection via COM port appears to be the most simple and aviable one. It is compartable with duplex radio channel, has high signal level at transmitting side needed to be decreased up to TTL level, provides transmitting rate up to 115 Kbps achievable not for any modem. Using of LPT port allows to increase the transmitting rate up to 2 Mbps but it is comlicated to mate with radio channel. The problem of current constant component for NRZ code is also ought to be solved in one of two ways – applying the modulation transforming (modem technology) or applying the Manchester coding (network technology).

The mobile null-modem connection via MMW channel was realized in this work (Fig.1). Two 15 ИЭ-00-013 displays were primarily linked by wires via consequent ports and were able to operate in accordance with RS-232 protocol at data rate from 75 till 9600 bps in semiduplex and duplex regimes. The single line or complete frame was transmitted without reverse response and error correction in contrast to LINK protocol that allowed to follow the signal easily in any point of the channel.

60 GHz transmitter included the horn antenna, Gunn diode oscillator, *p-i-n* –modulator and submodulator interfaced with display. Triply printed rectenna with Schottky diodes (3A147C –type) [4] built in the portable radio set "Радиус" (27 MHz) was used as receiver. Rectenna was connected with low frequency amplifier (LFA) operated within 300-3400 Hz. The sequence of positive and negative pulses resulted from differentiation of NRZ code in transformator connection of rectenna with LFA appeared in LFA output at data rate from 300 till 2400 bps. Data regeneration was similar to data reading in floppy drivers. The regenerator was designed to amplify positive and negative pulses, normalize, summarize them and restore the form of initial signal.

The second portable radio set was installed on transmitting side and allowed the users to communicate not only on MMW but also on SW (27 MHz). SW-band was necessary for MMW antennas aligning [5]. Test frame was successfully transmitted between MMW antennas separated at the distance of 6m without errors.

Null-modem communication of two IBM PC was performed by the direct pulse transmission via duplex MMW channel. Such communication at short distances (~10m) is successfully operable and alternative to the known complicated systems [2,3].

So we may conclude that MMW radio communication opens new opportunities for local computer network accomplishment. All multi-accessed computer radio sets are subjected to cross interference. Applying wideband noise-type signals and special data transmission procedures allow to avoid this interference. MMW

simplifies this problem due to directional antennas and significant MMW attenuation in air, especially within the range 58-62 GHz, so the combined multi-access communication at the common frequency becomes possible.

As soon as "radio networks are still in a formative and fragmentary stage of research" [6] so the millimeter wave development appears to be one of significant directions.

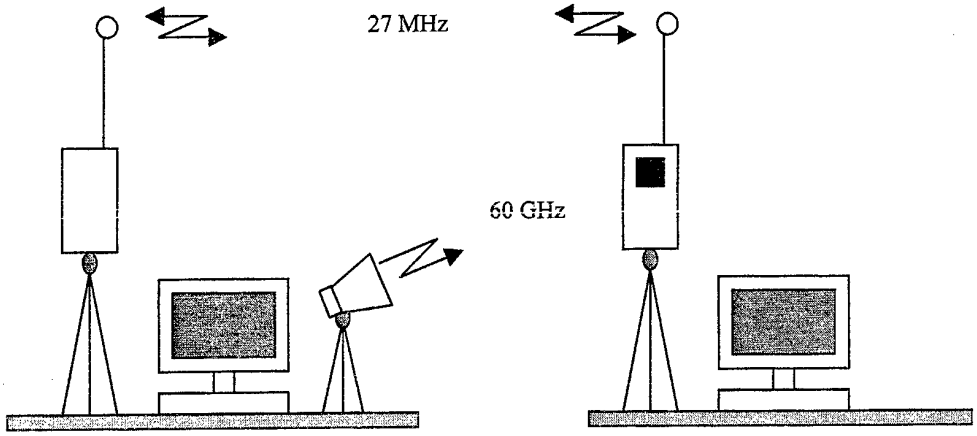


Figure 1.

References

1. Н.Н.Каменский и др., "Инженерно-технический справочник по электросвязи. Радиорелейные линии", Связь, М., с.112, 1970.
2. H.Meinel, "The Market for Short-haul Line-of-sight Millimeterwave Transmission Links", IEEE MTT-S Digest, pp.487-489, 1996.
3. T,Ninomiya et al., "60-GHz Transeiver for High-speed Wireless LAN System", IEEE MTT-S Digest, pp.1171-1174, 1996/
4. Н.М.Зайцев, В.Е.Любченко, Е.О.Юневич, "Антенно-связанные диоды Шоттки в приемных устройствах миллиметрового диапазона", Радиотехника и электроника, Т.43, №5, с.568-570, 1998.
5. V.E.Lioubtchenko, "Proc.XI Int.Microwave Conf.", Warsaw, Vol.3, p.73, 1996.
6. D.Bertsekas, R.Gallager, "Data Networks", 2nd Ed, Prentice-Hall, Englewood Cliffs, N.J., p.352, 1994.

ON ENERGY POTENTIAL OF MILLIMETER-WAVE RADAR

B. A. Rozanov, G. V. Cheslavsky
N.E.Bauman Moscow State Technical University
5, 2nd Baumanskaya street, Moscow, 105007 RUSSIA
Tel.: (007)(095) 263-65-98, Fax.: (007)(095) 267-75-96,
E-mail: rozanov@rl-1.bmstu.ru, gleb@mx.bmstu.ru

One of the most serious problems of a short-pulse millimeter (MM) wave radar is deficit of its energy potential. The radar range upper limit about a few kilometers is caused mostly by two factors: (1) low energy of transmitting signal pulses restricted by generator overheating or breakdown of waveguiding structures and (2) decreasing of signal energy received because of small aperture of antenna necessary to keep [1,2] high survey rate.

It is possible to keep high survey rate and energy potential of the radar when decreasing wavelength l if both the transmitting antenna gain and the receiving antenna area are fixed. This may be done if a multi-beam receiving antenna fills the transmitting antenna beam so that the radar angular resolution is determined by received beamwidths. The idea may be realized by different ways. The direct one is using a matrix receiver placed at the focal plane of a mirror or a lens receiving antenna. State of art of MMIC technology allows to build compact multi-element matrix receivers for frequencies up to 100 GHz [3]. The other way is using phase-array antennas where the multi-beam operation mode may be created by beam-forming circuit [1,2]. Splitting the transmitter energy to a set of beams can also be performed by frequency-switching antennae.

Energy of a pulse signal transmitted by the radar may be enhanced by extending the pulse duration. using quasi-continuous signals instead of short pulses allows to increase energy potential of a MM-wave radar by 15÷20 dB [4]. An advantage of the quasi-continuous signals is possibility to estimate the Doppler frequency of the reflected and received signal with high frequency resolution. Difficulties connected with employing the quasi-continuous signals are rather complicated isolation between the transmitter and receiver(s) and problem of ranging targets. Ranging of targets may be done in the case by phase modulation of the signal transmitted although in results in increase of number of the Doppler channels.

Some block-schemes of millimeter-wave radars using simple quasi-continuous signals were considered in [1,2,5] where a principle of measuring distances to targets by pulses of duration $\dot{O} = 2R_{max}/c$ and period/pulse ratio $Q=2$ was proposed as well. Here R_{max} is the measuring target distance for the radar and c is the ligth speed. To ensure good isolation of the receiver when transmission the sounding pulse the receiver is switched off for time T. Distance R to the target may be determined as $R=\tau/2c$ if the received pulse duration τ is measured (see Fig. 1). Analysis of possible increase of a MM-wave radar range when using this type of long sounding pulses is main subject of the paper.

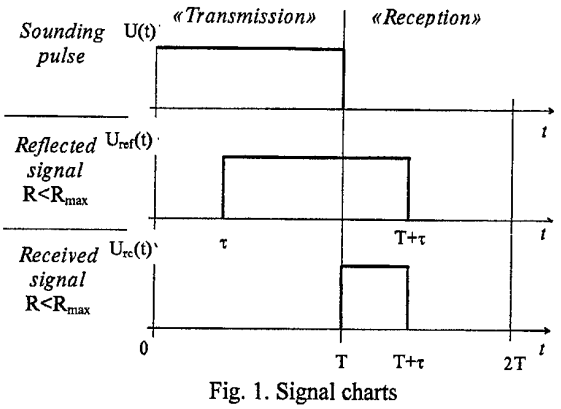


Fig. 1. Signal charts

A mathematical model was developed for computer simulations of quasi-continuous 3-mm band radar operating in maximum-duration pulse mode and capable to detect and resolve targets as well as estimate other their parameters. The algorithm allows to study some features of the radar operation and compare various methods of signal processing as well. Taking into account that duration, amplitude and Doppler frequency of the signal received within *(T, 2T)* time interval are not defined *a priori*, the optimal signal processing scheme at the first step should be multi-channel one covering proposed intervals of the unknown parameters.

The simulations of the long-pulse radar performance were done using a multi-channel filter model based on the fast Fourier transform (FFT). The radar detection profiles $D=f(R/R_{max})$ calculated for a single radar pulse at wavelength λ=3 mm for proposed maximum distance R_{max}=15 km (the value corresponds to pulse duration T=100 mS) are presented in Fig. 2. Every curve of Fig. 2 is the averaged one after over 1000 simulations. All the profiles were obtained for false alarm level $F = 10^{-4}$. Values of signal-to-noise ratio a for a target at maximum

distance R_{max} are specified for every curve. It is proposed that the ratio change with distance R according to the main ranging equation. Comparison of the calculated detection profiles with similar profiles of the ideal prototype of the pulse radar (see Fig.2) showed that *a priori* energy gain of 15 dB over a short-pulse radar was diminished to 12÷14 dB because of loss when signal processing.

It is possible to increase the detection probability by repeating the radar pulses sending to the same direction. The radar detection profiles for various number of received pulses are given in Fig. 3 for the case of non-coherent signal integration.

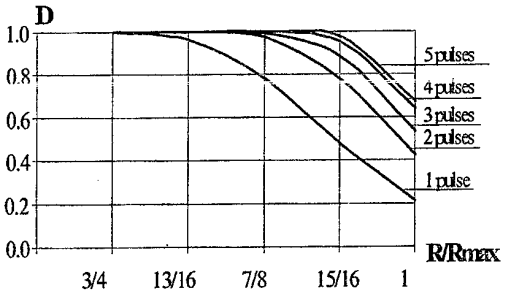


Fig. 3. Detection profiles at range R on 1 to 5 probing pulses for a quasi-continuous radar implementing the algorithm of non-coherent detection

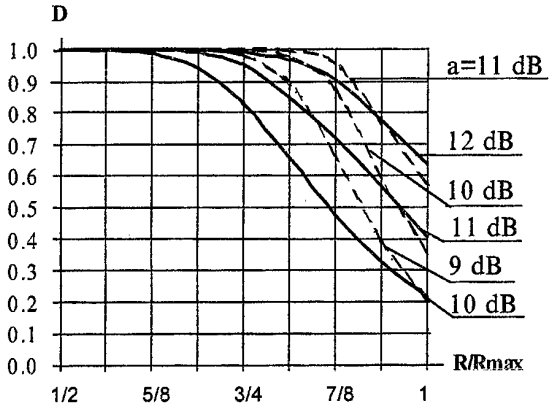


Fig. 2. Detection profiles at range R for radars: for quasi continuous radar implementing an FFT algorithm (---------), and for impulse radar ( )

Results of the analysis using the FFT algorithm allow to signal amplitude (by amplitude of the central component of the signal spectrum), the target velocity (by position of response from the target at the Doppler frequency axis, the position is determined by means of weighted signal processing), and distance to the target

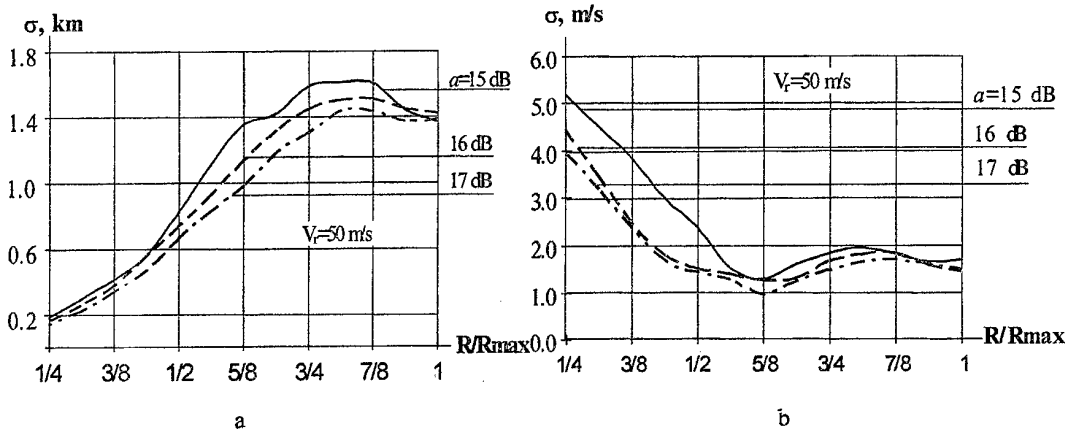


Fig. 4. Averaged estimates for: a) range; b) speed of a single target on one probing step using an FFT algorithm in function R/R_{max}

(indirectly, by width of the signal frequency band). A single sounding pulse can give preliminary estimates of the target parameters (Fig. 4) and accuracy of the estimates may be improved after next pulses. The set of estimates permits to decrease *a priori* uncertainty of the target Doppler frequency and to reduce number of the Doppler channels necessary for the phase-modulated signal.

Provided the transmitter power of 1 W is available, the transmitting antenna diameter is of 0.6 m, the receiver noise temperature is of 2000 K, the false alarm level is of 10^{-4}, probability of true target detection is of 0.65, and the atmosphere losses are of 0.3 dB/km it is possible to detect a target having effective echoing area more that 20 m^2 at maximum distance of 15 km.

References

1. Розанов Б. А. Радиолокационные станции миллиметрового диапазона волн с высоким разрешением: возможности и ограничения. "Электромагнитные волны и электронные системы", выпуск 2, №1, 1997г.
2. Розанов Б. А. Радиолокационные станции коротковолновой части миллиметрового диапазона волн с квазинепрерывными сигналами. "Вестник МГТУ" № 4, 1996г.
3. Kane B., Weinreb S., Fischer E., Byer N. High-Sensitivity W-Band MMIC Radiometer Modules. Microwave and Millimeter-Wave Monolithic Circuits Symposium, 1995. -59 p.
4. Bhartia P., Bahl I. J. Millimeter wave engineering and applications. New York: John Wiley and Sons, 1984. -714 p.
5. Розанов Б. А., Чеславский Г. В. Обработка сигналов в радиолокационной станции с квазинепрерывным излучением. "Вестник МГТУ" № 4, 1997г.

OPTIMUM SYNTHESIS OF TRANSMITTING-RECEIVING SECTIONS OF AN UNDERGROUND RADAR*

Orlenko A.A., Kholod P.V.
Usykov Institute for Radiophysics and Electronics of the National Academy of Sciences of Ukraine
12 Ak.Proskura St., Kharkiv, Ukraine
tel.: 44-84-70, 44-86-34, e-mail: orlenko@ire.kharkov.ua, kholod@ire.kharkov.ua

When sensing layered earthly covers, one of possible ways of achievement of a high penetration into the ground is the application of ultra broadband outgoing pulses [1,2,3]. Nowadays plenty of the publications is devoted to problems of the transient radiolocation, in which the various aspects of this problem are mentioned. The generalizing works belong to H. Harmuth [1,2]. At the same time there is a problem of optimum synthesis of transmitting-receiving sections of underground radars with an extended dynamic range. One of ways of this problem solution is the use as the receiver the device realizing a principle of accumulation of the radar-tracking responses.

After the basic opportunity of division (detecting) not synchronized signals [2] was proved, there was an interest to the realization of this idea in practice. The device for the selection of a periodic signal (with a period T) from noise or from signals with other period can be realized by the storage. The basic storage units (Fig.1) are the delay line, the hybrid device implementing functions of the summer, the amplifier and the coupler.

Let's assume, that the periodic signal with the amplitude A acts on the input of the selective device with a

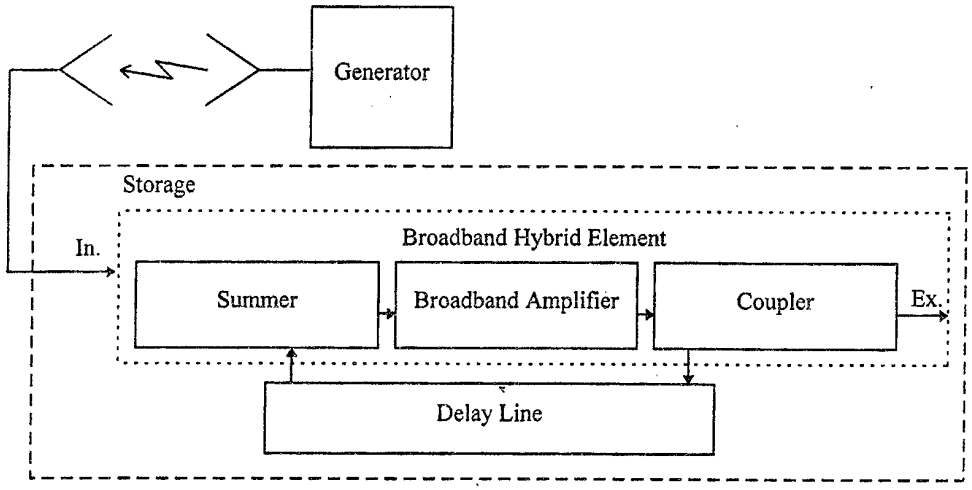


Fig.1. The block diagram of a transmitting-receiving section of an underground radar

delay line without any attenuation. Then if the repetition period of the signal T is equal to the delay time of the storage, the signal of some detained period will be summarized with the signal of the next period. Signals with a period distinct from T would have the least amplitude when composition. This summation of the useful signal results in the filtration effect.

If some attenuation takes place in the circuit, so as a result of one run of the signal on the delay line its amplitude A becomes equal to qA, where $q<1$, after n runs of the initial signal, the amplitude of the stored signal will be

$$A\left(1+q+q^2+\ldots+q^n\right)=A\left(1-q^n\right)/\left(1-q\right).$$

* This work is in part supported by the STCU fund. Project #366.

If one assumes, that the quantity of the stored pulses is great, one can neglect by the value q^n and the amplitude of the stored signal will equals to $A/(1-q)$. Thus, with $q=0.9$ the total amplitude will be $10A$, and with $q=0.99$ it will equals to $100A$. As it is possible to see, in the second case the selectivity is much higher, than in the first one, however a practical design in this case will require a high stability of parameters of elements of a transmitting-receiving system. Thus, if the value q will become equal or more than 1, the system would transmute into the generator. Achievement of high stability of elements of a system working in a ultra wide frequency range is the difficulty soluble technical problem suffices. Consequently, when constructing similar systems it is necessary to determine the characteristics of outgoing pulses.

The research of systems realizing the principle of accumulation of a useful signal was executed by the employees of Institute for Civil Aircraft in Riga [4,5,6].

Using the number of the theoretical calculations made by Finkelstain [3,7,8], let's analyze the requirements to the parameters of outgoing pulses providing a stable operating of the receiver and determine the basic ways of maximum ratio signal/noise achievement.

By the example of the estimation of a time position of the signal, we shall consider the influence of the start moment fluctuation of the generator on the characteristics of the videopulses receiver with accumulation. Suppose the intervals between the moments of occurrence of the adjacent pulses form a sequence of independent random values having some distribution within the interval 2τ about some average pulses repetition period $\overline{T}$. The spectrum of a such signal has the form of a comb near the frequencies $\omega = 2\pi k/T$, where $k = 1,2,3,...$ With $\omega\tau << 1$ the width of the tooths of the comb will be equal to $\Delta\omega_к = 4\pi k\tau/\sqrt{3}T^2$ [3].

To express τ in terms of the root-mean-square deviation of the videopulses repetition frequency $\sqrt{\overline{\Delta\omega_П^2}}$, we shall find the variance of the period

$$\overline{\Delta T_П^2} = \int_{-\infty}^{\infty}(t-T)^2 \tfrac{1}{2\tau}dt = \tfrac{1}{3}\tau^2.$$

Then, using the approximate equation [7]

$$\left|\frac{\sqrt{\overline{\Delta T_П^2}}}{T}\right| \approx \left|\frac{\sqrt{\overline{\Delta\omega_П^2}}}{\omega_0}\right|,$$

where $\omega_0 = 2\pi/T = \overline{\omega_П}$, we have

$$\Delta\omega_k = 2k\omega_0\frac{\sqrt{\overline{\Delta\omega_П^2}}}{\omega_0}.$$

Thus, the width of the spectral lines is directly proportional to the relative instability of the repetition frequency and the number of a harmonic. For the elementary storages, because of the instability most essentially influences higher harmonics, line broadening of the signal spectra around of the n-spectrum is expressed as

$$\Delta\omega_n = 2n\omega_0\frac{\sqrt{\overline{\Delta\omega_П^2}}}{\omega_0},$$

where $n = \omega_{\max}/\omega_0$.

Proceeding from above, it is possible to determine the optimum quantity of the pulses stored. By taking advantage obtained in [8] expression for optimum width of tooths $\Delta\omega_{0.7onm} = 0.4\omega_0/N$, where N is the quantity of the stored pulses, it is possible to find,

$$N = \frac{0.2}{n\dfrac{\sqrt{\overline{\Delta\omega_П^2}}}{\omega_0}} = \frac{0.2\sqrt{3}}{n\tau}T.$$

The calculated dependences of N as the function of τ are given on Fig. 2. On the basis of the obtained plots, it is possible to prove a choice of the values of the instability, the pulses repetition period, upper frequency of a spectrum of an outgoing signal and a quantity of the stored pulses. So, for an outgoing signal of a radar with the upper boundary frequency 1 GHz, with the pulse repetition frequency 1 MHz, and the quantity of the stored

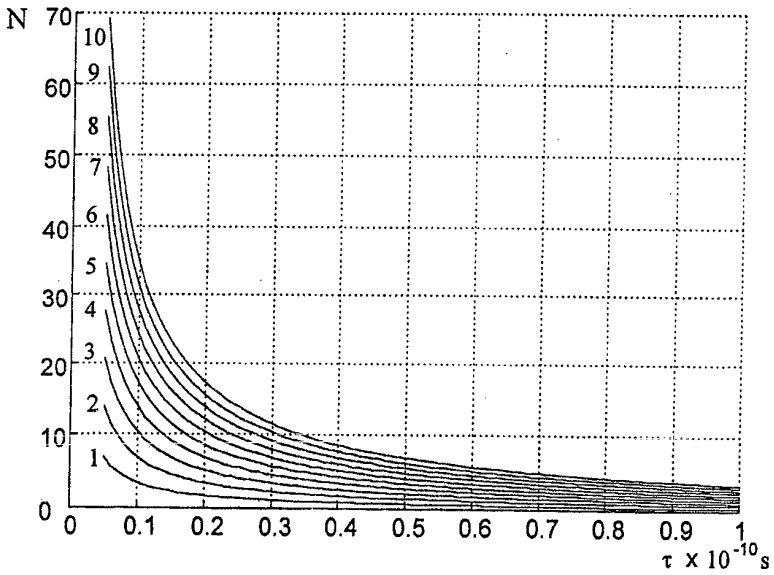


Fig 2. Dependence of the quantities of the stored pulses N as the function of the instability parameter τ with various values of the pulse repetition frequency ($\times 10^5$)

pulses $N = 10$, the instability of the pulses repetition period should not exceed the value $\tau = 35$ ps. For the accumulation of 35 pulses, the instability with $\tau \le 10$ ps are admitted.

The disadvantage of existing analog storages of a videopulse signal is their small efficiency (small quantity of stored pulses in comparison with a potentially possible one) due to:

1. limited width of a bandwidth of a feedback circuit (the necessary value of a bandwidth grows with an increase of an amount of stored pulses [8]);
2. non-linearity of the amplitude characteristic of a selective device (even the small non-linearity of the amplitude characteristic results in rather essential decrease of the efficiency of the device);
3. presence of parasitic reflections in a delay line.

The presence of a parasitic pulse reaction in the delay line caused by reactance of the line, and also instability of the pulses generator result in accumulation of a parasitic signal. Its level depends on value of instability of start of the video pulses source and can runs into large values, especially with a plenty of the stored pulses N and a high feedback factor β. It leads to reducing the dynamic range of the storage. Besides the instability of the start of the pulses generator restricts the value of the feedback factor of the storage, which, on the one hand, should get out optimum from the point of view of a reception of a necessary advantage in a signal/noise ratio with the certain amount of the stored pulses, and with another hand — to provide steady work of the storage.

Thus, to increase of the quantity of optimum stored pulses it is expedient to use of the multistage storages, that is equivalent to an application of one storage with the large feedback factor [1].

References

1. H F.Harmuth, Nonsinusoidal waves for radar and radio communication, Radio i svyaz', Moscow, p. 375, 1985.
2. H.F.Harmuth, «Sequency theory foundations and applications», Mir, Moscow, p. 574, 1980.
3. M.I.Finkelshtain, «Comb filters», Sov. Radio, Moscow, pp. 123, 1969.
4. Yu.S.Lezin, «Optimum filters and storages of pulse signals», Sov. Radio, Moscow, pp.319, 1969.
5. V.I.Karpukhin, «The analogous-discrete storage of pulse signals», In: Trudy RKINGA, Riga, pp. 19-25, 1976.
6. A.A.Guschin, V.A.Larner, I.I.Zil'berman, «Analysis of ways of construction of storages with charging connection», In: Trudy RKINGA, Riga, pp. 46-51, 1982.
7. M.I.Finkelshtain, «Spectral decomposition of a pack of pulses», Radiotekhnika, Vol. 17, No 4, pp.18-23, 1961.
8. M.I.Finkelshtain, A.V.Zelenkov, «About an allowable frequency bands of a feedback circuit in the spectrum analyzer of a recirculator type», Izvestiya vuzov, Radioelektronika, Vol. 11, No 2, pp.141-148, 1968.

THE PROBLEMS OF THE POSSIBLE NON-LINEAR RADIOLOCATION OF THE OBJECTS OF LOW PERCEPTION

S. A.Gayvoronskaja, V. I.Sergeev
Voronezh Construction Bureau of Antenna Design
Russia, 394000, Voronezh, P. O. Box 175, VCB AD
tel/fax (073-2) 33-29-92, e-mail: sergeev@vcb-ad.vrn.ru

The problems of radiolocation and particularly of the objects of low perception radiolocation have become urgent in the light of the employment of new materials in projection of flying apparatus which diminish naturally the effective area of dissipation of the object. Besides, the development of the small aviation limits essentially the possibility of the effective flight control through low effective area of dissipation of the flying apparatus and low efficiency of the radiolocational detection means when operated in the millimetrical range.

The purpose of this work is to determine the possibility og using the effect of the parametrical absorption of the electromagnetic wave energy by the material object with monostatic radiolocation in the millimetrical range.

The parametrical absorption effect implies that [1] while exposing an object to electromagnetic pulse burst with definite parameters (given pulse quantity pulse repetition period, pulse duration, oscillation frequency and irradiation power) the resulting oscillation will obtain sufficient power to concentrate on the superhigh harmonic while resolving into harmonical series the energy necessary to stimulate the monatomic structure of an object in the point of the resonant addition of the pulse burst. It is also necessary to take into account the resonant irradiation pulse addition on an object surface (when calculating on refracted near-surface wave). In the process, the energy shortage would appear at the expense of the permitted electron transitions (in case the quantity of the energy is not sufficient. The shortage will be reduced by the irradiation field energy. The energy redistribution on the front of the electromagnetic wave will increase the effective scatter area of an object.

To solve the problem which is being discussed in the presented work it is necessary to consider two variants of determining the received signal power: so-called, «direct» and «reflected».

In case of the «direct» variant (Fig.1) the radar beam is scattered by the troposphere. The power of the received signal scattered by the troposphere in the radiator direction is fixed on the receiving antenna.

In case of the «reflected» variant (Fig.2) it is thought that the power on the receiving antenna is the same as in the point A removed from the radiator at 2R distance (R is the distance from radiator till the troposphere scattering electromagnetic wave), when the power attenuation coefficient of the signal scattered by the troposphere in the radiator direction is known.

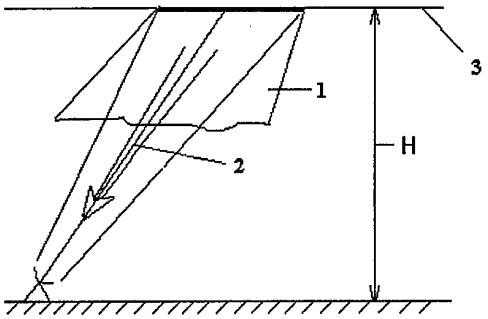


Fig. 1. Scheme of the monostatic radiolocation ("direct" method)
1 - a dispersion from the troposphere toward the radiator;
2 - an inverse signal received by the receiving antenna;
3 - a dispersing layer (in this instance - the troposphere), for which the weaking factor is known;
H - a height of the electromagnetic wave dispersion.
χ - is the angle of deviation from the normal.

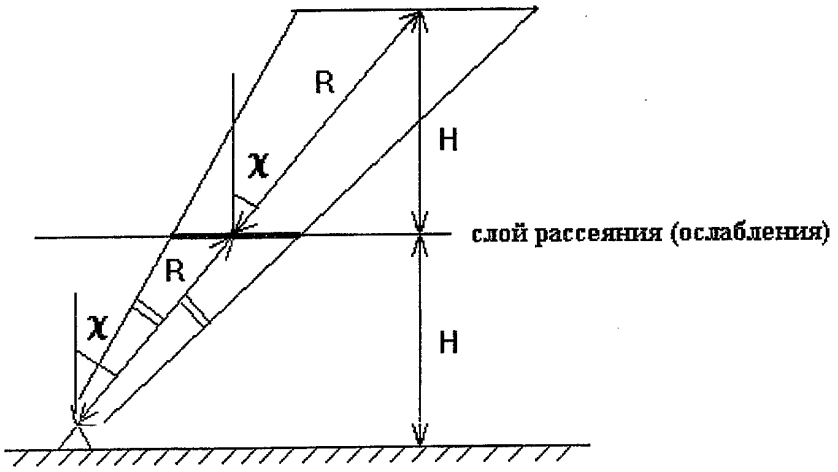


Fig.2. Scheme of the monostatic radiolocation ("reflected" method).
R is the distance from radiator till layer of the electromagnetic wave dispersion/

In the expression for determining the received signal power the shadow energy (that is the energy absorbed or scattered by an object itself but not by the troposphere) is taken into account. There are two cases:

1. $E_м \le E_з$. Then the absorption energy is included in the shadow energy -$E_з$.
2. $E_м > E_з$. Then the shadow energy is included in the absorption energy.

The received signal power for the «direct» variant is determined by the expressions:

I. $E_м \le E_з$

$$P_{прм} = \frac{E_{изл}\left(4\pi R_1^2 - D\,\sigma_{эпр}\right)}{\pi^3 \tau_v}\left(\frac{D\,\lambda}{16RR_1}\right)^2 F^2 \cos\chi \quad , \tag{1}$$

where $E_{изл}$ is the radiator energy; τ_v is the single pulse duration; R_1 is the distance from radiator till object; D is the directive antenna gain; F^2 is the coefficient of scattering in the radiator direction which has the physical sense of the attenuation coefficient; $\sigma_{эпр}$ is the effective scatter area of an irradiated object, that is the irradiated surface area.

II. $E_м > E_з$

$$P_{прм} = \frac{E_{изл} - E_м}{(8\pi)^2 R^2 \tau_v}\left(\frac{D\,\lambda}{8\pi R}\right)^2 F^2 \cos\chi \tag{2}$$

where $E_м$ is the absorption energy which is caused by the parametrical absorption effect.

For the reflected variant the following expressions are used:

I. $E_м \le E_з$

$$P_{прм} = \frac{E_{изл}\left(4\pi R_1^2 - D\,\sigma_{эпр}\right)}{\pi^3 \tau_v}\left(\frac{D\,\lambda}{16RR_1}\right)^2 F^2 \cos\chi \tag{3}$$

II. $E_м > E_з$

$$P_{прм} = \frac{E_{изл} - E_м}{\tau_v}\left(\frac{D\,\lambda}{8\pi R}\right)^2 F^2 \cos\chi \tag{4}$$

To realize the opportunities of using radiolocation expressions (1)-(4) considering the parametrical absorption effect it is important that the irradiation power sufficient for parametrical absorption effect is in line with the energy determined as following:

$$P_0 = \frac{E_0 F \sigma_{эпр} h \rho N_A N_{эл} \sqrt{\varepsilon \mu^3}}{M_{AT} k_н S_k S_{k=1}} \times$$

$$\times \sum_{m=1}^{i} exp\left[\frac{4\pi L_0 (1-m)}{\lambda_{np}} \sqrt{\frac{1}{2}\left(-1+\sqrt{tg^2\delta+1}\right)}\right] Q_A^{-m} \times \begin{vmatrix} 1, m = [1, i-1] \\ Q_A, m = i \end{vmatrix} \qquad (5)$$

where E_0 and F are the energy and frequency sufficient for stimulation of one electron with the definite set of quantum numbers or for realization (including assumed realization) of a electron transfer; h is the thickness of the surface (near-surface) layer; ρ is the density of surface layer material of an irradiated object; N_A is Avogadro number; ε, μ are the dielectric permittivity and magnetic permeability of the electromagnetic wave spreading layer (surface or near-surface), they can vary in case of the resonant accumulation of the pulse energy in an object with changing the refracted oscillation frequency f_{np}; $N_{эл}$ is the quantity of the reacting electrons on the one energy level of a chemical element single atom; M_{AT} is the molar mass of an irradiated substance calculated for atoms; S_k is the linear coefficient, the matrix of pulse resolving into Fourier series for determining the irradiation pulse power on the k-harmonic of the carrier frequency; $S_{k=1}$ is the linear coefficient, the matrix of pulse resolving into Fourier series for determining the irradiation pulse power on the carrier oscillation frequency; $k_н$ is the coefficient showing the power quantity fell on the wave spreading in the surface (near-surface) layer in case of normal or inclined falling of the irradiation pulses on an object; $\lambda_{пр}$ is the length of the oscillation wave refracted in a material object; $tg\delta$ is the loss factor; L_0 is the length of the closed curve of the refracted wave spreading in an object as a surface wave.

As a result, the maximum possible quantity of the absorbed energy can be calculated as:

$$E_м = S_л - \frac{E_0 F \sigma_{эпр} h \rho N_A N_{эл} \sqrt{\varepsilon \mu^3}}{M_{AT} k_н S_k S_{k=1}} \cdot (iT_0 - t_n) \times$$

$$\times \sum_{m=1}^{i} exp\left[\frac{4\pi L_0 (1-m)}{\lambda_{np}} \sqrt{\frac{1}{2}\left(-1+\sqrt{tg^2\delta+1}\right)}\right] Q_A^{-m} \times \begin{vmatrix} 1, m = [1, i-1] \\ Q_A, m = i \end{vmatrix} \qquad (6)$$

where i is the quantity of the irradiation pulses in the burst necessary to obtain the energy for the effect; $S_л$ is the linear coefficient with the dimensions of energy quantity and corresponding the reaction process of an observed object to the external exposure; T_0 is the pulse repetition period; t_n is the pause duration in the pulse burst.

In conclusion, in the presented work there have been calculated the analitical equation's which take into account the possibility of parametrical absorption effect application in the field of the non-linear radiolocation owing to the increasing of the effective scatter area of an object at the expense of energy redistribution on the front of the electromagnetic wave. The results are supported by the performed engineering calculations and experiments.

Literature

1. Egorov B.M. and others. The phenomenon of the electromagnetic wave energy parametrical absorbtion by material object. Diploma RANS N 31, 1996 / Bul.VAC RF N 6, 1996.

BRIGHTNESS VARIATIONS RESISTANT ALGORITHMS OF OBJECT LOCATION ON RADIOMETRIC IMAGES

V.I. Antyufeev, V.N. Bykov, B.I. Makarenko, A.M. Grichaniuk
Kharkov military university, 6 Svoboda square, Kharkov, 310043, Ukraine

The millimeter wave band is perspective for application in matching correlation systems, using radiometric sensors to form sensor maps mostly owing to the weatherwide possibility and ability to provide rather high spatial resolution at a comparatively small antenna size. But the intensity of radiothermal radiation of this band differs by strong uncertainty caused by variations of seasonal, weather and other conditions and which are not giving in to probabilistic description. We proposed to use a reference map representation on various scales depending on a brightness variability degree for synthesis of zone-type object locating algorithms, which are resistant to brightness variations and based on a zoned model of sensor map.

The uncertainty of radiometric image brightness component is possible for describing with the help of allowable transformations group G of brightness $g:\mathbf{R}\to\mathbf{R}$, which allows to allocate to a resistant brightness component and is determined experimentally. In the measurement theory the allowable transformations group allows unequivocally to determine a scale type on set X, which is understood ordered triple $\langle \mu, \nu, f\rangle$, where $\mu=\langle X,\{R_k\}\rangle$ is empirical system with the relations, $\{R_k\}$ is a preference relations set on X; $\nu=\langle \mathbf{R},\{\rho_k\}\rangle$ is numerical relations system; f is homomorphism of system μ in system ν (named also numbering), i.e. function $f: X\to\mathbf{R}$, keeping the relations $\{R_k\}$. If in a scale caused by group G homomorphism f is constructed the set all homomorphisms can be described as follows: $F_G(f)=\{g\circ f,\ g\in G\}$. This set also refers to as a G-orbit of an element f. The isomorphism between set of orbits and set of systems with the relations is established.

The simplified statement of a problem looks as follows. Let's represent $N_1\times N_2$ sensor map matrix as

$$\mathbf{y}=\mathbf{a}+\mathbf{n}$$

where $\mathbf{a}$ is the sensor map matrix without noise component; $\mathbf{n}$ is the matrix which elements are independent among themselves noise components on multichannel radiometer output. Let's form $K=(N_1-M_1+1)(N_2-M_2+1)$ $M_1\times M_2$ fragments

$$\mathbf{y}^{ml}=\left\|y_{ij}^{ml}\right\|=\left\|y_{i+m,j+l}\right\|,\quad \mathbf{T}_s^{ml}=\left\|a_{i+m,j+l}\right\|,\quad \mathbf{n}^{ml}=\left\|n_{i+m,j+l}\right\|,\quad i\in\overline{1,M_1},\ j\in\overline{1,M_2}$$

and we shall proceed to their vector representation by unwrapping on rows:

$$\mathbf{y}^k=\mathbf{T}_s^k+\mathbf{n}^k,\quad k\in\overline{1,M},\quad M=M_1M_2$$

where (M_1,M_2) is the reference map matrix dimension. Let $\mathbf{K}$ be the diagonal covariance matrix of vector $\mathbf{n}^k$ and H_k be the event consisting that k-th sensor map fragment $\mathbf{y}^k$ coincides with the reference map. Let the distribution $\{p_k\}_{k=1}^K$ is defined on set $\{H_k\}_{k=1}^K$. If a performance criteria be a posterior probability of shift parameter k the problem is formulated as follows: it is required by comparison of the reference map with all K sensor map fragments and on the basis of the information about statistical performances of noise vector $\mathbf{n}^k$, prior distribution $\{p_k\}_{k=1}^K$ and given group G to choose optimum under criteria

$$P_{ps}(H_k/\mathbf{y}^k)=\frac{p_k}{(2\pi)^{M/2}\prod_{i=1}^{M}\sqrt{K_i^k}}\exp\left[-\frac{1}{2}\sum_{i=1}^{M}\left(y_i^k-ge_i\right)^2\Big/K_i^k\right]$$

hypothesis H_j, i.e. to find number j for which

$$u_j = \min_{k\in K}\min_{g\in G}\left[\sum_{i=1}^{M}\ln K_i^k - 2\ln p_k + \sum_{i=1}^{M}\left(y_i^k - e_i\right)^2 \Big/ K_i^k\right]. \quad (1)$$

Difference from known statements consist in the following: the matrix $\mathbf{D}^k$ is given diagonal; the group G is submited and the reference map space $E = \{\mathbf{e}\}$ is extended up to G-orbit $F_G(\mathbf{e})$ of a vector $\mathbf{e} \in \mathbf{R}^M$; at comparison of each sensor map fragment $\mathbf{y}^k$ with reference map $\mathbf{e}$ we must found at first optimum reference map $\hat{\mathbf{e}} = g\mathbf{e}$ (maximum similarity reference map), i.e. the problem is decided

$$u_j^k = \min_{g\in G}\sum_{i=1}^{M}\left(y_i^k - ge_i\right)^2 \Big/ K_i^k = \min_{g\in G}\left\|\mathbf{y}^k - g\mathbf{e}\right\|^2_{\mathbf{D}^k},\ \mathbf{D}^k = \left(\mathbf{K}^k\right)^{-1}. \quad (2)$$

Let's assume in (2) $\kappa = g\mathbf{e}$ and form restriction $g \in G$ in terms of restriction for a vector κ. Let's construct map $r: X \to \overline{1,N}$ (N is number of reference map zones), $r(x_i) = r_i = j$, which compare to an i-th reference map element the number of a zone j, to which it belongs. We shall name a vector $\mathbf{r} = (r_1,\ldots,r_M)$ as a ranks vector of reference map elements. Let's construct the linear operator $h: \mathbf{R}^N \to \mathbf{R}^M$ having $M \times N$ matrix $\mathbf{H}$ with elements $h_{ij} = \delta_{r_i j}$. Let's enter into consideration a vector $\pi \in \mathbf{R}^N$ which components are equal numberings of zones brightnesses. Then any numbering vector of reference map $\kappa \in \mathbf{R}^M$ can be expressed through a vector π as follows: $\kappa = \mathbf{H}\pi$. We shall designate through $C_\pi \subset \mathbf{R}^N$ allowable numbering set on zones which is determined by a type of a scale, in which reference map is represented. Then the allowable numbering set for a vector $\kappa \in \mathbf{R}^M$ can be described as follows: $C_\kappa = \left\{\kappa \in \mathbf{R}^M \middle|\ \kappa = \mathbf{H}\pi, \kappa \in C_\pi\right\}$. The problem (2) accepts a form $\hat{\kappa}^k = \arg\min_{\kappa\in C_\kappa}\left\|\mathbf{y}^k - \kappa\right\|^2_{\mathbf{D}^k}$ and is equivalent to a problem

$$\hat{\pi}^k = \arg\min_{\pi\in C_\pi}\left\|\mathbf{y}^k - \mathbf{H}\pi\right\|^2_{\mathbf{D}^k}. \quad (3)$$

Usually at comparison of vectors $\mathbf{y}^k$ and κ^k vector $\mathbf{y}^k$ previously is normalized, i.e. $\left\|\mathbf{y}^k\right\|_{\mathbf{D}^k} = 1$. Therefore we shall require that optimum numbering κ^k also was the normalized vector. Then the problem (3) will be transformed to following:

$$\hat{\pi}^k = \arg\min_{\pi\in C'_\pi}\left\|\mathbf{y} - \mathbf{H}\pi\right\|^2_{\mathbf{D}^k} \quad (4)$$

where $C'_\pi = \left\{\pi \in \mathbf{R}^N \middle|\ \left\|\mathbf{H}\pi\right\|^2_{\mathbf{D}^k} = 1\right\}$.

In case of reference map representation in a nominal scale the decision of a problem (3) has a form [1]

$$\hat{\pi}^k = \left(\mathbf{H}'\mathbf{D}^k\mathbf{H}\right)^{-1}\mathbf{H}'\mathbf{D}^k\mathbf{y}^k \Big/ \left\|\mathbf{P}\mathbf{y}^k\right\|_{\mathbf{D}^k} \quad (5)$$

where $\mathbf{P} = \mathbf{H}\left(\mathbf{H}'\mathbf{D}^k\mathbf{H}\right)^{-1}\mathbf{H}'\mathbf{D}^k$. The equality (5) can be presented as follows:

$$\hat{\pi}_i^k = \frac{1}{n_i^k}\sum_{j\in N_i} D_j^k y_j^k,\ i \in \overline{1,N};\ n_i^k = \sum_{j\in N_i} D_j^k. \quad (6)$$

By substituting optimum reference map meaning for a k-th sensor map fragment determined by expression (6) in (1) we shall find that the decision functions of nominal and classical zoned algorithms coincide:

$$u^j = \min_{k\in\overline{1,K}}\sum_{i=1}^{N} n_i^k D_i^k,\ D_i^k = \frac{1}{n_i^k}\sum_{j\in N_i} D_j^k\left(y_j^k - \overline{y_i^k}\right)^2.$$

For order and hyperorder algorithms which are based on reference map representation in order and hyperorder scales the appropriate algorithms deciding a problem (4) are found in [1].

Is proved, that centrality of a vector $\mathbf{y}^k$ attracts centrality of optimum numbering $\hat{\kappa}$ for all algorithms. It's shown that if the sensor map fragments are normalized in the metrics $\mathbf{D}^k$ than to receive normalized reference map it is necessary to normalize the received decision.

To estimate efficiency of algorithms, which is understood as probability P of correct object localization, were carried out statistical tests. Sensor map of zoned structure having the dimension $N_1 = N_2 = 16$ and reference map having the dimension $M_1 = M_2 = 4$ and number of zones $N = 3$ was simulated. To estimate the characteristics of zoned algorithms at random variations of zones brightness levels of sensor map its zones brightness levels were simulated according to expressions

$$T_m = T_{m0}(1+\nu_m), \quad m \in \overline{1,N}$$

where T_{m0} is mean brightness meaning of a m-th zone; ν_m is dimensionless Gaussian random variable with zero mean and standard deviation χ_m. The algorithm efficiency estimation was determined by the ratio of correctly located situations to common number of algorithm starts in a series from 400 tests. The algorithms using reference map representation on absolute, order, hyperorder and nominal scales are tested.

The results of statistical tests of zoned algorithms are given in a fig. 1 at $\chi_1 = \cdots \chi_N = \chi$ and for the following set of parameters: $T_{10} = E_1 = 240K$, $T_{20} = E_2 = 250K$, $T_{30} = E_3 = 260K$, $D_1^k = \cdots = D_M^k = \sigma^2$. At the large signal to noise ratio ($q = (E_3 - E_2)/\sigma \approx 3{,}3$ for $\sigma = 3K$) the efficiency of all algorithms decreases with growth of χ, but the speed of its decrease for nominal algorithm is much lower, than others (fig. 1a). A prize of absolute algorithm at small meanings of χ is insignificant.

In case of the small signal to noise ratio ($q \approx 1{,}4$ for $\sigma = 7K$) in the field of small meanings of parameter χ the absolute algorithm which is for this case an optimum algorithm surpasses others in efficiency (fig. 1b). But at increase of zones brightness variations (increase χ) the best performances has the nominal algorithm and the absolute algorithm in this area has the worst characteristics. The efficiency of nominal algorithm even grows in this area at increase χ, that it is possible to explain by increase zoned variance at discrepancy of a configuration of reference map zones and compared sensor map fragment. The order algorithm occupies an intermediate situation on efficiency between two specified algorithms.

It is clear, that the algorithm with intermediate meanings of efficiency can be received by use as decision function of average weighted meaning of decision functions of order and nominal algorithms.

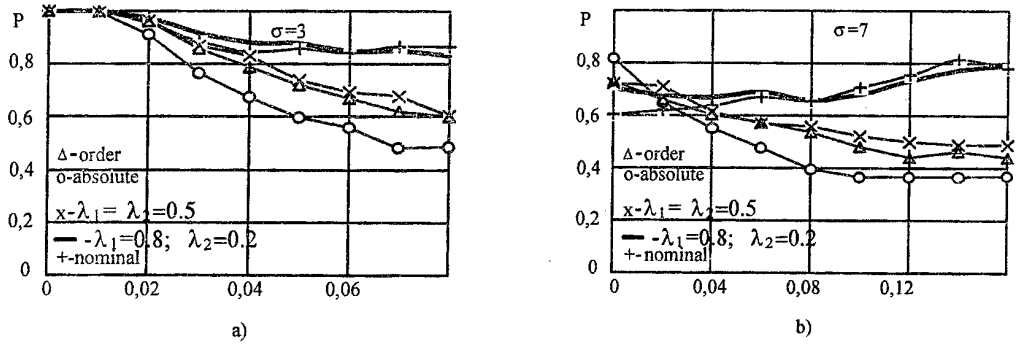


Figure 1. Dependence P from χ

References

1. Антюфеев В.И., Макаренко Б.И., Султанов А.С., "Синтез устойчивых к вариациям яркости изображения алгоритмов локализации целей в двумерных КЭСН. Сообщение 2. Выбор эталона максимального сходства и синтез оптимальных алгоритмов", Электромагнигные волны & Электронные системы., Т. 2, №6, 1997.

RECONSTRUCTION OF THE CONTINUUM OBJECT FROM THE SAMPLED RADIO IMAGE

A.S. Viltchinsky, B.I. Makarenko, E.D. Prilepsky, M.G.Shokin
Kharkov military university, 6 Svoboda square, Kharkov, 310043, Ukraine
Ph: 402887

The most complete information on the object may be obtained by its reconstruction from the measured image. The relation between an object $g(\mathbf{r})$ and an image $f(\mathbf{r})$ is given by the linear integral equation [1]

$$\int S(\mathbf{r},\mathbf{r}')g(\mathbf{r})d\mathbf{r} = f(\mathbf{r}'),\ \mathbf{r} \in D, \tag{1}$$

where $S(\mathbf{r},\mathbf{r}')$ is the system pulse response (the function of the point scattering (FPS); D is the domain of an image definition. The transformation kernel of eq. (1) reflects smoothing properties of an system or a measurement method as a whole.

The relationship of the type (1) describes experiments concerning different branches of science and technology [1-3]. The problem of reconstruction of the object $g(\mathbf{r})$ from the measured image $f(\mathbf{r}')$ is known [2] to be unstable towards the noise. Any smallest noise in the image can lead to the complete destruction of information about the object. The cause of this is in the fact that the eigenvalues of the operator corresponding to the system decrease in the region of high spatial frequencies. When the inverse transformation from image to object is made, the noise components falling at a region of high frequencies will unlimitedly grow leading to the complete destruction of information about the object.

There is a lot of methods for obtaining the stable approximate solution to eq. (1) [1-3]. Most of these methods are based on the replacement of the operation of the problem (1) by an approximate regularized operator having the spectrum (eigenvalues) which neither vanishes nor tends to zero for high-frequency components. The regularization parameter, i.e. the degree of closeness between exact and regularized operators is set a priori and has no direct connection with initial problem.

In the present work the incorrectness of the initial problem (1) is overcome by means of the image sampling. Actually, instead of equation (1) we consider the sampled in image analog

$$\int S(\mathbf{r},\mathbf{r}_n')g(\mathbf{r})d\mathbf{r} = f(\mathbf{r}_n'),\ \mathbf{r}_n' \in D. \tag{2}$$

Here $\mathbf{r}_n'$ are the sampling points. The equation (2) in contrast to eq. (1) has a stable solution even with an exact operator. Moreover, the object reconstruction error appears to be unambiguosly related to the sampling interval in eq. (2) and with its decreasing the error increases. In other words, the sampling interval plays the role of a regularization parameter and its magnitude directly determines the object reconstruction error component, caused by noises in image.

There is another reconstruction error component which is also connected with the sampling interval. The component is independed of the noise. We shall call it the degradation error. With increasing the sampling interval the number of degrees of freedom in image decreases and this leads to a loss of information about small details of the object. So, with decreasing the sampling interval the degradation error decreases and the error due to noise increases.

Hence, the optimum sampling interval can be determined for every set of objects when the noise level and a priori information about FPS are given. For this one can use, e.g. the minimum criterion of the total error, or the minimum criterion of one error component when the level of the other is set, or lastly the information criterion (e.g. maximum of information about the object which can be obtained from the image).

Now let us consider one-dimensional analog of eq. (2) connecting the object $g(x)$ to its uniformly sampled on the interval Δx image $f\{x'_n\}$

$$\int S(x'_n - x)g(x)dx = f(x'_n). \tag{3}$$

We denote $f(x'_n) = f_n$; $S(x'_n - x) = S_n(x)$. The functions $S\{x'_n\}$ are assumed to be linearly-independent. For a definite set of continuous objects $g(x)$ with the noise level in samples $\{f_n\}$ given and with FPS known, one needs to reconstruct the object and determine an optimum sampling interval.

The space of assumed objects $g(x)$ can be split into a subspace L of functions $g_L(x)$ and its orthogonal complement $\overline{L}$, i.e. a subspace of functions $\overline{g}_L(x)$ orthogonal to $g_L(x)$,

$$g(x) = g_L(x) + \overline{g}_L(x). \tag{4}$$

The equation (3) defines only the object component $g_L(x)$ while $\overline{g}_L(x)$ cannot be found from it. To determine $\overline{g}_L(x)$ (if necessary) one should have some additional primary information which is not contained in eq. (3). In view of the above we shall call $g_L(x)$ the basis solution of eq. (3). The set of functions $\{S_n(x)\}$ forms a basis (in the general case nonorthogonal) in the subspace L. Then, the values $\{f_n\}$ may be considered as projections of the initial object $S_n(x)$ onto space L spanning the system $\{S_n(x)\}$. The basis solution of eq. (3) can be given as

$$g_L(x) = \sum_n q_n S_n(x), \tag{5}$$

where coefficients $\{q_n\}$ do not equal to zero simultaneously. Substituting the expression (5) into (3) we obtain a set of equations to determine the coefficients $\{q_n\}$

$$\sum_m K_{nm} q_m = f_n, \tag{6}$$

where elements of the matrix $[K_{nm}]$ depend of the indices difference

$$K_{nm} = \int S(n\Delta x - x)S(m\Delta x - x)dx = K(n-m). \tag{7}$$

Making the Fourier transformation of eq. (6), we find

$$Q(\omega) = \lambda^{-1}(\omega)F(\omega), \tag{8}$$

where $Q(\omega)$ and $F(\omega)$ are the Fourier images of the coefficient set $\{q_n\}$ and sampled image $\{f_n\}$, respectively, and are equal to

$$Q(\omega) = \sum_n q_n \exp(-i\omega n\Delta x), \quad F(\omega) = \sum_n f_n \exp(-i\omega n\Delta x), \tag{9}$$

and $\lambda(\omega)$ are eigenvalues (spectrum) of the operator with elements $K(n-m)$ (7):

$$\lambda(\omega) = \sum_n K(n)\exp(-i\omega n\Delta x). \tag{10}$$

Using the expressions (5) and (9) we find the basis solution

$$g_L(x) = (2\pi)^{=1}\Delta x \int_{-\pi\Delta x^{-1}}^{\pi\Delta x^{-1}} \lambda^{-1}(\omega)F(\omega)\Psi(x,\omega)d\omega, \tag{11}$$

where the function $\Psi(x,\omega)$ is equal to

$$\Psi(x,\omega) = \sum_n S(n\Delta x - x)\exp(in\omega\Delta x). \tag{12}$$

Now we couple functions $\Psi(x,\omega)$ and $\lambda(\omega)$ to the frequency characteristic (FC) of the system. Shifting the origin of coordinates in the formula (12) we obtain

$$Z(x,\omega) = H^*(\omega,\gamma)\exp(i\omega n\Delta x), \tag{13}$$

here $H(\omega,\gamma)$ is the FC of the system and equals

$$H(\omega,\gamma) = \sum_k S\big((k-\gamma)\Delta x\big)\exp(-i\omega k\Delta x), \tag{14}$$

where $\gamma = \left\{x\Delta x^{-1}\right\}$ and $k = \left[x\Delta x^{-1}\right]$ are the fractional and integer parts of $x\Delta x^{-1}$, respectively. We make use of expressions (7), (10) and (14) and obtain the relation between the function $\lambda(\omega)$ and FC

$$\lambda(\omega) = \Delta x\int_0^1 |H(\omega,\gamma)|^2 d\gamma. \tag{15}$$

The physical meaning of the formula (15) is clearly seen. The spectrum of the $\{K_{nm}\}$ matrix is got by the averaging of the modules square of FC over the initial point of the digitized sample. Substituting values of $\Psi(x,\omega)$ (15) into formula (11) we finally obtain the basis solution

$$g_L(x) = (2\pi)^{-1}\int_{-\pi\Delta x^{-1}}^{\pi\Delta x^{-1}}\left(\int_0^1 |H(\omega,\gamma')|^2 d\gamma'\right)^{-1} F(\omega)H^*(\omega,\gamma)\exp(i\omega n\Delta x)d\omega, \tag{16}$$

where $x = (n+\gamma)\Delta x$; n is the integer and γ -fractional part of $x\Delta x^{-1}$.

It is interest to compare the obtained basis solution (16) with known regularized ones. For instance, in the Tikhonov method [2] regularized solution $g_T(x)$ is given as

$$g_T(x) = (2\pi)^{-1}\int_{-\infty}^{\infty}\left(\int_0^1 |H(\omega,)|^2 + \alpha^2\right)^{-1} F(\omega)H^*(\omega)\exp(i\omega x)d\omega,$$

where FC $H(\omega) = H(\omega,0)$; α is a regularization parameter damping small values of FC in the high-frequency region. In the basis solution $g_L(x)$ (16) the sampling interval Δx is the regularization parameter. The damping of small values of FC in the high-frequency region is achieved by means of convolution of the spectrum in the periodicity interval $|\omega| \le \pi\Delta x^{-1}$ and the estimation of isolated nodes of FC is done by averaging it over the sampling interval Δx.

References

1. Г.И. Василенко, А.М. Тараторин, "Восстановление изображений", Наука, М., 304с., 1986.
2. А.М. Тихонов, В.Я. Арсенин, "Методы решения некорректных задач", Наука, М., 288с., 1986.
3. "Обработка изображений и цифровая фильтрация" /Пер. с англ. Под ред. Т.Хуанга/, Мир, М., 270с., 1979.

INFLUENCE OF OIL FILM ON SPECTRAL AND POLARIZATION FEATURES OF S- , KA- AND V-BAND WATER SURFACE BACK SCATTERING

V. Lutsenko, S. Homenko, A.Uzlenkov, V. Kirichenko
Institute of Radiophysics and Electronics of NAS of Ukraine
12 Acad. Proscura St.,Kharkov,310085,Ukraine
Tel: 380 572 448 340; Fax 380 572 441 105; E-mail: homenko@ire.kharkov.ua

The last years oil slicks statistics looks dangerously. So, in period from 1970 to 1996, there are1082 small and medium sized and 364 large incidents with emergency oil floods took place. Cost of works for liqudation of pollution are exceeded the cost of oil in 3...4 orders.

In addition to emergency oil floods, the dumpings of polluting substances in neighbourhoods of bulk-oil terminals, in port and resort zones happen. The amount of such incidents, apparently, grows and poorly gives in to the account.

Thus, the problem of operating detection and liquidations of petroleum pollutions is in the number of rather actual problems.

The solution of this problem implies development and implementation of remote monitoring, both remote marine lines, and coastal zones, with engaging of various methods of oil pollutions detection: optical, radiometric, radar's. As first two methods have serious restrictions in application, most perspective is the radar's method.

It is known, that the possibility of detection of slics by radars is based on effect of decreasing of amplitude resonance - scattering waves due to oil films. It is exhibited in re duction of scattered signal amplitude.

Except for the phenomenon of wave's decreasing, it is possible to assume, that the availability of a film will influence not only amplitude component of sea disturbance, but also on a phase velocity resonance-scattering waves, that should be exhibited in spectra of scattered radio signals. The latter can be for an additional indication of pollution presents.

The purpose of experiments which are carried out under laboratory conditions, was the study of spectral reflectance, and also polarizing and band features of backscattering of radiowaves by an interface of mediums (water - air, petroleum - air) for want of generations waves by an air stream (or mechanical method in a more dense medium).

The laboratory experiments were conducted in a wave tank with sizes 0.75 m * 0.7 m and with depth of liquid no more than 3 cm. That has ensured the "deep water" condition for waves with less then 6 cm lengths and has removed a problem of long wave generation. The velocity of an air stream, was measured on a shear of the nozzle, was adjusted in limits from 0 up to 21 m/s, and the frequency of mechanical wavemaker was adjusted in limits from 0.1 up to 100 Hz.

The measuring complex worked on three lengths of waves (10 cm, 8 mm and 4 mm) in a continuous mode of a radiation.

The stand for a research of features of backscattering from a water surface is consists of: wavetank on rotary desktop; wave generation device; a measuring complex; an equipment for registration; the simulator for calibration of a measuring complex; the reflexless camera.

In the first series of experiments the surface of water was irradiated under an angle about 40^{O} by MM waves with vertical, horizontal and sloping orientations of polarization and the reception of two orthogonal polarized components (vertical and horizontal) of scattered signalwas carried out. The outcome between channels was not worse 20 dB. Besides the exposure of a surface on a wave 10 cm by vertical - polarized signal and reception of a scattered signal on horizontal polarization was carried out. Is found that irrespective of a direction of an exposure (on a wind or against a wind) the depolarizing factor makes -8 ...-9 dB and practically does not depend on the velocity of the air stream.

The intensities of scattered signals on vertical and horizontal polarizations with exposure of the surface by sloping polarization are about identical; the difference does not exceed 1 dB on velocities of the air stream less then 3m/c. Factors of cross correlation (between components agree and orthogonal polarized for radiated signal) made 0.5...0.7 (sloping-polarized signal was radiated); and - 0.35...0.15 (horizontal - polarized signal was radiated). It is necessary to mark a decrease from 0.5 to 0.15 factor of cross correlation of components vertical and horizontal orientation, for want of exposure of a surface by a signal with sloping polarization for

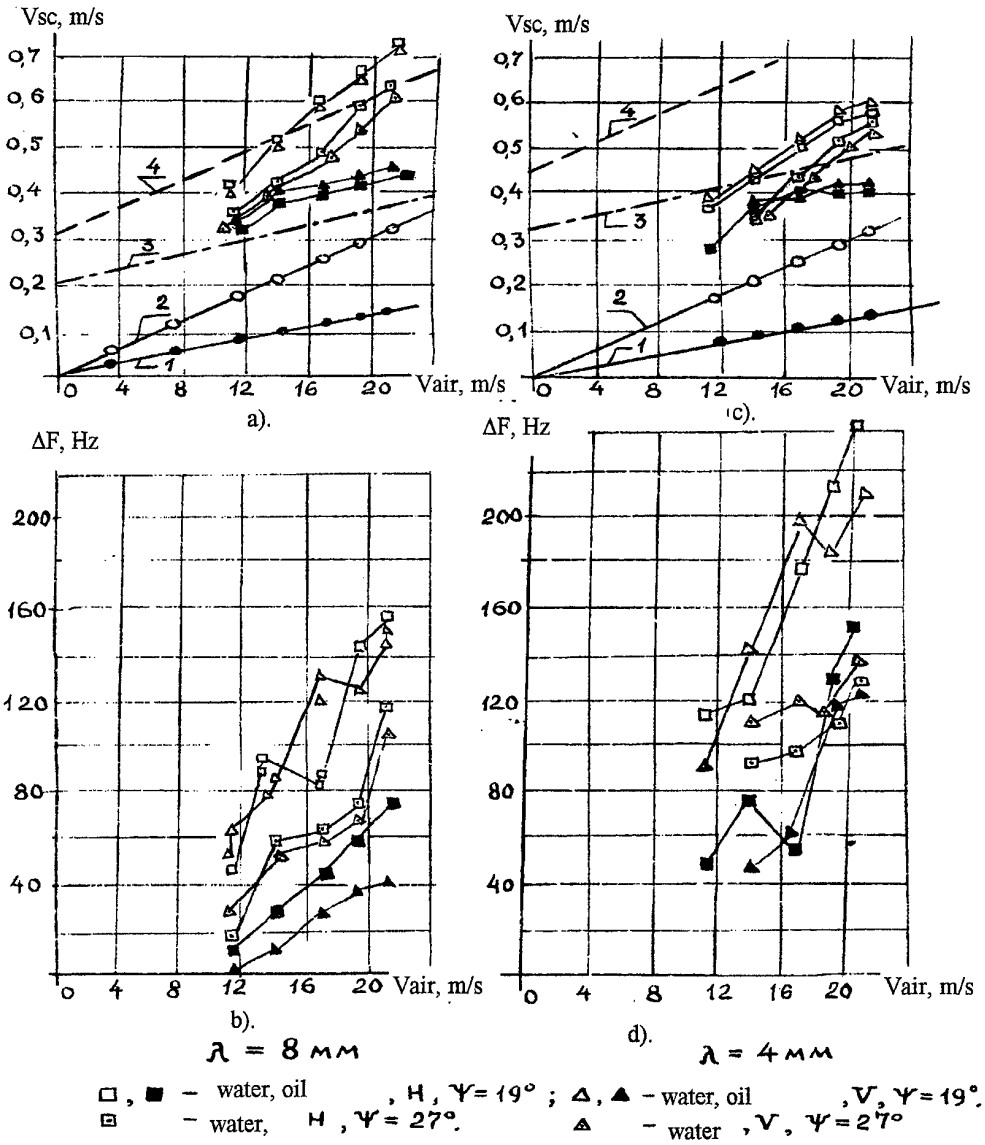


Fig. 1 - Dependence of a central frequency displacement and width of a spectrum from the velocity of the air stream.

increase of a velocity of an air stream from 1.5 up to 7 m/c. The study of spectral structure of scattered signals on 8 mm wave shows, that a width of a spectrum and frequency central displacement on horizontal and vertical orientations are identical.

The purpose of the second series of experiments is establishment of dependence of spectral reflectance of signals, scattered by the water surface and by the surface of petroleum (transformer oil), from a velocity of an air stream, polarization of a radiation and reception.

It is necessary to mark, that some parameters of experiments, surch as the velocity of the air stream (11...21 m/s) and grazing angles ($19^{\circ}...27^{\circ}$), was different than in the first series.

On fig.1 are presented dependence of a central frequency displacement (in accordance with equivalent velocity of scatterers) and width of a spectrum from a velocity of an air stream on waves of 8 mm and 4 mm accordingly. The various badges designate outcomes obtained for reflections from water and oil.

On fig.1a,c the regression dependences, which was obtained on experimental data of a surface layer wind drift velocity of oil - 1 and water - 2 are presented. It is visible, that for oil declination of dependence of a

central frequency displacement from a velocity of a wind approximately the same, as well as at dependence of a wind drift, while for water he is higher. It can be caused by that apart from mechanisms of scattering connected with resonance waves and a wind drift, can be present other mechanisms, in particular, scattering on water sparks, which will be derivated for want of large velocities of an air stream.

On fig.1a,c - lines 3, 4 the settlement significances of a central frequency displacement are shown in accordance with velocity of scatterers,defined with allowance for of phase velocity resonance - scattering waves of a wind drift for petroleum and water accordingly. The good correspondence of settlement assotiations and experimental outcomes exists. For water the divergence is more, especially on a wave with length 4 mm, that, as was indicated earlier, is connected to the more complicated phenomena of shaping of a scattered signal. At the same time, effect of reduction of a Doppler frequency displacement for scattering of Ka- V-band waves by oil in relation to clean water is observed.The magnification of a grazing angle results in a decrease of a Doppler frequency displacement. The behaviour of back scattering spectrum width dependence from a velocity of an air stream for oil and water surface (fig. 1 b,d) is similar.On a wave 10cm the indicated displacement of frequency both for water, and for oil practically does not depends on a velocity of an air stream and approximately corresponds to settlement significance of a phase velocity is resonance dispersing waves, which for this wave lenght range is poorly changed at transition from water to oil.

Thus, the experimental detected effects are connected with modification of resonance wave's phase velocity and can be used for increase of oil slick contrast.

TWO-PARAMETRIC REPRESENTATION OF NONSTATIONARY RANDOM SIGNALS IN RADARS

Konstantin A. Lukin and Anatoly A. Mogila
Institute of Radiophysics and Electronics,
National Academy of Sciences of Ukraine.
12 Acad. Proskura St., 310085 Kharkov, UKRAINE
E-mail:lukin@ire.kharkov.ua; fax: +38 0572 441105;

There are two general cases when one has to deal with radar returns which are essentialy nonstantionary and random. First of them takes place when one has to use random waveforms as a probe signal, while target is moving either randomly or regularly. The second case occurs for radars using deterministic signals, while the target's movement is both random and fast. Aside from classic example of moving point-like targets (aircrafts, heliocopters, etc.) a good example of that we have when getting microwave images via SAR technique of a forest or water surfaces under windy conditions. To perform a processing of such returns with aim of extracting useful information or to perform a "time-filtering" of images obtained one has to use an adequate methods. Time-Frequency Distribution and Wavelet Decomposition of nonstationary signals are the most popular approaches to solve those problems. However, for the Time-Frequency Distribution approach the type of sliding window and parameters to be adjusted in adaptive analysis are the most sadle and unclear points for a particular application. The absence of recommendations how to choose an appropriate decomposition basis, as well as how to assign frequencies to component functions are the biggest disadvantages (but not the only ones) of the wavelet time-frequency analysis.

In the paper we present a different approach to the above problem based upon the axiomatic theory of random processes and the machinery of Hilbert's metric spaces. We suggest a new two-parametric representation of nonstationary random signals with finite energy exploiting both introduction of a sliding time window of finite duration and decomposition of random process realisations over an ortogonal normalized basis of the corresponding Hilbert's functional space. The whole procidure of the two-parametric signal representation is mathematically jusified and provides integro-summatory representations converging for both the realisations of the random process and random processes itself.

The theory developed provides mathematical tools for the efficient analysis of the following characteristics of nonstationary random signals:

- Evaluation of the signal's amplitude and energy in the time-frequency plane.
- Evaluation of the correlation either between different spectral components at given times or between the same spectral components at different times, as well as combined correlations of those types;
- Adaptive procidure for an optimization of both the sliding window duration and its shape, as well as number of the spectral components to be used for adequate discription of the nonstationary random signals according to a certain criteria, e.g. minimum of mean square error.
- Adaptive filtration of the nonstationary random processes with given correlation or spectral properties.
- Algorithm for sinthesizing of random nonstationary signals with given correlation or spectral properties.

Examples of application of the approach suggested to the analysis Doppler's signals filtered out of radar returns scattered by moving man and fire are presented.

Possible areas of application for the two-parametric representation of nonstationary random signals are discussed.

MATHEMATICAL MODELS AND SPATIAL CHARACTERISTICS OF COHERENT AND INCOHERENT IMAGING SYSTEMS

Ivan Prudyus, Sviatoslav Voloshynovskiy, Taras Holotyak
Radio Engineering Faculty, State University "Lvivska polytechnika"
S. Bandery Str., 12, Lviv, 290646, UKRAINE
E-mails: {iprudyus, svolos, t.holotyak@polynet.lviv.ua}

At resent time 2D system of antenna elements is considered as main tool for coherent and incoherent imaging. These types of imaging systems can be applied in radar and hydroacoustic, ultrasonic image formation, in radio astronomy and Earth science problems.

Spatially distributed arrays of antenna elements (sensors) located on the plane that are designed for object image acquisition based on the emitting or reflecting radiation receiving play an important role in multidimensional image processing. Process of image formation is considered under assumption that object is placed in far zone and falling radiation has the features of plain wave. Except these, lets assume that received signals cover the narrow band near the certain central frequency. Then the antenna array elements (sensors) satisfy the measurement of local electromagnetic or acoustic field distribution. Further data processing provides the estimation of spatial distribution of complex signal or intensity on the object surface. The main task of imaging system consists in obtaining the mentioned above spatial distribution with high precision, i.e. with high spatial resolution.

In incoherent systems the information source is radiation emitted by object and observed by receiving antenna system. In coherent system signal is a result of transmitting energy reflection from the object surface and its estimation by receiving aperture. The image formation process as 3D real object or scene projection into the 2D image plane can be described by the next observation equation

$$g(\theta,\varphi) = \int_{\Omega} h(\theta',\varphi') \cdot f(\theta-\theta',\varphi-\varphi')\, d\theta'\, d\varphi' + n(\theta,\varphi) \qquad (1)$$

where $g(\cdot,\cdot)$ is obtained image distorted by antenna system and noises, $f(\cdot,\cdot)$ denotes original image, $h(\cdot,\cdot)$ is impulse characteristic of observing system or its blurring function, $n(\cdot,\cdot)$ denotes additive noise, Ω is the region of operator $h(\cdot,\cdot)$ support, θ and φ are the spatial units.

Presentation of observation equation (1) in spatial frequency domain gives simplified model of image formation process that consists in image and imaging system spatial spectra multiplication

$$\tilde{G}(m,p) = \tilde{H}(m,p) \cdot \tilde{F}(m,p) + \tilde{N}(m,p), \qquad (2)$$

where $\tilde{G}(m,p)$, $\tilde{H}(m,p)$, $\tilde{F}(m,p)$ and $\tilde{N}(m,p)$ are the Fourier transforms from g, h, f and n, respectively.

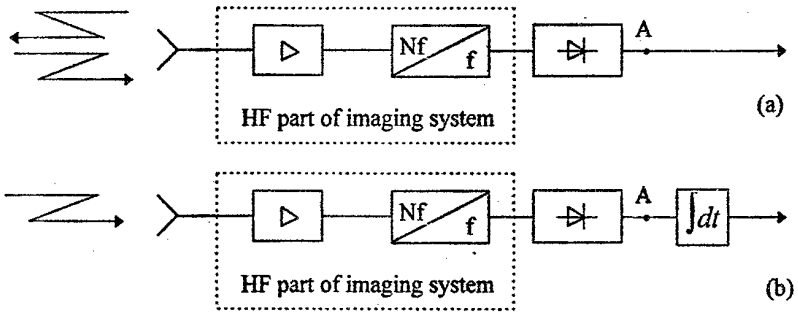


Figure 1. Block diagrams of coherent (a) and incoherent (b) imaging systems.

For description of both kinds of imaging system the spatial characteristics, i.e. impulse response of imaging system (blurring function) and spatial spectrum, were chosen [1]. Peculiarities of these characteristics are determined by physics of image observation process. Mentioned imaging systems can be presented by block diagrams given in Figure 1.

Taking into account Eq. 1 signal in point A for both systems under condition of noise absence can be expressed as

$$\left|g(\theta,\varphi)\right|^2 = \left|\int_{\Omega} h(\theta',\varphi')\cdot f(\theta-\theta',\varphi-\varphi')\,d\theta'\,d\varphi'\right|^2 . \tag{2}$$

Analysis of the above equation shown, that resulted signal depends not only from signals obtained by receiving system from different directions but from their cross-correlation term. The integrator presence in incoherent (passive) systems caused the cross-correlation term reduction conditioned by integration of phase multiplier that has uniform distribution. Therefore, the output signal of incoherent system can be written as

$$\left|g(\theta,\varphi)\right|^2 = \int_{\Omega}\int \left|h(\theta',\varphi')\right|^2 \cdot \left|f(\theta-\theta',\varphi-\varphi')\right|^2 d\theta'\,d\varphi'\,dt \tag{3}$$

According to these conclusions, spatial characteristics of passive imaging system were determined. Imaging system impulse response in this case is the directional power pattern

$$h_{IC}(\theta,\varphi) = \left|\Im\{E(x,y)\}\right|^2, \tag{4}$$

where $E(\cdot,\cdot)$ denotes the field distribution in antenna aperture, $\Im\{\cdot\}$ is the Fourier transform, x and y are aperture units. The result of inverse task solution for incoherent system will be the distribution of emitted energy intensity $\left|f(\theta,\varphi)\right|^2$. Spatial spectrum of this type of imaging system [2] is expressed by next equation

$$H(m,p) = \left|\Im\{h(\theta,\varphi)\}\right|, \tag{5}$$

where m and p are the spatial frequency space units.

In the case of coherent systems, that uses different antennas for transmitting and receiving, image formation describes by next equation

$$\left|g(\theta,\varphi)\right|^2 = \left|\int_{\Omega} h_T(\theta',\varphi')\cdot h_R(\theta',\varphi')\cdot f(\theta-\theta',\varphi-\varphi')\,d\theta'\,d\varphi'\right|^2 , \tag{6}$$

where $h_T(\cdot,\cdot)$, $h_R(\cdot,\cdot)$ denote impulse response (blurring function) of transmitting and receiving antenna systems respectively.

Coherent (active) systems provide estimation of complex reflection coefficient of investigating object surface $f(\theta,\varphi)$. For the active systems with one antenna for transmission and receiving observation equation (2) can be written as

$$\left|g(\theta,\varphi)\right|^2 = \left|\int_{\Omega} h^2(\theta',\varphi')\cdot f(\theta-\theta',\varphi-\varphi')\,d\theta'\,d\varphi'\right|^2 \tag{7}$$

Coherent systems may be described by the same characteristics, but, unfortunately, problems with cross-correlation term definition do not permit to do this.

To demonstrate the peculiarities of incoherent system spatial characteristic's computer simulation was performed. Figure 2 is presenting some types of aperture geometry, which impulse responses and spatial spectra are given in Figure 3 and 4 respectively.

First one is conventional square aperture that characterized by low level of side-lobs and filled till cut-off frequency of spatial spectrum. The second of the simulated example is sparse ("cross-like") antenna array that is widely used in modern imaging system. These antenna systems are characterized by simplicity of constructive constrain satisfaction and possibility of smart antenna design. Except these, sparse antenna arrays provide significant reduction of antenna element number. Sparseness of antenna array causes increasing of side-lobes level and zero-zones rising in spatial spectrum that evoke image spatial harmonics losing. However, these antennas satisfy higher image spatial spectrum observation in comparison with conventional antennas under same

number of antenna element condition. In this case the possibilities of unique obtained image interpolation are restricted by two factors: the *a priori* information image needed to be restored and signal to noise ratio. Image restoration for these tasks requires more sophisticated algorithms [3].

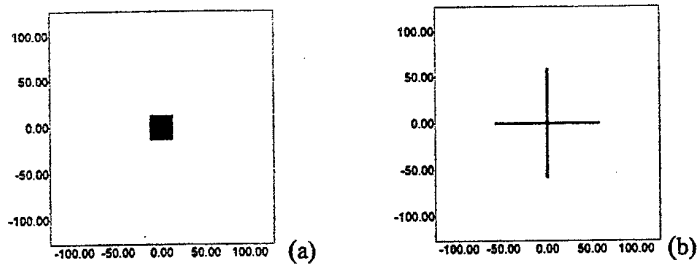


Figure 2. Antenna array geometries: with square aperture (a); "cross-like" (b).

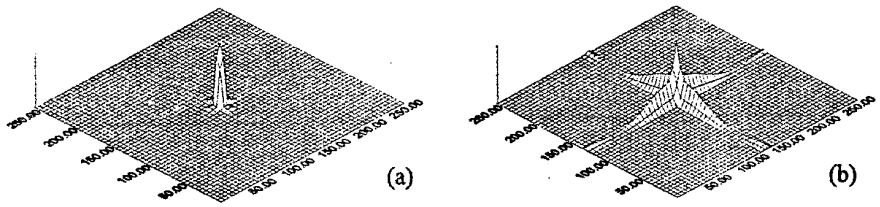


Figure 3. Directional antenna patterns of the square aperture (a) and "cross-like" (b) antenna arrays.

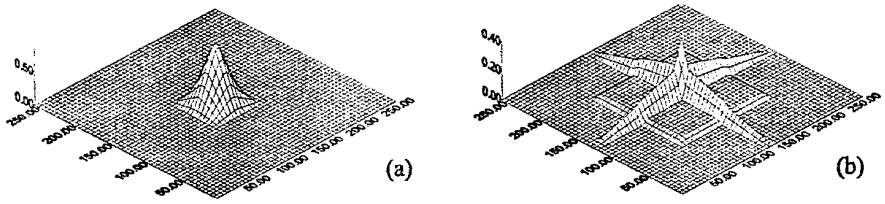


Figure 4. Spatial spectra of the square aperture(a) and "cross-like" (b) antenna arrays.

In this paper the effort of generalized approach description of image observation process was made. Block diagrams of both types of imaging systems (coherent and incoherent) are given. Peculiarities of passive imaging system permit to formulate expressions for receiving system spatial characteristics (impulse response (blurring function) and spatial spectrum). Coherent systems were described by observation equation. Computer simulation of incoherent system spatial characteristics was performed. The necessity of image restoration for sparse antenna array was shown.

References

1. I. Prudyus, S. Voloshynovskiy, T. Holotyak, "Computer Modeling of Radiometry Imaging System with Different Types Of Antennas", Proc. of 2nd International Conference "Antenna Theory and Techniques", Kyiv, Ukraine, May 20-22, 1997, pp. 101-103.
2. I. Prudyus, S. Voloshynovskiy, T. Holotyak, "Investigation of Spatial Antenna System Characteristics in Active and Passive Imaging Systems", Proc. of IEEE International Conference on Modern Problems of Telecommunications, Computer Science and Engineers Training TCSET'98, Lviv, Ukraine, February 23-28, 1998, pp. 124-125.
3. I. Prudyus, S. Voloshynovskiy, T. Holotyak, "Sparse Antenna Arrays in Radar Imaging Systems", Proc. of 3rd Conference on Telecommunications, Modern Satellite, Cable and Broadcasting Services TELSIKS'97, Nis, Yugoslavia, October 8-10, 1997, pp. 46-49.



MM AND SUBMM WAVE RADIO ASTRONOMY

OBSERVATIONS OF TOTAL SOLAR ECLIPSES AT SHORT MILLIMETER WAVES

B.A. Rozanov, N.A. Zharkova
Bauman Moscow State Technical University
5, 2-nd Baumanskaja str, Moscow 107005, Russia
(095) 263-65-98, (095) 267-75-96, Rozanov@RL1-7.bmstu.ru
V.G. Nagnibeda
St. Petersburg State University
7/9, Universitetskaja whart, St.Petersburg 199034, Russia

The Solar chromosphere is the source of the main part of solar millimeter wave radiation. Its observations are very interesting for investigations of this very dynamic unhomogeneous layer near the solar temperature minimum.

The lunar edge section method during the Sun eclipses gives some possibilities for analysis of solar compact objects (the limb, active regions, filaments and so on) with high angular resolution using relatively low angular resolution instruments. Thus a small millimeter wave radio telescopes may be useful for solar eclipse expedition observations.

Such an instrument with antenna dish diameter of 0.6 m (RT-0.6) was designed at the Bauman MSTU, in 1987 [1,2]. The antenna is equatorial mounted and moved in right ascension by short-stepping quartz-controlled motor. The telescope is equipped with 3.4 mm wavelength heterodyne radiometer. Its sensitivity is of 0.1 K by 0.5 GHz band width and 1 s integration time. The total weight of the telescope is of 20 kg. Therefore it is useful for aircraft trips.

Unfortunately due to small contribution of all local sources to total solar radiation flax at short millimeter waves the fluctuations of the terrestrial atmosphere make serious difficulties for observations. To suppress influence of the terrestrial atmosphere fluctuations and to increase contrast of the solar sources the conic scanning of the antenna beam around the solar disk centre direction with period of 25 ms was used. The beam width is of 21' and the scanning circle angle diameter is of 15'. Thus all solar disk could be observed practically simultaneously. The method of observations consists of the solar center tracing by the scanning radiotelescope during all eclipse phases. The reference voltage is connected with scanning phase. The output signals of the receiver square law detector and of the reference generator can be recorded on a dual-track tape for the following computer processing.

The total observation time of an eclipse is 4...5 hours. Therefore the result include a trends and interference's from the weather, radio signals, the instrument and electrical supply instabilities etc. To eliminate the effects some test procedures are fulfilled before, after and during eclipse observation.
For example, from measured antenna temperatures in direction of the Sun, out of the Sun at the same zenith angle and of blackbody absorber at ambient physical temperature one can determine out-of-atmosphere antenna temperature of the Sun which is invariant for the antenna (Fig.1).

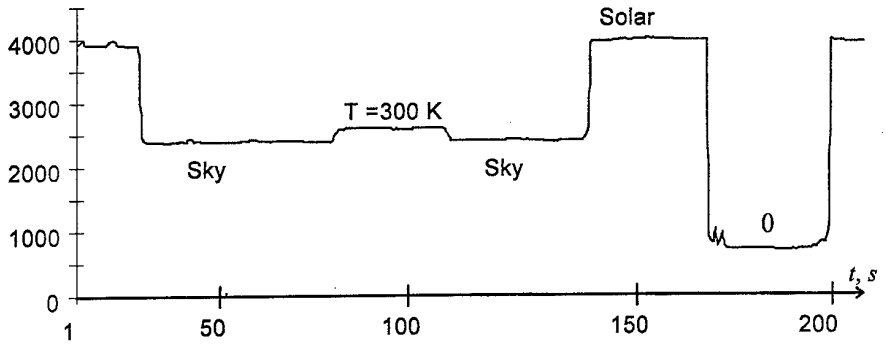


Fig.1.

The following signal processing includes the receiver output integration and dual-channel space-and-time quadrature synchronous detection. Thus the total solar flux P, the differential flux δP_y of the «upper» and «lower» solar parts (relative to the eclipse axis on the Sun) and the differential flux δP_x of the «right» and «left» solar parts (relative to the orthogonal axis) can be obtained. The quiet Sun flux signal modulated by the atmosphere attenuation fluctuations is suppressed in the differential signals. The combination of the three signals allows to estimate a local source position. Test curves time dependencies of P, δP_y , δP_x during solar pass through the telescope beam (without solar tracing and scanning) are presented at Fig.2. The calibration steps (Fig.1) can be seen at Fig.2 too.

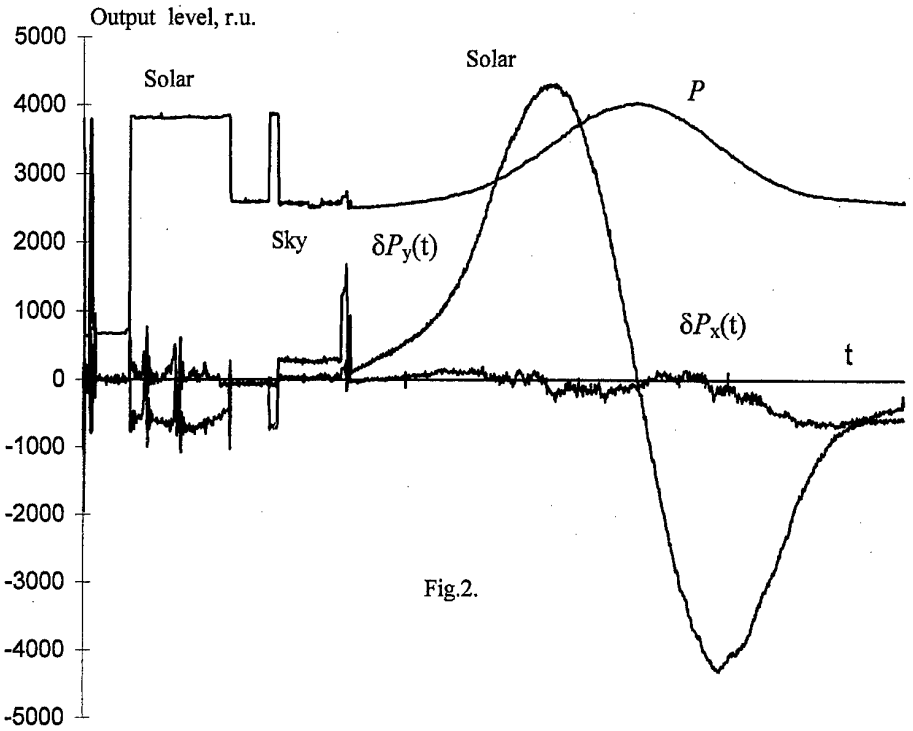


Fig.2.

The radio telescope RT-0.6 has been used for observations of a number solar eclipses: in Sayan (September 1987), in Chersky settlement (July 22, 1990), in La Paz, Mexico (July 11, 1991), in Murmansk (May 21, 1993), in Fan Thiet, Vietnam (October 24, 1995), in Chita-region (March 9, 1997), in El Supi, Venezuela (February 26, 1998), Simultaneously with all the eclipses the Solar, maps at λ=3.4 mm were obtained with angle resolution 2.5 by RT-7.5 MSTU radio telescope in Moscow region. The Mexico (1991), Chita (1997) and Venezuela (1998) eclipses observation were successful.

The eclipse 11 July 1991 curves are presented at Fig.3 and for large scaled central part of the eclipse at Fig.4 [1]. Analogous curves were obtained for other eclipses [3]. The analysis of the curves permit to get some characteristics of solar millimeter wave radiation (radio-radius, temperature profile of the solar-edge and others). The persistent variations of non shielded solar part activity makes obstacles for a weak local sources structure observations. Some phenomena observed have no satisfactory interpretation:

- the fast variations of the Sun radiation in differential canals;
- the splashes of differential Solar flax during full eclipse phase;
- some pulses of full flax of the Sun invisible in very sensitive differential canals.

It exist rather low probability that some of the results are artifacts. Therefore we search new methods of observations and processing to understand the effects.

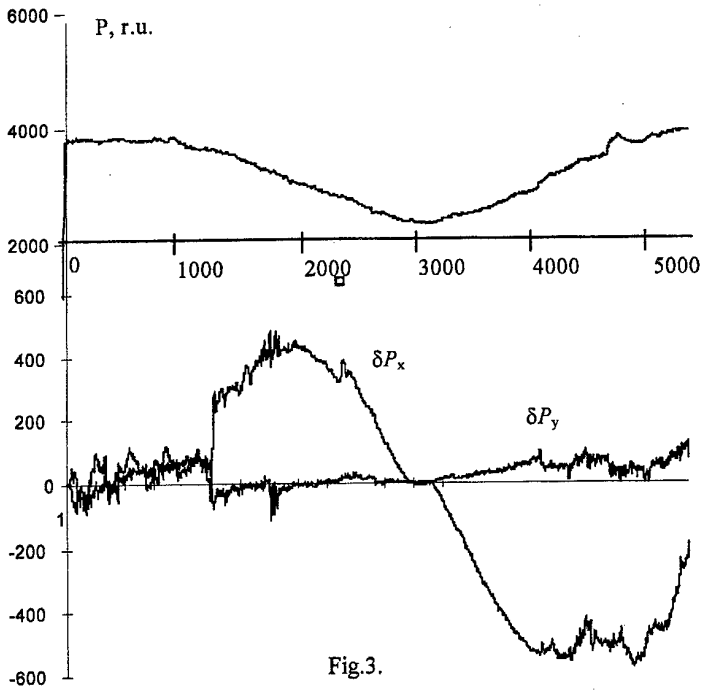


Fig.3.

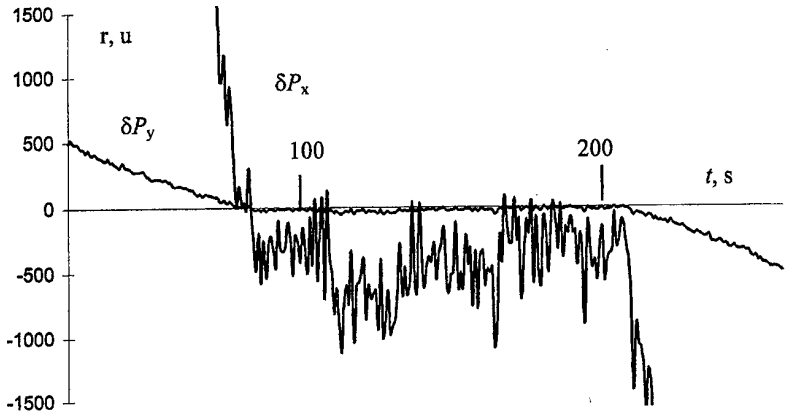


Fig.4.

References

1. B.A Rozanov. , V.G. Nagnibeda G.N Solovyov., N. S. Lebedyuk, , N.A Zharkova, V.V. Piotrovich, Yu.A. Fedorova. Observation of the Sun radiation in the short millimeter wave range / Vestnik MGTU, ser. «Instruments», N4, 1994,p.4-15. (In Russian).
2. B.A. Rozanov, V.G. Nagnibeda, G.N. Solovjev N.A Zharkova, , Y.A. Fedorova. The Solar eclipse July 11, 1991 Observation at 3.4 millimeter wavelength in la Paz, Mexico. /Radioastronomical researches, Nizhny Novgorod, 1995, p.119-125.
3. B.A. Rozanov, V.G. Nagnibeda, N.A Zharkova, V.A. Efremov. Observation of total Sun eclipse March 9, 1997 at millimeter waves / Vestnik MGTU, ser. «Instruments», N4, 1997,p.23-26. (In Russian).

THE INTERFEROMETRIC METHOD OF IMAGE FORMATION AND ASSOCIATED MATHEMATICAL PROBLEMS

Yu.V.Kornienko

Institute of Radiophysics and Electronics of National Academy of Sciences of Ukraine
310085, Kharkov, 12 Acad. Proskury St., Ukraine

Increase of informativeness of the images obtained by means of astronomical instruments in all wavelength ranges is invariably an actual problem of observational astronomy. The informativeness of an image is formed of the resolution, with which the image is obtained, and the precision, with which the brightness of each element of the image is measured. From this, two traditional problems arise immediately: the increase of the resolution and decrease of measurement errors.

The present report is devoted to these questions considered in connection with the interferometric method of image formation, suggested not so long ago [1, 2].

As it is known, the principal limit of the resolution of an astronomical instrument is put by the diffraction of the coming wave on the instrument aperture. However, when observing from the Earth surface, this limit is seldom achievable because of phase distortions of wave in the Earth atmosphere. At one time there were hopes of subsequent computer processing such images. However, gradually it became clear, that the loss of information, caused by the atmospheric distortions at conventional ways of observation, is irreplaceable, and therefore the efforts of investigators should be directed to the struggle against the atmospheric distortions immediately at the time of the observation.

There exist a set of ideas on how one has to form an astronomical image in order to reduce or exclude the influence of the phase distortions. They differ in wavelength range and class of objects for which they are more aplicable, as well as in the degree in which their authors are ready to break off with traditions and move in unknown direction. One of such methods, apparently, the most radical, is the interferometric method of image formation, suggested in [1,2]. In its initial form this method is intended for image formation in the optical range. It is based on the fact, that by virtue of the van Cittert - Zernike theorem, the brightness distribution over the object surface and the coherence function of the field of the wave coming from it are related by Fourier-transformation (for an infinitely remote object and free space of wave propagation). The coherence function depends on the pair of points in the plane, passing through the observation point perpendicularly to the direction to the object. However, this dependence has the special form: actually the coherence function depends not on both radius-vectors of these points separately, but only on their difference. Therefore, measurment of the coherence function for the different pairs of points with the same value of the base vector has to deliver the same value (that is infringed only by errors of the measurement and phase distortions in the propagation medium.)

It means that the information on the brightness distribution over the object surface is coded in the field of the incoherent wave coming from the object with some redundancy which gives rise to certain noise immunity of the coding and opens the possibility to restore the information damaged by the atmospheric distortion. The idea to obtain the object image by direct measurement of the coherence function and subsequent Fourier-transformation of it, is known in radio astronomy long ago and is the only real way of imaging objects in the long wave range. The idea of excluding the phase distortions produced by the atmosphere, on the basis of van Cittert - Zernike theorem, was stated in [3]. However, for the long time it was not clear, how this ideas may be extended to the optical range distinguished in other physical principles of signal detecting and parallel nature of measuring the energy flow from all the elements of the object image.

This question was resolved, when in [1,2], and then in [4] the optical scheme of the interferometer (interferometric telescope) was suggested, enabling one to perform the parallel measurement of the coherence function values for all points of the frequency domain accessible for the given aperture, with redundancy, sufficient to exclude unknown phase distortions caused by atmospheric inhomogenities. (In principle, the most correct variant of this scheme is the one suggested in [2].) Though such a statement of the problem is typical to the optical range, actually this problem and its solution have the direct relation to the radio wave range because of advance of radio astronomy to short-wave end of the radio wave range and inevitable hereafter transition to optical methods of image formation.

Furthermore, it is important to have in mind that, though this method is found on the way of struggle against the atmospheric distortions, it is also actual for design of orbital telescopes since the phase distortions and problems associated with them will inevitably arise in the space because of deformation of the construction at attempt to build an optical (radiooptical) system of the largest technically accessible size.

The essence of the interferometric method for image formation consists in that the image is built not directly in focal plane of the telescope, as in conventional method; instead of this input aperture of the interferometer is divided to some subapertures, and each pair of the subapertures transmits the proper frequency window in the space spectrum of the image. However, the contributions of these pairs are not added together, as in conventional way, when a traditional telescope is used, but are registered independently. For this purpose the periscopic system is used, which transfers the frequency windows formed by different pairs of subapertures to different areas of the frequency domain. The exits of this periscopic system in the aggregate form the output aperture of the interferometer, which, for correct functioning, has to be a nonredundant one. (The input aperture not only may, but also has to have some redundancy.) The interferogram formed by the output aperture is registered. In low-frequency part of the object space spectrum it does not differ from the object image, but has the microstructure, considerably distinct from the image of the object. Image reconstruction consists in exclusion of the unknown phase distortions and finding non-distorted values of the object brightness Fourier transform.

To do this, one has to solve the algebraic system of the equations relating the results of the coherence function phases measurement with the true values of the image Fourier-components phases and phase distortions in the atmosphere. The number of the equations in this system grows with increase of the number of the subapertures faster than the number of the unknowns (including phase distortions on the subapertures). This enables one to exclude completely, at sufficient number of the subapertures, the phase distortions, and to reconstruct the undistorted image of the object with resolution limited only by diffraction of the wave on the interferometer aperture.

The first question, arising in connection with this method, is: in what degree this idealized picture can be carried out in practice, when the results of measurement of coherence function are accompanied by the noise of registration inevitably present at any measurement. It is known quite a number of ideas on improvement of astronomical imaging, which are irreproachable in the theoretical aspect, but fail the test in real observations because of measurement errors. For example, there exists principal possibility to restore a long-exposition astronomical image to diffraction limit of resolution by means of Wiener filter. However, it requires precision of brightness measurement, overstepping limits of real possibility. Therefore, the question on the immunity of the interferometric method to the registration noise influence requires the special theoretical research. Though this research calls for certain efforts from a theorist, it is not conjugate with principal difficulties of mathematical nature and can be performed by means of simple mathematical methods [5].

The next range of questions, associated with more serious mathematical difficulties, is concerned to optimization of the input and output apertures of the interferometer. There exists much freedom to choose the configuration both for the input and output aperture. However, various configurations of aperture should not be thought to be equivalent neither in informational, nor in design aspects. Therefore, the problem arises of optimal choosing the configuration both for the input and output aperture. When choosing the configuration of the input aperture, the following reasons play the role. It is natural to aspire to ensure transmittance of the given spatial passband by means of whenever less number of the input subapertures.

The important moment in the design of an interferometric telescope, especially a space one, is the requirement to ensure its operational ability in the case of some apertures failure. It may be achieved if the redundancy of the input aperture is more than one for all space frequencies transmitted. As an example, the ring aperture in a square or hexagonal lattice may be mentioned. However, such an aperture has too high multiplicity of transmission for some space frequencies and hence is not optimal. It points on the necessity of more detailed investigation of the question about optimal synthesis of the input aperture configuration.

The next question concerns the synthesis of nonredundant output aperture, and leads to the problem of the most compact arrangement of its subapertures. The initial phase volume of the electromagnetic flow, passed by the input aperture, by virtue of the idea of the interferometric synthesis, is divided on parts with new space arrangement considerably less dense. As a result, the phase volume embracing the output flow appears to be much grater than the initial one. In some cases it entails the increase of the registration noise level, so this phase volume is to be made whenever less. It leads to the problem of constructing a nonredundant aperture of the least possible size, consisting of the given number of the subapertures, which is equivalent to the problem of locating the most possible number of subapertures in the given area of the integer lattice. These problems require the serious mathematical consideration and, consequently, strict mathematical formulation. An attempt to formulate them in the correct mathematical terms is undertaken below.

Let there be a lattice on the plane, square or hexagonal, and in this a compact area A is given. It is possible to locate the centres of the interferometer subapertures in the points of this area; for short, let name these subapertures by elements. Let number these elements by numbers from 1 to k; denote the radius-vector of the i-th element by r_i; the set of differences $r_i - r_j$ for all i, j (they belong to the same lattice)

let name by area of the (space) frequencies P passed by the interferometer. Let number these frequencies by numbers from 1 to m.

If some value Ω occures among differences $r_i - r_j$ m times, let say, that this space frequency is passed with the multiplicity m. The aperture, transmitting all frequencies from area P with multiplicity $m \leq 1$ is called nonredundant one.

Then the main problems of optimization of the input and output interferometer apertures, according to the said above, are:

(1) for the given area A of the integer lattice find such an arrangement of the input aperture elements, at which all frequencies from the given area P would be transmitted with the multiplicity not less then given m, whereas the number of the elements used should be the least possible;

(2) in the square of the given side n or the hexagon of the given radius r, build the nonredundant mask of the largest possible number of elements k.

The first of these problems is investigated very poorly. In connection with the second problem there is a set of results obtained, which are of theoretical and practical interest, but most of the questions remain so far unsolved. To discuss them, firstly let specify the terminology. The symmetry transformation of the area A maps a nonredundant aperture to other nonredundant aperture, may be, different from the initial one. Thus, the apertures of interest form the sets, within which they are mutually congruent, i.e. differ only in the position, but not in the form. To simplify the terminology, any representative of a class of mutually congruent apertures let call by mask. (One can easily see that such a class contains not more than eight apertures in the case of square area A and not more than six in the case of regular hexagonal one.) The nonredundant mask which, being added with any element, becomes redundant, let call a full nonredundant mask. The full nonredundant mask in the area A will be named a maximal nonredundant mask, if there exist no nonredundant masks, consisting of greater number of elements. One may convince with the direct check, that for any area (except the smallest ones) there exist full nonredundant masks with different numbers of elements and that the number of maximal nonredundant masks for the given area A is usually more than one.

In these terms it is easy to formulate some results, new or known previously, and questions, yet expecting their solution.

1. How many different full nonredundant masks may be constructed in the square of the side n and in the hexagon of radius r? Such estimmations are absent in the literature.
2. How many maximal ones occur among them and how many elements they contain? Some estimations are contained in [6].
3. The same questions concerning to hexagon of radius r. Some reasons on this are presented in [7].
4. In what way one can effectively find the maximal nonredundant masks for the given square or hexagon? There is no answer to this question. However, the effective methods of constructing nonredundant masks with number of elements, close to the largest possible, are known [6,7].

The shortage of considerable theoretical results in this direction prompts an investigator to proceed an empirical way and set up machine experiments, able to shed some light on certain sides of these questions. Some results in this direction are presented in the next report.

Refetrence

1. Yu.V.Kornienko, V.N.Uvarov, "Signal accumulation at observation of an astronomical object through the turbulent atmosphere" (in Russian), Comptes Rendus of Academy of Science of Ukraine, Ser. A, No. 4, p.60-63, 1987.
2. F.Roddier, "Redundant versus nonredundant beam recombination in an aperture synthesis with coherent arrays", J. Opt. Soc. Amer., A4, No. 8, p.1396-1401, 1987.
3. R.C.Jenison, "A phase sensitive interferometer technique for the Fourier transform spatial brightness distributions of small angular extent", Mon. Notic. Roy. Astron. Soc. No. 118, p.278-384, 1958.
4. Yu.V.Kornienko, "Interferometric approach to the problem of turbulent atmosphere effects in astronomical observations" (in Russian), Kinematics and Physics of Stellar Bodies, v. 10, No. 2, p.98-106, 1994.
5. Yu.V.Kornienko, V.A.Leyferov, V.V.Pugach, "Informational efficiency of a multibeam interferometer in the observation of an object through the inhomogeneous medium " (in Russian), Radiofisika i Elektronika, v. 2, No. 2, p.132-136.
6. J.P.Robinson, "Golomb rectangles", IEEE Trans., IT-31, p.781-787, 1985.
7. L.E.Kopilovich, "Nonredundant apertures for optical interferometric systems: maximization of the number of elements", Journal of Modern Optics (in press), 1998.

OPTIMIZATION OF NON-REDUNDANT APERTURES ON INTEGER GRIDS

L.E.Kopilovich
Institute of Radiophysics and Electronics of NAS of Ukraine
12 Acad.Proskura St., Kharkov,310085,Ukraine
Tel: 380 572 448 689; Fax: 380 572 441 105; E-mail:ire@ire.kharkov.ua

Systems with non-redundant apertures (NRAs) are widely employed in astronomy, from optical up to radio wave range. At the same time, the problem of constructing the maximum-element NRAs is not yet solved. Such NRAs have been built on the small-size grids using methods of random search [1,2]; obviously, when applying such methods as well as statistical ones, the difficulty of obtaining a maximum-element NRA rapidly increases with the growth of the number of the elements.

One may consider a NRA as a collection of subapertures on an integer 2-d grid whose centres are located at pairwise different distances. At this point, one may solve the maximization problem using the methods of the combinatorial analysis. In principle, such a problem may be reduced to the case of a square grid since it is clear from general considerations that the maximum number of the NRA elements on a grid of convex form has to be approximately the same as on the equivalent square grid.

It is known that the problem of constructing a n-element NRA on a nxn grid S_n is not solved in the general case [3]; on the other hand, if $n = p$ is a prime, the p-element set [4]

$$\left\{\left(i, i^2 \bmod p\right)\right\},\ i = 0,1,\ldots,p-1, \tag{1}$$

forms a NRA on the grid S_p, and it was shown in [5] that one can build n-element NRAs on S_n with all $n \le 1000$. Thus, optimizing the NRA one implies the construction of such an aperture with the number of the elements exceeding n as much as possible.

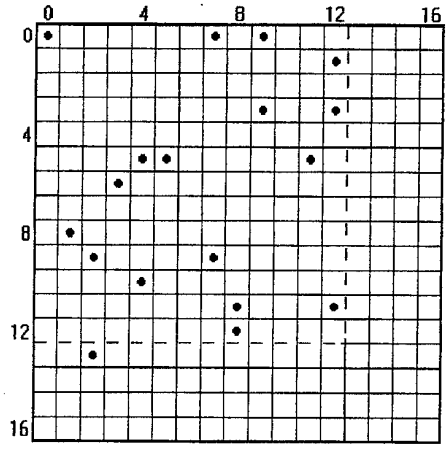
In the present report, the following approach to the construction of NRAs on 2-d grids is used. A definite class of non-redundant (in the above-stated sense) sets (NSs) is to be chosen, and these sets are then passed to the square grids so as to retain their non-redundancy. With this, the optimization is carried out by looking through the sets of the initial class.

As initial classes of NSs the cyclic difference sets (CDSs) [6] with the parameters $V, k; \lambda = 1$, and Bose-Butson relative difference sets [4] with the parameters $m, n; k; \lambda = 1$ were taken. Such CDSs exist for any $k = q+1$, where q is a power of a prime, while RDSs exist for any $k = q$; at this point, in the first case $V = k^2 - k + 1$, and in the second case $V = m \cdot n = k^2 - 1$. One can write these sets in the form of an increasing sequence $\{d_j\}$, with $d_1 = 0$; note also that $d_k < V$ and such a set forms a NS on a segment $[0, V-1]$. The important fact is that a set belonging to one of the DS types generates an ensemble of equivalent sets of the same type, with the same parameters V and k.

Now let us take such a segment in which a CDS or a RDS are arranged and fold it (by a procedure inverse to the scanning) to the square. One can prove by contradiction that with this, the set elements pass to a NS on the square, and since $d_k < k^2 - 1$ such a set goes into the S_k; and taking from the ensemble of the equivalent DSs those with relatively small d_k's one may expect to be successful in constructing a m-element NS in the grid S_n with $m > n$.

To define a NS having the maximum number of the elements, collections of equivalent CDSs and RDSs with given k were folded on square grids of various size, and then the number of the elements on them and on their subgrids were counted up. At this point, it was often found that the best results were obtained for inner squares. An example of such a construction is given in Fig.1 where a CDS with $k = 18$ was folded to the S_{17} and with this a maximum NS was obtained for S_{13}. A diagram presented in Fig.2 illustrates the dependence of a quantity $m - n$ on n where m is the maximum number of the NS elements on the grid S_n obtained in such a way (as dots, in Fig.2 are represented data of [2] with $n = 5,7,8,9$ which exceed our

results). Apparently, the true dependence of $m-n$ on n is to be more smoothed out, but its character reveals clearly: m is consistently exceeding n. The NS tables on square grids S_n with $n \le 50$ are given in [7].



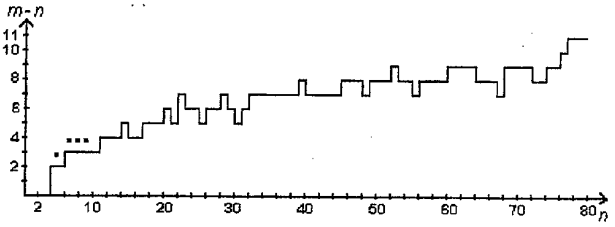
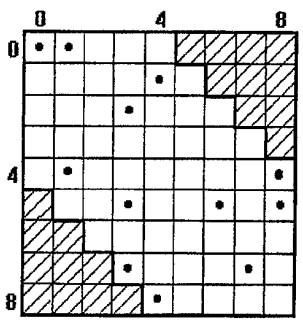


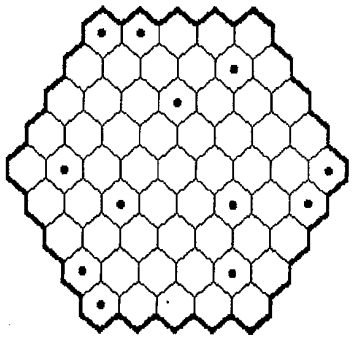
Fig. 2

Fig. 1

Constructing maximum-element NRAs on the hexagonal grids is also of interest because the hexagon is a better approximation to the circle than the square is. To construct a NRA on such a grid, one can make use of a scheme of transition from a square to a hexagon [8]. A singled out section of the square S_n in Fig.3a passes



a



b

Fig. 3

to the hexagon H_r of a radius r (with $n = 2r+1$) by means of a linear transfomation which retains the distinction in the distances between the set elements. Thus, for obtaining maximum NS on a hexagon, the preceding procedure is to be carried out, but now the number of the set elements located in this section of the square must be counted up.

The calculations show that maximum number of the elements of the NS on the hexagon H_r, with $r \le 25$, is not less than $2r+1$; with greater r, the quantity $s = m-(2r+1)$ gradually decreases, however, the dependence of $m-n$ on n, where now n is the side length of a square equivalent to H_r, is nearly the same as in Fig.2. Note that using CDS for constructing NSs on the hexagons gives one better results than employing RDSs.

In [7] Tables of NSs on the hexagons H_r, with $r \le 25$ are presented. Yet note that most of the maximum NRAs on the hexagons obtained with the method possess third-order symmetry, as one can see in Fig.3a or from the example of 61-element NRA on H_{30} (see Fig.4).

The method suggested may be applied to constructing NRAs on 2-d grids of any size, but the best results apparently would be achieved for grids equivalent to square grids S_n with n being close enough to some prime; as to large n lying far from the nearest prime, it seems likely that one would obtain substantially worser results.

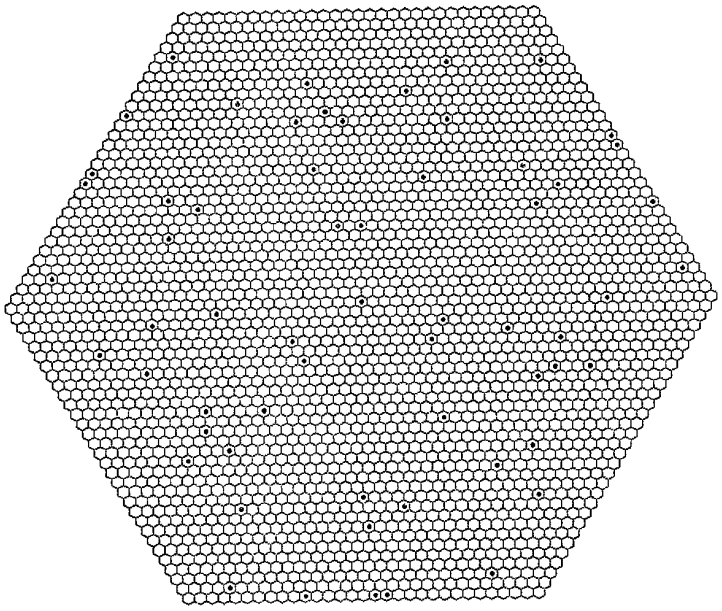


Fig. 4

References

1.Golay M., "Point arrays having compact nonredundant autocorrelations", JOSA, Vol. 61, No. 2, pp. 272-273, 1971.
2.Robinson J.P., "Golomb rectangles", IEEE Tr., Vol. IT-31, No. 6, pp. 781-787, 1985.
3.Golomb S.W., Taylor H., "Two-dimensional synchronization patterns for minimum ambiguity", IEEE Tr., Vol.IT-28, No. 4, pp. 600-604, 1982.
4.Elliott J. E. H., Butson A. T., "Relative difference sets", Illinois J. Math., Vol. 10, No. 4, pp. 517-531, 1966.
5.Kopilovich L. E., "Construction of nonredundant masks over square grids using difference sets", Opt. Communs, Vol. 68, No. 1, pp. 7-10, 1988.
6.Baumert L. D., "Cyclic Difference Sets", Lect. Notes in Math., Vol. 182, Springer, Berlin, pp.166, 1971.
7.Kopilovich L. E., "Nonredundant apertures for optical interferometric systems: maximization of the number of elements", J. Mod. Optics, 1998 (in Press)
8.Golomb S. W., Taylor H., "Constructions and properties of Costas arrays", PIEEE, Vol. 72, No. 9, pp. 1143-1163, 1984.

A CALCULATED CHOICE IN THE PROBLEM ON THE INPUT APERTURE OF AN OPTICAL MULTIBEAM INTERFEROMETER

L.V.Stulova
(12 Proskura st., Institute of Radio Physics and Electronics, National Academy of Sciences of Ukraine, Kharkiv, 310085, Ukraine)

Abstract.

In a numerical experiment on rational arrangement of receiving elements of the input aperture of an optical multibeam interferometer, the bounded bases of a one-fold covering ensuring registration of all spatial frequencies enbounded in a practically interesting small square area of the u, v-plane and only in it are designed.

For a case of a twofold covering of such an area, a more compact arrangement of receiving elements is found, than it is realized by the known Mills cross.

Introduction

In the present work, variants of economical arrangement of the receiving elements of the optical interferometer input aperture have been calculated, which can also be used in design of multielement radiotelescopes in both millimetric and submillimetric wave band.

The multibeam optical interferometer offered in Papers [1] and [2] measures the coherency function of the light flow in a given spatial area. The measurements are performed with the help of the primary (input) aperture that represents a system of pairs of subapertures for measuring the spatial spectral signal components. Investigation of problems on arrangement optimization for the subapertures in the optical interferometer was pursued by L.E.Kopilovich in paper [3].

Problem formulation, numerical results and discussion

In the Paper read, an integer square grid with the side of length n was constructed in the aperture plane on the basis of Paper [3]. To the grid there corresponds a domain of spatial frequencies in the u, v-plane (compare with Paper [4]). In certain grid nodes, dot subapertures are placed. An arrangement of the receiving aperture points that are to be occupied by the subapertures (basis) was calculated so that the system of all their point-to-point independent two dimensional intervals (differing either in length or in angle) fills the whole u, v-plane domain corresponding to the grid, without a gap (more detailed about the bases see in Papers [3], [5], [6]). On the basis choice being optimal, there evidences the aperture covering by as few number of the elements as possible. This quality is determined by the basis redundance factor. In the considered case of square grids, the basis redundance factor is measured by the ratio of number of basis elements to the length of the grid side (see Papers [3], [7]).

By the direct calculation with regard to the conditions imposed on quantitative distributions of the elements both on the grid "rows" and on its "columns", the bounded basis (i.e. a basis in which the elements do not come beyond the covered grid sides) containing as few quantity of elements as possible is found for a number of small grids.

For a grid with length of the side equal 4, the minimal number of the bounded basis elements appeared to be equal to 12 with 4 various possible variants of their arrangement (Fig. 1) that were determined. It was found out that with a smaller number of the elements of the bounded basis the whole region of the domain of spatial frequencies (u,v) corresponding to the given grid does not get covered. As it is visible from Fig. 1, three of the four found variants of basis are symmetric about the diagonal.

The coverings by symmetric variants of the basis can be extended to squares with any length n of the side of the grid, with preservation of their features in the sense that total of the elements of the symmetric bounded basis for the appropriate square with the side n does not exceed 3n and, accordingly, almost the same factor of redundancy not exceeding 3, and also a number of symmetric variants of basis no smaller than three is kept.

For a square with the side 5, 85 various arrangements for 15 elements of the basis were found (and again a smaller number of elements would not cover the whole grid); the factor of redundancy is equal 3, and again there were three (and only 3) variants symmetric about the diagonal.

For the square with the side 6, counting has shown that the known in the literature (see Paper [7]) bounded basis consisting of 16 elements has the unique variant of arrangement of elements and is minimal on their number.

Thereby, the given basis is factoring (i.e., it is equal to product of two onefold linear bases and is to be constructed by the following way: on two mutually crossed sides of the grid, either of the two being considered as a one-dimensional aperture, their one-dimensional linear bases are constructed, and other subapertures of the two-dimensional basis is to be located in points placed in the crossings of the grid lines going through the subapertures of the two linear bases). Note that all the calculated bounded bases found above (all except the last one) were not factoring, and the factoring bases for the appropriate squares had the greater number of elements.

With increasing n, the consumption of calculation time is sharply increased. In this connection exhaustion of all the basis variants would be too burdensome. The numerical experiment now was aimed to find a single basis arrangement variant. Thereby, the condition was maintained that the quantity of its elements should be as small as is possible.

Thus, it was numerically found that for a square with the side equal to 7 (3n is equal to 21) there is an asymmetrical basis including 20 elements (Fig. 2). Its redundancy factor is equal to 2.857. It was shown that with increasing n (the side of the grid) the number of the elements of the non-factoring bounded basis can really become smaller than 3n as well.

Let us pay attention to bases with an arrangement of the elements being similar to the first variant in Fig. 1. Here, as it is visible from that Figure, the number of the elements in the diagonal is equal to n -1. Calculation for a square with the side 8 showed that it is possible to reduce (relatively) by 1 the quantity of the elements located along the diagonal, i.e. the number of the elements in the diagonal will now be equal to 6; thereby, a part of the elements "leaves" the diagonal, but with a small "dispersion" about the latter (see Fig. 3). And the general number of basis elements will now be already equal 3n -1.

Further calculation showed that, for squares of greater length, the number of diagonal elements tends to decrease with simultaneous increase of their dispersion about the diagonal. For example, an arrangement of 48 basis elements of the square with the side that is equal to 17 (Fig. 4) is given. The factor of redundancy is equal to 2,824. Such calculation of the bounded bases is possible for squares with arbitrary large length of the side n when taken into account that a part of the basis elements remains in the diagonal, and the other part - in the grid sides. The given calculations (performed by the author for squares with side length up to 36) have not revealed a basis that would have a less number of elements than have the bases constructed in articles [5] and [7] by means of simple procedures of multiplication of linear bases or with the help of TDS (twodimensional difference sets). But it is necessary to take into account that the bases constructed in articles [5] and [7], exist not for an arbitrary square side lenth n, but only for certain n, and, in addition to that, the majority of them are not bounded, i.e. some of their elements are beyond the sides of the grid. And when it is desirable to have freedom in choice of the sizes and shape of the input aperture, especially when its compactness is required, as well as to have freedom in choice of the received spatial frequency band region, the results for bounded bases obtained by the calculations in the Paper read, can appear necessary.

It is pertinent to note here also some calculation results for a double covering of a square grid with the side 4. It was found that the minimal number of elements of such a basis (with no more than two basis elements being beyond the covered grid sides) is equal to 16, as well as in the Mills cross without the central element for correspondent u, v-plane. But as it is visible from Fig. 5, the given basis with redundancy factor equal to 4, which is identical to that of the Mills cross, also provides more compact arrangement of elements than in the latter. This basis can also be naturally extended both to squares with arbitrary side (number of the elements of such a basis will be no more than 4n), and also to rectangular grids with arbitrary sizes.

The author is sincerely indebted to L.E.Kopilovich for setting up the problem.

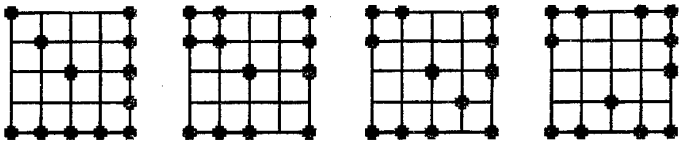


Fig. 1

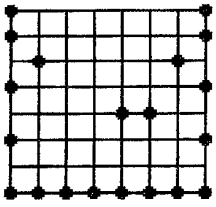


Fig. 2

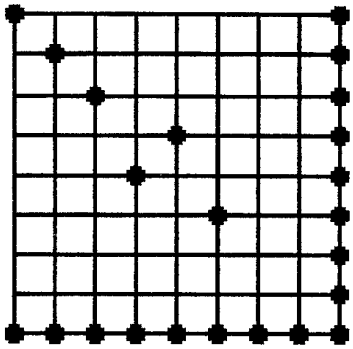


Fig. 3

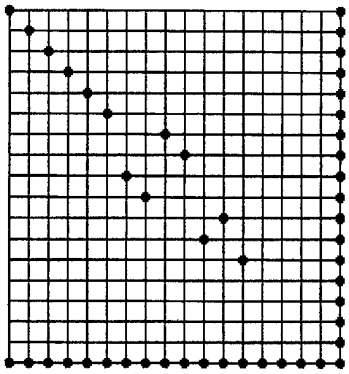


Fig. 4

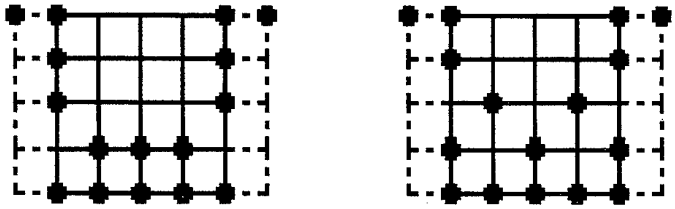


Fig. 5

References

1. Yu.V.Kornienko. "Interferometric Approach to the Problem on Turbulent Atmosphere Effects in Astronomical Observations. I", Kinematika i fizika nebesnych tyel., Vol. 10, No 2, pp. 98-102, 1994.
2. Yu.V.Kornienko , V.N.Uvarov. "Accumulation of the Signal During Observation of the Astronomical Object Through the Turbulent Atmosphere", Doklady AN USSR, Ser. A, No 4, pp. 60-63, 1987.
3. L.E.Kopilovich, "Optimum Synthesis of Optical Multibeam Interferometer for Viewing Through Inhomogeneous Atmosphere", Kinematika i fizika nebesnych tyel, Vol.11, No 5, pp. 85-91, 1995.
4. V.I.Turchin. "The Method of Aperture Synthesis; the Basic Relations and Processing of Information in Systems of the Aperture Synthesis (A review) // Izvestiya vuzov, Radiofizika, , Vol.26, No.11, pp.1335-1344, 1983.
5. L.E.Kopilovich. "Optimization of Two-Dimensional Systems Aperture Synthesis Systems", Radiofizika i elektronika, Vol.33, No.9, pp.1918-1923, 1988.
6. L.E.Kopilovich. "New Approach to Constructing Two-Dimensional Aperture Synthesis Systems", IEE Proc., Ser. F, Vol. 139, No 5, pp. 365-368, 1992
7. L.E.Kopilovich. "On Optimizing the Arrangement of Receiving Elements in Aperture Syntesis Systems", Izvestiya vuzov., Radiofizika, , Vol. 31, No.3, pp.347-352, 1988.

CONSTRUCTION OF NONREDUNDANT APERTURES FOR INTERFEROMETRIC RADIOTELESCOPE BY METHOD OF RANDOM SEARCH

Yu.V.Kornienko
Institute of Radiophysics and Electronics of National Academy of Sciences of Ukraine
310085, Kharkov, 12 Acad. Proskury St., Ukraine

The question about the utmost possibilities to increase the number of subapertures when constructing a nonredundant aperture in the given area of the square or hexagonal lattice is not still resolved. There exist effective regular methods of constructing such apertures (see the reference to the previous report.) However, it is not known, in what degree they enable one to approach the utmost possibilities. There also exist upper estimations of largest possible numbers of elements $S(n)$ in a square nonredundant aperture of side n for some values of n. However, there is no further information in the literature on behaviour of this function. It is known yet less about the function $H(r)$ determining the largest possible number of the elements in a nonredundant mask in the form of a regular hexagon of radius r.

For not so large values of n (up to 5 or 6) and r (up to 2 or 3) this question may be solved by the direct exhaustion of all full nonredundant masks and choosing from them maximal ones. It requires the volume of calculations though rather large but yet feasible for computers accessible at present. However, as the size of the aperture increases, the volume of such calculations grows quickly. It limits the prospect of such research for large n or r not only now, but also hereafter.

In this situation, as a compromise, the random search of full nonredundant masks may be accepted, and choosing among them ones containing the largest number of elements k. This way never guarantees finding masks with the largest possible k; on the other hand, it does not close this opportunity, what sometimes may be peculiar to some regular methods. By the results of such a search one may judge indirectly about number of maximal nonredundant masks for given n or r, investigating the probability of their repeating.

In this work an attempt is undertaken to investigate the possible number of elements for squares of side n up to 20 elements and hexagons of radius r up to 15 steps of the lattice. Excess of the values k obtained over n or $2r + 1$ are presented on fig. 1 and 2, and examples of configurations found, on fig. 3 and 4. Asteriscs mean the new values of k and points - the values known previosly.

As one would expect, the ratio of the number of masks with the largest k found, to total number of nonredundant masks found, for the given n or r decreases quickly with growth n or r. As a result, the search of maximal masks for $n > 30$ or $r > 15$ becomes difficult. Whereas, for majority of values of n and r shown on fig. 1 and 2, one may believe that the values of k found are the greatest possible, i.e. coincide with the corresponding values of functions $S(n)$ and $H(r)$.

The apearance of the plots on fig. 1 and 2 may give rise to suppose, that the functions $s(n) = S(n) - n$ and $h(r) = H(r) - (2r + 1)$, at least on the investigated part of the numerical axis, are monotonic and may be roughly approximated by the function $ln(N)$, N being the number of the mask elements. The deterioration of the results obtained at $r = 9$ and at the largest values of n and r on fig. 1 and 2 may be treated as a consequence of insufficient number of tests.

When several different masks was obtained for some values of n or r, one of them was chosen arbitrarily to display on fig. 3 and 4. Usually, a symmetric one was chosen in order to demonstrate such a possibility. The mask for $n = 7$ $k = 11$ is the only known and may be unique.

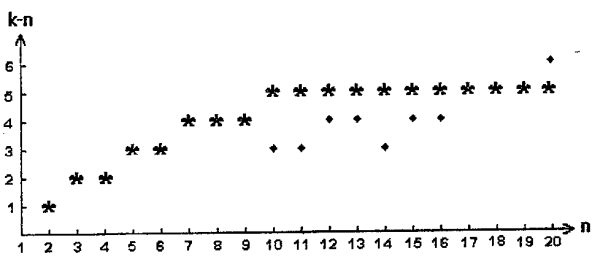


Fig. 1. Number of elements for square masks of side n.

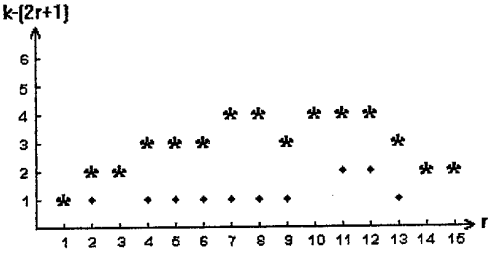


Fig. 2. Number of elements for hexagonal masks of radius r.

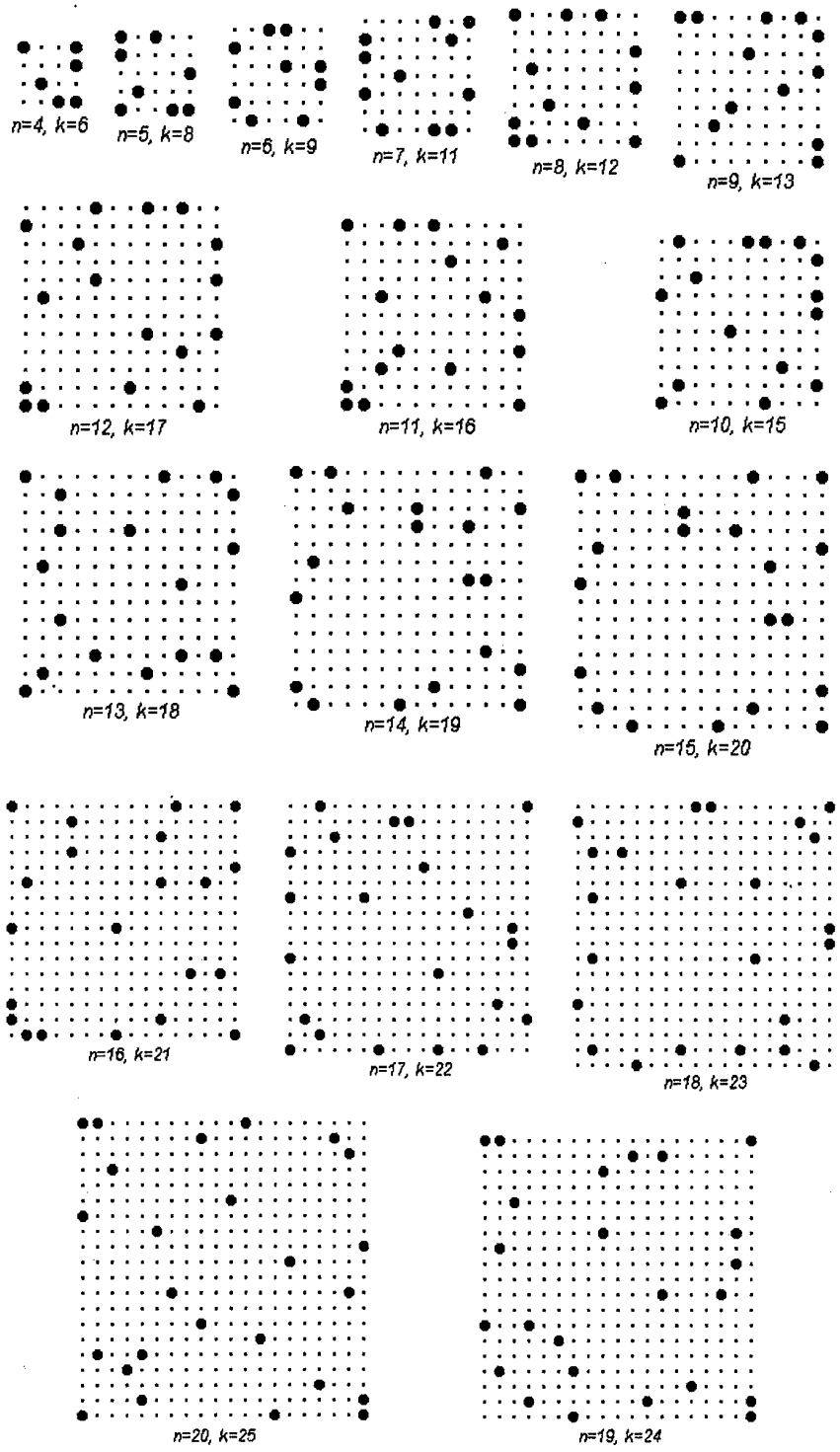


Fig. 3. Square nonredundant masks of side n from 4 to 20.

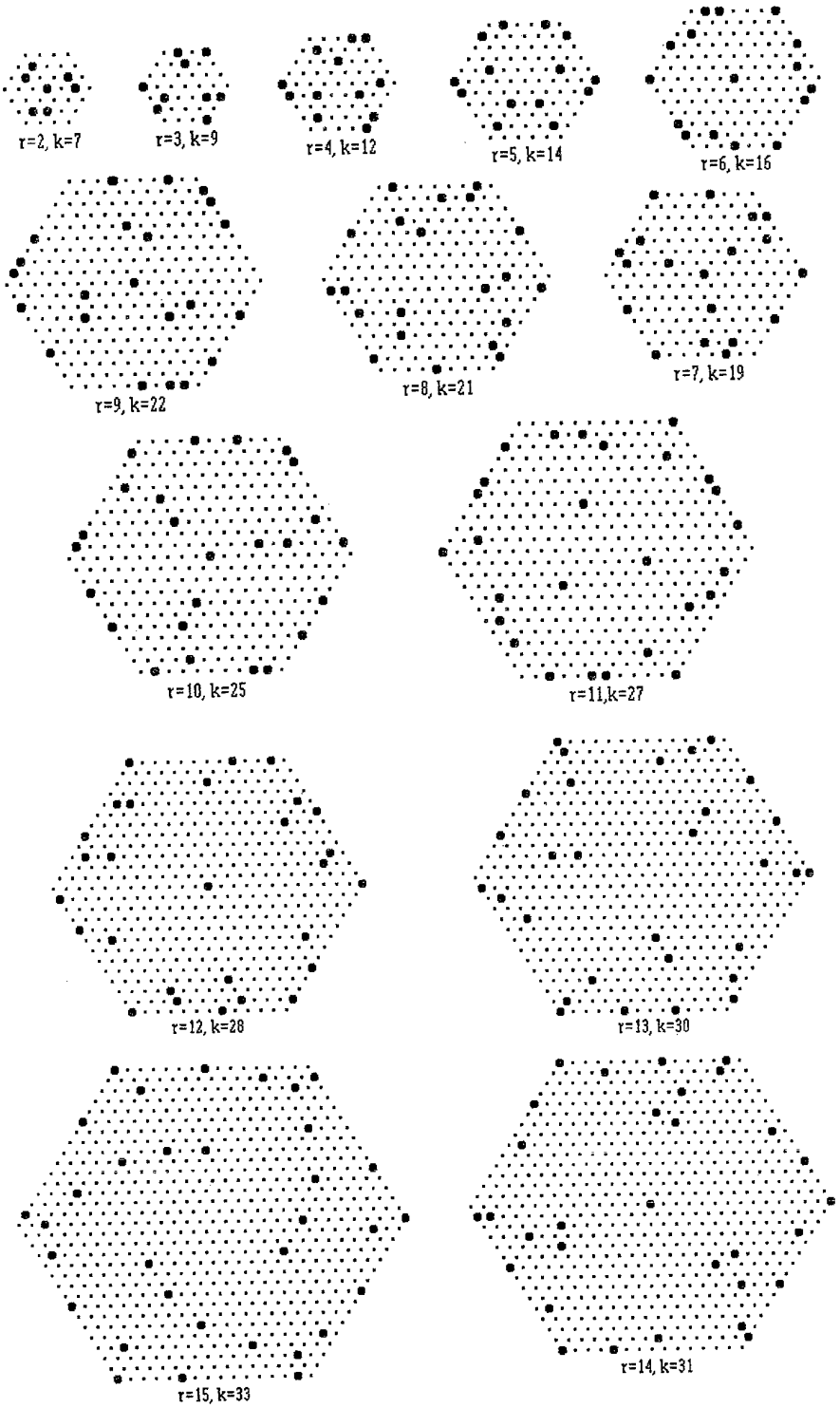


Fig. 4. Hexagonal nonredundant masks of radius from 2 to 15.

IMMUNITY OF THE INTERFEROMETRIC METHOD FOR IMAGE FORMATION TO PHASE DISTORTION OF THE WAVE FRONT

Yu.V.Kornienko
Institute of Radiophysics and Electronics of National Academy of Sciences of Ukraine
310085, Kharkov, 12 Acad. Proskury St., Ukraine

As it is known, at astronomical observation through the Earth atmosphere, the phase distortions of the wave front cause to restriction of angular resolution of the telescope with a value of order about one angular second. Subsequent processing of such images does not give radical solution of the problem. It indicates on necessity to search new ways for astronomical imaging. One of such ways is the interferometric method of image formation. It consists in measurement of coherence function by means of a multibeam interferometer (further development of the idea of Michelson's stellar interferometer) and enables one, due to redundancy of coding the information about the object in the wave coming from it, to exclude completely the unknown phase distortions and reconstruct the undistorted image. However, the question arises on its practical feasibility in real conditions of observation when the influence of the noise becomes actual.

The present work is devoted to quantitative evaluation of the information efficiency of multibeam interferometer and its immunity to the phase distortions.

1. Informativeness of an image. Let I be the true image of the object, J, the result of the coherence function measurement, with the values, correspondingly, I_i and J_i in i-th sample point, and R_{po} be the *a posteriori* density of probability, that the true image is I, if the result of measurement is J. Then the quantity of the information about the object, available as a result of observation, let be characterized by the Fisher's information matrix:

$$F_{ik} = E\frac{\partial^2 \ln R_{po}(I, J)}{\partial I_i \partial I_k}. \tag{1}$$

As the *a posteriori* density of probability $R_{po}(I, J)$ is given by the Bayes formula, and then comprises the *a priori* density of probability as a factor, substituting the Bayes expression for R_{po} in (1), one obtains $F_{ik} = F_{ik}^0 + F_{ik}'$, F_{ik}^0 being the quantity of *a priori* information (by Fisher), available before the observation, and F_{ik}' the quantity of information, obtained in the course of observation. Thus, this quantity is additive: if the series of independent observations is carried out, characterised by the values $F^1, F^2, ..., F^n$ of the matrix F, one's knowledge on the value I, obtained as a result of these observation is characterized by sum $F^1 + F^2 + ... + F^n$.

For practical purposes, when dealing with images, it is more convenient to construct, proceeding from the Fisher's information matrix, another additive quantity, scalar and non-dimensional, i.e. one-component and invariant to the chois of the basis in the space of images and to change of units, in which I is measured:

$$S = \sum_i \sum_k F_{ik} I_i I_k . \tag{2}$$

Here we shall be interested only in that part of information about the object, which is contained in the phases of the Fourier-components, and characterize it with the appropriate Fisher's matrix J.

2. Information efficiency of the interferometer. The system of equations for true phases φ_ν of the Fourier-transform of the astronomical object image consists of the equations of form

$$\varphi_\nu + \delta_i - \delta_k = \psi_{ik}, \tag{3}$$

δ_i and δ_k being the phase distortions on i-th and k-th subapertures, and ψ_{ik} the value of the coherence function phase, obtained as a result of measurement by this pair of the subapertures. This system is redundant, but under-determined, because three parameters in its solution are available for arbitrary choise: the additive constant in the phase distortions δ and general inclination of the phase front (two components). To exclude this uncertainty, let supplement the system, consisting of the equations (3), with conditions of equality of these parameters to zero:

$$\lambda \sum \delta_i = 0, \quad \mu \sum x_i \delta_i = 0, \quad \mu \sum y_i \delta_i = 0, \tag{4}$$

x_i, y_i being the coordinates of i -th subaperture. Let write the system obtained in the form

$$A|X\rangle = |Y\rangle, \tag{5}$$

where X is the vector with components being the required non-disturbed phases φ and the atmospheric phase distortions δ, Y is the vector, consisting of the values ψ measured, A is a matrix determined completely by the configuration of the interferometer, i.e. space arrangement of its subapertures. (All the elements of this matrix, except corresponding to (4), are equal 1, -1 or 0.) Right part of this system, being the result of measurement, contains the random errors, which are supposed to be distributed normally and independently with the same variance. The optimal way to solve it is the method of least squares. For this let multiply both parts of (6) on A^+, the matrix, conjugate with A, obtaining the system

$$M|X\rangle = |Z\rangle, \tag{6}$$

Its solution is the most probable value of vector X. Here $M = A^+A$, $|Z\rangle = A^+|Y\rangle$.

If the aperture of the interferometer consists of n subapertures and transmits l of space frequencies, vector X consists of $l+n$ components (l phases of the image Fourier-components and n phase distortions), vector Y, of $n(n-1)/2$ components, matrix A, of $n(n-1)/2$ lines. and columns.

Let the right part of (5) be known with error $|\eta\rangle$. It results in apearance of the error $|\xi\rangle$ in the solution of the system (6), which, by virtue of linearity (6), satisfies relation $M|\xi\rangle = A^*|\eta\rangle$, from which follows $|\xi\rangle = M^{-1}A^*|\eta\rangle$. Therefore, the covariance matrix $C = \overline{|\xi\rangle\langle\xi|}$ of this errors is of the form

$$C = M^{-1}A^*\overline{|\eta\rangle\langle\eta|}AM^{-1}, \tag{7}$$

where the line means averaging over the ensemble of realizations of the registration noise. The matrix $\overline{|\eta\rangle\langle\eta|}$ is the covariance matrix of the errors $|\eta\rangle$. At the assumption accepted here on the statistical properties of $|\eta\rangle$, it is equal DE, where E is the unit matrix, and D the variance of the vector $|\eta\rangle$ components error. Therefore and by virtue of (7)

$$C = DM^{-1}, \tag{8}$$

where D characterizes the intensity of the registration noise, and M^{-1} the influence of the interferometer configuration on the error of X. However, we are interested not of all unknowns, taking part in the system (6), but only of that of them, which relate to the object under observation, i.e. φ. The covariation matrix of their errors is equal

$$C_\varphi = DG, \tag{9}$$

where G is submatrix of M^{-1} and may be obtained from it by deletion of all lines and columnes, associated with unknown δ. As the errors are distributed normally, the Fisher's matrix F required is inverse to C_φ and equal G^{-1}/D.

The matrix $H = G^{-1}$ depends only on the configuration of the interferometer and characterizes its efficiency at observation through the atmosphere. We shall name it the information efficiency matrix.

The direct calculation of this matrix for some simplest interferometer configurations has shown that immunity of the method to the influence of the atmospheric distortions is unexpectedly high.

However, the question arises, in what degree this fact may be related to other configurations of the input aperture. To answer to it, the way of analytical calculation of the matrix H is required, that presents certain difficultiesbecause for the interferometer designed rationaly and consisting of tens of subapertures, the number of the elements in this matrix amounts to $10^5 - 10^6$.

3. The explicite expression for the interferometer information efficiency. On the basis of the said above let present the matrix M, the inverse one to it, and the unit matrix E in the form

$$M = \begin{pmatrix} \Phi & B \\ B^+ & \Delta \end{pmatrix}, \quad M^{-1} = \begin{pmatrix} H^{-1} & \beta \\ \beta^+ & \gamma \end{pmatrix}, \quad E = \begin{pmatrix} E_\varphi & 0 \\ 0 & E_\delta \end{pmatrix}, \tag{10}$$

where E_φ and E_δ are the unit matrices respectively above the subspace of the phases φ and the one of the distortions δ of the space of the unknowns. Then the identity $MM^{-1} = E$ may be written in the form

$$\Phi H^{-1} + B\beta^+ = E_\varphi, \quad \Phi\beta + B\gamma = 0, \tag{11}$$

$$B^{+}H^{-1}+\Delta\beta^{+}=0,\quad B^{+}\beta+\Delta\gamma=E_{\delta}, \tag{12}$$

where $\Delta = nE_{\delta} - (1-\lambda^2)U + \mu V$, U is a matrix, consisting of the units only, and V - matrix with elements $V_{ik} = x_i \cdot x_k$. Solving this equation system relatively to H (at $\mu = 0$), the expression (irrespective of λ) is obtained

$$H = \Phi - \frac{1}{n} B B^{+}. \tag{13}$$

The calculation of this matrix elements requires only the account of the mutual disposition of the subapertures and has merely geometrical nature. It yields the result

$$H_{ik} = \Phi_{ik} - w_{ik} / n, \tag{14}$$

where w_{ik} is the "mutual weight" of the i-th and the k-th space frequencies, which is an easily computable characteristic of the configuration, and and always satisfies the relation

$$w_{ik} \le \min(w_i, w_k), \quad w_{ii} = w_i. \tag{15}$$

w_i being the number of the subapertures, participating singly in transmission of the i-th space frequency.

4. The interferometer immunity factor. The immunity of the interferometer to phase distortion may be characterized by the local immunity factor on the i-th space frequency,

$$k_i = H_{ii} / \Phi_{ii} \tag{16}$$

and integrated factor of immunity, related to all space frequencies in aggregate (in the assumptions of equal information importance of all space frequencies)

$$K = SpH / Sp\Phi. \tag{17}$$

These factors by virtue of the definitions and (18) satisfy inequality

$$0 < k_i \le 1, \quad 0 < K \le 1, \tag{18}$$

the equality being reached only in absence of the atmosphere (because in this case $H = \Phi$).

As the element Φ_{ii} is equal to multiplicity m_i of transmission of the i-th space frequency by the interferometer, from (14) at $j = i$ one may obtain

$$k_i = 1 - w_i / m_i n \tag{19}$$

From here, in particular, follows (taking into account $w_i \le 2m_i$), that for any rigid configuration of the interferometer (i.e. such one which leaves no degrees of freedom in the solution of the system (6), except that are inevitable for all configurations) the inequality takes place

$$k_i \ge 1 - 2/n \tag{20}$$

The similar inequality may be obtained also for the integrated immunity factor K.

From this one can see that the interferometer of rigid configuration, containing tens of subapertures, is practically tolerant to interfering influence of the Earth atmosphere.



MM AND SUBMM DEVICES BASED ON THE PLANAR AND QUASI-OPTICAL TRANSMISSION LINES (Passive and Active Components, Antennas)

Preceding Page Blank

A New De-embedding Method for Microstriplines with Coaxial Adapters

Jürgen Marquardt and Jens Passoke
Institut für Hochfrequenztechnik der Universität Hannover
Appelstr. 9A, 30167 Hannover, Germany, Tel.: +49 511 762 5267, Fax.: +49 511 762 4010
e-mail: marquardt@mbox.hft.uni-hannover.de, passoke@ mbox.hft.uni-hannover.de

Abstract

A new de-embedding method for microstriplines with coaxial adapters is suggested. The method uses the field calculation to determine the scattering parameters of the coaxial adapter. Based on these datas an equivalent circuit of lumped elements is derived, which describes the physical reality of the adapter. This de-embedding method also provides a definition of the characteristic impedance of the microstripline. The values of the characteristic impedance presented in this paper have been verified experimentally and differ from those derived by two dimensional definitions of characteristic impedance.

Introduction

Modern network analyzers cover the frequency range from dc to 50 GHz and even higher with a singular coaxial port. Planar circuits, for example patch antennas or MMIC's, can be measured with the help of adapters between the coaxial and microstrip lines, if the characteristics of the adapter two-port and the characteristic impedance of the microstrip line are known. A typical measurement configuration is shown in figure 1. The standard calibration method of such adapters uses the known values for the characteristic impedance on both sides of the adapter two-port. This is a valid procedure for the coaxial line, but the characteristic impedance of the microstrip line depends on frequency because of the inhomogeneously filled cross-section. The characteristic impedance therefore used to be calculated separately by using the secondary values voltage, current and transmitted power, calculated from a two dimensional analysis of the microstripline [1], [2] and [3]. Another method uses the determination of characteristic impedance via the effective dielectric constant [4]. However, in [5] and [6] another procedure is suggested: the determination of the characteristic impedance with the help of a three-dimensional field calculation in a line excited by an idealized voltage source.

We would like to suggest yet another method which can be employed for the de-embedding of the planar circuits without any previous definition of characteristic impedance. The first step is the determination of the scattering parameters of the adapter. This can be done by measurement or numerical calculation of the three-dimensional electromagnetic field. The next step is the creation of an equivalent circuit of lumped elements corresponding to the physics of the adapter. The best fit to the scattering parameters is found by variation of each element together with the characteristic impedance of microstripline. So this procedure delivers not only the element values but first of all a definition of the characteristic impedance, which requires the knowledge of scattering parameters of an adapter from TEM transmission line to microstripline but needs no reference to a two-dimensional definition of current or voltage.

The De-embedding Method

The data from the device under test (DUT, see figure 1) connected with homogenous microstriplines are modified by the electromagnetic characteristics of the port discontinuities. Therefore the first step is to determine the scattering matrices of the ports and to convert them into chain matrices. By inverting these chain matrices and pre- and postmultiplying the measured matrix of the total circuit with the inverted matrices the chain matrix of the DUT can be determined. But this can be done only, if the scattering matrix of the ports and the characteristic impedance of the microstripline is known.

One possibility to characterize the port discontinuities is to measure the complex scattering parameters of the whole configuration (figure 1). By transforming the data into the time domain and gating them, solely the impulse response of the port is derived. After retransformation into the frequency domain one gets the scattering matrix of the port. An alternative is the numerical computation of the electromagnetic field of the transition to get the scattering matrix. This was done using the High Frequency Structure Simulator (HFSS) from Hewlett Packard. According to the transmission line theory lumped elements can only approximate the electromagnetic behaviour of a homogenous line, if the length fulfills the following condition:

$$l \leq \frac{\sqrt{6}\lambda}{2\pi} \qquad (1)$$

For this a abrupt transition between a 50 Ω coaxial line (3.58 mm Semi-Rigid filled with PTFE) and a 50 Ω microstripline (1.27 mm substrate height with the relative permittivity ε_r=10.8) was used. Considering the length of the field distortion into the homogenous lines, the use of lumped elements describing the discontinuity is valid up to 10 GHz. In figure 2 the scattering parameters of the transition between the coaxial line and the microstripline are presented in this frequency range (1 to 10 GHz). They were calculated and measured in planes with a distance to the transition plane being larger than the length of the field distortion and then transformed into the transition plane. The difference between measurement and simulation is lower than 0.011.

The simplest circuit to describe the field distortion in the transition plane consists of two lumped elements, one capacity and one inductivity. The determination of these elements was done by adapting the scattering parameters using the following error condition:

$$\zeta = 1/(2i)\sum_i \sqrt{\sum_{kj} |\underline{S}_{kj} - \underline{S}_{kj,LC}|^2}, \qquad k,j = 1,2 \qquad (2)$$

In the case of frequency independent elements and 10 frequency points, there are 12 variables to optimize. This was done by using a Quasi-Newton-Algorithm. The results for the scattering parameter $\underline{S}_{11}$ are given in figure 3, which containes only a part of the Smith-Diagram for passive circuits. In principle there are four possibilities to create a circuit with two lumped elements, that is: LC or CL both with frequency dependent (a) or constant (u) element values. The value for ζ is lower than 0.0004 with frequency dependent lumped elements, and lower than 0.0079 with constant lumped elements.

Results

The results for the lumped elements of the abrupt transition are presented in figure 4 and 5. The inductivity shows negative values for low frequencies. In the region of the field distortion the linear electric constants of the homogenous transmission lines are no longer valid, so the negative inductivity represents a correction factor.

Figure 6 shows the characteristic impedance of microstripline based on the TEM equivalent definition. The deviation between the different configurations is lower than 0.4 Ω, so they are plotted as one curve. Obviously an equivalent circuit with only two elements is sufficient to describe the transition and because of the smallness of these values the configuration is arbitrary. For comparison curves are shown in figure 6, which are gained via the traditional two dimensional definitions [1], ...[3] and via the effective relative permittivity [4]. However, it can be generalized that the three dimensional definition leads to the best value of the characteristic impedance and with the knowledge of this characteristic behaviour of the microstripline the de-embedding of other transitions with a longitudinal dimension is possible.

References

[1] Owens R. P.; „Predicted Frequency Dependence of Microstrip Characteristic Impedance Using the Planar-Waveguide Model", Electronic Letters Vol. 12, No. 11; pp. 269-270; 1976

[2] Pues, H. F., Van De Capelle, A. R.; „Approximate Formulas for Frequency Dependence of Microstrip Parameters"; Electronic Letters Vol. 16, No. 23; pp. 870-872; 1976

[3] Jansen, R. H., Kirschning, M.; „Arguments and an Accurate Model for the Power-Current Formulation of Microstrip Characteristic Impedance"; AEÜ 37; pp. 108-112; 1983

[4] Hammerstad, E.; Jensen, O.; „Accurate Models for Microstrip Computer Aided-Design"; IEEE MTT-S Internat. Symp. Dig. ; pp. 407-409; 1980

[5] Rautio, J. C.; „A De-Embedding Algorithm for Electromagnetics"; MIMICAE Vol. 1 No. 3; pp. 282-287; 1991

[6] Zhu, L..; Wu, K.; „Revisiting Characteristic Impedance and ist Definition of Microstrip Line with a Self-Calibrated 3-D MoM Scheme"; IEEE Microwave and Guided Wave Letters; vol. 8 no. 2; pp. 87-89; 1998

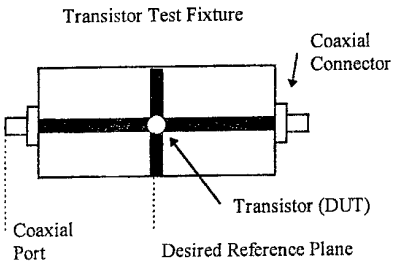


Figure 1: Example for an embedded DUT with coaxial connectors

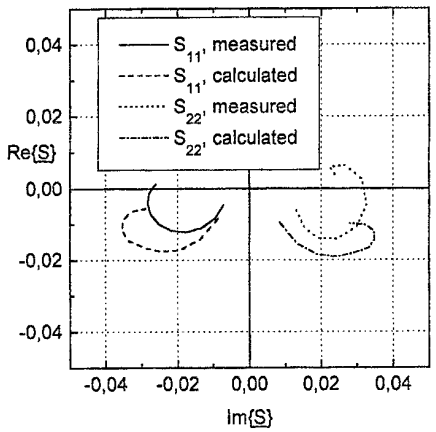


Figure 2: Measured and calculated scattering parameters of the considered adapter

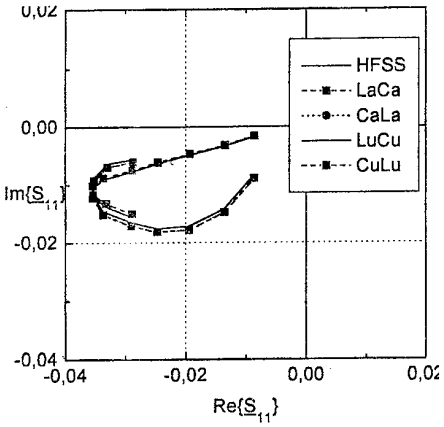


Figure 3: Calculated and adapted scattering parameter $\underline{S}_{11}$

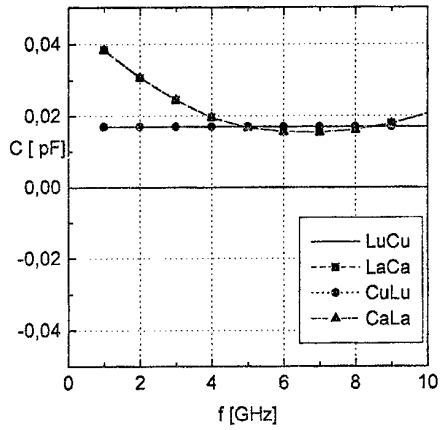


Figure 4: Lumped capacity

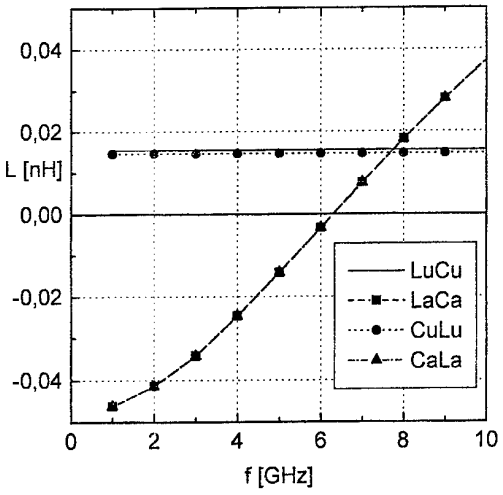


Figure 5: Lumped inductivity

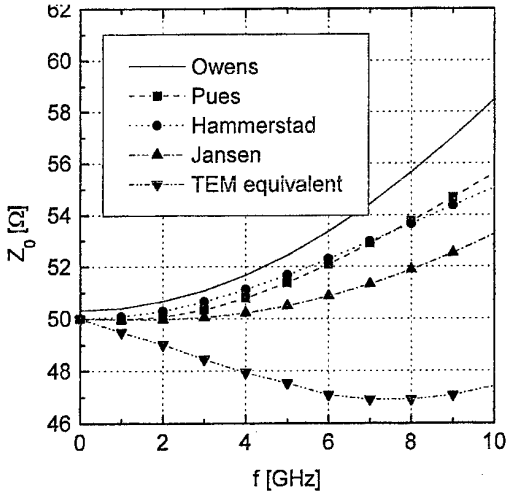


Figure 6: Characteristic impedance of microstripline

COUPLED-MODE FORMULATION FOR DOUBLE-STRIP NRD WAVEGUIDES BASED ON SINGULAR PERTURBATION TECHNIQUE

Koki WATANABE and Kiyotoshi YASUMOTO
Department of Computer Science and Communication Engineering, Kyushu University
6-10-1 Hakozaki, Higashi-ku, Fukuoka, 812-8581 Japan
Tel. +81-92-642-3858, Fax +81-92-631-4839, E-mail koki@csce.kyushu-u.ac.jp

The phenomena of wave propagation in coupled waveguides are commonly understood by the coupled-mode theory. In this theory, the coupling effects are characterized only by the coupling coefficients between the modal amplitudes, and therefore it can be easily applied even when the number of waveguides increases. Several formulations of the theory have been known such as the conventional coupled-mode theory (CCMT) and improved coupled-mode theory (ICMT)[1]. The total fields are expressed as a linear combination of the individual waveguide modal fields in these formulations. Therefore, these formulations are correct in first-order of perturbations, so that they are just valid within the weak-coupling region.

However, the strong-coupling is useful for miniaturizing the devices based on the coupled waveguides because of the small coupling length. Also, it yields wider bandwidth performance. For the analysis in the strong-coupling region, the coupled-mode formulation based on singular perturbation technique was proposed for coupled optical waveguides[2]. This formulation includes higher-order corrections of the perturbed modal fields and enables us to evaluate effects of higher-order rather than the first-order perturbations. In this paper, we apply this formulation to the analysis of a double-strip nonradiative dielectric (NRD) waveguide. NRD waveguides[3] are currently the topic of major interest in millimeter-wave integrated circuits, and the double-strip NRD waveguide is one of the most important components in applications.

The structure under investigation is illustrated in Fig. 1. It consists of two straight dielectric strips a and b with widths $2d_a$ and $2d_b$, and relative permittivities ε_a and ε_b, respectively. They are held between two parallel perfect conductor walls with separation distance t and situated parallel to each other with a separation distance $s_a - s_b - d_a - d_b$ in a surrounding dielectric with relative permittivity ε_s. Let us take the z-axis along the direction of propagation, and x-axis parallel to the conductor surfaces. We shall consider only guided transverse magnetic (TM) waves propagating in the positive z-direction. Each strip is supposed to allow only one fundamental mode to propagate. In our analysis, the time-harmonic wave is considered and the permeability is assumed to be uniform and equal to that of free space.

Considering that the tangential components of the electric field are zero on $y = 0, t$, the y-component of the magnetic fields in $0 \le y \le t$ are expressed as $\psi(x,z)\sin k_y y$ with $k_y = \pi / t$. Then, the wave function $\psi(x,y)$ for the total field satisfies the following Helmholtz equation:

$$\left[\frac{\partial^2}{\partial x^2} + \frac{\partial^2}{\partial z^2} - {k_y}^2 + {k_s}^2\left(1 + \Delta\varepsilon_a w_a(x) + \Delta\varepsilon_b w_b(x)\right)\right]\psi(x,z) = 0, \qquad (1)$$

where, for $\nu = a, b$,

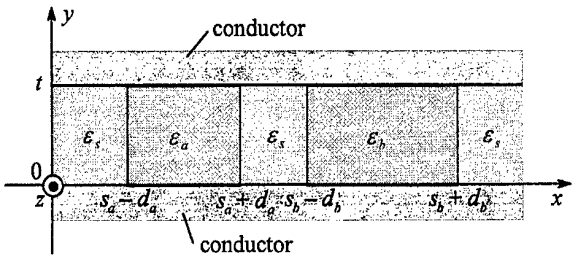


Figure 1: Cross-sectional view of a double-strip NRD

$$\Delta\varepsilon_\nu = \frac{\varepsilon_\nu - \varepsilon_s}{\varepsilon_s}, \quad w_\nu(x) = \begin{cases} 1 & \text{for} \quad |x - s_\nu| \le d_\nu \\ 0 & \text{for} \quad |x - s_\nu| > d_\nu \end{cases}, \tag{2}$$

and k_s is the wavenumber in the cladding. We decompose the wave function $\psi(x,y)$ as

$$\psi(x,z) = \psi_a(x,z) + \psi_b(x,z), \tag{3}$$

and then Eq. (1) is also decomposed as

$$\left[\frac{\partial^2}{\partial x^2} + \frac{\partial^2}{\partial z^2} - k_y{}^2 + k_s{}^2\left(1 + \Delta\varepsilon_\nu w_\nu(x)\right)\right]\psi_\nu(x,z) = -\delta k_s{}^2 \Delta\varepsilon_\nu w_\nu(x)\psi_\mu(x,z) \tag{4}$$

with $\nu, \mu = a, b$, $\nu \neq \mu$. The right side term of Eq. (4) expresses the effect from the adjacent waveguide, and it is treated as a perturbation term. Accordingly, we introduced a nondimensional small parameter δ to identify that this term starts from the order of δ in magnitude. From the uniqueness theorem, it is verified that the composite wave function $\psi(x,z)$ satisfies Eq. (1) when the decomposed wave functions $\psi_a(x,z)$ and $\psi_b(x,z)$ are solutions to Eq. (4). We seek an approximate solution in the form of a Poincaré-type asymptotic expansion:

$$\psi_\nu(x,z) = \sum_{n=0}^{\infty} \delta^n \psi_{\nu,n}(x,z). \tag{5}$$

The propagation wave fields in coupled waveguides are characterized by more than two physical scales in the propagation direction. They are the space scales of the wavelength combined into the basic oscillations and the space scales of the slower drifts in the modal amplitude due to coupling. To maintain the asymptoticness of the perturbation expansion, we introduce the multiple space scales: $z_n = \delta^n z$ ($n = 0, 1, 2, \cdots$). Substituting Eq. (5) into Eq. (4), expanding, and equating coefficients of equal powers of δ, we can derive the respective order of δ^n of perturbation by equating the coefficient of each power of δ to zero. The equations in the respective orders are obtained as

$$L_\nu \psi_{\nu,n}(x, z_{s,0}) = \begin{cases} 0 & \text{for} \quad n = 0 \\ -\sum_{l=1}^{n} T_l \psi_{\nu,n-l}(x, z_{s,0}) - M_\nu \psi_{\mu,n-1}(x, z_{s,0}) & \text{for} \quad n \ge 1 \end{cases} \tag{6}$$

where the linear operators appeared in this equation are defined as follows:

$$L_\nu \equiv \frac{\partial^2}{\partial x^2} + \frac{\partial^2}{\partial z_0{}^2} - k_y{}^2 + k_s{}^2\left(1 + \Delta\varepsilon_\nu w_\nu(x)\right) \tag{7}$$

$$T_n \equiv \sum_{l=0}^{n} \frac{\partial^2}{\partial z_l \partial z_{n-l}}, \quad M_\nu \equiv k_s{}^2 \Delta\varepsilon_\nu w_\nu(x) \tag{8}$$

and the notation $z_{s,n}$ denotes the sequence of the space scales: $z_n, z_{n+1}, z_{n+2}, \cdots$.

Noting that each strip allows only one fundamental mode to propagate, the solution to the zero-order wave equation can be expressed as

$$\psi_{\nu,0}(x, z_{s,0}) = a_\nu(z_{s,0}) u_{\nu,0}(x), \tag{9}$$

where $a_\nu(z_{s,0})$ is the modal amplitude and $u_{\nu,0}(x)$ is the zero-order modal profile function of the waveguide ν. The dependence of $a_\nu(z_{s,0})$ on z_0 is given by $a_\nu(z_{s,0}) = a_\nu(0, z_{s,1}) e^{-j\beta_\nu z_0}$ with the propagation constant β_ν. For the higher-order problem, the wave equations are given by inhomogeneous equations. Generally speaking, inhomogeneous equations are soluble only when the solvability conditions[4] are satisfied. The solvability condition for the n-th order wave equation is given in the form of

$$\frac{\partial}{\partial z_n} a_\nu(z_{s,0}) = -j\chi_{\nu a,n} a_a(z_{s,0}) - j\chi_{\nu b,n} a_b(z_{s,0}), \tag{10}$$

where $\chi_{pq,n}$ ($p, q = a, b$) give the n-th order coupling coefficients and can be derived by straightforward calculation. Using Eq. (10) and letting $\delta = 1$, we can derive the dependence of $\boldsymbol{a} = \begin{pmatrix} a_a & a_b \end{pmatrix}^t$ on the original space scale z as

Table 1: Error rates of the approximate propagation constants of double-strip NRD waveguides with $\varepsilon_a = \varepsilon_b = 9.5$, $\varepsilon_s = 1.0$, $t = 2.25$ mm, $2d_a = 2d_b = 1.0$ mm, and varying waveguide separation for frequency $f = 60$ GHz.

$s_a - s_b$ [mm]	β_{ex} [m^{-1}]	Error Rate			
		$\beta^{(0)}$	$\beta^{(1)}$ (CCMT)	$\beta^{(2)}$	ICMT
1.5	2689.5531	3.4×10^{-2}	6.2×10^{-3}	7.3×10^{-4}	1.0×10^{-2}
2.0	2622.8564	9.7×10^{-3}	4.5×10^{-4}	5.0×10^{-5}	1.4×10^{-3}
2.5	2605.3722	3.0×10^{-3}	3.2×10^{-5}	2.2×10^{-6}	1.6×10^{-4}
3.0	2600.0301	9.6×10^{-4}	2.0×10^{-6}	8.2×10^{-8}	1.7×10^{-5}
1.5	2534.7609	2.5×10^{-2}	4.9×10^{-3}	9.2×10^{-4}	2.3×10^{-2}
2.0	2574.5205	8.9×10^{-3}	4.4×10^{-4}	4.9×10^{-5}	1.8×10^{-3}
2.5	2589.8708	3.0×10^{-3}	3.3×10^{-5}	2.1×10^{-6}	1.5×10^{-4}
3.0	2595.0543	9.6×10^{-4}	2.0×10^{-6}	8.2×10^{-8}	1.7×10^{-5}

$$\frac{\partial}{\partial z}\boldsymbol{a} = -j\boldsymbol{K}\,\boldsymbol{a}\,, \tag{11}$$

where the (p,q)-entry of the matrix $\boldsymbol{K}$ is $\beta_p \delta_{pq} + \sum_{n=1}^{\infty} \chi_{pq,n}$.

In order to estimate numerically the accuracy of the present formulation, we consider a specific example of the double-strip NRD waveguide with $\varepsilon_a = \varepsilon_b = 9.5$, $\varepsilon_s = 1.0$, $t = 2.25$ mm, $2d_a = 2d_b = 1.0$ mm, and frequency $f = 60$ GHz. Table 1 shows the error rates of the approximate propagation constants as compared with those of exact theory for varying waveguide separations. The approximate propagation constants $\beta^{(n)}$ are the eigenvalues of $\boldsymbol{K}$ truncated with n terms, and the error rates are calculated by

$$(\text{error rate}) \equiv \frac{\beta^{(n)} - \beta_{ex}}{\beta_{ex}} \tag{12}$$

with the exact propagation constant β_{ex}. It is observed that our results are in good agreement with the exact ones and that the accuracy increases by improving the approximations. Alternatively, the present formulation is compared with ICMT formulated in Ref. 1. For CCMT, the coupled-mode equations becomes equal to those of the present formulation with first-order correction. The present formulation with second-order correction shows superior results to both of CCMT and ICMT. Table 1 shows that ICMT is inferior even to the CCMT. Because ICMT is formulated for optical waveguides and it is therefore valid when the permittivity difference between the core and the cladding is small.

In this paper, we have analyzed a double-strip NRD waveguide by using the coupled-mode formulation based on singular perturbation technique. The results of the present formulation are in good agreement with the exact one, and the error rates decrease according to the successive order of perturbation. Also, we compared the results with those of CCMT and ICMT, and it is shown that the present formulation with second-order corrections is superior to both of CCMT and ICMT. The analytical steps of the present formulation are straightforward, and therefore the coupled-equations are systematically derived in respective order of perturbation.

References

1. W. P. Yuen, "On the Different Formulations of the Coupled-Mode Theory for Parallel Dielectric Waveguides", J. Lightwave Technol., Vol. 12, No. 1, pp. 82-85, 1994.
2. K. Yasumoto, "Coupled-Mode Formulation of Parallel Dielectric Waveguides Using Singular Perturbation Technique", Microwave and Opt. Technol. Lett., Vol. 4, No. 11, pp. 486-491, 1991.
3. T. Yoneyama and S. Nishida, "Nonradiative Dielectric Waveguide for Millimeter-Wave Integrated Circuits", IEEE Trans. Microwave Theory and Tech., Vol. MTT-29, No. 11, pp. 1188-1192, 1981.
4. A. H. Nayfeh, "Introduction to Perturbation Techniques", Wiley, New York, 1981.

A Microstrip Array Fed by a Non-Homogeneous Stripline Feeding Network

Naftali I. Herscovici* *Cushcraft Corp.*, Manchester, NH
Nirod K.Das, *Weber Research Inst., Polytechnic Univ.*, Farmingdale, New York
Josh Klugman, *NCC Norsall*, New Rochelle, New Jersey

1. Introduction

Miniaturization of microwave and millimeter wave systems often includes the integration of the antenna with the transceiver. One of the array configurations most suitable for such integration is the aperture coupled microstrip array. The radiating element present a number of advantages over the microstrip fed, or probe fed patches:

- The crosspolarization level is very low (theoretically null in the principal planes).
- The typical effects of the interaction between the radiating elements and the corporate feeding network (shift in the resonance frequency, radiation of the feeding network, etc.) are eliminated.

The separation between the radiating elements and the feeding network can lead in many cases to a multilayer structure that include the stripline as the main transmission line. The special case in which the feeding network is a one-layer microstrip circuit, was extensively treated in the literature [1,2]. There, the back radiation, caused by the slot, even being small, can interact with the rest of the circuit and create uncontrollable mutual coupling between slots. This is why a parallel plate (either stripline or shielded microstrip) would be preferable to use as transmission line, provided the excitation of the parasitic parallel plate mode can be avoided or significantly reduced. This is usually done by shorting the two ground-planes in 'strategic points' on the circuits. This method works for weak sources of parallel plate mode (transmission line discontinuities, fabrication tolerances). However, when a perpendicular probe or a slot excites the stripline this method does not give good results [3].

This paper describes the implementation of a new approach in the suppression of the parallel plate mode in striplines. A microstrip-to-stripline-to microstrip coupler was built and tested to illustrate the idea. Finally a sixteen-element microstrip array fed by this new type of feeding network was built and tested at C-band. The building of this array at C-band was a first step towards the application of this technology at higher frequencies, where the integration of the antenna with the rest of the system is required.

2. Theory

Any multilayer configuration involves striplines and sources that definitely are exciting the parallel plate mode. Electrical posts usually suppress this mode. Beyond the fabrication complexity involved, these posts create imperfect waveguides, and imperfect cavities (around slots) which might considerably affect the predictability of the circuit performances. One way to avoid the posts would be by using asymmetric striplines (the two substrates are of different dielectric constants). This solution is acceptable as long as coupling to both sides of the stripline is not necessary. However, in multilayer configurations the coupling to both sides is needed, and the side adjacent to the lower dielectric substrate will have a lower coupling level.

The new solution proposed involves the use of an asymmetric stripline only in the vicinity of the microstrip-to-stripline coupling slot. A small area surrounding the slot (a small plug) is designed to have a higher dielectric constant than the rest of the circuit. The discontinuity between the area surrounding the slot and the rest of the circuit excites the TEM parallel plate mode, but at a much lower level.

3. A non-homogeneous asymmetric coupler

The non-homogeneous two-port coupler shown in Figure 1 was built and tested. This multilayer configuration consists of two microstrip-to-stripline transitions connected back-to-back through a homogeneous stripline. This is a two-port circuit, with all other transmission line ends terminated in stubs. All lines are 50 Ω and the substrates are 31 mils Polyflon Cuflon (ε_r =2.1). The coupling slots are 2.4 cm by 0.1 cm. The microstrip as well as the stripline stubs are 1.5 cm long. The plug insert is 3 cm in diameter and 25 mils in height. The remaining gap between the plug and the ground-plane (6 mils) is filled with bonding film (ε_r =2.5). Figure 2 shows the measured insertion loss and return loss of the coupler

These losses include: dielectric losses, conductive losses, surface wave losses (for microstrip) the slots radiation and the power lost to the parasitic parallel plate mode (for stripline). The first three type of losses can be easily computed and subtracted from the total loses (≅ 0.3 dB). These losses are inherent and depend only on the type of the material used and should be excluded in the evaluation of the coupler performances. Overall, two frequency bandwidths (which show a very low level of losses) are of interest: 2.18- 2.45 GHz and 3.5- 3.8 GHz. The first one exhibit very low losses and the matching of the two ports is expected to produce an insertion loss, better than 0.5 dB. In the second band, the coupler is very well matched already (S_{21}<-15 dB) and considering the dielectric and ohmic losses, the insertion loss is at an acceptable level.

4. The 4×4 array

Finally a 4×4 elements microstrip array was built. All patches are 2.3 cm by 2.3 cm and are printed on a 31 mil Polyflon Cuflon (ε_r=2.1). Each patch is fed by a slot in the common ground-plane 1 cm long and 0.1 cm wide. The feeding network is stripline made of two 31 mil layers of Polyflon Cuflon. The slot areas are replaced by high dielectric plugs (Rogers 6010, ε_r=2.1). The diameter of the plug is 2 cm. Since the commercial available 6010 is 25 mils thick (or thicker than 31 mils) the 6 mils gap was filled with Teflon bonding film. The stripline-feeding network is fed through a slot by 50 Ω microstrip line printed on a 31 mil Polyflon Cuflon. The stacked layouts of the antenna are shown in Figure 3. The radiation patterns of this array are shown in Figure 4. A crosspolarization level of more than 30 dB is noticed in the H-plane and about 26 dB in E-plane. Another 4×4 microstrip array fed by a corporate microstrip feeding network was also built to evaluate the efficiency of the multilayer array. At resonance, the gain of the multilayer array is smaller by about 1 dB.

5. Conclusions and Future Work

Using the high-dielectric plugs instead of via-holes eliminates the need for ohmic contact, which sometimes is difficult to insure in the vias. This technologic process requires one less plating round which considerably reduces the price of the product. All the layers are simultaneously processed and bonded together in the same way, striplines circuit are.

A 4×4 microstrip array fed by a feeding network which makes use of this new technology was built and tested. The implementation of this technique at 66 GHz is being considered.

REFERENCES

[1] D.M.Pozar, "A Reciprocity Method of Analysis for Printed Slot and Slot-Coupled Microstrip Antennas", IEEE Trans. on Antennas and Prop., Vol. AP-34, No. 12, pp.1439-1446, December 1986.

[2] P.L.Sullivan and D.H.Schaubert, "Analysis of an aperture coupled microstrip antenna", IEEE Trans. on Antennas and Prop., Vol. AP-34, No. 8, pp. 977-984, August 1986.

[3] N.Herscovici, "Analysis of Aperture Coupled Microstrip Transmission Lines and Antennas ", Doctor of Philosophy Thesis, Department of Electrical and Computer Engineering, University of Massachusetts at Amherst, September 1992.

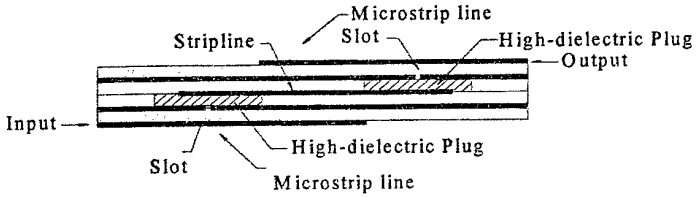


Figure 1 - The non-homogeneous multilayer coupler.

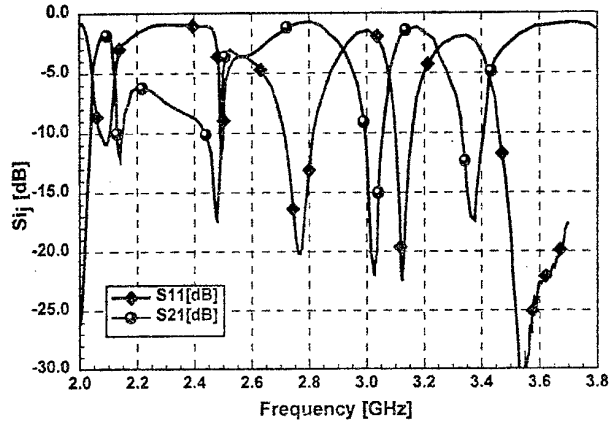


Figure 2 – The measured insertion loss and the return loss of the coupler shown in Figure 1.

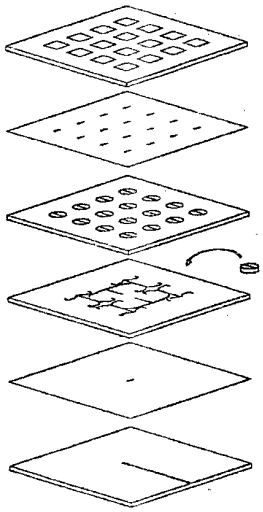


Figure 3 – The stacked layout of the multilayer antenna.

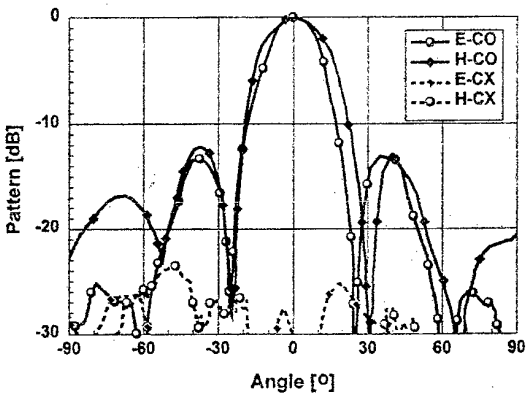


Figure 4 – The radiation patterns of the antenna shown in Figure 4.

PROPERTIES OF OVERSIZED CORRUGATED WAVEGUIDES AT MODERATE DIAMETER-WAVELENGTH RATIO.

D.A.Lukovnikov,A..A.Bogdashov, G.G.Denisov
Institute of Applied Physics, Russian Academy of Sciences
46 Ulyanov St., Nizhny Novgorod, 603600, Russia,
Tel. (8312)384236, Fax(8312)362061, E-mail<luk@appl.sci-nnov.ru>

Waveguides with transversal dimensions large compared to wavelength become necessary at millimeter wavelengths in order to reduce ohmic losses and to prevent breakdown in high-power applications. Such waveguides are called "oversized" or "overmoded" since more than one waveguide mode can there propagate .

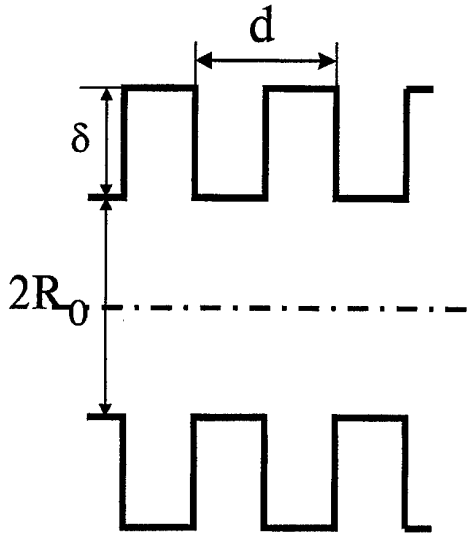


Fig.1. Geometry of corrugated waveguide

The corrugated oversized waveguides (Fig.1) are especially attractive for the application in antenna feeds because the lowest hybrid eigenmode HE_{11} in corrugated waveguide produces a radiation pattern with very low sidelobes and cross-polarization. Besides under a certain set of parameters (the electrical depth of corrugation about a quarter of wavelength and period less than half-wavelength) this wave in rather wide operating band has the attenuation much lower, than for any other linearly polarized wave in smooth waveguide [1,2]. This very interesting effect of ohmic losses decrease for certain waves in oversized waveguides is mainly considered for travelling HE_{11} wave which has the simplest structure and has frequency far above the cutoff

$$2R_0 >> \lambda/2 \quad , \tag{1}$$

and far from Bragg stop-bands:

$$d < \lambda / 2 \quad . \tag{2}$$

However in different practical applications the guide parameters may differ. For example corrugated guide sections at frequencies near Bragg stop-bands can be used in resonators for high-power microwave oscillators (Bragg resonators), waveguide mode filters, frequency stop-band filters, etc [3,4,5]. This case

corresponds to guide period, equal to half the longitudinal wavelength. Corresponding guide waves are also known as π-type oscillations. The effect of ohmic loss decrease for these waves has been studied in [6]. It was demonstrated, that in periodical guide there are π-type waves with ohmic quality growing approximatelly as a cube of guide radius, so this effect has also place.

In antenna feeds design the guide diameter-lambda ratio may also differ. So it is sensible to study the properties of a hybrid HE_{11} wave of a corrugated waveguide at different magnitudes of diameter-lambda ratio in order to define more certainly the field of parameters where the effect of ohmic loss decrease is valid.

In theoretical publications [1,2] where the condition (1) is satisfied the corrugated wall was replaced by an effective surface (wall) reactance. This so-called impedance approach neglects the space harmonics except the basic one and for moderate diameter-lambda relation is not accurate enough. So more precise mode-matching technique [6] was applied.

The corrugated waveguides were numerically and experimentally studied for different magnitudes of diameter-lambda ratio. Is is demonstrated at an example of rectangularly corrugated circular waveguide with the wavelength about 12 mm. Corrugation period was taken 2+2=4 mm (about third part of wavelength), corrugation depth 3 mm (about quarter lambda). For field structure and ohmic losses calculations the point at dispersion curve corresponding to phase run of 0.65π by the guide period was chosen. The results of calculations are collected in table:

Table 1

R_0, mm	λ, mm	δ/λ	Q_Ω	$Q_\Omega/Q_\Omega(TE_{11})$	Reflection at open guide end
36	**12.21**	**0.245**	**1747700**	**8.95**	$\mathbf{0.8\times10^{-5}}$
24	**12.08**	**0.248**	**533400**	**4.20**	$\mathbf{4.6\times10^{-5}}$
12	**11.52**	**0.260**	**85200**	**1.48**	$\mathbf{3.9\times10^{-4}}$
8	**10.81**	**0.277**	**35.620**	**1.03**	$\mathbf{4.5\times10^{-4}}$

The ohmic quality is more common characteristic compared to ohmic decrement [6]. It is given by the following formula:

$$Q_\Omega = \frac{2\pi\sqrt{f\sigma}\int\limits_{V_D}\left(|E|^2+|H|^2\right)dV}{c\int\limits_{S_W}|H_\tau|^2\,dS}, \qquad (3)$$

where V_D - guide period volume, S_W side wall surface, c - light velocity. The wall material has everywhere been taken copper ($\sigma = 5\times10^{17}\,s^{-1}$).

For different waveguide diameters (from 6 to 2 lambda) a lowest order fast eigenwave was studied. As follows from the numerical results, the field polarization of the HE_{11} wave remains practically linear at all mentioned diameters (the cross-polarization maximum intensity varies from .1 to 1 percent of the main one). The effect of ohmic loss decrease is also observed. For the diameter of 6 lambda the ohmic losses of HE_{11} is 9 times less than for TE_{11}

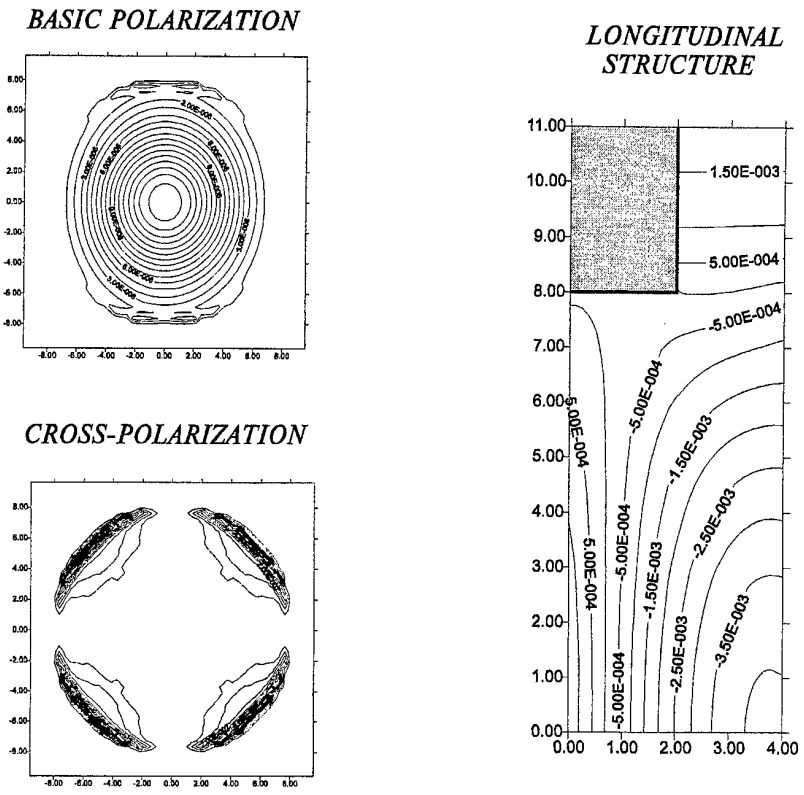


Fig.2 Eigenmode field structure of corrugated guide (R_0=8 mm, d=2+2=4mm, δ=3 mm: f=27.73 GHz, Q_Ω=35.620 (versus 34.321for TE_{11}) reflection at open guide end 4.5×10^{-4})

wave, for the diameter of 4, 2 and 1.5 lambda - correspondingly 4.2, 1.48 and 1.03 times less than for the TE_{11} wave of a smooth guide with the same radius. The field structure for the last case is shown at Fig.2. The calculations performed show, that the waves win slightly overmoded corugated waveguides keep the attractive properties as low ohmic losses and linear polarization.

References

1. P.J.B.Claricoats, A.D.Olver and S.L.Chong *Attenuation in corrugated circular waveguides,* Proceedings of IEE, V.122, №11,1975, pp.1173-1186.
2. J.L.Doane *Propagation and mode coupling in Corrugated and Smooth-Wall Circular Waveguides* Infrared and Millimeter Waves.Editored by K.J.Button. V.13, Pert 4, pp.123-170.
3. V.L.Bratman, G.G.Denisov, N.S.Ginzburg, M.I.Petelin *FEL's with Bragg Reflection Resonators...,* -IEEE Journal of QUantum Electronics, 1983, V.QE-19, №3, pp282-296.
4. G.G.Denisov, M.G.Reznikov. *Corrugated Resonators for Microwave Oscillators*, Izv. VUZ'ov Radiofizika, 1982, V.25, №5, pp.562-599 (in Russian).
5. G.G.Denisov, D.A.Lukovnikov, S.V.Samsonov *Resonant reflectors for free electron masers.* International Journal of Infrared and Millimeter waves, 1995, vol.16, №4, pp.745-752.
6. G.G.Denisov, D.A.Lukovnikov *"Ohmic Quality of Resonators Shaped by Corrugated Gude Sections at Frequencies near Bragg Stop Bands"* International Journal of Infrared and Millimeter Waves, 1997, vol.18, №3, pp.595-603.

INTEGRATED P-I-N-STRUCTURES DESIGNED FOR MM AND SUBMM WAVE QUASI-OPTICAL MODULATORS

V.V.Grimalsky, Ya.I.Kishenko, I.P.Moroz
Kiev Nat. University, Radiophysical Faculty. 252601 Kiev, Vladimirskaya str., 60, Ukraine.
E-mail: liz@astrophys.ups.kiev.ua

S.V.Koshevaya
Nat. Institute for Astrophysics, Optics, and Electronics. 72000 Puebla, Pue., Mexico.
E-mail: svetlana@inaoep.mx

Theoretical and experimental investigations of integrated p-i-n structures designed for quasi-optical millimeter and submm modulators in oversized waveguides are presented. These structures possess the transparency in regime without injection and good operational characteristics in presence of injecting current. Also a possibility to control the transverse structure of initial beam by means of non-uniform injection current is numerically demonstrated.

Silicon surface-oriented p-i-n-structures are well known as basic elements for microwave modulators in single-wave waveguide channel. These structures are made of silicon plate where the set of injecting p^+-i, n^+-i junctions is formed in the one side of the plate (see Fig.1). Integrated p-i-n-structures with deep injecting junctions (b = 10...25 mkm) are the most perspective because they combine the preferences of planar geometry (wide operating frequency range) and volume p-i-n diodes (the great value of modulation under moderate controlling currents). These structures demonstrate good operational characteristics in λ_0 = (8...2) mm wavelength region. But for shorter wavelengths $\lambda_0 \le 2$ mm, the transverse sizes of single-mode metallic waveguides become smaller, and, therefore, the limitations connected with possible integral power levels and the degree of dissipation occur. Apparently, in the range of wavelengths $\lambda_0 \le 2$ mm the perspective transmission line is multimode oversized metallic multimode waveguide with the typical transverse sizes $\ge$ 0.5cm. In this case, there are no serious limitations for integral microwave power levels transmitted by waveguide and the losses can be decreased too. Surface-oriented integrated p-i-n-structures also can be utilized in quasi-optical modulators placed into oversized waveguides but their characteristics differ from ones in single-mode waveguides ($\lambda_0 \sim 8$ mm).

The main demands are the next:

1. The quasi-optical modulators must provide the transmission coefficients that are close to unity for all modes of oversized waveguide in wide frequency range, when the controlling current is absent.
2. The degree of modulation must be quite great for the moderate densities of controlling current.

By another words, the integrated p-i-n-structures designed for quasi-optical modulators must transmit microwave beams without essential distortion in regime without controlling current and provide modulation of these beams in the presence of it. This leads to limitations for transverse sizes and shape of injecting p^+-i and n^+-i junctions, and for the thickness of structure.

Of course, these integrated p-i-n-structures can effectively control only linearly polarized modes (LP_x) because when the incident wave beam has component of electric field directed along the electrodes the reflection coefficients can be quite large even without injection. Besides, the thickness of i-layer (base) w between injecting electrodes must be no greater than the diffusion length $L_D = (D \cdot \tau)^{1/2}$: $w \le L_D$ where D is the ambipolar diffusion coefficient, τ is the lifetime of carriers in i-region. Really for silicon structures $w \le 100$ mkm. Additionally, the degree of surface metallization γ must be no more than 0.3 ($\gamma \equiv (d-w)/d$ where d is the distance between the centers of electrodes, see Fig.1). For the sake of good transparency in regime without current, the following condition must be satisfied: in x-direction (across the electrodes) the highly conducting elements must have sizes that are smaller than $\lambda_0/2$. Therefore, for the structures with $d \le 100$ mkm and $d-w \le 30$ mkm, the highly doped and metallized regions do not act on the process of reflection in regime without current.

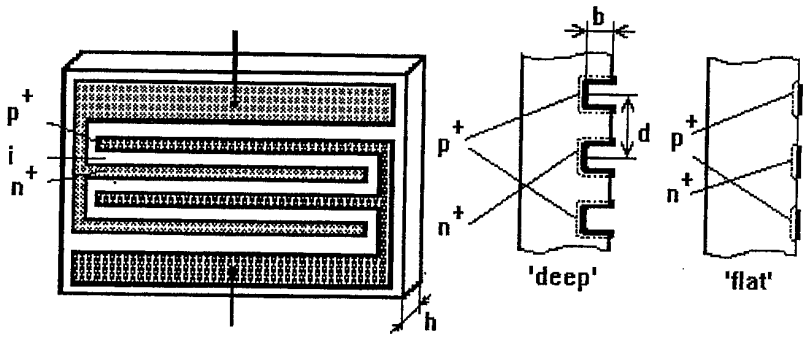


Fig.1

The most rigid demands are connected with the thickness of p-i-n-structure. As well-known, the integrated p-i-n-structures designed for modulation of $\lambda_0 \approx 8$ mm wave range microwaves have the thicknesses $h \leq 100$ mkm. Here the transmission coefficients are in regime without current: $T_0 \geq 0.9$ in wide frequency range, and condition $2\pi \cdot \varepsilon^{1/2} \cdot h/\lambda_0 \leq 0.3$ is satisfied where $\varepsilon = 12$ is dielectric permitivity of silicon. In quasi-optical modulators ($\lambda_0 \leq 2$ mm) it is impossible to provide the high transparency by means of decrease of thickness, because the mechanical strength becomes weak. Therefore, it is preferable to use p-i-n-structures with the resonant thickness $h \approx \lambda/2 \equiv \lambda_0 \varepsilon^{-1/2}/2$. For $\lambda_0 = 2$ mm this gives: $h \approx 300$ mkm. But another problem appears: the structures with resonant thickness have narrow frequency range of transparency. To make the operating frequency range wider, one can use two clarifying layers with dielectric permittivities $\varepsilon_c \approx \varepsilon^{1/2}$ and with equal thicknesses $h_c \approx h$, these layers must be applied to the both sides of p-i-n-structure. In this case, the necessary width of frequency range is realized (the optimal thickness h of p-i-n-structure is unessentially decreased: $h \approx 250$ mkm for $\lambda_0 = 2$ mm).

The modulation properties of integrated p-i-n-structures were investigated numerically. The main attention was concerned to the transmission of linearly polarized Gaussian microwave beams through the integrated structures placed into oversized waveguide. The distribution of concentration of electrons and holes influenced by controlling current in p-i-n-structures was derived from solving of ambipolar diffusion equation added by boundary conditions in injecting p^+-i and n^+-i junctions and free surfaces. Using the value of concentration one can calculate the value of dielectric permittivity of semiconductor plate and can obtain the transmission and reflection coefficients for each mode consisting microwave Gaussian beam.

The results of simulations showed that in regime without injected carriers the Gaussian beam passes optimized p-i-n-structure with clarifying layers without any transverse distortion. Note that the possible errors for the determining of optimal thicknesses of layers can be in the limits of 20%. Also the calculated dependencies of transmission coefficients $T(I_0)$, or insertion losses $\alpha = -10\ lg\ (T)$, demonstrate the satisfactory controllability of Gaussian microwave beams by these structures where I_0 is the value of controlling current in p^+-i and n^+-i junctions, see Fig. 2, curve 1. Here the simulation data are presented for silicon structure with thickness $h = 250$ mkm, the degree of surface metallization is $\gamma = 0.27$, the depth of injecting junctions is 20 mkm, the thicknesses of two clarifying layers ($\varepsilon_c = 3$) are $h_c = 250$ mkm.

A possibility to transform the transverse shape of wave beams by means of non-uniform distribution of charge carriers in p-i-n-structure was also numerically investigated. In a case when the different parts of the p-i-n-structure are controlled separately, LP_x modes of initial beam are transmitted through structure differently. Therefore, the transverse structure of initial beam can be essentially changed.

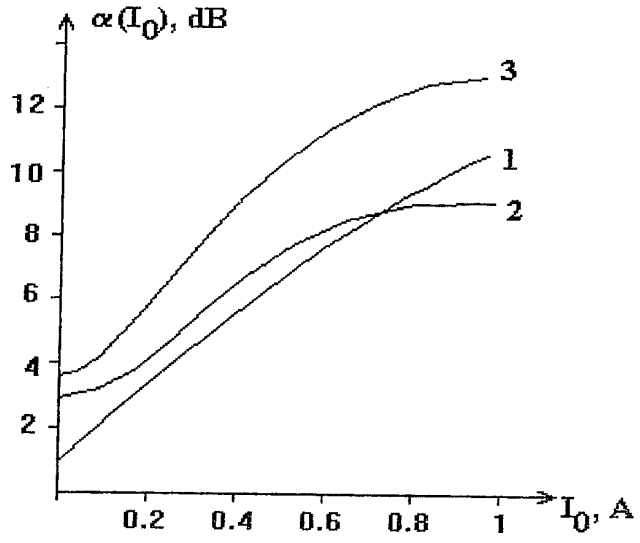


Fig.2

The integrated p-i-n-structures with sizes 3.4x3.4 mm were investigated experimentally in microwave region $\lambda_0 = 2$ mm ($f_0 = 140$ GHz). They had 'ribbon' p^+, n^+ regions (43 n^+ regions and 42 p^+ ones). The degree of surface metallization was $\gamma = (d-w)/d = 0.27$. The pair of these structures overlapped the waveguide cross-section 7.2×3.4 mm with additional diaphragm. Thickness of p-i-n-structures was h = 340 mkm. The backward travelling wave oscillator and avalanche diode were chosen as microwave sources. Two types of structures were under investigation: with 'flat' p^+-i, n^+-i junctions formed in the surface of silicon plate, and with injecting junctions created in the depth b = 20 mkm ('deep' junctions). The experimental dependencies of insertion losses a on controlling current I_0 are presented in Fig.2, curves 2, 3 correspond to structures with 'flat' junctions and 'deep' ones, respectively. One can see that the degree of modulation is much higher for structures with 'deep' junctions.

The utilization of additional dielectric layers (like teflon) gave the possibility to decrease the initial insertion losses for 1...2 dB.

The integrated structures with 'deep' junctions were also investigated in $\lambda_0 = 0.8$ mm wave region ($f_0 = 400$ GHz). There the modulational properties were approximately the same as in $\lambda_0 = 2$ mm but the initial losses were greater ($\alpha_0 = 4.2$ dB).

The testing of integrated p-i-n-structures with two-dimensional matrices of p-i-n-diodes (16×16) showed that these structures have the better high-speed characteristics but the modulational properties become worse. This can be explained by the penetration of essential part of microwave energy through the regions between the elementary diodes.

WIDE-RANGE SYSTEM OF TURNING MIRRORS FOR THE WAVEGUIDE LASER RESONATOR

V.A. Svich, V.M. Tkachenko, A.N. Topkov, V.A. Maslov, I.M. Militinskiy
Kharkiv State University, Department of radiophysics
4, Svobody Sq., Kharkiv 310077, Ukraine
Tel. (0572) 457-157, Fax (0572) 433-393, E-mail Vyacheslav.A.Maslov@univer.kharkov.ua

The folding resonators having two and more waveguides and quasioptically concerned by the system of turning mirrors (STM) are used for decreasing of laser overall dimensions. STM consisting of one or two mirrors [1] is usually used. In the first case the mirror is arranged on the axes crossing of matched waveguides. It can be both flat and spherical. The flat mirror is placed on the minimum distance from the ends of waveguides for decreasing of energy losses of modes, which are the results of diffraction on the open sections. Energy losses are proportional to $\left(\frac{\lambda l}{a^2}\right)^{\frac{3}{2}}$ for resonators with dielectric waveguides operating on the EH_{11q} mode. Here l is the distance between waveguides along optical axis [1]. The highest possible resonator compactness is reached due to the application of STM consisting of two plane mirrors. These mirrors are arranged at an angle of 45° with respect to the axes of matched waveguides. In this case the waveguides are mutually parallel.

It is possible to reduce diffraction losses at the EH_{11q} mode in the STM containing a spherical mirror with radius of curvature $R = \frac{2\pi\omega^2}{\lambda}$, where $\omega = 0.6435\ a$. This mirror is arranged at the distance $R/2$ from the ends of the matched wavegudes [2]. Such system causes considerable losses of pumping radiation while used for optically pumped submillimeter lasers.

The energy losses in the considered variants of STM strongly depend on the wavelength. This circumstance limits the working range of the wavelengths. We proposed the system with two spherical mirrors, which effectively operates in the sufficiently wide range of wavelengths [3].

The optical scheme of STM, matching wavegudes 1 and 2, is presented in figure 1. The system consists of spherical mirrors 3, 4 and plane mirror 5. The mirror 5 provides the parallel waveguide arrangement as well as a small angle between the normal to the reflected surfaces of spherical mirrors and the optical axis of STM that decreases extraaxis aberration.

We shall consider the propagation of radiation beam from 1 to 2. The distribution for the complex amplitude of field on the end 1, facing the system of matched waveguides can be decribed by $U_1(x_1, y_1)$. If to neglect the finite mirror dimensions of waveguide matched system in calculation, but to use the Rayleigh-Sommerfeld diffraction formula for the description of the field propagation between apertures of mirrors and waveguides, we'll get the following expression for the complex amplitude of the field on entrance end of waveguide :

$$U_2(x_2,y_2) \approx \frac{\exp\left\{-\frac{i\pi\alpha_2(x_2^2+y_2^2)}{\lambda f_4}\right\}}{\lambda^2 f_3 f_4} \int_{-\infty}^{+\infty} U_1(x_1,y_1)\exp\left\{-\frac{i\pi\alpha_1(x_1^2+y_1^2)}{\lambda f_3}\right\}\times$$

$$\times \int_{-\infty}^{+\infty} \exp\left\{-\frac{i\pi}{\lambda f_3}\left[2(x_1x+y_1y)+\frac{2(x_2x+y_2y)f_3}{f_4}+\left(\gamma_1+\frac{f_3}{f_4}\gamma_2\right)(x^2+y^2)\right]\right\} dx\,dy\,dx_1\,dy_1, \quad (1)$$

where $\alpha_1 = \frac{l_1 - f_3}{f_3};\ \alpha_2 = \frac{l_2 - f_4}{f_4};\ \gamma_1 = \frac{L_1 - f_3}{f_3};\ \gamma_2 = \frac{L_2 - f_4}{f_4};\ l_1 + l_2 = L\ ,$

x, y are the aperture coordinates of mirror 5; $x_1, y_1; x_2, y_2$ are the coordinates of waveguide ends 1 and 2, turned to phase correctors 3 and 4, accordingly; l_1, l_2 are the distances along the optical axis of resonator between phase correctors 3, 4 and turning mirror 5, accordingly. Here the sign of near equality is set since (1) received by neglecting of all quadratic formes which set up from quantities γ_1 and α_1. This is justified if to bear in mind the following constraints on the linear forms consisting of given quantities. Setting in (1)

$$\left|\left(\gamma_1+\frac{f_3}{f_4}\gamma_2\right)\frac{(x^2+y^2)}{\lambda f_3}\right| \langle\langle 1 \tag{2}$$

we shall obtain the value of internal integral in the form

$$\delta\left(\frac{y_1}{\lambda f_3}+\frac{y_2}{\lambda f_4}\right)\cdot\delta\left(\frac{x_1}{\lambda f_3}+\frac{x_2}{\lambda f_4}\right),$$

where δ is the Dirac's delta function. Bearing in mind the filtration property of this function we shall find from (1):

$$U_2(x_2,y_2)\approx\frac{f_3}{f_4}\exp\left\{-\frac{i\pi}{\lambda f_3}\left(\alpha_2+\alpha_1\frac{f_3}{f_4}\right)(x_2^2+y_2^2)\right\}U_1\left(-\frac{f_3}{f_4}x_2,-\frac{f_3}{f_4}y_2\right). \tag{3}$$

From (3) it can be seen that for

$$\left|\left(\alpha_2+\alpha_1\frac{f_3}{f_4}\right)\frac{(x_2^2+y_2^2)}{\lambda f_4}\right| \langle\langle 1 \tag{4}$$

the distribution of complex amplitude on the entrance of waveguide 2 will repeat this distribution on the waveguide exit 1 within the accuracy of a scale multiplier $K=\frac{f_3}{f_4}$. The following conditions of choosing focal lengths of spherical mirrors by the given transversal dimensions of waveguides and mirrors are given:

$$a_n\sqrt[3]{\frac{a_n}{\lambda_{\min}}} << f_{n+2} << \frac{a_{n+2}\,a_n}{\lambda_{\max}}, \tag{5}$$

$$f_{n+2} << \frac{a_5\,a_n}{\lambda_{\max}}, \tag{6}$$

$$\left|(f_3+f_4)-(l_1+l_2)\right| << \frac{f_3\,f_4\,\lambda_{\min}}{a_1\,a_2}, \tag{7}$$

$$\frac{\left|L_n-f_{n+2}\right|}{f_{n+2}} << 1, \quad n=1,2, \tag{8}$$

$$\left|f_4^2(f_3-L_1)+f_3^2(f_4-L_2)\right| << \frac{16\,a_1^2\,a_2^2\,\lambda_{\min}}{\lambda_{\max}^2}, \tag{9}$$

where a_1, a_2 are the radii of waveguides 1, 2; a_3, a_4, a_5 are the aperture radii of mirrors 3, 4, 5; l_1, l_2 are the

distances along optical axis from the mirrors 3, 4 up to the mirror 5; L_1, L_2 are the distances along optical axis from the waveguides 1, 2 up to the mirrors 3, 4, accordingly; λ_{min}, λ_{max} are the minimum and maximum wavelengths of working range STM. The relationship (7) means that the distance along optical axis between focusing mirrors should be close to a sum of their focal lengths. The lengths L_1, L_2 should be close to focal lengths f_3, f_4. The sum of lengths l_1 and l_2 should be close to the sum of f_3 and f_4. If quantities $(L_1 - f_3)$ and $(L_2 - f_4)$ are opposite in sign, then they are limited by a condition (8). If they have the same signes, then they are limited by much stronger condition (9). The diameters of matched waveguides correspond in the following way $a_1 / a_2 = K$.

The given system was assembled and tested in the middle part of SMM range on the wavelength λ=0.57056 mm (the generation line of molecule CH_3OH with the pumping on transition 9P16 of CO_2-laser). The turning mirrors were made of stainless steel with aluminium spraying and had the following parameters: $f_3 = f_4 =$ 80 mm; $a_3 = a_4 = 21$ mm, $a_5 = 10$ mm. This system was used for matching copper waveguides with internal diameter $2a = 19.8$ mm. Power losses of radiation in the waveguide channel with STM were 4.5 % higher than in the channel made of same waveguides joined close to each other. These losses, within the accuracy of error measurements, are equal to the heat losses in the turning mirrors. Hence, the sections of free space of STM almost did not introduce additional losses.

The waveguide matching with help of two flat mirrors was simulated for comparison. The waveguides were moved apart along the optical axis on 40mm (minimum section of free space at such waveguide matching is equal $4a$). In this case the losses were 29 % higher than in the channel made of the same waveguides joined close to each other. It is obvious, that all additional losses were caused by diffraction on the free space section.

The proposed system was successfully used for making the compact wide range SMM laser with optical pumping.

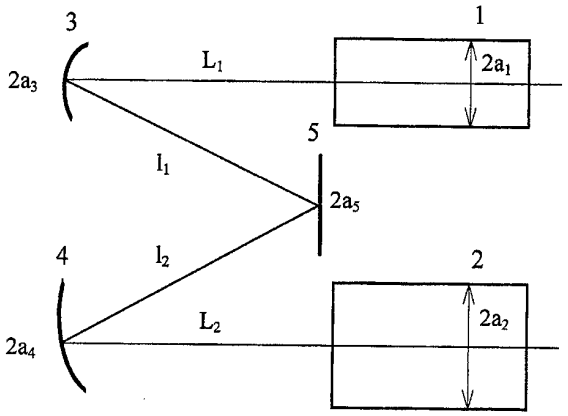


Figure 1. Geometry of folding resonator

References

1. P.E. Jackson, D.R. Hall, C.A. Hill, "Comparisons of waveguide folding geometries in a CO_2 z-fold laser ", Applied Optics, Vol. 28, No. 5, pp. 935-941, 1989.

2. J.Banerji, A.R.Davie, P.E.Jackson et. al., "Transmission and coupling losses in a folded waveguide", Applied Optics, Vol. 28, No. 21, pp. 4637-4643, 1989.

3. Пат. 2025008 Российская Федерация. Резонатор / Епишин В.А., Рябых В.Н., Ткаченко В.М., Топков А.Н., Юндев Д.Н. - №4947849/25; Заявл. 21.06.91; Б.И. - 1994. - №23. - С. 171.

SHORT PULSE GENERATION IN A CAVITY WITH AN ACTIVE LAYER AND A DIELECTRIC MIRROR

L. V. Yurchenko[1] and V. B. Yurchenko[1,2]
[1] Institute of Radiophysics and Electronics, National Academy of Sciences
12, Proskura St., Kharkov, 310085, Ukraine
Tel. 380 572 44 8349, Fax 380 572 44 1105, E-mail: yurchenk@ire.ire.kharkov.ua
[2] Electrical and Electronics Engineering Department, Bilkent University
Bilkent, Ankara, 06533, Turkey
Tel. 90 312 266 4307 Fax 90 312 266 4126 E-mail: yur@ee.bilkent.edu.tr

In this paper, generation of anharmonic and chaotic signals in a cavity with an active layer has been numerically investigated. The active layer can be formed by a laser medium, by a semiconductor of N-type current-voltage characteristics, by an array of Josephson junctions or semiconductor devices like tunnel or Gunn diodes, or field-effect transistors in active state [1].

When the coupling of the electromagnetic field and the active layer is sufficiently strong, self-excitation of high-frequency anharmonic oscillations with transition to dynamical chaos can be observed in the systems of this kind.

Particularly, we studied the dynamics of such oscillations in a cavity with a GaAs active layer and with a dielectric mirror intended for transmitting the electromagnetic signals into the outer free space. The dielectric mirror is also operating as a resonant filter when reflecting the electromagnetic field back into the cavity or transmitting it into the free space.

One-dimensional model of the cavity is considered, with the cavity width A being much greater than the length D. The dielectric mirror of thickness d and of refractive index n is placed at $x = 0$ $(-d < x < 0)$ and the active layer is at the cavity wall $x = D$. The response of the active layer to the incident field is assumed to be instant, i.e. the cut-off frequency of the active medium is greater than the maximum frequency of the process considered.

In practice, the layer can be an array of active devices of N-type current-voltage characteristics like those of Gunn diodes. Assuming the spacing between the devices is sufficiently small and the external voltage $V_0(t)$ is applied to every device, we can introduce the equivalent bias electric field $E_z^{(0)}(t)$ directed along the array and consider the latter as a continuous layer [2] with the surface current density $J_S(t)$ arising due to the total field $E_z(D,t) = E_z^{(0)}(t) + E_z^{(1)}(D,t)$ where $E_z^{(1)}(D,t)$ is the microwave field excited at the wall $x = D$.

In the case of a GaAs layer, the current-voltage characteristic is approximated as [3]

$$J_S = J_S(E) = J_{S0}G(E) = J_{S0}\left[(E + 0.2E^4)/(1 + 0.2E^4) + 0.05E\right] \qquad (1)$$

where $E = E(t) = E_z(D,t)/E_S$ is the normalized electric field in the active layer and the parameters are $J_{S0} = 50A/cm$ and $E_S = 1kV/cm$ (the carrier density $n = 10^{15}cm^{-3}$ and the frequency $f = 10GHz$ were used to estimate the skin-layer thickness and hence the value of J_{S0} given above).

The electric field in the cavity, $E_z(x,t)$, is a solution to the one-dimensional wave equation subject to the relevant initial and boundary conditions. The boundary condition at the active layer $x = D$ is nonlinear and takes on the form

$$\left.\frac{\partial E_z}{\partial x}\right|_{x=D} = -\left(\frac{W_0}{c}\right)\left(\frac{\partial J_S}{\partial E_z}\right)\left.\frac{\partial E_z}{\partial t}\right|_{x=D} \qquad (2)$$

where c is the speed of light, W_0 is the free-space impedance, and $J_S = J_S(E)$ is the surface current density defined above.

Eq.(2) follows from the generic boundary condition

$$H_y(D+0) - H_y(D-0) = J_S \tag{3}$$

where $H_y(D+0) = 0$, H_y is the y-component of the magnetic field that, due to the Maxwell's equations, satisfies the relation $\mu_0 \left(\partial H_y/\partial t\right)\Big|_{x=D} = \left(\partial E_z/\partial x\right)\Big|_{x=D}$.

Notice that nonlinear factor $\partial J_S/\partial E_z$ in Eq.(2) is the differential conductance of the active layer. The latter is negative when the total field $E_z(D,t)$ falls in the negative differential resistance region.

The boundary conditions at the dielectric mirror are linear and follow from the continuity of the tangential components of the electric field at the dielectric surfaces.

For the further analysis, we follow [4] and make use of the Riemann solution available to the one-dimensional wave equation. By considering the field in the cavity ($i = 1$), in the dielectric mirror ($i = 2$), and in the free space ($i = 3$), we take the solutions $E_z^{(i)}(x,t) = f_i(v_i t + x) - g_i(v_i t - x)$ where $f_i(.)$ and $g_i(.)$ are unknown functions, $v_{1,3} = c$ and $v_2 = c/n$, and apply the boundary conditions at the active layer, at the surfaces of the dielectric mirror, and at infinity.

In this way, we arrive at the multiple delay difference equation as follows

$$f(\tau) = \left\{G\left[E_0^{(0)}\right] - G\left[E(t,\tau,\tau_1,\tau_2,\tau_3)\right]\right\} G_0/n_1 + E_1(\tau_1,\tau_2,\tau_3) \tag{4}$$

where

$$E(t,\tau,\tau_1,\tau_2,\tau_3) = E^{(1)}(\tau,\tau_1,\tau_2,\tau_3) + E^{(0)}(t), \tag{5}$$

$$E^{(1)}(\tau,\tau_1,\tau_2,\tau_3) = n_1\left[f(\tau) - \eta^2 f(\tau_1) - \eta f(\tau_2) + \eta f(\tau_3)\right], \tag{6}$$

$$E_1(\tau_1,\tau_2,\tau_3) = \eta^2 f(\tau_1) - \eta f(\tau_2) + \eta f(\tau_3), \tag{7}$$

$E(t,\tau,\tau_1,\tau_2,\tau_3)$ is the total electric field in the active layer at the moment $t = (n\tau - D)/c$, $E^{(1)}(\tau,\tau_1,\tau_2,\tau_3)$ is the microwave field in the layer, $E^{(0)}(t)$ is the bias field defined by the Kirchhoff law of the bias circuit (if the latter contains the source E_{ext}, the load resistor R, and no reactive components, $E^{(0)}(t)$ is defined by the equation $E + RJ_S(E) = E_{ext}$), $E_0^{(0)}$ is the initial value of $E^{(0)}(t)$ (further, we assume $E^{(0)}(t) = E_0^{(0)} = \text{const}$), $G_0 = W_0 J_{S0}/E_S$ (for the parameters given above, $G_0 \le 20$), $\tau_1 = \tau - h$, $\tau_2 = \tau - L$, $\tau_3 = \tau - L - h$, $h = 2d$, $L = 2D/n$, $n_1 = n + 1$, and $\eta = (n-1)/(n+1)$.

The initial value of the field in the cavity is chosen as a small fluctuation determining the function $f(\tau)$ at the initial interval $(\tau_0 - L - h, \tau_0)$ as required for solving Eq.(4).

When the solution of Eq.(4) found, the normalized radiation field transmitted through the dielectric mirror is obtained as

$$U_1(t) = (n/n_1) f(\tau - 0.5L - d) \tag{8}$$

and the current in the active layer is computed as

$$J_S(t) = J_{S0}\left[G(E_0^{(0)}) + J_1(t)\right] \tag{9}$$

where

$$J_1(t) = n_1\left[f(\tau) - \eta^2 f(\tau_1) + \eta f(\tau_2) - \eta f(\tau_3)\right]. \tag{10}$$

For a thin dielectric of a small refractive index chosen to be sufficient for supporting self-oscillations, a train of short radio pulses is shown to be generated in the system (Figure 1). The period of pulsing is found to be equal to a single round trip of the field in the cavity. Meanwhile, the carrier frequency of each pulse, f, is obtained to be up to a hundred times greater than the frequency of the pulse repetition, f_p.

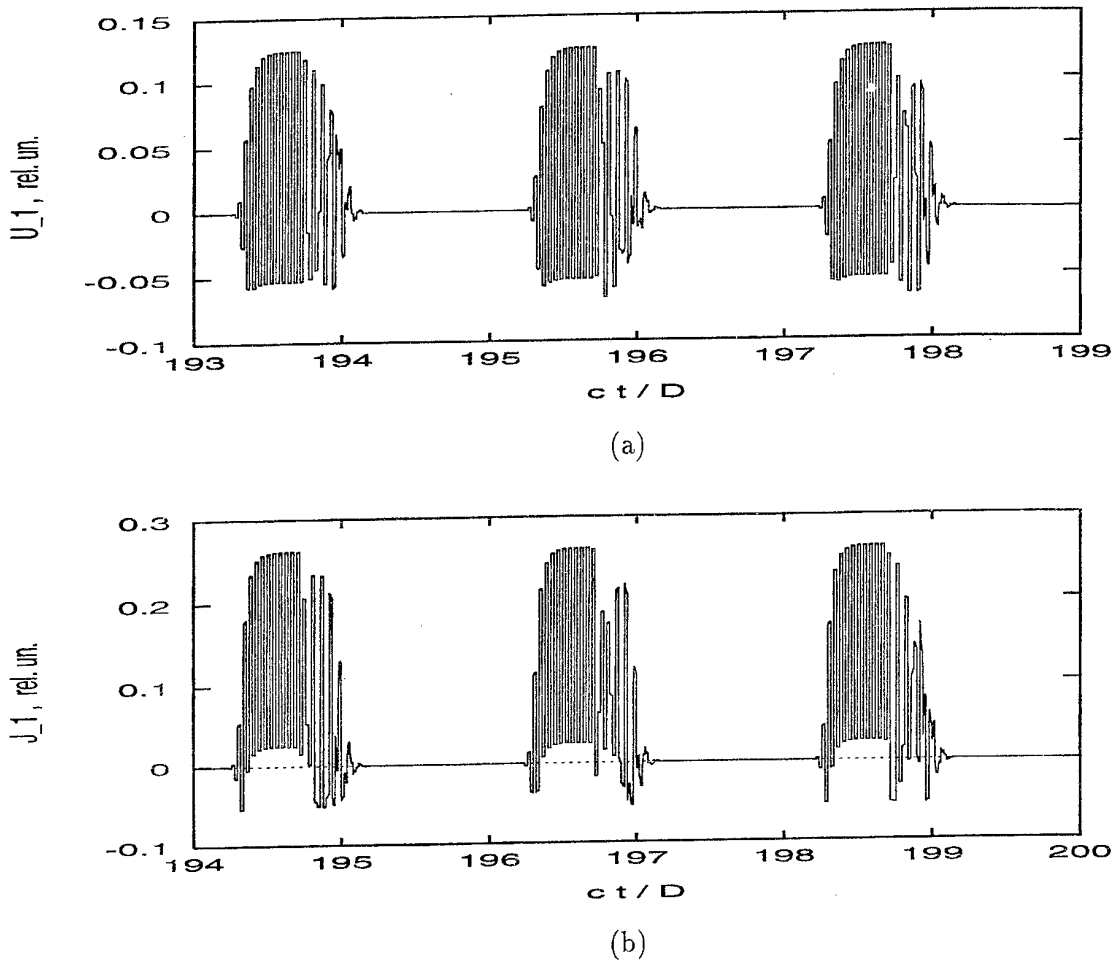


Figure 1: (a) The normalized radiation field $U_1(t)$ and (b) the current $J_1(t)$ in the bias circuit as functions of the relative time ct/D (moments of time in (a) and (b) are not synchronized)

A particular solution for the cavity of the length $D = 15mm$ with the dielectric mirror of thickness $d = 0.15mm$ and of refractive index $n = 3$ is obtained providing $f_p = 10GHz$ and $f = 500GHz$, with the pulse duration $t_p = 0.4 \times 10^{-10}s$. The solution was obtained with the parameters given above and the values of $E_0^{(0)} = 3$ and $G_0 = 1$.

References

1. J. C. Wiltse and J. W. Mink, "Quasi-Optical Power-Combining of Solid-State Sources", Microwave J., Vol. 35, pp. 144–156, 1992.
2. L. V. Yurchenko and V. B. Yurchenko, "Noise Generation in a Cavity Resonator with a Wall of Solid-State Power-Combining Array", in: The 11th International Microwave Conference MIKON-96, Warsaw, Poland, May 27–30, 1996, Conference Proceedings, Telecommunication Research Institute, Warsaw, Vol. 2, pp. 454–458, 1996.
3. J. Xu and M. S. Shur, "Velocity-Field Dependence in GaAS", IEEE Trans. Electron Devices, Vol. ED-34, pp. 1831–1832, 1987.
4. K. A. Lukin et al., "Method of Difference Equation in the Resonator Problem with a Nonlinear Reflector", Soviet Physics – Doklady, Vol. 34, pp. 977–979, 1989.

RESONANT REFLECTION OF ELECTROMAGNETIC WAVE FROM THIN STRIP GRATING

I.K.Kuzmichev[#] and S.N. Vorobiov[♦]
[#] Institute of Radio Physics and Electronics of National Academy of Sciences of Ukraine
12, Academic Proskura St., Kharkiv 310085, Ukraine
Phone: +38-0572-448-421 Fax: +38-0572-441-105 E-mail: ire@ire.kharkov.ua
[♦]Institute of Radio Astronomy of National Academy of Sciences of Ukraine
4, Chervonopraporna St., Kharkiv 310002, Ukraine
Phone: +38-0572-448-503 Fax: +38-0572-476-506 E-mail: prosvirnin@rian.kharkov.ua

Abstract. The conditions of the resonant reflection of the plane electromagnetic wave by the thin grating consisting of inclined metal strips have been confirmed and investigated experimentally. The good agreement and coincidence of the experimental and theoretical data have been obtained.

Electromagnetic fields scattered by gratings of identical thin metal strips have properties allowing to apply successfully such structures in antenna equipment and super-high-frequency arrangements. Applications of strip gratings as selective surfaces are rather variously. In particular, the grating consisting of inclined metal strips can be used as a directional coupler or a translucent screen with an adjustable division level that can vary widely (from almost zero up to unity) by certain relation between strips width, the angle of the strip inclination to the grating plane and its period. The wave reflection from the grating is strongly pronounced resonant because it is caused by an interference interaction of fields in the spaces between strips (i.e. in the grating domain).

The phenomenon of the total resonant reflection of the plane H-polarized wave from the thin grating of inclined strips had been detected in [1] (by the precise solving of the problem of the electromagnetic wave diffraction by the periodical grating) and investigated in [2]. The aim of this work is to check experimentally the existence of such resonances in real equidistant gratings and to determine the accuracy of the coincidence of the theoretical results with data measured in practice. It would permit to appreciate the validity of assumptions of the grating mathematical model (perfect conductivity and infinitesimal strip width) and then to construct complex electrodynamical systems operating in the millimeter wavelength range using resonant reflection conditions.

Physically the total reflection resonance existing in the infinite periodical grating can be interpreted as an excitation (caused by the normally incident plane wave) of two structure eigenwaves propagating along the grating (i.e. in the direction perpendicular to the strip edges) to meet one another. Thus, near the grating the high Q-quality conditions of standing waves take place, and, consequently, the grating becomes "unsusceptible" to the coming incident field that excites structure eigenwaves. In other words, the grating with thinly disposed strips for such incident plane wave behaves as an ideally reflecting screen [2].

The numerical analysis carried out in [2] yields the conclusion that the grating consisting of seven elements, having parameters $d/l = 1/4$; $\psi = \pi/4$ ($2d$ is the strip width, l is the grating period, ψ is the angle of the strip incline read from the normal to the grating plane), reflects ≈ 80 percents of the energy of the incident wave, i.e. the modulus of the reflection coefficient in the field is $|\Gamma| \approx 0{,}9$. Remind, that for the total resonant reflection the existence of one only, basic propagating wave in the wave spectrum of the periodical grating is quite necessary. It means that there is one dominating beam in the radiation pattern of the reflected field for the finite structure.

For experimental investigations we have made the grating with following parameters: $2d$ = 1,835 mm, l = 3,67 mm, $\psi = 45^0$; the width of strips made of copper foil was 0,3 mm (the d/l ratio and angle ψ value were the same as mentioned above data from [2]) and the number of strips equalled to twelve. It is a rather thin grating (the distance between strips exceeds the visible size of the strip) without waveguide domains between neighbour strips [1,2]. The number of strips in the grating was chosen according to the following circumstances. At first, the equidistant structure with the elements number exceeding ten is equivalent in electrodynamical characteristics to the infinite periodical grating with the relative accuracy of $\delta \approx 1$ percent (if we use the criterion from [3] for the appreciation of the correspondence), and for the grating of seven elements, as noted in [2], value $\delta \approx 12$ percents. It means that the resonant reflection regime for the grating of twelve strips would be more clear than for the structure of seven elements. In addition, when the number of structure elements increases then the radiation along the grating (which is parasitic in our case) decreases [2,3]. At second,

if such grating is placed into the open resonator (in which the fundamental type of oscillation $\mathbf{TEM}_{00q}$ exists) then the field "spot" must "illuminate" not less than three structure strips in order to excite conditions of resonant reflection in the grating. Note that if there is one of the higher types of oscillation in the open resonator ($\mathbf{TEM}_{20q}$ or especially $\mathbf{TEM}_{40q}$) the field distribution in the plane of the grating disposition exceeds essentially the size of the "spot" of the fundamental type oscillation field of such system. At third, it would be desirable to investigate rather small grating (i.e. the number of strips must be not too big) meaning its following application as a component of electrodynamical system.

Measurements were carried out within the wavelength range $\lambda = 4{,}0...4{,}6$ mm. The block diagram of the measuring set is shown in Fig.1. The grating of 50×50 mm^2 size placed into the absorbing screen can move perpendicular to the radiating horn antenna. The signal reflected from the studied grating, through the phase shifter, the directional coupler 2 (DC2) and II and III arms of the E-plane tee comes to the receiving channel consisting of the detector, the measuring amplifier and the oscilloscope. The frequency of the oscillator Г4 -142 is controlled by placing the wavemeter into the receiving channel. When the screen containing the grating moves (Fig. 1) the signal on the oscilloscope screen differs according to the sinusoidal law (it is connected with the reflection from the grating). Repeated reflections from the antenna (that is a pyramidal horn) and from different objects that are found in its radiation field are excluded by the screening using absorbing coatings.

The experiment was carried out in the following way. The grating-containing screen is moved and placed so, that the reflected signal in the arm III of E-plane tee would have the maximum value. Then by means of the attenuator 2 (AT2) and the phase shifter one reaches the compensation of the signals in the arm III of E-plane tee (the first signal is reflected from the grating and comes to arm II of E-plane tee, and the second signal is the base one from the oscillator in the arm I of E-plane tee) fixing the reading of the AT2 which equal to a_1 values. Then the calibration of the measuring set has to be done. The studied grating is replaced by the perfectly reflecting cooper plate and again the balancing of the E-plane tee by using the phase shifter and the AT2 (which reading now are a_2) is carried out. As a result, the modulus of the coefficient of the reflection in the field $|\Gamma|$ from the studied grating is obtained easily by the formula [4] : $|\Gamma| = 10^{a/20}$, where $a = a_2 - a_1$. In Fig.2 you can see measured values of the coefficient of reflection $|\Gamma|$ against the dimensionless frequency parameter $\kappa = l/\lambda$. Fine-scale oscillations of the experimentally obtained curve $|\Gamma(\kappa)|$ (points in the Fig.2 denote measured values of $|\Gamma|$) are caused, apparently, by unexcluded re-reflections from objects which are rather far from the experimental set. Close to real, averaged dependence $|\Gamma(\kappa)|$ is depicted in the Fig.2 by the solid curve which being analysed shows that in the frequency interval $\kappa_{refl.} = 0{,}85...0{,}87$ there exists the resonant wave reflection in the grating. The measured frequency value $\kappa_{refl.} = 0{,}86$ coincides with one obtained theoretically (their difference is less than five percents; and it should be noted that we allowed for the shifting of the calculated value of $\kappa_{refl.}$ for the grating with the greater number of strips).

Consequently, the mathematical model of the grating and processes of wave scattering occurring in it are practically adequate to those radiophysical conditions which took place in our experiment, and, thus, known assumptions of the mathematical model had proved to be correct. The precise electrodynamical method of the solving of the boundary value problem [2] and the experiment carried out carefully had resulted in the good coincidence of the calculated and measured physical characteristics of the phenomenon of the resonant wave reflection.

In conclusion we would like to note that the results obtained are of great interest when constructing complex electrodynamical systems, in particular, based on open resonator in which the thin grating of inclined strips (placed into it in the special way) is used as a selective tuning and controlling element.

References

1. S.N. Vorobiov, L.N. Litvinenko and S.L. Prosvirnin, "Wave diffraction by the periodic structure consisting of inclined metal strips", Journal of computation mathematics and mathematical physics, Vol.26, No.6, pp.894-905, 1986 (russian pagination).
2. S.N. Vorobiov and S.L. Prosvirnin, "The phenomenon of the total reflection of electromagnetic waves from the thin grating consisting of inclined metal strips", Soviet physics-technical physics journal, Vol.58, No.3, pp.458-468, 1988 (russian pagination).
3. S.N. Vorobiov, "Electromagnetic wave scattering by non-equidistant finite extent grating consisting of inclined strips", Journal of communication technology and electronics, Vol.32, No.4, p.687-695, 1987 (russian pagination).

4. Z. Frait and C.E. Patton, "Simple analytic method for microwave cavity Q determination", Review of Scientific Instruments, Vol.51, No.8, pp.1092-1094, 1980.

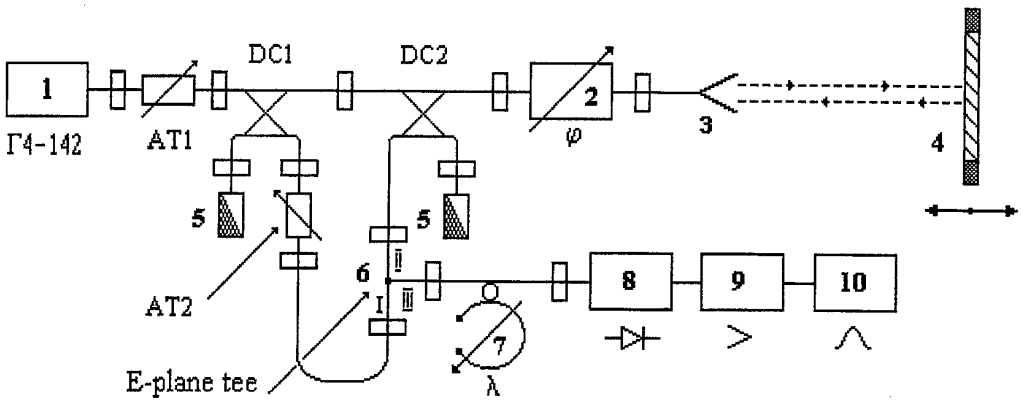


Figure 1. Block - diagram of the experimental and measuring set.
1 - M band oscillator Г4 -142 (53...78 GHz), 2 - phase shifter, 3 - horn antenna,
4 - screen containing the studied grating, 5 - matched load, 6 - E-plane tee,
7 - wavemeter, 8 - detector, 9 - measuring amplifier, 10 - oscilloscope,
AT1 - attenuator, AT2 - polarization attenuator, DC1 and DC2 - directional couplers.

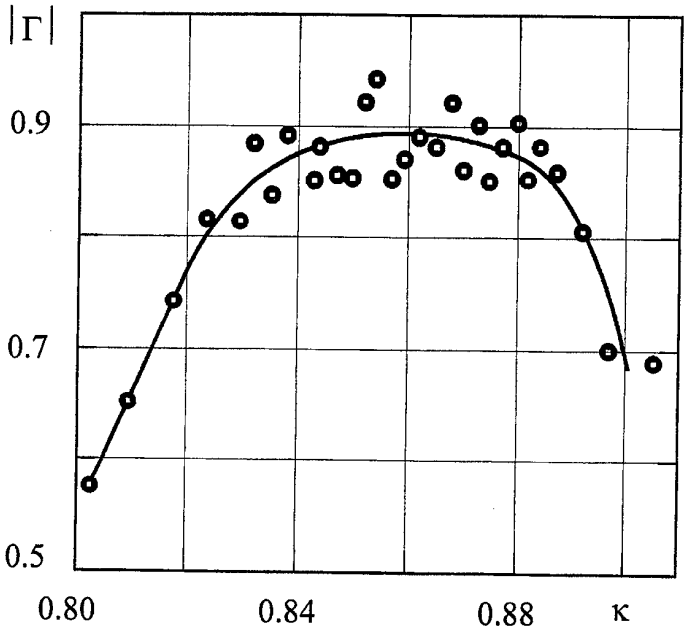


Figure 2. Modulus of the reflection coefficient $|\Gamma|$ versus the frequency parameter κ.

ON THE DIFFRACTION COUPLING ORGANISATION IN OPEN RESONATORS

D.G.Afonin, A.K.Malyshkin

Physics Departament of Moscow State University

Vorob'evy Gory, Moscow, Russia, 119899, tel.095-939-20-94 (E-mail: Afonin@radi1.phys.msu.su)

Open resonators (OR) with spherical mirrors near concentric geometry are considered with the purpose of organization and investigation of diffraction coupling with outer transmission-line systems (or with neighbor OR) at the expense of diffraction loss on mirror apertures.

Using the method of small perturbations, scattering matrices and OR equivalence conditions, analytic expressions for calculation of losses for one wave pass between mirrors and field distribution for several lowest oscillation types were obtained. It was showed, that changing the tuning of OR near concentric geometry, effective regulated diffraction coupling with outer transmission-line systems is executed.

In the other approach to solve this problem, solutions of parabolic equation for several oscillation types were used; in this case values of transmission coefficient between neighbor OR at different values of Q-factor were derived.

The system of diffraction coupled two-mirror ORs with spherical mirrors near concentric geometry was experimentally investigated, with the help of automatic device, in the millimeter region of wavelength. Such system was made in a form of two metallic blocks, on which mechanically made spherical mirrors are put close to each other. So, two such blocks, placed next to each other, formed a chain of diffraction coupled two-mirror ORs.

The spectrum of such system, distribution of field of excited oscillation types was experimentally investigated; the Q-factor and the coefficient of transmission from one OR to another were measured.

In the chain of 3 such coupled ORs the spectrum consisted of 3-4 oscillation types, the Q-factor changed within the limits 300÷1000, real transmission coefficient was 0.2÷0.7. Properties of diffraction coupling in such ORs were investigated in more detailed manner.

COMPUTER ANALYSIS OF SIDE RADIATION OF NARROW-BEAM ANTENNA ARRAY

N. N. Gorobets, Yu. N. Gorobets, V.I. Kiyko
Kharkov State University, 4 Svoboda Sq., Kharkov -310077, Ukraine
Phone: (0572) 45-71-75, Fax: (0572) 47-18-16, E-mail: Nikolay.N.Gorobets@univer.kharkov.ua

In the millimetre and submillimetre bands of the electromagnetic waves the physical sizes of antenna systems, providing high directivity, can be sufficiently small because the directional characteristics are determined by the electrical sizes of the radiating systems. Therefore the obtaining of the high directional characteristics, in particular the low side lobe levels at the expense of decreasing the gain and the aperture efficiency, is become possible. It is known [1] the more aperture efficiency the more the side lobes, that is observed on the sources amplitude distribution which is near to uniform one in the radiating aperture. On the other hand for many applications, especially in the radiometrical systems of remote sensing of Earth's atmosphere and surface from airspace carriers, the problem of providing minimum side lobes exists. In the case of the antenna arrays is possible to ensure the pattern without side lobes in general by using binomial distribution in cophase array [1]. Also it is possible to realize the optimal, in Dolf-Chebishev's sense, antenna arrays in which the minimum pattern main lobe width is provided under given side lobe levels. However in this case the decay of the side lobe levels is very slow that is not desirable for many use at practice. It is possible also to decrease side lobe levels by using the tree-parameter amplitude distribution in the equidistant antenna array [2]. In this paper on the basis of the computer analysis the influence of different factors - decreasing sources field amplitude at edges of the antenna, changing array radiating aperture shape, sectionaring of the arrays and changing antenna array edge by giving to it the comb shape - on the side lobe levels of narrow beam antenna array is investigated.

The idealized variants of the antenna array were discussed. It is supposed that array radiator has isotropic pattern, mutual influence of the radiators in the array is not considered and the array characteristics are entirely described by the complex factor of the system of the radiators. Such idealization essentially simplifies analysis and allows to study the basic effects of forming the pattern side lobes of the above mentioned variants of the antennas independently from the type of the solitary radiator.

The algorithm and computer program of calculation of the complex factor do not put on some limitation at the radiators position, their number and amplitude-and-phase distribution of the field sources in the radiating aperture. That allows to study the influence of all the possible factors on the side lobe levels and the decreasing laws under increasing the lobe number.

Let us consider the influence of amplitude distribution type on the side radiation of the array. The phase distribution is assumed uniform. The amplitude distributions is assumed symmetrically decreasing to edges of the antenna by the sinusoidal law

$$A_v = A_0 + (1 - A_0)\sin\left(\frac{N-|v|}{2(N-2)}\pi\right),$$

or exponentially

$$A_v = e^{-\alpha(|v|-1)}.$$

First of all the dependence on the relative field (current) amplitude at the edges of the antenna, i.e. pedestal A_0 of the amplitude distribution, of the side lobe levels was analyzed. The standard dependence of the first side lobe level (SLL) of the pattern on A_0 calculated for waveguide-slot array with a square aperture is shown on Fig. 1. Here the antenna consists of 32 linear waveguide-slot antennas, in every one of which 30 longitudinal slots were cut through. One can see that sinusoidal amplitude distribution provides in the main observation planes the monotonous decreasing of the first side lobe level from -13.2 dB on the uniform amplitude distribution to -23.2 dB on A_0=0.1. It is necessary to note that for A_0 < 0.15 the velocity of decreasing the first side lobe level under decreasing A_0 is slowed down. Decreasing side lobes level on the increasing its number is approximated with formula:

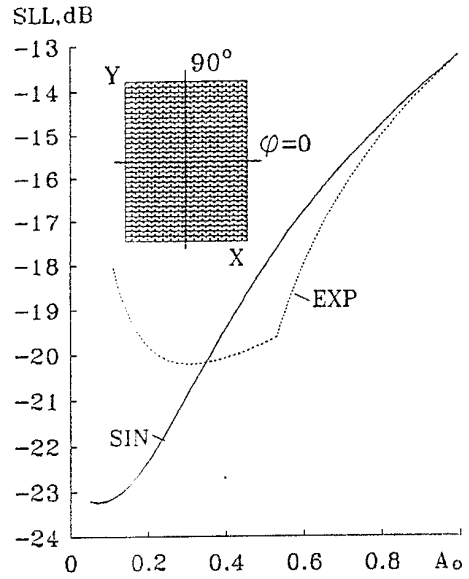


Figure 1. The maximum side lobe level for rectangular array vs field value at the array edge.

$$\frac{E_n}{E_{\max}} = (0.1753A_0 + 0.0405)n^{-\left(0.6576+\frac{0.0651}{A_0}\right)}$$

The pattern of the antenna on the sinusoidal distribution on A_0=0.3 is shown on the Fig. 2.

On the exponential amplitude distribution the law of the side radiation forming is differed from the previous case both quantitevely and qualitatively. On decreasing A_0 the velocity of decreasing even and odd side lobes is distinguished one from the other and besides the decreasing levels of the odd lobes with decreasing A_0 is more quick than levels of even ones. On A_0< 0.3 the odd lobes levels is very small, but even ones on decreasing A_0 increases. As a result the level of maximum side lobe on the exponential amplitude distribution, which is near to uniform amplitude distribution, is determined by. the first side lobe level, which decreases monotonously on decreasing A_0 from 1.0 to 0.55 (dotted line on Fig. 1). On A_0< 0.55 the second side lobe has maximum level (on A_0< 0.3 this lobe increase). In this case minimally possible side lobe levels approaches -20.3 dB at A_0= 0.3. The pattern on A_0= 0.3 is shown on the Fig. 3.

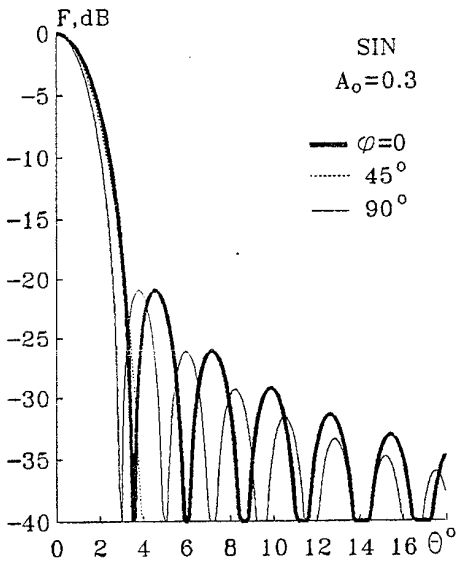


Figure 2. The patterns of the rectangular array with sinusoidal amplitude distribution.

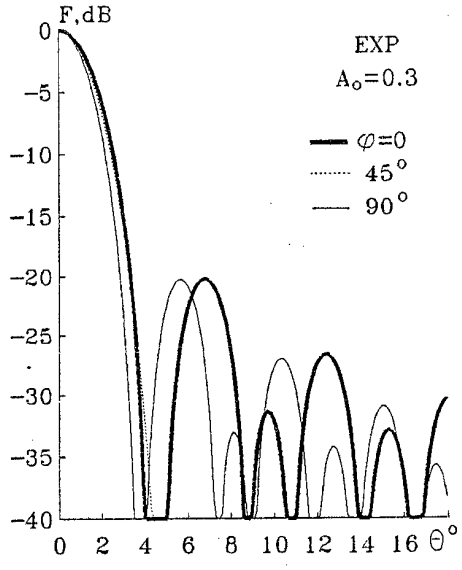


Figure 3. The patterns of the rectangular array with exponential amplitude distribution.

Thus, if permissible sides lobe level is more than of -20 dB the use of the exponential amplitude distribution is better, because it ensures more great aperture efficiency and smaller width of the pattern main lobe [3]. For smaller permissible side lobe levels it is necessary to use the sinusoidal amplitude distribution.

The dependence on the pedestal A_0 of the side lobe level in the diagonal observation planes $\varphi=\pm 45^0$ has a form as in the main planes, but their values is less at -16 ... -25 dB.

Let us see the influence of the radiating aperture shape at the its side radiation characteristics. The worked out computer program allows to except the part of the radiators thus that the aperture can acquire the rhombical, hexagonal, octagonal or circular shapes. The complex factors of such radiators system were calculated in the main and diagonal observation planes. Also the side lobe level was analyzed. It is know [1] that in antennas with such shape of aperture the side lobe levels are decreased because effective amplitude distribution of the equivalent linear antenna in all the observation planes is tapered even under uniform exciting radiators. The relative field amplitude is decreased proportionally to the number of radiators.

The calculations show that in the case of circular array with uniform sources distribution the side lobe levels are decreased to -17.8 dB, i.e. it is less at 4.6 dB as compared with an array of square shape. The number of radiators in the circular array is approximately decreased at 40% as compared with square one. In practice such side lobe level is not sufficiently low. Therefore the influence of tapering field sources amplitude of the waveguide-slot array on its side radiation was investigated. Fig. 4 shows the dependencies of the levels of the maximum side lobe level from pedestal A_0 on the tapering sinusoidal and exponential amplitude distributions. One can see that in this case the maximum side lobe level one may to decrease to -25.dB on the sinusoidal distribution and to -23.5 dB on exponential one.

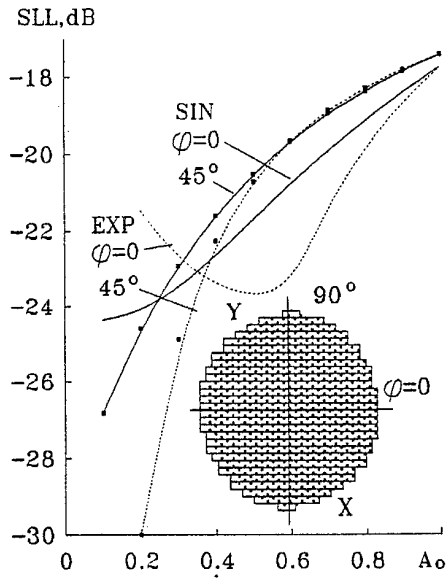


Figure 4. The maximum side lobe level for circular array vs field value at the array edge.

The influence of the amplitude distribution type (tapering sinusoidal and exponential) on the pattern of the circular array is the same as in the case of the square array (Fig. 5-6). However the absolute value of the maximum side lobe is less.

The possibility of decreasing pattern side lobes of the plane antenna arrays at the expense of decreasing radiators number on the edges of array was considered. In particular it is impossible to decrease the length of the linear antennas in the waveguide-slot arrays over one. The examples of three variants of the investigated arrays is shown on Fig. 7-9. The computer analysis showed that in the case of Fig. 7 on the uniformly excited radiators by means of choosing length of the smallest linear antenna the first side lobe level can be decreased from -13.2 dB to -20.5 dB, that is smaller level than for circular array. Using tapering amplitude distribution allows to decrease this minimum level some more at 4 dB. In the case of Fig. 8 on the uniform excitement the minimum side lobe level approaches -19.5 dB. For the circular array with notches (Fig. 9) the minimum side lobe level approaches -30 dB in the plane of $\varphi = 0$ and -23 dB in the plane of $\varphi = 45^0$. Identical side lobe level at all the observation planes are equalled of -22.5 dB.

Thus on the basic of the computer analysis the attainable first side lobe levels of the pattern of the plane antenna array were determined.

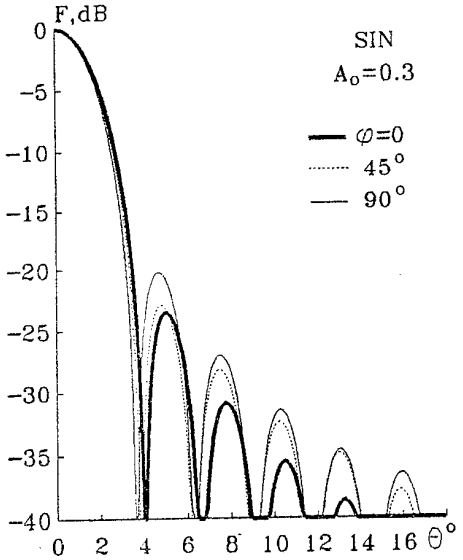


Figure 5. The patterns of the circular array with sinusoidal amplitude distribution.

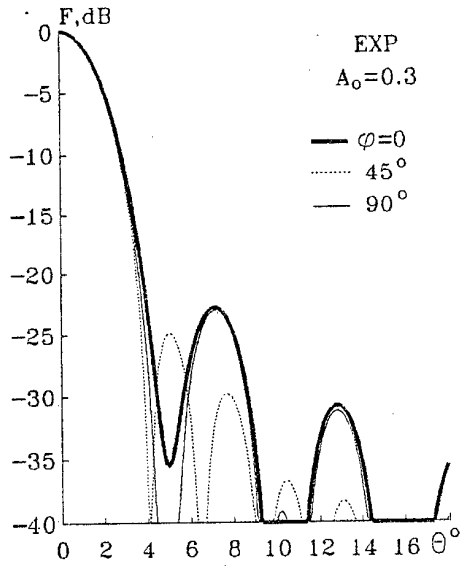


Figure 6. The patterns of the circular array with exponential amplitude distribution

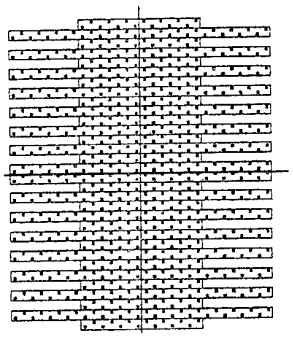


Figure 7. The scheme of the .rectangular array with rarefied aperture in single plane.

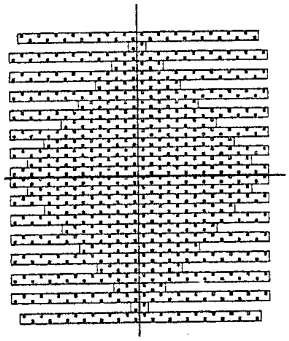


Figure 8. The scheme of the .rectangular array with rarefied aperture in two plane.

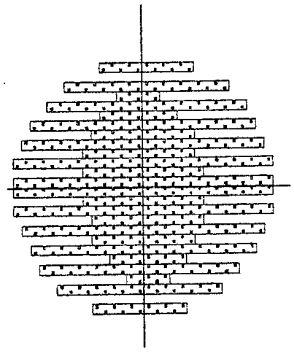


Figure 9. The scheme of the .circular array with rarefied aperture.

References

1. Yu.V. Shubarin. "Microwave Antennas", Kharkov University Publ., 1960, -283p. (in Russian).
2. N.N.Gorobets, Yu.N.Gorobets, A.B.Zholobenko. Tree- parametric representation of amplitude distribution in linear antennas. 3-th Crimean conf. and exhibition "Microwave-technique and satellite receiving, conf. proceedings "Sevastopol, Ukraine, 20-23 Sept., 1993, v.5, p.613-616. (in Russian).
3. N.N.Gorobets, Yn.N.Gorobets, V.I.Kiyko. Decreasing side lobes of plane antenna array. Kharkov State University Transactions, N 405 - Radiophysics and Electronics, Kharkov, 1998, pp.3-10 (in Russian).

INFLUENCE OF SIDE RADIATION ON ONE - REFLECTOR ANTENNA PARAMETERS

N.N. Gorobets, S.S. Vyazmitinova
Kharkov State University, 4 Svoboda Sq., Kharkov 310077, Ukraine
Phone: (0572) 45-71-75, Fax: (0572) 47-18-16, E-mail: Nikolay.N.Gorobets@univer.kharkov.ua

The side lobes of antenna's directive pattern cause a decrease of its gain coefficient, degradation of noise protection of radioelectronic systems equipped with this antenna, harmful effect of the electromagnetic irradiation on the environment. Especially important is reduction of side lobes of the directive pattern of antennas of radiometric systems for remote sensing of atmosphere, hydrosphere and Earth surface. In this connection the investigation to find opportunities to reduce the side irradiation of one of the main types of sharp-directed mm-band antennas - reflector antennas - is topical and urgent for many practical applications in scientific instrument-making and technique. The subjects of investigation in this work are levels and law of reduction of side lobes of directive pattern of parabolic reflector antenna.

The electrodynamic model, algorithm and computer program for calculating the direction characteristics of the antenna being investigated are described in the [1-2]. The system «reflector -irradiator» is being calculated, and the developed programs allow investigation of any variants of reflector-parabolic, spherical, intermediate variants between parabolic and spherical [1], axes-symmetric and with removed irradiation at any variant of waveguide or horn irradiator.

The Fig. 1(a,b) present the dependence of the first side lobe level (SLL) and the gain coefficient (G) of the axes-symmetric one-reflector parabolic antenna with an irradiator in the form of open end of round waveguide on the diameter of irradiator, referred to the wave length.

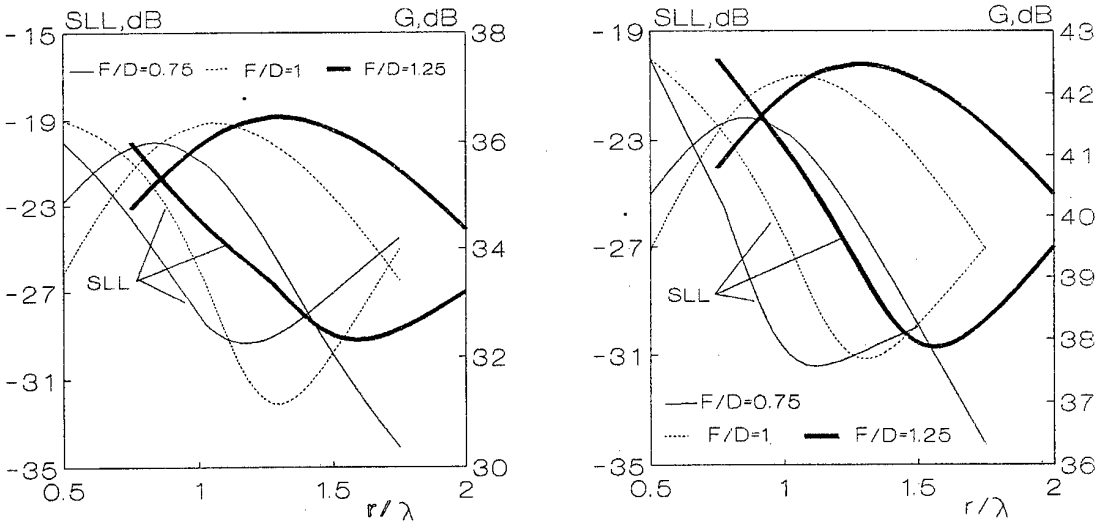


Figure 1. Dependence of the first side lobe level and the gain coefficient antenna from diameter of irradiator.

The diameter of the irradiating aperture of the reflector is 25λ (Fig.1a) and 50λ (Fig.1b). The focus distance of paraboloid varies from 0.75λ to 1.25λ of reflector's diameter (D). As it is seen from the pictures all curves have in the investigated interval $r/\lambda \in [0.5, 0.2]$ one minimum, which with increase of the value F/D swings to bigger values of r/λ. And what is more, the absolute values of argument r/λ, corresponding to the minimum of dependence of the first side lobe level on the dimensions of the irradiator, at all examined values of the parameter F/D and the dimensions of the reflector D/λ =25; 50; 100 remain with graphical accuracy.

In that way, the displayed results testify, that beginning from certain value of reflector's dimension D/λ there is only weak or almost no dependence between the side lobe levels and the D/λ and this level is mainly defined by the focus distance of the reflector and aperture of the irradiator. It is also interesting to mark , that as it turned out a certain dependence exists between the value $(r/\lambda)_{opt}$, where the gain coefficient is the maximum, and the value $(r/\lambda)_{\min SLL}$ corresponding to the minimum of side lobes of direction pattern . It is easy to follow this dependence and according to the results displayed on the fig. 1a,b it appears as :

$$(r/\lambda)_{\min SLL} \approx (r/\lambda)_{opt} + 0.3$$

On the face of it, this is nothing but empirically (by numerical experiment) ascertained formula. However, because by the given D/λ and F/D the side lobes level is determined first of all by the value of r/λ, i.e. by electric dimensions of irradiator's aperture, let's correlate the received result with characteristic properties of irradiator's operation mode .The field of the irradiator, working in the mode of excitation by principle type of wave in the H-plane, up to a constant factor, can be written down in the form [3] :

$$E_{0\psi} \approx \omega\mu kr\{\cos\theta + \frac{\lambda}{\lambda_L} + \Gamma(\cos\theta - \frac{\lambda}{\lambda_L})\} * J_1(\frac{2\pi}{\lambda_g} r) \frac{J_1'(kr\sin\theta)}{1-(\frac{\lambda_g}{\lambda}\sin\theta)^2} \cos\psi$$

where k is the wave number ; r is radius of irradiator's aperture; λ , λ_L , λ_g are wave length in the free space, wave length in the waveguide and the critical wave length; $J_1(x)$ and $J_1'(x)$ is Bessel cylinder function of the first order and argument derivative; θ and ψ are polar and azimuth angles of spherical coordinate system, Γ is a coefficient of wave reflection from the open end of waveguide.

As it is seen from the given example, spreading of irradiator's field on random spherical surface, which center is made to agree with the center of irradiator's aperture, is determined by the property of the argument derivative of Bessel cylinder function of the first kind of unit index in the interval of argument variations, limited by the first and second equation root $J_1'(x) = 0$, which are approximately equal to $x_{11} \approx$ 1.84 and k =5.33. In this interval $J_1'(x)$ is function, regular in all points with one extremum (maximum) [4].

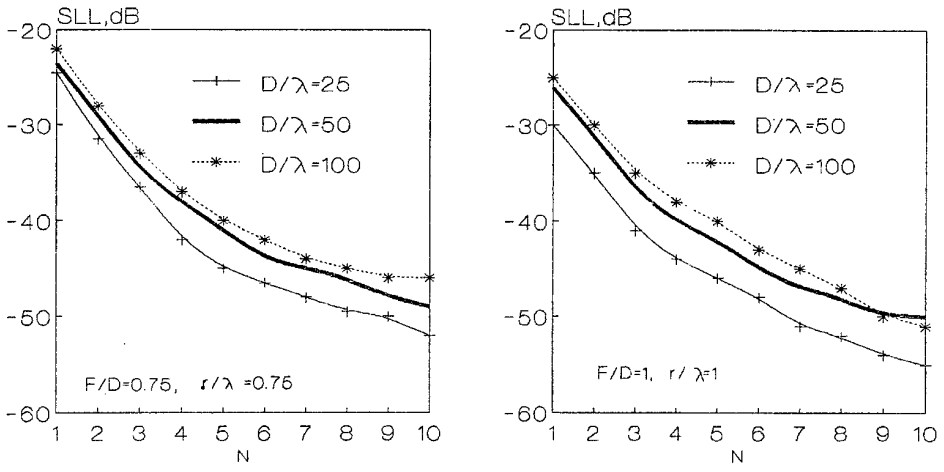
Thus, the efficiency of energy radiation by the open nd of waveguide as well as spatial spreading of this energy do not remain constant in the given interval of argument variations of function $J_1'(x)$, i.e. they depend on the electrical dimensions of irradiator's aperture r/λ. At that, as it follows from the received results, the maximum of the gain coefficient is reached by argument values, which approximately correspond to the extremum $J_1'(x)$, i.e. in the mode of the highest efficiency of energy radiation by the irradiator, and the minimum of side lobes level is reached by some higher argument values. Because the function $J_n'(x)$, as well as the function $J_n(x)$, *(n=0,1,2,...)* have intermittently occurring roots, so the latter means, that the minimum of the side lobes level is reached by such electric dimensions of irradiator's aperture, when a principal opportunity to excite the maximum type of waves occurs , and these waves correspond to the first root of argument derivative of Bessel function of the second index.

In order to characterize more precisely the directive pattern of the antenna out of the direction of the main maximum, let's analyse the law of side lobes reduction. But before we must mark one characteristic property of directive pattern, namely : a width of all side lobes is practically equal as to the level of radiation minimum, anyway as long as application of the method of physical optics for their calculation is rightful. The marked characteristic property of the directive pattern allows while studying the character of reduction of side lobe levels to use as an argument not even the angle coordinates but simply the number of a lobe, what makes the investigation much more easier.

On the Fig. 2(a,b) the dependences on the number of side lobe levels relative to the main lobe of directive pattern are given for reflectors with different electric dimension. The Fig.2a corresponds to $F / D = 0.75$, the Fig.2b to $F/D = 1$. At this for each series of curves, given on the one and the same figure, works the equality $r / \lambda = F / D$. As it is seen from the figures, the law of reduction of side lobe levels by $r / \lambda = F / D$ does not practically depend on reflector's dimensions and can be described with a simple formula:

$$SLL(N) \approx A \exp(\alpha * N)$$

where A is the level of the first side lobe (in decibel relative to the main lobe of directive pattern), N is the number of a side lobe, α is a constant, determining the speed of reduction .



a b

Figure 2 . Dependences of side lobes levels on it's number.

As the figures show, in the limits of each series of curves the spread in values of the multiplier does not exceed several decibels, and the value of constant can remain for all three values $F / D = 0.75, 1.0, 1.25$. Approximately it can be written down : $A \approx -(23...25)$ dB, $\alpha \approx 0.11...0.13$. It also turned out, that in case, when the reflector system is optimized for the minimum of the side lobes, the law of reduction of side lobes works with the same accuracy, but $A \approx -(30...32)$dB.

Thus, basing on analysis of the results of investigation of the main electrodynamic properties of antenna by method of physical optics we can make the following conclusions:

the maximum of the gain coefficient and the minimum of side lobes level are guaranteed by various values of irradiator with the difference of 0.3; at this the maximum of the gain coefficient is reached by the argument values, corresponding to the maximum of the derivative versus the Bessel cylinder function of the first kind of the unit index, and the minimum of the side lobes level corresponds to the argument derivative of Bessel function with the index 2;

the law of reduction of side lobes levels with growth of their number both in E- and in H-planes has exponentially decreasing form.

References

1. Gorobets N.N. , Vyazmitinova S.S. Computer analysis of multibeam reflector antennas. In book «Processing of raster display in automatic systems», 1991, Tula, pp.119-122.(in Russion).
2. Gorobets N.N., Vyazmitinova S.S. Numerical investigations of main parameters of one-mirror antenna with axes-symmetric reflector. Vestnik Kharkovskogo universiteta 1998, N 405, pp. 15-19.(in Russion).
3. Kjun R. Microwave antennas. L. Sudostrojenije, 1967.-p.517.(in Russion).
4. Handbook of mathematical functions (edited by M. Abramoviz and Irene A.Stegan.- M.:Nauka, 1974. - p.832.(in Russian).

MILLIMETRE-RANGE MULTI-CHANNEL TWO POLARIZATION HORN ANTENNA

N.N.Gorobets, V.M.Dakhov
Kharkov State University, 4 Svoboda Sq., Kharkov 310077,Ukraine
Phone: (0572)45-71-75, Fax: (0572)47-18-16, E-mail: Nikolay.N.Gorobets@univer.Kharkov.ua
I.V.Cherny
Center for Program Studies, Russian Space Agency, 84/32 Profsoyusnaya, Moscow 117810, Russia
Fax: 7-(095)-420-2275, E-mail: icherny@cpi.rssi.ru

In trassing or panorama (scan or multibeam) radiometers of mm-range for airspace or ground location an information is usually received by two orthogonal (vertical and horizontal) linear polarizations in several wave ranges. Realization of an antenna with high directivity characteristics and high polarization isolation in a wide wave band for such radiometers meets great difficulties.

One has developed and experimentally investigated a six-channel exciter of a conical horn antenna operating on two polarizations in the range from 18GHz to 182GHz. The exciter is a consequent system of regular circular waveguides cuts corresponding to frequency sub-ranges of diameters connected by conical transition with the corner angle about 90^0 (Fig.1). Information is picked off 5 channels on orthogonal parts of rectangular waveguides with standard cross-sections 11×5,5; 7,2×3,4; 5,2×2,6; 3,6×1,8 and 2,4×1,2mm^2. The latest channel is realized on a circular waveguide with a diameter equal to 1,2mm, where the information is picked by only one (vertical or horizontal) polarization.

The developed exciter was used in conical horn antenna wih a radiating diameter equal to 120mm. The matching characteristics, polarization isolation and horn patterns were investigated experimentally for the exciter in a wide frequency range. Voltage standing-wave ratio (VSWR) of the horn measured without the exciter in the range from 20 to 21 GHz is less then 2,0; for frequencies higher than 21GHz it is less than 1,2 and only for frequencies less than 19,8GHz VSWR of the conical horn with the developed multichannel ecxiter for all waveguide channels is much higher, oscillating in a wide frequency range. Particularly, VSWR variation for the waveguide channel 11×5,5mm^2 is from 1,2 in HF part of the waveguide frequency operating range to 10 in LF range.

Note, that as the antenna is for wideband radiometer, the oscillation of antenna VSWR depending on the frequency is averaged efficiently. Experiment proved the possibility of sufficient improving of the antenna matching in a narrow frequency range within the limits of the waveguide operating frequency range, by means of post waveguide transformer of full resistances.

Isolation of orthogonally polarized channels is an important characteristics of microwave polarization radiometers. It is essentially determined by electromagnetic coupling of the orthogonal rectangular waveguides in the exciter. Fig.2 shows the results of coupling coefficient $|\Gamma|^2$ measurement for 1st and 2nd as well as for 2nd and 1st exciter channels, correspondently, by the waveguide channels with 11×5,5mm^2 cross-section. One can see that in the LF region of the operating frequency range the orthogonal isolation is not worse than -24...-34dB when in HF region it is -5...-15dB. The antenna polarization isolation between orthogonal channels is determined by product of coupling coefficient $|\Gamma|^2$ between the orthogonal waveguides and a ratio of the antenna gain factor G_m on cross-polarized and main components of the field in main pattern maximum $\left|\Gamma_{vg}\right|^2 = \dfrac{G_{m\ \text{crosspol}}}{G_{m\ \text{copol}}}\left|\Gamma\right|^2$.

The developed multichannel antenna patterns were also investigated. The pattern measurements were made in a regime of excitation of the investigated antenna. Generator block of VSWR and attenuation-meter was used as a signal source. In the measurement equipment the detector section and the indicator block of the same VSWR-meter were used in a regime of attenuation measurement.

Fig.3 shows the antenna patterns on the first channel, measured on frequencies 18,2; 18,7 and 19,2GHz in H plane. Fig.4 shows the same in E plane. One can see that within the limits of the mentioned waverange the measured patterns are differed slightly. Side lobes in angle sector $-30^0...30^0$ are absent. Unlike the plane H, the pattern main lobe in E-plane of observation has a table-like shape. Its width on the level -10...-15dB is almost the same in the both orthogonal observation planes, varying slightly within a 5%-range of the operating frequency range.

The antenna pattern was measured also in a regime of the signal frequency scanning in the mentioned above frequency range. The measurement results proved conclusions obtained from patterns measurements by classical method for discret frequencies.

The developed multichannel two-polarization horn antenna could be used itself or as an feed for sharp-directed reflector antenna of trassing or scanning radiometer-spectrometer or scatterometer of mm waveband.

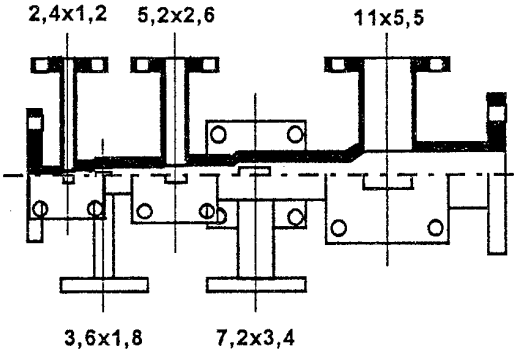


Fig.1. Sketch of the horn antenna exciter

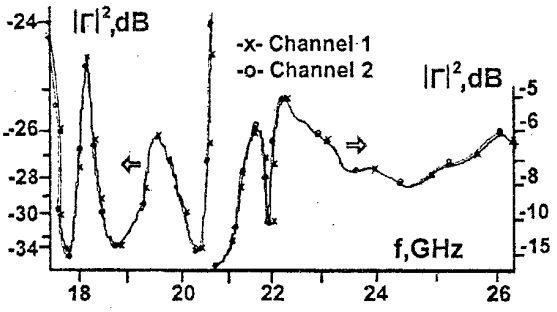


Fig.2. Dependence of the polarizational isolation of the orthogonal waveguide channels of 11x5,5mm² on frequency

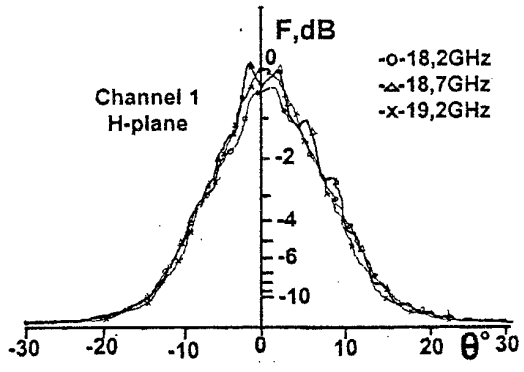


Fig.3. The horn antenna pattern in H-plane

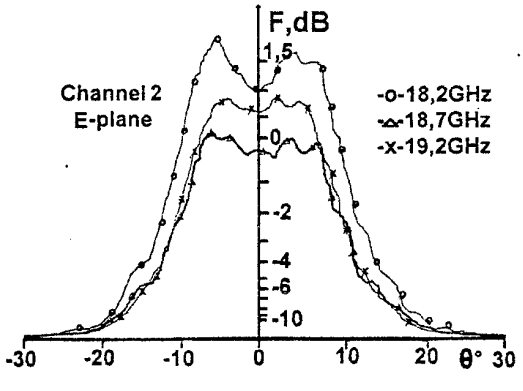


Fig.4. The horn antenna pattern in E-plane

THE PRINCIPLES OF ELECTRODYNAMICS OF PLANAR PERIODIC STRUCTURES

V.V.Khoroshun
Kharkov State University
Svobody Sq. 4, Kharkov, 310077, Ukraine
Tel. (0572) 126727

1. Electromagnetic properties of objects, concering which the discontinuous (periodic) boundery conditions one can use, are studied in electrodynamics of periodic structures (EPS). It concerns both the external and internal problems of EPS. Thus it is a generalization of classical electromagnetics and contains it as a limiting case for smooth surfaces.

2. The basic model of EPS is gyrotropic layer with nonzero thickness, which has one or two side modulated by some periodic law. Dielectric and metallic gratings, including those consisting of wire and infinitely thin strips, are particular cases of such physical model.

3. The basic equation of periodical structure (PS) determines the directions of higher order modes of diffraction spectrums. It is indepenendent of both the geometry and the material of PS as well as the structure of its period. In classical optics it names intensity rise condition in higher order diffraction harmonics and it is of the following form

$$\sin\alpha_n = \sin\varsigma + n\frac{\lambda}{l}, \quad (n = 0,\pm1,\pm2,K) \qquad (1)$$

where α_n, ς, l and λ are n-th harmonic diffraction angles, incident angle, structure period and wavelength of incident EM field, respectively.

4. In order to optimize the spectral characterictics of PS, it is necessary the phase synchronism condition

$$\frac{d}{l} = \frac{m}{2\left|n + (l/\lambda)\sin\varsigma\right|}, \quad (m = 1,2,\ K\ m_k) \qquad (2)$$

and the surface resonance condition

$$\frac{l}{\lambda} = \frac{|n|}{1 - sign(n)\cdot\sin\varsigma}, \quad (n = \pm1,\pm2,K) \qquad (3)$$

be satisfied.

Taking into account (3), formula (2) becomes

$$\frac{d}{l} = \begin{cases} \dfrac{m(1-\sin\varsigma)}{2n}, & (n > 0) \\ \dfrac{m(1+\sin\varsigma)}{2|n|}, & (n < 0) \end{cases} \qquad (4)$$

(here d is grating slot width).

5. In general, two systems of three-dimensional summatory equations are the mathematical model of planar PS. These systems are solved by any sufficiently effective method (AMSh method [1] and its modification for oblique incidence case [2,3], Lewin-Malin's method [4,5], modified Fourier's method and others).

As an example in Fig. 1-3 the numerical results obtained by modified AMSh method are presented. Fig. 1-3 show variation of reflection $|a_0|$ and transmittance $|b_0|$ coefficients of dominant and higher order modes $|b_n|$ versus the l/λ in case of EM scattering by periodic grating consisting of infinittely thin, perfectly conducting strips with period l and slot width d. The incident EM wave is assumed E-polarized and incidence angle is equal $\pi/3$. Formulation of the problem is analogous to one

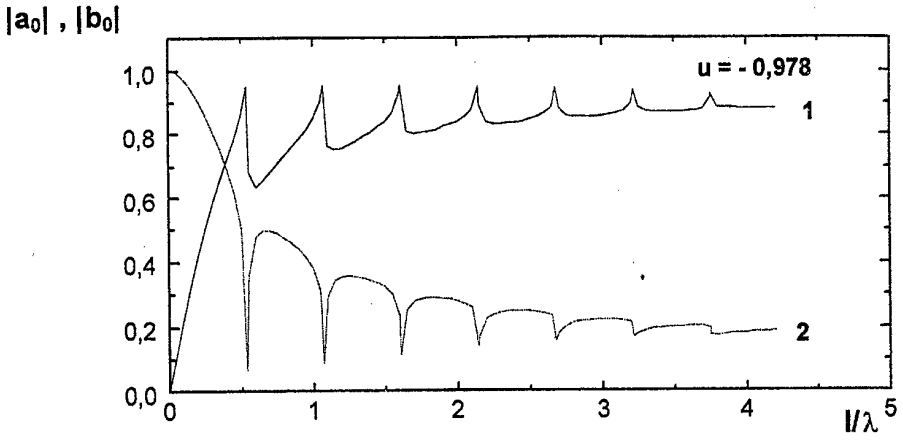


Fig.1. Dependence of reflection $|a_0|$ and transmittance $|b_0|$ coefficients on parameter l/λ for $\theta = 0{,}933$ and $\zeta = \pi/3$

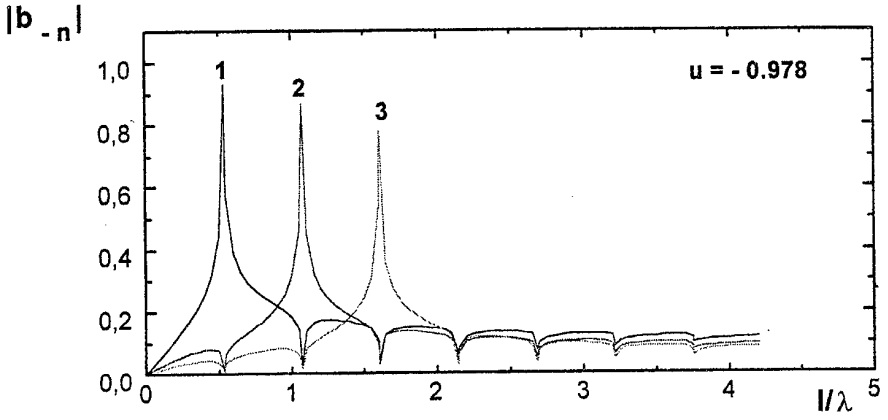


Fig.2. Dependence of transmittance coefficients $|b_{-n}|$ $(n = 1, 2, 3)$ on parameter l/λ for $\theta = 0{,}933$ and $\zeta = \pi/3$

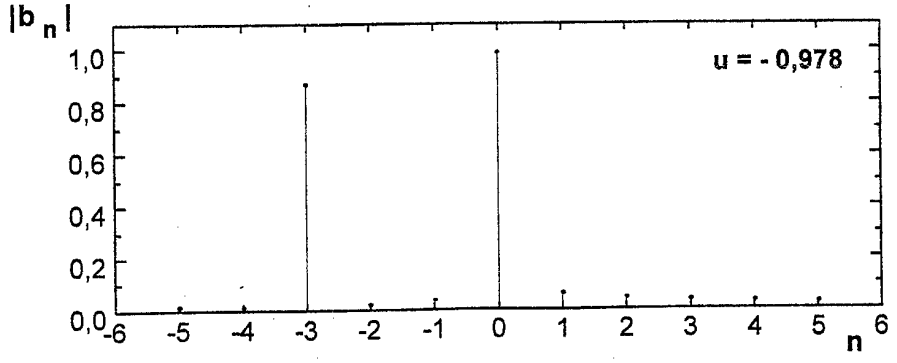


Fig.3. Amplitude spectrum of transmitted field for $l/\lambda = 1{,}608$, $\theta = 0{,}933$ and $\zeta = \pi/3$

accepted in classical optics, namely: in the case of scattering plane EM wave (oblique incidence $\zeta=\pi/3$ on a periodic grating) it is necessery to determine main maximum rise condition in **n=-3** diffraction order.

It follows from (3), that value $\tau = 1.608$ will be sliding point for harmonic **n=-3**. According to (4) value $\theta=d/l=0.933$ and, respectively, $u = \cos\pi\theta = -0.978$ will be correspond $\tau = 1.608$. Solution of SLAE-2 has been obtained by modified AMSh method and dependenses of amplitudes of diffraction spectrum have been built for above-mentioned parameters.

The dependences of reflection $|a_0|$ and transmittance $|b_0|$ coefficients of main modes versus l/λ are represented in Fig.1. Fig.2 shows amplitude of first three negative harmonics $|b_{-n}|$ as a function of parameter l/λ. Fig.3 shows amplitude spectrum of transmited field, consisting, except dominant harmonic the others $N=\pm5$ harmonics. The main maximum for harmonic n=-3 is visible distinctly. Diffraction of H-polarized plane wave on strip grating may be considered in the same manner.

Fig.4 represents variation of transmittance coefficients of n-th mode $|b_n|$ as a function of parameter $\tau=d/(\lambda/2)$ for sliding points of harmonics order n=-1, -2, -3 that is for $l/\lambda=0.536$, 1.071 and 1.608 respectively.

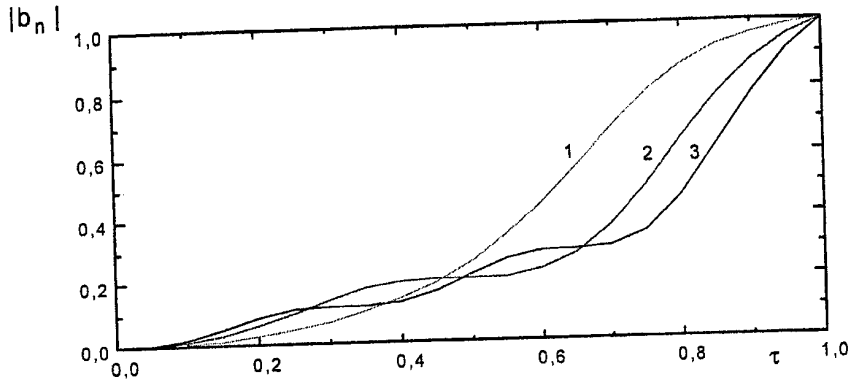


Fig.4. Dependance of transmittance coefficients $|b_n|$ on parameter τ

6. The main statements of planar PS electrodynamics are successfully applied for solution of various problems in which the periodical condition for one or two curve-coordinate is used(cylinder with longitudinal or(and) diametrical slots, sphere with one or several circular openings and others).

References

1. Z.S.Agranovich, V.A.Marchenko, V.P.Shestopalov,"On the diffraction of electromagnetic waves by plane metallic gratings", Zhurnal Technicheskoy Phisiki /in Russian/, Vol.32, No.4, pp.381-394, 1962.
2. V.V.Khoroshun, "On the modification of the method of the Riemann-Hilbert-problem in case of oblique incidence of plane electromagnetic wave on strip gratigs", Vestnik Kharkovskogo Universiteta. Radiophisika i electronika /in Russian/, No.405, pp.137-141, 1998.
3. V.V.Khoroshun, "On the modification of the method of the Riemann-Hilbert problem", Mathematical Methods in Electromagnetic Theory, International Conference Digest, Kharkov, Ukraine, 1998.
4. L.Lewin, IRE Trans., MTT-9, No.4, 1961.
5. V.V.Malin, "On the theory of strip gratings of finite period", Radiotechnika i elektronika /in Russian/, Vol.8, No.2, pp.211-220, 1963.
6. V.V.Khoroshun, "Optimization of the spectral characteristics of strip-type arrays", Telecommun. and Radioeng., Vol.45, No.3, pp.131-133, 1990.

OPTIMIZATION OF THE EIGENMODES SPECTRUM OF PARALLEL-PLATE WAVEGUIDE WITH KNIFELIKE DIAPHRAGM

V.V.Khoroshun, I.E.Pedchenko, N.A.Syvozalizov
Kharkov State University
Svobody Sq. 4, Kharkov, 310077, Ukraine
Tel. (0572) 126727

Phase synhronizm and surfase resonance conditions are used to optimize the spectral characteristics of strip grating excited by plane E- or H - polarized wave [1]. The same method of optimization is applied for optimization of eigenmode spectrum of parallel-plate waveguide consisting discontinuity in the form of infinitely thin and perfectly conducting fin. In this paper discontinuity problem is treated as the scattering problem of the incident guided wave.

The initial boundery value problem reduces to two systems of summatory equations, are solved by AMSh method [2], modified AMSh method [3] and the singular integral equation technique [4,5]. The solution of the problem is obtained in the form of infinitely nongomogeneous sets of linear algebraic equations of the second kind, therefore in this case reduction technique is applicable and one can obtain solution with any given accuracy in advance.

Comparative analysis of numerical algorithm efficiency is obtained by above-mentioned methods. Numerical results are discussed. Recommendations how to find the optimal parameter of investigated structure are given. The investigated structure may be considered as key one for antipodal finlines.

References

1. V.V.Khoroshun, "Optimization of the spectral characteristics of strip-type arrays", Telecommun. and Radioeng., Vol.45, No.3, pp.131-133, 1990.
2. Z.S.Agranovich, V.A.Marchenko, V.P.Shestopalov,"On the diffraction of electromagnetic waves by plane metallic gratings", Zhurnal Technicheskoy Phisiki /in Russian/, Vol.32, No.4, pp.381-394, 1962.
3. V.V.Khoroshun, "On the modification of the method of the Riemann-Hilbert-problem in case of oblique incidence of plane electromagnetic wave on strip gratigs", Vestnik Kharkovskogo Universiteta. Radiophisika i electronika /in Russian/, No.405, pp.137-141, 1998.
4. L.Lewin, "The use of singular integral equations in the solution of waveguide problems", In: Advances in Microwaves, Vol.1, ed.L.Young, Academic Press, New York, pp.212-284, 1966.
5. V.V.Malin, "On the theory of strip gratings of finite period", Radiotechnika i elektronika /in Russian/, Vol.8, No.2, pp.211-220, 1963.

SUPER NARROW-BAND LOW-DIMENTIONAL ULTRA-HIGH FREQUENCY FILTER ON THE BASIS OF WAVEGUIDE-DIELECTRIC RESONATOR

A.A. Zvyagintsev, A.V. Strizhachenko, V.V. Chizhov, V.V. Popov
Microwave Physics Department, Kharkov State University,
Svoboda Sq. 4, Kharkov, 310077, Ukraine; tel.: (0572)-45-74-24,
(0572)- 457319, E-mail: Aleksander.V.Strizhachenko@univer.ua

Modern microwave equipment (ME) promoted several requirements to ultra-high path functional assemblies parameters, particularly, a requirement to low-dimentional frequency-selective devices creation.

In present work the calculation and design of super narrow-band low-dimentional ultra-high frequency filter on the high-Q waveguide- dielectric resonator (WDR) basis it is proposed. Ultra-high filter represents resonator as a section of evanescent rectangular waveguide with flangeds, that includes one or more dielectric inserts, entirelly filled resonator along narrow wall and partially -along wide wall. To satisfy contradictory promotions: narrow bandpass (0,05%-0,1% from central frequency f_0) in the combination with low primary losses α_0 (α_0 <1 dB), it is possible with using a system, whose eigen Q not less than $50*10^3$ units. In such case it is succeeded to reach by the using of the material with low losses (e.g., leukosapphire - $tg\delta = 6*10^{-6}$ under t $=20^0$ C) and with turning of resonator on 90^0 concerning input path (H-plane). Such resonator eigen Q essential rise in comparison with usual WDR it is possible to explain by turning out, in main degree, the conducting currents, passed earlier in metal, that surrounds dielectric, with displacement currents, that permit to decrease the average power of losses in metal walls.

Filter resonant frequency temperature compensation is provided with using of two processes: the process of clearance changing between leukosapphire inserts and the process of filter frequency drift due to dielectric permittivity changing dependence upon the temperature. These two processes mutually compensated each other and, in such case, it is possible to realize the filter resonant frequency temperature compensation.

Designed and produced filters have the following parameters:

- frequency band	- 3 cm;
- passband (on 1 dB level)	- 8 - 10 MHz;
- primary losses α_0	- 0.8 - 1 dB;
- attenuation upon drift Δf from $f_0 + \Delta f$:	
a) dual link filter, not less than	- 20 dB;
b) triple link filter, not less than	- 30 dB;
- central frequency drift f under t = -50^0 C;$+50^0$ C -	-2MHz;
- mass	~ 150 g.

The designed filters will be of using as input circuits of radars receiver-transmitter pathes [1 - 3].

References

1. V.N. Velikotskiy, V.Ya. Dvadnenko, V.A. Korobkin, I.N. Yarmak, "SHF-resonator", A.c. 4622279/09, published in Bull. of Ach., 1991, No.20.
2. V.N. Velikotskiy, V.Ya. Dvadnenko, Yu.P. Yurchenko V.A., I.N. Yarmak, " Mm-band filter on the basis of leukosapphire resonators", Proceedings of 1st Ukranian Symposium "Physics of mm and submm radiowaves", Kharkov, 1991.
3. V.A. Korobkin, V.Ya. Dvadnenko, V.N. Velikotskiy, "Low-dimentional high-Q resonator with leukosapphire using", Radiotechnika i Elektronika, Vol.31, No.6, pp.1243-1245, 1986.

□

SURFACE WAVE HTS RESONATORS

G.A.Melkov, Y.V.Egorov, A.N.Ivanyuta and V.Y.Malyshev.
Kiev Taras Shevchenko University
Adress: 64,Vladimirskaya str.,Kiev,252017,Ukraine
Tel. (044) 266-05-32,Fax (044) 266-06-00, E-mail melcov@boy.rpd.univ.kiev.ua

Nowdays microwave electronics and measuring technics use microstrip and parallel-plate resonators. They must contain two superconducting films to have high quality Q. Besides the manufacture of such resonators for short-wave part of millimeter of waveband is accompanied by both the difficulties of design and increase of losses in the input microstrip and coaxial circuits.

For that reasons we have elabarated several microwave resonators using a single metal or HTS surface (existence of other surfaces only decreases Q). All resonators operate on the surface waves, running along metal. That can be surfase waves running along a solitary metal surface with a finite conductivity (Zennek waves) or surface waves along metal (even ideal) covered with dielectric. As a result, the microwave resonators can be formed with the properly sized pieces of an HTS wire, rod, plate, single-side film on a dielectric substrate.

Theoretical analysis of the resonant frequencies has been carried out by decomposition method [3,4]. Resotator, which use two dielectrics is placed in waveguide has been considered. . Such resonator is shown on Fig.1.

Firstly, the own waves of waveguide which has section shown on Fig.1 were described for determination of the resonant frequencies of such resonator. Waveguide has been devided into four partial areas:

I. $0<x<a, 0<y<(b-l)/2$;
II. $0<x<a, (b+l)/2<y<b$;
III. $0<x<D, (b-l)/2<y<(b+l)/2$;
IV. $D<x<a, (b-l)/2<y<(b+l)/2$;

The fields of own waves of waveguide were distributed on fields of LM and LE waves.[4]. Only 20 first waves were used in every area. The tangent components of electrical and magnetic fields were equaled on borders of areas.

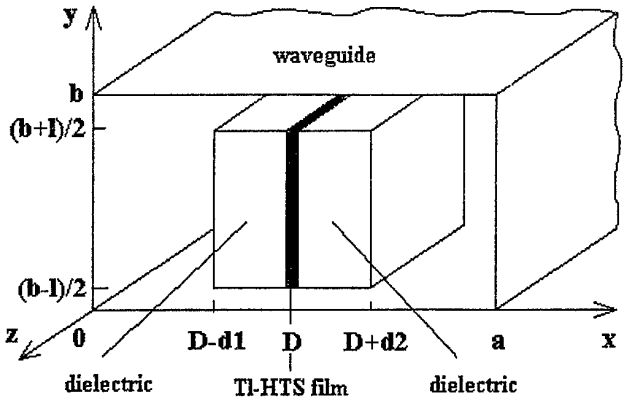


Fig.1 Resonator in waveguide.

Herewith the fields and the spreading-constants of the own waves of such waveguide were found. . The resonator in waveguide has been devided into three partial areas:

I. $z<-w$;
II. $-w<z<w$;
III. $z>w$;

The fields in the first and the third area were distributed on fields of empty waveguide. The fields in second area were distributed on fields of loaded waveguide. It was considered that $z=0$ - magnetic wall . The tangent components of electrical and magnetic fields were equaled on borders. So the resonant frequencies

of such resonator were found. The dependence resonant frequency for the first mode of such resonator on its length is shown on Fig.2-3. Also it is shown results of measurements of a resonant frequency. It is seen that results of theories and experiment coincide with accuracy before 5%.

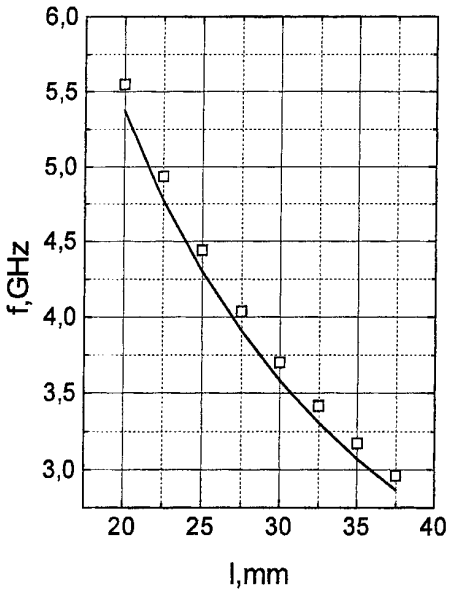


Fig.2 Resonant frequency of film with single dielectric. thickness 1mm, dielectrical permeability ε=9.8, D=11,75mm, w=1.9mm. Solid line – theory, squares - experiment.

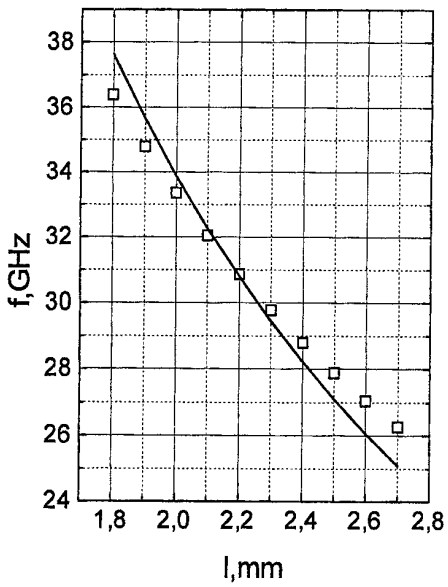


Fig.3 Resonant frequency of film with two dielectrics, d_1=0.2mm, d_2=0.5mm, ε_1 =25, ε_2 =9.8.D=1mm, w=1.9mm.

Unloaded Q-factor of such system was calculated with formula

$$\frac{1}{Q_0}=\frac{1}{Q_n}+\frac{1}{Q_b}+\frac{1}{Q_f}$$

where

Q_n- Q-factor is appearing because of losses in narrow walls,

Q_b- Q-factor is appearing because of losses in broad walls,

Q_f- Q-factor is appearing because of losses in HTS film.

Every Q-factor was calculated on formula

$$Q_i=\frac{\omega W}{P_i};$$

ω -frequency of oscillations;

W -energy of system;

P_i -loss power.

The dependence Q-factor on frequency is shown on Fig.4. We suggested, that surface impedance of HTS film square-law has been depended from frequency. From Fig.4 it is seen that unloaded Q-factor is defined in the main by Q-factor of HTS film.

Thereby new class of resonators on base of surface wave was created. The resonant frequencies and Q-factors of this resonator were counted and measured. Such resonators are easy in fabrications, have high Q-factor and can use for measuring of surfase impedance because own Q-factor is defined by Q-factor of HTS film.

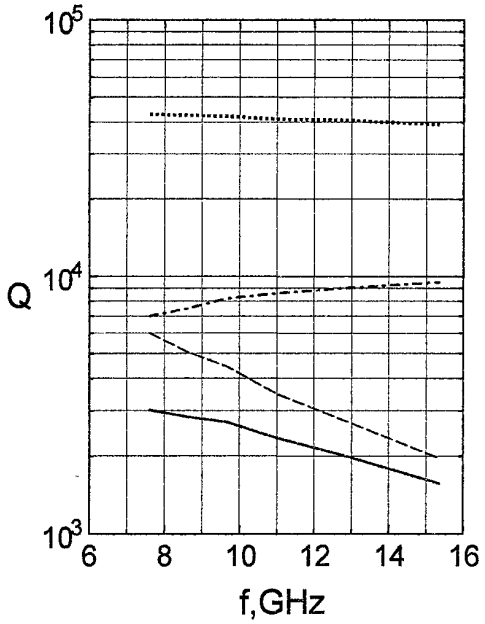


Fig.4. Theoretical dependence unloaded Q-factor of resonator on frequency for case Fig..2. Solid line-Q_θ; dash line-Q_f; dash-dotted line-Q_b; dotted line-Q_n;

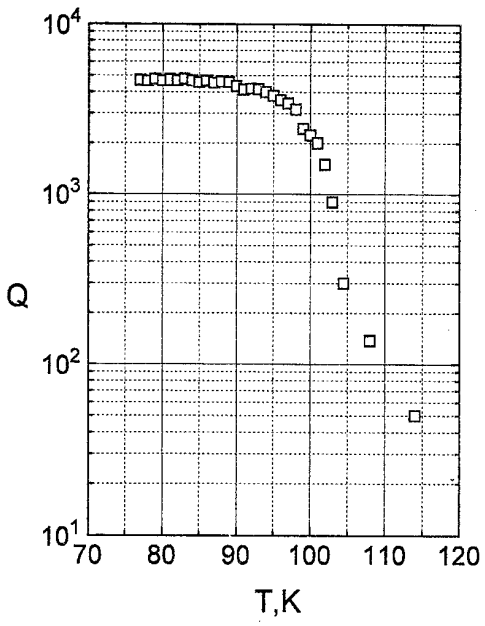


Fig.5 Experimental dependence Q-factor of resonator with Tl-film (Fig.1) on temperature. f=8.7GHz, d_1=0.5mm, d_2=0.5mm, ε_1=25, ε_2=9.8. D=11.75mm, w=1.9mm.

References

1..*Левин В.* Теория волноводов.-М.:Радио и связь,1981.
2.*Ваинштейн Л.А.* Электромагнитные волны.-М.:Радио и связь,1988.
3.*Адамс М.* Введение в теорию оптических волноводов.-М.:Мир,1984.
4.*Михайлевский В.С. и др.* Линии передачи сложных сечений.-Р.: Ростовский государственный университет,1983.
5.*Chang K.,Khan P.J.* Analysis of a narrow capacitive strip in waveguide// IEEE Trans. on MTT – 1974.-vol.22-No5.-P.536-541.

THE PHASED ARRAY ANTENNA FOR THE RADAR OF A MILLIMETRIC AND CENTIMETRIC RANGE

B.N.Bakhvalov, A.V.Gomozov, L.V.Kostenko
Joint-stock company NIIRI
271, street. The academician Pavlov, Kharkov, 310054, Ukraine
Ph. 262325, Fax: 264112, e-mail: niiri@ cnti.kharkov.ua

The phased array antennas (PAA) find broad application in radars and other radio engineering systems of various assignment for scanning of the directional diagram in angular coordinates. Defect of known PAA is that they usually contain a plenty of emanating elements and controlled phase shifters, that essentially increases sizes and cost of an antenna. Other defect of PAA is that for the circular review on an azimuth frequently it is necessary to rotate PAA together with a receive-transmitting cabin, and the high-power electric motor is necessary for this purpose.

A new engineering solution on construction of PAA for the ground radar of detection and controlled direction of millimetric and centimetric range is offered below, in which the mentioned above defects are eliminated.

A problem of the offer is the construction of PAA, in which, at the expense of fulfilment of the array antenna as two fixed concentric rings of feedhorns on the flat horizontal aperture and the use of a flat metal reflector rotated on an azimuth, it is ensured significant reduction of an amount of emanating elements and phase shifters for want of preservation of directed properties of an array antenna and diminution of a demanded potency of the electric motor of rotation on an azimuth.

The delivered problem is decided by observance of the following offers concerning horn emanating elements with wave guides and controlled phase shifters contained in the phased array antenna of the radar:

the array antenna is executed as two concentric rings of feedhorns on the flat horizontal aperture, and the radius of the internal ring twice is less, than the external;

in structure of the antenna in addition are included a flat metal reflector of the elliptic form, inclined to the horizontal plane under an angle 45°, and an electric motor of rotation of the reflector on an azimuth.

The offered configuration of accommodation of horn emanating elements on the flat horizontal aperture allows considerably to reduce total number of such elements and phase shifters but to preserve directed properties of the antenna. For this purpose the interference far-out sidelobes of the directional diagram of the array antenna are suppressed by the directional diagram of horn emanating element. The array antenna of feedhorns and the receive-transmitting cabin of the radar are motionless, and for the circular review on an azimuth only a flat metal reflector of little weight rotates.

The offered device ensures of reductions in 10 and more time of an amount of emanating elements and phase shifters of the array antenna for want of preservation of its directed properties and significant diminution of a demanded potency of the electric motor of rotation on an azimuth, that essentially reduces cost of the antenna.

A technical essence and principle of an operation of the offered device are explained on fig.1, where the simplified sketch of the offered array antenna is represented.

Structure of an offered antenna on fig.1 includes the following basic elements:

outside ring of horn emanating elements 1 of conic feedhorns of identical polarization;

the internal ring of horn emanating elements 2 (radius of the internal ring twice is less, than at the outside ring);

flat metal reflector 3 of elliptic form;

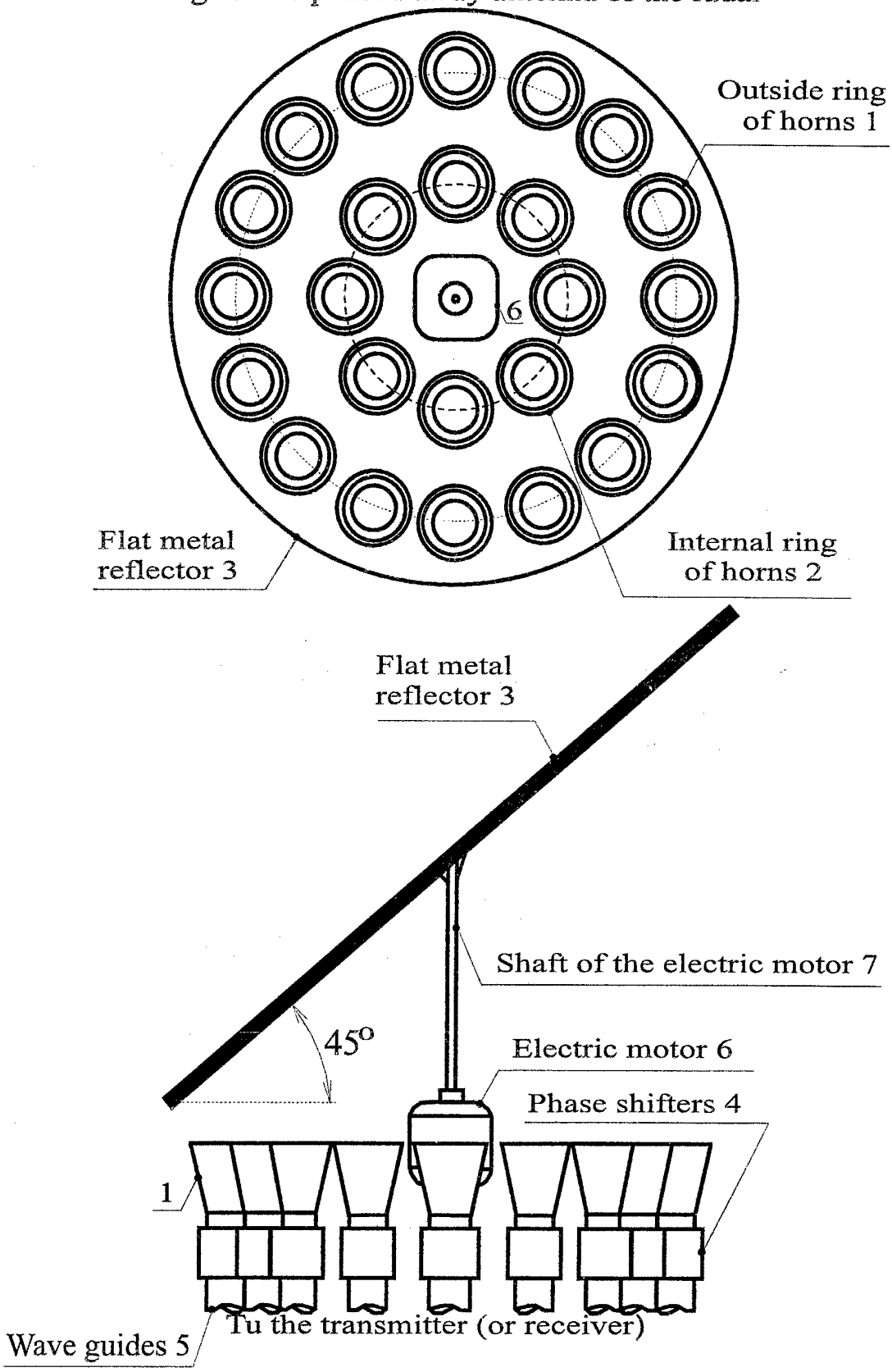
controlled phase shifters 4 of emanating elements;

round wave guides 5;

electric motor 6 rotations of the reflector on an azimuth;

shaft of the electric motor 7.

Fig.1. The phased array antenna of the radar



It is offered not to rotate on an azimuth the emanating elements of the array antenna and the receive-transmitting cabin of the radar, and to place the aperture of the array in a horizontal plane on the roof of a fixed body of the cabin of the radar. For want of it the array of feedhorns will radiate vertically up. For maintenance of the review in a narrow sector of rather small elevation angles above a surface of the ground it is offered to use the flat metal reflector, inclined under an angle 45° to the horizontal plane of the aperture of feedhorns. The circular review of space on an azimuth is offered to be realized by rotation the reflector on an azimuth with the help of an electric motor. The reflector is possible to execute as a grid of wires with a small-sized cell for little weight. For want of review on an azimuth only the reflector rotate, and the array of feedhorns and the receive-transmitting cabin of the radar are motionless. It allows considerably to reduce a demanded potency of the electric motor of rotation on an azimuth.

For reduction of an amount of emanating elements the array antenna for want of preservation of a former size of the aperture and breadth of the main petal of the directional diagram it is required to increase distances between adjacent elements. It is known, that in this case there are heavily interference petals of the directional diagram, which essentially worsen directed properties of the antenna and reduce security of the radar from radio interference coming on these petals. For elimination of these defects it is offered to place emanating elements on two concentric rings on the flat aperture for want of preservation of former outer size of the aperture of the array antenna. The distance between adjacent elements of a ring still remain rather small and it will not reduce in emerging significant interference petals of the directional diagram of the antenna. The interference far-out sidelobes will appear in this case only because of a significant distance on a radius between two rings. These interference far-out sidelobes are offered to be suppressed by the directional diagram of a single feedhorn. For this purpose the size of the aperture of the single feedhorn emanating element should be selected rather large, that also will reduce total of emanating elements. In an outcome the interference sidelobes of the directional diagram of the antenna will be suppressed and the antenna will save the directed properties in spite of considerably smaller amount of emanating elements and their phase shifters.

The conducted accounts have shown, that the directional diagrams of the offered antenna in horizontal and vertical planes practically are identical. The accounts have shown also, that the offered array antenna does not concede to the equivalent prototype on directed properties and level of the sidelobes of the directional diagram, but contains considerably smaller amount of emanating elements and phase shifters.

In the offered device for circular review on an azimuth it is not required to rotate the array antenna and the receive-transmitting cabin of the radar, and it is required to rotate only the reflector of little weight, therefore there is required a considerably smaller potency of the electric motor of rotation on an azimuth .

Scanning of the directional diagram of the offered antenna in a small azimuth and elevation sector is realized by a modification of shifts of phases of controlled phase shifters. The difference consists only in magnitude of these shifts of phases, which can easily be determined from known geometry of the antenna.

It is necessary to mark, that in the offered antenna for want of linear polarization of feedhorns the polarization of emitted radiowaves during the circular review on an azimuth will be changed from horizontal up to vertical, but it does not hinder work of the radar.

The reflector, inclined to for a horizontal on 45°, with the electric motor of its rotation on an azimuth are necessary for a realization of the circular review on an azimuth. In the offered device it is not required to use gyratings of a concatenation of wave guides, as the array antenna is motionless, and rotate only the reflector.

The accounts have shown, that in the offered array antenna the least level of a side radiation will be in case, when the radius of the outside ring of feedhorns twice is more, than the radius of the internal ring, therefore is recommended to select the indicated ratio of these radiuses. It is expedient to use only two rings of feedhorns on the aperture of the array, that as magnification of an amount of rings does not result in reduction of a side radiation, but only increases an amount of emanating elements and phase shifters . The accounts have shown also that it is not enough of one ring of feedhorns because then a level of a side radiation will increase considerably.

Thus, the offered device ensures reduction in 10 and more time of an amount of emanating elements and phase shifters of the array antenna for want of preservation of its directed properties and significant diminution of a demanded potency of the electric motor of rotation on an azimuth, that essentially reduces cost of the antenna.

Ring antenna array of millimiter wavelenght band

V.N.Rudenko, E.I.Solokha, V.I.Gomozov, L.V.Kostenko
Joint-stock company Research institute of radio engineering measurements
310054 Ukraines, Kharkov, street. The academician Pavlova, 271
Ph. (0572) 26-52-00, fax (0572) 26-41-12
E-mail: niiri@ cnti.uanet.kharkov.ua

General principles of construction of linear (flat) antenna arrays (LAA), are aplicable and for ring (nonplanar) antenna arrays (RAA). The conducted researches have shown, that the directional properties of RAA are much worse than those of LAA of identical geometric sizes, especially it concerns RAA of millimeter wavelength band. This deterioration of directional properties is exhibited in the extension of the main maximum (MM) of the directional diagram (DD), in growth of side petals (SP) and in a displacement of direction of MM relatively the designed one.

Except for deterioration of directional properties at existing RAA,problem of scanning is complicatedly decided which will be realized with the help as unguided, and with the help of controlled devices

Let us consider possible ways of development of RAA, at which are loosed the marked defects.

Investigating directed properties RAA, we mark, that majority from developed RAA have, above marked, drawbacks for the following reasons:

1. Phase distribution (PD) on an equivalent linear antenna array (ELAA) will be quadratic.

2. The peak distribution (PD) on ELAA will be not uniform, but with rise on edges.

3. Angles of orientation of main maxima (MM) DD of antenna elements (AE) do not coincide one with another.

For elimination of quadratic PD on ELAA on outputs of each AE the phase shifter (PS) with fixed significance of a phase v is installed, at which the condition of equal phase of flat aperture should be executed.

As fixed PS it is possible to use lines of transfers of certain length.

Obviously, that ELAA will be unequidistant, as to edges ELAA a distance between projections of phase centres (PC) AE d will decrease. It is equivalent to increase of peak distribution PD to edges, even if AE on an arc of a circle are excited uniform by amplitude of a current (voltage). For elimination of this defect it is necessary after the block, of fixed PS to place the block of amplifiers with a small level of noise and with, adjusted,(only to set-up and AT scheduled tasks RAA) factor samplifications. It will allow to generate such PD, for want

of whichis reached as an acceptable breadth DD q, and is minimum possible level of a side radiation (F).

For a diminution of distortions DD, called not by a parallelismdirections MM DD AE, it is offered in quality AE to useantenna modules (ÀÌ), each of which consists from two antenna emitters (AE), which PC are deleted on fixed distance d. Using the phase shifter with a fixed phase, it is possible to achieve that MM DD ÀÌ will be directed on MM DD ELAA.

All transferred systems are executed as a quadripole with an amount of inputs equal to an amount connected AE.The amount AE is determined by required parameters of performancesdirectednesses: by a breadth DD on a level of a half potency andby allowable magnitude of side petals. The scanning will be realizedin a plane of a disposition RAA.

From the made accounts and outcomes of modelling RAAit is possible to make the following conclusions:

1. With growth of a radius modified RAA a breadth DD qdecreases, and the level of a side petal F will increase, and,for want of small amount ÀÌ such modification q and F results to stabilization an amplfication factor G, and for want of plenty ÀÌ fasterthe growth F results in decrease G.

2. Weight peak factors and for smallthe amounts ÀÌ are changed in small limits: from 1 up to 2.,whereas for a plenty ÀÌ the same factorsare changed from 1 up to 16.

3. Breadth DD of one ring RAA in a vertikal plane,makes magnitude, order q of ~ 70, and level of a side petalF ~ 0,25 (-12ldB).

4. For simplification of a construction RAA it is offeredscanning DD to realize by switching group ÀÌ, withwhich help is formed MM of a required breadth..

Developed modified RAA can find applications:

for a rough bearing; for want of it one is used onlygroup AE;

- for a point bearing; for want of it two groups AE and are usedthe peak monoimpulse method direction finding will be realized;

- for a solution of navigational problems with the help of of companions two groups AE are used, which DD are directed inthe opposite parties.

References

1. D. I. Voskresencky and other. Convex scannings of an antenna. (Fundamentals of the theory and methods of account).-M: Sov. radio, 1978.-304 p.

Electromagnetic Modelling of Microwave High Power Multiplexers (KARKOV, UKRAINE, SEPTEMBER 15-17, 1998)

B.I.Makarenko*, A.S.Soroka*, I.S.Tsakanyan*
*Scientific-Research Institute of Radio Engineering Measurements Joint Stock Company
Acad. Pavlov Street, 271, Kharkov, 310054, Ukraine,
Tel. 7(0572)26-23-25, Fax.7(0572)26-41-12

High electrical requirements are presented to multiplexer used for combining of high power transmitters with different frequencies and receiving frequency separation. In this case isolation between receiver input and transmitter outputs and multiplexer matching with transmitter must be the best. De-signing such high power multiplexer (HPM) is usually complicated and demands laborious regulation.

It have been shown that required electrical characteristics of multiplexer one could provide by applying rejectors with higher "closed" modes and hybrid junctions with three mode coupling region, simultaneously obtain decreasing mass and size characteristics and more simple design.

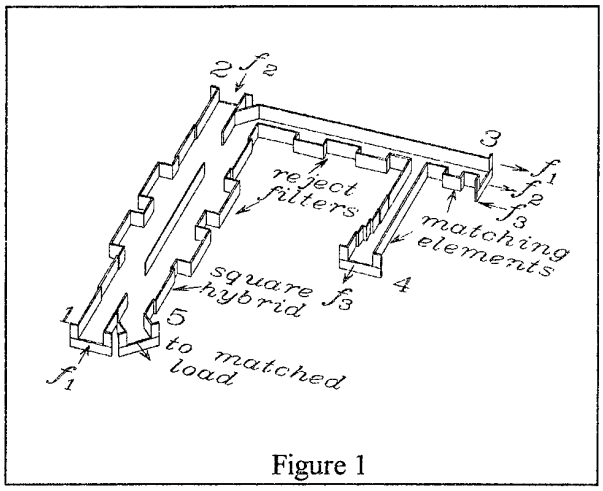


Figure 1

The multiplexer represents tenport waveguide H-plane arrangement (see Fig.1) intended for combining two trans-mitter signals with frequencies of f_1 and f_2 and separating these signals from re-ceiving signal with frequency of $f_3 \gg f_2 \geq f_1$. The structure have not any tuning elements, so high exactness of structure geometry have been provided on the stage of mathematical modelling.

We have elaborated mathemati-cally exact HPM models in the system of electrodynamic simulation SES-04 [1], which based on the decomposing principle of solving the boundary electromagnetic problems. The base elements as structural components was follows waveguide H-plane irregularities: semiinfinite bifurcati-on, step of cross waveguide section, T-junction and angled bend. The diffraction problems for H_{p0} mode in rectangular waveguide with set of such discontinuities was solved by the moment method.

In proposed HPD the identical pairs of square hybrids and reject filters are used for combining two signals of microwave frequencies f_1 and f_2 which differ on 100 MHz. The matching of hybrids was realized with the help of asymmetrical widening of threemode coupling region. The reject filters consist of two open coupling twomode waveguide resonators which formed by asymmetrical waveguide widenings for reflecting signal f_2. The reject filter reflecting signal f_3 to the waveguide 4, cut-off at the frequencies f_1 and f_2, is used for separating receiving and transmitting signals.

The HPM model has following calculated characteristics: direct losses of signals f_1 and f_2 in the band of 40 MHz - 0.08 dB, VSWR of transmitter inputs 1 and 2 are less than 1.22, isolation between them - 35.6 dB, nonuniformity of the group time delay is less than 1.5 ns; VSWR of input port 3 is less than 1.24 for the signal f_3 in the band of 40 MHz, losses - 0.064 dB, passing damping between port 3 and ports 1 and 2 are near 39 dB, nonuniformity of the group time delay for the f_3 is less than 0.4ns.

So HPM having simple and stiff construction provides low losses in operating bands and high isol-ation between transmitters, full isolation of receiver from transmitters, good matching.

REFERENCES

[1] A.A.Kirilenko,M.V.Lukhanin,V.I.Tkachenko, SES-04 and its applications in applied electromagne-tics. -In: Theory, elements and components of antenna feedlines/ Kharkiv, Test Radio, 1989. -P.146-165.
[2] B.I.Makarenko and others. Multistep Directional Couplers with Multimode Coupling Region. -In: Proc. 5th Int. Symp. on Recent Advances in Microwave Technology, Kiev, 1995. -P.295-298.

SIMULATION of MULTICHANNEL WAVEGUIDE POWER DIVIDERS (KARKOV, UKRAINE, SEPTEMBER 15-17, 1998)

A.S.Soroka*, A.O.Silin*, V.I.Tkachenko**, I.S.Tsakanyan*
*Scientific-Research Institute of Radio Engineering Measurements Joint Stock Company
Acad. Pavlov Street, 271, Kharkov, 310054, Ukraine,
Tel. 7(0572)26-23-25, Fax.7(0572)26-41-12;
**IRE NASU, 12 Ac.Proskura St., Kharkov, 310085, Ukraine, Tel. 7(0572)44-84-28

Three types of microwave waveguide multichannel power dividers based on H-plane hybrid junctions (Fig.1), E-plane T-joint (Fig.2), H-plane launcher on higher waveguide modes (Fig.3) are represented in the work. Mathematically exact investigation of such devices have been done by means of the system of electrodynamic simu-lation, which consisted in decomposing of boundary problem on a set of elementary dis-continuites of irregular wave-guide. These were: angle bend, half-infinity bifurcation in H-plane and the same discontinuities in E-plane. The diffraction problems of H modes at above mentioned elements have been solved in assuming the metal surface to be ideal conducted. Multimode S-matrix of bifurcation and step were calculated by the method of moment. Noncoordinate problem of waveguide bend was solved by the semiinvertion method. Recomposition of original structures was carried out by the method of S-matrix.

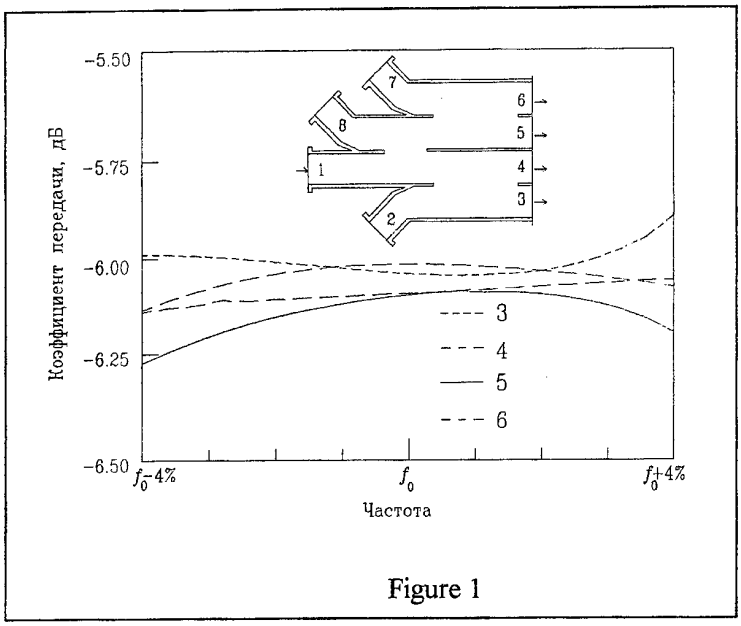


Figure 1

Fig.1 shows the H-plane crossection of 4-channel divider which represents three hybrids with treemode coupling region in single construction. The divider has simple compact technological construction. The output ports of the first hybrid are the in-put ports of the second and third ones. Mat-ched loads are connec-ted to the ports 2,7,8. So the divider has one input port 1 and four output ports 3,4,5,6. It should be noted that the resonance of reflection coused by H_{30} mode arises out of the operating frequency band. So there is not necessity for its suppression. In the frequency range more of 8% hybrid has the VSWR not exceeding 1.24, the irregularity of power division less than 0.3 dB,

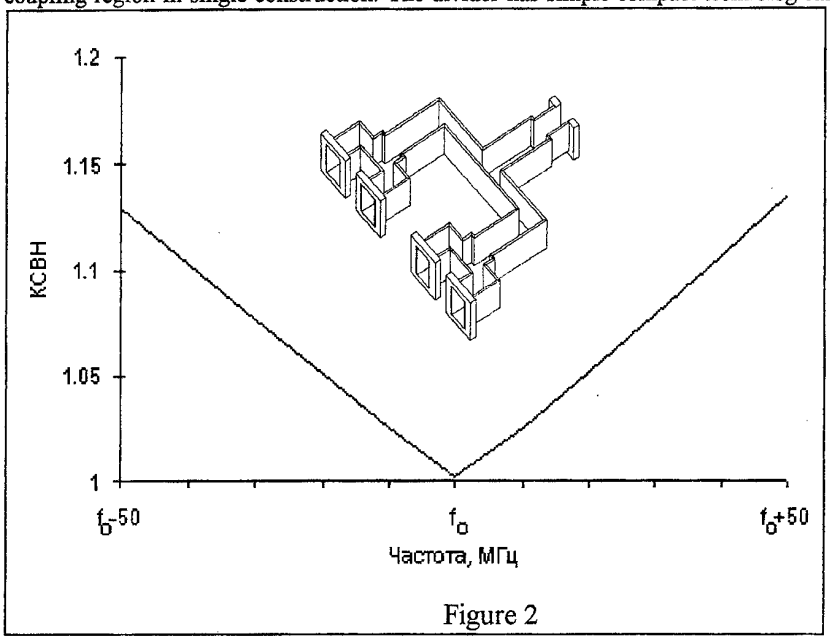


Figure 2

isolation not worse than 19.3 dB. Besides Fig. 1 shows the dependence of irregularity of power division on frequency in the operation range. The curves 3, 4, 5, 6 correspond to the different values of VSWR in output netrks: 3 - 1.1, 4 - 1.2, 5 - 1.26, 6 - 1.15.

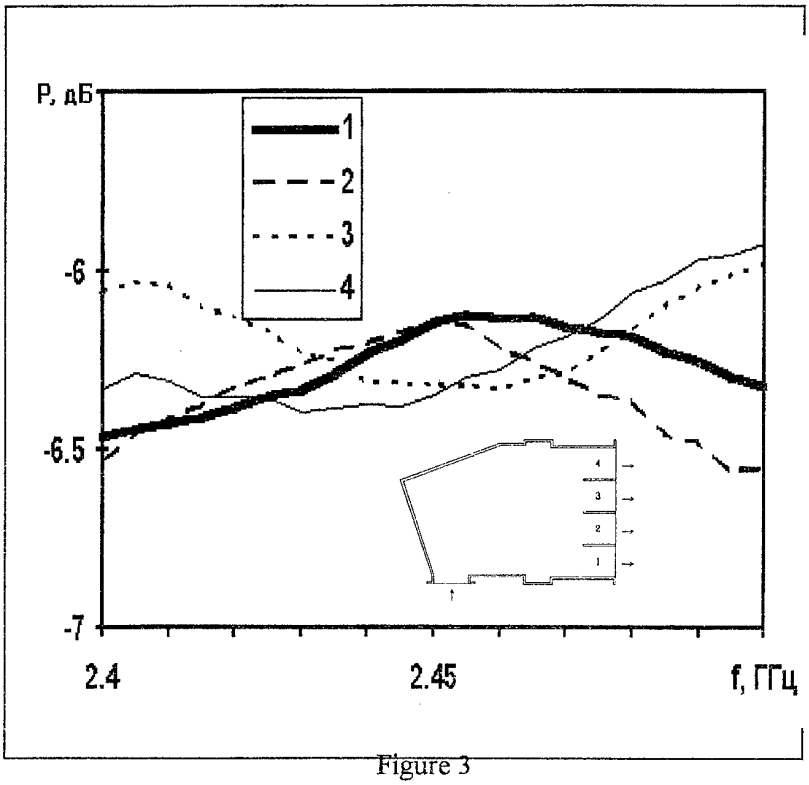


Figure 3

The 4-channel divider represents three E-plane hybrids in a single device (see Fig. 2). Matching of single T-junction provides by reduced cross section of side ports and their length divisible by $\lambda_g/4$ and step-like expansion of the waveguide entrance. In a result in given band of frequencies calculated input VSWR of such junction does not exceed 1.025, while for unmodified junction VSWR makes 2.6. Frequency dependence of input VSWRof designed divider is shown on fig. 2.The 4-channel divider on the base of E-tees provideds VSWR less than 1.13 in the range f_0 ±50 MHz and irregularity of power division not exceeded 0.04 dB.

Fig.3 shows the H-plane crossection of divider based on the H_{40} mode launcher which represents a bend joint of multimode rectangular waveguides. The idea of such a divider was moved in [1,2] and now have been realised. The launcher consists of three nonsymmetrical bends and provides transformation of input power (H_{10} mode in waveguide) with efficiency of W_{41}≥95% in frequency range 8%, VSWR is less than 1.3. For the sake of increasing transformation efficiency we have used steplike H-plane flare of oversized waveguide, so it would supported H_{50} mode at the frequency slightly higher than central frequency. For the sake of high purity of H_{40} mode it should created another steplike discontinuity. The analysis of such multimode structures carried out in details in [3,4] showed that efficiency increased to the value of W_{41} =99.48 with VSWR = 1.085. The results of experimental investigations for the 4-chan-nel experimental device are shown on Fig.3). After optimal adjusting the irregularity of power division was not worse than calculated value.

High accuracy of mathematical models allows to apply precise technology for manufacturing such devices without any adjusting elements. So such devices have high electrical strength, compactness and reliability.

REFERENCES

1. À.À.Kirilenko, M.B.Lukhanin, V.I.Tkachenko " SES-04 and its using for applyed electrodynamics", In "Theory, elements and devices of feeder networks", Kharkov, "Test-Radio", 1989.- P.146-165.
2. A.A.Kirilenko, L.A.Rud, V.I.Tkachenko "New type of microwave power dividers ", In Proc. 5-th Int. Sympos. on Recent Advances in Microwave Technology. Vol.II, Kiev, Ukraine, Sept. 11-16, 1995.
3. B.I.Makarenko, A.S. Soroka, A.O..Silin, I.S.Tsakanyan "Waveguide hybrid junctions with three-mode coupling region ","Radiotekhnika", Moscow, 1996., N8, p. 65-70.
4. V.I.Òkachenko, I.S.Tsakanyan "Waveguide multichannal power dividers based on the effect of mode transformation", "Radiotekhnika", Moscow, 1996., N8, p.71-76.

ON APPLICATION OF MULTICOMPONENT COPPER ALLOYS FOR MAKING MICROSTRIP LINE CONDUCTORS OF EHF MICROCIRCUITS

V.A. Bessonov, S.A.Barantsev, I.I. Uliyanova
Scientific Research Technological Institute of Instrument Engineering
40/42, Primakova Str., Kharkov, 310010, Ukraine
Tel.(8-0572)126048, Fax (8-0572) 271568

Microstrip lines, the fragments of lines to transmit EHF (extreme high frequency) energy, are one of a basic component in EHF microcircuits. Microstrip lines with a variety of geometric dimensions and configurations are also used as a integral part in the following EHF microcircuits: guided power dividers, filters, time-phase formers and others [1].

The main requirements asked for microstrip lines are a proper value of characteristic wave impedance, minimum losses in electromagnetic energy, maximum permissible value in transmitted power, high adhesion to an insulator substrate and long-term parameters stability during the microstrip lines operation.

The well-known multilayer structures such as Cr-Cu-Au, Cr-Cu-Sn-Bi and others used for making microstrip line conductors suffer from numerous drawbacks. The most essential of these are inadequate interlayer adhesion and great value of a contact resistance between the layers leading to decrease in reliability of the microstrip lines under their exploitation [2].

For the first time the author [2] initiated to develop the production process for microstrip lines with thickness range from 5 to 6 μm on the basis of BrNMnT5-2-0.1 industrial copper alloy. Yet the principal limitation for using this alloy as a material for microstrip line conductors proved to be a comparatively low value of the quality factor for test resonators (it is less than 150 nominal units) which is substantially inferior to that of microstrip lines with the conductors based on pure metals. Thus the purpose of our work is to develop new compositions for the copper alloys in order to reduce electromagnetic energy losses in microstrip lines providing invariability of a high conductor adhesion to an insulator substrate, fine weldability and solderability of these microstrip lines.

In the present work for making microstrip lines it is proposed to use the multicomponent fractionatable copper alloys Cu-Mg-Cr-Ti and Cu-Mg-Ge-Sn during thermal evaporation of which the "gradient" films with required parameters are being formed.

The experiments on obtaining the conductors based on these multicomponent alloys were performed using UVN 71P-3 vacuum-pumping installation under the following conditions: the temperature of a polycor substrate was approximately equal to 300°C, the pressure in a vacuum chamber less than $2x10^{-5}$ torr and with necessary freezing oil vapours by means of a nitrogen-gas trap. The film sheet resistivity was measured by a four-probe method using IUS-3 device. The film adhesion to a polycor sybstrate was determined by a direct breaking method with MR-0.5-1 tensile-testing machine. Electromagnetic energy losses in the microstrip lines was estimated by a resonance method on the basis of comparison with the value of a quality factor for a half-wave microstrip resonator. The weldability of the microstrip line conductors was determined on a breaking stress of the gold wire having 40 μm in diameter and welded to the conductor by a thermocompression method with KONTAKT-3A bonder. The solderability of the conductors based on Cu-Mg-Ge-Sn system was estimated by determinating a contact angle formed by the surfase of POS-61 solder relative to the conductor plane. The thermal stability for the microstrip line conductors was determined in terms of a relative change in their electric resistance after keeping the conductors in a thermostatically controlled chamber at the temperature of 125°C within 1000 h.

It is known that the layers directly adjoining a substrate exert the most considerable influence on the value of electromagnetic energy losses in microstrip line conductors. Therefore in the present study a special attention was given to the determination of an optimum regimes for the alloys evaporation.

The dependence of the adhesive ability for the microstrip line conductors and the quality factor for the microstrip line resonators on a magnesium percentage in Cu-Mg-Cr-Ti and Cu-Mg-Ge-Sn copper alloys ranged from 2.5 to 0.2 mass.% was investigated (Table 1).

Table 1. The effect of magnesium contents on the quality factor and adhesion of the copper alloy films

Mg contents, mass.%	Adhesion to polycor substrate, kg/cm^2	Quality factor, nominal units
2.5	300	160
2.0	270	180
1.5	250	200
1.0	220	220
0.5	200	250
0.2	150	250

Under reduction of a magnesium percentage in the initial copper alloy the quality factor value for the microstrip line resonator was established to rise steadily and come up to 250 nominal units with a magnesium percentage in the initial alloy being equal to 0.5 mass.%

Subsequent reduction of a magnesium fraction in the conductor underlayer (a layer directly adjoined a substrate surfase) leads to essential decrease in the adhesion between the film and polycor substrate.

Over a final stage of the alloys evaporation the layers of Cr-Ti and Ge-Sn are formed, which ensure fair thermal stability, weldability and solderability of the microstrip line conductors. The effect of Cr, Ti, Sn and Ge alloying additions on the thermal stability, weldability and solderability of the microstrip line coductors based on the multicomponent copper alloys was studied (Table 2).

Table 2. The effect due to the alloying additions in the copper alloys on some characteristics of the microstrip line conductors

Name of alloy system	Percentage of alloying additions, mass.%				Thermal stability, δR/R, %	Welda bility, P, g	Contact angle of wetting, deg.	Quality factor, nominal units
	Cr	Ti	Sn	Ge				
Cu-Mg-Cr-Ti	2	0.05	-	-	2.0	9	-	270
	5	0.1	-	-	1.0	10	-	245
	10	0.2	-	-	0.5	12	-	240
Cu-Mg-Ge-Sn	-	-	8	1	0.6	10	20	250
	-	-	12	2	0.5	11	15	240
	-	-	15	3	0.4	12	10	240

Increase in the contents of Cr, Sn, Ge ad Ti up to 10,15,2 and 0.2 mass.% respectively is seen to lead to substantial rise in the thermal stability, weldability and solderability of the microstrip line conductors based on these copper alloys without marked reduction in the quality factor for the microstrip line resonators.

In such a way, as a result of the performed investigation, it has been found that the microstrip line conductors produced from the multicomponent copper alloys based on Cu-Mg-Cr-Ti and Cu-Mg-Ge-Sn systems of the optimum contents have a long-term stability and can be used in EHF microelectronic devices.

References

1. G.I.Veselov, E.N.Yegorov, U.N.Alehin,"Microelecuronic SHF-Devices", Vysshaya Shkola Publisher, Moscow, p.p.3-28,1988.
2. V.A.Bessonov, "Study and Development of Manufacturing Process for Microcircuit Thin Film Elements Based on Multicomponent Copper Alloys", Technology of Instrument Engineering, No.1, p.p.78-80,1996.

WAVES IN IRREGULAR RECTANGULAR WAVEGUIDE WITH INHOMOGENEOUS ANISOTROPIC IMPEDANCE OF WALL

V. F. Borulko
Dept. of Radiophysics, Dniepropetrovsk Univ.,
13 Naukovy St., Dniepropetrovsk 320625 Ukraine
Tel: 38 0562 467995, Fax 38 0562 465523 E-mail: garry@rff.dsu.dp.ua

Rectangular waveguides with transversally magnetized ferrite film situated on wide wall are used in microwave isolators and nonreciprocal phasers [1]. Periodic structures are widely used because of variety of physical effects observed in them [2] – wave reflection, mode conversion, coupling of surface and space waves. Additional opportunity can be achieved if parameter perturbation becomes no periodic [3]. Wider physical and engineering results give structures combining some parameter perturbations of different nature [4].

In the present paper we theoretically consider coupling of transverse electric waves $TE_{n,0}$ and $TE_{0,m}$ propagating in rectangular waveguide formed by planes $x = 0$, R and $y = 0$, L. The wall with $y = 0$ is supposed to have frequent and not deep corrugation and thin magnetized ferrite film on it. Such surface may be approximately described by small anisotropic surface impedance [5]. Diagonal elements of impedance tensor w are caused by gyrotropy of transversally magnetized film and by a tilt of corrugation relatively longitudinal axis. If surface is lossless, tensor components are satisfied to following relations:

$$w_{zx} = -w_{xz}, \qquad w_{zz} = w_{xx}^{*}. \tag{1}$$

In particular case of corrugation without film w_{zz} and w_{xx} are real but if only magnetized ferrite film is on plane surface values of w_{zz} and w_{xx} are purely imaginary. We assume that the tensor components as functions of the coordinates may be represented in the form of a sum of sinusoidal addends spatially oscillated along longitudinal coordinate z. We suppose that all components of impedance are functions versus not only longitudinal coordinate but also transversal one. Thus, they are expressed in the form of two-dimensional expansions

$$\begin{aligned}
w_{xx} &= \beta \sum_j \sum_{s=1}^{\infty} w_{xxjs}(\beta z)\exp\left[i\psi_j(z)\right]\sin(\pi s/R) \\
w_{xz} &= \beta \sum_j \sum_{s=0}^{\infty} w_{xzjs}(\beta z)\exp\left[i\psi_j(z)\right]\cos(\pi s/R) \\
w_{zx} &= \beta \sum_j \sum_{s=0}^{\infty} w_{zxjs}(\beta z)\exp\left[i\psi_j(z)\right]\cos(\pi s/R) \\
w_{zz} &= \beta \sum_j \sum_{s=1}^{\infty} w_{zzjs}(\beta z)\exp\left[i\psi_j(z)\right]\sin(\pi s/R)
\end{aligned} \tag{2}$$

where $\psi_j(z) = \int \kappa_j(\beta z)dz$ are longitudinal phase of perturbation harmonics and βw_{xxjs}, βw_{xzjs}, βw_{zxjs}, and βw_{zzjs}, are amplitudes of perturbation harmonics. Perturbation amplitudes and longitudinal wavenumbers κ_j smoothly vary along z.

We suppose that smallness of perturbation amplitudes and smoothness of parameter variation are determined by the same small nondimensional parameter β [6]. Simultaneously with longitudinal coordinate z we introduce "smooth" scale $\zeta = \beta z$ [6].

All components of electromagnetic field can be expressed per longitudinal components of electric Π_e and magnetic Π_m Hertz potentials. Boundary-value problem contains small perturbations in the boundary conditions at $y = 0$. Solution is searched by means of complex form [7] of Krylov-Bogoliubov-Mitropolsky asymptotic method [6]. According to this method, the expressions for Π_e and Π_m have form of asymptotic expansions in orders of parameter β

$$\Pi_m(z)=a_1\exp(i\theta_1)\cos(\gamma_x x)+a_2\exp(i\theta_2)\cos(\gamma_y y)+\sum_q \beta^q v_q(a,\theta,\psi,\zeta)$$

$$\Pi_e(z)=\sum_q \beta^q u_q(a,\theta,\psi,\zeta) \tag{3}$$

where a_1 and a_2 are complex amplitudes of waves propagating in the waveguide; $\theta_1 = -h_1 z$ and $\theta_2 = -h_2 z$ are longitudinal space phases of these waves; $\gamma_x = n\pi/R$ and $\gamma_y = m\pi/L$ are transversal wavenumber of the waves; u_q and v_q (q = 1,2,....) are 2π-periodical in θ and ψ functions to be found. As zero-order approximation, it takes solution for the TE_{n0} and TE_{0m} modes in regular waveguide with perfectly conducting walls. The longitudinal wavenumbers h_1 and h_2 are found from solution of unperturbed boundary-value problem. If at some values of z wavenumber mismatch $\eta = h_1 - h_2 - \kappa_p(\beta z)$ becomes small spatial parametric resonance can be observed (p is a number of spatial perturbation harmonic that causes wave coupling on incident frequency).

The complex amplitudes a_1 and a_2 of considered waves are supposed to be functions versus z and satisfy to the following equations:

$$\frac{da_l}{dz}=\beta B_1^{(l)}(a,\zeta,\alpha)+\beta^2 B_2^{(l)}(a,\zeta,\alpha)+\ldots, \quad (l=1,2) \tag{4}$$

where $\alpha=-\theta_1+\theta_2-\psi_p$ is phase mismatch from a resonance, $B_q^{(l)}$ $(q=1,2,\ldots)$ are functions chosen from condition of absence of infinitely growing members in u_q and v_q when $z\to\infty$ and $\eta\to 0$. Substituting expansion (3) into boundary-value problems for Π_e and Π_m using (4) and equating members with identical smallness order we get succession of equations for u_q and v_q. In each smallness order we search solutions under "frozen" a_l and ζ. They must be valid for both small values of η and not small ones.

The first order of β gives boundary-value problem for functions u_1 and v_1

$$\frac{d^2u_1}{dz^2}+k^2u_1=0,$$

$$\frac{d^2v_1}{dz^2}+k^2v_1+\exp(i\theta_1)\cos(\gamma_x x)\left(-2ih_1B_1^{(1)}+\eta\partial B_1^{(1)}/\partial\alpha\right)+$$
$$+\exp(i\theta_2)\cos(\gamma_y y)\left(-2ih_2B_2^{(1)}+\eta\partial B_2^{(1)}/\partial\alpha\right)=0,$$

$$\nabla_t^2 u_1\Big|_{x=0,R,y=L}=0,$$

$$\nabla_t^2 u_1\Big|_{y=0}+\sum_{l,j,s}D_{1ljs}a_l\exp(i\theta_l+i\psi_j)\sin(s\pi x/L)=0,$$

$$\left(\frac{1}{\varepsilon}\frac{\partial^2 u_1}{\partial y\partial z}+i\omega\frac{\partial v_1}{\partial x}\right)\Big|_{x=0,R}=0,$$

$$\left(\frac{1}{\varepsilon}\frac{\partial^2 u_1}{\partial x\partial z}-i\omega\frac{\partial v_1}{\partial y}\right)\Big|_{y=L}=0,$$

$$\left(\frac{1}{\varepsilon}\frac{\partial^2 u_1}{\partial x\partial z}-i\omega\frac{\partial v_1}{\partial y}\right)\Big|_{y=0}+\sum_{l,j,s}D_{2ljs}a_l\exp(i\theta_l+i\psi_j)\cos(s\pi x/L)=0,$$

where D_{1ljs} and D_{2ljs} are expressed in terms of space harmonics of surface impedance. Solutions for u_1 and v_1 have form of a sum of space harmonics. Function u_1 consist of only nonresonance addends but v_1 contain also

resonance addends that proportional to $\exp(i\theta_1)$ and $\exp(i\theta_2)$ and "potentially" resonance addends that proportional to $\exp(i\theta_1+i\alpha)$ and $\exp(i\theta_2-i\alpha)$. The condition of boundedness of solution for v_1 allows us to obtain differential equation system for complex amplitudes a_1 and a_2 of coupled waves

$$da_1/dz = A_1\, a_1 + G_1\, a_2 \exp(i\alpha),$$
$$da_2/dz = A_2\, a_2 + G_2\, a_1 \exp(-i\alpha), \tag{5}$$

where

$$A_1 = -\left[h_1^2(w_{zx0,2n} - w_{zx00}) + ih_1\gamma_x\,(w_{zz0,2n} + w_{zz00}) + \gamma_x^2\,(w_{xz0,2n} + w_{xz00})\right]/(4\omega\mu\, h_1 L)$$

$$A_2 = -\gamma_y^2\, w_{xz00}/(2\omega\mu\, h_2 L)$$

$$G_1 = -\gamma_y^2\left\{i(h_1-\eta)\gamma_x\, w_{zz,-p,n}/[\gamma_x^2 + \eta(2h_1-\eta)] + w_{xz,-p,n}\right\}/[\omega\mu(2h_1-\eta)L]$$

$$G_2 = -\left(ih_1\gamma_x\, w_{xx,p,n} + \gamma_x^2\, w_{xz,p,n}\right\}/[\omega\mu(2h_2-\eta)L)$$

In general case this system has been solving numerically, but for some particular cases, analytical solutions have been found. If the perturbations are smooth only and wave coupling is absent ($G_1 = G_2 = 0$) solution is obtained in "adiabatic" form. Parameters A_1 and A_2 describe attenuation and additional phase shift. For TE_{n0} wave these effects contain both reciprocal and nonreciprocal parts and are widely used [1]. Parameters G_1 and G_2 describe spatial coupling of waves having linear mutually orthogonal polarizations. This coupling is caused by combination of phase synchronism and transversally inhomogeneous or diagonal components of surface impedance. In this case, phase synchronism can be realized in the three forms – wave degeneracy, bragg reflection or bragg conversion. Degeneracy causes nonresonant coupling of waves with the same propagation directions. Bragg transformations have resonance nature. If parameters A_l, G_l (l = 1,2) and η are constant the equation system (5) has an analytical solution in the form of a sum of exponential functions [7]. For strictly sinusoidal perturbations of tensor components of surface impedance, analytical solution described Bragg reflection or/and mode conversion has been derived. A combination of a transversal perturbation of surface impedance and degeneracy supplies rich set of polarization transformation. In the work polarization parameters of eigenwaves have been investigated. Possibilities of wave transformations are still wider if amplitudes of space harmonic of impedance perturbations smoothly vary along longitudinally coordinate z. For these cases numerical solution have been obtained. If η is not small, system of coupled differential equations (5) contains rapidly oscillated coefficients. So its solution using standard algorithms like Runge-Kutta method is faced with difficulties. By special change of variables the system (5) may be re-written in a form which contains only slowly (i.e. smoothly along z) varying coefficients.

Great variety of physical effects observed in considered structure makes it perspective in engineering of millimeter waves.

References

1. B.Lax, K.J.Button, "Microwave Ferrites and Ferrimagnetics", McGraw-Hill, New York, 1962.
2. C. Elachi, "Waves in active and passive periodic structures: A review" Proceedings of the IEEE. Vol. 64, No. 12, pp. 1666-1698, 1976,
3. A.Katzir, A.C.Livanos, J.B.Shellan, and A.Yariv, "Chirped Gratings in Integrated Optics", IEEE J. Quantum Electron., Vol. QE-13, No. 4, pp. 296-304, 1977.
4. K.Araki and T.Itoh "Analysis of periodic ferrite slab waveguides by means of improved perturbation method" IEEE Trans. Microwave Theory Tech., Vol. MTT-29, No. 9, pp. 911-916. Sept. 1981.
5. N.A.Kuzmin "Approximate boundary conditions in the electrodynamics of stratified tensor media," Radio Science, Vol. 4, No. 8, pp. 703-708. Aug. 1969.
6. N.N.Bogoliubov, Yu. A.Mitropolsky, "Asymptotic Methods in the Theory of Nonlinear Oscillations". New York: Gordon and Breach Science Publ., 1961.
7. V.F.Borulko, "Waves in nonregular rectangular waveguides with helical corrugation and gyrotropic filling", Proc. of the 1998 URSI International Symposium on electromagnetic Theory, Thessaloniki, Greece, 25 – 28 May 1998, Vol. 1, pp. 54-56

TWO-DIMENSIONAL BRAGG RESONATOR WITH NONPERIODIC RADIAL PERTURBATION OF PARAMETERS

V. F. Borulko, V. E. Ivanilov
Department of Radiophysics, Dniepropetrovsk University.
13 Naukovy St., Dniepropetrovsk 320625 Ukraine
Tel: 38 0562 467995, Fax 38 0562 465523 E-mail: garry@rff.dsu.dp.ua

Attention to Bragg structures causes by richness of physical effects that can be observed in them [1] – wave reflection, mode conversion, coupling of surface and space waves. Additional variety of effects is realized if parameter perturbation becomes no periodic [2].

In present work two-dimensional waveguiding structure nonperiodically inhomogeneous along radial coordinate is considered. Permittivity assumes to be presented in the form of a sum of sinusoidal spatially oscillated harmonics of perturbation. Amplitude ε_j and wavenumber κ_j of each harmonic smoothly vary along radial coordinate.

$$\varepsilon = \varepsilon(\rho) = \varepsilon_s + \beta \sum_j \varepsilon_j(\beta\rho)\exp[\, i\psi_j(\rho)], \tag{1}$$

where $\psi_j(\rho) = \int \rho_j(\beta\rho)d\rho$ is longitudinal phase of perturbation harmonic. We suppose that smallness of perturbation amplitudes and smoothness of parameter variation are determined by the same small parameter β [3]. Simultaneously with radial coordinate ρ we introduce "smooth" scale $\zeta=\beta\rho$.

In the present paper waves with components E_z, H_ρ, H_φ are considered. The function E_z should satisfy to the equation

$$[\, \Delta + k^2(\rho)\,]E_z = 0 \tag{2}$$

In view of symmetry of the structure we shall introduce potential function $\Pi(\rho)$ by a relation $E_z = \rho^{-1/2}\Pi(\rho)\exp(in\varphi)$. For $\Pi(\rho)$ it is obtained the equation

$$\frac{d^2\Pi}{d\rho^2} + \left[\, k_0^2\varepsilon(\rho) - \frac{n^2 - 1/4}{\rho^2}\,\right]\Pi = 0 \tag{3}$$

At $\beta = 0$ a solution of the unperturbed boundary value problem is obtained as a sum of divergent and convergent cylindrical waves

$$\Pi(\rho) = a_1\rho^{1/2}H_n^{(2)}(k_s\rho) + a_2\rho^{1/2}H_n^{(1)}(k_s\rho) = a_1\exp[\, i\theta(\rho)\,] + a_2\exp[\, -i\theta^*(\rho)\,], \tag{4}$$

where $H_n(\rho)$ are Hankel functions, $\theta(\rho)$ is complex space phase and $k_s = k_0\sqrt{\varepsilon_s}$ is the wavenumber of the unperturbed medium. In contradistinction to traditional bragg structures [1,2] in the considered task unperturbed radial wave number h is not a constant and is defined through cylindrical functions as follows:

$$\begin{aligned} h(t/k_s) &= ik_s\frac{d}{dt}\{\ln[\, t^{1/2}H_n^{(2)}(t)\,]\} = k_s\{i\frac{1}{2}\frac{d}{dt}\ln[\, tM_n^2(t)\,] + 2/[\, \pi tM_n^2(t)\,]\} = \\ &= k_s\{i/(2t) + i[\, J_n'(t)J_n(t) + Y_n'(t)Y_n(t)\,]/M_n^2(t) + 2/[\, \pi tM_n^2(t)\,]\} \end{aligned}, \tag{5}$$

where t is auxiliary dimensionless variable. For an evaluation $h(\rho)$ it is enough to have subprograms for Bessel function of the first and second kind. For the qualitative analysis it is desirable to know a behavior of $h(\rho)$ at the

large and small values ρ. For deriving of the suitable approximate formulas we make use of known representations for $M_n^2(t)$ [4]. At large ρ the following asymptotical expressions are valid:

$$tM_n^2(t) \approx \frac{2}{\pi}\{1+\frac{1}{2}\frac{(4n^2-1)}{(2t)^2}+\frac{3}{8}\frac{(4n^2-1)(4n^2-9)}{(2t)^2}+...\}$$

$$\mathrm{Re}[\ h(t/k_s)/k_s\ ] \approx 1-\frac{4n^2-1}{8t^2}-\frac{(4n^2-1)(4n^2-25)}{128t^4}-...$$

$$\mathrm{Im}[\ h(t/k_s)/k_s\ ] \approx -\frac{4n^2-1}{8t^3}\left(1-\frac{1}{t^2}\right)$$

At small values ρ the following approximate formulas is obtained:

$$tM_n^2(t) \approx [\ \frac{(m-1)!}{\pi}\ ]^2\left(\frac{t}{2}\right)^{1-2n}$$

$$\mathrm{Re}[\ h(t/k_s)/k_s\ ] \approx \pi 2^{2-2n}[\ (n-1)!\ ]^{-2}t^{2n-1}$$

$$\mathrm{Im}[\ h(t/k_s)/k_s\ ] \approx \left(\frac{1}{2}-n\right)\Big/t$$

At fixed small β there is such a value of the radial coordinate $\rho=\rho_0(\beta,n)$, that for $\rho>\rho_0$ values h and $k_s^2-(n^2-1/4)/\rho^2$ are possible to consider as smoothly varying along ρ.

A solution of the equation (3) is sought as an asymptotical series on degrees of a parameter β

$$\Pi(\rho)=a_1\exp(i\theta)+a_2\exp(-i\theta^*)+\beta u_1(a,\theta,\psi,\varsigma)+\beta^2u_2(a,\theta,\psi,\varsigma)+..., \qquad (6)$$

where u_q $(q=1,2,...)$ are sought functions, a_1 is amplitude of the divergent cylindrical wave and a_2 is amplitude of a convergent wave. The functions $\exp(i\theta)$ and $\exp(-i\theta^*)$ strictly satisfy to the unperturbed equation and are defined by the formula (4). Substituting expansion (6) in the equation (3) utilizing (1) and (4) and equating addends with identical degrees of a parameter β a sequence of the differential equations for functions u_q is obtained.

Bragg wave coupling occurs when difference of wavenumbers of propagating waves is close to wavenumber of one of the spatial perturbation harmonics ($\eta=2\,\mathrm{Re}(h)-\kappa_p$ is mismatch of wavenumber). A solution suitable near to a space parametrical resonance is searched with the help of complex form [2] of the asymptotic method of Krylov, Bogoliubov and Mitropolsky (KBM) [3]. The complex amplitudes a_1 and a_2 of cylindrical waves are supposed to be functions versus ρ and satisfy to the following equations [2]:

$$\frac{da_m}{d\rho}=\beta B_1^{(m)}(a,\varsigma,\alpha)+\beta^2B_2^{(m)}(a,\varsigma,\alpha)+..., \quad (m=1,2) \qquad (7)$$

where $\alpha=-\theta-\theta^*-\psi_p=-2\,\mathrm{Re}(\theta)-\psi_p$ is phase mismatch from a resonance, $B_q^{(m)}$ $(q=1,2,...)$ are functions chosen from condition of absence of infinitely growing members in u_q when $\rho\to\infty$ and $\eta\to 0$. Substituting expansion (6) into equation (3) using (7) and equating members with identical smallness order we get succession of equations for u_q. In each smallness order we search solutions under "frozen" a_n and ζ. They

must be valid for both small values of η and not small ones. As a first approximation on β we have following inhomogeneous differential equation for u_1:

$$\frac{d^2u_1}{d\rho^2}+\left[k^2-\left(n^2-1/4\right)/\rho^2\right]u_1+\exp(i\theta)\left(-2ihB_1^{(1)}+\eta\,\partial B_1^{(1)}/\partial\alpha\right)+\exp\left(-i\theta^*\right)\times$$
$$\times\left(2ih^*B_2^{(1)}+\eta\,\partial B_2^{(1)}/\partial\alpha\right)+\left[a_1\exp(i\theta)+a_2\exp\left(-i\theta^*\right)\right]\sum_j k_0^2\varepsilon_j\exp\left(i\psi_j\right)=0 \tag{8}$$

At $\eta=0$ functions $B_q^{(m)}$ are found from a condition of absence in u_q resonance addends proportional $\exp(\imath\theta)$ and $\exp(-\imath\theta^*)$. To ensure single-valued determination of $B_q^{(m)}$ for not small η we additionally demand absence of "potentially" resonance addends that proportional to $\exp(\imath\theta+\imath\alpha)$ and $\exp(-\imath\theta^*-\imath\alpha)$.

Taking into account that $-\theta^*-\alpha=\theta+\psi_p$ $\theta+\alpha=-\theta^*-\psi_p=-\theta+\psi_{-p}$ we find $B_1^{(m)}$. In a first approximation on β a system of the linear differential equations for complex amplitudes a_1 and a_2 is obtained. The system describes coupling of divergent and convergent cylindrical waves with an identical angular dependence.

$$\frac{da_1}{d\rho}=\beta a_2G_1\exp(i\alpha),$$
$$\frac{da_2}{d\rho}=\beta a_1G_2\exp(-i\alpha), \tag{9}$$

where $G_1=-ik_0\varepsilon_{-p}/(2h-\eta)=-ik_0\varepsilon_{-p}/[\ \kappa_p+2i\,\mathrm{Im}(h)\ ]$

$$G_2=ik_0\varepsilon_p/(2h^*-\eta)=ik_0\varepsilon_p/[\ \kappa_p-2i\,\mathrm{Im}(h)\ ]$$

The solution for u_1 does not contain resonance addends and has the form

$$u_1=\sum_{j\neq p}C_{1j}\exp\left(i\theta+i\psi_j\right)+\sum_{j\neq -p}C_{2j}\exp\left(-i\theta^*+\psi_j\right), \tag{10}$$

The system in the form (9) at a constant values of G_m and η has an analytical solution as a sum of exponential functions [2]. This solution is a basis of a method of a numerical integration (9) at smoothly varying G_m and η. For particularly case of piecewise constant value of permittivity the asymptotic solution was compared with rigorous one obtained by transfer-matrix method.

Find solution has been used for investigation of resonator properties of considered structure. Obtained results can be useful for designing of generator elements of millimeter and submillimeter bands.

References

1. C. Elachi, "Waves in active and passive periodic structures: A review" Proceedings of the IEEE. Vol. 64, No. 12, pp. 1666-1698, 1976,
2. V. F. Borulko, "Polarization and mode conversions in nonperiodically corrugated waveguides with a gyrotropic filling", Proc. of the 1995 URSI International Symposium on electromagnetic Theory, St.Petersburg, Russia, May 23-26, 1995, pp. 729-731.
3. N. N. Bogoliubov, Yu. A.Mitropolsky, "Asymptotic Methods in the Theory of Nonlinear Oscillations". New York: Gordon and Breach Science Publ., 1961.
4. M. Abramovitz and I.Stegun "Handbook of Mathematical Functions". National Bureau of Standards, 1964.

POLARIZABLE - SPECTRAL CHARACTERISTICS OF REVOLVING LINEAR POLARIZER

V.N. Polupanov, Y.M. Kuleshov, B.N. Knyaz'kov, M.S. Yanovsky
IRE NAS of Ukraine, 12 Ac. Proscura st.,Kharcov, 310085, Ukraine
Tel.38(0572)448-335, Fax.38(0572)441-105, E-mail: Kiseliov @ ire.Kharcov.ua.

We shall consider the transformation of polarizing and spectral performances of a wave, polarized on a circle, incident on revolving an ideal linear polarizer (LP). The turn of a LP rather frequently is applied to the various purposes. So, in particular, it can be used for the definition of own parameters of polarizers [1], and also for optimization of coupling of a resonator of an optical quantum generator with a load [2]. The spectrum on output LP, revolving in a field of circular polarizing wave, is of interest, as at such "elementary" approach it is possible to detect essential singularities of going on physical processes.

A normalized vector of the Maxwell polarized on a circle to the right (to the left) wave, which moved along the axis Z, we shall note as [3]:

$$E_1 = \frac{1}{\sqrt{2}}\begin{bmatrix}1\\ \pm i\end{bmatrix}\exp\{i\omega(t-\frac{z}{c})\} \quad . \tag{1}$$

The polarizing matrix (matrix of the Jones) of ideal LP which axis of passage is oriented under an angle θ to axis X, looks as follows:

$$\Pi = \begin{bmatrix}\cos^2\theta & \cos\theta\cdot\sin\theta\\ \cos\theta\cdot\sin\theta & \sin^2\theta\end{bmatrix} \quad . \tag{2}$$

Vector of the Maxwell E_2 on the output of LP in the matrix form

$$E_2 = \Pi \bullet E_1 = E_{2id} + E_{2ort} \quad , \tag{3}$$

where:

$$\mathrm{E}_{2\mathrm{id}} = \frac{1}{2\sqrt{2}}\begin{bmatrix}1\\ \pm \mathrm{i}\end{bmatrix}\exp\{\mathrm{i}\omega(\mathrm{t}-\frac{\mathrm{z}}{\mathrm{c}})\} \quad , \tag{4}$$

$$\mathrm{E}_{2\mathrm{ort}} = \frac{1}{2\sqrt{2}}\begin{bmatrix}1\\ \mp \mathrm{i}\end{bmatrix}\exp\{\mathrm{i}[\omega(\mathrm{t}-\frac{\mathrm{z}}{\mathrm{c}})\pm 2\theta]\} \quad . \tag{5}$$

From (4) and (5) it is visible, that the wave on the output of ideal LP in a considered case is a sum of two polarized on a circle orthogonal component. Thus component polarized on a circle identic, as the wave on the input of LP, has a constant a phase, and the phase of orthogonal polarized wave is determined by orientation of LP and direction of rotation of a vector of polarization of an entering wave. Polarized on a circle in opposite directions of a waves it is lawful to name orthogonal, as it corresponds to the definition on the sphere of Poincare.

The work of LP in a form of a wire grate it is possible, using [4], to describe as follows. The radiation incidend on LPconsists of four equal, uniformly polarized on a circle, groups of fotons, which are separate equally into two parts - passed and reflected. In these parts the polarization of one group of fotons varies on orthogonal during interaction with LP, and the polarization second - is saved. At this it appears, that with LP effectively interact only those fotons, which polarization will be transformed. Last follows that the phase of a passed and reflected radiation, which polarization was transformed, is determined by an angle of a turn of LP around of an axis of an incident beam, and the phase of a radiation passed through LP without transformation of polarization, or reflected from it, as from a mirror, does not depend on of the orientation of an axis of an anisotropy of LP.

In our case, when the LP is evenly revolves with frequency Ω, the angle of orientation is equal

$$\theta = \pm\Omega t \quad . \tag{6}$$

As a result, for orthogonal polarized wave the formula looks so:

$$E_{2ort} = \frac{1}{2\sqrt{2}}\begin{bmatrix}1\\ \mp i\end{bmatrix}\exp\{i[(\omega \pm 2\Omega)t - \frac{z}{c}]\} \quad . \qquad (7)$$

The sign at 2Ω is determined by relative direction of rotation of LP and wave on its an input. The power of each of component E_{2id} and E_{2ort} four times below than a power of a wave acting on an input of LP if not to take into account of an negligible modification of an energy E_{2ort} because of a modification of the frequency.

The singularities of a spectrum of oscillations on an exit of revolving LP allow to use it as phaseshifting element of polarizing phase shifters and of phase frequency shifters (FS) [5].

In a sense, the construction of FS with the LP is further development of idea, what used in continuous waveguide phase shifter [6]. In it for improving spectral performances and wideband the half-wave section is divided on two quarter wave, between which is installed LP, oriented under by an angle 45^0 to quarter-wave sections. LP rotates together with the last. Such scheme has appeared rather effective and has allowed considerably to improve spectral - frequency characteristic of FS [7]. In offered FS with a polarizer as phaseshifting element is used already only LP.

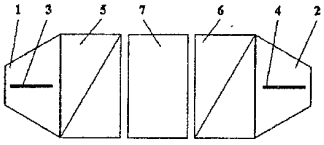


Figure 1. The scheme of the FS with a linear polarizer

The scheme of waveguide variant FS with LP is showed in a Fig. 1. LP consists of two passages 1 and 2 from a rectangular waveguide to round with absorber plates 3 and 4, two quarter-wave differential phase sections 5, 6 and phaseshifting section 7, what revolving around of a longitudinal axis of the waveguide. Section 7 is carried out as a length of a round waveguide, inside which is installed the element selecting linearly polarized component from circular polarization wave.

In the polarizing phase shifter of Fox [8] the phaseshifting element is the half-wave differential phase section that revolving. However this section is necessary for adjusting on the special measuring equipment, that is labour-consuming and durating operation.

The spectral parameters of a gear are improved that the properties of the LP are saved in a band of working frequencies rather high. In quality waveguide variant of the LP it is possible to apply various variations of constructions. In quasioptical devices as a LP the wide application was found by wire grates.

In a table 1 the formulas, defining relative level of amplitudes spectral component on an exit FS with LP and with half-wave section in an dependence from disorder δ of differential phase sections, are showed. The account is carried out similarly [9].

Table 1.Relative levels of amplitudes on an exit of FS

Relativ level	**Useful signal**	**Mirror side**	**Carrying**
Type of fase section	$\omega + 2\Omega$	$\omega - 2\Omega$	ω
$\lambda/2$	$1-3\delta^2/4$	$-\delta^2/4$	$-\delta^2$
Linear polarizer	$1-\delta^2/4$	$-\delta^2/4$	$-\delta$

It is visible, that the amplitude of a useful signal on an exit of the FS with the LP, on a comparison with the FS with a half-wave section, is reduced three times slower, the amplitudes of mirror side are identical, and the amplitude of the carrying in the FS with the LP in $1/\delta$ time is higher. In a Fig. 2 and 3 the dependeces of a relative level of spectral components, what calculated on the formulas of tab. 1,are showed.

For a research of spectral performances of a FS with the LP [5] was used the construction of the FS on the basis of the phase shifter of Fox with a half-wave differential section, in which the mica plate of half-wave differential phase section was replaced by a absorbing plate carried out from micarta, covered by carbon. The measurements were carried out in a millimeter range of waves (cut of a waveguide 5,2x2,6 mm^2) on the strategy described in [9]. The outcomes of measurements are reduced in a table 2.

It is visible, that the FS has a small level of mirror side, in spite of the fact that the quarter-wave sections were adjusted on a wave of 8,15 mm.

The phase shifter and the FS with the LP are realized by us also on the basis of hollow of dielectric

beamguide [10]. The flat polarizing grate from parallel thin wires is applied as a LP. In the phase shifter with the LP the linear dependence of a shift of a phase of a passed wave from an angle of a turn of the LP is

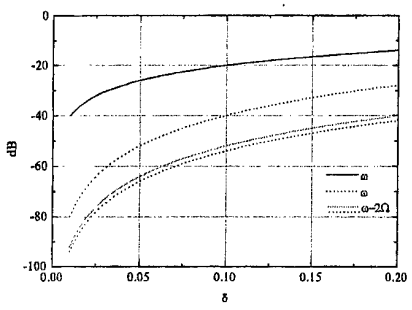


Figure 2. The dependence of a relative level carrying and mirror side on an output of the FS from disorder of a phase sections
--- - FS with a linear polarizer;
- - - - FS with a half-wave phase section

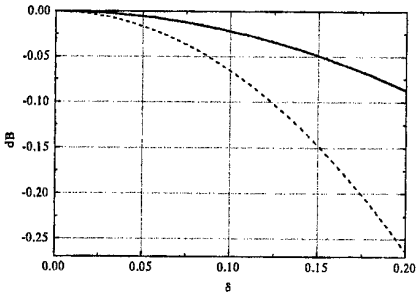


Figure 3. The dependence of a relative level of a useful signal on an exit of FS from disorder of a differential sections
----- - FS with a linear polarizer;
- - - - СЧ with half-wave phase section.

Table 2. The level of spectral components on an output of the FS

λ, mm	$N_{\omega+2\Omega}$, dB	N_{ω}, dB	$N_{\omega-2\Omega}$, dB
8,15	**-8,2**	**-38**	**-45**
6,4	**-6,8**	**-22**	**-50**

ensured, that allows to use it as a masterpiece.

In a quality of the LP the gyrating in a round waveguide a discharge in a plasma with electronic concentration $N_e > N_{ecrit}$, where N_{ecrit} - electronic denseness of the plasma appropriate to frequency of cut-off of a microwave, is possible also to use [11]. The FS with such LP, fulfilling a functions of the phaseshifter element, will have the increased speed.

References

1. V.K. Kiseliov, Y. M. Kuleshov, D.D. Litvinov, V.N. Polupanov, "A possibility of a measurement of the parameters of polarizing wire grates", Izv. VUZov, Radioelectronica, Vol.17,No.7, pp119-121, 1974, (in rus.).
2. Inventor's Certificate No.1111657 (USSR), "A waveguide gas laser", Yu.E. Kamenev, Y.M. Kuleshov, V.K. Kiseliov, D.D. Litvinov, V.N. Poluoanov,-ISM, B129, No.6, p.3, 1990, (in rus.).
3. A. Djerrard, J.M. Birch, "Introduction in matrix optics", Mir, Moscow, 341 p., 1978, (in rus.).
4. V.N. Polupanov, M.S. Yanovsky, B.N. Kniaz'kov, "About physical principles of work of the polarizing phase shifter", Radiotehnika, Resp. mezved. n.-t. sb., Vyscha shkola, Vyp. 51, pp. 71-75, 1979, (in rus.).
5. Inventor's Certificate No.228100 (USSR), "The phase shifter of revolving type", V.N. Polupanov, Y.M. Kuleshov, Publ. in Bull. Inv. No. 31, 1968, (in rus.).
6. Inventor's Certificate No.178870 (USSR), "The waveguide phase shifter of continuous type", M.S. Yanovsky, B.N. Kniaz'kov, Publ. in Bull. Inv. No. 4, 1966, (in rus.).
7. M.S. Yanovsky, B.N. Kniaz'kov, "About a possibility of a diminution of spectral distortions and extention of a range of phase shifters of continuous type", Radiotehnika, Vol.21, No.7, pp.69-71, 1966 (in rus.).
8. A.G. Fox, "An adjustable wave-guide phase changer", PIRE, Vol.35, No.12, pp.1489-1498, 1947.
9. F.N. Petrosian, V.A. Gol'ba, "The strategy of a research and tuning of phase shifter of continuous type", Tr. VNIIFTRI, Vyp. 70-(130), pp.83-88, 1963, (in rus.).
10. Inventor's Certificate No.302054 (USSR), "Dielectric beamguide of a submillimeter range of waves", A.N. Ahiyezer and others, Publ. in Bull. Inv. No. 8, 1972, (in rus.).
11. Inventor's Certificate No.141510 (USSR), "The frequency shifter of plasma type", M.S. Yanovsky, Y.M. Kuleshov, B.N. Kniaz'kov, Publ. in Bull. Inv. No. 19, 1961, (in rus.).

CONSIDERATION OF OPTIMUM SECTIONAL WAVEGUIDE TAPERS FOR QUASI-OPTICAL TRANSMISSION LINES

V.K. Kiseliov
Institute for Radiophysics and Electronics of the National Academy of Sciences of Ukraine
Address: 12, Ac. Proskura St., Kharkov, 310085, Ukraine
Tel: 38 0572 448335, Fax: 38 0572 441105, E-mail: kiseliov@ire.kharkov.ua

The broadband matching considerations must be embodied in the short - millimeter / submillimeter designs based on quasi-optical principles and involving quasi-optical transmission lines of the class "Hollow Dielectric Waveguide" (HDW) [1-3] to keep the HDW quite high broadbandness and provide the minimum-loss transition with the space saving. The thorough study [4] of commonly used waveguide tapers joining the different-size optical waveguides in a smooth way revealed that the adiabatic transition could be shortest achieved by using parabolic tapers. Unfortunately, when extended in the axial direction, a parabolic surface is too difficult in manufacture even in planar form. Evidently the things are much worse when dealing with 3-D optical and quasi-optical waveguides of circular, rectangular, and other cross-sectional shapes. In this case, a linear taper like a conical horn is only possible. However for the adiabatic transition in the optical and quasi-optical areas, it must be very extended. As known, the dissipation loss is proportional to the taper length and grows correspondingly. In this connection, a sectional waveguide taper (SWT) that represents a succession of ordinary linear tapers approximating a desired parabolic shape is considered to be an acceptable solution providing, on one hand, a high manufacturability of the tapers of this kind and, on the other, approaching (at a proper number of the sections) the necessary characteristics of ideal parabolic tapers.

A new method of the design of adiabatic optimum sectional waveguide tapers (OSWT) for quasi-optical circular waveguides of the HDW class is presented with the calculation formulas for an optimum, in terms of minimum extension and dissipation loss, subdivision of a parabolic taper into a finite number of the linear sections. This method is validated by the comparison of the synthesized OSWT with the both linear and parabolic analogs.

A sectional waveguide taper joining two quasi-optical circular hollow dielectric waveguides HDW_1 and HDW_2 of characteristic sizes (diameters) D_0 and D_n represents, as shown in Fig.1, a succession of linear sections LS_m, $m = 1, ..., n$ approximating the proper parabolic surface. Both the waveguides and the taper have the similar cross sections and the same interface nature. The working (fundamental) mode of both waveguides is HE_{11}. The standard quasi-optical conditions $ka_0 \gg 1$, $ka_n \gg 1$, where $a_0=D_0/2$, $a_n=D_n/2$, and $k=2\pi/\lambda$ are valid. Using a ray model [5] of the mode propagation in a quasi-optical system we assume that every mode is asymptotically equal to the ray family with common propagation characteristics or ray invariants. In the model terms, the SWT adiabatic condition can be formulated as the following system of the "nonsepareted propagation" conditions of the local plane waves or ray families corresponding to the fundamental mode of each SWT section.

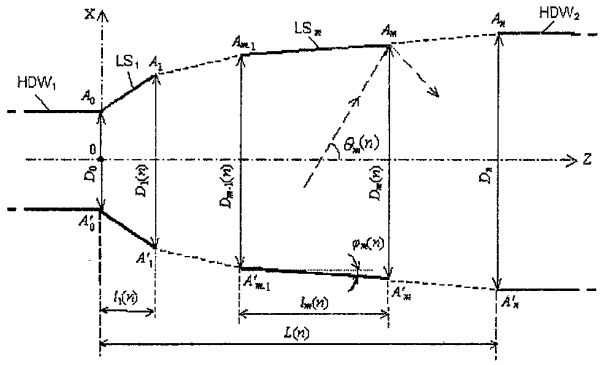


Figure 1. Sectional waveguide taper

$$\varphi_m(n) \le \theta_m(n), \quad m=1,\dots n, \tag{1}$$

Here $\varphi_m(n)$ is the angle which the m-th section generator makes with the Z axis; $\theta_m(n)$ is the local angle which the generator of the ray cone corresponding to the fundamental mode of the widest cross section $A_m - A'_m$ of the m-th section makes with the Z axis in the XOZ plane. System (1) determines the optimum SWT geometry and provides the calculation of the principal geometrical parameters.

In view of $ka_m >> 1$, (1) gives the narrow angle θ_m and, consequently, narrow φ_m. Here φ_m becomes wider as ℓ_m decreases and θ_m grows with the wavelength. Hence the minimization of each linear section LS_m and, consequently, the total SWT length is determined by equations (1) which for HE_{11} and for zero-order $1/ka_m$ are written as

$$(D_m(n)-D_{m-1}(n)) / (2\, l_m(n))=\tilde{U}_1\cdot\lambda_{min}/(\pi D_m(n)), \quad m=1,\dots,n, \tag{2}$$

where $\tilde{U}_1=2.405$ is the fundamental mode parameter.

System (2) yields the SWT length as a nonlinear function of the intermediate diameters $D_m(n)$. The minimum of this function determines the OSWT geometry, and in its turn is determined by the unique set of $D_m(n)$ values

$$D_m(n) = D_0 + m(D_n - D_0)/n = D_n[q + m(1-q)/n], \quad m=1,\dots,n, \tag{3}$$

where $q = D_0/D_n$ is the OSWT unitless parameter. Using (2) and (3) one can find the rest OSWT parameters

$$l_m(n) = \pi\cdot D_n^2(1-q)[q+m(1-q)/n]/(2n\lambda_{\min}\tilde{U}_1), \quad m=1,\dots,n, \tag{4}$$

$$\varphi_m(n) = \tilde{U}_1\lambda_{\min}/(\pi\cdot D_n[q+m(1-q)/n]), \; m=1,\dots,n, \tag{5}$$

$$L(n)=\sum_{m=1}^{n} l_m(n)=\pi\cdot D_n^2(1-q^2)[1+(1-q)/(n(1+q))]/(4\lambda_{\min}\tilde{U}_1). \tag{6}$$

Formulas (3) - (6) calculate all the principal geometrical parameters of the n - section OSWT joining two circular HDWs with the fundamental mode HE_{11}.

The break points $A_0,\dots, A_n$ of the SWT generator (Fig.1) lie on the parabola whose axis is parallel to the Z axis and whose vertex is at point C_n with coordinates : $X(C_n)=-D_n(1-q)/(4n)$, $Z(C_n)=-\pi D_n^2[q+(1-q)/(2n)]^2/(4U_{11}\lambda_{min})$. The symmetrical points $A'_0,\dots, A'_n$ lie on another parabola which runs along the Z axis but whose vertex is at point C'_n with coordinates $X(C'_n)=-X(C_n)$, $Z(C'_n)= Z(C_n)$. Both parabolas have the same focus-to-directrix distance $p= U_{11}\lambda_{min}/2\pi$ independent of n and q. Hence these parabolas are identical. Their focal planes coincide but their foci are symmetrically displaced by $\Delta_n = \mp D_n(1-q)/(4n)$ from the Z axis. In the limit $n=\infty$, the enveloping parabolas merge giving the contour of the adiabatic parabolic taper.

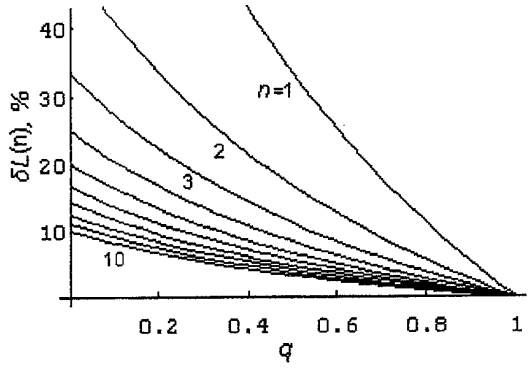


Figure 2. The relative difference between the lengths of the OSWT and the adiabatic parabolic taper

The relative difference $\delta L(n)$ between the lengths of the OSWT and the adiabatic parabolic taper is shown as a function of q and n in Fig.2. At first, $\delta L(n)$ rapidly falls an n rises. But at $n \geq 10$ this difference is less than 10 percent even for $q << 1$ implying that the diameters of the joined waveguides differ widely. Evidently a minimum number of the OSWT sections is determined by q for each specific application, and in actual practice it is, as a rule, much less than 10.

The SWT optimization is performed not only for a minimum number of the sections but also for a minimum of the power loss $A_{dB} = B_{dB} + C_{dB}$ of the fundamental mode over the taper. In this case, the dissipation loss B_{dB} is primarily due to the leakage of some power out of the channel through the air-dielectric interface, and C_{dB} is caused by the fundamental mode conversion into the higher parasitic modes. As a rule, the dissipation loss rises with the taper length. The conversion loss does the reverse, but it reveals itself by sharp splashes attributed to the mode coupling phenomenon occurring, in particular, in quasi-optical tapers based on a metal-dielectric waveguide [7]. As long as the excitation of the parasitic high-order modes in an adiabatic linear taper based on a HDW in the form "circular channel inside dielectric" is

sufficiently prevented [7], the conversion loss may be neglected. Then $A_{dB} \cong B_{dB}$, so that the loss calculation formulas [6] taking no account of the mode conversion are valid.

The dissipation losses of each OSWT section add up to give the dissipation loss of HE_{11} wave over the n - section OSWT as follows

$$B(n) \cong 0{,}88 \cdot \frac{U_{11} \cdot \lambda^2 \cdot \pi}{n \cdot D_n \cdot \lambda_{\min}} \cdot \eta' \cdot \sum_{m=1}^{n} \frac{(1-q) \cdot \left[q + \frac{2m-1}{2n}(1-q) \right]}{\left[q + \frac{m-1}{n}(1-q) \right]^2 \cdot \left[q + \frac{m}{n}(1-q) \right]}, \; dB, \qquad (7)$$

where

$$\eta' = \frac{1}{2} \frac{\left[(\varepsilon'+1)^2 + (\varepsilon')^2 tg^2\delta \right]^{1/2}}{\left[(\varepsilon'-1)^2 + (\varepsilon')^2 tg^2\delta \right]^{1/4}} \cdot \cos\left[-arctg \frac{\varepsilon' \cdot tg\delta}{\varepsilon'+1} + \frac{1}{2} arctg \frac{\varepsilon' \cdot tg\delta}{\varepsilon'-1} \right], \qquad (8)$$

$\varepsilon = \varepsilon' - i\varepsilon''$ is the complex permittivity of the HDW channel walls, tg $\delta = \varepsilon''/\varepsilon'$ is the dielectric loss tangent.

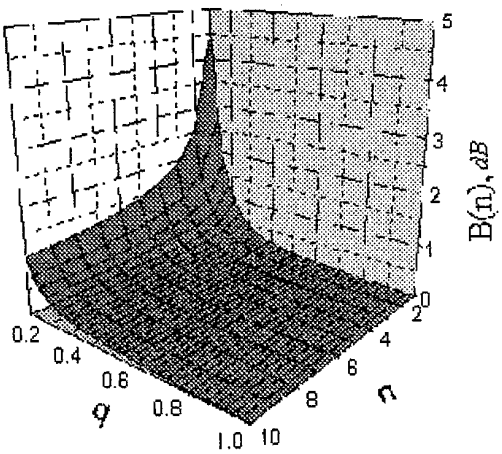


Figure 3. The OSWT loss as a function of n and q parameters

At n = 1, (7) converts to the loss formula for a minimum-length adiabatic circular conical taper. In the limit $n \to \infty$, we have the loss formula for the corresponding parabolic taper.

Fig.3 shows the OSWT loss predicted by (7) for $\lambda=\lambda_{min}$, $D_n/\lambda=100$, $\varepsilon'=3$, and $tg\delta=0.1$.For $q< 0.5$, the OSWT loss initially falls down as n rises. At $n > 7$, it nearly flattens out and slowly approaches the loss level of the parabolic taper. For $q > 0.5$, the loss is practically independent of the sections number. However, as has been said above, the requirement of a minimum taper length may move this boundary towards the larger q. If, for instance, the condition $\delta L(n) < 10\%$ of the OSWT expedience is taken then, as follows from (6) and Fig.2, the q range is as wide as $0 < q \le 0.8$.

The obtained results can be easily extended to any arbitrary shape of the joined HDW channels with any interface nature, provided the dispersion equation is solved and the transverse wavenumbers are known. The latter is necessary for finding the angle of propagation of the local plane waves involved in adiabatic conditions (1). And then based on the above stated line of argument for finding the OSWT parameters for a circular HDW one can design the OSWT for the required HDWs.

References

1. E.A.Marcatili and R.A.Schmeltzer., "Hollow Metallic and Dielectric Waveguides for Long-Distance Optical Transmission and Lasers", Bell System Tech. J., vol.43, N.7, pp.1783-1809, 1964.
2. Yu.N.Kazantsev and O.A.Kharlashkin, "Circular Waveguides of "Hollow Dielectric Channel" Class", Radiotekhnika i Electronika, vol.29, N.8, pp.1441-1450, 1984.
3. A.Ya.Usikov, E.A.Kaner, N.D.Truten', et al., "Electronics and Radiophysics of Millimeter and Submillimeter Radiowaves", Naukova Dumka, Kiev, pp.140-157, 1986.
4. W.K.Burns, A.F.Milton, and A.B.Lee , "Optical Waveguide Parabolic Coupling Horns", Applied Physics Letters, vol.30, N.1, pp. 28-30, 1977.
5. A.W.Snyder and J.D.Love, " The Theory of Optical Waveguides", Russian translation, ed. by E.M.Dianov and V.V.Shevchenko. Radio i svyaz, Moscow, pp.589-600, 1987.
6. V.K.Kiseliov and T.M.Kushta,"Tapers for Submillimeter Quasi-Optical Lines", In: "Applications of Millimeter and Submillimeter Radiowaves", Inst. of Radiophysics and Electronics of the NAS of Ukraine, Kharkov, pp.128-131, 1990.
7. V.K.Kiseliov and T.M.Kushta, "Mode Conversion in Circular Conical Tapers for Quasi-Optical Submillimeter Lines", In: "Physical Researches by Using Millimeter and Submillimeter Radiowaves", Inst. of Radiophysics and Electronics of the NAS of Ukraine, Kharkov, pp.94-97, 1991.

STOCHASTICALLY RESONATOR FOR THE ACCUMULATION OF MILLIMETER WAVE RANGE ELECTROMAGNETIC FIELD ENERGY

E.M.Ganapolskii
Institute for Radiophysics and Electronics of NAS of Ukraine
310085, Kharkov, 12 Ak.Proskura St .
Tel.(0572)448553. E-mail: ire@ire.kharkov.ua

Let us consider elecrodynamic system made in the form of cavity having the characteristic dimensions which are much greater than the electromagnetic wave length in free space, and surrounded with the well conducting walls - the super dimensional resonator. The excited in this resonator microwave short impulse is propagated in cavity and multiple reflected from metal walls. As a result of this the filling of the cavity resonator by electromagnetic field takes place. When the spectrum of the resonator natural frequencies is sufficiently rarefied the space distribution of this field belonging to the any natural frequency conforms to the definite mode of oscillations and the lifetime of this field in resonator τ is proportional to the quality Q of oscillation mode . It follows that the resonator must have the great quality for the attainment of the great value of an electromagnetic field lifetime. For example, for $\tau = 3$ μs and angular frequency $\omega = 2\pi \times 36$ GHz by the ratio of impute and output microwave signal power of 100 dB the resonator quality of 3×10^4 is needed. But the bandwidth of such resonator is occurred very narrow about 1 MHz. From here it follows that the use of classic cavity resonator with the rarefied spectrum for the long accumulation of microwave signal energy in the wide frequency range is impossible.

It was established in present work at first that the mentioned above principal contradiction between the requirements for increasing of the energy lifetime of signal and attaining of the wide frequency bandwidth of resonator one can resolve on the base of the stochastically mechanics principles use. The ideas which lie in the base of this problem solving connected with the fundamental conceptions of stochastically dynamics of material particles such as locally instability and mixing [1]. Under a locally instability it is understood the exponentially divergence of the particle motion trajectories.

The propagation of electromagnetic wave in the system with the characteristic dimension $D >> \lambda$, where λ is the wavelength in the free space as it is known one can describe in the geometrical optic approximation on the Hamilton-Jacoby equations base, i.e. on the base of the same equation which is used for the describing of the material particles motion. One can see from here that the electromagnetic wave propagation processes in electrodynamic system where this inequality is fulfilled is the physical analogy of the material particles motion in closed volume. If the convex surfaces which scatter the electromagnetic waves are placed inside the electrodynamic system that system obtains the properties of locally instability and mixing of the propagated in it electromagnetic wave. Such system maybe named as a electromagnetic K-system [2] isomorphic to Sinaj`s billiard.

The space area bordered of metal walls where the electromagnetic wave is propagated represents the resonant structure or cavity resonator having the set of resonant frequencies corresponding to the various distributions (modes) of an electromagnetic field. In the super dimensional resonator the number of resonant frequencies in the resonant volume is determined by the known asymptotically Kurant`s formulas [3]. By the increasing of the cavity resonator volume or by frequency increasing the spectrum of cavity is bunched. In this case it necessary to take into account the finite conductivity of the cavity walls. Therefore, by the resonator frequency or volume increasing one can arrive to that the resonant curves corresponded to the neighboring resonance's are recovered. In this case we will get the quasi continuous spectrum instead of the discrete one which is characteristic for the cavity resonator with the ideally conducting walls and resonant properties in this case disappear. But the obtaining of the quasicontinuous spectrum which consists of the near frequencies set of the resonant structure is belonged to the its potential possibilities and one can not be realized in the usually resonators having the proper geometrical form, for example sphere, cylinder or rectangular parallelepiped. This is connected with the mode degeneracy caused of the resonator space symmetry which results in the spectrum rarefy. For confluence of various resonant curve it is needed the significant increasing of the resonator dimensions. Besides this, by excitation of electromagnetic field in such resonator it is really impossible to provide the same and simultaneous interaction with the all resonator modes in given frequency interval. This problem is solved by the use of the field stochastization in electromagnetic K-system due the locally instability and mixing.

The resonator having the scattering surfaces which is the analogy of Sinaj's billiard «Star» type was chosen as a such K-system. This resonator was named as stochastically resonator. Firstly, the own mode oscillation degeneracy is fully removed in stochastically resonator. Secondly, the excitation of a some mode by mixing is reproduced to the all another modes in the frequency band of impute signal. Due to this the quasicontinuous spectrum can realized in stochastically resonator by the moderate resonator dimensions. The electrodynamic system obtains by this a very wide frequency band and in the same time the energy lifetime is determined by the its effective quality which is equally to the ratio of the reserved energy to the one dissipated over the oscillation period. This quality, which in the given case have the value of the order D/δ where δ is the skin-layer deep, is not belonged to the separate oscillation mode as in an usually resonator and to all oscillations excited in the system.

The idea of the microwave electromagnetic field stochastization was realized by the creation of the new wide frequency band device possessing the long keeping (delay) of the microwave signal energy in the eight millimeter wave range. The spherical cavity was chosen as a K-electrodynamic system. The well conducting metal spheres served as scattering objects for electromagnetic wave are placed into the spherical cavity. (Fig.1). The cavity body was made of brass and the spherical surface was covered by silver and polished. The three eccentric placed metal spheres with the covered by silver surface were used for the full removal degeneracy of the spherical resonator own oscillation modes and the field stochastization. The diameter of spherical cavity is of 95 mm and the diameter of metal spheres is 30 mm. The accumulation energy device can operate in two regimes: «on reflection» and «on transmitting». In the first regime just the same coupling element is served for the impute and output the electromagnetic energy and in second regime for the energy impute and output the coupling elements are separated. They are made identical and represent the wave guide sections of standard cross-section 7.2 $\times$ 3.4 mm^2 which is connected with the spherical resonator by means of coaxial line. This coaxial line has the loop coupler with the wave guide on the one end and the one fourth wave vibrator for the stochastically resonator excitation on the second end. The Teflon plug was used as insulator between the inner and external connector of coaxial line to reduce to a minimum of the coaxial line loss.

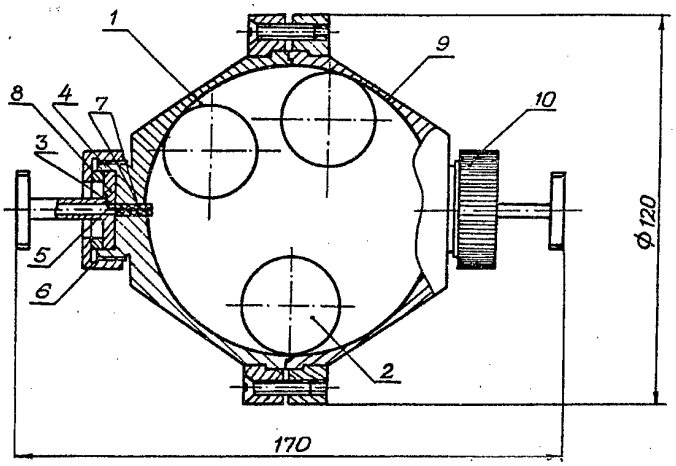


Figure1. The spherical stochastically resonator with the scattering metal spheres.
1 - the inner cavity, 2 - metal sphere, 3 - Teflon insulator of the coaxial line exciter, 4 - the exciter wave guide flange, 5 - the inner connector of the coaxial exciter, 6 - the antenna, 7 - the hole in the resonator body for the exciter, 8 - the plate on the resonator body served for the control of the polarization plane of the antenna, 9 - the stochastically resonator body, 10 - the part of exciter fixing.

The device construction foresees the possibility to control of the coupling value and obtaining of the optimal value of it both for the receiving of the wide frequency band and for achieving of the minimum of the microwave electromagnetic energy loss by an accumulation. This is realized by means of the length changing of the antennas dipole immersing into the resonator cavity and the mutually orientation of the planes where the loops of impute and output vibrators are placed. For this aim the wave guide section has on the end the plain flange made in the form of a disk which borders to the plate on the external surface of the device body and due to this can turned about the wave guide axis.

The measurements shown that in the spherical resonator, as it was assumed, the degeneracy of the own mode oscillations takes place and due to this the spectrum of spherical resonator is rarefied to the full when the every line corresponds to the definite oscillation type. Owing to the high resonator quality the lines in such spectrum are narrow with the frequency width less than 1 MHz. When the metal spheres are placed eccentricity

into spherical cavity the frequency characteristics of resonator is changed radically. Instead of the isolated narrow resonant lines the nonregular following one after another on the frequency and overlapping resonant lines are appeared. The such character of frequency dependence corresponds to the full removing of the mode degeneracy in the spherical resonator. The mean distance between these resonance's is some MHz. Hence, if the spectrum width of the impute impulse exceeds this frequency distance the resonator frequency characteristic for impulse is smooth and the stochastically resonator obtains the character of the wide frequency band device with the very great of the order of the waveguide frequency band. Thus, the described stochastically resonator in the frequency range 34 - 37 GHz has the relative frequency band exceeded of 10% for the impulse signals having the pulse width less than 0.2 μs.

The measurements of characteristics of the stochastically resonator used for the microwave energy accumulation were carried by means of the transmitting and receiving set. With this aim the short impulse of the width of 0.1 μs and impulse power of 1 kW of microwave energy from the eight millimeter range impulse magnetron is applied on the impute of stochastically resonator which was operated in this case in regime «on reflection». The accumulated in the stochastically resonator signal arrives in broad band receiver of this range which contains the mixer, klystron local oscillator, waveguide gas-filled switching tube, intermediate frequency amplifier, signal selection unit and oscilloscope indicator. The regime of receiver was chosen in such way that in normal state the receiver was closed and was opened then on the short time - «time window» by means of selection impulse from special unit. The width of «time window» was 10μs and the time interval between the «time window» and the impute impulse position one can change in the limits to 5μs in order that to avoid the receiver sensitivity suppression by the high power impute impulse.

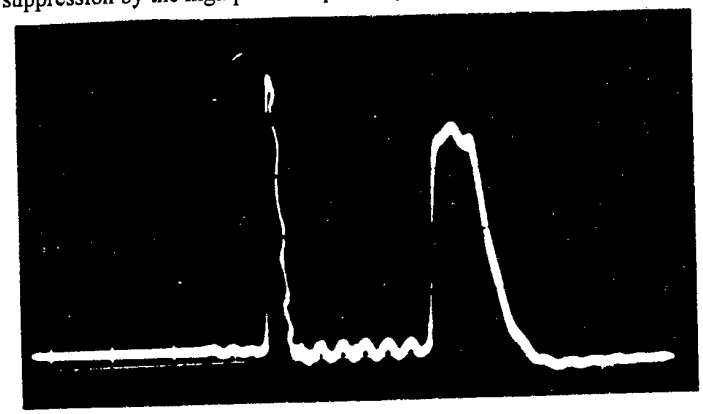


Figure.2. The oscillogram of the accumulation (delay) effect of microwave impulse of the eight millimeter range in stochastically resonator. The impulse impute power is 1 kW at the frequency 36.7GHz , the receiver sensitivity is 10μμW, the accumulation time $\tau \geq 5$ μs. by the ratio of impute and output power of 140 dB.

Thus, the wide band accumulation device of eight millimeter wave range was created in the work. This device can accumulating and long time keeping the energy of the microwave electromagnetic signal. The new principle of the electromagnetic energy accumulation in the electrodynamic system has been put in the base of the device. The electrodynamic K-system is represented in this case the stochastically resonator where due to the locally instability by scattering of electromagnetic waves on the convex surfaces of metal spheres the field stochastization takes place. As a result of such stochastization the device resonant properties remove really but at the same time the super high quality of electromagnetic cavity is conserved. This permits to achieve the microwave field accumulation for a long time in the wide frequency band of millimeter wave range. The created device can be used with success for the automatic control of the millimeter wave range radar system potential.

References

1.G.M. Zaslavsky Stochastitchnost` dynamitcheskich system. M. Nauka, 272 p. 1984

2. E.M.Ganapolskii Electromagnitnaya K-systema s dlitel`nim uderzhaniem energii SVCH sygnala. Doklady AS SSSR, v.319,p.1128-1131, 1991.

3. L.A. Vainschtein Otkritie resonatori i otkritie volnovody M. Sovietskoe Radio, 475p.1966.

OPEN HEMISPHERICAL IMAGINE DIELECTRIC RESONATOR WITH WHISPERING GALLERY MODES

Z.E.Eremenko, Yu.F.Filipov, S.N.Kharkovsky
Institute for Radiophysics and Electronics National Academy of Science of Ukraine
12 Str. Proskura , Kharkov, 310085 , Ukraine
Tel.: 380 572 448 593; Fax: 380 572 441 105; E-mail : eremenko@ire.kharkov.ua

The imaging dielectric resonators with whispering gallery modes (WGM's) for the creation of new class millimeter waves solid-state oscillators, devices for the investigation of high temperature superconductors were suggested [1-3]. They contain a dielectric element as a semidisk or a cylinder or a hemisphere and a flat metal mirror. The latter is a necessary element for placing in the resonator field active elements, conductor samples of materials. There is an important question about the dependence of the resonant frequencies and Q-factor of these resonators on impedance of the resonator mirror. In the present paper new investigation results of the open hemispherical imaging dielectric resonator (HIDR) with WGM's are represented.

Consider the homogeneous isotropic dielectric hemisphere with radius R . It is limited at $\theta = 90^0$ by flat metal mirror (insert , Fig.1). The mirror has a surface impedance $Z = \sqrt{\frac{\omega_q}{2\sigma}}(1-i)$, where σ is a metal conductivity, ω_q is a resonant frequency. The influence of small impedance value $Z << 1$ lead to frequency shift, which for TM modes is

$$\omega - \omega_q \approx \frac{(1+i)c(n-m)!}{\pi R(n+m)!}(2n+1)(n+1)^{2m-2}(n-m+1)^2\sqrt{\frac{\omega_q}{8\sigma}},$$

where n and m are the variation number along polar and azimuth coordinates, respectively.

Let us consider the numerical and experimental investigation results of TM_{nm1} WGM's in the resonator. The relative deviation of their resonant frequencies $\Delta\omega / \omega_{q1} = \left(\omega_{q2} - \omega_{qi}\right) / \omega_{q1}$ due to the mirror conductivity is shown in Fig.1.

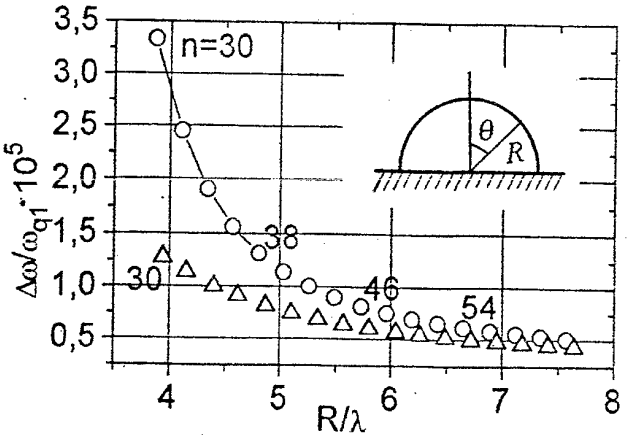


Fig. 1. The dependence the relative deviation of the resonance frequencies on parameter R/λ . O TE_{n81}, Δ TM_{n9i}

In the Fig.2 it is represented the dependence of unloaded Q-factor of TM_{nm1} modes on relative hemisphere radius R/λ (λ is the wave length in the open air) for teflon resonator ($\varepsilon' = 2.08$, $\tan\delta = 1.78 \cdot 10^{-4}$) with $R = 39mm$. The value Q_{01} is calculated for ideal case of the metal mirror $(Z = 0)$, and Q_{02} is obtained real case of copper one (conductivity $\sigma = 1.5 \cdot 10^{-7} c^{-1}$) for two values of $m = 9,17$. Here by the

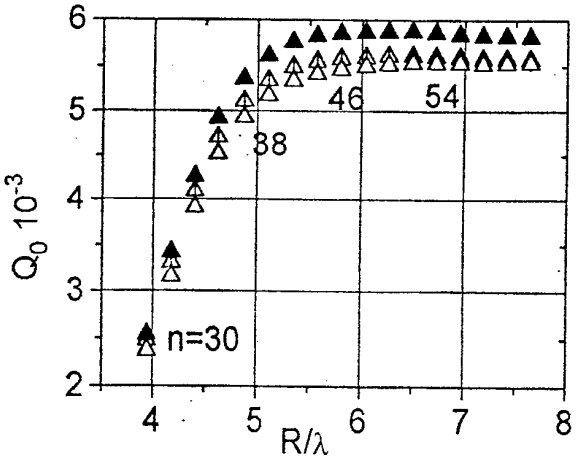


Fig.2 The dependence of Q-factor of TM modes on parameter R/λ
▲ Q_{01}, ▲ $Q_{02}(m=9)$ △ ,$Q_{02}(m=17)$

vertical limited lines it is shown trust intervals of experimental measured Q_{02} mode values. TM modes there exist in HIDR only with odd index sum $(n+m)$. The characteristics of HIDR TE modes are the same as TM ones., but TE modes exist in HIDR only with even index sum $(n+m)$. The numerical investigation of mode characteristics of HIDR, which is made of polycortexes ($\varepsilon' = 9.6$; $\tan\delta = 3 \cdot 10^{-4}$) shows that they are the same as in teflon one.

The theoretical analysis and the experimental results of the WGM's in HIDR investigation show that their spectral characterictics can be obtained with the sufficient precision by means of the integral equation method at the small mirror resonator impedance. In compare with the modes of the dielectric ball the WGM's in hemispherical resonator have the following differences: their spectrum has low density, e.g. TE amd TM modes exist only with even and odd index sum $(n+m)$, accordingly; their resonant frequencies are higher, but the value of deviation in the case of copper mirror is -0.001%, i.e. it is neglected; their unloaded Q-factor is smaller and its difference can be 8 --- 10 %.

The unloaded Q-factor WGM's of HIDR is decreased at the increasing azimuth index m. The mirror hemishperical dielectric resonator with WGM's can be used as an oscillator system of devices in millimeter band (solid state oscillators, devices for study material and so on).

References

1. Yu. F. Filipov , and S.N. Kharkovsky "Quasioptical Imaging Dielectrical Resonator", In:Kvaziopticheskaya Tehnika Millimeter i Submillimeter diapozonov, Kharkov, IRE, 1989, pp.28-34 (in Russian)
2. E. Kogut, V.V. Kutuzov, Yu. F. Filipov, and S. N. Kharkovsky " Whispering Gallery Modes in Quasioptical Hemisphere Dielectic Resonator" , Izvestiya Vuzov, Radioelectronka, vol. 40, no.2, 1997, pp.19-26 (in Russian)
3. N. Kharkovsky, A. Ya. Kirichenko, and A.E. Kogut, " Solid- State Oscillators with Whispering -Gallery Mode Dielectric Resonators", Microwave and Optical Technology Letters, vol.12, no.4, 1996, pp.210-213

THREE - MIRROR OPEN RESONATOR WITH A SATURATING PARAMAGNETIC

I. Gudim, N. Popenko

Usikov Institute of Radiophysics and Electronics NAS of Ukraine

12 Acad. Proskura vul., 310085 Kharkiv, Ukraine. Tel.(380572)-448594,

fax: (380572)441105. E-mail: buran@ire.kharkov.ua

The three-mirror open resonator (OR) [1 - 3] is formed by two metal mirrors and one dielectric mirror - total internal reflection (TIR) facet of a dielectric prism placed between the mirrors. Such an OR is of several advantages compared to a two-mirror OR which are brought about by the boundary «dielectric - air». One of them is a regulated coupling between an OR and a sample which determines the effectiveness of using this OR for measuring the characteristics of high-loss samples, e.g. [4]. For instance, one of the promising semiconductor in the modern solid electronic is a semimagnetic semiconductor. Its properties to a large extent are determined by an ion Mn+. Studying of characteristics of these substances by electron spin resonance methods at low and super-low temperatures will allow to determine the conditions of the phase transfer «paramagnetic - spin-glass», to forecast their new properties and to give recommendation for their composition and technological conditions of growth. Such investigations require a measuring system in the form of a three-mirror OR which would allow to measure the electron spin resonance spectra and the time of electron relaxation of semimagnetic high loss samples. And also when the substances are investigated by the magnetic resonance method at super-low tempetatures, the location of a sample near the dielectric mirror allows to decrease substantially the heatstream into the working chamber of the evaporation refrigarator ^{3}He [5]. The latter is of vital importance for providing normal working conditions of a super-low temperature complex.

The paper is to devoted investigation into non-linear processes in three-mirror OR with a paramagnetic under conditions of saturating electron spin transfer in millimeter wave range. The characteristics of this non-linear dissipation system have been calculated for different concentrations of paramagnetic centres, time of electron relaxation and coupling coefficient between OR and sample.

The OR under the investigation is a described above type of a three mirror OR, which has a paramagnetic layer near the TIR facet. The situation in which the electron spin transfer is saturated by EHF field, is in the focus. In approximation of the middle field we have received the equation that unites the amplitude and frequency of electromagnetic radiation at the entrance to the three - mirror open resonator and the amplitude of the resonator field with saturating of electron transfer. The behaviour of such a system may be described in the framework of a theoretical model [6].

We are considering the propagation of plane electromagnetic waves in this OR. Plane waves are propagating between semi-transparent metal mirrors with the reflection coefficient R and the transmission coefficient T and its TIR facet:

$$H_j(z,t) = H_j \exp\left[i(\omega t \pm kz)\right] + c.c\,, \tag{1}$$

After falling on the first semi-transparent metal mirror, an incident wave is propagating further in the direction of the TIR facet and after being reflected from it goes to the second metal mirror. The full cycle of a wave going through the OR is finished when it comes back to the first metal mirror. The resonance oscillation is set in the three-mirror resonator when the following boundary conditions are fulfilled:

$$\begin{vmatrix} H_I(0) \\ H \end{vmatrix} = \begin{vmatrix} \sqrt{T} & \sqrt{R}r(H)e^{i\beta} \\ -\sqrt{R}r(H)e^{i\beta} & \sqrt{T} \end{vmatrix} \tag{2}$$

where H - field amplitude in the resonator, H_I - amplitude of incident electromagnetic wave; β - phase shift per single passing; r(H) - reflection coefficient from the non-linear boundary formed by the TIR facet and a paramagnetic sample placed near it. The value r(H) is determined on the basis of the solving problem of diffraction of plane elecrtomagnetic wave from the four-layer system: dielectric - dielectric - paramagnetic - dielectric, under condition when the electron spin transfer is saturated. In this case for the elementary spin system, comprising N spins of one type with spin number s=1/2 the paramagnetic permeability is described by the expression [7] and the non-linear properties of a paramagnetic are determined by its dependence on the alternating magnetic field H. Among the parameters of the paramagnetic there are static paramagnetic permeability, time of the spin-lattice and spin-spin relaxation and concentration of paramagnetic centres. For electro-dynamic system changing parameters, on which its properties depend, are reflection coefficient of mirrors, distance between the mirrors, coupling coefficient between OR and samples.

In the general case the equation which connects the waves propagating in the resonator looks as follows:

$$H = \frac{H_I\sqrt{T}}{1 - Rr(H)^2 \exp(i2\beta)\exp(-\alpha L)} \qquad (3)$$

The numerical analysis of such a system for different concentration of paramagnetic centres, time of relaxation and also coupling coefficient between OR and sample was carried out. As a result, it was estimated that for a certain proportions of concentration of paramagnetic centres, time of relaxation and constant coupling coefficient between OR and sample, beginning with certain value of incident waves, several roots of solving the equation (3) appear (Fig. 1b). That is why, when behaviour of electron spin system of paramagnetic is studied for saturation condition in the area of bistability, interpretation of the results will be incorrect. So when non-linear processes in electron spin system are studied, to interpret the obtained results correctly it is necessary to choose the regime of electro-dynamic system far from the point corresponding (Fig. 1b).

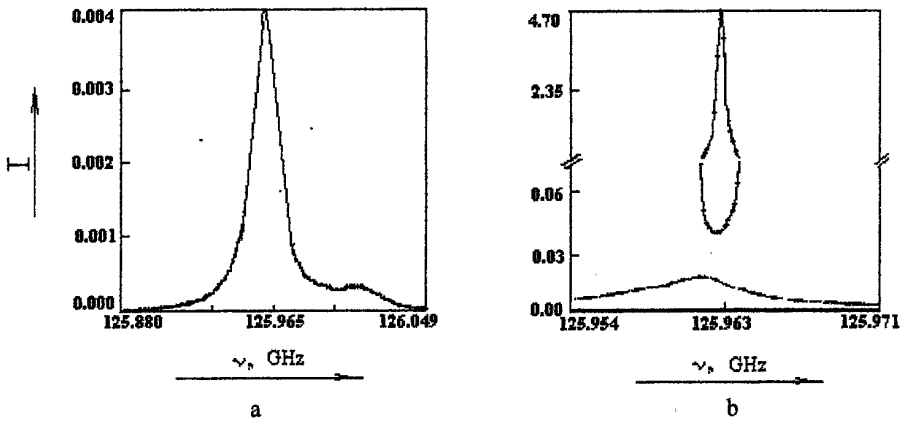


Fig. 1. Resonance curvatures for the OR with a saturating paramagnetic:
a - $H_I = 0.15$; b - $H_I = 0.25$ (coupling coefficient between sample and OR is constant).

For the three-mirror resonator this problem is solved quite easily. As the results have shown, stable regime of the system is chosen by changing coupling coefficient between sample and OR. The results of this calculation are convinient to be presented as plane of parameters (concentration of paramagnetic centres, coupling coefficient between sample and OR, incident EHF field intensity). In this case it is divided into two areas: stability and bistability (Fig.2).

For a sample under the investigation location of boundary between these areas is determined by value of magnetic permeability. Analysis of its dependence on EHF field value for different concentrations of paramagnetic centres and relaxation time has shown that: 1) field intensity necessary for going into non-linear regime increases proportionally to concentration of paramagnetic centres in the samples; 2) changes in relaxation time leads to changes in value of non-linear area and also in steepness of the dependence. It is necessary to note

that influence of spin-lattice relaxation time is substantially greater than that of spin-spin. For samples with bigger time of spin-lattice relaxation $T = 8*10^{-3}$ s. the boundary between the two areas moves to the area of big intensity values (Fig. 2b). For samples with smaller relaxation times $T = 10^{-3}$ s. form of the boundary of the given areas gets much more complicated (Fig. 2a), which is determined by strenthening of non-linear properties of the system.

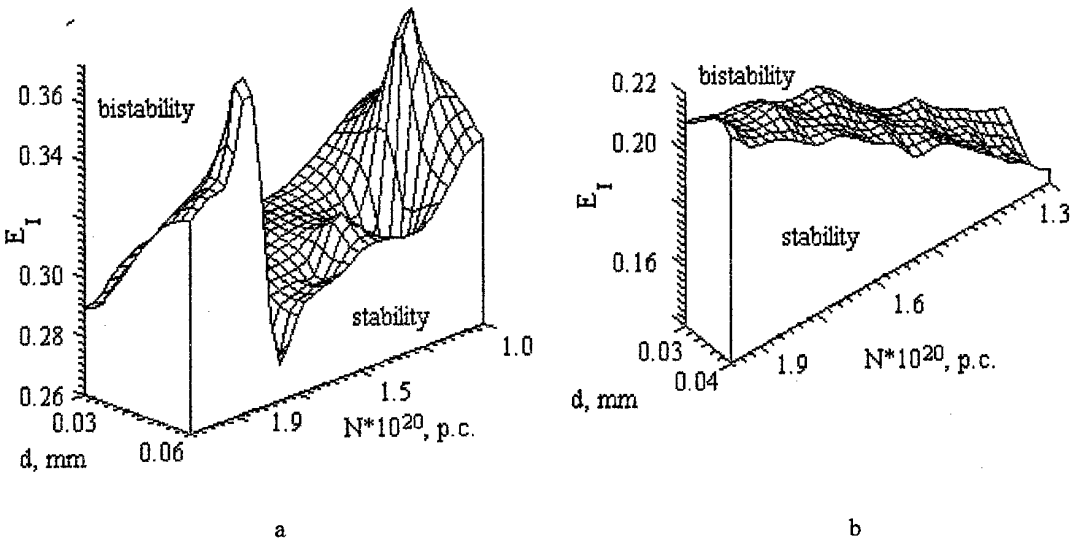


Fig. 2. The parameter plane such as concentration of paramagnetic centres, incident wave, coupling coefficient between OR with the sample (distance between the TIR facet and the sample) for different time of spin-lattice relaxation: a - $T=10^{-3}$s., b - $T=8*10^{-3}$s.

Thus, in this paper in approximation of middle field the parameters of three-mirror OR with saturating paramagnetic placed near the dielectric mirror, by which the transfer from stable regime to bistable one is observed, have been defined. Usage of this parameter plane allows to determine the coupling coefficient between the OR and the sample, by which for sample with set concentration of paramagnetic centres and spin-lattice and spin-spin relaxation times in the whole area of changes in the incident field, the resonance system will be working in stable regime.

Acknowledgements. The author thanks prof. S. Tarapov for the valuable discussions.

References.

1. A. Vertiy, N. Popenko, Yu. Popkov, S. Tarapov, V. Shestopalov «Three-mirror OR in MM Range», Izvestiya VUZov, Radiophysics, Vol.27, No.6, pp.775-782, 1984, (in Russian)
2. A. Vertiy, N. Popenko, S. Tarapov, V. Shestopalov, «Investigation into OR with Prism of Total Internal Reflection», Izvestiya VUZov, Radiophysics, Vol.25, No.6, pp.684-687, 1982, (in Russian).
3. A. Vertiy, G. Zvyagina, N. Popenko, «Quasi-optical Resonator with Dielectric Frame», Izvestiya VUZov, Radiophysics, Vol.31, No.5, pp.591-610, 1988, (in Russian).
4. N. Popenko, I. Gudim, S. Tarapov, «Open resonator for Measuring High-losses Dielectric», Internetional Journal of Infrared & MM Waves, Vol.17, No.11, pp.1879-1893, 1996.
5. A. Vertiy, G. Zvyagina, I. Ivanchenko, N. Popenko, S. Tarapov, «Resonance Cell of Super-low Temperature Spectromrter», Instruments and Experimental Techniques, No.2, pp.107-110, 1988.
6. H.M. Gibbs. Optic Bistability; Controlling Light with light. Academic Press. Orlando, FL, 1985.
7. C. Poole. Electron Spin Resonance. John Wiley & Sons. New York. 1983.

DIFFRACTION RADIATION OSCILLATOR WITH THE LONG-FOCUS SMALL-APERTURE OPEN RESONATOR

M.Demchenko, I.Ivanchenko and V.Korneynkov

Usikov Institute of Radiophysics & Electronics NAS of Ukraine
12, Ac.Proskura St., 310085 Kharkov, Ukraine. Tel. +380(572)448594,
fax: +380(572)441105, e-mail: buran@ire.kharkov.ua

Introduction

Of the average power millimeter-wave oscillators the diffraction radiation oscillators (DRO) [1] operating on the Smith-Purcell's effect have a prominent place. The oscillators of this type are sometimes referred to as free electron lasers [2]. The combination of good spectral and power characteristics allows them to be effectively used in antenna equipment, radiospectroscopy, defectoscopy, plasma diagnostics, medicine, etc. A great variety of DRO modifications is widely used at present. An efficiency of their practical applications will depend largely upon the solution to the problems such as: a decrease in their dimensions and, consequently, in their weight and cost of these devices. It is necessary to save a radiation spectrum quality and the high power characteristics. This problem can be solved by reducing dimensions of the DRO electrodynamic system in the form of a open resonator (OR) which provides for a positive feedback. This had been previously achieved by using a short-focus quasi-optical OR analog as an oscillatory circuit. In these resonators the radii of aperture and curvature of reflectors and the separation between them are comparable to the operating wavelength. This led to the development of a series of the compact DRO which are on a par with the basic DRO in terms of their characteristics [3]. However, the reduction of the interaction space of the electron flow with the resonance electromagnetic field in the DRO gives rise to an increase of starting currents as well as to the steepness of mechanical and electronic frequency change. In this paper a new DRO modification with an oscillation circuit as a small-aperture long-focus OR is proposed.

Investigation method and results

The proposed OR is formed by a cylindrical reflector and a spherical reflector with the slot-type coupling element (3.6*1.8 mm^2) placed in the reflector geometry centre. The reflected diffraction grating (RDG) is 10mm wide and is positioned in the central part of the cylindrical reflector. The reflectors aperture radius W and their steepness radius R are W=12mm and R=110mm respectively. This OR geometry accounts for an operating interval for the reflectors' separation of $L = (0.7 - 6.0)\lambda$.. In the above OR the quasi-optical condition $W^2/L\lambda << (L/W)^2$ (where λ is the wavelength) is violated as well as for short-focus OR whereas the Fresnel numbers are of the same order both in the typical quasi-optical OR and in its short-focus analog. To determine subsequently the DRO output characteristics with the electrodynamic system of this kind it is necessary to know the amplitude and phase resonance field distributions near the RDG. A relatively low Q-factor of the modes for this system ($Q \approx 400 - 700$) and the small reflectors separation L do not allow the traditional small disturbance method to be used [4]. The novel «dielectric antenna method», developed by the authors for the space structure field investigation within the short-focus OR [5] will not be effective in this particular case.

Therefore, we have developed an original experimental method to investigate the OR spectral characteristics and resonance space field distributions inside it, where the Sommerfeld's wave is used for the oscillation excitation within the system. This wave is propagated along a metal wire (the diameter D=0.09 λ) and scattered by an electrical dipole (the dipole length is l=0.25 λ and its diameter is d=0.04 λ) coupled with such a transmission line. Sommerfeld's line together with the dipole is placed on the mechanical scanner, which makes it possible to meet the required conditions for the investigation of both the spatial amplitude and phase field distributions within the OR. The study of the «cold» OR was performed in the 4-mm wavelength band. It was found that the OR spectrum consists of four modes within the interval $L = (0.75 - 1.5)\lambda$.. When the reflectors separation increases, the spectrum is rarefacted due to a sharp increase in the diffraction losses for the

higher modes. Under $L > 3.6\lambda$ conditions only a fundamental TEM_{00q} mode remains and it is not excited for $L > 6\lambda$..

The resonance field intensity distributions were recorded in the OR cross-section at a distance 0.75λ from the RDG plane that was flush with the reflector plane. Fig.1 shows the normalized field distributions along the resonant beam radius. The field pictures correspond to the TEM_{00q}, TEM_{02q}, TEM_{20q} and TEM_{40q} modes. In this case, in contrast to the quasi-optical OR (with the similar geometry) the fundamental mode with any reflectors separation exists. The field stain of this mode is within the RDG boundaries. Therefore, when this mode is used as an operating one within the DRO the latter is similar to the orotron. The TEM_{02q}

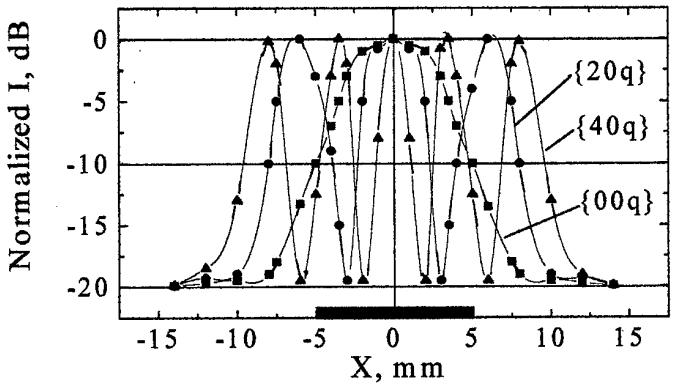


Figure1. Normalized field distributions of TEM_{00q}, TEM_{20q} and TEM_{40q} modes

mode is also excited within OR under $L > 1.13\lambda$. conditions. As regards the TEM_{20q} mode as the basic DRO working mode, the lateral field stains are on the division boundary of the RDG with the reflector surface and their field intensity is equal to that for the central stain. This can be explained by the fact that the cylindrical reflector steepness compensates the phase shift of the reflected wave from the equiphase reflecting surface of the RDG and from the smooth reflector surface [6]. It results in the intensity redistribution in the mode field stains and we observe the three field stains with a practically equal amplitude (see Fig.1). It also refers to the TEM_{40q}

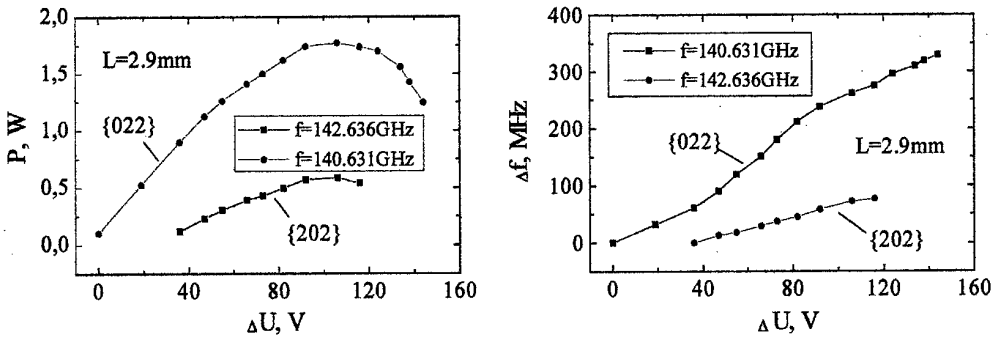


Figure2. The DRO output power and electronic frequency change for the TEM_{022} and TEM_{202} modes as the functions of an accelerating voltage

mode field structure. The DRO cross-section contour is performed at the foot of the Fig.1 by the black rectangle.

The obtained field distributions show that the fundamental mode field stain within the small-aperture sphere-cylindrical OR with the long-focus reflectors is both slightly deformed and stretched along the RDG and the stain dimension is nearly half of the RDG length. It implies that a decrease of space interaction volume of the

electron flow with the resonance field (in contrast to the DRO with the short-focus OR) does not occur here, and, therefore, the power characteristics of the basic DRO should remain unchanged for the same electron flow densities. It has to be noted that the inhomogeneous field distribution along an interaction space (when the DRO operates on the highest modes) will lead to the emergence of the partially degenerated zones in the DRO spectrum [7].

The modified DRO was developed on the basis of the «cold» OR investigation. The output power take-off is done by means of the open waveguide ($1.6*0.8mm^2$) placed on the spherical reflector periphery when the fundamental mode field intensity decreases ε times as compared with the field intensity in the OR axis. The frequency band of the electromagnetic radiation is (100 - 160)GHz. The accelerating voltage varies from 2.05kV to 4.6kV. The reflectors separation varies within the interval of (2.0 - 7.7)mm. The DRO operates on the TEM_{00q}, TEM_{20q} and TEM_{02q} modes. In Fig.2 the dependences of the output power and electronic frequency change for the TEM_{022} mode (the upper curves) and TEM_{202} mode (the lower curves) respectively as functions of an accelerating voltage are shown. The steepness of the electronic frequency change for the TEM_{022} mode tend to

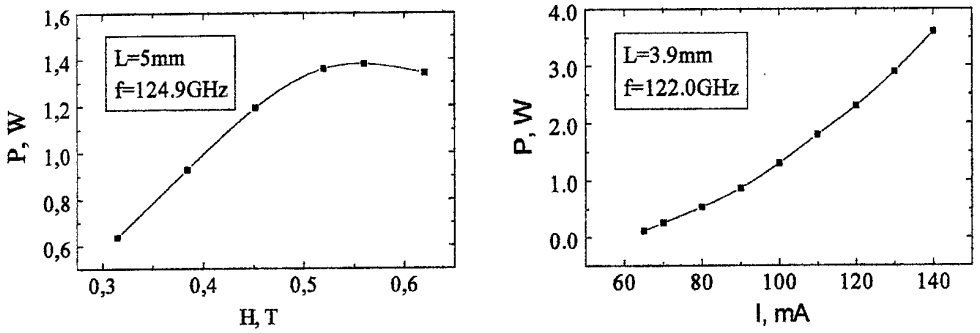


Figure 3. The DRO output power as a function of the focusing magnetic field and the working current

vary from $3\,MHz/V$ to $1.5\,MHz/V$ and it is $0.95\,MHz/V$ for the TEM_{202} mode. In Fig.3 the DRO output power as a function of the focusing magnetic field (left-hand graph) and of the working current (right-hand graph) is shown. One can see that the saturation at the magnetic field is observed at H=0.5T, and therefore, the samarium-cobalt magnetic system mass is about 4kg for the DRO with the 32mm separation between magnet poles. In this case the output power of 3.6W is achieved for the working current of 140mA.

Conclusion

A small-aperture long-focus OR is proposed by the authors as a positive feedback circuit in the new modification of the millimeter DRO. It has been shown that the TEM_{00q}, TEM_{20q} and TEM_{02q} modes can be used as the working modes in this oscillator. The output power of small-size DRO increases in comparison with the basic DRO. The starting currents and the steepness of the mechanical and electronic frequency changes are the same as in the basic DRO. The practical application of the compact DRO with the small long-focus reflectors tend to increase the functional capabilities of the microwave oscillators, and the new prospects are opened up for the development of the multicascade systems in the field of the microwave diffraction electronics.

References

1. V.P.Shestopalov, «Diffraction electronics», Visha shkola, Kharkov State University, pp.145-220, 1976.
2. R.P.Leavitt, D.F.Wortman, C.A.Morrison, «The orotron - a free-electron laser using the Smith-Purcell effects», Appl.Phys.Lett., Vol.35(5), No.345, pp.363-365, 1979.
3. A.V.Nesterenko, A.I.Zvyk, V.P.Shestopalov, «Diffraction radiation oscillator miniaturization», Doklady Academii Nauk SSSR, Vol.277, No.1, p.84-88, 1984.
4. S.P.Gavrilov, I.Ya.Gudim, I.V.Ivanchenko, «The scattering field research of OR excitement element as a dielectric antenna», In: Preprint No.95-10, IRE NAS Ukraine, 1995. - 31p.

MILLIMETER WAVE LINEAR ANTENNA ARRAYS BASED ON RIDGE DIELECTRIC AND GROOVE WAVEGUIDES

A.P.Yevdokimov and V.V.Krizhanovsky
Institute of Radiophysics and Electronics of the National Academy of Sciences of Ukraine
Address : 12, Ac. Proskura st , Kharkov , 310085 , Ukraine
Tel 38-0572-448326 , Fax 38-0572-441105 , E-mail yevdok@ire.kharkov.ua

Various open structures such as open resonators and open waveguides are widely used in the modern millimeter-wave equipment. Plane and linear dielectric waveguides are among them. Their advantages are both the high parameters available and the low cost compared to the analogous traditional devices. For example, antenna arrays on the basis of the conventional slotted waveguides with the aperture of 10 - 20 wavelengths are rather expensive because of the high accuracy required to make the slots, especially in the wide waveguide wall in the vertical polarization case.

The vertical- and horizontal-polarized linear antenna arrays have been designed on the basis of a ridge dielectric waveguide, and they have been introduced in the airborne radar systems. The characteristic length of these arrays is 1500 mm, the operation waveband is 8 mm. The operation principle rests on the scattering of the waveguide mode on the periodically spaced radiators arranged as a diffraction grating. The mentioned radiators represent rectangular waveguide hollows oriented along the waveguide axis in the vertical polarization case and perpendicular to it in the horizontal polarization case. The fabrication of the diffraction grating makes no problem. The grating provides a high decoupling between the across polarized modes which is no less than 40dB. The pattern width of the antennas based on a ridged dielectric waveguide is from 30 ^{0} to 80 ^{0} depending on the type of the diffraction grating used. These antennas are very good for the side observation radars. The low cost of such antennas is determined not only by the ease of manufacture of the ridge dielectric waveguides and the mentioned diffraction gratings, but also by the possibility of the fine tuning of the amplitude and phase distributions. This possibility somewhat decreases the required accuracy of the component fabrication.

The antennas based on a ridged dielectric waveguide are preferable for the aperture dimensions no more than 200 wavelengths. The further aperture increase rises the losses. For example, they are more than 1.5dB for the teflon waveguides. In the radar mode of operation this reduces a the radar potential by 50% . In order to decrease the losses, it seems advisable to replace the ridge dielectric waveguide by the metal groove waveguide. The groove waveguide is remarkable as it is a structure which may be suitable for antennas operating on the wavelengths up to 2 mm due to comparatively large groove dimensions.

The development of the linear antenna arrays on the basis of a groove waveguide arises a number of the problems concerned with the field structure investigation, loss measurements, the excitation of the fundamental mode with a high efficiency, the investigation of the interaction of the fundamental mode with the periodic scatterers. The latter problem is concerned with the investigation of the efficiency of the fundamental mode cotransforming into a leaky wave for the regimes with converting and non converting of polarization, and with the study of the transformation of the fundamental mode into higher ones.

For the first time the groove waveguide was suggested in / 1 /. It consists of two metal planes with rectangular grooves. Later it was suggested a triangular shape of grooves / 2 /. It was found that it allows for the decrease of losses. The fundamental mode of the groove waveguide is H_{10}-wave. Decreasing of its losses is achieved mainly due to increasing of the distance between the metal planes up to 3 wavelengths. The triangular shape of the grooves used eliminates a sharp edge that also leads to losses decreasing. The depth and height of the grooves have smaller influence on the losses. For our purpose it is not admissible to increase the distance between the metal planes very much because of a probability of the excitation of higher modes in the presence of the diffraction grating. So this distance was chosen near to a single wavelength for the frequency band of 36.72 - 69GHz. It equals 5.2mm while the depth and height of the grooves are 1mm and 3.4mm, respectively. In order to determine the effect of the sharp edges of the groove on the losses, two models of the waveguide have been studied. The first model assumes a rectangular shape of the groove, whereas edges with the angle of 45 ^{0} are considered in the second model. The height of the groove in the second model is 4.8mm. In the both models the groove waveguides are fitted by means of a horn transaction to a waveguide with the cross section dimensions of 7.2mm x 3.4mm. Losses in these transactions are not more than 0.15 - 0.2 dB in the frequency band of 46 – 55 GHz. Our measurements have shown that the groove waveguide with the rectangular shape of

the grooves have losses twice lower in comparison with a metal waveguide having cross section dimensions of 7.2mm x 3.4mm. The groove waveguide without the sharp edges has losses lower at 30% in comparison with the groove waveguide with the rectangular shape of the grooves. It is supposed that the walls of the both waveguides are made from the same metal. Summarizing this results it should be stated that the linear antenna aperture can be increased by factor two in comparison with the antenna on the base of the ridged dielectric waveguide.

The most complicated problem, related with the groove waveguide, is the fundamental mode transforming into a leaky wave. Several types of reflecting diffraction gratings inserted between metal planes close to the groove have been investigated from this point of view. The leaky wave from the diffraction grating comes across the groove, then through the space between the opposite metal planes, and then it is radiated through the slot between the edges of the metal planes. Diffraction gratings with different period values and with various forms of the shape have been studied. The energy characteristics have been measured for two groove waveguide models. It is very important to achieve a maximum of transforming efficiency, especially for short apertures. The second aim is to minimize the influence of the diffraction grating on the fundamental mode field structure and on the fundamental mode phase velocity. The energy characteristics measured resemble that for resonant structures, like the ridged dielectric waveguide. The different rate of coupling between the fundamental mode and the diffraction grating allows for the design of linear antenna arrays with apertures from 20 to 400 wavelengths for the operation on the horizontal polarization. The efficiency of the transformation into a leaky wave may be as high as 95%. An antenna model has been investigated with a diffraction grating of 215mm in length for frequency of 49.25GHz. The width of the radiation pattern in this case is 1.6^{0}, and the sidelobes level is -13dB. Such an antenna can be easily realized in the short-wave region of the millimeter waveband. It would be much cheaper than the classic antennas, especially in the case of large apertures.

The main feature of the diffraction grating used for the fundamental mode transformation into a leaky wave with horizontal polarization is that the grating provides the interaction with longitudinal components of electric field. In opposite to this situation a diffraction grating sensitive to the transverse components must be used in the case of the vertical polarization. Taking into account that the distribution of the transverse components is even, composed diffraction gratings are needed. Two types of such diffraction gratings have been investigated. Both of them consist of two separate diffraction gratings, shifted on the half period in the longitudinal direction what is needed to provide 180^{0} phase shift in the radiated field. The first grating has the shape of a rectangular resonant cavity. However, due to its low efficiency this grating is admissible for large apertures only. The second diffraction grating has an elementary radiator in the form of a dipole. Its efficiency is rather high, but there are frequency bands with sharp resonances. Radiation patterns have been investigated for frequencies of 36.72 GHz and of 50 GHz. The width of the pattern is 1.6^{0} with the sidelobes of -12dB for the frequency of 50GHz. For the frequency of 36.72 GHz the radiation pattern is 2.25^{0} in the width with -14dB sidelobe level. The main beam of the radiation pattern makes an angle of 24.6^{0} to the normal of the aperture. This corresponds to a relative phase velocity of 0.75 when the diffraction grating period is 7.0mm. In general the diffraction gratings with a dipole are suitable for the design of antenna gratings for both cases of small and large apertures.

Acknowledgment. This work was supported in part by EC under contract BIC15CT960816.

References

1. F.J.Tischer, ``The Groove Guide, a Low-Loss Waveguide for Millimeter Waves``, IEEE Trans., Vol. MTT-11, №5, pp. 291-296, 1963.
2. T.H.Ho, D.J.Harris, ``Millimeter Wave Groove Guide with V-Shaped Grooves``, Electronic Letters, Vol. 20, №19, pp. 777-778, 1984.

MILLIMETER WAVE PLANAR COSECANT ANTENNA ARRAY FOR AIRBORN RADAR FOR THE UKRAINIAN MINISTRY OF EXTREME SITUATIONS

A.P.Yevdokimov and V.V.Krizhanovsky
Institute of Radiophysics and Electronics of the National Academy of Sciences of Ukraine
Address : 12, Ac. Proskura st , Kharkov , 310085 , Ukraine
Tel 38-0572-448326 , Fax 38-0572-441105 , E-mail yevdok@ire.kharkov.ua

There is an increasing interest in cosecant antennas for aircraft-installed radars aimed at earth remote sensing. As known [1 - 3], cosecant radiation patterns are generally produced by mirror antennas. But, for one thing, mm-wave mirror antennas are too bulk and cumbersome to be used aboard the aircraft and, in addition, they must be supplied with like radomes. For another, the practical application of a cm-wave mirror antenna in the ice-surveying airborn radar complex revealed its susceptibility to the engine and fuselage action resulting in pronounced pulsations in the cosecant pattern. When exceeding 0.5 dB these pulsations modulate the earth image, so that the special preprocessing of the signal is necessary. In this situation, the aim is to combine the planarity of the antenna geometry with the smoothness of the pattern in the observation range.

The developed system must fit the state-of-the-art point of the mm-wave antenna designs. And along with the desired electrodynamical characteristics, it is claimed to be well suited to a minimum of weight and size, aerodynamical conditions, elevated vibrations, temperature and pressure drops, waterproofing.

Custom Antenna Specifications :	
Working frequency :	36.8 GHz ± 400 MHz
Polarization :	linear vertical
Pattern shape in elevation range $2\Delta\varphi$:	cosec φ
Elevation range :	4 0 deg
Pattern width in azimuth range $2\Delta\Theta$:	0.5 deg
Sidelobe level in azimuth :	-- 2 0 dB
Smooth gain area in elevation range :	8 dB
Antenna gain :	37 dB
Loss :	no more than 1.5 dB
SWR :	no more than 1.3
Working aperture :	1000 mm x 230 mm
Antenna dimensions (tentatively) :	1000 mm x 320 mm x 55 mm
Weight (tentatively) :	12 kg.

To avoid the sweating occurring in the pressure equalizing as the aircraft climbs, the system must be equipped with a renewable silica gel cartridge.

From the planarity standpoint, diffraction radiation antennas [4] qualified as a new antenna class are best suited. The electrodynamical scheme of this antenna represents a surface-wave transmission line in the form of a dielectric waveguide combined with a scattering diffraction grating. The operation principle is based on the conversion of the waveguide surface waves into the volume waves when passing the periodically arranged scatters. However the ready-to-use engineering solutions of the cosecant pattern forming by a planar structure are not known yet. To this end, a special research has been made.

The efforts were undertaken to develop a mathematical model that can predict the cosecant pattern for the given coverage when a surface wave excited by a planar dielectric waveguide passes aperiodic scatters. In our case, 36 reflection elements aperiodically arranged as a diffraction grating of length 25 λ and width 1 m were regarded as a former of the cosecant pattern covering a 40-degree range. Evidently the aperture required for forming the exactly cosecant pattern exceeds 20 λ . The groove parameters of this reflection - type diffraction grating (1, Fig. 1) are selected proceeding from the desired polarization (in our case, vertical linear). The surface wave source is a planar dielectric (teflon) waveguide [2] of length 25 λ and width 1 m. The waveguide width is determined by the antenna beamwidth in azimuth, which is 0.5 degree. For a 3-mm thickness of the planar dielectric waveguide with the chosen parameters of the diffraction grating , the cosecant pattern maximum is off the normal to the antenna plane by 105 degree towards the excitation waveguide [3] with size 7.2 mm x

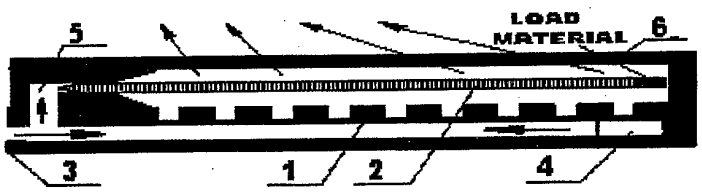


Fig.1 The antenna design.
1. Diffraction grating. 2. Dielectric waveguide made of Teflon. 3. Feeding waveguide. 4. Parabolic reflector. 5. Waveguide bend. 6. Radio-transparent blister.

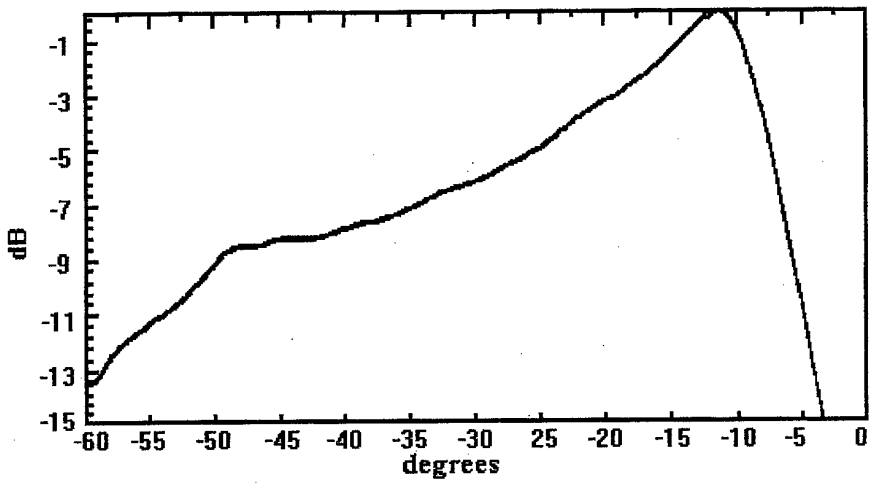


Fig.2 Theoretical antenna pattern.

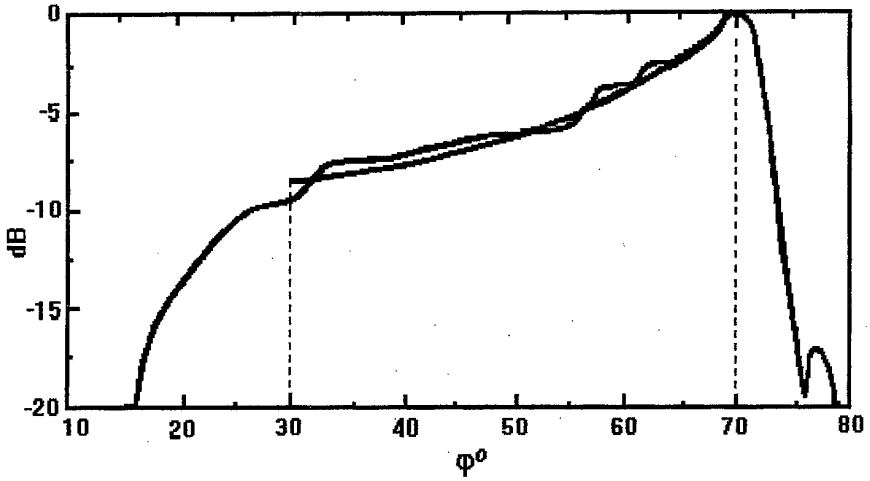


Fig.3 Experimental antenna pattern in the tilt plain (solid line) along with ideal pattern shape (dashed line).

3.4 mm. As shown in Fig. 1, planar waveguide (2) is excited by planar horn - parabolic exciter with 1-m aperture. H_{10} wave is transmitted by waveguide (3) to a 170deg plane horn. Then it is reflected by parabolic reflector (4), passes 180deg waveguide bend (5) and excites waveguide (2). Periodic grating (1) converts the surface wave into the volume wave that passes radiotransparent radome (6). The arrows in the figure indicate the spatial orientation of the field scattered by different parts of the diffraction grating in the process of the cosecant pattern forming.

The simulated cosecant pattern is shown in Fig. 2. It is sufficiently close to an ideal cosec φ function. The difference between cosec φ and the measured cosecant pattern produced by the real antenna enclosed in a radiotransparent radome is attributed to the radome presence (see Fig. 3).

In the design process, once more variant of the cosecant antenna for the airborn radar complex has been engineered. The difference between the two models lies in the following data:

Antenna gain : 37. 5 dB
Loss : 1.2 dB
SWR : 1.14
Dimensions : 1000 mm x 32 0 mm x 48 mm
Weight : 15 kg .

The rest characteristics coincide with those listed before.

The other model for the Ukranian Ministry of Extreme Situations for the airborn radar complex aimed at earth remote sensing follows the above-stated scheme. The only difference is the absence of 180 - deg waveguide bend (5, Fig. 1) combined with parabolic reflector (4) exciting planar dielectric waveguide (2). In this case, the antenna aperture size in azimuth is doubled , so the antenna pattern width is 0.25 deg x 40 deg , and the antenna gain at the pattern maximum is 3 dB larger.

Both antennas were tested and now they are used according to their destination together with airborn radar systems.

1. Rudolf Kiihn. Mikrowellenantennen , Veb Verlag Technik, Berlin, 1964.
2. A.L.Drabkin, V.L.Zuzenko, and A.G. Kislov, "Antenna - Fider Devices". Moscow: Sov. Radio, 1974 (in Russian).
3. Radar Handbook , Editor-in-Chief Merrill I. Skolnik , McGraw-Hill Book Company , 1970.
4. A.P.Yevdokimov and V.V.Krizhanovsky , " A New Direction in Antenna Array Technology ", Izv. VUZov , Radioelektronika , Vol. 39, No.9, 1996 , pp. 54-61 (in Russian).

AUTOMOBILE RADARS FOR COLLISION AVOIDANCE

A.P.Yevdokimov, V.V.Krizhanovsky
Institute of Radiophysics and Electronics National Academy of Sciences of Ukraine
Address : 12 Ac. Proskura St , Kharkov , 310085 , Ukraine
Tel . 38-0572-448326 , Fax 38-0572-441105 , E-mail yevdok@ire.kharkov.ua

In the recent time an interest increases to a near - range radars, which may be mounted on a various kinds of vehicles. In the first turn it is connected with requirements of the traffic safety. Such radar, installed on a vehicle, supplies the driver with additional information about obstacles and other vehicles in a conditions of low visibility or limited time of surrounding situation survey. It must be noted that the problems related with the development of oscillators, detectors and other microwave devices have been solved much more quickly than that, related with processing and proper using of direct information about the distance and the relative velocity of surrounding objects. In this field some tendencies are only deliberated. The most perfect and the most complicated systems stipulate representation of the radar image of surrounding situation in an observable form on a computer display. Evidently, such systems should form controlling signals for executive devices of the automobile. They should permit driving on the base of the visual information from the display only. These systems have advantages under conditions of zero visibility (fog, snowfall), but at the same time under the conditions of limited visibility the driver will be forced to switch his attention permanently from road situation to display and vice versa. The driver may become early overtired, moreover, the information from the display is not useful while dazzling. The simplest and therefore cheap radar systems have another task. They must give a notice of various obstacles with the help of a sound or light alarm, that does not divert attention from the road situation. In this case various measuring sets with the digital indication are also not needed for quick orientation in surrounding situation, though they may be mounted on automobiles and used for motion parameters control in usual circumstances.

We have designed two models of an automobile radar with the maximum range of operation of 100m and a sound form of the alarm signal. On our opinion the sound form of indication diverts driver's attention from surrounding situation in the lowest extend and keeps its properties of additional source of information while dazzling. Both radars operate in 76-77GHz band. The transmitter is designed on the base of a Gunn oscillator with the doubling of the fundamental frequency. Its frequency bandwidth is of 0.3GHz in the regime of linear frequency tuning by varactor. These models of radar differ in methods of signal processing that comes from the detector and in the form of the alarm signal. In the first case an analog method of processing is realized. Four filters are used in order to distinguish various obstacles in distance. Cutoff frequency distribution is logarithmic type, so quite admissible accuracy of distance measuring is received. As signal processing is parallel in time, the question of the number of filters is not principal, and an acceptable size and weight only limit their number. The signal from the lower distance filter blocks all signals from higher distance filters. Thus the alarm signal is available only from the nearest obstacle. Sound frequency of 1000 Hz is used for the alarm signal. It was found that the variation of the modulation frequency from 5 Hz to 50 Hz is a convenient way to indicate the distance to an obstacle. Radar sensitivity is sufficiently high to discover automobiles, people, and trees on the maximum operating distance. Power supply of the radar is based on a 12V, 0.2A source.

In the second case the signal from the detector after amplifying comes to an analog-digital converter. The frequency of the conversion is close to 1MHz. This is quite sufficient for signal recording with the bandwidth up to 0.2MHz. After processing the alarm signal is formed, that carries information about all obstacles.

In the nearest future radar models will be designed with the prime cost that is not higher than 100$. The authors have in their disposal original Gunn oscillator circuits, plane antennas and other microwave devices.

References

1. S.A.Zelubowski, ``Low Cost Antenna Alternatives for Automotive Radars``, Microwave Journal, 1994, №7, pp.54-63.
2. A.P.Yevdokimov, V.V.Krizhanovsy, ``Antenna for Automobile Radar``, In: Proceedings of the Second International Conf. on Antenna Theory and Techniques, Kyiv, Ukraine, Kyiv Polytechnical Inst., pp.168, May 1997.

AIRBORNE RADIOMETER BROADBAND QUASI-OPTICAL SCANNING ANTENNA SYSTEM

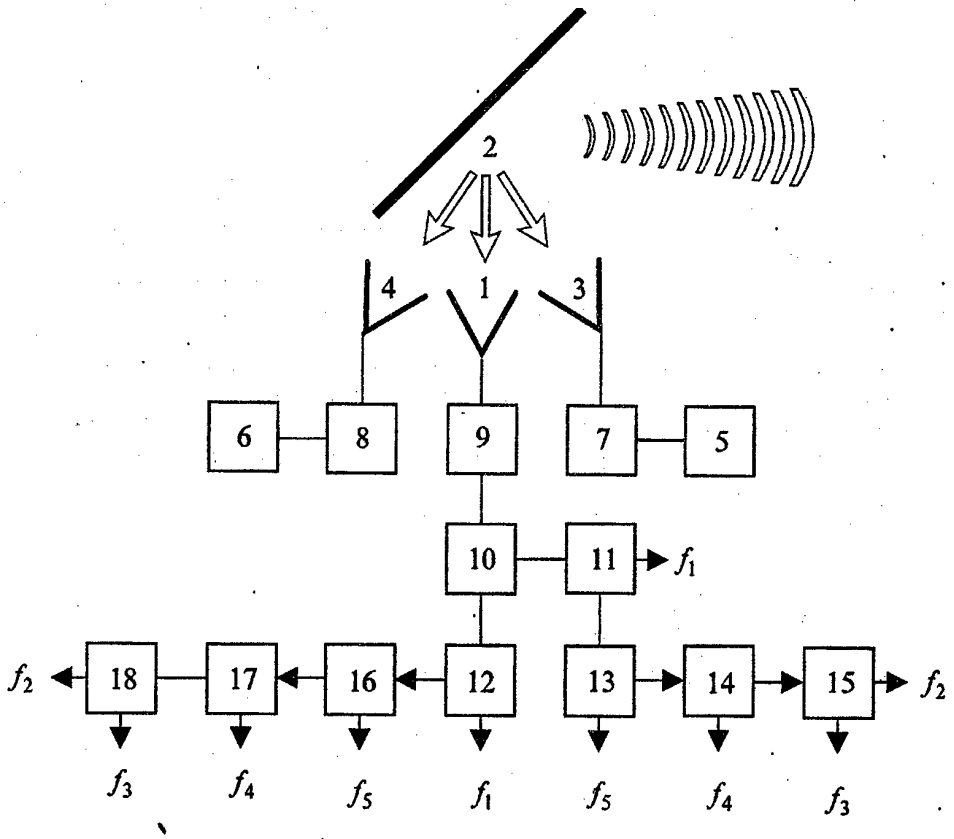
Grigoriy I. Khlopov, Vladimir A. Komyak, Alexei A. Kostenko, and Sergei P. Martynuk

Usikov Institute for Radiophysics and Electronics of National Academy of Sciences of Ukraine 12, Proskura st., Kharkov, 310085, Ukraine
Tel. +380 (572) 44-85-74

The modern methods of the remote sensing of the Earth by microwave radiometers are based on wide-band analysis of microwave radiation with a complete polarization reception and a wide-angle scanning of Earth surface at a constant incidence angle of a beam in a scan band.

In present paper, the airborne radiometer scanning quasi-optical antenna system for broadband operating in ranges: f_1= 90,0 GHz; f_2= 36,5 GHz; f_3= 18,7 GHz; f_4= 10,95 GHz; f_5= 6,6 GHz simultaneously for two orthogonal polarizations is described. In this connection, quasi-optical methods are most expedient for design of antenna feeder systems and the principal problem is reduction of system dimensions.

As a basic transmission line we used an updated quasi-optical Gubo line as the shielded Gauss beamguide in a metal pipe with periodical phase correctors. It was shown, that properties of such transmission line under specific conditions do not much differ from the well-known Gubo line. At the some time, this line has all advantages of shielded waveguides which is especially important for radiometer shielding.



Figure

The horn-parabolic antenna 1 (see Figure) with periscopical plane reflector 2 for a wide-angle scanning was used. Three linear step motors are arranged on periphery of the reflector for reduction of mechanical moments at scanning, and the center of reflector is fixed by a support. Rods of linear motors are controlled by on-board computer. Such construction provides an orientation of the reflector in any given direction with small mechanical moments and the reversal beam scanning over an arc with a sector angle 52^0 and length 85^0. In extreme positions of the scanning sector the antenna beam is directed to apertures 3, 4 of "hot" and "cold" reference loads 5, 6 with the reflector for a calibration of the radiometer.

Loads are broadband devices based on waveguide with cross-section of $36\times15\ mm^2$, which is dominant-mode for the range f_5= 6,6 GHz and oversized for more high frequency ranges f_1= 90,0 GHz; f_2= 36,5 GHz; f_3= 18,7 GHz; f_4= 10,95 GHz. This systems provides a calibration with the greatest possible accuracy and minimum loss of a scanning time. For isolation of calibration channels during the operating scanning cycle, reference loads are disconnected from antennas with waveguide commutators 7, 8.

By virtue of the chosen scanning method, the polarization plane of the antenna is twicted, and because of the antenna feeder system contains a polarization compensator 9 as a rotating joint formed by a combination of plane and parabolic mirrors. The received signals compensaton is provided by the polarization twisting in accordance with an on-board computer synchronously with a beam scanning. Then signals enter a polarizing splitter 10 in a form of the one-dimensional small-period diffraction grating in the diagonal cross-section of the cross-shaped junction of beamguides. The similar device permits to divide signals with vertical and horizontal polarizations into two independent identical channels with the high polarization isolation (>50 dB).

Each polarization channel contains a frequency multiplexer formed by a combination of quasi-optical and waveguide filters for a separation of five frequency channels. The quasi-optical filters 11, 12 are Fabry-Perot resonators on the basis of double wire grating in the diagonal cross-section of the cross-shaped junction of beamguides. High gain-frequency slope of a similar device provides transmission of f_1 signal in the direct port and reflection of f_2, f_3, f_4, f_5 signals in side port. Step-by-step circuit of waveguide T-bridged filters 13, 14, 15 (16, 17, 18) are used for a separation of f_2, f_3, f_4, f_5 frequency channels.

The radiometer broadband quasi-optical scanning antenna system is located horizontally along a aircraft axis and the plane reflector reradiates the antenna beam in a direction of the Earth (incidence angle is 52° with respect to normal) through a hatch in the fuselage. The horizontal arrangement of the antenna and screening of a parabolic reflector provide an essential reduction of the background clutter.

Thus, considered antenna system provides:

- small mechanical moments while antenna is scanning;
- "cold" and "hot" radiometer calibration;
- reduction of the background clutter and level of the antenna distant side radiation.

The main characteristics of the antenna system are shown in the table.

Table

No	Characteristics	Range Medium Frequency				
		f_1	f_2	f_3	f_4	f_5
1	Total Losses of Antenna-Feeder System, dB	-0,56	-0,73	-1,30	-1,30	-1,30
2	Gain of Antenna, dB	55,5	47,7	41,9	37,2	32,7
3	Aperture Boundary Power Level, dB	-9,9	-9,8	-9,5	-8,8	-7,3
4	Half-Power Beamwidth, Angle Degree	0,33	0,81	1,57	2,70	4,46
5	10 dB-Power Beamwidth, Angle Degree	0,56	1,38	2,70	4,60	7,44

The offered airborne radiometer broadband quasi-optical antenna system allows to carry out microwave radiometry in a wide frequency range and to increase an accuracy of measurements using internal calibration and dynamic correction of polarization characteristics of the scanning system.

EXCITATION OF THE WHISPERING-GALLERY-MODES AT THE SHIELDED HEMISPHERICAL DIELECTRIC RESONATOR

S.N.Kharkovsky, V.V.Kutuzov, A.E.Kogut, V.A.Solodovnik
Usikov Institute of Radiophysics and Electronics National Academy of Sciences of Ukraine
12 Ac. Proscura Str., Kharkov, 310085, Ukraine
Tel. (0572) 448-593, Fax (0572) 441-105, E-mail : ire@ire. kharkov.ua

Dielectric resonators (DR) with whispering gallery modes (WGM's) are used at the wide range of frequencies (from microwave to optical). These modes are formed by the grazing traveling waves in quasioptical DR (D > $10\lambda_d$, where D is diameter of resonator) inside dielectric with small incidence angles, their reflection factor being close to 1. WGM's electromagnrtic fieldes are localized between the external and inner caustics. Near this region the electromagnetic fields are evanescent. Therefore these modes have a high value of Q-factor. Variouse advanteges of the DR with WGM's suggest their utilization in the microwave and millimeter wave devices such as the filters [1], power combiners [2], solid-state oscillators [3], sensors for study of various materials [4].

One of the most important limits of the DR using is the problem of their coupling with other elements and circuits because of the open nature of these resonators and parasitic wave radiation. The open nature of the DR with WGM's leads to the system sensitiveness to the external medium and elements. It can display in non-control modification frequency and Q-factor value of the WGM's and influence at other circuits. One of this problem solution is the shielding of the DR [5,6].

The problem of the open DR (ODR) compatitibility with other circuits may be solved by the design way in the case of the absorber screen using. Absorbing screen worsens of the shielded dielectric resonator (SDR) characteristics (size, mass, Q-factor value) in comparison with the ODR.

The perspective of the SDR construction with the coaxial situated cylindrical DR and with reflective screen is represented in the famous theoretical papers [5,6]. The high Q-factor modes determined by the occurence of the localization of their fields in dielectric exist in this system. The investigations find the problem of the excitation of these modes in real condition, which are arised through the dense spectrum of the SDR modes and difficulty introduction of the couplers in the field of the WGM's. Besides it can note that the calculation of the characteristics of the own modes of the cylindrical resonators is possible by the approximation method.

In this paper we investigate the problem of the excitation high Q-factor WGM's of the hemispherical SDR the field of which is localizating in the dielectric and compared characteristics of the WGM's SDR with characteristics of the WGM's hemispherical ODR.

The excitation of the high Q-factor WGM's of SDR was investigating experimentally in resonator which is shown in Fig.1 (insect). Teflon dielectric hemiball 1 ($\varepsilon = 2.08$, radius R_d= 39 mm) and metallic hemisphere 2 (radius R_s= 42 mm) are situated on the local flat mirrors 3, 4 with coupling slot with the external waveguide. In the experimental model of SDR there was a possibility to easy change the position of the radiation source and passive slot on the radial coordinate. In this case it's a possible the effective coupling of the radiation source with the resonator field, the first; the cleaning of the modes spectrum, the second; measurement of the radial field distribution, the third. The WGM's $TM_{nml}(E_r \neq 0)$ or $TE_{nml}(E_r = 0)$ (n,m,l are field variations along the polar, azimuthal and radial coordinaters accordingly) are excited in the investigated resonator.

The characteristics measurements of the lowest (l=1, m=1) WGM's are carried out by the sweep generator in the frequency range 27-37 GHz. The highest WGM's are suppresed by the methods which are described in papers [3,7]. The coupling values are installed on the frequency characteristic of the VSWR (voltage standing wave ratio) and are controlled by the smaller absorber body method. The values of the own Q-factor are determined by the full resistance method [8].

The frequency dependences of the VSWR in the channel with the investigated resonators are obtained for the coupling slots with the different width by direct measurements. The dependence of the relative amplitude A/A_m of resonance from the standardized radial coordinate of the passive slot center to the dielectric hemiball radius r_o / R_d for the TM WGM's of the ODR (circuits) and SDR (points) is shown at Fig. 1. As can be seen the modes fields of these resonators are concentrated in dielectric between the caustics of WGM's of ODR. The frequency dependence of unloaded Q-factor TM WGM's of the ODR (circuits) and SDR (points) is shown at Fig. 2. The monotonous decreasing of Q-factor of the hemispherical ODR,when the frequency is decreased, is connected with the own radiative losses increasing. The Q-factor of the ODR WGM's at the high frequency

border is approximated to the level which is closed by the dielectric Q-factor (in this case dielectric Q-factor is equal 5.6×10^3). The unloaded Q-factor of the WGM's of the hemispherical SDR is approximetly constant in the investigated frequency range and it is determined only dielectric losses.

Thus, the WGM's are excited effectively at the hemispherical SDR through the coupling slot. Their fields are localized inside dielectric. Therefore unloaded Q-factor of the WGM's of SDR is determined only by the dielectric losses in the wide frequency range. However the unloaded Q-factor of the ODR modes with the frequency decreasing is decreased because of the radiative losses increasing. It allows to reduce the sizes of dielectric at SDR with comparison ODR with constant Q-factor.

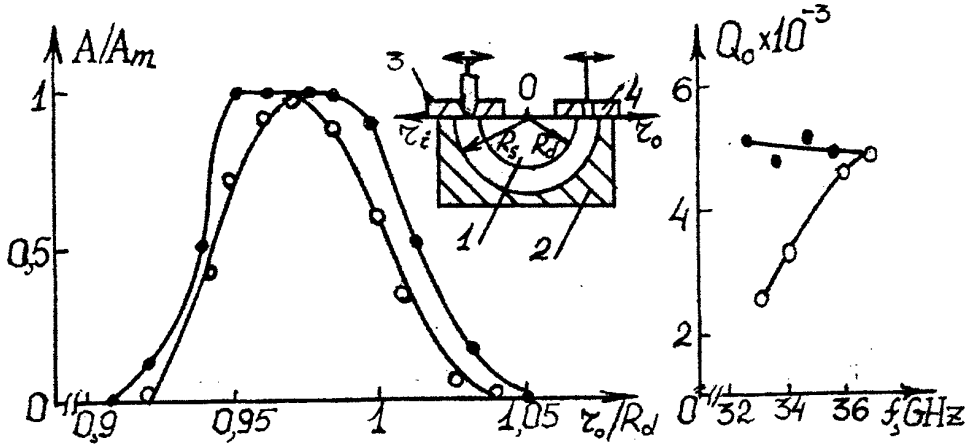


Fig.1. The dependence of the relative amplitude A/A_m of resonance from the standardized radial coordinate of the passive slot center to the dielectric hemiball radius r_o / R_d for the TM WGM's of ODR (circuits) and SDR (points).

Fig.2.The frequency dependence of unloaded Q-factor for TM WGM's of ODR (circuits) and SDR (points).

References

1. D.Gros, P.Guillon, "Whispering gallery dielectric resonators modes", IEEE Trans. Microwave Theory Tech., Vol.38, No.11, pp. 1667-1673, 1990.
2. X.H.Jiao, P.Guillon, Ph. Auxemery, Cros, "Dielectric resonators suitable for use in planar intergrated circuits at short millimeter wavelengths", IEEE Trans. Microwave Theory Tech., Vol.37, No.2, pp. 432-437, 1989.
3. S.N.Kharkovsky, A.Ja.Kirichenko, A.E.Kogut, "Solid-state oscillators with whispering-gallery mode dielectric resonators", Microwave and Optical Techn. Letters, Vol. 12, No.4, pp. 210-213, 1996.
4. V.B.Braginsky, V.S.Ilchenko, K.S.Bagdasarov, "Experimental observation of fundamental microwave absorption in high-quality dielectric crystals", Physics Letters A, Vol.120, No.6, pp. 300-305, 1987.
5. V.F.Vzyatyshev, V.I.Kalinichev, V.I.Kuimov, "Physical phenomena in shielded dielectric rod resonator and problem of its design", Radio Engineering and Electronics Physics, Vol.30, No.4, pp. 705-712, 1985. 6. E.N.Ivanov, D.G.Blair, V.I.Kalinichev, "Approximate approach to the design of shielded dielectric disk resonators with whispering galleru modes", IEEE Trans. Microwave Theory Tech., Vol.41, No.4, pp. 632-637, 1993.
7. A.E.Kogut, V.V.Kutuzov, Yu.F.Filipov, S.N.Kharkovsky, "Whispering-gallery modes of the quasioptical hemisphere dielectrical resonator" (in Russian), Izv. Vuz. Radioelectronika, Vol.40, No.2, pp. 19-26, 1997.
8. E.L.Ginzton, "Microwave measurements" (in Russian), In. Lit., Moscow, pp. 620, 1960.

OPEN RADIATING SYSTEMS FOR MICROWAVES AND MILLIMETER WAVES

V.K. Korneenkov, V.I. Lutsenko, V.S. Miroshnichenko, V.I. Uzlenkov
Institute of Radiophysics and Electronics, Ukrainian Academy of Science
Address: 12, Akad. Proskury Street, Kharkov, 310085, Ukraine
Tel. (0572) 44-84-22, Fax (0572) 44-11-05, E-mail homenko@ire.kharkov.ua

The open resonant radiating systems [1] have a number of advantages on a comparison with the closed systems, namely: they have a rarefied spectrum, high Q-factor, and also provide natural radiation of a part of power generated by crystal diodes in surrounded space without conventional losses in waveguides and matching devices of source of oscillation and antenna. The use of multifunctional modules based on open radiating systems allows to reduce number of a necessary microwave elements and units, to increase their technical and operating performances. Especially it concerns devices of broad application, such as systems of communication and notification, security systems, and systems of warning of collisions of a vehicles.

In this report the planar open radiating system consisting from two segments of parabolic reflectors, joined by planar dielectric waveguide with a metal substrate, is considered. A periodic structure of metal tapes is located on opposite side of the planar dielectric waveguide. Two crystal diodes are located in focal points of reflectors (see Figure 1). Such open radiating system provides an excitation of crystal diodes, control of oscillation frequency, formation of the pencil-beam diagram of radiation, reception and transformation of reflected signals in one device having acceptable mass, dimensions and electrical parameters. The formation of the required diagram of radiation is provided by diffraction of a wave E_1 of the planar dielectric waveguide on a periodic structure with accordingly selected dimensions of elements and aperture. At one-frequency mode of operation of an open radiating system the receiving and transmitting of signals are performed in normal direction to a surface of a periodic structure, however the device has potential capabilities to form multi-beam diagram of radiation, and to operate on two independent frequencies.

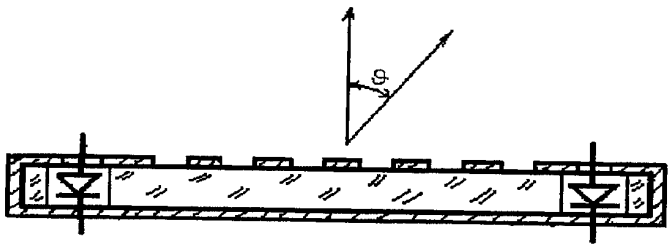


Figure 1. A planar open radiating system.

Experimental model of a planar open radiating system in 8-mm waveband has the following geometry: size of the radiating aperture - 100×50 mm^2; period of the structure - 7,5 mm; width of slots of the structure - 2,5 mm; total number of periods of the structure - 12; aperture of parabolic reflectors - 50×2 mm^2; focal length of reflectors - 12 mm. As crystal diodes located in focal points of reflectors, the active diodes AA718 are used. The diagram of radiation of an experimental model with one diode in horizontal plane has three beams with intensity, accordingly: -10 dB, 0 dB, -6 dB. The beam width is $\Delta\theta_x = 8{,}5^\circ$ (see Figure 2), the electrical tuning of frequency of experimental model - 175 MHz/V, the width of spectral line of radiation - 50 kHz.

The effective conversion of energy of a wave E_1 of the planar dielectric waveguide to radiating waves happens on a section from 1-st to 7-th slot of a structure. That was determined, when we have closed by absorber the radiating slots of planar open radiating system.

The diagram of radiation of the planar open radiating system in vertical plane (in parallel plane to slots of a structure) - has one beam, however there is a fall in radiation at an angle $\theta_y = 10^\circ$ (see Figure 3).

At combined (transmitter - receiver) mode of operation it is possible to transform the frequency of receiving signals at replacement one of the crystal diodes on mixed diode. The displacement of diode from focal point of reflector allows to obtain optimum conditions for transformation of a frequency of receiving signals.

The considered planar open radiating system is perspective for use in near-distance radar, in particular, in systems of warning of collisions of a vehicles [2].

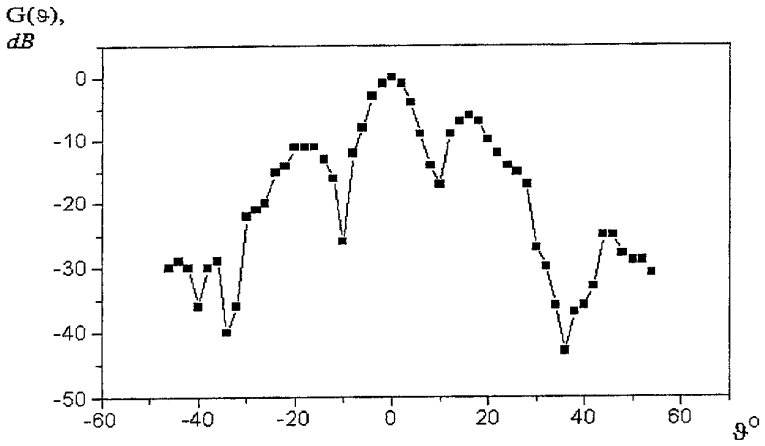


Figure 2. The radiation pattern of the planar open radiating system in horizontal plane

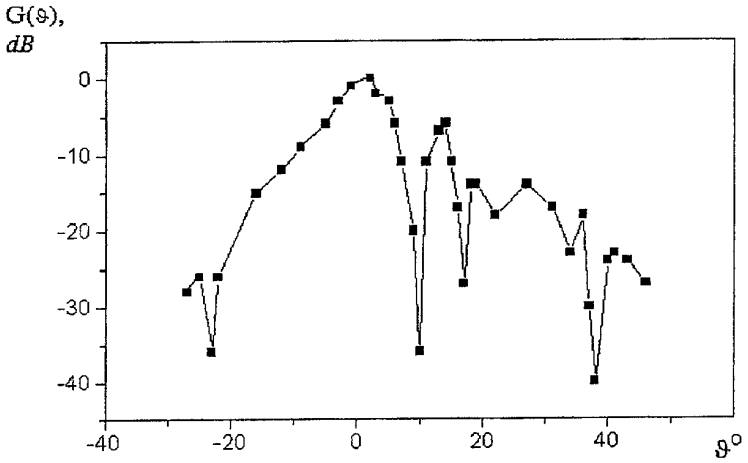


Figure 3. The radiation pattern of the planar open radiating system in vertical plane.

The small-size omnidirectional radiating modules for microwaves and millimeter waves are of interest for security systems, an environment space monitoring , fire safety. An example of such device is developed by us the omnidirectional active antenna (see Figure 4). This active antenna consists from two coaxial ring-type dielectric resonators separated and limited at their ends by means of conductive disks; inside each resonator on the axis is located the crystal diode, that joined with conductive disks. The coupling elements are made as counter slants of external surfaces of resonators. The narrowing of beam of radiation in vertical plane is achieved, when the conductive disks as truncated biconical cylinders are used, and the additional annular lens is installed in an aperture, that corrects a phase of radiating wave.

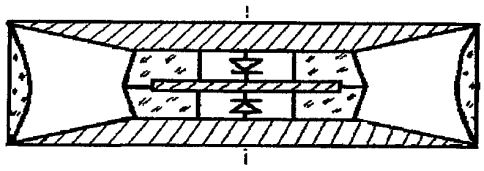


Figure 4. The omnidirectional active antenna.

The experimental models of the active antenna were developed for 8-mm wavelength. As a source of oscillations the Gunn diodes of a type 3A728Г were used, and for transformation of signals were used mixed diodes of a type 3A121A. The parameters of the experimental model of the active antenna are: the external diameter of the biconical aperture - Ø78 mm, the inner diameter of the aperture is the same that external diameter of a dielectric resonator - Ø30,5 mm, altitude of the external aperture - 23,5мм. The inner diameter of a dielectric resonator is Ø12,5 mm, material of the dielectric resonators - teflon. On frequency 40,1 GHz the all radiated power of the active antenna was about 25 mW, and the beam width in vertical plane didn't exceed $\Delta\theta = 15^{\circ}$ (see Figure 5).

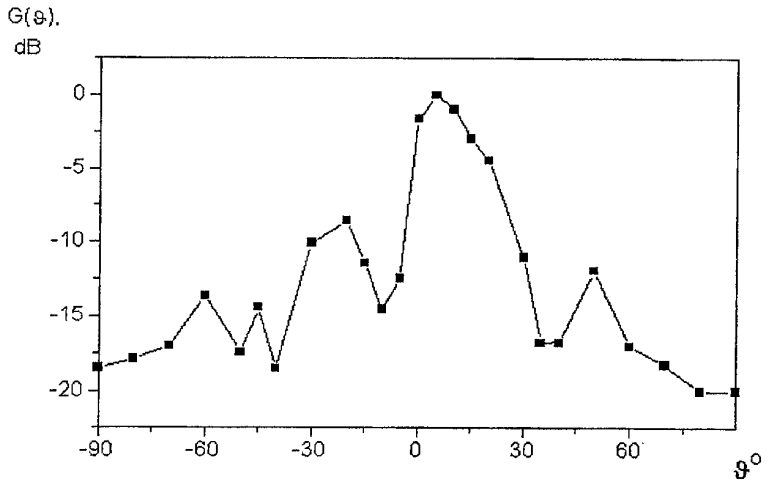


Figure 5. The radiation pattern of the active antenna in vertical plane.

The formation of the uniform diagram of radiation in horizontal plane is provided with a circular symmetry of the active antenna relatively to vertical axis. If necessary the extension of the beam width in vertical plane and the reduction of a «dead» zone near to a vertical axis may be achieved, when the external surfaces of ring-type dielectric resonators are made as a hyperbolic cylinder, that allows to construct a ring-type dispersing lens in an aperture of antenna.

It is necessary to mark, that in the considered active antenna there is a capability of further increase of radiated power, when additional ring-type dielectric resonators with crystal diodes are arranged on main vertical axis.

References

1. V.K.Korneenkov, V.I.Lutsenko, V.S.Miroshnichenko, "Principles of construction of the open radiating systems for millimeter waveband". Proceedings of the 7-th Int. Crimea Microwave Symposium, 15-18 September, 1997, Sevastopol, Crimea, Ukraine, V.2, pp.498-501, 1997.
2. P.L Lowbridge, "Low Cost Millimeter Wave Radar System for Intelligent Vehicle Cruise Control Applications " Microwave J., No.10, pp. 20-48, 1995.

THE MAIN TYPE OF OSCILLATIONS IN WAVEGUIDE BRANCHING OF THREE ORTHOGONAL BELOW CUTOFF WAVEGUIDES.

Yu. G. Makeev

Institute of Radiophysics and Electronics Ukrainian Academy of Science
12, Acad. Proskura st., Kharkov, 310085, the Ukraine, tel. (0572)-44-83-78, fax. (0572)-44-11-05,
e-mail ire@ire.kharkov.ua

At present time the branchings on the base of two below cutoff orthogonal waveguides are used for unbroken measurements of electrical parameters of dielectric and ferrite materials, ferroelectric films . They can be widely applied for creation of various filters, microwave generators and etc. in all parts of microwave range. The free oscillations in such structures are well studied for two-dimensional oscillations (number of electromagnetic field variations in one of structure directions is equal to zero). There are known the results of investigations of three-dimensional oscillations in the waveguide branchings, formed with two orthogonal rectangular waveguides. It was shown that in such structure the hybrid oscillation could exist. For case when waveguides, forming branching, are empty or they are filled with homogeneous and isotropic dielectric these oscillations turn into unconnected each with other H_{mng} and E_{mng} oscillations (where *m, n, g* is a number of field variations along coordinate axes of waveguide structure).

In present work the main type of oscillation of waveguide branching, forming with three orthogonal below cutoff rectangular waveguides, is considered. It was shown that this type belongs to class HE_{mng} oscillations. Calculation of obtained as a result of electrodynamic problem solving equations and experimental measurements showed that the most low-frequency oscillation in considered branching is HE_{110} oscillation, that for one-wave approximation can be considered as H_{110} oscillation.

Electrodynamic calculation of eigen frequencies of HE_{mng} oscillations (where *m, n* are odd numbers and *g* - even numbers) and, as private case, H_{110} oscillation was made on base of method of partial regions with following projection of obtained as a result of performance of boundary conditions expressions on eigen vector functions of waveguides, forming branching.

Investigating branching was divided into four partial regions: three regions were semi-infinite parts of waveguides with dimensions of cross-section of the fist waveguide *a x b*, the second - *b x c* and the third - *a x c*. The forth region was the region of waveguides crossing. The beginning of coordinate system was placed in the center of branching. Under solving of problem it was used the property of symmetry of system. It simplified the solving of problem very much. Calculation was made in assumption that losses of electromagnetic energy in the waveguide walls were equal to zero. Electromagnetic field in the waveguide parts was presented as a sum of electrical and magnetic types of waves that damped in the longitudinal direction. In region of branching field was written as a sum of fields of waveguides, formed the branching. For description of fields in all regions Hertz vectors were used. So electrical and magnetic Hertz vectors for the first region were written as:

$$\vec{\Pi}_1^e = \vec{z}_0 \sum_{n,g} A_{ng} \cos p_n y \cos p_g z \exp(-\gamma_{ng}(x - a/2))$$

$$\vec{\Pi}_1^h = \vec{z}_0 \sum_{n',g'} A_{n'g'}' \sin p_{n'} y \sin p_{g'} z \exp(-\gamma_{n'g'}'(x - a/2)), \quad \text{where} \tag{1}$$

$\vec{z}_0$ is the orth in direction of axis *z*; $A_{ng}, A_{n'g'}'$ are the amplitudes of electrical and magnetic types of waves;

$p_n = \frac{n\pi}{b}$; $p_g = \frac{g\pi}{c}$; $p_{n'} = \frac{n'\pi}{b}$; $p_{g'} = \frac{g'\pi}{c}$ are the diametrical wave numbers; *n*, n' are odd numbers; *g*, g' are even numbers; $\gamma_{ng} = (p_n^2 + p_g^2 - k^2)^{1/2}$, $\gamma_{n'g'}' = (p_{n'}^2 + p_{g'}^2 - k^2)^{1/2}$

are longitudinal wave numbers; $k = 2\pi / \lambda$; λ - resonance wavelength. For the second and the third regions Hertz vectors may be written as analogous to (1). In the region of branching electrical Hertz vector is:

$$\vec{\Pi}^{e}_{IV} = \vec{z}_0 \sum_{n,g} D_{ng} \cos p_n y \cos p_g z \frac{ch(\gamma_{ng} x)}{ch(\gamma_{ng} a/2)} + \vec{z}_0 \sum_{m,g} E_{mg} \cos p_m x \cos p_g z \frac{ch(\gamma_{mg} y)}{ch(\gamma_{mg} b/2)} -$$

$$- \vec{z}_0 \sum_{m,n} F_{mn} \cos p_m x \cos p_n y \frac{ch(\gamma_{mn} z)}{ch(\gamma_{mn} c/2)} , \quad \text{where} \qquad (2)$$

D_{ng}, E_{mg}, F_{mn} are the amplitudes of damped electrical types of wave along axes x, y, z, accordingly; $\gamma_{mg} = (p_m^2 + p_g^2 - k^2)^{1/2}$; $\gamma_{mn} = (p_m^2 + p_n^2 - k^2)^{1/2}$. Magnetic Hertz vector for this region may be written as analogous to (2).

Matching of tangent components of electrical and magnetic fields was made under all surface of regions. So the boundary condition for the first and the third regions was written as:

$$\vec{y}_0 E_y^I + \vec{z}_0 E_z^I = \vec{y}_0 E_y^{IV} + \vec{z}_0 E_z^{IV} \quad \mathrm{I}_{x=a/2};$$

$$\vec{y}_0 H_y^I + \vec{z}_0 H_z^I = \vec{y}_0 H_y^{IV} + \vec{z}_0 H_z^{IV} \quad \mathrm{I}_{x=a/2}.$$

The system of equations, obtained as a result of boundary conditions performance, was projected into eigen vector functions of electrical and magnetic types of waves of waveguides forming branching. For equations, obtained under boundary conditions performance on boundary of I, IV regions these functions may be written as:

for magnetic types of waves

$$\vec{y}_0 \cos p_n y \cos p_g z$$

for electrical types of waves

$$\vec{y}_0 p_n p_g \cos p_n y \cos p_g z + \vec{z}_0 (k^2 - p_g^2) \sin p_n y \sin p_g z.$$

Such, it was obtained the system of four linear algebraic equations of the second kind (SLAE-II) accordingly to $4mng$ unknown amplitudes of electromagnetic field of resonator. Eigen resonator frequencies were determined from condition of equality this system determinant to zero. In determinant elements in the same time parameters, that characterize electrical and magnetic types of waves, are contained, i.e. in common case oscillations in such resonator are hybrid. In case when $g = 0$ the system of equations disintegrates into two independent systems for H_{mn0} and E_{mn0} oscillations of resonator.

The main oscillation type of considering resonator is H_{110} oscillation. Equation, describing the behaviour of resonance frequency of H_{mn0} oscillation (and H_{110} in detail) for case when in each of waveguides, forming the branching, one damped wave exists, and in region of branching there is its sum, has next form:

$$[\frac{1}{16}\gamma_{ng}a\gamma_{mg}b(1+th\gamma_{ng}a/2)(1+th\gamma_{mg}b/2)-\frac{p_m^2}{p_m^2+\gamma_{ng}^2}\frac{p_n^2}{p_n^2+\gamma_{mg}^2}]x$$

$$x[\frac{1}{16}\gamma_{mg}b\pi^2(1+\frac{a^2}{b^2})(1+th\gamma_{mg}b/2)(1+cth\gamma_{mn}c/2)+\frac{p_n}{\gamma_{mn}}\frac{a}{c}\frac{p_mp_n-\gamma_{mg}^2}{p_n^2+\gamma_{mg}^2}]=$$

$$=[\frac{1}{4}\gamma_{mg}b(1+th\gamma_{mg}b/2)+\frac{p_n^2}{p_n^2+\gamma_{mg}^2}][\frac{1}{4}\gamma_{mg}b(1+th\gamma_{mg}b/2)(\gamma_{ng}^2-p_mp_n)+$$

$$+\frac{\gamma_{mg}^2-p_mp_n}{p_n^2+\gamma_{mg}^2}]\frac{a}{c}\frac{p_m}{\gamma_{mn}}\frac{1}{\gamma_{ng}^2+p_m^2} \qquad (3)$$

Analysis of this equation shows that under $c\to\infty$ it coincides with known expression, describing H_{mn0} oscillations in waveguide branching of two rectangular waveguides. Analogous result was obtained under analysis of complete system of equations.

We made calculation of equation (3). In Fig.1 the curves of dependence of normalized resonance wavelength of H_{110} oscillation (λ/λ_{cr}) upon value *a/c* for three values *a/b* are shown. The upper curve corresponds to *a/b* = 1; the middle curve - *a/b* = 1.5; lower curve - *a/b* = 2. As a critical wavelength we chose wavelength $\lambda_{cr}=2a$.

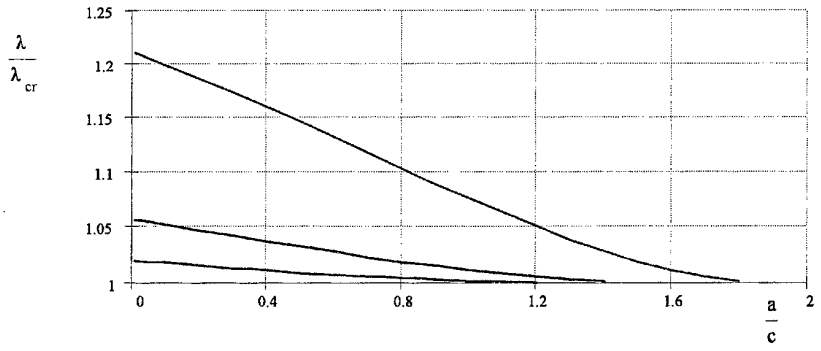


Fig. 1. Dependence of resonance wavelength of H_{110} oscillation upon geometrical dimensions of branching

Table 1. The change of λ/λ_{cr} upon *m (n)* under $g = 0$ when $a = b = c$.

m(n)	1	5	11	21	31	41	51
λ/λ_{cr}	1.07621	1.07065	1.06963	1.06981	1.06973	1.06976	1.06974

Difference of experimentally measuring value of resonance wavelength and calculating value under one-wave approximation was ~ 6.0%.

Thus on the base of method of modes matching on the surface and application of projecting method to obtained equations the problem about free oscillations of six -shoulders waveguide branching was solved. It was shown that the main type of oscillation in this branching was hybrid. Experimental investigation of this type of oscillation was carried out. The complete calculation for such oscillation was made, too.

CHARACTORS OF WAVEGUIDE-DIELECTRIC RESONATOR

Yu.G. Makeev, A.P. Motornenko

Institute of Radiophysics and Electronics of National Academy of Science of Ukraine
12, Acad. Proskura st. Kharkov, 310085, the Ukraine
tel.:(0572) 448-378, fax:(0572) 441-105, e-mail ire@ire.kharkov.ua

In present time a waveguide-dielectric resonators (WDR) are widely used for creating of active and passive packs and devices at the microwave band [1-2]. On the basis of the WDR measurement methods of electrical parameters of the dielectric and ferrite materials have been developed [3-4].

The classic construction of the WDR represents a piece of a rectangular or circular waveguide filled with a dielectric element (DE). The most common dielectric full fill the cross-section of the waveguide. To diminution the sizes and weights the pieces of evanescent waveguides are used. On addition of a metal short-circuit plunger to the construction the WDR functional possibilities of it are augmented. Using those WDR the compact and stable semiconductor generators of the SHF- and UHF-band were worked [5]. Notice that the WDR with a short-circuit plunger can form the basis for a measuring a frequency dependence of a permittivity and a loss dielectric tangent angle of various materials as well as surface resistance the films of a metal and a semiconductor.

Today the WDR electric characteristics on the rectangular waveguide with the DE partially filling the cross-section of a waveguide have been studied adequately [6].

In this paper the generalised results of an investigation for the WDR with the DE of the thickness h mounted inside the cylindrical evanescent waveguide with a radius a and a short-circuit plunger placed at the arbitrary distance L from the DE are presented. On the other hand of the DE the waveguide was infinite. The electromagnetic energy losses in metal parts of the resonator and in the DE volume have been neglected

The electrodynamic problem was solved with partial regions method. The resonance structure was divided into three regions: I region is a piece of a hollow waveguide up to the DE; II region is a part of a waveguide with the DE and III region is a piece of a hollow waveguide with the short-circuit plunger. Case was considered for which the sections of a hollow waveguide were below cut-off for the resonance type of oscillation and in the waveguide section filled with dielectric the resonating wave propagated.

The electromagnetic fields in all regions were represented as a sum of all types of waves in the considered structure. The fulfilment of the boundary condition led to a system of functional equations which was transformed with projection method. As a projection basis eigen vector functions of a hollow waveguide were chosen.

The equation describing resonance frequency behaviour of the $H_{mn\delta}$-oscillation type in considered structure has following form:

$$\frac{\Gamma_{mn}}{\gamma_{mn}}\left[1+th(\gamma_{mn}L)\right]-\left[\frac{\Gamma_{mn}^2}{\gamma_{mn}^2}th(\Gamma_{mn}L)-1\right]tg(\Gamma_{mn}h)=0, \qquad (1)$$

where $\Gamma_{mn}=\sqrt{k^2\varepsilon-\left(\frac{\nu_{mn}}{a}\right)^2}$; $\gamma_{mn}=\sqrt{\left(\frac{\nu_{mn}}{a}\right)^2-k^2}$; $k=2\pi/\lambda$; λ is resonance wavelength, ν_{mn} are roots of the equations $J'_{mn}(\nu_{mn})=0$; J'_{mn} are derivative of Bessel function of the first kind for the m-th order; ε is permittivity of DE.

It is easy to verify that with removal the short-circuit plunger from the DE dispersion equation (1) is converted to known expression [1-3]

$$\frac{\Gamma_{mn}}{\gamma_{mn}}=\begin{cases} tg\dfrac{\Gamma_{mn}h}{2} \\ -ctg\dfrac{\Gamma_{mn}h}{2} \end{cases} \qquad (2)$$

As seen from (2) even and odd oscillations exist independently of one another. The availability of the short-circuit plunger leads to coupling of the oscillations. The equation for the $E_{mn\delta}$-oscillations type can be obtained analogously.

Q-factor of investigated resonance structure for the $H_{mn\delta}$-oscillation types was calculated as a ratio between the story energy in the resonator and the power of total losses in all partial regions [1,2].

$$Q = \frac{\varpi W_\Sigma}{P_\Sigma},$$

(3)

where ϖ is circular frequency.

The total story energy in the WDR for the $H_{0n\delta}$-oscillation is obtained as

$$W_\Sigma = A_{0n}^2 \frac{\pi\varepsilon_0}{4}(\nu_{0n}a)^2\zeta_{0n}\{\frac{1}{2\gamma_{0n}}(K_{0n}\cos\alpha_{0n} - K1_{0n}\sin\alpha_{0n})^2 +$$

$$+\frac{\varepsilon}{2\gamma_{0n}}[K_{0n}^2(2\alpha_{0n} + \sin 2\alpha_{0n}) + K1_{on}^2(2\alpha_{0n} - \sin 2\alpha_{0n})] + \quad (4)$$

$$+\frac{1}{4\gamma_{0n}}\frac{\Gamma_{0n}^2}{\gamma_{0n}^2}\frac{1}{ch^2(\gamma_{0n}L)}(K_{0n}\sin\alpha_{0n} - K1_{0n}\cos\alpha_{0n})^2(sh2\gamma_{on}L - 2\gamma_{0n}L)\},$$

where $\alpha_{0n} = \Gamma_{0n}h/2$; $K_{0n} = \sin\alpha_{0n} + \frac{\Gamma_{0n}}{\gamma_{0n}}\cos\alpha_{0n}$; $K1_{0n} = \cos\alpha_{0n} - \frac{\Gamma_{0n}}{\gamma_{0n}}\sin\alpha_{0n}$;

$\zeta_{0n} = J_0^2(\nu_{0n}a)$.

The power of the losses consists of the losses power in the metal walls of the partial regions and the losses power in the dielectric.

The expression for the losses power of the $H_{0n\delta}$-oscillation type is written in the form

$$P_\Sigma = P_1 + P_2 + P_3 + P_d, \quad (5)$$

where

$$P_1 = A_{0n}^2\xi_{0n}\frac{a}{\gamma_{0n}}\nu_{0n}^4(K_{0n}\cos\alpha_{0n} - K1_{0n}\sin\alpha_{0n})^2;$$

$$P_2 = A_{0n}^2\xi_{0n}\frac{1}{\Gamma_{0n}}\nu_{0n}^4[K_{0n}^2(2\alpha_{0n} + \sin 2\alpha_{0n}) + K1_{0n}^2(2\alpha_{0n} - \sin 2\alpha_{0n})];$$

$$P_3 = A_{0n}^2\xi_{0n}\frac{1}{ch^2\gamma_{0n}L}(K_{0n}\sin\alpha_{0n} - K1_{0n}\cos\alpha_{0n})^2\left[\frac{\nu_{01}^4}{\gamma_{01}}(sh2\gamma_{0n}L - 2\gamma_{0n}L) + 2\frac{R_1}{R}\frac{\gamma_{0n}^2}{a}\nu_{0n}^2\right]$$

;

$$P_d = A_{0n}^2\frac{\pi\omega\varepsilon\varepsilon_0}{8}tg\delta(\nu_{0n}a)^2\xi_{0n}\frac{1}{\Gamma_{0n}}[K_{0n}^2(2\alpha_{0n} + \sin 2\alpha_{0n}) + K1_{0n}^2(2\alpha_{0n} - \sin 2\alpha_{0n})];$$

$$\xi_{0n} = \frac{\pi R}{(2\omega\mu_0)^2 K1_{0n}^2}J_0^2(\nu_{0n}a);\ R = \sqrt{\pi f\mu_0/\sigma_1};\ R_1 = \sqrt{\pi f\mu_0/\sigma_2};\ \text{f is resonance}$$

frequency; σ_1 is conductivity of waveguide walls material; σ_2 is conductivity plunger material.

Under analysis of the Q-factor value of the WDR the total Q-factor was represented as sum s of the partial Q-factors [1,2]:

$$Q_\Sigma = \left(\frac{1}{Q_1} + \frac{1}{Q_2} + \frac{1}{Q_3} + \frac{1}{Q_d}\right)^{-1} \quad (6)$$

The numerical calculation of the electrical characteristics of the WDR was made for the lowest frequency oscillations $H_{01\delta}$ and $H_{11\delta}$. The Q-factor was calculated for the resonator, made from copper (conductivity $\sigma_1 = \sigma_2$ = 5.8 $x10^7$cm/m), and dielectric element of this resonator, made from phtoroplast (ε=2..08,

$tg\delta = 10^{-4}$). The experimental investigations of electrical characteristics were made with the two model of the WDR:

–in the SHF-band (a=6.5 mm; h=4 mm, 8.7 mm, 20 mm);

–in the UHF-band (a=2.3 mm; h=1.44 mm, 4 mm, 8 mm).

The dependencies of the resonance frequency, partial and eigen Q-factors of the WDR under changes of the distance between the DE and the short-circuit plunger for the several thickness of the DE were obtained. Dependencies of electrical parameters of WDR from thickness of the DE for two short-circuit plunger positions (L= 0; L = ∞) were analysed.

The changing of the eigen Q-factor the WDR for the various loss dielectric tangent angle and the surface resistance of the waveguide was analysed, too. An investigation of a distribution of the electromagnetic field in the WDR from parameters h and L for chosen oscillations type with the computer simulation was made.

One of important WDR characteristics is number of electromagnetic field variations along longitudinal axis. Every field variation accords to eigen WDR oscillation. These oscillations differs each from other with index δ values. Results of equation (1) solution for several values of ε, h under constant waveguide radius and distance from short-circuit plunger to DE (a =L = 2.3 mm) for $H_{11\delta}$ oscillation are presented in Table 1.

Table 1. Resonance frequencies values of $H_{11\delta}$ oscillation.

ε	h (mm)	f (GHz)
2,0	1,5	35,596
	4,0	30,825
	8,0	28,628; 33,1
5,0	1,5	25,055
	4,0	19,995; 28,075
	8,0	18,226; 21,438; 26,246; 32,091
10,0	1,5	18,252; 36,693
	4,0	14,232; 20,258; 28,803
	8,0	12,909; 15,243; 18,742; 23,023; 27,788; 32,835
25,0	1,5	11,738; 24,543; 31,689
	4,0	9,033; 12,946; 18,52; 24,917
	8,0	8,172; 9,669; 11,914; 14,661; 17,723; 20,98; 27,821;31,334; 34,878
50,0	1,5	8,344; 17,598; 29,915
	4,0	6,395; 9,184; 13,158; 17,723; 22,568; 27,555; 32,616; 37,69
	8,0	5,78; 6,843; 8,438; 10,388; 12,563; 14,876; 17,277; 19,737; 22,237; 24,765; 27,313; 29,875;32,448; 35,027; 37,604

This table shows that WDR with dielectric with small values ε and small thickness h has the most thin spectrum of oscillations.

Obtained results are used for creation of microwave generators, filters, measuring sections on WDR basis. They give possibility to choose the best construction of microwave devices.

References.

1. M.E. Ilchenko, V.F. Vzyatyshev, e.c., Dielectric resonators, Radio and Communication ,Moscow, pp.328, 1989.
2. B.F. Kapilevich, E.P Trubekhin, Waveguide-dielectric filtering structures, Radio and Communication, Moscow, pp.272, 1990.
3. T.I. Vasil'eva, A.A Kirilenko, E.A. Sverdlenko, Determination of dielectric parameters after resonance at lock modes, Izvestiya VUZov "Radiophysics", vol.32, N9, pp.1181–1184, 1989.
4. Yu.G. Makeev, V.A. Korobkin, Resonance method of determination of magnetodielectrics parameters in the cylindrical waveguide, Instruments and Experimental Techniques, N1, pp.139–141, 1978.
5. Yu.G. Makeev, A.P Motornenko, A.A Zorkin, Semiconductor microwave generator on basis of waveguide-dielectric resonator, Instruments and Experimental Techniques, N6, pp.86–89, 1995.
6. A.G. Yuschenko, Field presentation and calculation of resonance frequencies of partially filled with dielectric the waveguide resonators, Radiotekhnika and Electronika, N4, pp.870–873, 1989.



MM AND SUBMM WAVE SPECTROSCOPY

Preceding Page Blank

WIDE-RANGE MILLIMETER-WAVE SPECTROMETER FOR HIGH-RESOLUTION INVESTIGATION OF MOLECULAR ROTATIONAL SPECTRA

E.A.Alekseev, V.V.Ilyushin, S.F.Dyubko
Institute of Radio Astronomy of the Ukrainian Academy of Sciences
4 Chervonoprapornaya St., 310002 Kharkov, UKRAINE
Tel. +380 (572) 448 449, Fax. +380 (572) 476 506, e-mail nns@rian.kharkov.ua

This paper contains the brief description of the essential improvement of the automated millimeter-wave spectrometer previously described in [1]. This spectrometer is built according to so-called "classic scheme", i.e. radiation from a scanning source passes through an absorbing cell containing investigated gas inside, and then is received by a receiving system. A computer-controlled millimeter-wave frequency synthesizer is used as the scanning radiation source. The spectrometer was intended for high-resolution detail spectral investigations only [2,3]. However for initial studies of molecular rotational spectra it is necessary to record very wide frequency ranges. For this purpose we have undertaken modernization of the spectrometer hardware and software. The results of such modernization are presented below.

The frequency synthesis in the millimeter range is achieved by means of two-step frequency multiplication of the commercial reference frequency-synthesizer output (390-400 MHz) in two phase-locked loops. At the final multiplication step, the millimeter wave BWO is used, whereas the 3.4-5.2 GHz klystron oscillator is used at the first multiplication step. That is why previously continuous locked-in frequency range of the spectrometer was limited by the klystron voltage mode and was about a few MHz. Any additional realization was recorded after manual adjustment. In order to expand automatically recorded locked-in frequency range without any manual adjustment we equipped the spectrometer with special servosystem that provided mechanical adjustment of the klystron resonator. This servosystem includes servomotor and remote control system. After preliminary calibration it becomes possible to provide the wide-range continuous locked-in operation of the klystron oscillator. This gave possibility to realize the multimode operation of the spectrometer. At present there are three main modes. The first of them is the detail mode. The second one is the data collection mode, and the third one is the survey mode.

The detail mode is intended for the most common investigations. Records of molecular spectra are obtained with measurements of power variations on the output of the absorbing cell when the frequency on its input is changed point-by-point in the recorded range. Time interval between neighbour points is 200 ms. In order to eliminate background power level the output of the synthesizer is FM-modulated, and phase-lock detector is applied in the receiving system. That is why spectral lines are recorded as the first frequency derivatives from lineshapes. Intensities of absorption lines may be estimated with a full power channel.

The data collection mode is realized as a variant of detail mode and is used to record the most weak spectral lines that are usually observed with bad signal-to-noise ratio. In order to improve signal-to-noise ratio the fragment of spectrum is recorded with a number of passes. The results of all passes are averaged.

For both detail and data collection modes transition frequencies are determined by means of the least-squares approximation of experimental records of spectral lines with the Gauss, Lorentz or Voigt lineshape. The type of lineshape is chosen in accordance with experimental conditions. Approximation with Gauss lineshape is mainly used for high precision measurements of transition frequencies whereas Lorentz and Voigt lineshapes are used during the investigation of the pressure broadening of spectral lines. In the case of close neighbourhood of several spectral lines we approximated recorded multiplet with the sum of lineshapes of chosen type. The line frequencies and intensities of components varied independently whereas the width of components was the same.

The survey mode is intended for quick record of rotation spectra of molecules in the full frequency range of the spectrometer. After essential hardware improvement this mode was realized fully by software. The time interval between neighbour points is reduced to 40 ms. Line positions from the survey records are determined as follows. At first, in order to exclude slow background variations and high frequency noise a digital bandpass filter is used. Then scanning a frequency of a simulated lineshape sample over the realization we obtain cross-correlation function for a given record. As a simulated lineshape sample we use Gaussian with calculated Doppler linewidth. Then the standard deviation σ is calculated for record processed in this way, and all peaks that exceed 3σ are considered as absorption lines. The accuracy of frequency determination for an isolated line was not worse then a frequency step of experimental record. Naturally survey records are obtained with worse signal-to-noise ratio in comparison with other spectrometer modes, that is why the most weak lines in

this case are ignored. However the signal-to-noise ratio is still sufficient for initial study because it gives possibility to reveal the most important parts of spectra that have to be recorded using the detail mode or the data collection mode. The main attractive feature of the survey mode is a possibility of a quick obtaining of data for initial study of the investigated spectrum and of general obvious picture of the spectrum. Figure 1. presents an illustration of survey and detail mode of the spectrometer.

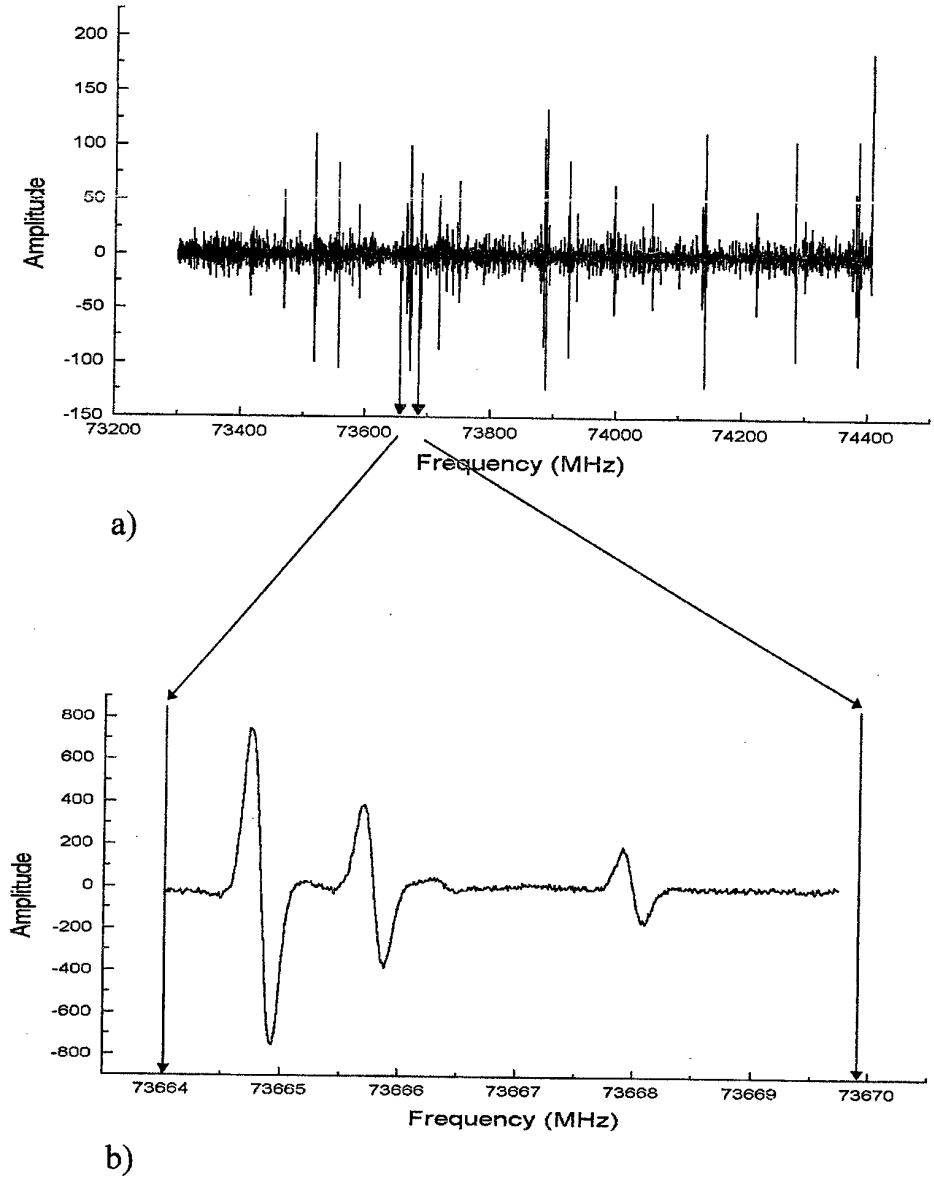


Fig.1 A fragment of survey record of acetic acid spectrum (a) and a part of the same spectrum recorded using detail mode (b). The same part of the spectrum is marked by the arrows on both records.

Using survey mode of the spectrometer we have investigated spectra of following molecules CH_3COOH [4], $CHClF_2$, CF_2Cl_2, CF_3CFH_2. For CF_3CFH_2 availability of survey records gave an opportunity to make the initial assignment of rotational spectra for three vibrational modes never investigated before.

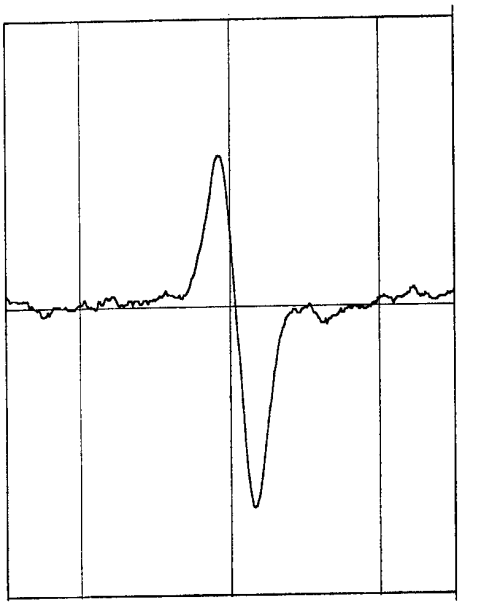


Fig.2. Record of J=3←2 transition of $^{14}N^{15}N^{16}O$ in the 02/0/0 vibrational state with 4.36×10^{-7} cm^{-1} absorbtion coefficient.

Main features of the spectrometer described above are following. The frequency range is 30-143 GHz and it is overlapped with series of BWOs (36-52, 52-78, 78-118, 118-143 GHz). Using frequency doubler we have possibility to expand frequency range up to 160 GHz. Maximum spectral resolution is limited by Doppler broadening of spectral lines and it is of about 50-200 kHz in dependence of molecule mass and frequency range. Sub-Doppler spectral resolution is achieved with the Lamb-dip observation. Observed Lamb-dip width is of about 10-20 kHz. In order to determine an accuracy of measurements of transition frequencies we have record the hyperfine structure of J=0←1 transition of HCN molecule that was previously measured in a molecular-beam maser with accuracy not worse than 1 kHz [5]. Our measurements have shown very good agreement with [5] and results of such comparison are presented in Table 1. In order to estimate the sensitivity of the spectrometer we have record a rather weak transition J=3←2 of $^{14}N^{15}N^{16}O$ molecule in the 02/0/0 vibrational state (Figure 2). Intensity of this line is 4.36×10^{-7} cm^{-1}. Taking into account the signal-to-noise ratio one can conclude that the sensitivity is estimated to be 10^{-8} cm^{-1}.

Table 1. Measured Frequencies of the J=1 ← 0 Transition of the HCN Molecule

J = 1 ← 0	our measurements	De Lucia, Gordy[5]	residual
F = 1 ← 1	88630.4160	88630.4157	0.0003
F = 2 ← 1	88631.8476	88631.8473	0.0003
F = 1 ← 0	88633.9357	88633.9360	-0.0003

References

1. E.A.Alekseev. Automated High Resolution Millimeter Wave Spectrometer.// Turkish Journal of Physics. - 1995. - Vol. 19. - P.1457-1461.
2. E.A.Alekseev, S.F.Dyubko, V.V.Ilyushin, S.V.Podnos. The High-Precision Millimeter-Wave Spectrum of $^{32}SO_2$, $^{32}SO_2$ (ν_2), and $^{34}SO_2$.// J.Mol.Spectrosc. -1996. - Vol. 176. - p.316-320.
3. O.I.Baskakov, S.F.Dyubko, V.V.Ilyushin, M.N.Efimenko, V.A.Efremov, S.V.Podnos, E.A.Alekseev. Microwave Spectroscopy of Vinyl Cyanide, Taking into Account the Hyperfine Structure.// J.Mol.Spectrosc. - 1996. - Vol. 179. - p.94-98.
4. V.V.Ilyushin, E.A.Alekseev, S.F.Dyubko, O.I.Baskakov, S.V.Podnos. Millimeter wave spectrum of acetic acid (A-type transitions) // Radio Physics and Radio Astronomy. - 1997. - Vol.2. - N 3. - p.359-372.
5. F.C.De Lucia, W.Gordy. Molecular-Beam Maser for the Shorter-Millimeter-Wave Region: Spectral Constants of HCN and DCN.// Phys. Rev. - 1969. - Vol. 187. - N.1. - p.58-65.

MILLIMETER WAVE SPECTROMETER AND ITS APPLICATION

A.N.Kopnin and V.V.Meriakri
Institute of Radio Engineering and Electronics, Russian Academy of Sciences
Address: 1 Vvedensky sq. Fryazino, Moscow region, 141120, Russia
Tel: (095)5269266, Fax: (095)7029572, E-mail: ask@ms.ire.rssi.ru

The near millimeter wave region (wavelengths λ=3.0÷0.8 mm) is rich in spectral lines of various light molecules and high -J rotational lines of molecular species [1-3] including transient molecules [4].

A millimeter and submillimeter-wave high sensitivity spectrometer suitable for observation of spectral lines of molecules and transient radicals and species at frequencies from 150 to 320 Ghz is developed [5]. Fig 1 shows schematic diagram of the spectrometer.

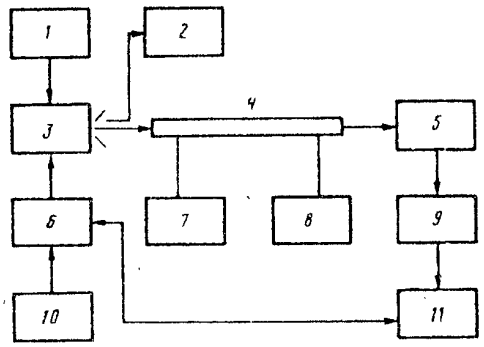


Fig. 1. Schematic diagram of the spectrometer.

Here 1 is radio frequency modulator, frequency changes from 3 to 100 Mhz. 10 is low frequency modulator. 3 is a backward-wave oscillator with supply 6. 4 is quasioptical absorption cell. The cell is made of a 120 cm-long silica tube with diameter of 5 cm. This cell is equipped with metal electrodes to induce a glow discharge with a current up to 5 ma. The second method for inducing discharge employs a high frequency oscillator (frequency of 120 Mhz and output power of 40 w).

Open resonator 2 allows to measure spectral frequency with accuracy up to 10^{-5} using known spectral line as standard.

Vacuum systems 7 guarantees pressure up to 10^{-3} mm Hg. Device 8 fills the cell 4 with gas under test.

Detector section 5 with d.c. amplifier 9 and computer interface 11 realized the minimum detectable absorption coefficient of this spectrometer about 10^{-8} cm^{-1} with resolution up to 10 Khz.

The spectral line of H_2S near frequency 190 Ghz depending on pressure was investigated. The maximum absorption at atmospheric pressure was 7.7 db/m at frequency 168.7 Ghz and the line half-width was equal to 5 Ghz; for comparison, at the pressure 1 mm Hg the half-width was 10 Mhz.

The result of these investigations allow us to suggest a method for monitoring the H_2S content in the vicinity of oil factories.

The spectral line width and intensity at frequency 325.153 Ghz depending on pressure from 10^{-2} mm Hg were investigated too. For example for pressure 0.1 mm Hg absorption is equal 0.5 db/m and half-width of line was 2 Mhz.

In addition, the spectral lines of transient molecules and radicals were investigated in the frequency region 150÷320 Ghz. Some results are summarized in Table 1.

The accuracy of the transition frequency measurements is 30÷50 Mhz.

For HCN and CH_3NC the total absorption in measuring cell were 20 and 12 db accordingly. For other molecules absorption was 1-5 db for concentration up to 1%.

The observations of spectral lines of transient molecules and species are of interest for radio astronomy environment control, and interstellar chemistry.

Table 1. Spectral lines of some molecules under test.

Molecule	Transition J	Frequency, Ghz	Dipol moment, Debye
HCN	2-1	177262	2.98
HCN	3-2	265886	2.98
HNC	2-1	181330	3.05
HNC	3-2	271980	3.05
CN	5/2-3/2	226980	1.45
CH_3CN	13-12	239160	3.91
CH_3CN	14-13	257560	3.91
CH_3CN	15-16	275960	3.91
CH_3NC	13-12	261370	
CH_3NC	14-13	281470	
CH_3NC	15-14	301580	
CS	3-2	146969	1.96

The spectrometer was used also for the investigation of composition of pyrolisis products of a wide group of proteines.

References

1. A.K.Garrison, W.Gordy, High-Temperature Molecular Beam Microwave Spectrometer. Physical Review, Vol.108, pp. 899-890, 1957.
2. M.Winnewisser, K.Sastry, R.Cook, W.Gord, Millimeter Wave Spectroscopy of Unstable Molecular Species. II Sulfur Monoxid, Journal of Chemical Physics, Vol.41, pp.1687-1691, 1964.
3. D.A.Helms, M.Winnewisser and A.Winnewisser, Millimeter Wave Spectrum of Barium Sulfide in Low Pressure Flame. Current Millimeter Wave Measurement of High-Temperature Species. Journal of Physical Chemistry, Vol.84, pp.1758-1785.
4. S.Saito, H.Ozeki, S.Yamamoto, Submillimeter Wave Spectroscopy of Transient Interstellar Molecules. 19th International Conf. On Infrared and Millimeter Waves, Digest, pp.183-184, Japan, Sendai, 1994.
5. A.N.Kopnin, V.V.Meriakri, Millimeter Wave Gas Spectrometer and Some its Applications. Izvestia Akademii Nauk. Seria fisicheskaya, Vol.61, No.12, pp2323-2328, 1997 (in Russian).
6. V.V.Meriakri, Spectroscopy of Millimeter and Submillimeter Ranges, Moscow University Physics Bulletin, Vol.47, No.3, pp.81-88, 1992.

THE REGISTRATION OF DISTORTIONS BY MICROWAVE COMPONENTS OF MEASUREMENTS OF THE MULTIFREQUENCY RADIOINTERFEROMETER OF MILLIMETER WAVES

M. V. Andreev
Department of Radiophysics, Dniepropetrovsk State University,
13 Nauchny pereulok, Dniepropetrovsk, 320050, Ukraine
Tel. (0562)46-79-95

In the last years modern industry all more often addresses to a problem of a construction of multifrequency radiointerferometers of millimeter waves, which can be used for a wide range of problems, in particular for parameter determination of layered dielectrics [1], non-destructive testing of composite materials, detection of discontinuities in different transmission lines [2,3], etc. For interpretation of the processed data in multifrequency radiointerferometers the use of additive exponential model is meant, that enables to apply well itself recommending methods of the parametric spectral analysis [2-4]. However an efficiency of this approach essentially depends from distortions of an interpreted signal which are brought in by measuring waveguide path.

The analysis of considered problem was carried out on the basis of the measuring-computer complex of the radiowave non-destructive testing of layered dielectrics RIMCH-04, permitting to conduct measurements of frequency characteristics of reflection from researched structures in a free space in 8-mm microwave range (26÷37.6 GHz) and determine parameters of layered dielectrics by methods of the spectral analysis [1]. The primary measuring converter in it are the directional detectors with cross-section of waveguide transmission line 7.2×3.4 mm^2, and the pyramidal horn of length 56 mm with the sizes of the aperture 40×30 mm^2 was used as the radiator.

The non-uniformity of a measuring waveguide path (see Fig. 1), which segments (rectangular waveguide, horn, free space) have different phase-frequency characteristics, results in phase distortions of the measured signal rather used additive exponential model of frequency characteristics of reflection [5]. It results in essential distortion of the form of peaks of interpreted signal in spectral time area, which positions and amplitudes determine parameters of layered dielectrics. The additional distortions introduce reverberation between a researched structure and aperture, and also change of a gain with modification of frequency.

The preprocessing of the measured data $\boldsymbol{R}_{\text{mes}}$ could allow to reduce distorting influence of a measuring waveguide path, however for realization of data preprocessing it is necessary to find out character of brought in distortions.

For research of character and sizes of brought in distortions carried out series of real experiments on measurement by RIMCH-04 of frequency characteristics of a complex reflection coefficient from a metal plane in frequency band 26÷37.6 GHz in N=59 equidistant frequency points. The outcomes of one from a series of the measurements of a module and phase of a reflection coefficient from a metal plane are represented in fig. 2. Then the approximating methods selected a main informative part of a measured signal $\boldsymbol{R}_{\text{mes}}$ and the behaviour of a residual term (connected to presence of brought in distortions and a random noise) was investigated.

The problem of approximating of the frequency characteristics of the measured data $\boldsymbol{R}_{\text{mes}}$ by model $\boldsymbol{R}_{\text{mod}}$ as a sum of exponents in form

$$R_{\text{mod}}(\omega) = \sum_{m=1}^{M} r_m \exp(-j\omega t_m) \qquad (1)$$

was considered at first. For approximating an indicated kind the method of search of quasisolution [5] was used. Approximating of the frequency characteristic of the measured data $R_{\text{mes}}(\omega)$ unary exponential curve $R_{\text{mod}}(\omega)=r_1\exp(-j\omega t_1)$ has allowed to receive an evaluation of distance up to a researched sample $z_1=ct_1/2\approx180$ mm (50 mm from them to be come on a free space). The error of approximating, defined on the formula

$$\rho = \|\boldsymbol{R}_{\text{mes}} - \boldsymbol{R}_{\text{mod}}\|^2 / \|\boldsymbol{R}_{\text{mes}}\|^2, \qquad (2)$$

has made on the average for the whole series of experiments about 0.4 (i.e. 40 %). And in time spectral area the residual signal $\boldsymbol{R}_{\text{mes}}$-$\boldsymbol{R}_{\text{mod}}$ was grouped as two peaks located in region z_1, that speaks about the extension of initial time peak. The measured signal in time-domain ($|G(z)|$ - solid line), estimated one peak in z_1 with amplitude r_1 ($|G(z)|$ - dashed line) and the residual signal $\boldsymbol{R}_{\text{mes}}$-$\boldsymbol{R}_{\text{mod}}$ in time-domain ($|\Delta G(z)|$) are represented in fig. 3.

The increase of order of the additive exponential model up to M=4 has allowed to compensate the considered remainder and also time peak, which appropriates the reverberation between a metal plane and a horn (z_1 = 167 mm, z_2 = 178 mm, z_3 = 189 mm, z_4 = 290 mm, $|r_1|$=0.160, $|r_2|$=0.249, $|r_3|$=0.222, $|r_4|$=0.072). Amplitudes of estimated peaks have been not equal ($|r_1|<|r_3|\approx|r_2|$), that speaks not only about the extension of initial time peak, but also about a skew of the form. At considered approximating the error of approximating has decreased up to a level 0.09 (i.e. up to 9 %), which corresponds to a level of a random measuring noise in the data. The further increase of order M of exponential model did not give the essential lowering of approximating error and resulted only in splitting estimated positions, that conducted to the physically unjustified increase of estimated amplitudes r_m ($z_m \approx z_{m+1}$; $|r_m|,|r_{m+1}| \to \infty$). For example, the increase of order of additive exponential model up to M=5 has given the following outcomes: z_1=161.1mm, z_2=161.4mm, z_3=187.9mm, z_4=188.1mm, z_5=291.8mm, $|r_1|$=4.92, $|r_2|$=4.99, $|r_3|$=9.49, $|r_4|$=9.39, $|r_5|$=0.073, ρ=0.07.

The researches on approximating the measurement data by Chebyshev's orthogonal polynomials (with complex coefficients) with successive increase of their order and analysis of change of approximating error were carried out. For deleting a determined part (which is connected to reflection of a plane electromagnetic wave from a metal plane) the measured data were normalized (are divided) on model $R_{mod}(\omega)=r_1\exp(-j\omega t_1)$ with use of obtained earlier estimates of parameters of exponential model of the first order. This analysis has shown predominant influence in the measured reduced data of the second degree of polynomials. The use of polynomials of the fifth order has allowed to reduce an approximating error till ρ=0.1, which corresponds to a level of a random noise in the data. The result of approximating the normalized data by Chebyshev's orthogonal polynomials of the fifth order are represented in fig. 4 (measured data - solid line, model data - dashed line).

The similar analysis which has been carried out only for a phase of the normalized measured data, has shown predominant influence of the second degree of polynomials, moderate - to the third degree of polynomials and practically absent - higher order in polynomials, that allows to make an appropriate conclusion about character of brought in distortions. For example, for the data from a fig. 4, the values of polynomial coefficients have made: a_0=-0.78, a_1=0.82, a_2=2.25, a_3=0.45, a_4=-0.01, a_5=-0.03; value of approximating error has made ρ=0.04. Using the considered approach for the model data appropriate to reflection from a metal plane in the waveguide with cross-section 7.2×3.4 mm, have given a similar results, and the coefficient at a polynomial of the second degree a_2 increased with increase of length l of a section of the waveguide before metal plane: for l=75 mm it was a_2=1.21, for l=100 mm it was a_2=1.61, for l=120 mm it was a_2=1.94.

The values of coefficients in Chebyshev's polynomials insignificantly vary at change-over from processing of one series of real experiment to other if the scheme of measurements did not vary. It allows to modify preprocessing the measured data of the multifrequency radiointerferometer which was written in [5]. The measured data can be normalized not on outcomes of additional measurements of the reflection characteristics from the standard reflector (metal plane), but on simulated relation which was obtained with the help of Chebyshev's polynomials and earlier estimated values of polynomial coefficients. It allows to reduce time of measurements and to reduce influence of the measuring noise which present in the measured reflection characteristic from the standard reflector. The considered approach was checked at use of the multifrequency radiointerferometer for parameter determination of a layer of a foam plastics which has test parameters: ε=1.20, d = 40.0 mm. At use of a normalization [5] the following values of parameters of a layer were obtained: ε=1.21, d = 39.5 mm; at use of a modified normalization estimations have made: ε=1.20, d = 40.1 mm.

The obtained outcomes allow to specify paths on reduction of distortion by waveguide measuring path in considered microwave radiointerferometers.

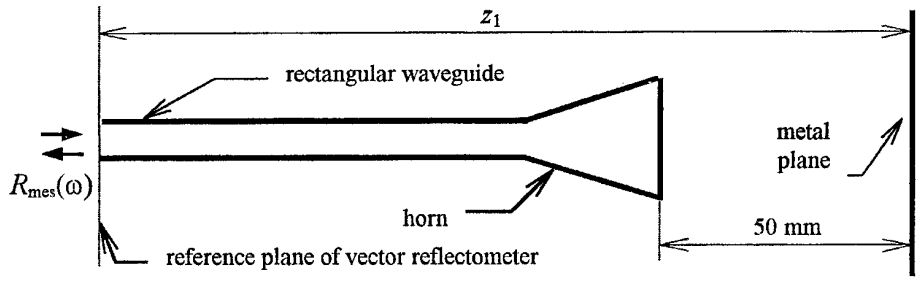


Figure 1. Measuring path of radiointerferometers

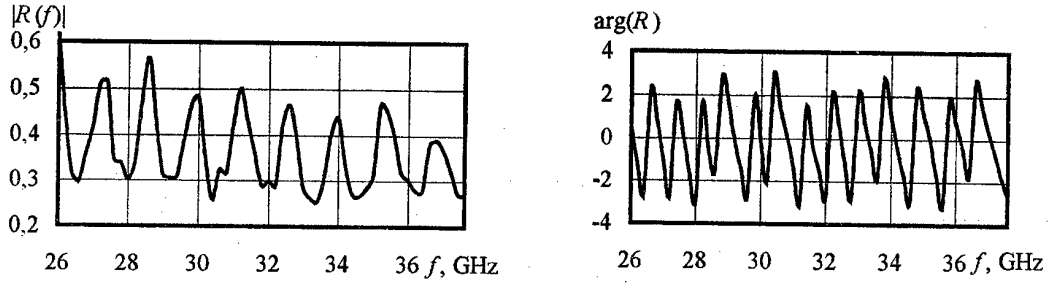


Figure 2. Measured complex reflection coefficient from metal plane

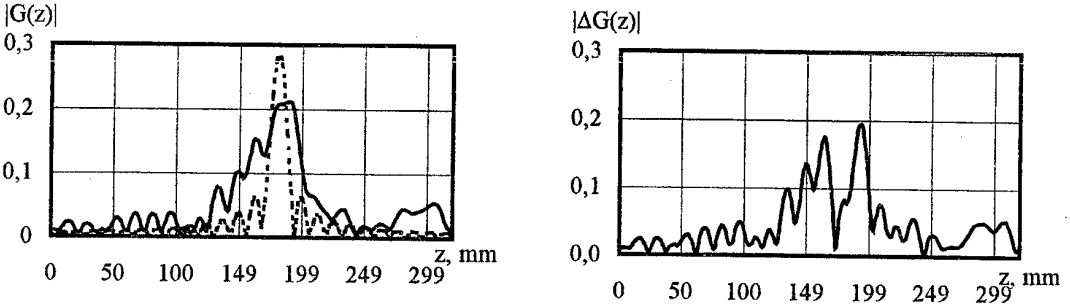


Figure 3. Measured signal and residual signal in time-domain

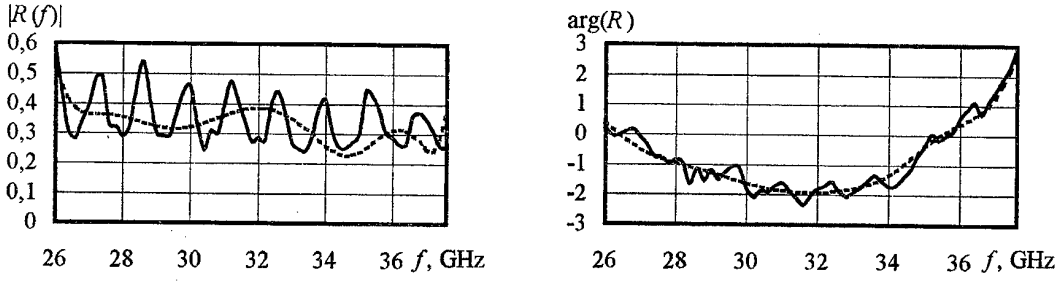


Figure 4. Approximating the measured normalized data by Chebysyhev's orthogonal polynomials

References

1. V. F. Borulko, O. O. Drobakhin, V. A. Karlov, "The measuring - computer complex RIMCH-04 for the non-destructive testing of layered dielectrics", Russian Non-destructive Testing (in Russia), No. 6, pp. 70-78, June 1993.
2. H. Vanhamme, "High resolution frequency-domain reflectometry", IEEE Trans. on Instrument. Measurem., Vol. IM-39, No. 2, pp. 369-375, Feb. 1990.
3. Z. A. Maricevic, T. K. Sarkar, Y. Hua, A. R. Djordjevic, "Time-domain measurements with Hewlett-Packard network analyzer HP8510 using the matrix pencil method", IEEE Trans. Microwave Theory Tech., Vol. MTT-39, No. 3, pp. 538-547, March 1991.
4. M. V. Andreev, V. F. Borulko, O. O. Drobakhin, "The solution of the inverse problem for multilayered dielectric structures", Proc. of Int. Kharkov Symp. "Physics and Engineering of Millimeter and Submillimeter Waves", Vol. 1, pp. 42-45, 1994.
5. M. V. Andreev, V. F. Borulko, O. O. Drobakhin, "About implementation of quasisolution method at determination of parameters of layers of dielectric layered structures. I.", Russian Non-destructive Testing (in Russia), No. 9, pp. 61-72, Sept. 1996.

TIME SPECTROSCOPY OF A FILM BOLOMETRIC RESPONSE TO MM-WAVES POWER AS A METHOD OF THE THERMODYNAMIC COEFFICIENTS DIAGNOSTICS IN A FILM STRUCTURES

A.M. Grishin #, Yu.V. Medvedev +, Yu.M. Nicolaenko +
Royal Institute of Technology,
S-100 44, Stockholm, Sweden
+ Donetsk Physical and Technical Institute of the National Academy of Sciences of Ukraine
72,R.Luxemburg, Donetsk, 340114,Ukraine.
E-mail: medvedev@host.dipt.donetsk.ua , grishin@gam.dipt.donetsk.ua

We have applied 4 and 8 mm band wave power for a pulse heating of the film and investigated a time function of a film overheating temperature with a help of time and temperature dependencies of a film electrical resistivity (R) [1]. The time function of R(t) is recorded by our equipment in a computer memory with a different size of a time scales. For a submicron thickness films we have neglected by film temperature gradient which can be appeared as a result of one side sink of a heat and have proved the conditions for a parallel heat flow propagation in the film structures. Theoretically film temperature (T_f) is described by one dimension equations:

$$c_f \rho_f v_f (\partial (T_f - T_s(x=0)) / \partial t) = -S\lambda_{fs}(T_f - T_s(x=0)) + P_j (T_f), \qquad (1)$$

$$c_s\rho_s(\partial T_s/\partial t)=\lambda_s \partial^2 T_s/\partial x^2, \qquad (2)$$

with initial $T_f = T_s = T_0$ and boundaries conditions: $\lambda_s(\partial T_s/\partial x) = \lambda_{fs}(T_f - T_s(x=0))$, x=0, and $\lambda_s(\partial T_s/\partial x) = \lambda_{st}(T_s(D) - T_0)$, x=D, where c_f ,c_s and ρ_f , ρ_s are specific heat capacity coefficient and density of both film and substrate, (v_f) is film volume, λ_{fs} and λ_{st} are thermoconductivity coefficients of the film-substrate and substrate-thermostat interfaces, D is the thickness of the substrate. The values of x=0 and x=D are corresponded to film-substrate and substrate-thermostat interfaces. We have selected a typical data for $YBa_2Cu_3O_{7-\delta}$ and $LaAlO_3$ materials at T=90K and of a stationary calculated digitally the time function of a film temperature corresponding to the transition process heat-transport steadying in a film-substrate-thermostat system after the constant joule power input in the film (see fig. 1).

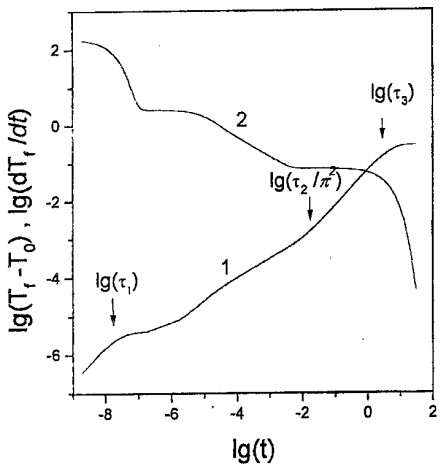


Fig.1. Time function of the film overheating temperature ($T_f - T_0$) (curve 1) and (dT_f/dt) - time function (curve 2) in two logarithmic scales. Digital calculation with a parameters values: c_f =181.3 J/kg K, ρ_f = 6.3 10^3 kg/m^3, c_s =163.4 J/kg K, ρ_s = 6.51 10^3 kg/m^3, λ_{fs} = 10^7 W/m^{2}K, λ_{st} = 130 W/m^{2}K, λ_s =18.14W/mK, size of structure is 9*3*0.5mm^3 and thickness of the film 0.17mkm .

The film temperature T_f (t) is very sensitives for all particularities of the heat transport in the system. It's clear seen from behaviour of dT_f/dt function (curve 2 of fig .1).

The most informative part of (T_f-T_0) time function is showed in fig.2a-c. They contain information about temperature amplitudes (ΔT_i) and time constants (τ_i) of the thermal equilibrium steady on the: film-substrate interface (fig.2a), thickness of substrate (fig.2b) and interface of the substrate-thermostat (fig.2c). Curves 2 on the fig.2a-c are corresponded to idealized process which can be described analytically.

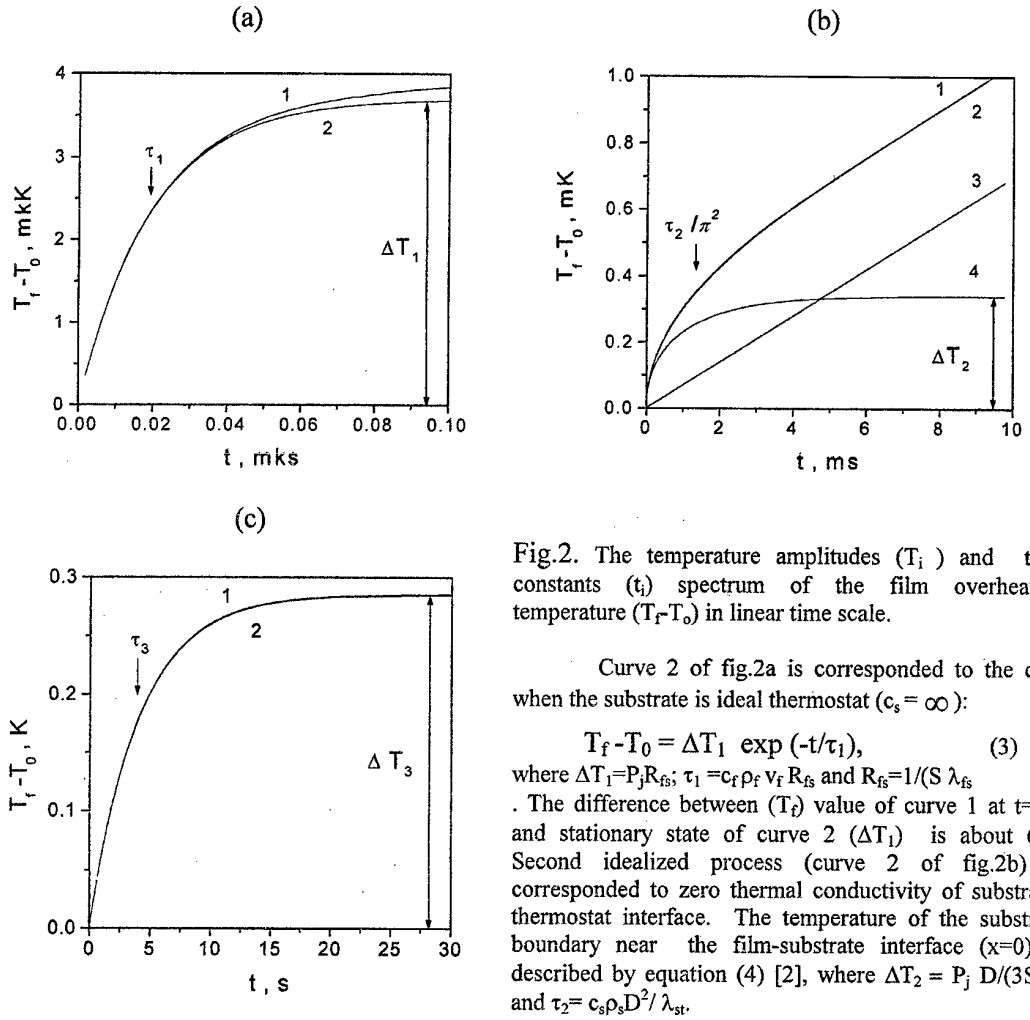


Fig.2. The temperature amplitudes (T_i) and time constants (t_i) spectrum of the film overheating temperature (T_f-T_o) in linear time scale.

Curve 2 of fig.2a is corresponded to the case when the substrate is ideal thermostat ($c_s = \infty$):

$$T_f - T_0 = \Delta T_1 \exp(-t/\tau_1), \qquad (3)$$

where $\Delta T_1 = P_j R_{fs}$; $\tau_1 = c_f \rho_f v_f R_{fs}$ and $R_{fs} = 1/(S \lambda_{fs}$. The difference between (T_f) value of curve 1 at $t = 5\tau_1$ and stationary state of curve 2 (ΔT_1) is about 6%. Second idealized process (curve 2 of fig.2b) is corresponded to zero thermal conductivity of substrate-thermostat interface. The temperature of the substrate boundary near the film-substrate interface (x=0) is described by equation (4) [2], where $\Delta T_2 = P_j D/(3S\lambda_s)$ and $\tau_2 = c_s\rho_s D^2/\lambda_{st}$.

$$T_s(t) = P_j t/(c_s\rho_s v_s) + \Delta T_2 \{1 - (6/\pi^2) \sum_{n=1}^{\infty} (1/n^2) \exp(-n^2\pi^2 t/\tau_2)\}. \qquad (4)$$

Curves (3) and (4) of fig. 2b demonstrate first and second members of the equation (4) separately. In third process (curve 2 of fig.2c) we have described the heating of the structure as a whole:

$$T_f - T_0 = \Delta T_3 \exp(-t/\tau_3), \qquad (5)$$

where $\Delta T_3 = P_j/S\lambda_{st} = P_j R_{st}$ and $\tau_3 = R_{st}(c_f \rho_f v_f + c_s \rho_s v_s)$. As it's seen from fig.2b and fig.2c the curves (1) and (2) are good coincided. It is a consequence of a strong inequalities of $\Delta T_3 >> \Delta T_2 >> \Delta T_1$ and $\tau_3 >> \tau_2 >> \tau_1$. They can be satisfied for many standard film structures with a small value of R_{fs} because R_{st} value can be changed in experiment in wide range. If we know the structure of (T_f-T_0) function the equation of (5) can be used for joule power determination in the case of microwave heating of the film. This procedure consists of control of relative value of (P_j) with a help of (ΔT_3) measurement and quantitative determination of (P_j) by mean of dc heating of the film. If the value of (τ_3) is more greater than substrate time constant (τ_2) in both longitudinal and transversal directions (P_j) can be calculated directly: $P = I^2(R + R_c)$, where R and R_c are electrical resistivity of both film and film current contacts..

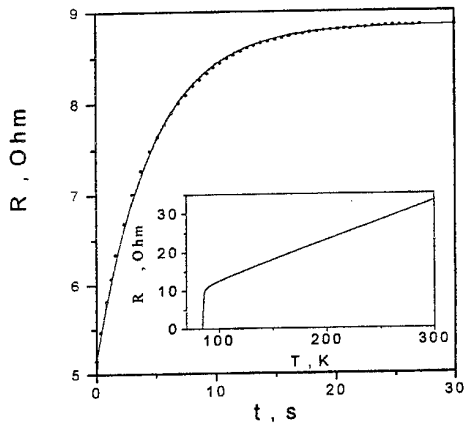


Fig.3. Time and temperature (insert) dependencies of electrical resistivity $YBa_2Cu_3O_{7-\delta}$ / $LaAlO_3$ film.

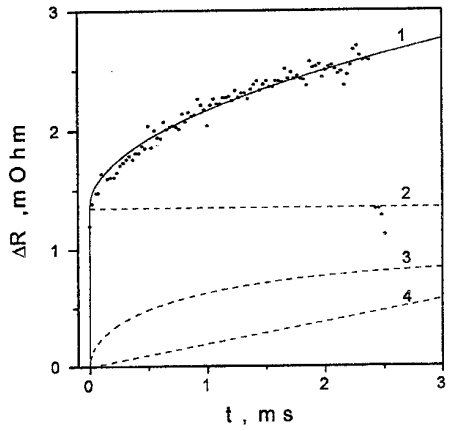


Fig.4. Time dependence of electrical resistivity of $YBa_2Cu_3O_{7-\delta}$ / $LaAlO_3$ film.

As a model structure we have applied the 0.2 mkm thickness $YBa_2Cu_3O_{7-\delta}$ film is produced by magnetron sputtering of a target on the monocrystalline $LaAlO_3$ substrate [3]. Temperature dependencies of R(T) is shown in insert of fig.3. The film has a linear region of I-V characteristics at temperatures more than 83.75K. The experimental time function of a film electrical resistivity is shown in fig.3 by points. First point of R(t=0) is corresponded to a moment of a microwave power input and initial temperature T_0 =85.0K. The solid line of fig.3 is approximation of the experimental data by equation: $R(t,T) = R(0,T_0) + \Delta T_3 (dR/dT)(1-\exp(-t/\tau_3))$, where $R(0,T_0)$=5.15 Ohm; ΔT_3 =0.376 K; dR/dT = 9.81Ohm/K and τ_3 = 4.6s. We have determined P_j =1.09mW from separate measurement and calculated $R_{st} = \Delta T_3 / P_j$ =338K/W and $c_f\rho_f v_f + c_s\rho_s v_s = \tau_3 / R_{st}$ =1.36 10^{-2} J/K.

The time function of electrical resistivity of fig.4 is measured in periodical series of rectangular power pulse regime at thermostat temperature T_0 =84.1K. Microwave pulses has a meander shape and duration of pulse is equal to t =2.38ms. A particularity of this dependence is additional high speed part of the film resistive response to microwave power. The amplitude of this response is shown in fig.4 by constant line (2). We don't described it in this work. Bolometric part of R(t) is corresponded to thermal flow steady on the thickness of the substrate we have approximated by the sum of linear (line 4) and saturated (curve 3) function according to equation of (4). For the linear function we have determined dR/dt=0.19 Ohm/s, and for saturated function: τ_2 =13.6 ms, dR/dT=2.68 Ohm at T=84.29K, ΔT_2 =0.339mK and P_j =0.96 mW at T_0 =84.1K Then the values of $R_s = 3\Delta T_2 / P_j$ =1.06K/W and $c_s\rho_s v_s$ =1.34 10^{-2}K is calculated. We have noted that T=84.29K is corresponded to minimal temperature of the substrate in the case of pulse heating of the film and pulse duration of t =2.38ms is corresponded to value of τ_2 / π^2 =1.38ms. The value of coefficients of both specific heat capacity (c_s =152.2J/kg K) and thermal conductivity (λ_s =17.47W/m K) of a lanthanum aluminate were obtained in good agreement with a other method data [4].

References

1. A.M.Grishin, Yu.V.Medvedev, Yu.M.Nicolaenko, Thermodynamic coefficients and thermal resistance of the film structure interfaces, Phys. and Techn. of Hight Pressure, 8, 1,pp.27-40,(1998).
2. H.S. Carslaw, J.C.Jaeger, Conditions of heat in solids, Oxford, Clarendon Press,(1959).
3. J.H.Xu, B.M.Moon, I.L.Zhou, K.V.Rao, G.G.Zhang Proc.ICMAS-92, Paris, 117, (1992)
4. P.C.Michael, J.U.Trefny, B.Yarar Thermal transport properties of single crystal lanthanum aluminate. J.Appl. Phys,72 1,1,pp.107-109,(1992).

J



MM AND SUBMM WAVELENGTH INSTRUMENT-MAKING FOR SCIENTIFIC RESEARCH (Hot-Plasma Diagnostics, Control of Technological Processes)

HETERODYNE SPECTROMETER FOR REMOTE SENSING OF THE ATMOSPHERIC OZONE

V.A.Gusev[1], E.P.Kropotkina[1], S.V.Logvinenko[1], A.N.Lukin[1], P.L.Nikiforov[2], S.B.Rozanov[1], A.M.Shtanjuk[2], S.V.Solomonov[1]
[1] P.N.Lebedev Physical Institute of the Russian Academy of Sciences
53 Leninsky prospect, Moscow V-333, 117924 RUSSIA
Tel.: (007)(095) 132-64-62, Fax: (007)(095) 135-24-08, E-mail: solomon@sci.lpi.msk.su
[2] Institute of Applied Physics of the Russian Academy of Sciences
46 Uljanova street, Nizhny Novgorod, 603600 RUSSIA
Tel.: (007)(831) 238-45-74, Fax: (007)(831) 236-19-59, E-mail: shtan@appl.sci-nnov.ru

Millimeter (MM) wave ground-based research on the atmospheric ozone and its anomalies is one of the most important aspects of remote sensing of the atmosphere. Measurements of pressure-broadened rotational spectra of ozone allow to retrieve vertical ozone distribution (VOD) for altitudes about from 15 to 75 km [1, 2]. The method has a number of essential advantages over the ground-based optical methods. Heterodyne receivers based on low-noise Schottky diode mixers were used almost in all instruments for remote sensing of ozone at MM waves [3]. So a receiver with planar diode mixer [4] was chosen for the new Lebedev Physical Institute (LPI) heterodyne spectrometer [2] which is being used for ground-based measurements of the 142.2 GHz ozone line in Moscow since November 1994.

Computer simulations [5] allowed to optimize performance of the spectrometer. It was found that high-accuracy retrieval of the VOD by method [6] is possible for altitudes of about 15-75 km at integration time less than 1 h if SSB system noise temperature is less than 800 K, the total analyzing band is more than 250 MHz, and the frequency resolution increases from 0.1-0.2 MHz at the line center to 10-20 MHz at its wings. Antenna beamwidth may be up to about 5°.The LPI spectrometer consists of three main parts: (1) low-noise cooled receiver, (2) two spectrum analyzers, and (3) an IBM PC with special software (Fig. 1). Noise signal from sky or a reference blackbody load is focused by an input lens of a quasioptical block. The rotating flat bow-tie chopper mirror of the block switches two input channels with frequency of 75 Hz. Signal frequency is down-converted to the first intermediate frequency (IF) band of 3.4-4.0 GHz in the first mixer. Both the signal and the first local oscillator (LO) pump at 138.5 GHz goes into the mixer through a diplexer and scalar horn. The diplexer and the first mixer are tuned for the DSB operation. To minimize input loss we don't use SSB filter but measure accurately the receiver gain in both sidebands. Free-space Gaussian beams were used at the receiver front-end to provide both low input loss (about 1 dB including horn) and antenna beam of about 3° at -10 dB level with no sidelobes at least down to -35...-40 dB. All fused quartz lenses have antireflecting quarter-wavelength teflon coating.

The first mixer and the FET IF amplifier are mounted in vacuum section of the liquid nitrogen cryostat. The mixer and horn support is centered to the cryostat window to avoid shifts across the beam axis under cooling. The mixer temperature under cooling is about 85 K.The IF amplifier is placed at the bottom of liquid nitrogen bath and connected to the mixer by a flexible RF cable. The cryostat's 3.2-litre bath, when filled, provides 2.5-3 days of the receiver operation.After additional amplification outside the cryostat, the IF signal is down-converted to the second IF band of 240 MHz central frequency and power-divided. One part of the signal is used to measure the atmosphere brightness temperature in broadband channel of the spectrometer including square-law and synchronous detectors, analog-to-digital converter (ADC) and a control chart recorder. The broadband data allow to determine tropospheric attenuation of the ozone line. Other part of the signal is divided between two filter-bank spectrum analyzers. The first one (SA 80) has 80 channels with the total bandwidth of 283 MHz. The channel widths increase in five steps from 0.2 MHz at the line center to 20 MHz at its wings. The second analyzer (SA 120) has 120 channels of 0.1 MHz (the total band of 12 MHz) and provides higher frequency resolution at the line center. High stability of both LOs are provided by phase/frequency locking systems (PFLS). The first LO is the OV-76 type carcinotron. Its PFLS includes three phase locking loops. The second LO of 3.45 GHz frequency is a standard G4-80 generator. Both the PFLSs are based on standard frequency synthesizers with reference quartz generators. The first LO short-term (0.2 s) relative stability is about $2 \cdot 10^{-8}$.

A calibration/observation procedure includes two calibration and two observation stages. At the first calibration stage, both input channels are closed by blackbody loads, the first one being in liquid nitrogen and the second one being warm. At the second calibration stage, the loads are swapped. At the first observation stage one channel is closed by the cold load and the second one is open, and at the second observation stage the cold load closes the other channel. Usually, a calibration stage takes 30 s and an observation one, 100 s. Several

observation cycles can be done after one calibration cycle. Accurately measured brightness temperature of the cold load is 112±2 K. To avoid distortions of the spectra, it is desirable to equalize brightness temperatures of the atmosphere and the reference cold load at the observation stages. It is taken into account that the calibration signal and the atmosphere background contribute to both sidebands but the ozone line does only to the upper sideband.

Integration of the signal is done digitally at the analyzer channel outputs by the PC, after A/D conversion of the signals in multi-channel 10-bit ADC interface units (Fig. 1) with scaling gain. A/D conversion time is 30 μs. Data processing includes averaging the individual ozone spectra, correction the averaged spectrum by tropospheric absorption and retrieval the VOD. Special test programs control the spectrometer operation. The control is carried out every time before starting observations. All parameters of the calibration/observation procedure are entered by an operator through the ADC units.

Two receivers were made and tested at room temperature and under cooling [2, 3]. The first one had the IF of 3.4-4.0 GHz and was used in the spectrometer, and the second one, of 1.3-1.7 GHz IF, was planned for future experiments. The tests were done without quasioptical block (0.35 dB input loss) in DSB and two SSB modes selected by the diplexer. The OV-68 type carcinotron was used as the first LO of 117-175 GHz range. No PFLS was used for the tests. The LO power was measured by thermistor at the diplexer idle output. The input receiver noise temperature was determined by standard *Y*-factor method using hot/cold blackbody loads.Some results are given in Figs. 2 and 3 where receiver and mixer noise temperatures T_r and T_{mx} together with the mixer conversion loss L_{mx} are presented versus the LO frequency. As far as we aware the SSB value T_{mx}=460±60 K obtained at the LO frequency of 147.5 GHz and IF of 3.7 GHz is the lowest one reported for uncooled Schottky diode mixers employing either honeycomb or planar diodes at frequencies above 115 GHz. Additionally, the T_{mx} values of 180±30 K SSB and 100±15 K DSB at the LO frequency of 135.2 GHz and IF of 1.5 GHz are the lowest ones reported for cryogenic planar Schottky diode mixers above 115 GHz. In the last case T_r =190 K DSB. The cooled receivers may operate quite satisfactorily at the LO power as low as 0.1-0.2 mW. Peaks and teeth at curves of Figs. 2 and 3 around 130 GHz originated probably from defects of scalar horns. Taking into account the quasioptical block loss the spectrometer noise temperature T_R is less than 1500 K SSB (about 800 K DSB) at 142 GHz. The value is sufficient for routine ozone measurements at signal integration time about 1 h. Under cooling the T_R value fell to 660 K SSB (about 400 K DSB). Some results of ozone observations at the LPI in 1996-98 are presented in [7].

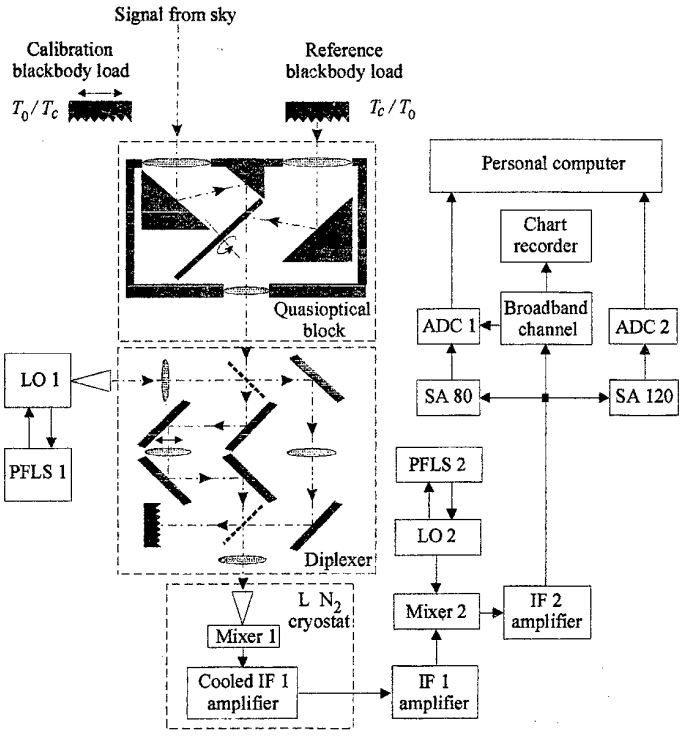


Fig. 1. A block-scheme of the spectrometer.

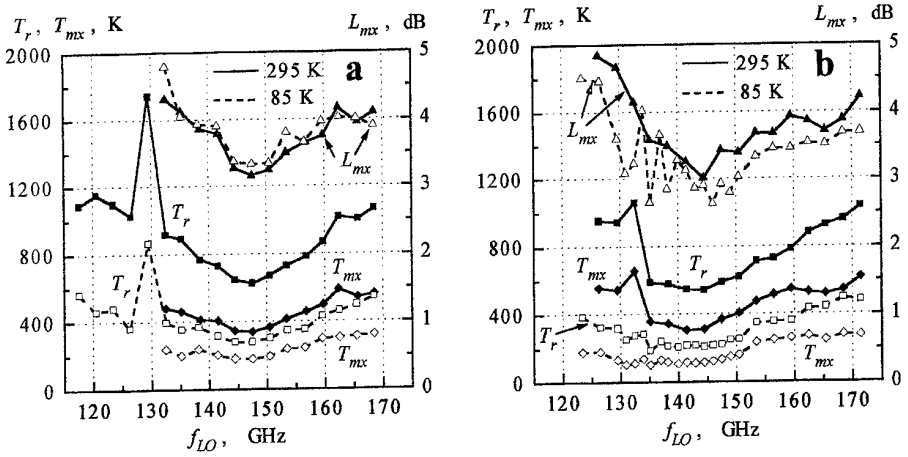


Fig. 2. DSB performance of receivers and mixers for IF of 3.7 GHz (*a*) and 1.5 GHz (*b*).

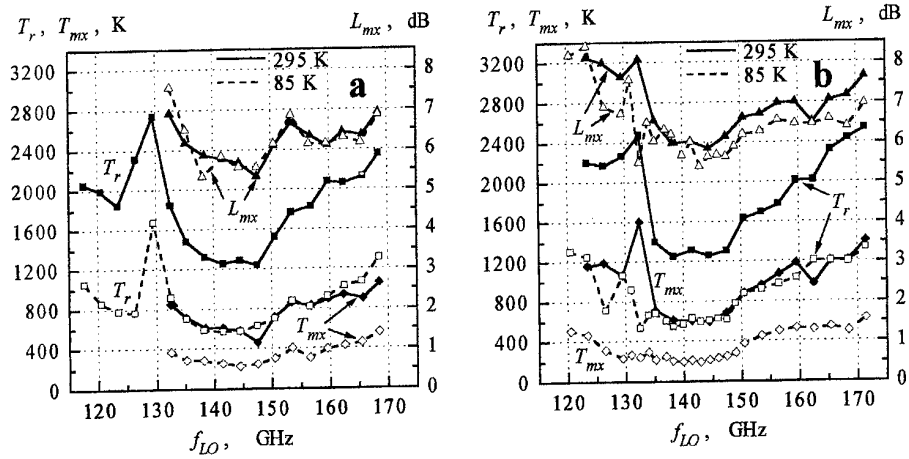


Fig. 3. SSB (upper sideband) performance of receivers and mixers for IF of 3.7 GHz (*a*) and 1.5 GHz (*b*).

The research was supported by Grant No.96-02-19093 from the Russian Foundation for Basical Research.

References

1. R.T.Clancy, D.O.Muhleman, "Ground-based microwave spectroscopy of the Earth's stratosphere and mesosphere", In: Atmospheric remote sensing by microwave radiometry, Ed. M.A.Janssen, J.Wiley & Sons, New York, Chapter 7, pp.335-381, 1993.
2. S.V.Solomonov, S.B.Rozanov, E.P.Kropotkina, A.N.Lukin, "Techniques of ground-based remote sensing of the ozone layer by millimeter-wave heterodyne spectroscopy", Proc. SPIE, Vol.3406, 1998.
3. S.B.Rozanov, A.N.Lukin, S.V.Solomonov, "Low-noise cooled planar Schottky diode receiver for ground-based ozone measurements at 142 GHz" Int. J. Infrared and Millimeter Waves, Vol.19, No.2, 1998.
4. S.B.Rozanov, "Low-noise beam lead Schottky diode mixers for 2 mm waveband", Rus. Radiotekhn. i Elektron., Vol.41, No.3, pp.362-369, 1996.
5. E.P.Kropotkina, S.V.Solomonov, "Submillimeter radiation spectra of the Earth`s atmosphere", Rus. Issledovaniya Zemli iz kosmosa, No.1, pp.81-88, 1988.
6. K.P.Gaikovich, "Tikhonov's method of the ground-based retrieval of the ozone profile", Dig. Int. Geosciences And Remote Sensing Symp., Pasadena, CA, Aug. 8-12, 1994. Vol.4, 1901-1903, 1994.
7. E.P.Kropotkina, A.N.Lukin, S.B.Rozanov, S.V.Solomonov, Remote sensing of the atmospheric ozone at millimeter waves, this issue.

OPTIMISATION OF UHF REFLECTOMETER DEVICE FOR STUDY OF PLASMA DENSITY PROFILE AND FLUCTUATION IN MAGNETICALLY CONFINED PLASMAS

A.I.Skibenko, V.L.Berezhnyj, O.S.Pavlichenko, V.L.Ocheretenko, I.B.Pinos, I.P.Fomin,
Institute of Plasma Physics, NSC KhIPT ,1, Academicheskaya St., Kharkov, 310108, Ukraine

In correlation reflectometry method [1-2] two microwave signals (usually of the same polarization) are launched into plasma, reflected by a cut-off layer, received and analyzed. The spatial coherence of fluctuations is studied by changing the frequency of the second microwave signal against the first one. There is a problem of separation of these two signals as for their frequencies are near to each other. This problem can be removed if one use the probing signals with the different frequencies but reflected from the same plasma layer. This could be done if one uses the magnetized plasma probing via microwaves with different polarization - O- and X- mode probing.

In this paper we describe the results of study of plasma fluctuation properties by using of dual polarization single line microwave plasma probing in the reflex discharge.

Experiments were done on the pulsed reflex discharge performed in the SS- vacuum chamber (length - 150 cm, diameter - 20 cm) that was put inside of magnetic solenoid producing nearly homogeneous magnetic field up to 1.2 T. Hydrogen plasma with the electron density $\bar{n}_e \le 10^{14}$ cm^{-3} and temperature $T_e \approx$ 30 eV was produced at the gas pressure in the range of 10^{-3} - 10^{-1} torr with time duration about 2 ms. (Fig.1)

The choice of appropriate frequency pairs for dual polarization probing of the same or adjacent plasma layers was done by calculation of radial distribution of O - and X - mode cut-off frequencies for a given magnetic field and parabolic electron density profile. Analysis of results of such calculations showed that the range of frequency difference between O- and X- probing signals at plasma radius scanning is larger when X- mode frequency is fixed and O- mode frequency is changing .

Dual polarization plasma probing was produced by means of single antenna optimized for O- mode launching. This antenna was connected via a rectangular waveguide to a special device allowing to fed a waveguide by both - O- mode and X- mode (via directional coupler mounted on the narrow side of waveguide). Such kind of devices were designed and constructed on the basis of metallic and dielectric rectangular waveguides and used for both - launch and receive - antennas. Two sets of such devices were constructed and tested (transition losses 5-12 dB): for the reflex discharge: O-mode - 30-45 GHz, X- mode - 45-75 GHz; for "Uragan-3M" torsatron : O-mode - 17-26 GHz, X- mode - 25-45 GHz.

Backscattering experiment on the reflex discharge was performed by means of 2 antennas put on a diagnostic ports in the central part of discharge column (angle between antenna axes was $\approx 4^{O}$). The measurement system layout is shown on Fig. 1. During the experiment on reflex discharge at B = 0.52T the O- mode frequency was changed in the range of 37 - 47 GHz for 2 values of X- mode frequency signals: 54,84 GHz and 74,84 GHz.

Typical signals of O- and X- mode reflectometers are shown on Fig.2. The low frequency envelope of such signals was used for reconstruction of time behavior of cut-off layer position and electron density profiles. The high frequency component of signal from reflectometer detector described as

$$A = A_0 \cos\Omega_0 t [J_0(\Delta\phi_1) - 2\Sigma J_{2k}(\Delta\phi_1)\cos 2k\Omega t] - 2[\Sigma J_{2k+1}(\Delta\phi_1)\sin(2k+1)\Omega t]\sin\Omega_0 t$$

was used for determination of amplitude of phase oscillations $\Delta\phi_1$ and analysis of electron density fluctuations (amplitude $\delta n/n$, phase spectra $G(\Omega)$, coherency γ, correlation length L_{cor}). The coherency γ was calculated from $\gamma = [G_{O,X}(\Omega)/G_O(\Omega)G_X(\Omega)]$, where G_O, G_X, G_{OX} - spectra of phase oscillations of ordinary and extraordinary waves and their cross-spectrum.The amplitude of density fluctuations $\delta n/n$ was defined as

$$\frac{\delta n}{n} = -\left[\frac{f_x f_{ce}}{f_{pe}}\frac{\delta r_c}{L_n} + \frac{\delta r_c}{L_n}\right];\ L_n = n\left[\frac{dn}{dr}\right]^{-1};\ L_B = B\left[\frac{dB}{dr}\right]^{-1};\ \delta r_C = \frac{\bar{\xi}}{2},$$

where $\bar{\xi}$ is amplitude of phase oscillations and was iquel 0.1-0.3. The correlation length L_{cor} of fluctuations was defined from relation $\gamma \propto \exp(-\Delta r / L_{cor})$. The dispersion relation $K(\Omega)$ of fluctuation was defined

from relation $K(\Omega)=\mathrm{arctg}(\mathrm{Im}G_{ox}/\mathrm{Im}G_{ox})/\Delta r$, where $\mathrm{Im}G_{ox}$ and $\mathrm{Re}G_{ox}$ are imaginary and real parts of phase crosspectrum $G_{0x}(\Omega)$, Δr – the distance between layers.

Firstly we have checked if the phase oscillations of o- and x- probing waves with quite distinct frequency difference (up to 17 GHz) are coherent when they are reflected from the same plasma layers. Fig.3 shows that these oscillations have similar spectra and that within of accuracy of the density profile measurements are highly coherent (Fig.4).

From the data of Fig.3 it is seen that observed fluctuation wavelengths Λ are in the range of 1-6 cm ($\Lambda/\lambda\cong 1.5$–7). The phase and amplitude response of the finite size microwave beam reflected from the *plane* plasma surface with density perturbations depends on the ratio of Λ/λ. We have extended this analysis for the case of reflection from perturbations moving on *cylindrical* surface. Backscattering coefficient [3]

$$\rho = \frac{\int_{-b_2}^{+b_2} \exp(-\frac{y^2}{p^2}) \exp i[-\frac{4\pi}{\lambda}(\xi - \frac{\eta}{2})]dy}{\int_{-b_1}^{+b_1} \exp(-\frac{y^2}{p^2})dy}$$

where y - distance from probing beam axis, $2b_1$ - the beam width, $2b_2$ - the width of beam that after reflection from a cylinder is coming back into antenna, $\xi = h\cos(2\pi\frac{y}{\Lambda}+\varphi_0)$, h, Δ, φ_0 - amplitude, wavelength and starting phase of fluctuations, $\eta = \sin\varphi_1 - \sin\varphi_2$, φ_1 and φ_2 are the incidence and reflection angles. The amplitude A and phase P response of reflected wave (Fig.5) were calculated as

$$A = \rho\rho^*,\ P = arctg\frac{\mathrm{Im}\,\rho}{\mathrm{Re}\,\rho}.$$

The main conclusion of these calculations is that in our case the accurate (within 10-20%) measurement of density fluctuation level is possible only at low frequency part of observed spectrum ($\Omega < 50$ kHz).

The main conclusion of this work is that the *dual polarization correlation reflectometry is a useful extension of correlation reflectometry* for magnetically confined plasmas.

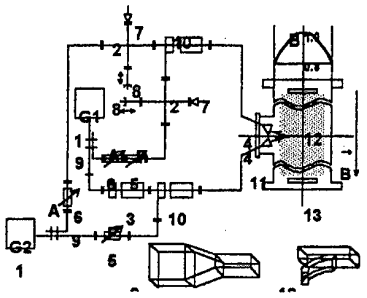


Fig.1 Layout of experiment and dual polarization reflectometer. 1-microwave oscillator; 2- magic T; 3- special taper; 4-antennae; 5-phase turner; 6- attenuator; 7- detector; 8- plunger; 9 – coupler; 10- dual polarization coupler; 11- discharge vessel; 12- plasma column; 13- cathode.

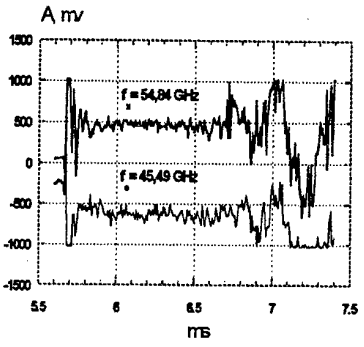


Fig.2 Typical outputs of dual polarization reflectometer

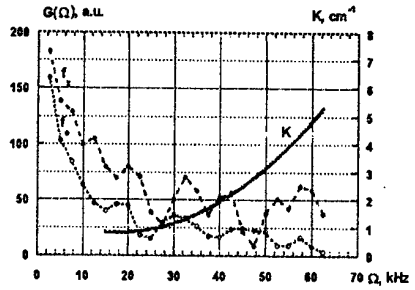


Fig.3 Spectra of phase fluctuations observed at O- and X-mode waves and the wave equation.

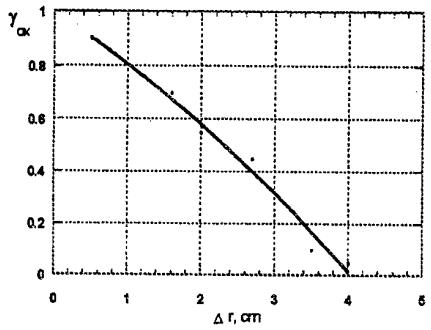


Fig.4 Cross-correlation between O- and X- mode phase fluctuations versus the distance between reflecting layers.

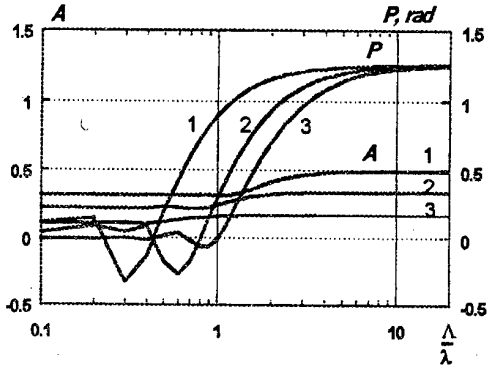


Fig.5 The amplitude **A** and phase **P** response of the finite size microwave beam with wavelength of λ reflected from the cylindrical plasma surface with density perturbations with wavelength Λ. [λ=1cm, h=0.2 cm, parameter of curves – $\rho = \frac{r_{cut-off}}{R}$ ($r_{cut-off}$ - radius of reflecting surface); 1 - ρ =0.9; 2 - ρ=0.7; 3 - ρ=0.4]

References

[1] C.R.Hanson, J.H.Harris at al, Nuclear Fusion, **32,** 1593 (1992)
[2] A.I.Skibenko, O.S.Pavlichenko at al, 23rd European Physical Society Conference on Controlled Fusion and Plasma Physics, Kiev (1996), Part III, p.1124
[3] G.D.Conway, Rev. Sci. Instrum., **64(10)**, 2782 (1993)

GRAPHITE-MADE UHF RESONATOR OF FABRY-PEROT TYPE FOR INVESTIGATION OF THE PLASMA DIVERTOR FLOW IN FUSION DEVICES AND THE SMALL-SCALE PARTICLES OF A SUBSTANCE

V.L.Berezhnyj, V.S.Voitsenya, V.L.Ocheretenko, A.I.Skibenko, I.P.Fomin
IPP of NSC KhPTI, Akademichna St.1, Kharkov, 310108, Ukraine

The UHF resonator device has some definite advantage comparatively to an interferometer scheme in measuring parameters of plasma flow[1]. The resonator allows to measure the plasma density of 2-4 orders in magnitude lower than the critical density for the given frequency, and it can be used for thin plasma layer (when layer thickness ~ wavelength) as well as for investigation of fluctuations in a plasma flow[2]. There is a reason to change the metallic mirrors of UHF resonator by ones made of graphite with an aim to lower the degradation of these element and to preclude the ingress of heavy metal impurities into the plasma, when the resonator are subjected to fluxes of plasma, neutron, gammas and heating in fusion devices. The measurement of carbon-graphite materials (CGM) plates reflectivity show that it compose 0.8-0.96 of metallic plate reflectivity on different frequencies (30-105 GHz). The results of plasma influence on reflectors made of CGM showed small increase of their reflectivity with stronger effect for shorter wavelength. The improvement of reflectivity can be explained by decrease of the surface roughness. The test of CGM element under heating up to 1000C (20 cycles) did not cause degradation of their surface and their reflectivity R increase up to 700-800C due to the graphite electroconductivity increase.To simulate effects of neutron irradiation the CGM reflectors were irradiated in the reactor up to $F=2x10^{22}/cm^2$. The R values were measured at l=337 μm and dropped at initial 0.9 to 0.78. Thus the CGM can be using for fabricating the UHF resonator mirrors[3].

To study the properties of resonators made of CGM the transmitted resonator was fabricated with graphite mirrors, with diameter d=70 mm, curvature radius ρ=100 mm and connection holes of 1.5 mm in diameter. The distance between mirrors, L, were variable in the range 10-100 mm. The frequency of the unloaded resonator (f=36.47 GHz) was not changed significantly when L was changed.

However, with L increasing there were observed some increase of the quality factor, Q, and decrease of the resonance amplitude, A. Important fact is that the measured Q for graphite-made resonator was only 5-10 times lower in comparison to Q of the identical copper resonator, in spite of much higher difference predicted on the base of the electrical conductivity ratio: $(\sigma_{Cu}/\sigma_C)^{1/2}=50$. It is evident from this fact the contribution of diffraction losses in the case of a graphite resonator is less than in the case of metallic one, where such losses determine the Q value.

For L=60 mm and with Q measured, the minimal density is $(n_eL)_{min}=10^{10}/cm^2$, and the maximum value of (n_eL) is determined by the frequency sweeping range. Taking into account the realignment range of a

Gan type solid diode (i.e., Δf=0.5-1.0 GHz) the $(n_eL)_{max}$ can be found as ~$7x10^{12}/cm^2$. Therefore, in reality the range of n_eL to be measured, with small influence on the resonator characteristics, will be limited by meanings: $1x10^{10}$-$(1-5)x10^{12}/cm^2$.

To check effects of heating on resonator properties, the measurements were carried out when temperature of one mirror varied up to 300C, using Ohmic current. We observed the increase of the resonance amplitude, A, (up to 30%) and the shift of the resonant frequency. These results can be explained, correspondingly, by increasing the graphite conductivity due to temperature growth and by some changing of L due to thermal expansion.

So, the heating of mirror will lead to errors related to measurement of the frequency shift, however, this error will be small and controlled for slow temperature change.

The possible application of graphite resonator consider for the investigation of the small-scale particles of the substance and the dust formations (their sizes, dielectric permittivity, density) at the conditions of the considerable temperature changes too.

If the dielectric sphere go in resonator volume the resonance frequency shift may be written[4]:

$$\Delta f = f\, 4\pi/v(\varepsilon-1)/(\varepsilon+2)\, r^3N,$$

where f, v- resonance frequency and volume, ε- dielectric permittivity, r- sphere radius, N- density. The determination of dielectric permittivity, radius and velocity of sphere carry out by using of two resonator, excited on different frequencies taking into account the resonator field attenuation stipulated by ball. Fig.5-6 shows resonance frequency on ε value (f=37 GHz, v=10 cm^3, r=0.1 cm) and on sphere radius (f and v- are same, ε=3).

Thus graphite UHF resonator can be advisable for measurement of plasma flow density and small particles parameters if resonators mirrors may be subjected to influence that lead to their surface degradation.

References

1. D.K.Akulina, J.I.Nechaev. UHF methods of plasma density measurements on FIAN stellarators. Stellarators, v.65 (1973) 100-133, Izdatel'stvo "Nauka", Moskow (in Russian).

2. A.I.Skibenko, O.S.Pavlichenko at al. Density Fluctuations Studies for the "Uragan-3M" torsatron via Microwaves. 23rd European Physical Society Conference on Controlled Fusion and Plasma Physics, Kiev (1996) PartIII, p. 1124.

3. V.S.Voitsenya, V.L.Berezhnyj, V.V.Chebotarev at al. On the possibility of using carbon-graphite materials for the inner elements of millimetre and sub-millimetre diagnostics of fusion plasma, Fusion Engineering and Design 34-35(1997)491-494.

4. L.A.Vajnshtejn. "Otkrytye resonatory i otkrytye volnovody". Izdatel'stvo "Sovetskoe radio", 1966, Moskow (in Russian).

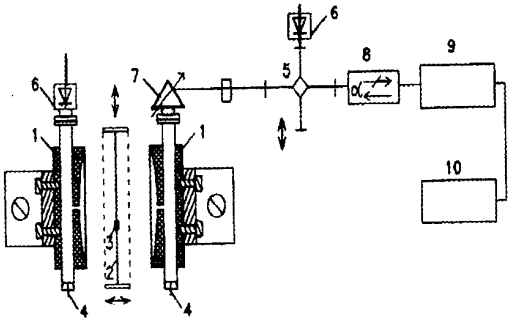


Fig.1. Resonator lay-out: 1-graphite spherical mirrors; 2,3-suspender and exasperating body; 4-waveguides; 5-magic T; 6-detector; 7-agreementing element; 8-isolator; 9-generator of modulation pulses.

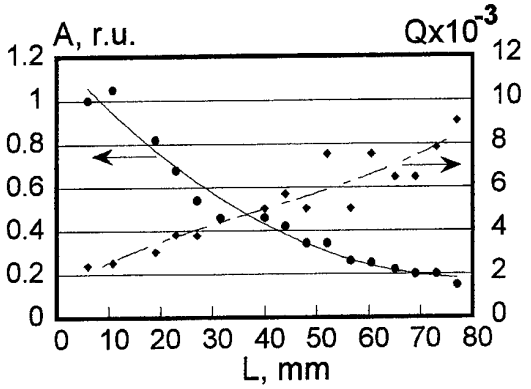


Fig.2. Dependence of amplitude and factor Q on the distance between mirrors.

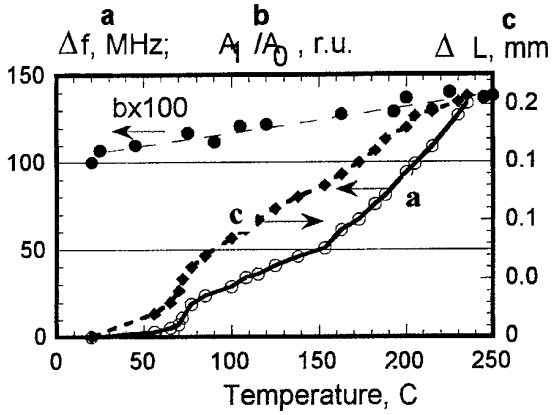


Fig.3. Dependencies of frequency shift, resonator and resonance amplitude on mirror temperature.

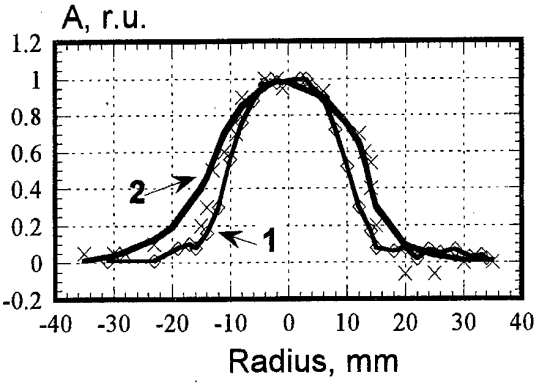


Fig.4. Radial distribution of UHF field at l=36mm (1) and l=58mm (2) from the mirror.

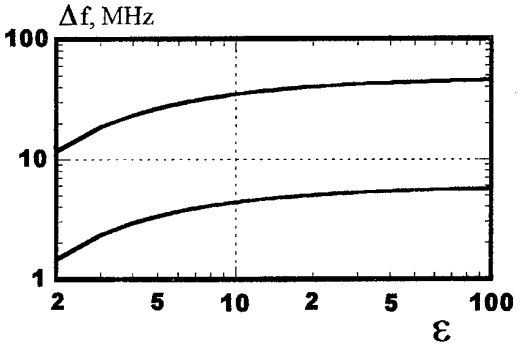


Fig.5. Frequency shift versus ε.

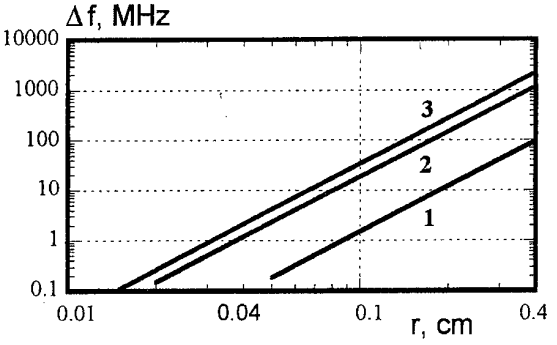


Fig.6. Frequency shift versus size of microparticles: 1 - ε=1.01; 2 - ε=3; 3 - ε=10.

EXTENSION OF FUNCTIONAL POSSIBILITIES OF MM-RANGE MODULATION RADIOMETERS

Yu.A.Skripnik*, A.F.Yanenko**
*Academy of Light Industry of Ukraine, 252601, Kiev, Nemirovich-Danchenko str. 2,
**Scientific Research Center of Quantum Medicine VIDHUK,
252033, Kiev, Vladimirskaya str. 61-b.

The problem of measuring the low values of power of electromagnetic oscillations peculiar to noise and monochromatic signals is very urgent for radioastronomy, physics, biology and medicine as well as for many other branches of science and engineering [1, 2, 3]. Usually, to measure the power of low-intensive non-modulated radiations the use is made of high-sensitivity measuring receivers, i.e. radiometers, designed according to compensation, modulation or correlation schemes. From the viewpoint of hardware realisation and accuracy, sensitivity and resolution, the most advantageous is the scheme of one-channel modulation radiometer [4].

With this in mind, the mm-wave range unit based on commutational transformation is considered in [3]. The device allows for measuring the power of noise signals at $1 \cdot 10^{-18}$ W/Hz level, and monochromatic ones at $1 \cdot 10^{-12}$ W. It is used for metrology estimation of equipment parameters in microwave resonance therapy [2]. High-sensitivity unit for measuring the objects' radiation power suggested in [5] provides an increase (by 1-2 orders) of sensitivity of the well-known circuits of modulation radiometers resulting in extension of their possibilities when such an equipment is used for scientific investigations in the field of radiowave measurements of radiation originating from the objects. However, today's research involve the problems of measuring not only the power of mm-range signals but also some other information parameters, i.e. frequency and phase shift, reflection and absorption coefficient, auto- and intercorrelative signal functions which brings about the necessity of designing complex measuring systems.

One of the most important characteristics of random signals is a correlation function of there signals. The correlation function among the values of the same random signal $x(t)$ is defined as an autocorrelation function and has the form

$$R(\tau) = \lim_{T\to\infty} \frac{1}{T} \int_{-T/2}^{T/2} x(t) \cdot x(t-\tau) \cdot dt ,$$

where τ is delay interval time of the random signal.

The cross-correlation function for the values of two random signals $x(t)$ and $y(t)$ is defined

$$R_{xy}(\tau) = \lim_{T\to\infty} \frac{1}{T} \int_{-T/2}^{T/2} x(t) \cdot y(t-\tau) \cdot dt .$$

When studying radiothermal emanation from biological and other objects, the necessity arises to measure autocorrelation as well as cross-correlation functions without loss of possibility of concurrent registration (measurement) of radiation power.

Classical scheme of correlation radiometer includes two identical high frequency transformation channels with outlets switched to a multiplier realising the function $x(t)x(t-\tau)$ or $x(t)y(t-\tau)$. Availability of two transformation channels considerably complicates the task of engineering implementation of the given radiometer, the more so in SHF range. On the basis of commutation-modulation transformation, the authors have designed one-channel radiometer scheme which is much more easily realised. The simplified scheme of modulation-correlation radiometer which measures random signals power and also permits to register their autocorrelation function is given in the figure. One-channel radiometer operates as follows.

Radiothermal radiation of the investigated object is received by antenna X1 and sent via commutator S1 to the first level of U1 transformation. Commutator S1 is switched at F_1 frequency

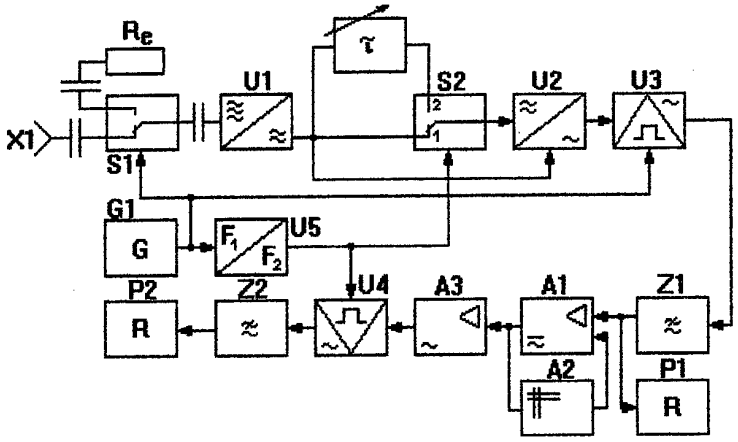
of the reference generator G1, and commutator S2 with F_2 frequency, and here $F_2 < F_1$. As a result, at the output of the first transformation level, packages of noise signals are formed by turn, at intermediate frequency, and here the signals dispersions are

$$\sigma_1^2 = S_{U1}(\sigma_a^2 + \sigma_{U1}^2), \quad (1)$$

$$\sigma_2^2 = S_{U1}\sigma_{U1}^2, \quad (2)$$

where $\sigma_a^2 = S_a T_x$ is dispersion of antenna's output signal and S_a is antenna's sensitivity, T_x is noise temperature of a signal;

S_{U1}, σ'_{U1} are transformation curvature and eigen noise dispersion of the 1-st transformation level.



Voltage of encircling frequency F_1 is formed at the output of the second transformation level in position 1 of the commutator S2

$$U_{U2}(t) = [(U_1 - U_2)/2]sign \sin 2\pi F_1, \quad (3)$$

where $U_1 = \sigma_1^2 \cdot S_{U2}$; $U_2 = \sigma_2^2 \cdot S_{U2}$, and S_{U2} is the second level transformation factor U2.

Voltage (3) is fed to a multiplier U3 and voltage of the reference frequency F_1 is fed to the second outlet of the same multiplier. We obtain at the output of low-end frequency filter Z1

$$U_{Z1} = S_{U3} \cdot K_{Z1}[(U_1 - U_2)/2](sign \sin 2\pi F_1)^2, \quad (4)$$

where K_{Z1} is a transfer coefficient of low-end frequency filter (LFF), S_{u3} is transformation coefficient of multiplier U3.

Taking into account (1), (2) and the fact that meander product $(sign \sin 2\pi F_1)^2 = 1$, the expression (5) can be written as

$$U_{Z1} = S_0\sigma_a^2 \quad (5)$$

where S_o is curvature of transient transformation of a radiometer channel.

As can be easily seen from (5), voltage at LFF1 output is proportional to the power of thermal radiation σ_1 of the object being investigated. The voltage is measured and registered by registration unit R1.

At the output of the second level transformation in position 2 of commutator S2 there is formed the voltage of encircling videopulse frequency F_1 proportional to correlation moments $R_1(\tau)$ and $R_2(\tau)$

$$U'_{U2}(t) = [R_1(\tau) - R_2(\tau)]/2(sign \sin 2\pi F_1),$$

and here $R_1(\tau) = S_{U2}\sigma_a^2\rho_a(\tau)$, where ρ_a is a normalised correlation function of a mixed eigen noises of the first transformer and antenna's signal, $R_2(\tau) = S_{U2}\sigma_2^2\rho_{U1}(\tau)$ and ρ_{U1} is the normalised correlation function of eigen noises of U1 transformer.

At the output of low-end frequency filter Z1, due to independence of antenna's noise signal and eigen noises of U1 transformer, the voltage will obtain the form

$$U'_{Z1} = S_0\sigma_a^2\rho_a(\tau) \quad (6)$$

Owing to the absence of delay in the unit τ ($\tau = 0$), the normalised correlation function attains the unity value $\rho_a(0) = 1$. Thus the earlier obtained voltage (5) corresponds to the maximal value of correlation moment, i.e., signal power.

In case of τ unit delay, correlation moment decreases and so does the value of correlation function $\rho_a(\tau) < \rho_a(0)$. Hence, for $\tau > 0$, voltage (5) is always higher than voltage (6).

Periodic switching of commutator S2 at frequency $F_2 < F_1$ at filter Z1 output, successively forms constant voltages (5) and (6) within time interval $\Delta t = 1/2F_2$. Amplification factor of the amplifier A1 is automatically adjusted by the unit A2.

Taking account of amplification factor K_{A1}, the pulse amplitudes obtain the values

$$U_{A1} = K_{A1} S_0 \sigma_1^2, \qquad 0 < t < 1/2F, \tag{7}$$

$$U'_{A1} = K_{A1} S_0 \sigma_1^2 \rho_a(\tau), \qquad 1/2F < t < 1/F. \tag{8}$$

Amplifier A3 defines and reinforces the variable component of the frequency F_2 voltage

$$U_{A3} = K_{A3}[(U_{A1} - U'_{A1})/2] sign \sin 2\pi F_2. \tag{9}$$

Variable voltage (9) enters U4 multiplier input, while rectangular voltage of the reference F_2 frequency is fed to the second input, which results in the voltage

$$U_{Z2} = S_{U4} K_{A3} K_{Z2} [(U_{A1} - U'_{A1})/2](sign \sin 2\pi R F_2)^2. \tag{10}$$

at the output of low-end frequency filter Z_2. Substituting the voltage values (7) and (8) into expression (10) we obtain

$$U'_{Z2} = S_0 S_{U4} K_{A1} K_{A3} K_{Z2} [1 - \rho_a(\tau)] \sigma_a^2. \tag{11}$$

Amplification factor K_{A1} is determined by the action of the unit A2 on the control input of the amplifier A1. Under conditions of inertial operation of the unit A2 (quick wear and tear and slow restoration) amplification factor is defined by the higher amplitude in a succession of voltage pulses (5) and (6). Due to the fact that voltage (5) is always higher than voltage (6), the amplification factor A1 can be written as

$$K_{A1} = U_0 / U_{Z1} = U_0 / S_0 \sigma_a^2 \rho_a(0), \tag{12}$$

where U_0 is output voltage of amplifier A1 in a limitation mode (U_0=const).

Substituting the value (12) into (11) we obtain the voltage

$$U''_{Z2} = S_{U4} K_{A2} K_{Z2} [\rho_a(0) - \rho_1(\tau)] / \rho_1(0) = \alpha [\rho_a(0) - \rho_1(\tau)] \rho_1(0),$$

which is registered by a recorder P2.

Successive variation of τ delay allows for registering the relative changes of correlation function $\rho_a(\tau)$ of the received signal. The latter makes it possible to analyse the structure of radiothermal radiation and also to identify its source in SHF and mm-wave length ranges. And what is important, the measurement result is not influenced by the level of receiving signal (σ_a^2), the level of eigen noises of transformer (σ_{U1}^2) and nonstability of transformation coefficients $S_0, S_{U4}, K_{Z1}, K_{A1}, K_{A3}, K_{Z2}$. Transformation coefficient is α stable and is determined in the process of radiometer calibration.

REFERENCES

1. Sit'ko S.P., Mkrtchian L.N. Introduction to Quantum Medicine. - K.: Pattern. - 1994. - 146p.
2. Sit'ko S.P., Yanenko A.F. Direct registration of non-balanced mm-range electromagnetic radiation of a human body // Physics of the Alive. - v.5. - №2. - 1997. - p.60.
3. Skripnik Yu.A., Yanenko A.F. Problems of measuring low-intensive mm-wave range radiation. Proc. sci./theor.conf. "SKIT-97" - Muk.: 1997; 1997, p.153-157.
4. Skripnik Yu.A. Measuring devices with commutation-modulation transformations. - K.: Vyshcha shkola, 1975 - p.250.
5. Skripnik Yu.A., Peregudov S.N., Yanenko A.F. High-sensitivity instrument for measuring the objects radiation power. Mat.of III Infern. sci./pract.conf. "Modern technologies in aerospace complex". - 1997, p.160-162.

INVESTIGATION OF A NEW QUASI-OPTICAL WAVEGUIDE MODELING METHOD FOR BACKWARD AND FORWARD SCATTERING STUDY IN MILLIMETER AND SUBMILLIMETER WAVE BANDS

V.K. Kiseliov, T.M. Kushta, and P.K. Nesterov
Institute of Radiophysics and Electronics of the National Academy of Sciences of Ukraine
12, Acad. Proskura St., Kharkov, 310085, Ukraine
Phone:38 0572 448335, E-mail: kiseliov@ire.kharkov.ua

We have previously proposed [1] a new quasi-optical waveguide modeling (QWM) method for RCS measurement under laboratory conditions. In the method, the object under investigation is situated into a quasi-optical waveguide structure which presents a circular hollow dielectric waveguide (HDW), and the main waveguide mode, HE_{11}, scattering parameters are determined. The parameters are related to the object under investigation RCS in a quite definite manner. The HDW presents a remarkable combination of useful properties because it is a guiding, forming and filtering quasi-optical structure that allows to place sufficiently large (as compared with wavelength) nonuniformities in its waveguide channel. Owing to the properties, in conjunction with HE_{11} mode field quasi-plane character and some other HDW merits, it turned out possible to simulate the conditions for electromagnetic wave scattering by an object placed in certain region inside the HDW that are close to the conditions existing when a uniform plane wave is scattered by the same object placed in free space. Therefore, HDW plays in the QWM method the role of the main component of a micro-compact range intended for the study of scattering characteristics of various physical objects under laboratory conditions in the short millimeter and submillimeter wave bands.

When describing electromagnetic wave scattering by physical objects (scatterers) in free space, the following important parameters are usually used: scattering cross section, C_{sc}; extinction cross section, C_{ext}; absorption cross section, C_{abs}; and radar scattering cross section, C_b (RCS).

Scattering cross section is defined by the known formula [2]

$$C_{sc} = \int_0^{2\pi}\int_0^{\pi} \frac{\left|\vec{X}\right|^2}{k^2} \sin\theta d\theta d\varphi = \int_{4\pi} \frac{\left|\vec{X}\right|^2}{k^2} d\Omega , \qquad (1)$$

where $\left|\vec{X}\right|^2 / k^2$ is the differential scattering cross section that characterizes the scattered electromagnetic wave angular distribution. In particular, if the real scatterer is replaced by a hypothetical one for which the vector scattering-amplitude $\vec{X}$ does not depend on direction and is set to be equal to the real scatterer scattering amplitude in the backward direction (θ=180°), i.e. $\vec{X} = \vec{X}\left(180^0\right)$, then we obtain the following formula for radar scattering cross section:

$$C_b = \frac{4\pi\left|\vec{X}\left(180^\circ\right)\right|^2}{k^2} . \qquad (2)$$

In this case, when considering the far zone field, the extinction cross section can be expressed by formula [2]

$$C_{ext} = \frac{4\pi}{k^2}\mathrm{Re}\left\{\left(\vec{X} \quad \vec{i}_x\right)_{\theta=0}\right. . \qquad (3)$$

The formula represents a special formulation of the optical theorem. The theorem is common for all kinds of scattering and expresses the fact that the extinction depends only on the scattering amplitude in the forward direction. At the same time, extinction is the result of both absorption in the body and scattering in all directions [2].

If the scatterer is surrounded by a nonabsorbing medium, the absorption cross section, C_{abs}, can be obtain merely from the relation

$$C_{abs} = C_{ext} - C_{sc}. \qquad (4)$$

For the correctness of the interpretation of the measuring results obtained with the help of QWM method, a one-to-one correspondence should be established between the measured coefficients of the waveguide

mode scattering by a scatterer placed into the HDW and the characteristics of plane wave scattering by the same object being in free space. For finding the correspondence, we have used the Lorenz's lemma [3] and the orthogonality condition for HDW guided modes.

From this one can obtain a waveguide analogue of extinction cross section for a scattering body, the analogy being defined through the waveguide parameters of the body:

$$C_{ext}^{w} = \frac{2N_i \mathrm{Re}\, c_{+i}}{I_{inc}}. \qquad (5)$$

Here I_{inc} is the maximum intensity of the mode incident on the body, C_{+i} the transmission coefficient of the mode.

This expression is waveguide analogue of the optical theorem (3). Moreover, the expressing allows to formulate the following conclusion: if one forms a quasi-plane wave within the limits of a scattering body placed into the HDW and reduces to a minimum the rereflections between the body and the waveguide walls, then one can define the scattering body extinction cross section by the measuring of the transmission coefficient of the incident wave.

By this manner, one can obtain also the expression for RCS presented in [1] for the scattering in a waveguide:

$$C_{b}^{w} = \frac{k^2 N_i^2 |c_{-i}|^2}{\pi I_{inc}^2}. \qquad (6)$$

Expressions (5) and (6) establish a connection between the direct and backward scattering characteristics in free space and in a waveguide. Under some aforementioned conditions, the characteristics are identical.

For the illustration of the QWM method effectiveness, the dependence on the diffraction parameter kb is presented in Fig.1 of the backward scattering effectiveness $\sigma_b^w = C_b^w / \pi b^2$ by a perfectly conducting sphere with radius b situated in a circular HDW with radius a. The dependence is calculated for the main mode HE_{11} and ka=38. An analogous dependence for the extinction effectiveness $\sigma_{ext}^w = C_{ext}^w / \pi b^2$ is presented in Fig.2. For comparison, in both figures the corresponding dependences calculated with the help of Mie theory for free space are presented. As can be seen, the QWM method gives a good conformity with the free space data even for comparatively large b/a values.

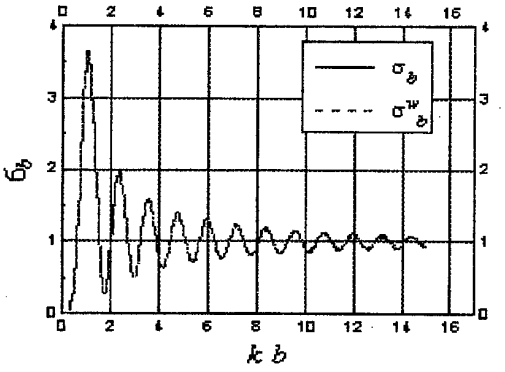


Figure 1.

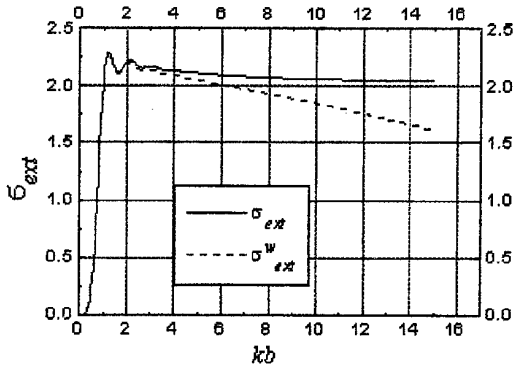


Figure 2.

We have designed a laboratory installation (its simplified diagram is presented in Fig.3) for the experimental study by the QWM method of the amplitude-and-phase characteristics of the physical objects and their scaled models forward and backward scattering in the short millimeter and submillimeter wave regions of electromagnetic waves spectrum. The installation is a quasi-optical waveguide micro-compact range (MCR) based on a circular 40mm in diameter HDW. The high-frequency part of the installation is executed with the use of HDW-based quasi-optical devices and components, as well as of standard waveguide microwave components. The low-frequency part is carried out with the use of IBM PC/AT – based hardware and software, as well as of unified modules executed in KAMAK standard. In the MCR, the homodyne principle with frequency transformation is used, the transformation being carried out with the Fox's waveguide continuous phase shifter. The parasite background signals compensation is made with the help of a regulable (by the phase and modulus)

quasi-optical loading installed in the lateral arm of the quasi-optical beam divider having a polarizing wire grating.

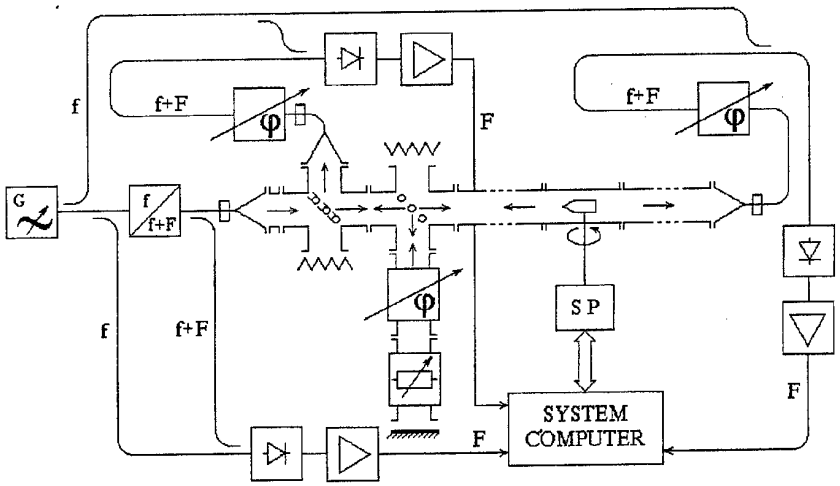


Figure 3. Quasi-optical waveguide micro-compact range

As an illustration, some measurement results obtained with the use of the MCR in the 4mm wavelength range are presented in Fig.4.

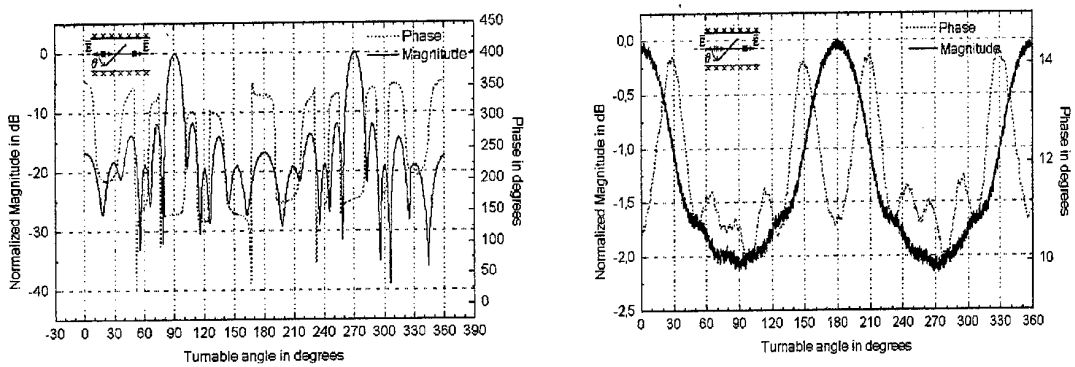


Figure 4. The amplitude-phase diagrams of the backward scattering (a), and forward scattering (b) of a 10x10mm metal plate placed into HDW (F = 74Ghz, H-H polarization)

Hence, as a result of the investigation, the possibility is theoretically and experimentally corroborated of the use of the proposed quasi-optical waveguide modeling method for the study of physical objects forward and backward scattering characteristics in the short millimeter and submillimeter wave bands.

References

1. V.K. Kiseliov and T.M. Kushta, «Principles of a New Compact Range Technique for the Submillimeter Wave Region», In: Proc. 19th Meeting & Symposium AMTA'97, Boston, Massachusetts, pp.524-528, November 17-21, 1997.
2. C.F. Bohren, D.R. Huffman, «Absorption and Scattering of Light by Small Particles», John Wiley and Sons, New York, pp.77-106,1986.
3. L.A. Vainshtein, «Electromagnitnyye volny», Radio i Sviaz', Moskva, pp. 289-306, 1988.

ABOUT DIGITAL PROCESSING SIGNALS OF THE DYNAMIC SPECTRUM FOURIE

V.K.Lapty
Institute of radiophysics and electronics by A. J. Usikov NAS of Ukraine
12 Ac.Proskura St,310085,Kharkov, Ukrain,Ph/Fax:+380(572)441105

Adoption dynamic spectrum (DS) - three- dimensional function a spectral denseness (SD) depending on frequency and time - for spectral representation of acoustic signals is new methodical basis on the signature analysis of acoustic processes [1]. For systems and processes with periodic excitation dynamic spectograms allows to receive representation not only about change intignations of spectral structure working system, but also about peak - frequency to the characteristic of system on transitive conditions, for example with reference to the mechanism, in condition of start (on rise of revolutions) or in a condition drop (on descent of revolutions). The typical example DS can be served by continuous registration of SD vibrations for the case when the electric motor depending number of revolutions after switching-off it from a source of the power supplies at gradual delay the rotation of rotor up to end stop [2].

Because difficulty of quantitative interpretation the spectral information of DS, their application is limited mainly for the qualitative characteristic of the processes and systems. The present message is devoted to a problem the digital processing of signals (DPS) [3] DS with the purpose simplify of their quantitative interpretation.

We shall present a target signal of researched system on a transitive conditions by a temporary sequence N of realizations of function $X_n(t)$, where the moments of time of realizations are chosen proceeding from necessity of maintenance constant discrete change of the period. If the period of target signal in each of N positions during time necessary for registration is kept constant, it is possible to consider function $X_n(t)$ periodic and in each position it is possible to spread out her in the Fourie row[4]

$$X_n(t) = \sum_k A_k \cos\left(\frac{2\pi k}{T_n} t + \varphi_k\right), \tag{1}$$

where: T_n -period of target signal on the moment of registration, A_k and φ_k -amplitude and phase of factors of decomposition. Let discrete the change of the period of a target signal is chosen ΔT, then $T_n = T_0 + n\Delta T$ and by results of researches can be generated the matrixes

$$((A)) = \begin{vmatrix} A_{11} A_{12} \cdots A_{1s} \\ A_{21} A_{22} \cdots A_{2s} \\ \cdots\cdots\cdots \\ A_{n1} A_{n2} \cdots A_{ns} \end{vmatrix};$$

$$((\varphi)) = \begin{vmatrix} \varphi_{11} \varphi_{12} \cdots \varphi_{1s} \\ \varphi_{21} \varphi_{22} \cdots \varphi_{2s} \\ \cdots\cdots\cdots \\ \varphi_{n1} \varphi_{n2} \cdots \varphi_{ns} \end{vmatrix}; \tag{2}$$

where: an index S - number of a harmonic for which made the truncation of the row (1). At a correct choice of an interval ΔT (correspond to the theorem of Shenon-Kotelnikov [5]) and if the experimental techniques are realized according to the accepted above assumptions that of a matrix (2) reflect DS of researched system in a transitive conditions, are its spectral " by a portrait " and rather full hercharacterize. The technique on the first sight is represented obvious, however its practical use for concrete systems, and evident representation of results the expenses of significant efforts require. So the analysis of multielement matrixes (2) hardly will allow by the

certain image to characterize system, or to compare among themselves characteristics of two systems. Therefore there is a necessity of graphic representation of results.

The difficulty quantitative interpretation the received information file of discrete spectrum in a graphic kind also puts under doubt expediency of use him as the quantitative characteristic of system. However, as has shown the analysis of structure the received spectral file, these difficulties overcome is alloved, and are caused by that submitted in a file DS harmonious components of various numbers k are non-comparable on frequency scale (frequency scale of components is equal to number of a harmonic) and beginning of readout of frequencies dependences of each discrete harmonic with frequency by a scale of the basic tone (period) of excitation.

We shall consider a matrix frequency of argument (3) characteristics under the formula (1), where on horizontal lines the dependence on discrete change of the period T_n, and on vertical lines dependence on numbers of harmonics k is given; the scale of the basic frequency of the period on horizontal lines is supposed linear

$$((\omega))=\begin{vmatrix} \frac{2\pi}{T_0} & \frac{2\pi}{T_0+\Delta T} & \frac{2\pi}{T_0+2\Delta T} & \cdots & \frac{2\pi}{T_0+n\Delta T} \\ \frac{4\pi}{T_0} & \frac{4\pi}{T_0+\Delta T} & \frac{4\pi}{T_0+2\Delta T} & \cdots & \frac{4\pi}{T_0+n\Delta T} \\ \cdots & \cdots & \cdots & \cdots & \cdots \\ \frac{2\pi k}{T_0} & \frac{2\pi k}{T_0+\Delta T} & \frac{2\pi k}{T_0+2\Delta T} & \cdots & \frac{2\pi k}{T_0+n\Delta T} \end{vmatrix} \qquad (3)$$

from (3) shifts of a beginning of readout of frequency for harmonics with number k concerning frequency of the basic tone at a linear scale of frequency of the basic tone makes

$$\delta\omega_k = (\omega_k - \omega_1) = \frac{2\pi \cdot \ k}{T_0} - \frac{2\pi}{T_0} = \frac{2\pi}{T_0}(k-1) = \omega_1(k-1) \ , \qquad (4)$$

The distinction of scale of frequency of harmonics with number k concerning scale of the basic frequency of the period makes

$$M_k = (\omega_{kn} - \omega_{k0}) \cdot (\omega_{1n} - \omega_{10})^{-1} = (\tfrac{2\pi k}{T_n} - \tfrac{2\pi k}{T_0}) \cdot (\tfrac{2\pi}{T_n} - \tfrac{2\pi}{T_0})^{-1} = k; \qquad (5)$$

where: ω_{kn}, ω_{k0} - frequency k of harmonic for n- th and 0-th discrete changes of the period; ω_{1n}, ω_{10} - frequency of the basic tone for n-th and 0-th discrete changes of the period. At the expense application artificial convertible operation for reduction the set of readout discrete Fourie of spectrum to uniform scale and beginning of readout of frequency conterminous with frequency the scale of the basic tone of excitation of sounding is exists an opportunity elimination of lack of the characteristic (2). This procedure requires introduction for each harmonic of settlement shift beginning of readout of frequency (shift of a beginning of lines to the right) (4) and change of scale of frequency for each harmonic (stretching of length of numbers of readout on lines by the appropriate scale increase of intervals between readout) (5). Performance above described procedure of reduction of a spectral information file to uniform rectangular system of coordinates (ordinate - module of amplitude of harmonic or phase, abscice - basic frequency of the period or period, aplicate - number of harmonic) limiting simplifies interpretation of the characteristic at complete preservation of its positive properties - information completeness and presentation.

In figure 1. it's the example of realization offered DPS DS with reference to spectral-frequency the characteristic of timbre of sounding of a grand piano is submitted. In figure 1. the designations are accepted: Ak - module of amplitude k-th harmonic; $-LogT$ - parameter of the period numerically to equal basic frequency of

the period of excitation of a signal; k - number of harmonics; by digits 1,2,3... are marked the numbers apropriate of harmonics.

The basic area for application of the offered form of representation DS, in our opinion, is the area of functional diagnostics (decision of the task for recognition of the image) [6] wide diapasone of periodic

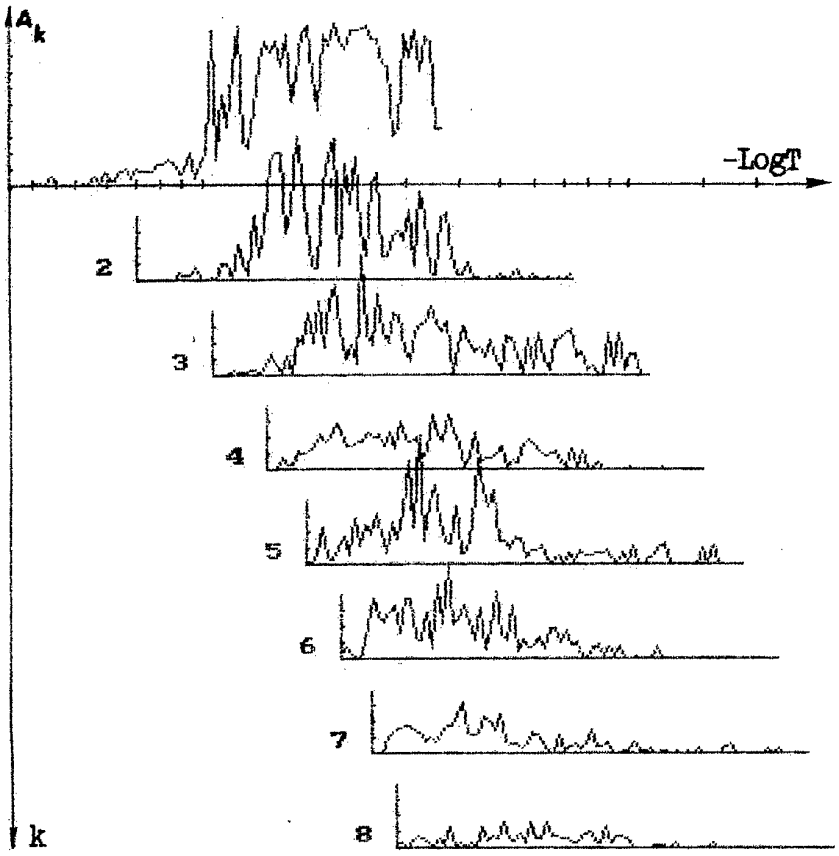


Figure 1. Example DPS of DS sounding of grand piano.

oscillatory systems with the expressed nonlinearity: in area vibrodiagnostiks, coherent radar-location, medicine, etc. A clear advantage for the offered spectral-frequency characteristic in relation to the initial traditional form DS is the comparability of all spectral components in uniform system of coordinates and simplicity interpretation of their dependences from everyone variable separately, and also opportunity of the analysis nonlinear properties of system [5,7] in all a range of change her period.

References

1."Vibroacustitcheskaja diagnostica zarogdajutchichsja defektov".Red. d.t.n., M. D. Genkin,Nauka, M., pp. 106,1984.
2. Firma Brjul & Kjer., "Kratkij katalog 1989/90." fig.861591, pp. 47.
3. "Primenenie zifrovoj obrabotki signalov." Red. E.Oppenheim, perevod s angl.Mir,M., pp.5,1980.
4. I.S.Gonorovskij, " Radiotechnitcheskie cepi i signaly". Radio i svjaz, M.,pp. 17, 1986.
5. A.P.Zinovjev, P.I. Filippov "Vvedenije v teoriju signalov i cepej". Vyschaja chkola, M., pp.41,222, 1975.
6. "Vibrazii v technike". Spravotchnik v 6 t., Izmerenia i ispytanija. T. 5 . Red. d.t.n., M. D. Genkin , Mashinostroenie, M., pp. 384,1981.
7. C.P.Nikias,M.R.Raguver "Bispectralnoe ocenivanie primenitelno k zifrovoj obrabotke signalov", TIIER, v.75, N7, pp. 5, 1987.

PROFOUND SPECTRAL-FREQUENCY ANALYSIS OF THE CARDIOGRAMS

V.K.Lapty
Institute of radiophysics and electronics by A. J. Usikov NAS of Ukraine
12 Ac.Proskura St,310085,Kharkov,Ukrain,Ph/Fax:+380(572)441105

Functional diagnoses of the heart based on the analysis of electrical biopotentials of working heart, has arisen in boundary scientific area between physics and medicine, and it has borrowed physical methods of research. Out the positions of the physics the periodic electrical biopotentials of the heart represent an output signal of some oscillatory system and, therefore, they can to analyse by appropriate methods. One of most effective modern methods performance of periodic oscillatory systems is the dynamic spectrum (DS), which itself representing three-dimensional function a spectral denseness (SD) dependet on time and registered on a transient regime operation of a system; for example, with reference to an electrocardiogram it corresponds to filing SD at a growing or decreasing load [1]. Let's consider a possibility of application DS as informative performance for the purposes of profound functional diagnoses of the heart because it an electrocardiogram.

In world practice of functional diagnoses of the heart is founded on the analysis of the electrocardiograms, describing stationary conditions of operations of the patient; the cardiogram to register wheile the patient heve a peace [2]. With the purpose of an improvement of the diagnosis qualitative tests with various aspects of a load of heart [2] are applied also. The application DS from functional to diagnose of the heart allows to use in diagnose purposes is spectral - frequency an information about biopotentials of heart as in a stationary condition it of work (in rest) and in a transient regime at monotone increase of a load and - or it decrease. For the adequate indicator of a load of heart can be reductions of frequency of heart(RFH) of the patient [2]. For the diagnose purposes the range of a modification of loads can be used from quiescency of the patient up to level limited by sublimiting value RFH for concrete category of the patients [2].

Electrical biopotentials of heart generally represent is the non-stationary process. The process can be reduced to stationary [3] in case limited time of observation and it have a constant load. In this case, as a first approximation , biopotentials of heart can be represented by the determined periodic process, and it express by temporal function $X(t)$. A discrete spectrum Fourier of function $X(t)$- (the value of factors of the Fourier series with number - n) has an aspect [5]

$$C_n = \frac{1}{T}\int_{t_1}^{t_2} X(t)\cdot\exp(-in\omega_1)dt, \qquad (1)$$

where $\omega_1 = 2\pi/T$; and t_1 and t_2 of a beginning and a extremity of an integration.

At discrete change of the period the aproach is fair for any value T, that allows to receive quasicontinuous on the period registration DS of load electrocardiogram, which represents the dependence of the discrete spectrum of the Fourier Cn of a sequence cardioimpulse from a modification of period T. Quasicontinuous DS the Fourier in coordinates phase and number of a harmonics can be graphically represented by a three-dimensional surface of amplitudes of discrete harmonics. Such performance differs from a traditional two-coordinate electrocardiogram by the increased selfdescriptiveness. However contour DS is defined only for discrete values of a period and numbers of harmonicses, that hampers it the interpretation. This shortage is formal can be eliminated as follows.

For everyone single cardioimpulse on the same frequency (period) $\omega_1 = 2\pi/T$ the spectral denseness [4] can be defined

$$S(\omega = n\omega_1) = \int_{t_1}^{t_2} X(t)\cdot\exp(-in\omega_1)dt, \qquad (2)$$

Spectral denseness $S(\omega)$ under the equation (2) differs from factors C_n under the equation (1) only by lack of a factor $1/T$, which can be considered as a scale factor. At a known period T from the cardioimpulse

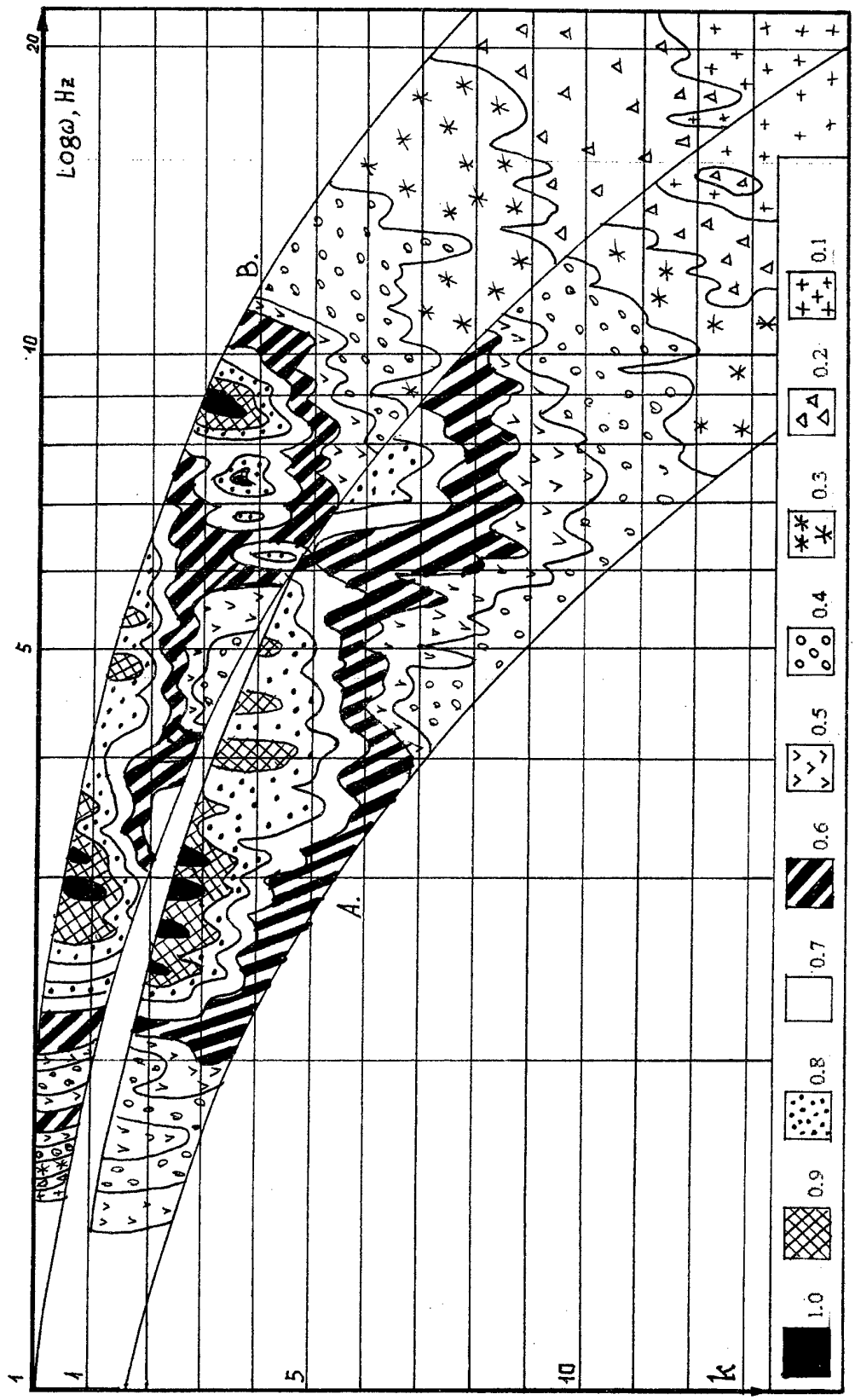


Figure 1. The topography of spectral denseness of electrocardiograms: A - normality, B - pathological.

SD $S(\omega)$ after process of scaling can be combined with enveloping of a discrete spectrum the Fourier C_n. Thus, there is a possibility, map of a load electrocardiogram with the help of DS in the form of a quasicontinuous contour. The discrete of a contour because of a modification of a period can be descrease to necessary values at filing an electrocardiogram or smoothed by an interpolation at its consequent handling.

On figure *1A* and figure 1*B* the examples generated as assotiations $S(\omega)$ for period (base frequency of a period) load electrocardiograms for healthy heart and pathology (ishemia of coronary vessels of the heart) accordingly are shown. Represented on fig.1 the surface for illustration continuous $S(\omega)$ are obtained by a linear interpolation of discrete Fourier spectrum C_n of sequence of cardioimpulses , generally they can be obtained by an integration of a signal of an electrocardiogram under the formula (2) for the given values of its T. DS are represented as the projection of a map of the module of amplitudes of spectral components on a plane laying on coordinate axises: abscissa - base frequency of a period $Log\ (\omega)$ and ordinates - number of a harmonics of a base frequency of a period k. Formal the analysis map shows, that a characteristic dominating site of surface representing DS of an electrocardiogram is the extreme area of surface (area of maximas). The localization of these areas on fig.1*a* (norma) is defined by coordinates on frequency 6-8 Hz and on a harmonics $k = 4$, and in a fig.1*b* (pathology) 2.5-3.5 and 7-9Hz and $k = 3,5$, that corresponds) to sublimiting loads on heart of the patient (for obviousness DS biased to move in begining of the coordinates on $Log\ \omega = 0, 8$ and $k = 1$). By defining diagnostic selfdescriptiveness of surface through it a total derivative in a three-dimensional frame [5] we shall reach to a conclusion, that the most informative area of a surface is the area of localization it extremes ; the periphery of a surface, switching and area of rest used for traditional functional diagnostics of heart, is less informative as here is only performance of a dissipation of dynamic appearances happening in extreme area of a surface. As diagnostic indications the quantitative modifications of coordinates of a displacement and strain of extremums in a case patology concerning a norm can be accepted. In reduced case histories on fig.1*b* a displacement of extremums of pathology surface is a compensate by a displacement of a beginning of a reference. This sketchy analysis illustrative DS of load electrocardiograms shows a simplicity of the interpretation DS at preservation of their high selfdescriptiveness. High diagnostic selfdescriptiveness and obviousness of performance of an electrocardiogram as a surface, and possibility of quantitative differentiation of a pathology from a norm specify on perspective application of the given approach at the analysis DS of the electrocardiogram for the purposes of the profound functional cardiodiagnostic.

References

1. "Vibroacustitcheskaja diagnostica zarogdajutchichsja defektov".Red. d.t.n., M. D. Genkin,Nauka, M., pp. 106,1984.
2. V.N. Orlov, "Rukovodstvo po electrocardiografii". Medicina , M., pp. 47, 1984.
3. V.I.Gaidukevitch, A.A.Melnikova, "Verojatnostnaja obrabotka oscilogram electritcheskich velitchin" Energia, M., pp.13, 1972.
4. I.S.Gonorovskij, " Radiotechnitcheskie zepi i signaly". Radio i svjaz, M.,pp. 17, 1986.
5. "Vibrazii v technike".Spravotchnik v 6 t., Izmerenia i ispytanija. T. 5 . Red. d.t.n., M. D. Genkin , Mashinostroenie, M., pp. 384,1981.



ELECTROMAGNETIC METROLGY

ELECTROMAGNETIC METROLOGY OF MILLIMETER AND SUBMILLIMETER WAVELENGTH BANDS AT LAST YEARS IN UKRAINE

Boris I. Makarenko
Scientific-research Institute of Radio Engeneering Measurements JSC (AT NDIRV)
271, vul. Academika Pavlova, Kharkiv, 310054, Ukraine
Fax: +380-0572-264112, E-mail niiri@onti.uanet.

In recent years, works on electromagnetic metrology were continued in Ukraine, including those covered by the present Symposium wave range. Because of the absence of state programs that could initiate the investigation, the organizing part played the Ukrainian URSI Committe and first of all A, C, and J Commissions and their Chairmen. Unfortunately, because of the known common difficulties in Ukraine, there were no radically new achievements in millimeter and submillimeter waves ranges. But, in my opinion, there are sufficiently interesting results that should be mentioned in this report and thet will be presented in greater detail by the authors of the relevant reports.

Works should be mentioned of professors A. Kleiman and V.Solovyov group (Scientific and Production Association "Metrologiya") on the development of hightly stable frequency standards and their metrologic characteristics measurement devices that can operate over millimeter and submillimeter wave ranges.

The theoretical base of such equipment is laid, in its base the main unit lies which assures measurement of frequency instability with the resolution of (1-3) 10^{-14} for measurement time of 1 s on the frequency of 5 MHz and spectral density of power of phase fluctuations with the resolution of -175 dB/Hz on the analysis frequency of 1 kHz and works in the carrier frequencies range of 1 to 100 MHz.

Frequency instability is measured for any time interval in the range of 10^{-6} to 10^{3} s, and spectral density of power of phase fluctuations is measured in the analysis frequencies band of 10^{-3} to10^{6} Hz. The use of realized metrological generators permits to carry out measurement up to frequencies of 300 GHz and higher.

The method of direct multiplication of frequency from standard sources has a number of essential limitations which makes impossible its use for standard frequencies transfer into submillimetric range and higher as when multiplication ratios are 10^{4} the phase noise increases intolerably.

The complicated problem of high-stable generators development for realization of such sources in the metrological systems take a particular place in the problems of submillimetric range systems realization.

The creation of sources for metrological systems and also for the united time, frequency and length standard is realized by the use of various-type generators which are stabilized by means of phase lock. Them suggested the method of phase lock multiringed optimal systems computation which permits to maximize the stabilized generator output signal S/N ration.

The principles of high-stable sources of oscillatios construction for metrological purposes are discussed. The result of the investigation of some metrological high-stable on frequency sources of oscillations are adduced. The inherent relative instability of output frequency of one of the realized metrological sources on the frequency of 70 GHz is (1-2) 10^{-14} for measurement time of 100 s.

Very interestingworks are conducted under the direction of professor S.Diubko at Kharkiv State University.

Important results relating to electromagnetic metrology were obtained in Quantum Radiophysics division over 1994/1998. Investigations of highly excited (Rydberg) atoms have resulted in the development of a precision radio spectrometer. New measurements of the transition frequencies of Na atoms were carried out with the instrument. Investigated have been nS-nP transitions in the range of quantum numbers n=22 to 32. Also, the fine structure of the D-term was measured at precision. Precision frequency measurements for these transitions permit determining the set of constants for the quantum defects which describe the energy spectrum of Na in the p-, d-, and f- states. These sets of constants are valid for calculating energy levels of Na from ground states up to the ionization limit. The results were published in [1]. Another development is the millimeter-wave radiospectrometer intended for high-precision investigations of molecular rotational spectra between 50 and 250 GHz. The accuracy of transition frequency determination is about 1-3 kHz for isolated lines with sufficiently high signal-to-noise ratios. This specrometer allows to perform measurements both with the Doppler-limited resolution and in the sub-Doppler mode. The main fields of application are molecular spectroscopy, molecular physics, astrophysics, environmental monitoring, etc. Precision measurements of the rotational spectra of astrophysical molecules which contain isotopic species of O, C, N, and S - atoms were performed in the 70 to 250 GHz frequencies range by using this unique, computer driven radiospectrometer (the measurement accuracy was within 1 kHz). The radiospectrometer is based on a frequency synthesizer with a narrow spectral width of the output radiation < 1 kHz and absorbing cell operated both in the ordinary absorption mode and the Lamb-dip mode (the width of recorded resonance was about 15-20 kHz). The group developed an original high-precision method to treat the experimentally observed rotational spectral lines. It has provided for an order of magnitude increase in the accuracy of measured frequencies compared with prior investigations.

The high-resolution measurements were carried out for the following species (the transition numbers are given in the brackets):

CH_3OH(68); CH_3OD(10); HCOOH(21); $C2H_5OH$(72); CH_3COH(46); CH_3CN(12); OCS(15);

CH_3NH_2(31);NH_2COH(27); $^{32}SO_2$(76); $^{34}SO_2$(53); $^{32}SO_2$[v=2](45); CH_2CHCN(187); NH_2OH(12).

Sets of the molecular constants have been determined, thus allowing to calculate the millimeter wave spectra of $^{32}SO_2$(76); $^{32}SO_2$[v=2](45); CH_2CHCN(187) with a 1 or 2 orders of magnitude better accuracy than in the previous studies. The results have been published in [5, 6, 7].

The works are progressing, and the spectroscope itself has achieved a highh level of perfection. Its elements and assemblies can find use also for other purposes in electromagnetic metrology for the ranges under consideration.

Research on the development of microwave generators based on superconducting resonators were carried out under F.F.Mende guidance (Institute of Low Temperature Phisics). The relative frequency

instability of 3 cm generator was about 10^{-2} with the noise level of 130 ... 140 dB/Hz at 1 kHz off the carrier.

Progress can be reported in the development of microwave measuring instruments which allow both to reproduce hight stable, spectrally pure signals with a telative instability lower than 5·10 minugh the frequency range, and to perfom frequencies and responses of radiation sources with a relative error not below 10^{-11}. The problems of precisely controllable sources and means of their metrological control in a wide range of carrier frequencies have been investigated at the R&D Assotiation "Metrologia".

Are of interest the works on power measuring in the ranges under consideration that are being conducted at Kharkiv State University under the supervision of professor V.Kuzmichov[3].

Some progress should be emphasized in active and passive elements perfection for measuring generators, receiving devices, electromagnetic wave transmission lines, and measuring channels [4] that is reported in other Sections reports of our Symposium. Undoubtedly, these achivements will contribute to the technology of electromagnetic metrology.

In an effort to more successful progress in the electromagnetic metrology of the ranges under consideration, it is necessery, in our opinion, to intensify in Ukraine first of all the works on frequency standards and their characteristics measurement, and to improve the characteristics of receiving devices as applied to electromagnetic metrology problems as well as radiation power measuring.

I Think that this Symposium work will give a new impetus to the development of the investigation in the foregoing and other directions.

References

1. N.G.Nahodkin, "Ukrainian URSI Commitee", Radio Physics and Radio Astronomy, v1, №1, p-p. 123-158, August 1996.
2. A.Kleiman, "The elaborationaud measurement accuracy problems of the frequency characteristics on the sources of high stability acscillations in the millimeter and submillimeter range and of the means of their tranceability".
3. V.Kuzmichov, "Thin-wire bolometers of inteuse electromagnetic radiotion, Proceedin of the third International Kharkov Symposium "Phisics and Engineering of millimeter and submillimeter wokes", Kharkov, Ukraine, September 15-17, 1998.
4. Под редакцией Р.А.Валитова и Б.И.Макаренко, "Измерения на миллиметровых и субмиллиметровых волнах. Методы и техника", Москва, "Радио и связь", 1984.
5. O.I.Baskakov, S.F.Dyubko, M.N.Efimenko, V.V.Ilushin, V.A.Efremov, S.V.Podnos, and E.A.Alekseev. Submitted to JMS, Re. No. 258-08-95.
6. E.A.Alekseev, S.F.Dyubko, V.V.Ilushin, and S.V.Podnos. Submitted to JMS, Re. No. 258-08-95.
7. O.I.Baskakov, S.F.Dyubko, M.N.Efimenko, V.A.Efremow, and S.V.Podnos. Proc. of Conf. on Molecular Spectroscopy, Dijon, France, 1995.

THINWIRE BOLOMETERS of INTENSIVE ELECTROMAGNETIC RADIATION

V. M. Kuzmichov
Department of Radio Physics
Address: Kharkov State University, Kharkov 310077, Ukraine
Tel. 45-71-57

The measurement spatial-power and polarization parameters of intensive and wide-aperture electromagnetic radiation by traditional methods causes large technical difficulties, that sometimes results in impossibility of measurement of some parameters, for example, polarization condition of pulsing radiation.

One of possible ways of the decision of the given problem is use of thinwire bolometers, tense as lattices with constant period. Such bolometers have not restrictions on the maximum size of the entrance aperture, little inertiated, have wide band and maintain high density of radiation intensity. The period of a lattice gets out of a condition of an allowable error of spatial integration of distribution of radiation intensity in section of a beam. As a rule, it is rare lattices, which period have more length of a radiation wave and diameter of a used bolometer. The basic part of radiation passes through a lattice and only the small part it cooperates with a bolometer.

The basic physical parameters of a bolometer, determining its transformation factor of electromagnetic radiation, are temperature factor of resistance α, factor of efficiency of absorption q, factor of heat exchange with external environment γ, specific heat capacity c, linear weight m and factor of heat conduction χ. At interaction with a bolometer the following parameters of radiation are taken into account: average linear falling capacity $\overline{P}$, specific linear average falling energy $\overline{E}/m$; integrated factor of non-uniformity of distribution of falling intensity on the area of the entrance aperture gauge or on whole length of a bolometer $\delta = 1 + \sigma_0^2$, where σ_0^2 — relative dispersion of the appropriate distributions; polarizated factor

$$k = \cos^2\varphi + k_D \sin^2\varphi, \qquad (1)$$

where φ — corner of a linear polarization direction of radiation concerning a corner of a direction of bolometer elements of a lattice; k_D — dichroizm factor of a bolometer, equal to the relation of the factors of efficiency of absorption for a perpendicular and parallel axis of a bolometer linear polarizations of radiation.

Trellised converters allow to measure the following parameters of laser radiation: continuous capacity, average capacity, energy of a pulse, profile distribution, position of power centre, root-mean-square radius, generalized area, integrated non-uniformity of intensity distribution, condition linear and elliptical polarization, distribution of intensity in section of a beam. A thinwire bolometer allows to register the form of a pulse and parameters of a focal stain of radiation.

Large levels of radiation result in essential heating of bolometer elements, when their basic physical parameters do not remain constant, occurrence of nonlinearity of the characteristic of transformation, amplifying non-uniformity of distribution of intensity on the area of the entrance aperture of a gauge, and systematic errors of measured parameters of radiation.

The signals of a lattice at influence of continuous capacity U_P and energy of a pulse U_E can be written down in the following kind

$$U_P = \eta_{op} F\left(\delta \overline{P} k\right) \overline{P} k; \qquad U_E = \eta_{OE} F\left(\frac{\delta \overline{E}}{m} k\right) \frac{\overline{E}}{m} k, \qquad (2)$$

where η_{op} and η_{oe} — transformation factors of a bolometer in linear mode of operations and linear polarization of radiation parallel to axes of elements of a lattice; $F\left(\delta \overline{P} k\right)$ and $F\left(\delta \overline{E}/m\right)$ — normalized, accord-

ingly on η_{ep} and η_{oe}, transformation factors of a bolometer in nonlinear mode of operations.

For linear temperature dependencies of the basic physical parameters of a bolometer the normalized factors of transformation simply turn out after the decision of the stationary and non-stationary equations of heat conduction, average on whole length of a bolometer. Dependencies $F(\delta\overline{P}k)$ and $F(\delta\overline{E}/m)$ for a platinum bolometer working in normal conditions, and radiation with wave length 10,6 micron approximates by polynomials of the second degree with an error 0,5 % as:

$$F(\delta\overline{P}k) = 1 + a_p\delta\overline{P} + b_p(\delta\overline{P})^2, \tag{3}$$

where a_p=-5,236·10^{-2} cm/W and b_p=2,185·10^{-3} cm^2/W^2. Polarizated factor k changes argument of function $F(\delta\overline{P}k)$. Is similarly written down and $F(\delta\overline{E}/m)$ with a_E=7,61·10^{-2} g/kJ and b_E=-9,68·10^{-3} g^2/kJ^2. For an any condition of radiation polarization limiting meaning of an effective power $\delta\overline{P}_{max} = 5$ W/cm, and effective energy $\delta\overline{E}/m = 2$ kJ/g.

The measurement of capacity and energy of a pulse of radiation is made by two lattices with angular directions of elements ψ_1=0 and ψ_2=π/2 and the signals them are summarized for exception of dependence from a condition of radiation polarization. Normalized transformation factor of a double lattice for capacity measurement will be

$$F_p(\delta\overline{P}) = (F_1k_1 + F_2k_2)(k_D + 1)^{-1}, \tag{4}$$

where the indexes 1 and 2 concern to the appropriate lattices. The systematic error of nonlinearity of the transformation characteristic of a bolometer at capacity measurement can reach -25 %, and energy of a pulse — + 12 % in the specified radiation intensity ranges. The given systematic error can be excluded, if one and too meaning of radiation intensity to measure simultaneously by two ways, have various nonlinearity of bolometer transformation. For example, energy of a pulse of radiation it is possible to measure on the maximum meaning and area of a target signal, and continuous capacity — on a stationary signal and on the area above a curve of heating or under curve of cooling of target signal at turning-on and turning-off of measured capacity.

Use of the given ways of measurements requires knowledge of the appropriate normalized factors of transformation, which can be determined at bolometer calibration. At calibration a target signal of a bolometer, radiation intensity by absolute calorimeter and profile distribution of radiation intensity in two interperpendicular directions, registered with each bolometer element is registered. Factor of non-uniformity δ is defined on expression:

$$\delta = S/4\pi\sigma_x\sigma_y, \tag{5}$$

where S — area of the entrance aperture of a bolometer; σ_x and σ_y — root-mean-square radii of a beam on two directions, calculated on profile distributions.

The measurement of a polarization condition of radiation is carried out by three lattices with angular directions of elements ψ_1=0, ψ_2=π/3 and ψ_3=-π/3. Normalization of target signals of lattices is made

$$U_{i,0} = \frac{3(k_D + 1)}{2}\frac{U_i}{\sum_{j=1}^{3} U_j}, \quad i=1, 2, 3 \tag{6}$$

For linear polarization of radiation the relation of sizes undertakes

$$\frac{U_{i+1,0}-0,5(k_D+1)}{U_{i+2.0}-0,5(k_D+1)}=U_{i+1,i+2}, \tag{7}$$

which defines corners of possible directions of radiation polarization relative to i-d of a lattice

$$\varphi'_{i.L}=\frac{1}{2}\text{arctg}\frac{1-U_{i+1,i+2}}{\sqrt{3}(U_{i+1.i+2}+1)}, \tag{8}$$

where L=1, 2, as tangent of a double corner in an interval of corners $[-\pi/2, +\pi/2]$ will have identical meaning for two corners. The index i in expression (7) cyclic passes meanings 1, 2, 3 and $U_{4,0}=U_{1,0}$ and $U_{5,0}=U_{2,0}$. The valid meaning of a corner $\varphi'_{i.L}$ is determined on comparison of lattices signals. In the given way of measurements the maximum systematic errors of measurements do not exceed ±0,75° for continuous capacity and ±0,22° of energy of a pulse, and maximum absolute root-mean-square deflection of a measured corner is close to relative one of registered lattices signals.

For elliptical polarization of radiation polarizated factors of interaction look like:

$$k_i=k_D-(k_D-1)\left[\xi^2_{xj}\cos^2(\psi_j-\psi_i)+\xi^2_{yj}\sin^2(\psi_j-\psi_i)+2\xi_{xj}\xi_{yj}\sin 2(\psi_j-\psi_i)\cos\alpha_j\right], \quad j=1, 2, 3, \tag{9}$$

where ψ_j — corner of an abscis axis of chosen rectangular system of coordinates; ξ_{xj} and ξ_{yj} — relative amplitudes of an electrical field of radiation rather x_j-d and y_j-d of axes of coordinates; $\cos\alpha_j$ — shift of phases between electrical making fields of radiation. The normalized signals define sizes ξ^2_{xj}, when the indexes i and j in expression (9) coincide,

$$\xi^2_{xj}=(k_D-U_{i,0})\Big/(k_D-1), \tag{10}$$

and the corners of directions of half-axes of radiation polarization will be:

$$\text{tg}2\varphi'_{iL}=\frac{3(k_D+1)-2U_{i,0}-4U_{i+1,0}}{\sqrt{3}(k_D+1-2U_{i,0})}. \tag{11}$$

The half-axes of ellipsis of radiation polarization will be:

$$\xi^2_{Li}=\frac{1}{k_D-1}\left\{(k_D-U_{i.0})\cos^2\varphi'_{iL}+(U_{i,0}-1)\sin^2\varphi'_{iL}+\frac{\sin 2\varphi'_{iL}}{2\sqrt{3}}\left[3(k_D+1)-2U_{i.0}-4U_{i+1,0}\right]\right\}. \tag{12}$$

The maximum systematic error of measurement of a large half-axis of ellipsis of radiation does not exceed -5 % for capacity, and corner of its direction ±0,75°. Relative root-mean-square deflection of meaning of a half-axis of ellipsis of radiation is close to one of lattices signals, and absolute root-mean-square deflection of corners of ellipsis half-axes is increased, when ξ^2_1 changes from 1 to 0,5.

Due to high optical resistance and high spatial sanction the thinwire bolometers can be used for determination of focal stain parameters of a intensive radiation with success.

Thus, the thinwire bolometers are perspective for measurement power, polarizated and spatial parameters of wide-aperture and intensive electromagnetic radiation.

MEASUREMENT OF THE GENERALIZED LASER BEAM CROSS SECTION AREA

V. M. Kuzmichev , S. N. Pokhil'ko
Department of Radiophysics, Kharkov State University
Adress: 4, sq.Svobody, Kharkov, 310077, Ukraine
Tel.45-73-01

A generalized area, S_0, of the cross section of a laser beam [1] with an arbitrary distribution of the optical power over the area of the beam cross section, $W(x, y)$, is an area of the cross section of an equivalent beam with a constant power density and the total power equal to that of the real beam.

The generalized area is defined by the expression

$$S_0 = \frac{\left[\int_S W(x,y)ds\right]^2}{\int_S W^2(x,y)ds}, \quad = S\frac{\overline{W}^2}{\overline{W^2}}\ ; \tag{1}$$

where S is the area of integration equal to the area of the entry aperture of the measuring device, $\overline{W}^2$ is the square mean incident optical power, $\overline{W^2}$ is the mean square incident optical power.

To calibrate nonlinear thin-wire bolometers for measuring energy parameters of laser emission [2], it is necessary to determine the relative parameter of non-uniform optical power distribution, δ, over the entry aperture of the device; the parameter δ is related to the relative variance of the power distribution $\sigma^2_{W_0}$ according to the relationship

$$\delta = 1+\sigma^2_{W_0} = 1+\frac{1}{S}\int_S\left[\frac{W(x,y)}{\overline{W}}-1\right]^2 ds = \frac{S}{S_0}\ ; \tag{2}$$

Relation (2) shows that the generalized area of a and the area of the entry aperture S of the measuring device are sufficient for determining the relative parameter of non-uniform optical power distribution.

If the distribution of the optical power can be expressed in the form

$$W(x,y) = W_x(x)W_y(y)\ , \tag{3}$$

then the relative parameter of non-uniform incident optical power distribution can be represented as the product of its x- and y-components

$$\delta = \frac{\overline{W_x^2}}{\overline{W}_x^2}\cdot\frac{\overline{W_y^2}}{\overline{W}_y^2} = \delta_x\delta_y \tag{4}$$

The aim of this paper is to validate the techniques for measuring the generalized area of laser beam with a grid-type measuring device containing thin-wire bolometer elements.

If the signals are recorded at each element of a grid-type bolometer with the orthogonal grid elements, then the respective components of the relative parameter of non-uniform optical power distribution are as follows

$$\delta_{x,y} = \frac{1}{n}\sum_{i=1}^{n}\left(\frac{u_{i,j}}{\overline{u}_{i,j}}\right) \tag{5}$$

where $u_{i,j}$ are signals from the x- and y-components of the bolometer, respectively, $\overline{ui,j}$ are their means.

If the power distribution W(x, y) stretches not along the coordinate axes, then relation (4) along with (5) results in diminishing the relative parameter δ and in increasing the generalized area S_0. The bias reaches its maximum when the distribution stretches along the $\pm\pi/4$ directions with respect to the bolometer grid element directions.

Given the magnitude of the relative parameter, and using expression (2), the generalized area of a laser beam is determined. A Gaussian beam of optical emission with the power distribution

$$W(x,y)=\frac{P}{2\pi\sigma^2}e^{-\frac{x^2+y^2}{2\sigma^2}} \tag{6}$$

where P is the total beam power, and σ is its root-mean-square radius, has the generalized area

$$S_0=4\pi\sigma^2 \tag{7}$$

according to relation (1), which is the area of a circle with a radius equal to two root-mean-square radii.

It is easy to show that a circular beam of a radius R with uniform optical power distribution has the root-mean-square radius $\sigma=R/2$ and its generalized area is

$$S_0=\pi R^2=4\pi\sigma^2 \tag{8}$$

We have determined that the generalized areas of the beams with the different optical power distributions are expressed by the same formula in terms of their root-mean-square radii. Thus, the conclusion can be reached that the generalized area of a laser beam with an arbitrary optical power distribution can be determined in terms of its root-mean-square radius.

The root-mean-square radii, σ_x and σ_y, along two perpendicular directions can be determined with a grid-type bolometer measuring device using the coordinates of the bolometer elements and the signal voltages along the coordinate axes normalized to their sum; the root-mean-square laser beam radius is determined as a geometric mean of σ_x and σ_y

$$\sigma=(\sigma_x\sigma_y)^{1/2} \tag{9}$$

Let us verify this conclusion using a circular beam with a uniform optical power distribution and a beam with a Gaussian distribution and two similar beams with spaced centers and equal powers. Numerical simulation was carried out on a dual grid of 16 bolometer elements each and of a period κ. The origin of the Cartesian coordinate system is placed at the center of the grid and its coordinate axes are parallel to the bolometer elements. The length of every bolometer element is $2l_0$, the period $\kappa=l_0/8$, and the area of the grid $S=4\cdot l_0^2$.

For beams with a uniform optical power distribution and a radius of 5κ, the relative parameter of the incident non-uniform optical power distribution δ was calculated using the distributions along the coordinate axes for determining σ_x and σ_y, employing the non-uniformity of the distribution along the coordinate axes for determining δ_x and δ_y, and using the relative variance of optical power distribution along the whole length of the bolometer grid as well.

The results of calculation are presented in Table 1.

In the second line of Table 1, there are the results for the beams the centers of which coincide, i.e. there is one beam. In the third line, there are results for two beams spaced symmetrically along the grid diagonal at a distance of $4\sqrt{2}\,\kappa$. The lack of coincidence among δ, δ' and δ'' is accounted for by a bias of about 1% in the spatial integration of this optical power distribution with one bolometer grid which results in diminishing δ for the first beam by about 2%, for the second and third beams by 4%, in diminishing δ' for all the beams by 2%, and in diminishing δ'' by 4% in accordance with relations (5) and (9). For the third beam, the diminishing in magnitudes of δ' and δ'' is due to stretching the optical power distribution along the grid diagonal.

For Gaussian beams with root-mean-square radii σ, equal optical powers, and spaced at a distance of d, the relative parameter of non-uniform optical power distribution δ can be easily obtained

$$\delta=S\cdot\frac{1+e^{-\frac{(d/\sqrt{2})^2}{2\sigma^2}}}{8\pi\sigma^2} \tag{10}$$

The results of calculation for $\sigma=2\kappa$ and three beams with the same center coordinates as in Table 1 are presented in Table 2.

For Gaussian beams the results are slightly better. The spatial integration for such beams is being carried out practically without a bias, which is confirmed by the determined magnitudes of σ_x/l_0 and σ_y/l_0 for one beam, and which nearly corresponds to the magnitude $\sigma=2\kappa=0.25$. For the first two beams, the magnitudes obtained δ, δ' and δ'' are nearly the same and for the third dual beam δ' is diminished by 11%, and δ'' is diminished by 17%, which is due to the diagonal arrangement of the beams and due to an increase in an arising bias in a value of δ'' with respect to the value of δ'.

If the conditions allow us to rotate the grid-type thin-wire bolometer measuring device around the beam optical axis, then the biases in the generalized area S_0 and the parameter δ reach at a minimum when the magnitudes σ_x/l_0 and σ_y/l_0 are at an extremum.

Thus, the technique for measuring the generalized area of the cross section of a laser beam is validated using a grid-type thin-wire bolometer measuring device with a dual grid with the perpendicular elements. The generalized area is determined in terms of the measured root-mean-square radius of a laser beam or in terms of the measured relative parameter of non-uniform optical power distribution over the surface of the entry aperture of the measuring device.

Table 1

beam center coordinates	$\delta = 1 + \sigma_{p0}^2$	σ_x/l_0	σ_y/l_0	$\delta = \frac{S}{4\pi\sigma^2}$	δ_x	δ_y	$\delta^* = \delta_x\delta_y$
$x_1 = 0;\ y_1 = 0$ $x_2 = 0;\ y_2 = 0$	3,228	0,3163	0,3163	3,181	1,705	1,705	2,906
$x_1 = -2\kappa;\ y_1 = 0$ $x_2 = +2\kappa;\ y_2 = 0$	2,452	0,4032	0,3163	2,497	1,354	1,705	2,308
$x_1 = -2\kappa;\ y_1 = -2\kappa$ $x_2 = +2\kappa;\ y_2 = 2\kappa$	1,991	0,4032	0,4032	1,958	1,354	1,354	1,833

Table 2

beam center coordinates	$\delta_{n0}(10)$	σ_x/l_0	σ_y/l_0	$\delta' = \frac{S}{4\pi\sigma^2}$	δ_x	δ_y	$\delta' = \delta_x\delta_y$
$x_1 = 0;\ y_1 = 0$ $x_2 = 0;\ y_2 = 0$	5,093	0,2499	0,2499	5,098	2,257	2,257	5,094
$x_1 = -2\kappa;\ y_1 = 0$ $x_2 = +2\kappa;\ y_2 = 0$	3,483	0,3515	0,2499	3,624	1,547	2,257	3,492
$x_1 = -2\kappa;\ y_1 = -2\kappa$ $x_2 = +2\kappa;\ y_2 = 2\kappa$	2,891	0,3515	0,3515	2,576	1,547	1,547	2,393

References

1. M.I.Gryaznov. Generalized Parameters of Emission Pulses. *Pulse Photometry*. Leningrad, Mashinostroyeniye/Mechanical Engineering. No. 6, pp. 35-41 (1979), (in Russian).

2. V.M.Kuz'michev and S.N.Pokhil'ko. Errors of Thin-Wire Bolometer of increased accuracy of laser pulse energy. *Ukrainian Journal of Metrology*. No. 4, pp. 33-35 (1997), (in Russian).

INTENSIVE LASER RADIATION ELLEPTICAL POLARIZATION MEASUREMENT BY THIN-WIRE BOLOMETERS

V.M.Kuzmichov, E.V.Kuzmichova
Department of Radiophysics, Kharkov State University
Adress: 4, sq.Svobody, Kharkov, 310077, Ukraine
Tel.45-73-01

The measurement of a condition of polarization of intensive and wide-aperture laser radiation by classical methods is practically impossible. One of probable paths of the solution of this measurements is the use of thin-wire bolometric grids convertors having high optical durability, small lag, absence of restrictions on a maximum size of the source aperture and being polarizing elements.

To measurement of elliptic polarization of laser radiation by three bolometric grids working in a linear mode, devote work [1]. Transition to more high levels of radiation, when the essential heat of bolometric elements and their main physical parameters (temperature factor of resistance α, factor of efficiency of an absorption q, factor of heat exchange with an external medium γ and specific thermal capacity c) do not remain constant, results in nonlinearity of performance of bolometer transformation, amplifying nonuniformity of distribution of an incident radiation on square of the source aperture of a meter, and systematic errors of measured parameters of radiation.

The given work justifies a technique of a measurement of main parameters of elliptic polarization of radiation (relative semiaxes of an ellipse and their angular directions in a cut of the optical beam) by three bolometric grids with nonlinear performances of transformation caused by linear temperature assotiations of main bolometer physical parameters. In the correspondence with [1,2] signals u_i from identical bolometric grids, which were turned around in cuts of the beam on a certain angle rather one another, for a continuous power it is possible to note

$$u_i = \eta_0 F(\delta \overline{P} k_i) \overline{P} k_i, \qquad i = 1,2,3, \tag{1}$$

$$k_i = k_D - (k_D - 1)[\zeta_{xj}^2 \cos^2(\phi_j - \phi_i) + \zeta_{yj}^2 \sin^2(\phi_j - \phi_i) + \\ + \zeta_{xj}\zeta_{yj} \sin 2(\phi_j - \phi_i)\cos\alpha_j] \qquad j=1,2,3 \tag{2}$$

are the interaction polarization coefficients between radiation and bolometers of i-grid, when x-axis of rectangle coordinat system aligns with the direction of j-grid elements; ϕ_i , ϕ_j - angles of direction of corresponding grids' elements; k_D - dichroism coefficient of cylindric bolometric elements, which is equal to the ratio of factors of efficiency of absorption for linear polarization of radiation, which is perpendicular and parallel to the bolometer axis; η_0 - transformation coefficient of each grid in linear mode of operation for the linear polarization of radiation, which is parallel to grids' elements; $\overline{P}$ - average incident linear power on bolometer, δ - non-uniformity distribution parameter of incident power and temperature along bolometer, which is equal to $\delta = 1 + \sigma_{p0}$, where σ_{p0} is a relative dispersion of incident power distribution on square of the source aperture of a meter or on total bolometer length; $F(\delta \overline{P} k_i)$ are transformation coefficient of i-grid in non-linear mode of operation, which are normalized on η_0, ζ_{xj} and ζ_{yj} - relative mutually perpendicular amplitudes of electrical field of radiation to x_j-axis, which are connected with relation $\zeta_{xj}^2 + \zeta_{yj}^2 = 1$; α_j - the phase shift between electrical components of radiation field for the coordinate system with x-axis x_j.

The constant period of elements of grids is selected by such, that for all possible measured distributions of power in a cut of bundle the error of the tree-dimensional integration by the grid did not exceed 1%.

For the grids with the direction angles of bolometric elements equal to $\phi_1 = 0$, $\phi_2 = \pi/3$ and $\phi_3 = -\pi/3$ it is easy to show, that the sum of signals is equal to

$$\sum_{i=1}^{3} u_i = \frac{3}{2}(k_D + 1)\eta_0 \overline{P}_u \tag{3}$$

and doesn't depend on a condition of polarization of radiation, where $\overline{P}_u$ - measured by bolometers average incident power per unit length.

Entering relative output signals of grids by ratio

$$u_{i,0} = \frac{u_i}{\eta_0 \overline{P}_u} = \frac{3(k_D + 1)}{2} \frac{u_i}{\sum_{k=1}^{3} u_k}, \tag{4}$$

which to within a systematic error called by nonlinearity of performance of transformation of bolometer are equal to polarizing factors of interaction k_i, and using (2), we have magnitudes ζ_{xi}^2, when the indexes i and j in expression (2) coincide

$$\zeta_{xi}^2 = \frac{k_D - u_{i0}}{k_D - 1} \tag{5}$$

and the angle of shift of phases α_i between the components of radiation electrical field with relative amplitudes ζ_{xi} and ζ_{yi} is determined from expression

$$\cos\alpha_i = \frac{3(k_D + 1) - 2u_{i,0} - 4u_{i+1,0}}{2\sqrt{3}[(k_D - u_{i,0})(u_{i,0} - 1)]^{1/2}} \tag{6}$$

In formula (6) index i cyclically passes significances $1,2,3$, that is $u_{4,0} = u_{1,0}$ and $u_{5,0} = u_{2,0}$. Obtained significances ζ_{xi} and ζ_{yi} allow to use their functional connection with angles of directions of semiaxes of an ellipse of radiation $\varphi_{il}^{'}$ concerning an angle of directions of elements of i-grid

$$tg\,2\varphi_{il}^{'} = \frac{2\zeta_{xi}\zeta_{yi}}{\zeta_{xi}^2 - \zeta_{yi}^2}\cos\alpha_i = \frac{3(k_D + 1) - 2u_{i,0} - 4u_{i+1,0}}{\sqrt{3}(k_D + 1 - 2u_{i,0})}, l = 1,2 \tag{7}$$

The relative semiaxes of an ellipse of radiation ζ_{il} are obtained from expression

$$\zeta_{il}^2 = (2 - u_{i,0})\cos^2\varphi_{il}^{'} + (u_{i,0} - 1)\sin^2\varphi_{il}^{'} + \frac{\sin 2\varphi_{il}^{'}}{2\sqrt{3}}[3(k_D + 1) - 2u_{i,0} - 4u_{i+1,0}] \tag{8}$$

Let's evaluate significances of systematic errors of parameters of elliptic polarization of radiation measured by platinum bolometers in normal conditions on radiation wave-length equal to $10,6\mu m$ and having the following dependence of normalized factor of transformation

$$F(\delta\overline{P}) = 1 - 5,236\cdot 10^{-2}\delta\overline{P} + 2,185\cdot 10^{-3}(\delta\overline{P})^2 \tag{9}$$

For the certain condition of elliptic polarization of radiation there were obtained coefficients k_i and, setting significance of an effective power $\delta\overline{P}$, the magnitudes $F(\delta\overline{P}k_i)k_i$, $u_{i,0}$ were defined. Than the magnitudes ζ_{xi}^2, $\cos\alpha_i$, $\varphi_{il}^{'}$ and ζ_{il}^2 were determined. The characteristic property of calculations consists in the following. Resulting the found angles $\varphi_{il}^{'}$ to angles relative to the first grid by expression

$$\varphi_{il} = \varphi_{il}^{'} + \phi_i, \tag{10}$$

we receive, that the angles φ_{il} coincide for all significances i and l. The found significances ζ_{il}^2 also coincide for all significances i. From this follows, that it is possible to make measurements of parameters of elliptic polarization of radiation relative rather any one grid.

On fig.1 are shown the dependences of an absolute systematic error $\Delta\varphi_{il}$ from the real angle φ of the big semiaxis of an ellipse of polarization, which are changed harmonically with period $\pi/3$. The amplitude of these deviations grows with magnification of ζ^2 and achieves maximum significance at

$\zeta^2 = 1$. For a small semiaxis of an ellipse the dependence $\Delta\varphi_{i2}$ will be similar, only it will be moved by phase on π and always is satisfied condition $\varphi_{i1} - \varphi_{i2} = \pm\pi/2$.

On fig.2 the calculated dependences of significances ζ_{i1}^2 from an angle φ are indicated. Dependences $\zeta_{i2}^2 = 1 - \zeta_{i1}^2$ will be same harmonic, but moved by phase on π. The amplitude of these harmonic deviations $\Delta\zeta_m^2$ grows with magnification ζ^2 and is maximum for $\zeta_1^2 = 1$.

On fig.3 are shown the dependences of amplitude $\Delta\varphi_m$ from effective power of radiation $\delta\overline{P}$. On fig.4 the dependences of measured average value ζ_{1i}^2 for $\zeta_1^2 = 1$ and amplitude of deviations $\Delta\zeta_m^2$ from magnitude $\delta\overline{P}$ are shown. The trend of these dependences is completely determined by function $F(\delta\overline{P})$.

The obtained results show, that the maximum systematic error of determination of a big semiaxis of n ellipse of polarization of radiation ζ_1 does not exceed -5%, and an angle of it direction - does not exceed $\pm 0{,}75^0$ in a range of an effective power $\delta\overline{P} = 0...5$W/cm.

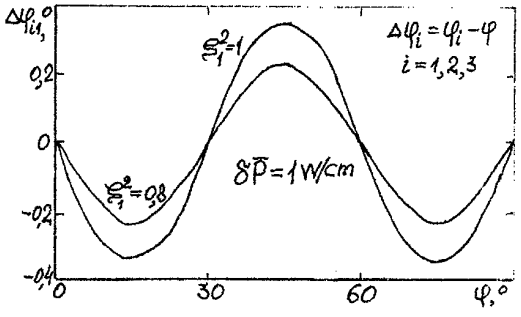


Figure 1. Dependence of systematic error $\Delta\varphi_{i1}$ from the real angle φ.

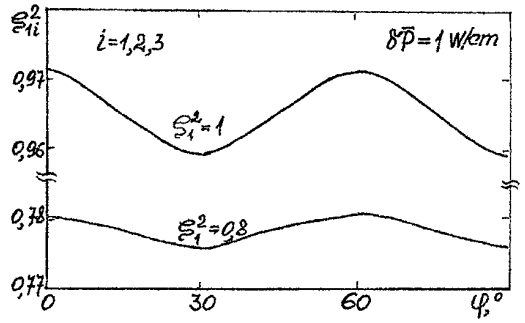


Figure 2. Measured results ζ_{1i}^2 from φ.

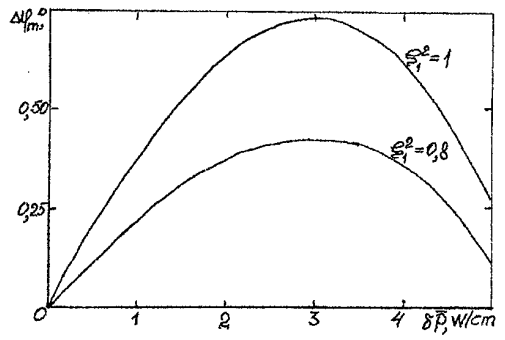


Figure 3. Dependence of amplitude $\Delta\varphi_m$ from $\delta\overline{P}$.

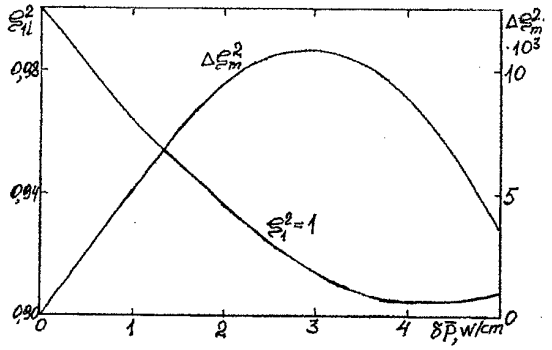


Figure 4. Dependence of average value ζ_{1i}^2 and amplitude ζ_m^2 from $\delta\overline{P}$ for $\zeta_1^2 = 1$.

References

1.A.B.Katrich, V.M.Kuzmichov, "Measurement of direction of polarization of an electromagnetic radiation.", Impulsnaya fotometriya, L:Mashinostroeniye, v.5, pp.129-131, 1978.
2. V.M.Kuzmichov, A.V.Zolotaykin, "Nonlinearity transformation performance of thin-wire bolometric meters of continuous power and energy of impulses of a laser radiation.", Izmeritelnaya technika, №12,pp.20-22, 1990.

NONLINEARITY OF THE CHARACTERISTIC OF TRANSFORMATION THINWIRE BOLOMETER OF FOCUSED LASER RADIATION

V. M. Kuzmichov, S.V. Pogorelov
Department of Radio Physics
Address: Kharkov State University, Kharkov 310077, Ukraine
Tel. 45-71-57

Parameters of focused laser radiation allow to estimate its radiatence, and by use in technology define quality of carried out processes, for example such, as cutting speed of metal, melt depth and width of a cut of a sheet material. The means of measurements of a focal stain laser parameters should have high optical durability and large spatial accuracy of determination of intensity distribution in section of a beam. In a visible range of a spectrum use photographic ways [1], moving of an opaque plate with a small aperture in cross section of a beam and method of a replaceable stops with receivers of radiation, and also way of an evaporating film on a transparent plate [2]. The listed ways require essential easing of radiation, are rather labour-consuming and result in significant errors of measurements results. Complexities of use of known ways of a focal stain parameters measurements are increased with transition in infrared range of spectrum.

One of possible ways of perfection of measurement methods of a focal stain parameters of continuous laser radiation is use of thinwire bolometers with diameters in units of micron, having high optical durability and large spatial accuracy at their moving in section of a beam.

The large density of radiation capacity result in significant temperatures of heating of irradiated bolometer areas and under these conditions its basic physical parameters (temperature factor of resistance α, factor of efficiency of absorption q, factor of heat exchange with external environment γ, the specific heat capacity c and factor of heat conduction λ) do not remain constant, that results in occurrence of nonlinearity of the transformation characteristic, amplifying non-uniformity of falling capacity distribution, and systematic errors of registered parameters of radiation.

In work [3] researches of a thinwire bolometer of a focal stain of the laser on the basis of the decision of the stationary equation of heat conduction with variable factors are begun. The given work is continuation of these researches by the decision of the non-stationary equation of heat conduction with variable factors.

In a rather large interval of temperatures the basic physical parameters of a bolometer have linear dependences: $\alpha(T)=\alpha_0+\alpha_1 T$; $q(T)=q_0+q_1 T$; $\gamma(T)=\gamma_0+\gamma_1 T$; $c(T)=c_0+c_1 T$ and $\lambda(T)=\lambda_0+\lambda_1 T$, α_0, q_0, γ_0, c_0 and λ_0 — meanings of parameters at temperature of environment, and α_1, q_1, γ_1, c_1 and λ_1 — factors of temperature dependence of these parameters. Under these conditions quasi-lineal non-stationary equation of heat conduction for bolometrical element, irradiated with Gaussian beam of radiation, will be:

$$\left(1+\frac{c_1}{c_0}T\right)\frac{\partial T}{\partial \Theta}=\frac{S_H}{\gamma_0}\frac{\partial}{\partial z}\left[\left(\lambda_0+\lambda_1 T\right)\frac{\partial T}{\partial z}\right]-\left(1+\frac{\gamma_1}{\gamma_0}T\right)T+\left(q_0+q_1 T\right)\frac{Pk\exp\left(-\frac{z^2}{2\sigma_H^2}\right)}{\gamma_0 L\sigma_H\sqrt{2\pi}}, \qquad (1)$$

where $2\cdot L$ — complete length of a bolometer; $z=x/L$ — relative coordinate of a bolometer, varied from -1 up to 1; t — time, and $\Theta=t/\tau$ — normalized time, where $\tau=m\cdot c_0/\gamma_0$ — thermal time constant of a bolometer with linear weight m; $S_H=\pi\cdot d^2/4\cdot L^2$ — normalized area of bolometer section with diameter d; $\sigma_H=\sigma/L$ — normalized root-mean-square radius of an optical beam with the valid meaning σ; $T=T(z,\Theta)$ — temperature of a bolometer in a point with coordinate z at the moment of time Θ; Pk — effective falling capacity on a bolometer; P — complete capacity of radiation falling on a bolometer; $k=\cos^2\phi+K_D\sin^2\phi$ — polarizable factor of interaction of radiation with a cylindrical bolometer, showing dependence of the factor of absorption efficiency on a corner between direction of linear polarization and axis of bolometer; K_D — dichroizm factor of a bolometer equal to the relation of the factors of absorption efficiency for perpendicular and parallel axis of a bolometer polarizations of radiation.

The equation was solved with the entry condition $T(z, 0)=0$ and boundary conditions $T(\pm1,\Theta)=0$.

The decision of the equation is received numerically through a method of final differences under the

obvious circuit [4], when the meaning of temperature is determined consistently in each point of a grid. The calculations were carried out up to $\Theta=10$, when the distribution of temperature differs from stationary distribution to thousand shares of percent. Relative increment of bolometer resistance was defined on expression:

$$\frac{\Delta R}{R_0} = \alpha_0 \int_{-1}^{1} \left[1 + \frac{\alpha_1}{\alpha_0} T(z,10)\right] T(z,10)\,dz = \eta_0 F(Pk,\sigma_н) Pk, \qquad (2)$$

where ΔR and R_0 absolute increment and initial resistance of a bolometer; η_0 — factor of bolometer transformation in linear mode of operations, when for small levels of effective falling capacity Pk normalized factor of transformation $F(Pk,\sigma_н) = 1$. From the last equality of expression (2) there was the meaning $F(Pk, \sigma_н)$. The transients of a bolometer depending on its diameter, level of falling effective power with certain root-mean-square radius of a beam turning out at calculations are analysed in work [5].

The calculations of normalized factor of transformation of a platinum bolometer with length 2L=1 cm are carried out for laser radiation with length of wave 10,6 micron, levels of effective falling capacity up to 1 W, diameters of bolometers d=3...20 microns and range of normalized root-mean-square radiuses of Gaussian beames $\sigma_н$=0,01...0,1. Errors of calculations by method of final differences did not exceed 10^{-8}K. The temperature dependences of physical bolometer parameters have the following numerical meanings:

$\alpha(T)=3{,}98\cdot10^{-3}\cdot(1-0{,}15\cdot10^{-3}\cdot T)\ K^{-1}$;

$q(T)=3{,}8\cdot10^{-2}\cdot(1+1{,}0\cdot10^{-3}\cdot T)$;

$\gamma(T)=3{,}0\cdot10^{-4}\cdot(1+1{,}2\cdot10^{-3}\cdot T)\ W\cdot cm^{-1}\cdot K^{-1}$;

$c(T)=13{,}35\cdot10^{-2}\cdot(1+0{,}187\cdot10^{-3}\cdot T)\ J\cdot g^{-1}\cdot K^{-1}$;

$\lambda(T)=0{,}69\cdot(1+0{,}3\cdot10^{-3}\cdot T)\ W\cdot cm^{-1}\cdot K^{-1}$.

Dependences of normalized transformation factors of bolometer F for its diameters 3 microns and 20 microns from effective falling capacity Pk and several meanings $\sigma_н$ are shown on fig. 1.

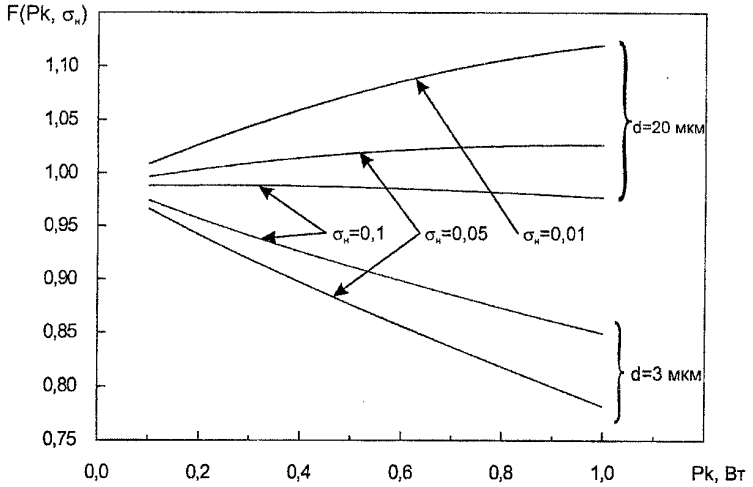


Fig.1. The dependence of normalized transformation factor of platinum bolometer with diameters 3 and 20 microns from effective falling capacity Pk and normalized root-mean-square radius of Gaussian beam $\sigma_н$.

For a bolometer diameter 3 microns running of heat from area of heating it is not enough and distribution of temperature close to distribution of falling capacity. In this case dominant role in meaning of transformation factor of bolometer has the temperature dependence of factor of heat exchange with external environment $\gamma(T)$. With increase $\sigma_н$ temperature in irradiated part of bolometer is lowered and normalized transformation factor is increased, but there is less unit. For $\sigma_н$=0,05 normalized transformation factor of bolometer decreases up to meaning 0,7818 at Pk=1W.

For diameter of a bolometer 20 microns running of a heat from area of heating already it is essential, especially for small meanings σ_H and the distribution of temperature becomes wider in comparison with distribution of falling capacity of radiation and maximum temperature is much less, than for bolometer with diameter 3 microns. In these conditions the absorption of radiation occurs in the field of maximum temperature and the basic heat exchange with external environment occurs from length of bolometer, exceeding an irradiated part. Under such circumstances dominant role in transformation factor of bolometer has the temperature dependence of the factor of absorption efficiency q(T). With reduction of meaning σ_H this process amplifies that conducts to increase of normalized transformation factor. And from meanings close to 1,00 at σ_H=0,1...0,05 in considered range of effective falling capacity it begins essentially to grow for σ_H=0,01 and reaches meaning 1,12 at Pk=1W.

At reduction of falling capacity up to zero the normalized transformation factors come nearer not to unit, and a little bit smaller meaning, that is determined by thermal losses through end faces of bolometer. These losses of a heat are increased with growth of bolometer diameter d and normalized root-mean-square radius of an optical beam σ_H and also with reduction of bolometer length 2L.

The deviation of normalized transformation factor of bolometer from unit gives meaning of a relative systematic error of measurement of capacity falling on it.

Maximum density of laser radiation capacity at which greatest temperature of bolometer heating reaches temperature of melting, can be appreciated on expression:

$$W_{max}^{E,H} = \frac{\left(\gamma_0 + \gamma_1 T_{pl}\right) T_{pl}}{\left(q_0^{E,H} + q_1^{E,H} T_{pl}\right) d}, \qquad (3)$$

where the indexes E, H concern to direction of linear polarization of falling radiation; T_{pl} — melting temperature of bolometer material. Meaning of quantity $W_{max}^{E,H}$ is inverse proportion to bolometer diameter d. It is necessary to take into account that dichroizm factor of platinum bolometer $K_D=q^H/q^E$ on radiation with wave length 10,6 micron practically linearly grows with increase of its diameter and at d=4 micron passes through unit. At d < 4 microns maximum density of capacity will for H-polarized radiation and for d=3 micron it will to make about 50 кW/cm². Compulsory dusting of bolometer increases this meaning.

Maximum capacity of Gaussian beam which can maintain a bolometer is defined by meaning W_{max} and root-mean-square radius of a beam σ on a parity:

$$P_{max}=2\cdot\pi\cdot\sigma^2\cdot W_{max} \qquad (4)$$

The spatial resolution of profile distribution of radiation intensity, registered by a thinwire bolometer, makes meaning close to its diameter.

Thus normalized transformation factor of platinum thinwire bolometer of focused laser radiation with wave length 10,6 micron in view of temperature dependences of its basic physical parameters is calculated and analysed. Such bolometer can be successfully used for diagnostics of a focal stain of intensive continuous laser radiation, thanking its high optical stability, large spatial resolution and small inertness.

References

1. G. Hird "Measurement of laser parameters", M.: Mir, 540 p. 1970.
2. O.E. Sidoryuk, E.N. Ushanova "Increase of measurement accuracy of focused laser diameter of beam", Measuring engineering, №6, p. 23-24, 1995.
3. V.M. Kuzmichov, A.V. Zolotaykin, A.S. Sochin "To the transformation characteristic of platinum bolometrical receiver of radiation", Pulsing photometry, L.: Mechanical Engineering, Ch.8, p. 166-168, 1984.
4. A.N. Tichonov, A.A. Samarskiy "The equations of mathematical physics", M.: Nauka, 724 p. 1966.
5. V.M. Kuzmichov, S.V. Pogorelov "Transients of thinwire bolometer of focal laser beam", Bulletin of Kharkov State University, № 405, Chapter "Radiophysics and electronics", Kharkov, p. 133-136, 1998.

MICROWAVE DIAGNOSIS OF PROTECTIVE COATINGS QUALITY

O.B.Ljashchuk
Ph.D., senior investigator
Z.T.Nazarchuk
Corr. member of NAS Ukraine, professor

Address: Physico-Mechanical Institute of the National Academy of Sciences of Ukraine,
Naukova Str. 5, Lviv, 290601, Ukraine
Tel. 380 (0322) 63-70-38, 380 (0322) 63-32-00
Fax. 380-0322-649427; E-mail panasyuk@ah.ipm.lviv.ua

Defect, thickness and structure measurement of protective coatings is a matter of interest in material science, as well as in aero-space and chemical industries, machine and ship building. Besides, it is very important in testing of oil and gas pipelines, oil tanks etc.

A microwave method within the range of super high frequency waves is one of effective methods for nondestructive testing of multi-layer dielectrics both on metal substrates and dielectric ones. Both theoretical and experimental research works on diagnosis of protective coating quality are being carried out at Karpenko Physico-Mechanical Institute of the National Academy of Sciences of Ukraine (Lviv).

The works include:

- development of new mathematical models, methods and algorithms for solution of direct and inverse problems of electromagnetic diagnosis of multi-layered dielectrics of both isotropic and anisotropic structures;
- design of high accurate measurement stands with horn-lens antennas for laboratory determination of multi-layer material characteristics;
- design of microprocessor devices of testing of multi-layer dielectric materials and coatings on both metal and dielectric substrates to be exploitated condition of production.

1. Theoretical Study

Theoretical basis of foregoing testing is solution of electrodynamical direct and inverse problems. While solving these problems the reflection or transmission coeficients as frequency function are considered as an initials data. In the case of one-side access to the tested objects reflection coefficients V are initial values. Describe the geometric and electromagnetic characteristics of the tested objects by some vector $\vec{p}$. Then we have the equation

$$V = A[\vec{p}], \tag{1}$$

where A is a wholly continuous operator with nonbounded inverse one. The direct problem on electromagnetic waves interaction with the object consists in solution of equation (1), that is in determining reflection coefficients V on the basis of known characteristics $\vec{p}$. Inverse problem of interaction of electromagnetics field with the object, as applied to the nondestructive testing, consists in determination of $\vec{p}$ on the basis of known V.

We shall consider M layers structure with the planeparallel division's boundaries. We shall assume that structure is in domain $0 < z < \sum_{m=1}^{M} h_m$, where h_m is thickness of layer number m. The lamination that would arise between the layers (non-glueing contact, etc.) or inside separate layers are also represented as layers with flat boundaries. The investigated structure is characterized by the number of layers, theirs thicknesses and the dielectric parameters.

Direct and inverse problems on electromagnetic waves reflection from the planestratifield dielectric were widely solved as to the isotropic [1-5] and anisotropic [6] dielectrics. Showed, in order to obtain the definite solution of the diagnosis problem, when prior information is not enough and the range of possible variation of coating parameters under defections is wide, it is necessary to solve the inverse problem. For numerical solution

of the inverse problems usually two methods, exhausting and regularization, are applied [7]. Exhausting methods allow to reduce the initial inverse problem of electromagnetic testing to a nonlinear programming problem which consists in finding the position of global minimum of some function. The minimum coordinates are parameters to be find. The method of global minimization developed at Karpenko Physico-Mechanical institute has shown itself to be effective in solution of inverse problems of microwave electromagnetic nondestructive testing of multi-layer glueing composite and polymer materials. The method is described in paper [3]. In the paper [4], using parallel calculations, it was effectively implied in defectometry of multi-layered materials with inner plane separation and interlayer ones.

Let us assume that, in the result of measurement in the selected frequency range f, we obtain reflection factor values V_e or voltage standing-wave ratio K_u. The latter are in some respective relation with the first. In the method of global minimization, the experimental coefficients are being compared with the theoretical ones $V_t(f_n, \vec{p})$:

$$F = \sum_{n=1}^{N} \left| V_t(f_n, \vec{p}) - V_e(f_n) \right|^2 . \qquad (2)$$

The point of the method of global minimization consist in the determination of the global minimum F. As it is shown theoretically in paper [9] (proof of a theorem of uniqueness and existance of the solution) as well by the help of numeric and nature experiments for thickness measurement and defectometry of multi-layered dielectric structures, the obtained global minimum F definitely corresponds to parameters under study. Thanks to multi-parametreness, obtained solution are stable to influence of errors of an experiment; to errors of the mathematical model describing V_t and to these of calculation, which-occur due, for example, to restriction of PC word length.

At Fig.1, the behavior of the minimization functional F is presented for the structure with parameters: ε_a =3.9; ε_b =3.2; ε_c =6; $\mathrm{tg}\,\delta_a = \mathrm{tg}\,\delta_b = 0.02$; $\mathrm{tg}\,\delta$ =0.5; $d_a = d_b = 20$ mm; $\gamma_1 = \gamma_2 = \gamma_3 = 0.5$ mm at five frequency selection from 36-42 GHz. It is seen that $F(h_1)$ is a multi-extremum function.

The problems of defectometry and structurometry may be solved completely only if computer-aided systems of microwave electromagnetic diagnostics are designed.

2. Experimental Study

The experiments have been performed on precision stands on the basis of meters: P2-61 (the range 8-12 GHz) and P2-69 (53-78 GHz). At picture 2, the general view of a measurement stand in the range 8-12 GHz is shown. It consists from a generator, an indicator of voltage standing-wave ratio $K_u(f)$, which is situated on the generator, and a measurement high frequency path, which has a waveguide bending in plane E at its edge. A table from perspex is fixed to the bending. In the middle of the with experimental samples, a pyramidal horn is situated. With quasi-plane front of irradiation, it is used in diagnostics of multi-layer composite materials. The measurement stand for the range 53-78 GHz on the basis of the device P2-69 is similar of P2-61. At Figs.3 $K_u(f)$ dependencies are shown for a five-layer glueing composite structures: a glass reinforced plastic plate

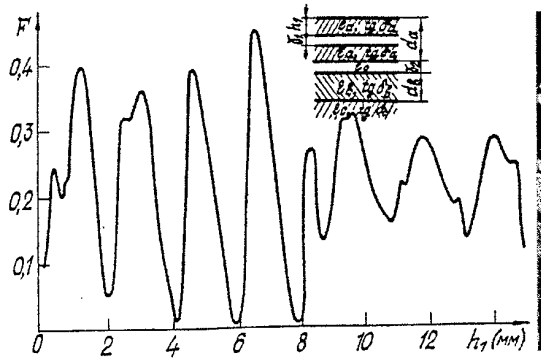


Fig.1.

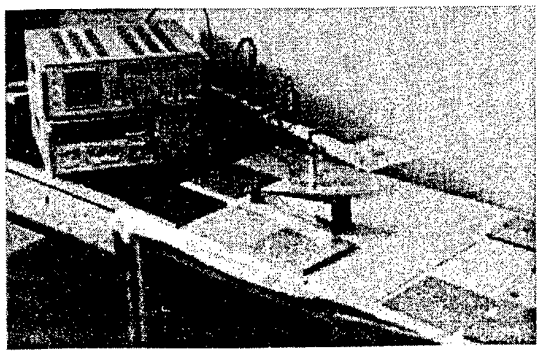


Fig.2.

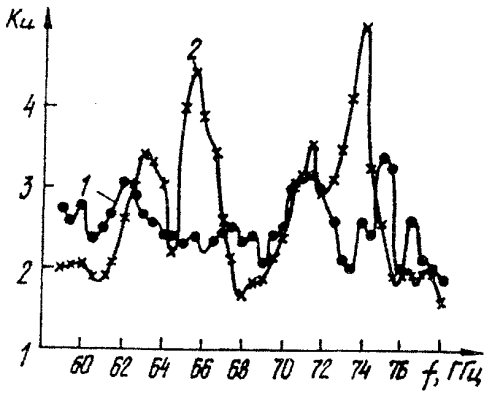


Fig.3.

(1 mm), cell glass reinforced plastic filler (14 mm), again a plate of glass reinforced plastic (1 mm), again cell glass reinforced plastic filler and again a plate of glass reinforced plastic (1 mm). Curves 1 correspond to samples with peelings (non-glueing contacts) between the glass reinforced plastic and filler 0.5 mm thick, and curves 2 correspond to the non-defect cases. It is seen that in order to provide definite testing it is necessary to solve the inverse problem using multifrequency sounding.

3. The Design of the Model of a Microprocessor Super High Frequency Device in Karpenko Physico-Mechanical Institute

Microprocessor SHF portable device for separation and plane inclusions diagnostics in protective coating and composite materials on metallic and dielectric bases (technical parameters)

- defects size: 2 and more μm;
- average diameter ≥2 mm;
- thickness of dielectric materials: 10 μm – 5 cm;
- thickness of the base – no limits;
- transmitted wave frequency range: 57-73 GHz;
- level of emission (radiation): <10 mV;
- simplicity in service;
- automatic calibration and solution of inverse problem for single-valued determination of defect location;
- exit to PC;
- signal and audible signaling of defects;
- weight – 5 kg.

References

1. O.B.Ljashchuk, "Theoretical investigation of plane electromagnetic wave on stratified dielectric structure", Registered manuscript in WINITI, Moscow N784, 40 p., 28.12.1984 (in Russian).
2. B.I.Kolodiy, O.B.Ljashchuk, "Numerical solution of direct problems of electromagnetic reflectometry of planestratified dielectric", Academy of Sciences of Ukrainian SSR, Physico-Mechanical institute. Preprint N128, Lviv, 30 p, 1988 (in Russian).
3. B.I.Kolodiy, O.B.Ljashchuk, "Determination of layers thickness in flat-layer dielectric by means of radio-wave methods", Defectoscopia, N8, p.88-91, 1987. (in Russian).
4. O.B.Ljashchuk, "Electromagnetic Diagnosis of Multi-Layers Polymer Materials Including Stratification Type of Defects", Defectoscopia, N9, pp.71-77, 1990, (in Russian).
5. B.I.Kolodiy, O.B.Ljashchuk, "The Direct and Inverse Problems of Electromagnetic Diagnosis of Plane-Layered Composite Materials Using a Rectangular Waveguide", Physico-Khimichna Mekhanika Materialiv Journal, N2, pp. 26-33, 1994 (in Ukrainian).
6. B.I.Kolodiy, O.B.Ljashchuk, "Direct and Inverse Problems of Electromagnetic Waves Reflection from the Anisotropic Dielectrics", Proc. MMET'96, VI International Conference on Mathematical Methods in Electromagnetic Theory, Ukraine, Lviv, pp.454-456, Sept. 10-13, 1996.
7. A.V.Tichonov, V.Ya.Arsenin, "Methods of Noncorrect Problems Solution", Nauka Publ. House, Moscow, 285 p., 1979 (in Russian).
8. B.I.Kolodiy, O.B.Ljashchuk, B.I.Fedorchak, Radiowave Thickness Measuring og Flat-Layer Dielectric Materials Using Globe Minimisation Method", Defectoscopia, N9, pp.67-71, 1990 (in Russian).

THE ERROR'S INFLUENCE ON THE ACCURACY OF INVERSE PROBLEMS SOLUTION FOR THE MICROWAVE ELECTROMAGNETIC DIAGNOSIS OF MULTILAYER MATERIALS

O.B.Ljashchuk
Ph.D., senior investigator

Address: Physico-Mechanical Institute of the National Academy of Sciences of Ukraine,
Naukova Str. 5, Lviv, 290601, Ukraine
Tel. 380 (0322) 63-32-00
Fax. 380-0322-649427; E-mail panasyuk@ah.ipm.lviv.ua

1. Formulation of Problem

Using polymer composite materials in many branches of engineering requires the determination of their electrophysical and geometrical parameters. Such testing can be effectively realised on the basis of investigated objects sounding by means of electromagnetic waves in the superhigh frequencies range.

Theoretical basis of foregoing testing is solution of electrodynamical direct and inverse problems. While solving these problems the reflection coefficients V (in the case of one side access to the tested objects) as frequency function are considered to be an initials data. Describe the geometrical and electrophysical characteristics of the tested objects by some vector $\vec{p}$. Then we have the equation

$$V = A[\vec{p}], \tag{1}$$

where A is a wholly continuous operator with nonbounded inverse one ($\vec{p} \in P$, P is metric space). The direct problem on electromagnetic waves interaction with the tested object consists in solution of equation (1) that is in determining reflection coefficients V on the basis of known characteristics $\vec{p}$. Inverse problem of interaction of electromagnetic field with the structure as applied to the nondestructive testing, consist in determination of $\vec{p}$ on the basis of known V. In practice it is important to study the influence of the errors of an initial data V and the number of sounding frequencies on the accuracy of desired parameters determination.

2. Direct and Inverse Problems

We shall consider the structure which consists of M-1 dielectric layers with thickness h_m (m=1,...,M-1) and located between two halfspaces x<0 and $x > \sum_{m=1}^{M-1} h_m$. It is assumed that every layer has the flat boundaries and is homogeneous and isotropic. The lamination that would arise between the layers or inside separate ones are also represented as layers with flat boundaries. The investigated structure is characterised by the number of layers M, their thicknesses h and electrophysical parameters. So, this structure may be described by the vector $\vec{p}$ in $3M$-dimentional space P:

$$\vec{p} = \left(M; \varepsilon_1, \operatorname{tg}\delta_1, h_1; \ldots, h_{M-1}; \varepsilon_M, \operatorname{tg}\delta_M\right), \tag{2}$$

where ε_m and $\operatorname{tg}\delta_m$ are relative permittivity and dielectric loss tangent of corresponding layers. The equation far electric intensity E has the form (incident waves are perpendicular):

$$\frac{d^2E}{dx^2} + km^2 E = 0, \tag{3}$$

$$km^2 = \omega^2 \mu_0 \varepsilon_m'; \ \varepsilon_m' = \varepsilon_0 \varepsilon_m (1 - i \operatorname{tg} \delta_m); \ \omega = 2\pi f . \tag{4}$$

Here m=0,1,...,M; m=0 and m=M correspond to upper and lower halfspace; ε_0 and μ_0 are absolute permittivity and permeability for vacuum. Using the continuity conditions for tangential electric and magnetic components and the radiation condition, one can find to [1] expression for reflection coefficient:

$$V = \frac{N_0 - Y_1}{N_0 + Y_1},$$

$$Y_m = N_m \frac{Y_{m+1}(\exp(z_m) + 1) + N_m(\exp(z_m) - 1)}{Y_m(\exp(z_m) + 1) + N_{m+1}(\exp(z_m) - 1)}, \tag{5}$$

$$z_m = 2i\omega h_m \sqrt{\varepsilon_m' \mu_0} \ , \ N_m = \sqrt{\varepsilon_m' / \mu_0} \ , \ Y_M = N_M .$$

Further we shall consider 2 dielectric plates located on semiinfinite dielectric subground. Let the plate 1 has the thickness d_1, there is the delamination in the plate with thickness γ_1 at distance h_1 from the plate surface, at which a sounding wave is incident. A defects in a from of a peeling γ_2 and γ_3 thicks are situated between 1 and 2 plates, and 2 plate and subground respectively. The calculation of V have been performed according to relationships (5) and (4). The dependence $|V(f)|$ for the $d_1 = d_2 = 20$ mm; $\varepsilon_1 = 3.9$; $\varepsilon_2 = 3.2$; $\varepsilon_3 = 6$ (subground); $\operatorname{tg}\delta_1 = \operatorname{tg}\delta = 0.02$; $\operatorname{tg}\delta_3 = 0.5$ for plate materials are presented in Fig.1. Lines 1-4 correspond for $\gamma_1 = 0.5$ mm and $h_1 = 1$ mm; 1) $\gamma = \gamma_3 = 0$; 2) $\gamma = 0.5$ mm; $\gamma_3 = 0$; 3) $\gamma = 0$; $\gamma_3 = 0.5$ mm; 4) $\gamma = \gamma_3 = 0.5$ mm. Similar regularities are observed for other multi-layer structures [2]. Therefore, in order to obtain the definite solution of the diagnosis problem, when prior information is not enough and the range of possible variations of parameters under detection is wide it is necessary to solve the inverse problems.

For numerical solution of the inverse problems usually two methods, exhausting and regularisation, are applied [3]. Exhausting methods allow to reduce the initial inverse problem of electromagnetic testing to a nonlinear programming problem which consists in finding the position of global minimum of a minimisation function

$$F = \sum_{n=1}^{N} |V_t(f_n, \vec{p}) - V_e(f_n)|^2 \ , \ \vec{p} \in P . \tag{6}$$

Here $V_t(f_n, \vec{p})$ and $V_e(f_n)$ are theoretical and measures reflection coefficients values taken over frequencies fn of sounding waves.

As an example we determine the delamination depth h_1 in multilayer materials with parameters are such as in foregoing direct problem (Fig.1, line 1, with $h_1 = 10$ mm). The global minimum (Fig.2) corresponds to the true delamination depth $h_1 = 10$ mm is F=2×10^{-9}. As it is seen from obtained results, function F is not unimodal and consequently the standard methods of nonlinear programming can't be appied to determination of the global minimum position F and consequently the desired parameters. A method of global minimisation (parallel computation) has been applied for the definite solution of the mentioned problems within a wide range of possible parameters variations, when prior information is not enough and errors (noise) of an experiment are present in [4].

3. The accuracy of inverse problems solution

In practice it is important to study the influence of the errors (mathematical models, calculations and experimentals) and the number N of sounding frequencies on the accuracy of desired parameters determination.

Using the statistical solutions theory, one can find the expression for minimisation function with error's influence (noise)

$$\overline{F} = \frac{1}{1+\nu} F + \frac{\nu}{1+\nu}, \tag{7}$$

where $\nu = D_{\Delta V} / D_V$; D – dispersion V_e (D_V – non noise; $D_{\Delta V}$ – with noise).

For numerical simulation some errors covered on the calculated values V_c of the reflection coefficients as follows:

$$V_e = V_c(1 + sq), \tag{8}$$

where s is the experimental data accuracy and q is a random values in the interval (-1,1) produces by the random number generator. The numerical values for the materials parameters are the some as for Fig.2. From the Table 1

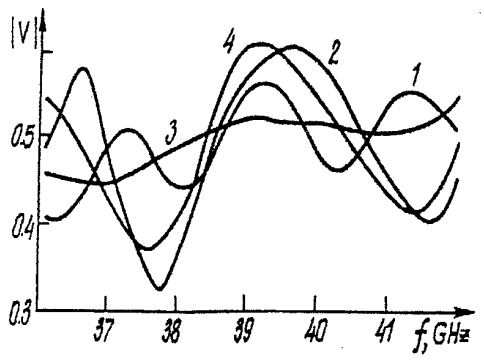


Fig.1.

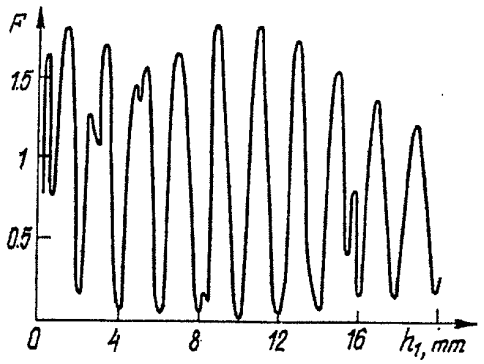


Fig.2.

it is seen that the global minimum values is increasing with errors increase, and the position of this minimum is shifting relatively to the true values of parameters. An increase of the sounding frequencies number permits to obtain more accurate values of an unknown parameters.

S,%	N	F
		h_1,mm
0	5	2.0×10^{-9}
		10.0
5	5	5.1×10^{-4}
		10.1
10	5	1.6×10^{-3}
	15	18.9 1.1×10^{-2}
	25	14.2 1.3×10^{-2}
		9.8
20	5	6.7×10^{-3}
	15	3.8 3.1×10^{-2}
	25	14.8 4.0×10^{-2}
		10.5

Tabl.1

References

1. J.Wait, "Electromagnetic waves in stratified media", Pergamon Press, Oxford - etc., pp.608, 1970.
2. O.Ljashchuk, "Theoretical investigation for reflected plane electromagnetic waves from multi-layer dielectric structures" (Depon. in VINITI, N784-85, Physico-Khimichna Mekhanika Materialiv Journal), Lviv, pp.40, 1985 (in Russian).
3. A.V.Tichonov, V.Ya.Arsenin, "Methods of Noncorrect Problems Solution", Nauka Publ. House, Moscow, 285 p., 1979 (in Russian).
4. O.B.Ljashchuk, "Electromagnetic Diagnosis of Multi-Layers Polymer Materials Including Stratification Type of Defects", Defectoscopia, No9, pp.71-77, 1990, (in Russian).

MEASUREMENT OF A DIELECTRIC PERMEABILITY OF SOLUTIONS BY A RESONATOR APERTURE METHOD

A.V. Koberidze
National Shevchenko University of Kyiv , Radiophysics Faculty
64 Volodimirska St., Kyiv, 252017 Ukraine
tel.: 380+44+266 05 51, E-mail: koba@ukrpack.net

The development of a resonator aperture method is continued. This method combines advantages of resonator and waveguide methods. It is close to a resonator method on the sensitivity, and on convenience and simplicity of use - to waveguide method. The general computational formulas were received in [1]. The similarity of these formulas to the similar formulas in resonator method testifies to correctness of selection of physical model and method of the solution.

The relation of parameters of the resonator (resonant frequency and Q-factor) from a microwave dielectric properties of medium, in which the wave through resonator aperture is radiated, underlies a resonator aperture method.

Relation of property of an aperture to radiate from a ratio between complex dielectric permeability's of medium inside and outside of the resonator is used for obtaining general computational formulas.

The practical implementation of a resonator aperture method can have some versions. Here are the basic elements, which can vary:

1. The type of the resonator and excited oscillation.
2. The shape and size of a hole (aperture).
3. The location of a hole.
4. Thickness of the aperture and position of a plane of separation of mediums.
5. Electrodynamics conditions of radiation:
   - •Into free homogeneous space;
   - •Into the waveguide with homogeneous filling;
   - •Into inhomogeneous medium.

The procedure of measurements also can differ. The measurement in relation to the resonator without a hole or in relation to the resonator radiating into another medium is possible.

At the theoretical analysis the method of small disturbances is used. The change of a flow of Poynting's vector can be made by change of any parameter of the resonator. We shall take into account change only of one parameter, namely integrity of volume. The variation of a flow of Poyntig's vector is equal to an emission power from volume. The resonator detuning is made by a small hole is equal:

$$\delta\omega = j\frac{\delta N_{s+\delta s}}{\varepsilon_0 \int_V EE^* dV} = j\frac{P}{W}.$$

Here P - power which is radiated from a hole; W - energy accumulated in the resonator; j - imaginary unit.

The simplest case is the radiation from a round hole into infinite homogeneous medium. Let small round hole is located in centre of a face wall of the prism $(a \times b \times l)$ resonator exited on H_{10P} the type of oscillation. The dielectric permeability of substance inside the resonator is equal to unit. In this case power P is equal:

$$P = \frac{8}{27}\frac{\omega_0^4 \varepsilon_0 d^6 \sqrt{\varepsilon}}{\pi c^3} H_{0x}^2$$

Here, H_{0x} -is amplitude of strength of a magnetic field along an axis OX tangent to a face walls prism resonator; ε - dielectric permeability of ambient substance.

Energy accumulated in the resonator, also can be expressed through this field part:

$$W = \frac{1}{8}\mu_0 H_{0x}^2 abl\left(1 + G^2\right)$$

$$G = \frac{l}{\rho a}$$

Finally for detuning of the prism resonator by a small face hole is received:

$$\delta\omega = j\frac{64\varepsilon_0\omega_0^4 d^6\sqrt{\varepsilon}}{27\mu_0 abh\pi c^3\left[1+\left(\frac{l}{\rho a}\right)^2\right]} = jA\omega_0^4\sqrt{\varepsilon}$$

We use further transition to complex frequencies and finally are received:

$$\varepsilon' = \frac{(\omega-\omega_0)^2 - (\Delta\omega-\Delta\omega_0)^2}{A^2\omega_0^8}$$

$$\varepsilon'' = 2\frac{(\omega-\omega_0)(\Delta\omega-\Delta\omega_0)}{A^2\omega_0^8}$$

$$A = \frac{64\varepsilon_0 d^6}{27\mu_0 abh\pi c^3\left[1+\left(\frac{l}{\rho a}\right)^2\right]}$$

These ratioes are obtained in conditions of some approximations:

- The Q-factor of the resonator without a hole is considered equal more than 100; it gives an error less than 1%.
- At Q-factor 100 imaginary parts of a dielectric permeability are less than half of a real part of a dielectric permeability; at large values of Q-factor the imaginary part can be more; it gives an error no more than 10%.

For connection of the resonator with a measuring line the second hole - hole of connection is used. The resonant frequency and loaded Q-factor can be measured in experiment. The accuracy of measurement strongly depends on parameters of connection. Obviously, the maximum accuracy is reached in conditions, when the connection with a measuring line is close to critical. The parameters of connection are necessary for transition from loaded Q-factor to the own Q-factor.

The resonator aperture method is convenient especially for use in technological processes for the control of parameters of fluids. It is expedient distinguishes absence of thin handsets for connection with a sample.

The obtained formulas were checked up in experiments with a water, water solutions of ethyl alcohol and sucrose. The measurements were made on frequencies 10 and 35 GHz. The proportionality of a real part of a dielectric permeability of the sixth degree of diameter of a hole is confirmed. The permeability values are obtained close to known.

References

A.V. Koberidze, «Resonator aperture as an antenna for measuring media variables», Proceedings of the Second International Conference on Antenna Theory and Techniques. Kiev, 20-22 May, 1997. P.224-225.

REALIZATION OF PRINCIPLE OF FOURIER HOLOGRAPHIC PROCESSING IN MULTIFREQUENCY MEASUREMENTS IN RANGE 126.6-145.4 GHz

O.O.Drobakhin, D.Yu.Saltykov, A.Yu.Velikiy
Radiophysics Department, Dniepropetrovsk University.
Address: Bildg. 13, Nauchny pereulok, Dniepropetrovsk, 320050, Ukraine
Tel. 0562 - 46 - 79 - 95

INTRODUCTION

Spectral analysis of complex reflection coefficient measured at many frequencies in wide band is powerful tool of diagnostics and non-destructive testing of dielectric structures. This approach is similar to time pulse probing. Widening of frequency band gives possibility of synthesizing shorter pulses thus structures with less thickness can be tested. For this purpose millimeter wave range is more preferable than centimeter range. In the latter range phase measurements can be realized as by means of signal transformation to lower frequencies with phase measurements at low frequencies as by means of 6-port reflectometer conception application.

In 2.5 mm wavelength range the first way requires many steps of transformation therefore it is not suitable. The shortage of the second way is lack of the set of standard loads. In this wavelength range the role of precise conjunction is steadily growing. The idea of time-domain signal synthesis without direct phase measurements is very attractive. It was shown [1] that if distance between reference discontinuity and a structure under test (SUT) was provided more value than SUT electric thickness, one could obtain a part of result of transformation into time domain coinciding with time-domain signal calculated by Fourier transform of complex reflection coefficient. Reference reflection can appear as before or after reflections of SUT.

In range 17-25.5 and 26-37.5 GHz described approach has been realized by recording square modulus of interference of informative reflection and reference reflection. The latter has been obtained by reflection from open end of waveguide [1] or horn throat [2]. But in range 126.6 - 145.4 GHz waveguide junctions can not be realized so thoroughly thus they can play the role of additional reference reflections.

THEORY OF THE METHOD

Let us analyze amplitude reflectivity $A(\omega)$ from SUT with complex reflection coefficient $R(\omega)$ in presence N reference reflections r_i with time delays t_i. r_i and t_i include not only reflections from aperture but reflections in waveguide junctions. Then $A(\omega)$ is given by

$$A(\omega) = k\left|\sum_{i=1}^{N} r_i \exp(+j\omega t_i) + R(\omega)\right|^2 =$$
$$= k\left\{\left|\sum_{i=1}^{N} r_i \exp(+j\omega t_i)\right|^2 + |R(\omega)|^2 + \sum_{i=1}^{N} r_i^* R(\omega)\exp(-j\omega t_i) + \sum_{i=1}^{N} r_i R^*(\omega)\exp(+j\omega t_i)\right\}. \quad (1)$$

After subtracting results of measurements under conditions of radiation into space without SUT

$$A(\omega) = k\left\{\left|\sum_{i=1}^{N} r_i \exp(+j\omega t_i)\right|^2\right\}, \quad (2)$$

expression (1) is transformed to

$$A(\omega) = k\left\{|R(\omega)|^2 + \sum_{i=1}^{N} r_i^* R(\omega)\exp(-j\omega t_i) + \sum_{i=1}^{N} r_i R^*(\omega)\exp(+j\omega t_i)\right\}. \quad (3)$$

Inverse Fourier transform of $A(\omega)$ contains autocorrelation function $r_A(t)=F^{-1}\{|R(\omega)|^2\}$($F^{-1}\{\ \}$ - inverse Fourier transform) and set of cross-correlation functions $r_i(t)=F^{-1}\{r_i^* R(\omega)\exp(-j\omega t_i)\}$ which appear at positive time and $r_i(t)=F^{-1}\{r_i R^*(\omega)\exp(+j\omega t_i)\}$ which are observed at negative time.

Cross-correlation functions $r_i(t)$ are not overlapping with autocorrelation function if t_i are greater than time τ of propagation in SUT. The condition of non-overlapping $r_i(t)$ and $r_k(t)$ is $|\ t_i - t_k\ | > \tau$. If any r_i has uniform frequency characteristics, any cross-correlation functions $r_i(t)$ coincides in form with time-domain response of SUT. If r_k is dominant then only $r_k(t)$ can be used and situation can be simplified. Thus the conditions for time intervals must be satisfied only for reference discontinuity r_k.

EXPERIMENTAL RESULTS

Experiments have been carried out in range 126.6 - 145.4 GHz with step 200 MHz. Generator G4-161 has been used as the source of the signal. The error of frequency setting up was ±1.5%, i. e. ~ 2 GHz. Ordinary scalar waveguide reflectometer with two directional couplers has been used. The size of rectangular waveguide cross-section was 1.6 × 0.8 mm. Voltmeters V7-27A/1 have served as power-meters.

Variations of incident wave power as function of frequencies were ±25%. But reflected wave power changed in ten times. In comparison, in frequency range 17 - 25.5 GHz for waveguide reflectometer with cross-section 11 × 5.5 mm variations of incident and reflection wave power did not exceed ±10%. Therefore the calibration this short-circuit load was need. From point of view of time-domain signals, division of experimental data by result of short-circuit calibration is similar to inverse filtering. In contrast to this situation, in 15-mm and 8-mm wavelength ranges this calibration procedure is not necessary.

In 15-mm and 8-mm wavelength ranges open end of rectangular waveguide is very suitable source of reference signal and its gain is sufficient for measurements at distances 15 - 20 cm (10 - 25 λ). Our experiments demonstrated that in contrast to wavelength range mentioned in 2.5-mm wavelength range open end of rectangular waveguide with and without flange was not applicable. This situation is explained as by presence of contact pins with resonance properties as by lack of gain.

The time-domain signal synthesized from frequency data for radiation of a horn in space without SUT is shown in fig. 1. The horn had sizes: length 50 mm, aperture sizes 21 × 26 mm. In purpose of flange adjustment additional waveguide section with length 50 mm was used. Electrical length of the horn and the waveguide section were approximately 73 and 81 mm due to different values of phase velocity. The structure of the signal displays that there are three essential reflections in experimental track. The first of them is in flange connection of the reflectometer and the waveguide section. The second one is in flange connection of the waveguide section and the horn. This discontinuity is situated closely to the horn throat. The third one evidently is in the horn aperture. Really the peak number 1 is cross-correlation of discontinuities in the horn throat and the aperture. The peak 2 is the result of interference of the horn discontinuity and the discontinuity in flange connection of the waveguide section and the horn.

The time-domain signal for metallic plate situated in 120 mm from aperture plane is presented in fig. 2. The peak 1 describes reflection from metallic plate. It has additional components 2 and 3 that shows complicated structure of reference reflections. The width of peak at 3 dB level is 12.8 mm, i.d. ~ 45 ps. Subtracting results of measurements without SUT does not allow to remove completely components of time signal in the original due to errors of frequency setting up. The time-domain signal for plexiglass layer with thickness 39 mm is shown in fig. 3. The peak 1 is reflection from front surface and the peak 2 is reflection from rear surface. Estimates of effective $\varepsilon' = 2.95$ and $\mathrm{tg}\,\delta = 0.037$. Attempt of foams measurements was failure. It was noted that reassembling measuring sometimes caused swap of dominant reference reflections. For instance sometimes reflection in the connection of the waveguide section and the horn was dominant.

References

1. O.O.Drobakhin, V.F.Borulko, and V.A.Karlov, " Millimeter Apparatus for Transmission Line and Dielectric Material Measurements by Multifrequency Methods", In: CPEM-96 Conference Digest, Germany, Braunschweig, pp.598-599, 1996.

2. O.O.Drobakhin, " Principle of Fourier holographic processing in multifrequency microwave measurements ", In: Conf. Proc. 1998 Int. Conf. on Mathematical Methods in Electromagnetic Theory, Ukraine, Kharkov, vol.1, pp.598-599, 1998.

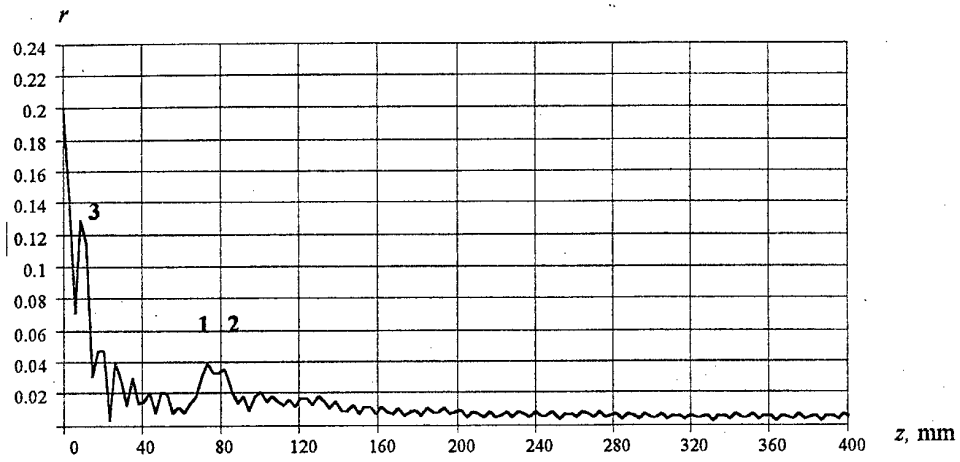


Figure 1. Time-domain signal for free space calibration

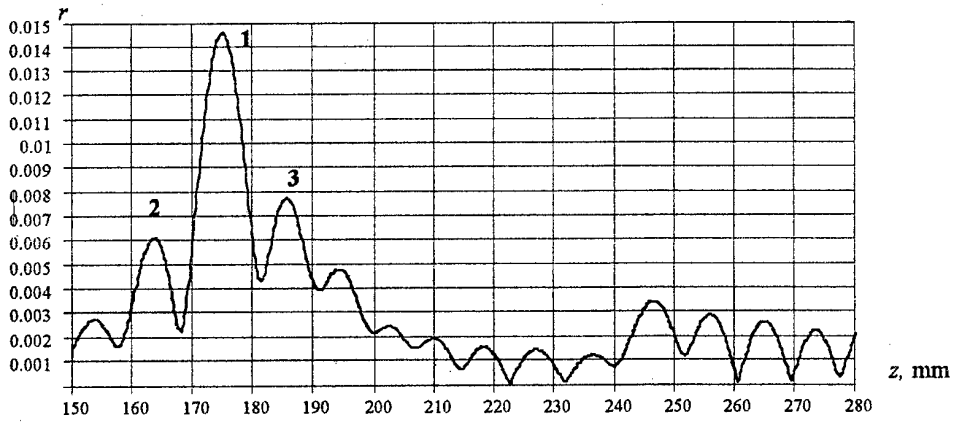


Figure 2. Time-domain signal for metallic plate

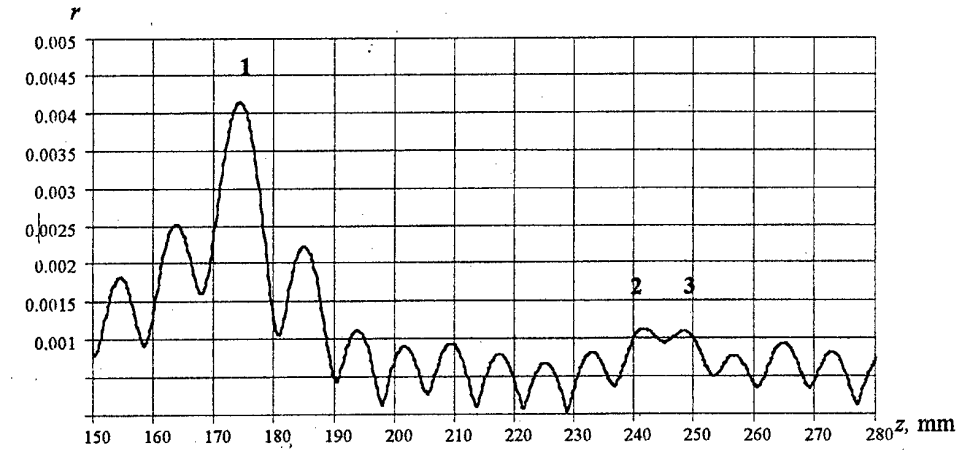


Figure 3. Time-domain signal for plexiglass layer

VIBRATORY STRING AS A PERTURBATION BODY IN ORDER TO MEASUREMENT ELECTROMAGNETIC FIELD OF MICROWAVE RADIATORS

A.Ya. Kirichenko, O.A.Suvorova
A.Ya. Usikov Institute for Radiophysics and Electronics,
National Academy of Sciences of Ukraine
12 Acad. Proskura St., Kharkov, 310085, Ukraine
Tel: 380-572-448323, E-mail: shig@rian.kharkov.ua

It is well know that perturbation method has been proposed and widely used by several scientists for measuring microwave field in cavity and open microwave resonators [1,2]. A perturbation method for measurement of free space microwave fields is described in [3]. Naturally, the application of this method for measurement of field in free space is more difficult. This method requires an examination of weak useful signal on the background of surroundings. Precise instruments are required for measurement of small values.

In this paper possibility of usage of vibrating string as an perturbation body for exploration of electric components distribution at near-field of radiator is described. Until the present time vibrating string method has been used only for exploration of electron beams. The arrangement of setup considered is shown in Fig.1.

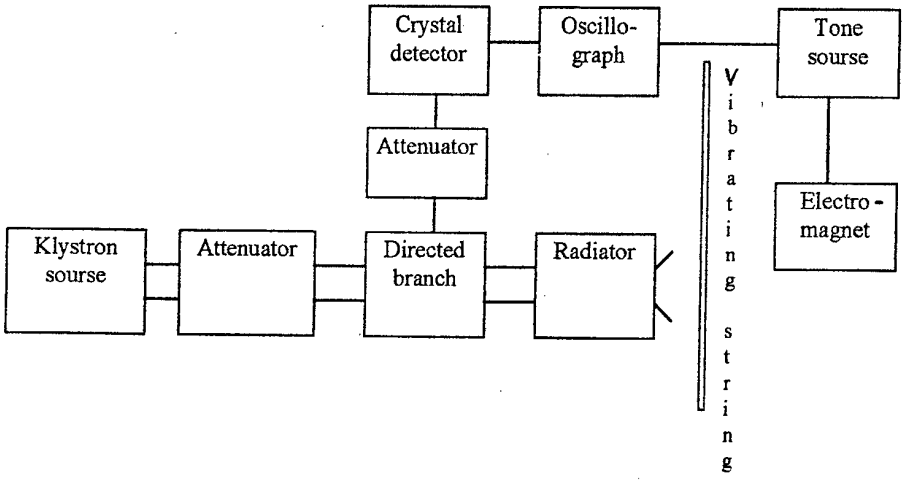


Figure 1 Experimental setup

First of all we inserted the infinitely long metal string, which is considerably thinner than radiation wavelength, to the field of radiator. The part of the field diffracted on the string reflects toward radiator and is received by radiator which works as receiving antenna. If amplitude of metal string oscillation exceeds the radiator size, it opens perspectives for signal scattering from test body. Thereupon it should be pointed out that measured speed grows as well as system reliability. By means of directed branch located in feeding channel of radiator the reflected from radiator aperture signal arrives receiver. In order to detect signal reflection from immobile objects and the reflection due to mismatch of the radiator with its waveguide, metal string oscillates.

The oscillation of string is realized at its resonance frequency by electromagnet which is fed by alternative current from the tone generator. The scanning of oscilloscope used as signal indicator in the receiver is realized at frequency of tone generator.

The metal string moves practically parallel with the plane for a wavelength less then 10 mm, if this string with length 150 to 200 mm oscillates in fundamental mode. It makes possible to observe amplitude and phase distribution of the field at the plane of sting oscillation at the screen of oscilloscope when the radiation field has linear polarization. The setup described operates at a wavelength about 8 mm.

In order to make an estimate of this method, the test measurement of radiation patterns has been performed. Figure 2 shows typical experimental curves for radiation pattern of open-ended rectangular waveguides with dimensions 7.2 x 3.4 mm. (curve 1) or 7.2 x 0.8 mm (curve 2) without flanges. Curve radiation pattern of routing waveguide with flanges is also plotted in this figure (curve 3). The radiation pattern is shown in two sections - E-plane (a) and H-plane (b). It is found that there are differences between these patterns.

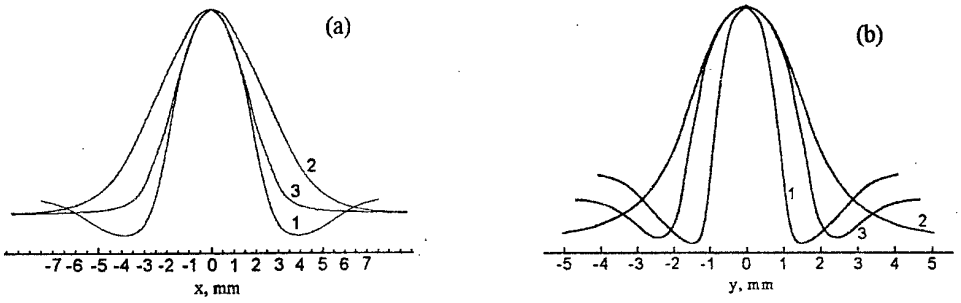


Figure 2. Comparison of E-plane (a) and H-plane (b) radiation patterns of open-ended rectangular waveguide

Figure 3 shows the variation field of surface wave of periodic structure. The measurements are fulfilled at frequency of 35 GHz at delayed wave 2.6.

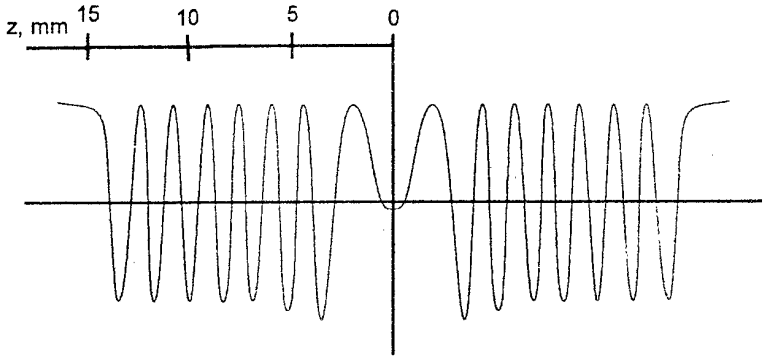


Figure 3. The variation of field along surface of periodic structure

In the same way we succeeded in defining radiating spot size and distribution of whispering gallery wave on the different mode in the dielectric half disk resonator. Thus, a vibratory string is a suitable instrument for measuring electromagnetic field of microwave radiators.

References

1. J.C. Maier, J.C. Slater, «Field-strength measurements in the resonant cavities», Journal of Applied Physics, vol. 23, № 1, pp. 68-77,1952
2. Yu. M. Tsipanyuk, «The test - body in open resonator», in digest «The Great Powerful Electronics», Moscow, Nauka, № 4, pp. 173-177,1965 (in Russian)
3. A.J. Cullen, J.C. Parr, «A new perturbation method for measuring microwave fields in free space», Proc. IEE, vol. 102B, №6, pp.836-844, 1955
4. I.K. Ovtchinikov , N.S. Zinchenko, «Method of vibrating probe for investigation of axial symmetric electron beams», Ukrainsky phisicheskiy jurnal, vol. 4, №2, pp.219-228, 1959, (in Russian)



BIOMEDICAL APPLICATIONS OF MM AND SUBMM WAVES

Preceding Page Blank

RADIOTHERMOGRAPH MILLIMETRES OF A RANGE FOR MEDICAL DIAGNOSTICS

B.Makarenko, V.Kudryashov, E.Khomenko, D.Martinenko

At diagnostics inflammatory of diseases and diseases, the regulations accompanied by infringement of temperature of a body of the person, as well as after traumas need to be supervised temperature on separate sites of a surface of a body. The change of these parameters occurs on concerning a small depth (from a share of mms up to units of centimetres). Change of temperature of a body render influence on own electromagnetic radiation in centimetric and millimetric a range radiowaveband.

This radiation can be registered with the help radiometer of a receiver, to process with the help PC and to display in kind of thermal cards on a screen of a monitor or paper. In a specified range of waves the space sanction, satisfying to requirements, can be received at measurements from the opened space [1].

For research of diagnostic opportunities of remote measurement of temperature of a body of the person is developed medical computer measuring instrument, using electromagnetic radiation. It consists from:

modulation radiometer of 8 mm of a range;

two- focus by an aerial of a system;

device of scanning;

PC AT.

Radio-Btumeter has following characteristics:

temperature sensitivity - 0.12 °K/s;

resolution on a surface of a body of the person no more smaller 15x15 mm;

quantity of colour gradation on whole dynamic range of measurement radiocontrast of temperatures at construction radiothermal of cards, not less than 16.

Received radiothermals of the image of object process with the help programme of realized space filters, that increases quality of the image and promotes allocation measurable

physiology of parameter. The software includes also means of visualisation, storage and editing radiothermal of the images, statistical processing, segmentation and classification of the images.

At the help Radio-Btumeter are investigated 20 ill with appropriate diseases, including with traumas (crisis the bottom extremities). The researches were conducted in branch of functional diagnostics Ukrainian SRI of Therapy and department IPKK of Kharkov. Radio-Btumeter placed on distance 1,2 m from object of research.

The measurement of temperature of a body is conducted by means of sequential moving of an axis of a receiving aerial on a given site of a body of the person. Management of moving of an aerial and the processing of results of measurements are conducted at the help Щ́,Ь. The registration of received data is carried out on magnetic disks. Processed statistics were deduced (removed) in a real time scale on a screen of a monitor.

By results of executed researches it should note, that thermography in millimetre a range of lengths of waves in difference from infrared thermovisions reflects the information on dynamic temperatures in depths in thousand time large (about 1 mm).

Therefore the protective and stabilising effect of surface layers of a leather renders smaller influence to results of measurement of differences of temperatures inside object. On quality of the image is weak an easy clothes influence, dry of cotton bandage, plaster and film bandage and even. Hence, the method radiothermography in millimetre a range can find application when undesirably worry ill, to infringe bandage, as well as in cases, when contact methods thermometry and infrared thermovisions are not applicable.

Literature:

Valieff I.B., Zakharthenko I.I. A system remote dynamic radiovision for medical diagnostics.

Radiotehnics, 1991, ь 8, pp.69 - 74.

USING OF EHF METHOD FOR INVESTIGATION OF RADIATION-INDUCED CHANGES IN DNA HYDRATION SHELL

O. V. Dubovitskaya, V. A. Kashpur, A. A. Krasnitskaya, V. Ya. Maleev
Institute of Radiophysics and Electronics of National Academy of Science of Ukraine
Address: Build. 12, Akademic Proskura Str., Kharkov, 310085, Ukraine
Tel. (0572) 44-83-19, Fax (0572) 44-11-05, E-mail maleev@ire.kharkov.ua

The DNA molecule is considered to be the most important target for the cellular effects of ionizing radiation. As such, much attention has been devoted to elucidating the mechanism of radiation action on DNA and by now the nature of radiation damage of its primary structure has been studied enough in detail [1]. Furthermore, it has been discovered that the extent of radiation influence on biomolecule depends on water amount in its hydration shell [2] which is known to play a dominant role in stabilizing DNA conformation [3]. Thus, it is to be expected that radiation-induced changes of the DNA structure may give rise to destruction of the hydration layer around phosphates, sugars and bases of DNA.

EHF method is sufficiently effective for obtaining information about the radiation-induced changes in the interaction of biomolecules with their water environment because the range of water absorption takes place at millimeter wavelengths (Debye relaxation process of polar water molecules). Since there is not at present sufficient knowledge about the γ-radiation effect on the dielectric properties of biomolecules, the purpose of this study is to obtain by means of EHF dielectrometry and some other electric measurements the data on the state of DNA ion-hydration shell at different doses of γ-radiation. It will permit to estimate a contribution of hydration changes to the radiation effects observed.

Materials and methods. Samples of calf thymus DNA (Serva, sodium salt, 38% hyperchromicity in concentrations of 0.75% for dielectrometric and of 0.2% for conductivity studies in a medium of 0.01 M NaCl were used. Irradiation was performed using ^{60}Co-γ-source with a dose rate 6 Gy/min. DNA solutions were irradiated at doses 19, 370, and 1650 Gy. Measurements were carried out at 20 ^{o} C.

The extent of radiation influence was checked by electrophoresis. A 1% agarose gell in 0.089 M Tris-borate buffer (pH 8.2) with addition of 0.003 M EDTA was used. The lengths of DNA fragments were estimated by some markers (see Fig. 1).

EHF measurements were fulfilled at 7.6 mm wavelength by differential dielectrometer described previously [4]. The basic element of the metering device is a dielectric cell consisting of two consequently disposed cuvettes of variable thickness. One cuvette contains a sample with known complex permittivity ($\varepsilon^* = \varepsilon' - i\varepsilon''$) and other is one under investigation. The initial experimental values are the differences of attenuation $\Delta\alpha$ and phase shift $\Delta\beta$ of these two substances. The differences of real $\Delta\varepsilon'$ and imaginary $\Delta\varepsilon''$ parts of complex permittivity at wavelength λ

$$\varepsilon' = \lambda/\lambda_c + (\lambda/2\pi)^2(\beta^2 - \alpha^2), \quad \varepsilon'' = 2(\lambda/2\pi)^2\alpha\beta .$$

Conducting medium needs of a conductivity correction $\varepsilon'' = \varepsilon''_{meas} - \sigma/f$ where f is frequency. Conductivity measurements were made by the use of an AC bridge at 10 kHz.

Since the Debye theory of dipole molecules is true for aqueous solutions with sufficient accuracy [5], in order to find some radiation-induced changes of dielectric parameters we can use the Debye equations to pass from description by ε' and ε'' values to that in terms of parameters ε_s and λ_s ($\lambda_s = 2\pi c \cdot \tau$ where τ is relaxation time of polar molecules)

$$\varepsilon_s = \varepsilon' + (\varepsilon'')^2/(\varepsilon' - \varepsilon_\infty) \text{ and } \lambda_s = \lambda\varepsilon''/(\varepsilon' - \varepsilon_\infty)$$

where ε_∞ is the high-frequency limit of dielectric constant. As free water molecules have absorption peak in the range of wavelength 7.6 mm and DNA molecules does not absorb there [6], $\Delta\varepsilon_s$ is only due to the change of the amount of the water molecules which are tightly bound to the DNA and does not absorb microwave energy in the millimeter range.

Supposing that the aqueous solution of biomolecules represents a medium of high permittivity ε_s with suspended particles of low permittivity we can use in the case of a low concentration c the following equation for the calculation of the hydration change $\Delta\omega$ (in the linear approximation)

$$\Delta\omega = A \cdot \Delta\varepsilon_s / pc - v$$

where v is specific volume of macromolecule, p is the form coefficient, and $A = 1/(\varepsilon_s - \varepsilon_\infty)_{water}$ [4].

Results and discussion. The results obtained in this study are shown in Table 1 and Figure 1. The conductivity value of 0.01 M NaCl solution σ is equal to 1.01×10^{-3} $(\Omega\cdot\text{cm})^{-1}$, ε' and ε'' values of the native DNA solution are equal to 17 and 28, respectively. The radiation action at 19 Gy practically had no influence on the parameters being investigated, however at doses 370 and 1650 Gy it gave rise to some small but reliably recorded changes of dielectric properties.

Table 1. Dielectric and hydration properties of γ -irradiation DNA

Parameters measured	Control solution of DNA	DNA solutions irradiated at doses (Gy)		
		19	370	1650
$\Delta\varepsilon'(\pm0.01)$	0,00	0,01	0,03	0,04
$\Delta\varepsilon''(\pm0.01)$	0,00	0,00	0,07	0,05
$\sigma(\pm0.01)\times10^3$, $\Omega^{-1}\cdot\text{cm}^{-1}$	1,15	1,15	1,14	1,17
$n(\pm1)$, water mol./nucl.	19	19	15	(18)

It can be seen from the Table 1 that the trustworthy increase of conductivity was observed at 1650 Gy. It was due to the liberation of counterions Na^+ from the polymer as a result of radiation-induced strand breakage. Taking into account the known values of conductivity coefficients it may easily be shown that the increase of the portion of dissociated Na^+ ions from 0.57 to 0.65 per nucleotide at 1650 Gy corresponds to the value $\Delta\sigma$ observed under conditions of this study (DNA concentration and ionic strength). It also follows that the average length of the fragments produced is equal to several hundreds of base pairs, supposing that a single-strand break (ssb) liberates 8.5 counterious [7] and the number of double-strand breaks is a function of ssb. It is in agreement with the electrophoresis data shown in Figure 1.

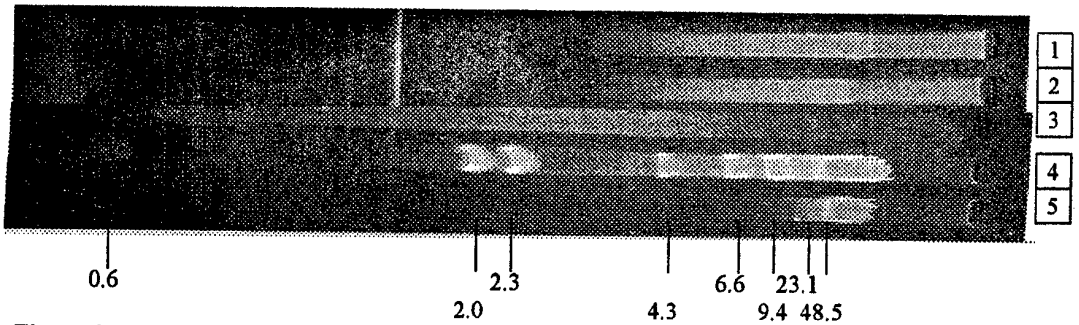


Figure 1. Electrophoregrams of DNA solutions: 1-control DNA solution; 2, 3-DNA solutions irradiated at 19 and 370 Gy respectively; 4-markers of λ -phage DNA-Hind III in thousands of base pairs; 5-λ -phage DNA

The amount of bound water molecules per nucleotide **n** is less by 4(~20%) for DNA irradiated at 370 Gy as compared with the degree of the native DNA hydration which was established by the dielectrometric method as 19 water molecules per nucleotide [5]. This result is obviously due to the destruction of water spin structure arising from the radiation modification of the native conformation of DNA molecule. The especially

important role belongs to distortions of double helix parameters, which have been resulted from the damage of 2-deoxyribosyl.

In recent years it has been found that such processes as breakage of linkages H-Cn′, production of radicals • Cn′ appearance of deoxyribosyl epimers, including those in a conformation similar to the C3′ -endo of deoxyguanosine in Z-DNA, take place in the sugar ring after γ -irradiation [1, 8]. If these conversions happen, the angle between the linkage C1′-N and its primary orientation reaches 80-100°. It essentially affects the location of base in space. The structure of DNA hydration shell appears to be appreciably changed too [3]. In the major groove, the conditions for the formation of water bridges between the methyl group of thymine and an adjacent phosphate oxygen, and the bridges between phosphate oxygen atoms of the chain will be disturbed. In addition, the conditions for the formation of bidentate water bridges between the nitrogen and oxygen atoms of two neighbouring base pairs will also be disturbed. In the minor groove, the alteration of base orientation will violate the water bridges between the O2- atoms of thymine and the N3-atoms of adenine. The state of water spine molecules, which are attached to the imperfect sites of backbone or hydration spine, will be changed too. In that way, DNA hydration must be reduced after γ -irradiation.

It should be noted, that in the case of poly(dG-dC) in which distortions of component orientation in comparison with their orientations in B-DNA are similar to above mentioned (e.g. the distance between adjacent phosphate oxygen atoms decreases from 8-9 $\mathring{A}$ to 4.4-5.2 $\mathring{A}$), the amount of bound water reduces from 19 molecules per nucleotide to 9 for the alternating copolymer [5].

The further rising in the dose of radiation to 1650 Gy did not lead to any increase of dehydration. It can be explained by the predominant influence of new hydration-active centers on the hydration which appear through the radiation modification of canonical bases. The amount of hydroxyl derivatives of purine and pyrimidine bases is equal to 10% of the total number of bases [9]. The notable feature of these compounds is the presence of hydroxyl groups OH and other hydroxyl centers which actively bind water molecules. However, the exact measurement of number n is difficult in this case because of the release of low molecular components of DNA. The amount of bases released at 424 Gy is 0.2% of their total number, but it grows rapidly with dose [10].

So, the changes of the DNA hydration under the exposure to radiation are due to the destruction of the water spine of macromolecule which is caused by distortions of the spatial structure of DNA and by modification of components at high doses. Dehydration can strengthen primary radiation defects of DNA structure, especially under the conditions of strong intermolecular interactions in the cell (e.g. to promote the formation of noncovalent scissions).

This work was supported by the State Foundation of Fundamental Investigations (Grant N 2.4/764).

References

1. V. A. Sharpatyi, " Radiation Modification of a Sugar Fragment in DNA", Radiobiology, Vol. 32, No. 2, pp. 180-193, 1992.
2. S. G. Swarts, M. D. Sevilla, D. Becker, C. J. Tokar, K. T. Weeler, "Radiation-Induced DNA Damage as a Function of Hydration", Radiat. Res., Vol. 129, pp. 333-344, 1992.
3. W. Saenger, "Water and Nucleic acids", In: Principles of Nucleic Acid Structure, Mir, Moscow, pp. 393-412, 1987.
4. V. A. Kashpur, V. Ya. Maleev, T. Yu. Shchegaleva, " Investigation of Globular Protein Hydration by a Differential Dielectrometric Method", Mol. Biol. (USSR) , Vol. 10, No. 3, pp. 568-575, 1976.
5. T. Umehara, S. Kuwabara, S. Mashimo, S. Yagihara, "Dielectric Study on Hydration of B-, A-, and Z-DNA", Biopolymers, Vol. 30, pp. 649-656, 1990.
6. V. Ya. Maleev, V. A. Kashpur, G. M. Glibitsky, A. A. Krasnitskaya, Ye. V. Veretelnik, "Does DNA Absorb Microwave Energy", Biopolymers, Vol. 26, pp. 1965-1970, 1987.
7. M. Adinarayana, E. Bothe, D. Schulte-Frohlinde, " Hydroxyl Radical-Induced Strand Break Formation in Single-Stranded Polynucleotides and Single-Stranded DNA in Aqueous Solutions as Measured by Light Scattering and by conductivity", Int. J. Radiat. Biol., Vol. 54, No. 5, pp. 723-733, 1988.
8. C. N. Trumbore, Y. N. Myers, C. K. Hyde, R. D. Hudson, C. N. Rhodes, J. K. Masselink, "Metal-Ion Assisted, Radiation-Induced Conversion of B- to Z-DNA in poly (dG-dC) and Two Natural DNAs", Int. J. Radiat. Biol., Vol. 66, No. 5, pp. 479-483, 1994.
9. A. F. Fuciarelli, B. J. Wegher, W. F. Blakely, M. Dizdaroglu, "Yields of Radiation-Induced Base Products in DNA", Int. J. Radiat. Biol., Vol. 58, No. 3, pp. 397-415, 1990.
10. E. S. Henle, R. Roots, W. R. Holley, A. Chatterjee, " DNA Strand Breakage is Correlated with Unaltered Base Release after gamma Irradiation", Radiat. Res., Vol. 143, pp. 144-150, 1995.

The physical evidence of the weak electromagnetic field action in the 30-300 GHz region upon biological systems.

L.I.Berezhinsky[1], G.I.Dovbeshko[2]

1-Prospekt Nauki, 45, Institute of Semiconductor Physics, NASU, Kiev-28, 252028, Ukraine; 2-Prospect Nauki, 46, Institute of Physics NASU, Kiev-22, 252022, Ukraine, fax:380-044-265-15-89, e-mail: galina@dpbs-3.kar.net;

Now the study of the low-dose (weak) millimeter (MMW) electromagnetic field action upon biological systems is of great interest due to their well-known biological and therapeutical effects [1-3]. From other hand, the number of natural and artificial sources of millimeter waves increasing every day. Despite the growth of information on biophysical experiments with the weak intensity of the electromagnetic field effects and its medical application, there exist a number of problems in fundamental interpretation of the data obtained. Obviously, it is determined by physical and chemical complexity of the objects under study, by scarcity of information about changes in their characteristics under electromagnetic radiation in real time regime and by absence of new approaches to the explanation of the effect.

In our work 1) using holographic interferometer [4], we have visualized the action of millimeter field upon blood, solution of biological molecules and tissues. With holographic interferometry we have registered the changes in refractive index of model solution. The changes in refractive index of biological solution in the millimeter field had both reversible and inversible features. 2) With optics and spectroscopy, we have detected the changes in vibrations modes of NH3 and COO terminal groups of aminoacids, which is responsible for the interaction of protein with other biological molecules in biochemical reactions. 3) The changes in protein luminescence kinetics process have been detected also. 4) The modification of tertiary structure of DNA molecules have been observed in model experiments.

Detectable changes in biological molecules under study depend on frequency, power and polarization of electromagnetic radiation.

1) MMW radiation effect upon 2% blood plasma water solution at 51.5 GHz frequency have been investigated. Changes in the refractive index of the sample under MMW action were registered and estimated. In our experiments the maximum change of refraction index during 15 minutes corresponds to $n = 2.59 \times 10^{-4}$, which is by an order higher than the temperature changes of refraction index.

With the account of this total value of MMW radiation effect will make up about 3x10-4. The changes in interference picture were irregular with time. The largest changes occurred during the first minute then they slowed down. During 6.5 min from the start of exposure the number of interference bands in the object's profile decreased essentially . After this period only slight changes were observed. The latter allows the assumption of the saturation effect. Since these changes were observed in the whole plasma volume, their nature was regarded as a macroscopic one.

The reversibility of the effect has been established: after MMW source was switched off, the interferogram had restored its original structure, construction period of original state was 3-4 min longer than the time of maximum change accumulation. The increase in plasma concentration up to 10% was essentially slowing down the process of changes, whereas the addition of 1.5% of CaCl2 into the solution was increasing the rate of interference picture shift more than twofold.

The estimation of the temperature effect by using of thermal conductivity equation and thermal balance equations showed the following. Thus, maximum solution heating in this period with no account of thermal exchange, i.e. under the condition unfavorable for thermal effect estimation may amount to 1 K. The calculation showed that even in the absence of heat exchange between the solution and environment under the radiation effect with the power density of 10 mW/cm^2 the temperature of solution with the volume of 1.5 cm^3 may raise round 1° C within 6 min. Lower temperature value (0.5-0.6° C) was obtained by us in the measurements with the use of thermosensor. Temperature coefficient of changes in water refraction index makes up 6×10^{-5} K. MMW irradiation and heating effects were opposite-directional. Thus, the numerical estimations and the experimental data demonstrate that refraction index changes under MMW action were conditioned by non-thermal changes of solution dielectric constant which may be described as a sum of contributions of electronic, vibrational and orientational components. Evidently, structural rearrangements took place in plasma solution and in its components – biomolecules. Therefore, low-energy MMW radiation initiates the processes of internal

rearrangements in solution, which may result in modifications of medium electronic polarizability observed from refraction index change.

2) Unique properties of biological molecules and crystals are determined mainly by weak bonds, in particular, by H-bonds. It is well known, that the energy of H-bonds is in the range from tens of kcal/mol to unites and less. As it was estimated with molecular mechanics calculations, the energy of the conformational transitions of the building blocks of biological macromolecules such as DNA bases is about 1-2 kcal/mol, sometimes 10-1000 times less [5,6]. This energy lies in the region of energies, which corresponds to MMW radiation. That is why we attempted to study the influence of the weak MMW radiation on the structure of biological molecules with infrared spectroscopy (IR). We have established [7,8] that some bands of α-glycine and β-alanine single crystals have changed under the action of weak MMW field with power density less than 10 mW/cm^2 at some resonance frequencies in the range of 37.5 to 78.5 GHz.

We have examined polarized IR spectra of single crystals of aminoacids, namely, α-glycine, β-alanine, L-histidine and DNA molecules and their changes in MMW electromagnetic field.

In the polarized IR spectra of aminoacids, the essential changes (intensity changes, redistribution of bands and its shapes and structure) occur under the MMW radiation. The most drastic changes were observed for the NH_3^+ and COO^- vibrations in all objects under study. Changes in the shape and halfwidth of NH_3^+ and COO^- bands could be explained in the assumption of the existence of multiwell potential field for proton energy in these groups. Changes of the dipole moments of $NH3^+$ and COO^- vibrations under the action of MW radiation are supposed to be connected with the changes of directions of H-bonds involved in corresponding vibrations. As it is known from [9], the intensity of deformational vibrations are changed slightly under the H-bond in contradiction of intensity of valent vibrations, which are drastically changed in the case of H-bond formation. In our experiments the intensity of valent and deformational vibrations, including in H-bonding is drastically changed in the aminoacid crystals under the MMW radiation. The values and directions of these changes depend on frequency, polarization and power of MMW radiation. From our experimental results we can conclude, that dipole moments are changed under the MMW radiation because of the changes in the electron charge on hydrogen atoms. Radiation with different frequencies and polarizations causes to both increasing and decreasing of bond vibration intensity. In this case, the changes of dipole moments are not accompanied by the changes of length of N-H bond, only the changes in directions of chemical bonds and these changes are proportional to the amount of dipole moment of the bond. Thus, the presence of H-bonds seems to be an indicator of properties of valent COO and deformational NH vibrations, which would be impossible to manifest without of H-bonds. Namely, H-bonds are sensitive for charge changes in hydrogen under external stimuli in the systems with many H-bonds and in the wide range of their energy.

3) Effect of MMW at 37.5 GHz upon spectral and kinetic parameters of albumin crystal luminescence with polyen structure additives has been investigated. Specimens luminescence spectrum consisted of two bands with maxima at 360 and 450 nm and halfwidths 20 and 30 nm, respectively. It was discovered that the intensity of shortwave polyen band (360 nm) was changed under the influence of MMW radiation. Longwave band remained almost unchanged by intensity, being a little affected in shape. Kinetic investigations demonstrated that luminescence damping constant of longwave band under MMW radiation: have been changed, namely, contribution of short time component decreased in three time at nonsubstantial changes of characteristic time.

4) The parameters of the spectra of the DNA samples, prepared in the electromagnetic field, were compared with the parameters of the spectra of the reference DNA samples. In the nonpolarized spectra of irradiated DNA, only very slight changes could be registered, but these changes were well pronounced in polarized spectra (fig.1). The drastic changes in polarized spectra were observed in the region of C=O stretching (1500-1700 cm^{-1}) and PO^-_2 symmetrical and antisymmetrical stretching (1100-1300 cm^{-1}) vibrations and in the range of "fingerprints" (480-650 cm^{-1}). A new structural band has been appeared near 1450-1500 cm^{-1} region for the DNA sample prepared in the electromagnetic field. In the 1500-1700 cm^{-1} region, the number of components for irradiated samples is less than for the reference sample, and three relative intensities of the bands are redistributed (fig.1).

The changes in spectral parameters of the bands for the irradiated DNA as compared with those for the reference DNA are greater for the angle of polarization of 0^0 (fig.1 a, b) than of 90^0. From the comparison of the polarized spectra of irradiated DNA for different angles of polarization (0,1, 3, 5,7, 10, 15, 90^0) and for different spectral regions with the same parameters for the reference DNA one can conclude, that the values and directions of dipoles of the C=O bonds in the DNA bases have been changed. Changes in the direction of the dipole moments are equal to or less than 1^0 .

The changes were observed in the spectral parameters of the polarized spectra for the DNA prepared in the weak electromagnetic field as compared to those for the reference Na-DNA. These changes are not connected with DNA B-form transition into A-form and consequent disordering. The changes in the rate of loosing water and in spectral parameters are opposite to those expected for B-A transition [10] .The values and

directions of transition moments of the C=O bonds of DNA bases have been changed. This can be caused by changes in the third order space structure of DNA molecule as a whole.

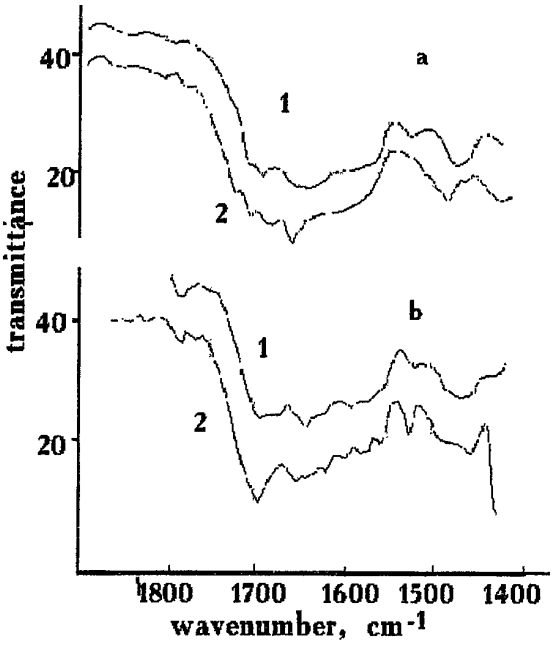


Fig.1. IR polarized spectra of DNA with 76% humidity on KRS-5 substrate, prepared in the weak electromagnetic field with 60.0 GHz frequency (1), and of the reference DNA (2) for 90^0 (a) and 0^0 (b) polarization angels.

References

1. V.S.Ulashchuk, New methods of physical therapy, Minsk, Belarusia, 1986.
2. Cheng Jiong,Kehui Gong,Qunrhu He, Jorn.trad.chin. Med., Vol.1, N1, pp. 9-11, 1986.
3. H.Frohlch, Biological coherence and response to external stimuli, Springer Verlag, Berlin, 1988.
4. L.I.Berezhinsky, N.Ya.Gridina, G.I.Dovbeshko, M.P.Lisitsa "Visual observation of mm- wave action upon blood plasma". Biophysics, Vol.38, N2, pp.378-384, 1993 (Rus).
5. D.N.Govorun, V.D.Danchuk, D.N.Govorun, V.D.Danchuk, Ya. R.Mishchuk, I.V.Kondratyuk, N.F.Radomsky, N.V.Zheltovsky, "Mirror symmetrical conformational states of canonical nucleic acids", Dokl .Ac. Nauk Ukraine, N2, pp.66-69, 1992.
6. S.G.Stepanyan, "High resolved vibrational spectra and structure of nucleic acid bases", FTINT AN UkrSSR, 16 P, 1998.
7. L.I.Berezinsky, G.I.Dovbeshko, G.S.Litvinov, V.V.Obuchovsky, N.B.Yanovskaya," Changes in polarized vibrational spectra of glycine-containing crystals under the action of millimeter radiation", Optics and spectroscopy, Vol.75, N5, pp. 625-636, 1993.
8. L.I.Berezinsky, G.I.Dovbeshko, G.S.Litvinov, M.P.Lisitsa, "Vibrational spectra of β-Ala under the millimeter waves", Molecular Materials, Vol. 87, N3, pp. 215-219, 1993.
9. A.V.Iogansen, "Infrared spectroscopy and spectral determination of H-bond energy", in: Hydrogen bond, Moscow, Nauka, pp. 112-155, 1981.
10. E.A.Andreev,T.V.Bolbuch, G.M.Glibitsky, V.N.Kharkyanen, " Influence of millimeter electromagnetic radiation upon the interaction with water and Na-DNA, *VII Conf. Spectrosc. Biopolymers*, Kharkov, 1-4 Oct., pp. 6-7, 1991 (Rus.).

DYNAMICS OF INDEXES WATER-ELECTROLITIC COMPOSITION OF THE BLOOD FOR PATIENTS WITH ALCOHOLIC PSYCHOSIS UNDER EHF-THERAPY.

M.IGNATOV, A.MALIHIN, V.DERKACH, L.ZOLOTUHINA

The Usikov' Institute for Radiophysics and Electronics of the Academy of Sciences of Ukraine,
.Ukrainian Scientific Research Institute of Clinical and Experimental Neurology and Psychiatry
12 Ac Proskura St., Kharkov, 310085, Ukraine
Phone 44-85-94, Fax (0572)- 441-105, E-mail: derkach @ire.kharkov.ua

Introduction

The disorders of water-electrolytic metabolism (calling a chain reaction of metabolic, hypoxical and hemodynamic disorders) take the important place in forming of painfulness clinical picture of alcoholic psychosis. It is determined in clinic on a degree of display a mental and neurological deficit [1-6]. However in practice, the researches of water-electrolytic metabolism at such patients practically will not be carried out, because it is difficulty to define its parameters. Significant interest presents an operative study of these factors and searching a new methods to normalization the systems, have a bearing on the processes of metabolism. During last year we have fulfilled the work, which purpose consists:

- in complex study of dynamics of exchange violations in organism, in particular, of water-electrolytic metabolism (on the basis of our new method of screening computer analysis[7]),
- in research of connection of these violations with a common picture of clinical and paraclinical manifestation of acute alcoholic psychosis,
- in a research of a possibility of normalization of indexes by using extra high frequency (EHF)-therapy.

The results of this work are submitted in present paper.

Technique and results

We have tested a method of EHF-therapy both as a mono method and in the complex with traditional method of treatment for the course treatment of acute alcoholic psychosis. 80 male patients of 30 to 55 with given pathology of a different degree of painfulness have been observed. They were divided into three groups: the first group got a traditional infusion therapy, the second - a combination of traditional treatment with EHF-therapy and the third - only EHF-therapy.

The integrated method of an inspection of the patients has been applied. It consists of a daily clinical neurological and clinical-psychiatric inspection, research of biochemical indexes of peripheral blood, measurement of arterial pressure and pulse. On the initial stages and in an extremity of treatment, paraclinical methods of a research EEG, REG and Echo-EG were applied.

The method of screening computer diagnostics of a patient condition allowed us operatively investigate various parameters of organism activity (metabolic, hemodynamic) and, in particular parameters water-electrolytic metabolism such as concentration Na^{+}, Ka^{+}, Ca^{++}, Mg^{++}, Cl^{-}, common water. This method allowed also to analyses distribution of water on vascular and perivascular sectors; osmotic and mechanical resistant of erythrocytes; hemodynamic and cerebral factors. As initial parameters the indexes of a clinical structure of blood, arterial pressure and a pulse were used.

EHF influence was carried out on the developed technique on biologically active dots and zones of Zaharina -Geda. As a source of low-intensity microwave radiation was used generator G4-142 with a variable frequency within range of 37.5 - 53.57 GHz, power level varied within 3 - 10 mkW/cm^2. Frequencies of electromagnetic radiation, to which an influence have been exerted, and areas of influence have been selected individually on the base of data of screening analysis of a peripheral blood. We used as a basic dots of the projections of principal lymphatic channel (at the left), of kidney, of livers, the projection of under collar-bone vein (at the right) or their composition. Course of treatment consisted of 4 - 8 seances (depending on state of patient) on 20 minutes daily. The treatment proceeded before reaching effect of normalization of basic indexes of habitability. The condition of the patients was inspected on a series of indexes during all treatment (before EHF- influence) and in the set aside phases (through one - two weeks).

The comparison of the clinical and paraclinical data at different patients has allowed dividing them into three groups in dependent on painfulness of alcoholic psychosis current. The first group consist of the

patients with the easy form alcoholic psychosis, the second group - from the patients with alcoholic psychosis of average painfulness and the third group - from the patients with the heavy form.

The indexes of water-electrolytic metabolism (before and after of the EHF-therapy session) have been analyzed and averaged on groups.

Some results are shown in Table 1.

components meas. units.	Structure of the blood components on groups of the patients						Indexes (norm)
	1- group easy form of delirium		2- group average form of delirium		3- group heavy form of delirium		
	up to EHF	after EHF	up to EHF	after EHF	up to EHF	after EHF	
Na^+-mmol/l	153.1 ± 2.3	146.9 ± 0.6	136.5 ± 1.5	141.0 ± 2.0	132.7 ± 1.5	151.4 ± 2.0	146.0 ± 1.6
K^+ - mmol/l	3.72 ± 0.6	4.13 ± 0.03	3.67 ± 0.05	3.81 ± 0.1	3.29 ± 0.1	3.84 ± 0.1	4.6 ± 0.61
Ca^{++} - mmol/l	4.45 ± 0.4	3.89 ± 0.15	5.47 ± 0.5	4.83 ± 0.05	5.6 ± 0.3	4.85 ± 0.15	3.2 ± 0.60
Mg^{++}- mmol/l	2.23 ± 0.03	2.47 ± 0.05	2.07 ± 0.01	2.35 ± 0.05	1.74 ± 0.15	1.88 ± 0.15	2.8 ± 0.1
Cl^- - mmol/l	99.43 ± 1.4	99.26 ± 0.5	95.35 ± 4.0	99.5 ± 1.5	97.3 ± 2.5	90.0 ± 5	85.0 ± 12
Fiber of plasma g/l	73.69 ± 5.0	65.06 ± 3.0	80.07 ± 4.0	78.45 ± 1.0	87.73 ± 2.0	75.43 ± 1.5	67.0 ± 5
Consumpt. O_2. cond. un.	570.23 ± 15	606.92 ± 20	536.66 ± 20	565.0 ± 15	474.1 ± 15	549.2 ± 10	692 ± 15
Coef. of esterificaton cond. un.	31.38 ± 2.1	33.05 ± 1.0	37.69 ± 1.31	34.96 ± 1.04	40.86 ± 2.0	34.45 ± 1.5	32 ± 0.1
Consumpt. O_2 on 100 g. of tissue cond. un.	1.63 ± 0.2	1.88 ± 0.15	1.56 ± 0.02	1.65 ± 0.1	1.13 ± 0.1	1.68 ± 0.15	2.0 ± 0.15
Common water cond. un.	55.93 ± 2.5	58.9 ± 1.5	51.44 ± 1.5	56.0 ± 1.5	47.89 ± 2.0	56.01 ± 1.0	60.0 ± 2.0
Volum of intarsticial liquid ml/g	5.29 ± 0.3	3.7 ± 0.25	6.76 ± 0.15	5.5 ± 0.3	9.44 ± 2.1	6.2 ± 1.5	4.5 ± 1.5

Table 1. Dynamics of indexes of water-electrolytic metabolism at the patients with acute alcoholic psychosis a different degree of painfulness before and after EHF-therapy.

In the result we established, that the EHF-therapy (both as a mono EHF-therapy and in combination with traditional methods) reduced in improving indexes of life-support on many parameters. The current of disease was softened. Such parameters, as water-electrolytic metabolism, content of common water, amount of interstitial liquid, assimilation of oxygen (O_2) at 100g of tissue had the positive tendency of a modification. It is necessary to note, that during a course of treatment process this had an oscillatory structure, it not always was unidirectional, frequently there were significant deviations in both legs (at the expense of a modification

hemo-concentration indexes). It testified to constant searching by a system of a metabolism a right path of functioning.

The important place in these processes has interaction of a complex " erythrocytes-hemoglobin" in relation to the leukocytes formula, which participates in regulation of ion concentration Na +, Ca ++. The modification of their concentration (especially Ca ++) on a comparison with a norm correlated with weight of hypoxical display at the investigated patients.

In whole, the carried out integrated researches of influence of EHF-therapy on the patients with acute alcoholic delirium (in dynamics) have shown that the EHF - influence (on our technique) gives positive medical effect as independently, and in a combination with traditional therapy. The process of way out from psychosis is accelerated, the indexes of homeostasis are normalized, the recovery are accelerated on 3 - 5 days on a comparison with control group of the patients receiving only medicament treatment. Besides the EHF-therapy is significant leveling a change of worse of the patients' condition connected to an accompanying pathology of interior organs.

It is necessary to note that the use only EHF-therapy reduces to full blockade of diseases (convalescence) at the patients with the easy forms alcoholic psychosis. The integrated therapy including EHF-therapy is recommended the patient with the heavier forms. By the very heavy patient, at which the expressed violations of water metabolism (drop of common water more than 10 % from a norm) EHF-therapy are marked can be carried out only after an emergency medical correction.

Reference

1. V.A.Berezovskiy, "Oxygen insufficiency", M.: 1963

2. I.I.Bloh,O.M.Morox,I.V.Nechiporenko," Modification of parameters of interchanging in erythrocytes, and development of membranopaty at the patients with paranoid schizophrenia", Ukr. vestn. Psihonevrologi, Kharkov, v.4, No.4, pp.14-15, 1996.

3. L.I.Zolotuhina, "Neurophysiology analysis of the therapy effect of KCG and MRT in dynamics of treatment of alcoholic psychosis", Ukr. vestn. Psihonevrolog, Kharkov, v.4, No.4, pp.166-168, 1996.

4. S.Kler"Kidney and homeostasis in the norm and at pathology", M.: Medicine, 1987

5. A.V.Malihin, "The amount of infusion therapy in a phase acute alcoholic delirium", Ukr. vestn. Psihonevrologi, Kharkov, v.4, No.4, pp.170-171, 1996

6. A.M.Cherny "Pathology of hypoxy condition", M.: Medgiz, 1961

7. A.V.Malihin, P.A.Volocsin, V.S.Mertsalov, Patent USSR N 1517937 1997.

EFFECTS OF LOW POWER MICROWAVE ELECTROMAGNETIC FIELDS ON BRAIN NEURODYNAMICS

Tatyana N. Sulima and Anatoly I. Fisun
Institute for Radiophisics and Electronics
12, Proskura Str., Kharkov, 310085, Ukraine
Tel. 44-87-41, Fax. 44-11-05, E-mail obel@ire.ire.kharkov.ua

1. Introduction

It is evident today that the low intensive microwave radiation can produce a wide spectrum of a therapeutic application. The treatment is more effective when microwave beam is injected into Chinese points. However mechanisms underlying for these effects are still only partially understood. In our opinion a solution of this problem can result from the investigation on the brain involving in the process of the body function normalization.

It is known that any physical stimulus applied to the acupuncture points can lead to the activation of antinociceptive endogenous brain system [1]. Thus injection of the microwave beam in bioactive point can produce undirect effect to the brain integrative process, in particular, the interaction between subcortical and cortical regulation systems.

The aim of this report is to the investigation of the action of the low power microwave radiation on the brain neurodynamics. The new technical equipment and modern method of the biosignal processing was elaborated for the realization of the purpose in hand.

2. Experimental techniques

The conception of the microwave radiation influence consists of two aspects in the present experiment. On the one hand, the frequency band was at most extended. With this in mind type-O carcinotron was used having the frequency periodic changing in the band from 50 GHz to 83 GHz and the power of 0.1–10 mW. The theoretical investigation shows that the biological important frequency is precisely in this region. Secondly, the interaction zone must be localized on the acupuncture point. The open end of the slot transmission line (STL) [2] was used as a feeding antenna. It shows up as a dielectric cylinder with a thin metallic screen and a longitudinal slot (See Fig. 1a). The STL has the small overall dimensions and the wide wavequide transmission band. This is just the key feature of this slot transmission line in comparison with others microwave transmission lines. The analysis of the dispersion equation of the STL (if take into consideration of the screen thickness) produces the next appraisal of the critical wavelength

$$\frac{\lambda_c}{2a} = \pi\sqrt{2\varepsilon\eta}$$

where a is slot line radius, ε is dielectric constant, $\eta = \ln\left(1/\sin(\theta/2) + \pi d / 2\sin\theta\right)$, 2θ is slot opening angle, $2d$ – screen thickness. For θ=3·10°, ε=1.5, d=0.01 mm and λ=5 mm the slot line radius is approximately 1.5 mm.

The electrical component of the electromagnetic field of STL is concentrated about the clearance between the borders of the screen (see Fig. 1b). Whereas the magnetic part is uniformly distributed across the whole width of the dielectric rod.

In such a manner the effective size of STL is less than sizes of the dielectric or metallic standard wavequides. The all numerical properties and easy concordance with a regular wavequide determine the selection of STL as a feeding antenna. This is just the condition of the ideal conformity to the local influence of the radiation upon the individual acupuncture point.

The 5 rabbits have been used as laboratory animals.

To investigate the brain activity, the electrodes have been implantated in the laterally symmetrical areas of Prefrontal and Sensomotoral of Neocortex, Dorsomedial nucleus of Hypothalamus, Periaqueductal Gray and nucleus Raphe Magnus.

Multichannel electroencephalogram [EEG] was recorded by 16-channal Electroencephalograf [Medicore, Hungary]. The digital biosignal processing was provided by the package "Neuroresearcher".

The brain neurodynamics was appreciated with a certain features derived from the application of the

spectral analysis [3].

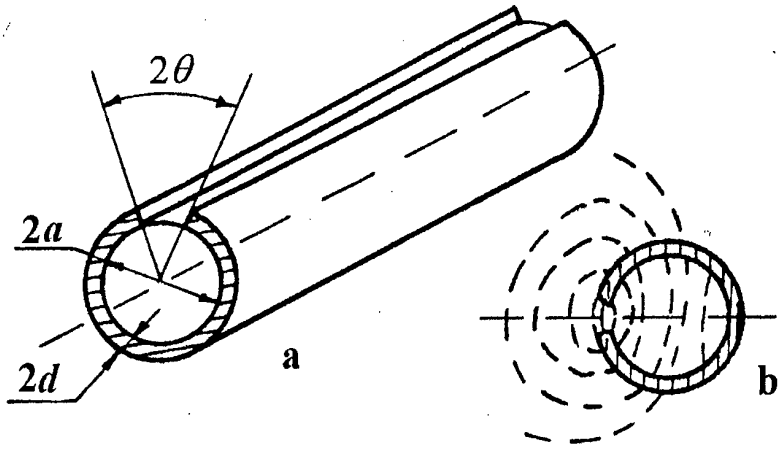


Figure 1.

To present a random signals in a frequency domain the Fast Fourier Transform were used. The following features were computed:

1. The auto-spectral density function, which displays the distribution of the variance or the power over the elementary frequency components of a single EEG signal $\{G_{xx}(f)\}$.

2. The cross-spectral density function, which demonstrates the covariance between the elementary frequency components of two EEG signals $\{G_{xy}(f)\}$.

3. The coherence spectral function which represents the mutual correlation of elementary components at each given frequency $\gamma_{xy}^2(f)$. It provides a quantitative measure of the linear dependency between two brain regions. We selected the Partial Coherence function $\gamma_{xy}^2(f)$ for the correct description of the relationship between the subcortical brain areas and neocortical fields [4].

Experimental conditions were approached as well as possible to the usual acupuncture procedure.

In the first step it was made the multichannal recording of EEG of the wakeful animal. Thereafter the acupuncture point at the animals ear was located from a low electrical resistance level. The microwave applicator was installed near the acupuncture point and the microwave radiation was switched on during 10 min. The dynamics of the brain activity was investigated during 1 hour after shutdown of the microwave action.

Secondly, the experimental setup was repeated in the same sequence after 7 days. In this experiment the microwave beam was replaced by needle and the acupuncture have been made during 30 min. The development of the analgesic effect was tested on reducing of the somatosensory evoked potentials on the painful stimulus.

3. Experimental results

Due to the outlined technical and experimental performances the following results have been obtained.

The application of the microwave radiation to the bioactive point of the rabbit's ear has produced a widespread changes of the electrical activity in all examinated brain areas. Its consisted in the altering of the functional relationships between the subcortical structure and neocortical areas. As can be seen, the Partial Coherence function of the Prefrontal Cortex spontaneous electrical activity, shown on Fig. 2,a and Fig. 3,a, has they maximum in the discreet frequency bands. The Dorsomedial nucleus of Hypothalamus gives its spectral deposit to the Prefrontal area in the frequency of f=1.75 Hz; 2.9 Hz (see Fig. 2,a). The Periaqueductal Gray gives one in the frequency of f=3.5 Hz; 6.44 Hz and Raphe Magnus gives its deposit in the frequency band 5–7 Hz.

This character of neurodynamics changed after exposition of the microwave electromagnetic fields. One can see increasing of the spectral deposits of Hypothalamus to the high level in whole frequency band (see Fig. 2,b). Simultaneously, the spectral deposit of Periaqueductal Gray reduced (see Fig. 3,b). Raphe Magnus increased its spectral deposit in the high frequency band – f=13–25 Hz.

The same neurodynamics changes have been recorded in the relationships between Sensomotoral Area and Hypothalamus and Formatio Reticularis. But they occurred in the high frequency band – f=13–25 Hz.

It was interesting to compare the action of the microwave radiation on brain neurodynamics with acupuncture one. This experimental setup was performed on the same animal, because neurodynamics has the individual variability.

As can be seen from Fig. 2,c and Fig. 3,c the spectral deposits of Hypotalamus and Periaqueductal Gray to Prefrontal Area increased in its own frequency bands after acupuncture procedure. But in comparison with microwave action on neurodynamics, the acupuncture can not alter a character of functional relationship between the brain regulation systems.

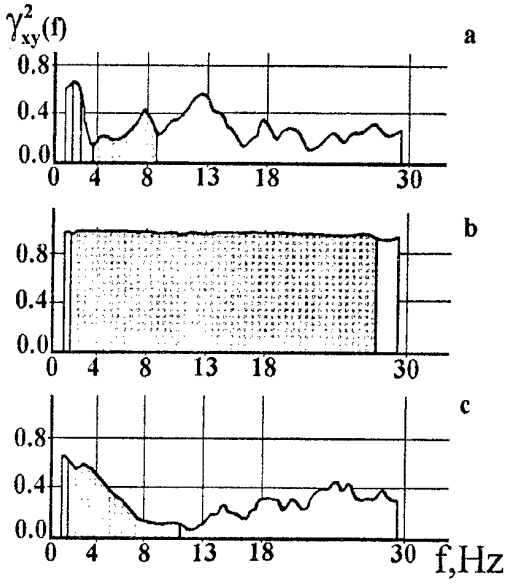


Figure 2.

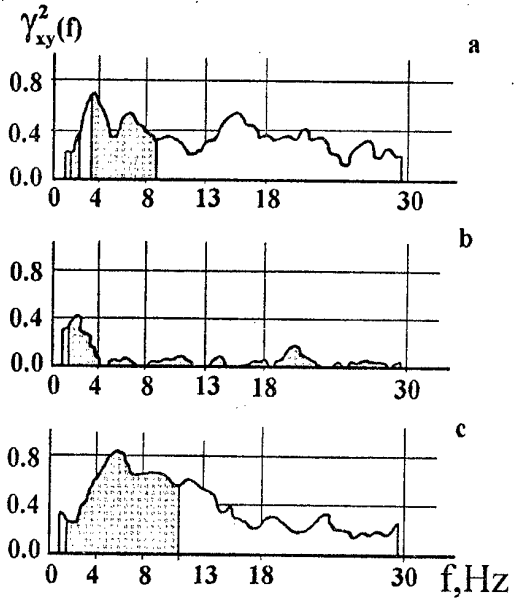


Figure 3.

4. Conclusion

The obtained in this work results can answer on the questions when had been placing in the preceding publication [5]. The microwave radiation injected into bioactive points can excitate the same transmission channels and brain structures as in the case of the acupuncture application. But the involving of antinociceptive systems in the brain integrative process is different. The microwave radiation produces a widespread activation of Hypothalamus and its dominant role in the process of the subcortical- cortical interaction. Those physiological phenomena are the basis of normalization of body function in the course of the microwave therapy.

References

1. L.V. Kaljuzhnyi "Physiological mechanisms of pain regulaion". AMS USSR. Moskow, Meditsina, 1984. (In Russian).
2. Shestopalov V.P. "Physical principles of millimeter and submillimeter technique". Vol. 1. "Open structure". Kiev, Naukova Dumka, 1985. (In Russian).
3. J.S. Bendat, A.G. Piersol "Random data.Analysis and Measurement Procedures". John Wiley & Sons, 1986.
4. G. Dumermuth, L. Molinari "Relationships among signals: cross-spectral analysis of EEG". In.: R.Weitkunat (Ed.) Digital Biosignal Processing. Elsevier Science Publishers B.V., 1991, pp. 361–398.
5. A. Vander Vorst, J. Teng, D. Vanhoenacker "The action of microwave electromagnetic fields on nervous system". In Proc. Internat. Conference "IEEE Antennas and Propagation Society", Nice, France, November, 1992, pp. 111–119.

RESEARCH OF CONTROLLING CONNECTION SYSTEMS OF CELL MACROMOLECUL MECHANISMS BY METHOD DIELECTROMETRY IN MM RANGE OF RADIOWAVES

Shchegoleva T.Yu., Kolesnikov V.G.
Institute of Radiophysics and Electronics of the National Academy of Sciences of Ukraine
12 Ac. Proskura St, Kharkov, 310085, Ukraine
The Problem Scientific-Research Laboratory of Molecular Mechanisms
4/32 Solanikovski lane, Kharkov, 310003, Ukraine
Tel.8-0572-448506,8-0572 23-04-38,Fax 8-0572 441105,E-mail tsch@ire.kharkov.ua

The research of macromolecul complexes work of a functioning cell during transmembrane transmission of a signal, during growth and regeneration, immune resistance and many other, enable to receive an information about state of their molecular mechanisms. The study of a structurally functional role of hydrate environment of macromolecule and their complexes at different levels of alive organization from macromolecule up to a cell allows to find a solution of this problem. It is supposed to study with the help of method dielectrometry in mm-range(EHF - dielectrometry) of radio waves in the field of a dispersion of a free water.

The development of this method was begun in on study of a condition a water component of biosystems and hydration parameters of macromolecule with use of mm-range of radiowaves in the region of dispersion of free water. This researches was carried out within 20 years in Institute of Radiophysics and Electronics of a National Academy of Sciences of Ukraine. As a result of conducted complexe of thease works the common model of macromolecule hydration, which quantitatively compared with their space organization on of International Protein Data Bank of the X-ray diffraction analysis is constructed.

. Types of a connected water and their character of binding in a object structure are quantitatively described. In a general view it can be circumscribed as follows. Macromolecule actuates as the constituent some strong-binding water forming more one hydrogenous bind with the protein.

There is some of water molecules which determin the given conformation condition (w_1), and fixed by its generated structure (w_3). It makes full nearest hydrate environment in a radius of hydrogenous bind.

It can be constructed on a particular space structure with accuracy 10 % in accordence with the developed scheme of representations under the data of X-ray diffraction analysis and also can be measured by a method of . EHF-dielectrometry with derivation of connected water types with accuracy 2%.

It is shown, that the major part of macromolecule hydrate environment is a replica of its structure, which includes part of water, as the structural element ensuring it space organization. This method enables to follow for a water structure replica[1]. It is proved on a series of experiments on modelling the largescale globe reorganizations, including affecting a doment structure, at different levels of organization from macromolecule up to cells and tissues for the analysis of changes in condition of a water component in these processes. In these processes the largescale restructurings, which have molecular memory functionally significant and stipulated by space organization, are detected.

It is used methodological approach on the analysis of macromolecul conformational transformations at different levels of organization according to the change of their hydrate environment developed by us. According magnitudes deviations of researched objects dielectric permeability, from the same magnitudes in an inactive condition by method EHF-dielectrometry will becarried out scrining of the cell response in action on various controlling complexes of a cell by the biologically active agents in real time, in eliminating destruction conditions of objects For the analysis the change of a condition of a water environment of a cell, to conformational transformations of it's components on specific binding of biologically active substances is used. The cells is not exposed to any additional actions, as the potency in waveguide tract does not exceed 10 мVt. The measurements are produced in dielectrometer A-17, developed by Research Laboratory of Controlling Complexes of a Cell.

Simulating various way of passing of a signal, during start of a system, and variants of blockade of these way, it is possible to describe the scheme of their action in an alive cell of selected objects in real time (within several hours). The first stage is the construction of a hypothetical model or models as a sequence of events (ramified web, interconnected by the act of the interaction,) in an analyzable system. By the second stage - scrining of the specific biologically active factors of action on key points of this model in monitoring of the

principal cells answers by a method EHF-dielectrometry. On this basis the new approach to study of work of molecular mechanisms of cells - research of a functioning system on modifications of it's hydrate environment characteristic is developed. It is obvious, that EHF-dielectrometry has significant advantages on a comparison with other methods, as the cells do not fail and are not modified in experiment.

In a cycle of works [2-4] on a construction of a connections system of molecular mechanisms of adenylate cyclase complex functioning during transmembrane transmission of a signal according the functional answers of an alive cell to directed biochemical actions on it the structural elements part of datas about hormon action when they blockade various links on transmembrane transmission of an information, alpha-, beta-receptor and G-protein in erythrocytes has already received. Some aspects of modulation of cell functions by exogenous calcium (Figure 1) and prostaglandines, and also series of cytoskeleton functions in erythrocytes, trombocytes, leycocytes and sperm has already been considered.

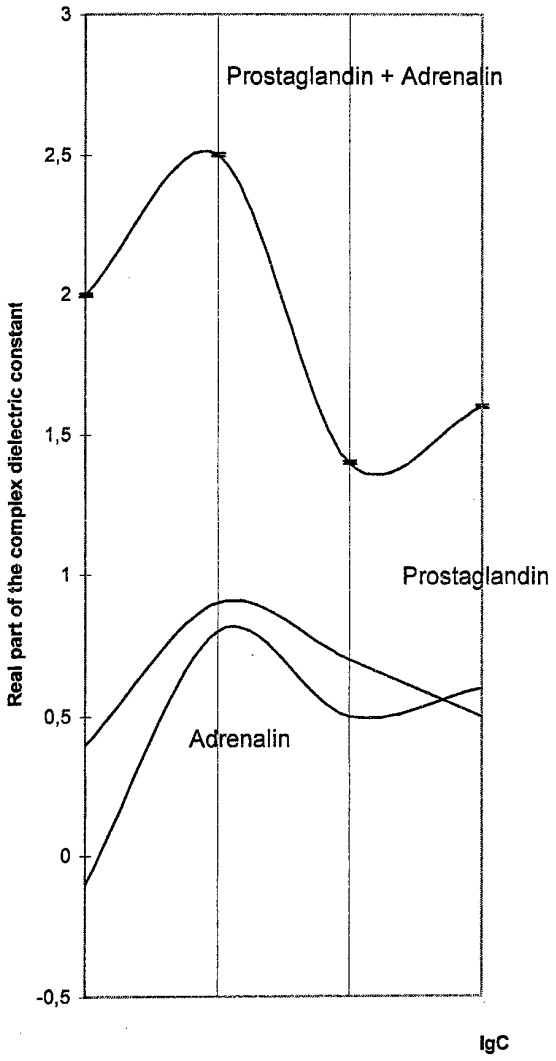


Figure 1. Modulation of cell functions by exogenous calcium (C - calcium concentration) and prostaglandines

The key moment of connection of a cytoskeleton web with adenilate cyclas system of transmembrane transmission of a signal are defined [5,6]. Functional system of communications of a erythrocytes adenylat cyclase complex bilding by EHF-dielectrometry i s represented on figure 2.

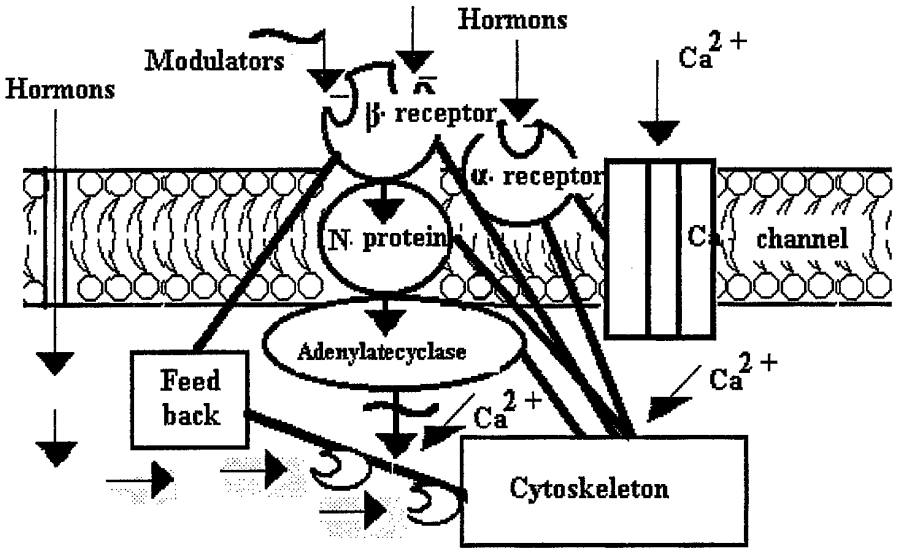


Figure 2. Functional system of communications of a erythrocytes adenylat cyclase complex.

The study of molecular mechanisms transmembrane transmission of a signal with the participation of adenylate cyclase system is rather important in a research of the functional answers of a cell and organism as a whole on various actions. That will allow to expand existing representations about biology of a cell and can be used in medicine, pharmacology, agriculture, ecology[6,7].

Reference

1.T.Yu. Shchegoleva, «Hydration environment and macromolecule structure». Advance of modern biology., 116,6,700-714, pp 1996.
2.T. Yu. Shchegoleva, V. G. Kolesnikov, « Change in the hydrate environs of erythrocytes on hormonal stimulation», Biophysics, Vol.41, No.5, pp.1093-1097,1996.
3.Ò. Yu. Shchegoleva, V. G. Kolesnikov, «The adenylat cyclase system and calcium channels», Biophysics, Vol .40, No.6, pp.1301-1304, 1995.
4.T.Yu. Shchegoleva, V.G. Kolesnikov, «Thermoinductive transitions in proteins»., Biophysics, Vol.42 No.4, pp.1301-1304,1997.
5.T.Yu. Shchegoleva, «Functional system of communications of a erythrocytes adenylat cyclase complex», Advance of modern biology, , Vol 117, No.4, pp .442-454,1997.
6.T.Yu. Shchegoleva. «Research of biological objects in millimeter range of radiowaves», Naukova dumca, Kiev, pp. 182,1996
7.M.V. Zubets, T.Yu. Shchegoleva, V.G. Kolesnikov, « Application of millimeter range waves in agriculture, Agrarian science», Kiev, pp.163,1996.

ABOUT POSSIBLE LOW-INTENSIVE COMBINED FIELDS OF VARIOUS PHYSICAL NATURE' MECHANISMS OF INTERACTION WITH BIOOBJECTS

Y.V.Chovnjuk [1,2]
Professor
[1]Scientific Research Centre "VIDGUK",Bildg. #61-B, Volodymyrskaya str., Kiev, 252033, Ukraine; Tel. # (044) 2444439
[2] Home address: P.O.Box #34, Kiev, 252040, Ukraine; Tel. #(044) 2638858

This work is devoted to the problem of treatment, analysis and modelling of tissue' interactions with weak electromagnetic fields of extra high frequency (EHF) and transformed in tissue hypersound. We make an attempt to systematize the existing idea of possible mechanisms of millimetre & hypersound waves' effects on the tissues and human functional state with the help of noise induced transitions' model [1-15].The idea of noise-induced coherence in neural networks [16] and of colored noise (not white one!) in the dynamics of aqueous protein solutions [17] is used here as well.

We investigate the dynamics of large networks (or cluster) of N globally pulse-coupled biocells (biotissue's elements) in a noise-induced synchronized state. The power spectrum of an individual element (biocell) within such cluster is shown to exhibit in the thermodynamic limit $(N \to \infty)$ a broadband peak and an additional delta-function peak (of EHF' electromagnetic/hypersound field) that is absent from the power spectrum of an isolated biocell. The power spectrum of the mean output signal exhibits only the delta-function peak, by the way. These results are explained analytically in an exactly soluble oscillator model with global phase coupling [18,19].It's shown, that the mechanism of manifestation of excitation of undamped oscillations of cells with a discrete series of possible stable amplitudes is a result of the effect of external periodical EHF' force which is non-linear along the coordinate (!) of motion of the excited oscillation system (biocell's model). One may investigate typical regularities of the phenomenon on the basis of two common models: a) a pendulum under inhomogeneous effect of the external periodical force; b) an oscillator under the effect of the incident EHF' electromagnetic/hypersound wave. It's shown that the phenomenon mechanism is connected with the phase capture and adaptive phase lock control providing for necessary energy contribution to the biocell's oscillation process. We used the principle of reversibility of modulation-parametric interactions [19] as well, which is the basis with the respect to effective control over equivalent impedances of oscillating biosystems (biocells' cluster).We also give a classification of oscillating biosystems with forces, which can change the effective reactive parameters and dissipation in biocells. There is an analytical V.N.Damgov's technique to investigate modulation-parametric processes in oscillating and self-oscillating biosystems under the action of weak EHF' external signals.

The response of biodynamical system to noise has received considerable attention recently. Most of the work has focused on cases where the noise was found to increase the coherence of the biosystem. One such case is stochastic resonance, where a particle in a bistable potential is subject to noise, in conjunction with a weak EHF' periodic force of electromagnetic/hypersound nature. The inclusion of noise facilitates the switching of the particle between the two wells and leads to an increase in the signal-to-noise ratio of the output signal. The non-equilibrium fraction of electromagnetic radiation of a human body in mm-range has a noise level about $\sim 0{,}5*10^{-22}\ W/_{Hz}$ [20]. We think these experimental results registered at the Scientific Research Centre of Quantum Medicine of Ministry of Health of Ukraine may be explained just with the help of a stochastic resonance' model in biotissue (S.P.Sit'ko' microwave resonance therapy method).

It's known, that the signal-to-noise ratio is further increased in the case of a chain of biooscillators with a bistable potential [21]. It has been shown that stochastic resonance is not limited to biosystems with a bistable potential but can occur also in a single excitable element (such as biocell, for example) [22] and in spattially extended excitable biosystems (biocell's cluster)[23].Furthermore, studies on the effect of noise in globally coupled maps [24,25], in mathematical models that display stable and unstable fixed points [26,27], and in globally coupled biooscillators [28] showed that noise can induce a coherent response even in the absence of an external periodic EHF' force of electromagnetic/hypersound nature.

Excitable elements underlie many biological functions and are often subject to complex external stimuli which can be aperiodic in time and/or exhibit random variations in amplitude (Debye's waves, for

example). An isolated biocell in the biotissue (in accupuncture's point, for example) is an excitable unit (Schwan's cell, for example) that is connected to a large numberof others (typically 1000-10000).They can be stimulated by EHF' signals from the external world or other parts of the biofibre. These signals are subject to a cytomembrane's noise, as well.

In this work, we investigate the dynamics of large networks(cluster) of N globally coupled excitable elements that exhibit a globally synchronized state above a critical noise threshold [29]. We focus on understanding how the dynamical behavior of an individual element (biocell) within the network (cluster) differs from that of an isolated elements (schwan's cell, for example), i.e., not coupled to any other elements, as well as on the mean output signal of all the elements (biocells' cluster).

The power spectrum of the individual element (biocell) within the cluster exhibits both a broadband peak and, in the thermodynamic limit, a delta-function peak that is absent from the power spectrum of an isolated element. The power spectrum of the mean output signal, in contrast exhibits only a delta-function peak in that limit. These results can be qualitatively understood analytically in a noisy oscillator model with global phase coupling [16]. The coherence in biocluster is induced solely by noise in conjunction with the global coupling (i.e. Ranvjue's in terceptors near the Schwan's cell boundaries), and not by a periodic external driving force of EHF as in standard stochastic resonance. It also doesn't depend on a constant dc drive, the oscillatory nature of the elements, special initial conditions, or an additional cellular mechanism, as well.

The physical mechanism can be qualitatively understood as follows: the noise induces the elements to exceed the threshold value and to fire (W.Horsthemke, R.Lefever et al. models and mechanisms). For sufficiently strong coupling, this results in a coherent synchronous state in the biocluster which produces a sharp peak in the power spectrum. As we increase N, the average noise decreases as 1/N which leads to a delta-function peak in the thermodynamic limit. An individual element (biocell) within the cluster is driven by the mean which results in a sharp peak that becomes a delta-function peak for infinite networks (clusters). Each biocell, however, experiences its own nonzero noise that produces a broadband peak. The broadband peak is independent of N and decreases for decreasing noise levels.

In summary, identical qualitative power spectra are reproduced by a simple oscillator model with global phase coupling, demonstrating that the excitable nature of the biocells is not crucial. Thus, these spectra should be present in any excitable and oscillatory stochastic system with a coherent state. The observed gain in coherence and synchronization in the cluster is achieved nearly instantaneously. This suggests the interesting possibility that Schwan's cells use noise to produce coherent signals (in mm-wave range!). The global output signal in that case should be markedly different from the output signal of an individual element. This behavior could potentially be investigated experimentally.

References

1. W. Horsthemke, Nonequilibrium Transitions Induced by External White and Colored Noise.- In: Dynamics of Synergetics systems Springer Series ni Synergetics, Vol. 6/Ed. by H. Haken.- Berlin, Heidelberg, N.Y.: Springer, 67 (1980).
2. W. Horsthemke, M. Malek Mansour, Zs. Phys. B24, 307 (1976).
3. L. Arnold, W. Horsthemke, R. Lefever, Zs. Phys. B29, 867 (1978).
4. W. Horsthemke, Noise-Induced Transitions.- In.: Stochastic Nonlinear Systems in Physics, Chemistry, and Biology/Springer Series ni Synergetics, Vol. 8/Ed. By L. Arnold, R. Lefever.- Berlin, Heidelberg, N.Y.: Springer, 116 (1981).
5. W. Horsthemke, R. Lefever, Phys. Lett., A64, 19 (1977).
6. R. Lefever, Dynamics of Cell-Mediated Immune Respouse.-In: Dynamics of Synergetic Systems/Springer Series ni Synergetics, vol. 6/Ed. By Haken.-Berlin, Heidelberg, N.Y.: Springer, 205 (1980).
7. R. Lefever, Noise-Induced Transitions in Biological systems.- In.: Stochastic Nonlinear Systems in Physics, Chemistry, and Biology/Springer Series ni Synergetics, Vol. 8/Ed. By L. Arnold, R. Lefever.- Berlin, Heidelberg, N.Y.: Springer, 127 (1981).
8. W. Horsthemke, J.C. Michean, R. Lefever, J.Chem. Phys. (in print).
9. R. Lefever, W. Horsthemke, Proc. Nat. Acad. Sci. USA, 76, 2490 (1979).
10. W. Horsthemke, R. Lefever, Zs. Phys., B40, 241 (1980).
11. K. Kitahara, W. Horsthemke, R. Lefever, Phys. Lett., A70, 377 (1979).
12. K. Kitahara, W. Horsthemke, R. Lefever, Y.Inaba, Progr. Theor. Phys., 64, 1233 (1980).
13. W. Horsthemke, R. Lefever, Biophys. J., 35, 415 (1981).
14. R. Blumenthal, I.P. Changeaux, R. Lefever, J. Membr. Biology, 2, 351 (1970).
15. L. Arnold, W. Horsthemke, J.W.Stucki, Biom. J., 21, 451 (1979).
16. W.J. Rappel, A.Karma, Phys. Rev. Lett., 77, 3256 (1996).

17. P.V. Lam, D.Bagayoko, Phys. Rev., E53, 1280 (1996).
18. V.N. Damgov, Ukrainian J. Phys., 38, 460 (1993).
19. V.N. Damgov, Ukrainian J. Phys., 42, 582 (1997).
20. S.P. Sit'ko, O.P. Yanenko, Physics of the Alive (Biophysics & Beyond) (Ukraine), 5, 60 (1997).
21. J.F. Lindner et al., Phys. Rev. Lett., 75, 3 (1995).
22. K. Wisenfeld, D. Pierson, E. Pantazelon, C. Dames, F. Moss, Phys. Rev. Lett., 72, 2125 (1994).
23. P. Jung, G. Mayer-Kress, Phys. Rev. Lett., 74, 2130 (1995).
24. K. Kaneko, Physica (Amsterdam), 55D, 368 (1992).
25. G. Pezez, H.A. Cerdeira, Phys. Rev. A, 46, 7492 (1992).
26. H. Gang, T.Ditzinger, C.Z. Ning, H. Haken, Phys. Rev. Lett., 71, 806 (1993).
27. W.-J.Rappel, S.H. Strogatz, Phys. Rev. E, 50, 3249 (1994).
28. V. Hakim, W.-J. Rappel, Europhys. Lett., 27, 637 (1994).
29. C. Kurrer, K. Schulten, Phys. Rev., E51, 6213 (1995).

EHF - RADIATION IMPACT ON DROSOPHILA MELANOGASTER VIABILITY

V.G.Shachbazov, B.M.Bulgakov, S.P.Sirenko, L.M.Chepel', A.I.Fisun and O.I.Belous.

Kharkov State University
4, Svoboda scv., Kharkov, 310077, Ukraine
Institute for Radiophisics and Electronics
12, Proskura Str., Kharkov, 310085, Ukraine
Tel. 44-87-41, Fax. 44-11-05, E-mail obel@ire.ire.kharkov.ua

The electromagnetic radiation of the extremely high frequency band (EHF) have gained widespread acceptance in the therapevtics of different diseases. However, the biological foundation for analysis of the interaction between human organism and EHF-radiation has yet to be studied. The influence of EHF-radiation on the hereditary factors, among other processes, has been the subject of investigation and much concentrated attention. This problem invites further investigation, as it is liable to fur-reaching implications.

The action of EHF-radiation is studied on the imago of Drosophila mel. of the three generations of the inbred groups of a wild high-active (HA) and low-active (LA) lines. A shoosing of the investigation objects is substantiated by a relatively short vital cycle of Drosophila mel.

The standard generator Г4-141 was used as a source of EHF-radiation. The special automatically swiping block is built into generator, which spans approximately from 37 to 53 GHz frequency band. The swiping frequency is 20Hz. The power density is no more than 10 mW per cm^2. The widely band effect was taken as the principle, because the biological important frequency reside in this band and have not thus far been properly calibrated.

The imago in the 2 days age are hibrized with specieses of one kind and generation after radiation. The crossing cheme is as $C \times C$, $C \times T$, $T \times C$ and $T \times T$, where T is test species and C is control species. The resulting posperity viability is estimated by the thermo-test (40^0C, 20min). The imago male and female irradiation for a time 30min have been influated on the biological reproduction. In the all experimental cases the reproductive capacity of the HA female's line had been increasing on the 6 – 15%. The first posperity imago heat-tolerance (HT) after EHF-radiation action is also increased. The HT increase is on the 13 –24% for a female and on the 9 – 23% for a male (see Fig. 1). This effect becomes to a regligibly small quantity for second and third generations.

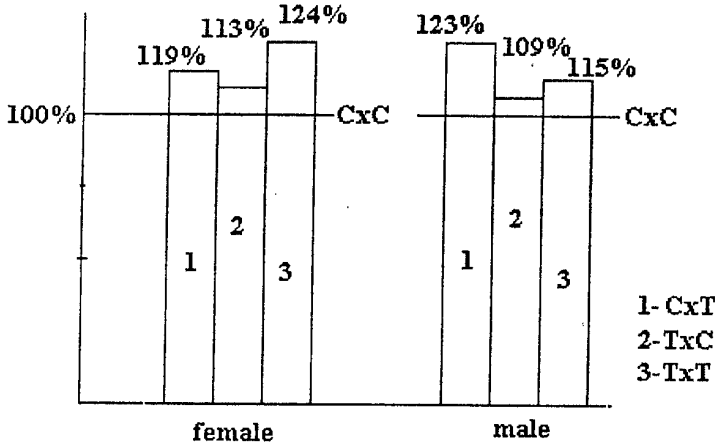


Figure 1.

At the shorts time expositions the reproductive capacity of HA female line had been increasing on the 22 – 50% (see Fig. 2) and HT of imago had been rising on the 13 – 50% (see Fig. 3) for all experimental conditions. The LA-lines has not, in this instance, the perceptible reaction on the outlined conditions.

Upgrading of the Drosophila mel. viability and reproductive capacity as a result of EHF-radiation can be dated to the physiological geterozis category. The physiological geterozis is a topical problem of the animals and plunts selection. However, this EHF-irradiation-produced effect of physiological geterozis up to the present has not described.

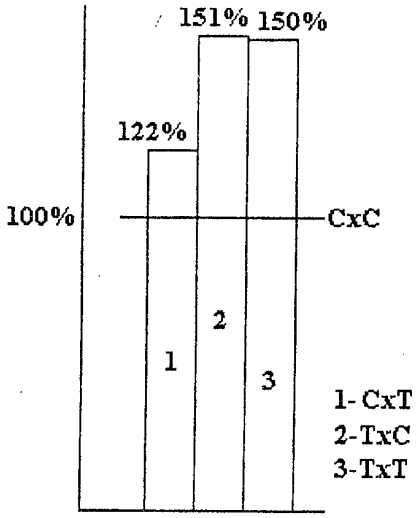


Figure 2.

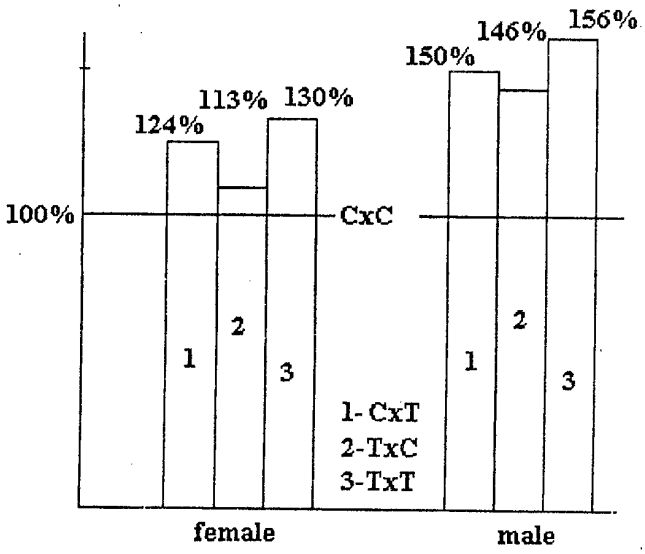


Figure 3.

USING OF EHF AND IR METHODS FOR STUDYING HYDRATION OF POLYCYTIDYLIC ACID

V.A. Kashpur, M.A. Semenov, N.N. Sagaidakova
Institute of Radiophysics and Electronics National Academy of Sciences of Ukraine
Address: 12, Ac. Proskura St, 310085, Kharkov, Ukraine
Tel. 0038-0572-448337, Fax 0038-0572-441105, E-mail: berez@ire.kharkov.ua

The use of dielectric measurements in the range of millimeter range (extremely high frequencies (EHF)) is important in a number of areas of biology and medicine. In particular, they allow one to study the state of water in biological solutions [1].

The methods of X-ray diffraction analysis, NMP, IR and CD spectroscopy, dielectrometry and others have established the presence of bound water around biomacromolecules [2]. Such solvent molecules attach to the hydration-active sites on the biopolymer surface through hydrogen bonding. In energy terms the water molecule may be considered «bound» if its energy of interaction with any hydration center exceeds the mean energy of water-water interaction in the liquid phase.

Numerous investigations demonstrated that without detailed knowledge of the features of the interaction of biomolecules with water there could be no complete understanding the properties and behavior of the macromolecules. Because the bound molecules have a lower mobility, the corresponding relaxation peak is observed near 100 MHz while the peak due to ordinary water locates around 20 GHz [3].

Unfortunately, the dispersion of dielectric permittivity of biomolecules is also observed near 100 MHz creating substantial difficulties in the interpretation of dielectric data. On the other hand, in the millimeter range the dispersion observed is only due to the relaxation of bulk water and hydration leads to a lowering of the dielectric permittivity of solution as compared with that of solvent [1]. This decrement can be used to study the interaction of biomolecule with water.

The present work is devoted to the investigation of the hydration environment existing around poly(rC) (polyribocytidylic acid). This polynucleotide is known to form different structures in aqueous solutions as a function of the pH, temperature and ion content [4]. At room temperature and neutral pH, poly(rC) is an ordered single-strand helix. In the range 3.7<pH<5.5 it forms a helical double-strand complex in which a proton is added to the ring nitrogen for each pair of bases (Fig.1). Below pH 3.5, through the addition of a second proton per base pair, a dissociation into two disordered chains with protonated cytosines occurs. It is believed that the hydrogen bond between the protonated and unprotonated rings mainly stabilizes the hemiprotonated complex.

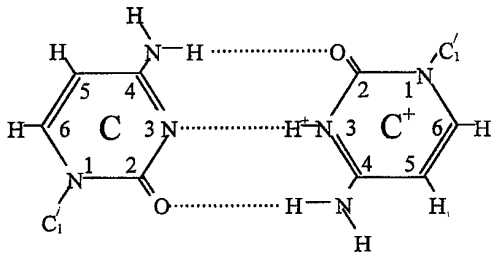


Figure 1. Hydrogen bonding between bases in the hemiprotonated complex.

The aim of the work is to elucidate the role of water environment in the formation of the different structures of poly(rC).

We used samples of poly(rC), K^+ salt, obtained from «Serva» (Germany) and «Reanal» (Hungary). The content of the K^+ ions in relation to the dry mass of the biomolecule was 6.7%(«Serva») and 8.5%(«Reanal»). Solutions in the range 3<pH<5.5 were prepared by the addition of HCl. For microwave measurements, 1% solution was used. For infrared studies, thin uniform films of poly(rC) were prepared and deuterated as described previously [5]. The wet films in the relative humidity (r.h.) interval from 0 to 96% were derived in the special cuvette. The degree of protonation was constant up to r.h.=86%.

Measurements in millimeter range were carried out by the differential dielectrometric method developed by us [6]. The decrement of the complex dielectric permittivity $\Delta\varepsilon^x = \varepsilon^*_{solvent} - \varepsilon^*_{solution} = \Delta\varepsilon^{/} - i\Delta\varepsilon^{//}$ was determined. The knowledge of the complex permittivity and conductivity σ measured at f=10kHz made it possible to calculate the effective dielectric constant of solution ε_s which is characteristic parameter of the Debye theory of fluids

$$\varepsilon_s = \varepsilon^{/} + \frac{\left(\varepsilon^{//} - \sigma/f\right)^2}{\varepsilon^{/} - \varepsilon_\infty} \quad ,$$

where ε_∞ is the high-frequency limit of dielectric permittivity. The validity of the Debye equation to the description of the relaxation of pure water was shown in a number of works [3].

The IR spectra were recorded with the UR-20 two-beam spectrometer, NaCl prism, spectral slit width 6 cm^{-1} at 1700 cm^{-1}.

Table 1 presents the results of dielectric measurements. The initial experimental values are the differences between the attenuation $\Delta\alpha$ and phase shifts $\Delta\beta$ of the solvent and solution. From these findings the analogous differences $\Delta\varepsilon^{/}$, $\Delta\varepsilon^{//}$ and $\Delta\varepsilon_s$ have been determined (for water $\varepsilon^{/}$=18 and $\varepsilon^{//}$=28.5 at 23^{0}C). Experimental errors for $\Delta\varepsilon^{/}$ and $\Delta\varepsilon^{//}$ are within 0.02 and 0.03, respectively.

The degree of hydration ω (g water per g solute) or n (the number of bound water molecules per nucleotide) may be found from the data obtained. Its value is proportional (in the first approximation) to the dielectric decrement and can be derived as

$$\omega = \Delta\varepsilon_s / p \cdot c \cdot \left(\varepsilon_s - \varepsilon_\infty\right) - v \ ,$$

where c is the concentration of poly(rC), v is the specific volume of poly(rC), p is coefficient depending upon the form of the polymers. According to the earlier paper [7], its meaning varies from 1.5 (sphere) to 1.66 (cylinder). Recently, it became possible to obtain the degree of DNA hydration (B form) using the dielectric measurements in the range of dispersion of bound water [3]. This value (n =19) is in agreement with our estimation of DNA hydration if the value of p is assumed to be 1.65. All the values of n in the Table have been calculated using this value.

The millimeter measurements demonstrate that at pH 8 the amount of water molecules which got into strong interaction with single-stranded poly(rC) is equal to 7-8.

Table 1. Results of the dielectric measurements (T=23^{0}C) of poly(rC)

Parameters measured	*pH 8* *c=1.18%*	*pH 4.5* *c=0.97%*	*pH 3.3* *c=1.3%*
$\Delta\alpha$ (nep/mm)	0.0161	0.0114	0.0151
$\Delta\beta$ (rad/mm)	0.0168	0.0164	0.0120
$\Delta\varepsilon^{/}$	0.07	0.10	0.04
$\Delta\varepsilon^{//}$	0.07	0.09	0.25
r/f	0.12	0.17	0.32
$\Delta\varepsilon_s$	1.34	1.26	2.16
$n(\pm 1)$	7-8	8-9	11

IR spectroscopy in wet films make it possible to study the stages of the formation of different structures of biopolymers and their hydration shells. Analysis of the changes in IR spectra occurring with wetting allows one to find the atomic groups which are hydration centers and to determine the order and degree of their fitting by water molecules.

To obtain such information on poly(rC) we derived IR spectra of the films for different humidities in the region of absorption of the intra- and the extraring vibrations of bases (1500-1750 cm^{-1}) and in the region of absorption of ribose and phosphates PO_2^- (900-1350 cm^{-1}). The dependences of the frequencies ν and intensities R on n were found from these spectra.

At the initial stage of sorption (0<r.h.<44%) the results of IR studies in the above regions point to the bonding of water molecules with such centers as atoms of the N_1, N_3 and, possibly, the groups C_2=O and NH_2 (base), O_4, and OH (ribose), PO_2^- (phosphate).

With further change in n in the interval 44%<r.h.<86% (to $n \cong 10$), the IR hypochromism and high-frequency shifts of the bands of the intraring vibrations and also the appearance of the band at 1292 cm^{-1} appear to be due to the ordering of cytosine rings and to the transition of poly(rC) to the fully ordered single-strand structure.

Thus, EHF (solution) and IR (wet films) results at pH 8 are close to each other and show that 8-10 bound molecules and necessary to form the ordered structure at poly(rC).

From the dielectric data presented in Table 1, it follows that at pH 4.5 the hydration of poly(rC) is 8-9 molecules of water per nucleotide (double-stranded helical structure).

The dependences of ν and R on n (pH 4.6, 0<n<2-3) for the absorption bands associated with the intra- and the extraring vibrations of cytosine may also be explained by hydration. The hydration centers are the same as those at neutral pH region and take part in the hydrogen bond between the cytosines of two opposite poly(rC) chains.

The rise of the intensity of the band at 970 cm^{-1} as well as the appearance of the bands at 1059 cm^{-1} and 1293 cm^{-1} (0<n<5) of ribose correspond to the formation of bonds between water molecules and the atoms $O_{4'}$ and OH. The water bridges connecting these atoms and phosphates, cytosines and atoms $O_{2'}$ and $O_{5'}$ of neighbouring strands are formed. This process stabilizes the double-helical complex.

Further wetting (2<n<7) leads to the changes in intensity and position of some bands associated with vibrations of bases and ribose. These effects indicate the formation of the double-helical conformation. Final stabilization of the complex takes place with increase in the water content to n=9.

This value fully agrees with the EHF findings. Thus, this amount may be considered to be necessary for the stabilization of double-helix poly(rA) both in solution and in films.

Dielectric measurements show that the poly(rC) hydration at pH 3.3 is 11 water molecules per nucleotide. Since in this case the double-stranded complex dissociates with elimination of base pairing, water bridges and ordered helical conformation, it might be anticipated that the hydration at pH 3.3 might not exceed the hydration at pH 8. The greater value which is observed is apparently due to the protonation of N_3 (65% at pH 3.3). It is known that the hydration number for proton is 10 [8], so that the poly(rC) chain, except N_3, binds 5 water molecules. This value is very close to IR data (n=6). However, the latter value may also be explained by aggregation of poly(rC) in acid region (pH<3).

We thank I.V. Sysa for help in EHF measurements. This work was supported by the State Foundation of Fundamental Investigations (Grant No2.4/759).

References

1. E.H. Grant, R.J. Sheppard, G.P. South, «Dielectric Behaviour of Biological Molecules in Solution», Clarendon Press, Oxford, pp.237, 1978.
2. V.Ya. Maleyev, M.A. Semenov, A.I. Gasan, V.A. Kashpur, «Physical Properties of the DNA-Water System», Biofizika, Vol.38, No.5, pp.789-811, 1983.
3. T. Umehara, S. Kuwabara, S. Mashimo, S. Yagihara, «Dielectric Study on Hydration of B-, A- and Z-DNA», Biopolymers, Vol.30, No.7/8, pp.649-656, 1990.
4. C.H. Chou, G.J. Thomas, «Raman Spectral Studies of Nucleic Acids», Biopolymers, Vol.16, No.4, pp.765-789, 1977.
5. M.A. Semenov, B.I. Sukhorukov, V.Ya. Maleyev, «Are Nitrogen Bases of DNA Hydrated at Low Humidity?», Biofizika, Vol.26, No.6, pp.979-984, 1981.
6. V.A. Kashpur, V.Ya. Maleyev, T.Yu. Shchegoleva, «Investigation of Hydration of Globular Proteins by Differential Dielectrometric Method», Mol. Biol., Vol.10, No.3, pp.568-575, 1976.
7. T.J. Buchanan, G.M. Haggis, I.B. Hasted, «The Dielectric Estimation of Protein Hydration», Proc. Roy. Soc., A213, No.1114, pp.379-391, 1952.
8. L.I. Antropov, «Theoretical electrochemistry», Moscow, pp.568, 1975.

Study of the weak electromagnetic field action upon the biological molecules and tissues by holographic interferometer.

L.I.Berezhinsky[1], G.I.Dovbeshko[2], N.Ya. Gridina[3]

1-Prospect Nauki, 45, Institute of Semiconductor Physics, NASU, Kiev-28, 252028, Ukraine; 2-Prospect Nauki, 46, Institute of Physics NASU, Kiev-22, 252022, Ukraine, fax:380-044-265-15-89, e-mail: galina@dpbs-3.kar.net; 3-Manuilsky str.37, Romodanov Institute of Neurosurgery, Med.Ac. Sci.Ukr., Kiev-50, 254050, Ukraine.

INTRODUCTION

The investigation of the biological effects of the low-energy electromagnetic (EM) fields has recently became an object of great interest in the fundamental science. This is caused by the fact that we live in the world, where the human beings undergo different types of EM irradiation from both artificial and natural sources. In addition, the low energy interactions are characteristic to the life processes and play very important role in the structure and functioning of the living matter [1].

The previous investigations mostly were performed on high levels of organizations of living matter, namely, they were performed with higher organisms and cells, because in these cases the effects of the EM fields are well pronounced. It has been found [2, 3] that with the use of the low-intensity millimeter wave (MMW) field of selected frequencies applied to organisms' biologically active points a corrective action on specific immunological and metabolic processes could be achieved.

As for MMW effects upon biomolecules, there is a gap in the researches, and the mechanism of the influence of MMW radiation on molecular level is not clear, although there are some experiments and hypotheses concerning this subject [4-6]. The series of our experiments on crystals of compounds, which can be regarded as building blocks of the living matter [7-9], indicated an essential role of disturbance of the dielectric properties by the MMW radiation. Here we present our results concerning visualization of the action of the MMW field and changes in refraction index (n) of tissues from different organs, native blood plasma water solutions and model biological molecules (proteins and DNA) under MMW irradiation..

METHODS AND MATERIALS

Experiments were carried out with the use of the holographic interferometer, whose optical scheme is given in Fig.1. The He-Ne laser (1) radiation (output power 1 mW at (λ=632.8 nm) is divided by beam splitter cube (2) into two beams: object beam and reference beam. In the object beam there is a mirror (3) and a collimator (4) consisting of negative and positive lenses and forming a parallel beam with 5 cm in diameter. The beam passes through the object under study (6), and then arrives at finely dispersed diffuse scatterer (9). According to Lambert's law, its every point is scattering the light in all directions. Therefore, the light from the whole surface of the scatterer arrives at every point of light sensitive thermoplastic (10). In thermoplastics plane object beam together with reference beams produced by mirror (11) and objective lens (12) form the hologram of the object under study. After the hologram is registered, a plane-parallel plate (5) is introduced in the object beam, resulting to the appearance of interference patterns in the thermoplastic plate. Picture of the object and interference patterns are observed by TV camera, combined with PCAT computer. With the help of glass plate (5), which introduces phase detuning, the regime of interference picture can be selected. Thus, at one inclination of the plate (5) the increase of refraction index will result in the increase of interference period, i.e. in the decrease of number of bands, while at another inclination (with the same sign of n) it leads to lessening of interference period and crowding of bands, i.e. to the increase of their number. In our experimental set-up the plate (5) was located so that the increase of solution refraction index in the flask would result in the decrease of the number of interference bands in sample field, and vice versa, the decrease of refraction index (e.g. at the expense of thermal expansion) would cause the increase of the observed number of bands in the sample field. In this case the number of interference bands outside the flask field remained unchanged and served for independent control over the objects alterations. If the dielectric characteristics of the object under study are the same before and after MMW action, then interference picture remains unaltered, and interference bands inside and outside the object's profile continue each other. On the contrary, the interference picture within the limits of object's profile will change, particularly the number of lines and the distance between them, if some external factor caused changes of the refraction index of the object.

Commercial generators (G4-141 and G4-142, USSR) that operate with backward wave tube at the frequency tuned within the range of 37,5-78,5 GHz and maximum output power density of 10 mW/cm^2 with frequency stability 5 MHz served as the sources of millimeter wave irradiation. To apply the irradiation, a flexible teflon waveguide with 2,8 x 5,6 mm^2 cross-section was used. One of its ends was put in the aperture of

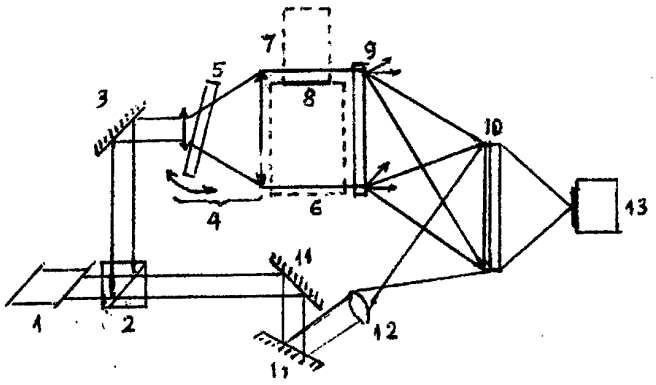


Fig.1.Experimental holographic set. 1-He-Ne laser, 2-beam splitter cube, 3-mirror, 4-collimator, 5- plane-parallel plate, 6-quartz flask (cuvette) with solution, 7- other flask with solution, 8-filter, which divides two flasks, 9-scattering layer, 10- thermoplastic recording plate, 11-reference beam mirror, 12-reference beam lens, 13-TV camera.

generator's metal output waveguide while the free end was lowered into a quartz cuvette (1x1x4, 3 cm^3) with the studied solution to a depth of 2-3 mm. Experiments were carried out at output power density on the end of teflon waveguide amounting to 10 mW/cm^2. The exposition was performed at the fixed frequencies selected to achieve maximum effects. Investigations were carried out at temperature 20° C controlled by thermocouple accurate to 0,2° C.

Na-DNA (Servo), human albumin (Reonal), homogenates of embryonic and mature tissues from different organs (kidney, thyroid, gland, spleen and liver) of experimental rats, blood plasma of human were used as samples

RESULTS AND DISCUSSION

The most strong changes in MMW radiation effect upon 2% blood plasma water solution at 51.5 GHz frequency have been detected and investigated. When MMW source was switched on, the increase of distance between object bands occurred. The changes in interference picture were irregular with time. The largest changes occurred during the first minute then they slowed down. Within the first 10 seconds the increase ranged up to half of the interference line and within 30 sec. it ranged up to a full band. Without MMW action the number of interference bands was the same in the field of the object and around it and equaled to 5. During 6.5 min from the start of exposure the number of interference bands in the object's profile decreased by four. After this period only slight changes were observed. The latter allows the assumption of the saturation effect. Since these changes were observed in the whole plasma volume, their nature was regarded as a macroscopic one. Changes in the refractive index of the sample under MMW action were estimated from equation: $L\Delta n = l\Delta k$, where L - the thickness of the sample (solution), Δn - changes in refractive index, l - wavelength of the source of light (laser), Δk - changes in the number of the interference bands in the samples field of view, which obtained as a result of external effect.

The reversibility of the effect has been established: after MMW source was switched off, the interferogram had restored its original structure, construction period of original state was 3-4 min longer than the time of maximum change accumulation. The increase in plasma concentration up to 10% was essentially slowing down the process of changes, whereas the addition of 1.5% of CaCl2 into the solution was increasing the rate of interference picture shift more than twofold. Experiments showed that a seven minute MMW radiation action on the pure water carried our at 41.5 GHz frequency resulted only in minor changes of interference picture, though a 5 minute exposure at 51.5 GHz frequency decreased the number of interference bands by one. Thus, weak mm-field effects also occurred in water, though their magnitude was small ($\Delta n=2x\ 10^{-5}$). These facts suggest that the

effect be mainly determined by the blood plasma components. MMW irradiation and heating effects were opposite-directional. Temperature rise in the flask detected by thermosensor within the period of MMW action with 10-mW/cm^2 power density amounted to 0,5- 0,6 K, which agreed with the data of other authors where the heating of biological aqueous solutions by MMW irradiation was investigated. So in view of the inevitable solution heating due to MMW radiation absorption it is appropriate to estimate the role of temperature effect. The estimation of the temperature effect by using of thermal conductivity equation and thermal balance equations showed the following. Thus, maximum solution heating in this period with no account of thermal exchange, i.e. under the condition unfavorable for thermal effect estimation may amount to 1 K. The calculation showed that even in the absence of heat exchange between the solution and environment under the radiation effect with the power density of 10 mW/cm^2 the temperature of solution with the volume of 1.5 cm^3 may raise round 1° C within 6 min. Lower temperature value (0.5-0.6° C) was obtained by us in the measurements with the use of thermosensor. Temperature coefficient of changes in water refraction index makes up $6x10^{-5}$ K. In our experiments the maximum change of refraction index corresponds to $n = 2.59x10^{-4}$, which is by an order higher than the temperature changes of refraction index. With the account of this total value of MMW radiation effect will make up about $3x10^{-4}$. Thus, the numerical estimations and the experimental data demonstrate that refraction index changes under MMW action were conditioned by non-thermal changes of solution dielectric constant which may be described as a sum of contributions of electronic, vibrational and orientational components. Evidently, structural rearrangements took place in plasma solution and in its components - biomolecules and water molecules, which in turn effected a solution dielectric constant. Thus, low-energy MMW radiation initiates the processes of internal rearrangements in solution, which may result in modifications of medium electronic polarizability observed from refraction index change.

By using the holographic interferometery we could visualize and study the interaction between different tissue under different condition. Products of cell metabolism could be extracted by filter 8 from cuvette 7 (Fig.1). Then we can study the interaction of these cell products with tissue and cells, which are put in cuvette 8 by means of interference picture. Study of value and sigh of changes in interference patterns we can follow for the interaction the products of metabolism from upper cuvetter 7 with tissues or cells in lower cuvetter 8. Value and other characteristics of interference patterns have been changed essentially when solution with tissue has been undergoing to MMW radiation. From the experiments we can conclude, that under MMW tissue has changed their interaction with environment cells and solution. This state was kept some period of time (3-5 minutes) and then it was restored. Hypothesis of charge changes of cells and their components under MMW is proposed.

REFERENCES.

1. H.Frohlich "Biological Coherence and Response to Extermal Stimuli, Herbert Frohlich (Ed.) Springer-Verlag Berlin Heidelberg New-York London Paris Tokyo, p. 268 , 1988.
2. Fundamental and applied aspects of millimeter electromagnetic field in biology and medicine, in Proc.I Symposium with Inter Part., Kiev, Soviet of Ministery, Temporal Scientific Center Otklik, p. 404, 1989.
3. Chengjiong He, Kehui Gono, Gunzhu He Effects of microwave accupuncture on the immunological functional cancer patients. J.Trad.Chin. Med. N7, pp.9-11. 1987.
4. A.A.Serikov "Weak Field Influence on Biomolecular Changes". Journal Biological Physics, vol.18, pp.65-77, 1991.
5. I.Ya.Belyaev, Y.D.Alipov and V.S.Shcheglov, "Chromosome DNA as a target of resonant interaction between E.coli cells and low-intensity millimeter waves". Electro and magnetobiology, vol.11(2), pp.97-108, 1992.
6. Litvinov G.S. Response of biomolecules and cells to millimeter wave electromagnetic field. Transactions of the First Congress of European Bioelectromagnetics Association. Vth European Symposium, Brussels, Belgium, Posters, p.46, 1992.
7. G.S.Litvinov, L.I.Berezhinsky, G.I.Dovbeshko, M.P.Lisitsa "Mm-wave radiation action on infrared reflection spectra β-alanine single crystal". Biopolimery i kletka N3, pp. 77-82 , 1991 (Rus).
8. Dovbeshko G., Berezhinsky L., Obuchovsky V. "Special case of nonlinearity of biological molecules" Proc.SPIE, vol.2795, pp. 306-311, 1996.
9. L.I.Berezhinsky, N.Ya.Gridina, G.I.Dovbeshko, M.P.Lisitsa "Visual observation of mm- wave action upon blood plasma". Biophysics, vol.38, N2, pp. 378-384, 1993 (Rus).

Method of EHF-therapy at treatment of endogene mental diseases

BacherikovA.N.,Derkach V.N.

The Usikov' Institute for Radiophysics and Electronics of the Academy of Sciences of Ukraine.
Ukrainian Scientific Research Institute of Clinical and Experimental Neurology and Psychiatry
12 Ac Proskura St., Kharkov, 310085, Ukraine
Phone (0572)448-594, Fax(0572)441-105,E-mail: derkach@ire.kharkov.ua

In a basis of the physical concept of influence of EHF-radiowaves the supposition about their information action on organism of person is put. According to this concept, the related cells exchange an information by means of electromagnetic waves of EHF range [1]. The functional violations, which arise in organism of person, reduce to decrease of a common emitted potency and shift of emitted frequencies from eigen frequency of organism or organ, that in turn reduces in violation of information connections between cells and, as a corollary, to the further development of pathologic process. To prevent this process it is possible by action onto biologically active zones (biologically active dots, zone Zaharina-Geda) by the electromagnetic radiation. This radiation makes an additional electromagnetic field, which stimulates and synchronizes work of all emanating of systems.The effectiveness of EHF-therapy (to the present time) is shown at treatment of diseases of gastrointestinal tract, cardiovascular systems, nervous and dermal diseases etc. It is necessary to note, that the known methods the properties such basic information structure as water do not take into account and do not use. Aside from the functional features of the organism are not taken into account completely. Is established [1], that the effect of EHF-therapy largely depends on a condition of water in tissue, its structural organization and percentage structure of a free and connected of phases. As the indicated physic-chemical (electrophysiological) properties of water are determined in temperature, it is natural to assume, that the effect of action EHF also will depend that of temperature of a surface layer of a skin in zone of action. Hence, alongside with a selection of therapeutic frequency the temperature condition of the biological tissue in zone of influence EHF is necessary individually to select.

We tested a method of treatment by EHF-therapy at which electromagnetic radiation acts on cooled segments of a skew field. Such approach allows more completely to use individual singularities of the patients organism, to increase effectiveness of a mode of EHF-therapy, and as a corollary to decrease period of treatment.

The essence of a method is what the action of low-intensity electromagnetic radiation is produced on cooled (up to temperature + 5 + 20C) site of a skew field. The cooling is reached by ventilation of zone of action by a cooled air. The EHF influence was carried out on the developed technique on biologically active dots and zones of Zaharina -Geda. As a source of low-intensity microwave radiation was used generator G4-141 with a variable frequency within range of 37.5 - 53.57 GHz, power level varied within 3 - 10 mkW/cm^2. Frequencies of electromagnetic radiation, to which an influence have been exerted, and areas of influence have been selected individually on the base of subjective feeling. Course of treatment consisted of 6 - 8 seances (depending on state of patient) on 30 minutes daily. The treatment proceeded before reaching effect of normalization of basic indexes of habitability. The condition of the patients was inspected during all treatment (before and after EHF-influence) and in the set aside phases (through one - two weeks).

Was marked, that the effectiveness of such method of EHF-therapy was increased apparently because in a biological medium, at the expense of a modification dielectric (ε and $\mathrm{tg}\,\delta$) and electrophysiological parameters of water at a modification of temperature, there are optimum conditions for resonance passage of electromagnetic waves and effective transmission of an information between biological structures. Alongside with it, under our judgement, the positive effect of such method of treatment is connected to double effect of action on organism:

- reflexogenic, which is connected to stimulating action on subcortical structure of a head brain, including on hypothalamus, and as a corollary on mechanisms of adaptation;
- local, which is connected to direct action on regeneration possibilities of tissues, that is exhibited as resorption, antiinflammatory, analgetic and anti-alergic reaction

The treatment with application of a new method of EHF-therapy was conducted 10 patients (women, of 25 to 40) with manic-depressive psychosis in a condition of depression. Depression at the patients in basic was determined following axial syndromes: suppressed mood, intellectual inhibition, psychomotor inhibition, bradylalia. At 8 patients had a place characteristic diurnal oscillation of mood, i.e. the softening of depressing; symptomatology in evening time, and at 2 patients the reduced mood varied within a day a little. In 4 cases an

alarm and despair periodically were more expressed, than other depression symptoms, at these patients also were marked appearances of irritability, fixed ideas, hypochondriac ideas. At all patients the expressed alarm, anguish was marked, that was accompanied by physical burdensome sensations, feeling of weight in epigastrial area or in the field of heart. Also at all patients the expressed violation of dream was marked (sleeplessness, length of sleep was 2 - 3 hours. The expressed drop of appetite reduced that the patients lost in weight 5 - 10 kgs. Suicidal ideas at 8 of 10 patients were marked, that testified to extreme painful of depression.

The study of parameters of a condition of vegetative nervous system (VNS) was shown that positive therapeutic effect of EHF-action was realized through normalization of adaptation process. The indexes of variation pulsomety of the patients before and after of treatment are shown in tables 1 and 2 for the illustration this process. The analysis of a rhythm of cordial activity was produced by a measurement of duration of each interval R - R in 100 cordial cycles with accuracy 0.01.

The following statistical indexes was calculated:

- M is mathematical expectation (show an average value of a duration of a cordial cycle);
- Mo is time interval, the index most frequently of met interval R - R (mode);
- AMo is amplitude of mode, the index of encountingly of an interval R - R correspond to Mo;
- ΔX is variation amplitude, the index of oscillations of duration of a cordial cycle, which together with a root-mean-square deviation (σ), reflects a degree of stability of a cardiac rhythm;
- IE is the effort index, it summarizes correlation of basic indexes of a cordial rhythm ;
- VEI is the vegetative equilibrium index, it indicates a relation between sympathic and parasympathic by parts of a vegetative nervous system;
- VCI is the vegetative cardiac rhythm index it testifies to a degree of an autonomy of regulation ;
- RI is the regulation index it reflects influence of a sympathetic nervous system on activity of sinoatrial node.

TABL1.

medical	mean	σ	V	As	Ex	П. norm	Mo
Befor	0.929± 0.02	0.041± 0.005	4.376± 0.5	-0.278± 0.164	-0.600± 0.402	2.782	0.9± 0.04
after	1.048± 0.03	0.109± 0.008	10.422± 0.5	0.102± 0.527	0.230± 0.309	0.395	1.0± 005

TABL2

medical	AMo	ΔX	VCI	IE	VEI	RI	HBP
Befor	42±4.6	0.16± 0.026	6.944± 0.6	145.83± 29	262.5± 42	46.667±4	17.214± 2.1
after	41±3.1	0.52± 0.04	1.923± 0.2	39.423± 7	78.846± 24	41±3.8	49.642± 3.3

As it is visible from reduced tables, at the patients during treatment the following basic tendencies are marked:

- translational magnification of indexes σ and average value;
- increase of values of a variation factor and kurtosis;
- magnification ΔX in 3 times;
- progressive decrease of indexes VCI, IE, VEI and, to a lesser degree,RI;

These dates testify about positive adapt influence of a new method of EHF-therapy. It also is confirmed by a diminution of EI with 146 up to 39, VCI with 7 up to 2, VEI with 263 up to 79 and RI with 47 up to 41, at a practically not varying index ÀMo.

The analysis of other vegetative indexes such as minute volume of blood (MO) and index Kerdo (KI) during treatment is shown an amplification of parasympathic influences of a vegetative nervous system.

It is possible to speak, that the EHF-therapy provides on the patient organism the adapt action on what indicates that fact, that already after 5-10 days happen normalization of vegetative indexes .. On stability of vegetative regulation after treatment the indexes of factor of a variation, AMO,Mo,σ indicate.

The similar results were obtained at a research of dynamics of the Danini-Asher's vegetativ reflexes (sinocariotid reflex) and Chermak's (oculocardiac reflex). Has appeared, that at majority of the patients had a place a decrease of vegetative reactivity (at 5 patients), at 3 patients - sympathic response, and at 2 patients perversion a response of VNS. After treatment at 7 patients the normalization of responses of these reflexes was marked, at 3 patients was saved increased sympathetic a reactivity.

1.PetrocjanA.E.,GulaevU.V.,ZigilevaE.A. Radiophisics and Electronics B1.-1995.-p.127-1331.

THE RESEARCH OF MOLECULAR MECHANISMS OF SPERM CONTROL SYSTEMS FUNCTIONING.

Zubez M.V.,Kolesnikov V.G.,Schegoleva T.Yu.
Ukrainian Agrarian Academy of Science,
2 Suvorova St, Kiev,252030, Ukraine
Institute of Radiophysics and Electronics of the National Academy of Sciences of Ukraine
12 Ac. Proskura St, Kharkov, 310085, Ukraine
The Problem Scientific-Research Laboratory of Molecular Mechanisms
4/32 Solanikovski lane, Kharkov, 310003, Ukraine
Tel.8-0572-448506,8-0572 23-04-38,Fax 8-0572 441105,E-MAIL tsch@ire.kharkov.ua

The sperms essentially differ from other cells by the structurally functional organization. The sperm membrane against a erythrocytes trombocytes and other, well investigated cells, has less receptors complexes or they are less active on literature datas. Availability in it adenilate cyclase system and beta-receptor is discussed. Especially important cell component of the sperm is cytoskeleton. However sperms rather short-lived cells, if the additional modes of preservation which in turn modify cells are not applied. The study of processes of sperm control should be produced in a rather short time interval - some hours. EHF-dielectrometry enables to decide of this problem.

The development of this method was begun in researches on study of a water component condition of biosystems and hydration parameters of macromolecule with use of mm-range of radiowaves in the region of free water dispersion. This researches was carried out within 20 years in Institute of Radiophysics and Electronics of a National Academy of Sciences of Ukraine. As a result of conducted complexe of thease works the common model of macromolecule hydration, which quantitatively compared with their space organization on International Protein Data Bank of the X-ray diffraction analysis is constructed. [1,2].

The types of connected water and their character of binding in a structure of macromolecule are quantitatively described. It is shown, that the major part of macromolecule hydrate environment is a replica of its structure, which includes part of water, as the structural element ensuring it space organization. In the present work the approach on the analysis of macromolecule conformational transformations at different levels of organization on a modification their hydration environment, developed by us, will be used. This approach has become a basis of the new methodology of the analysis of a cell controlling systems on directed action on it's macromolecule component by biologically active substances. This approach also made it possible to reveal connection between magnitudes of the cell response on action of various biologically active substances and hydrational parameters of macromolecule, participating in the process.

The essence of this approach is, that in the beginning of experiments the prospective inquiry scheme of a cell response on action biostimulators on exhaustive search of variants of blockade and modulation of function by scrining the prospective components of a cell, participating in the analyzable process, is developed on biochemical and immunological datas being available from the literature. Then, this inquiry is produced in vitro in the correspondence with the analyzable scheme on a modification of dielectric parameters of test microvolume in real time. The use of such approach already has allowed to receive part of datas about hormon action when they blockade various links on transmembrane transmission

of an information, alpha-, beta- receptor and G-protein in erythrocytes. Some aspects of modulation of cell functions by exogenous calcium and prostaglandines, and also series of cytoskeleton functions in erythrocytes, trombocytes, leycocytes and has already been considered.

In an assotiation from complexity of this scheme it can last from one till several hours, the time of a measurement of one test does not exceed 5 minutes. The information processing happens with sequential adjustment of the inquiry scheme during realization of experiment. The cells is not exposed to any additional actions, as the potency in waveguide tract does not exceed 10 мVt. The measurements are produced in dielectrometer A-17, developed by Research Laboratory of Controlling Complexes of a Cell.

As a result of a conducted cycle of works, which was undertaken in Ukrainian Academy of Agrarian Sciences, the series of structurally functional singularities of the sperm on transmembrane transmission of a signal, including the receptors membrane as adenylate cyclase system, so other types of receptors, conjugate with it and firmware in membrane is detected. The series of new basic outcomes concerning modulation of activity sperm α- and β-receptor by prostaglandines is obtained. Some systems connections between α-, β-receptor, cytoskeleton and interior structural organization of a cell in various aspects of transmembrane transmission of a signal are detected.(Fig.1)[3].

For it the study of receptor complexes of a sperm membrane was conducted and the selection of modes of defferenciation of their qualitative indexes for development basic new methodology and, on its basis the modes of express-testing, prediction and correction of sperm quality on all stages of its storage and use, is realized.(Fig.2) [3,4]. The found out rather high activity of a series of membrane receptor complexes, according to results of EHF-dielectrometry, gives a basis for an operating the express-tests on a large gang of indications, essential to process of cultivation engineerings of animals.Nucleous

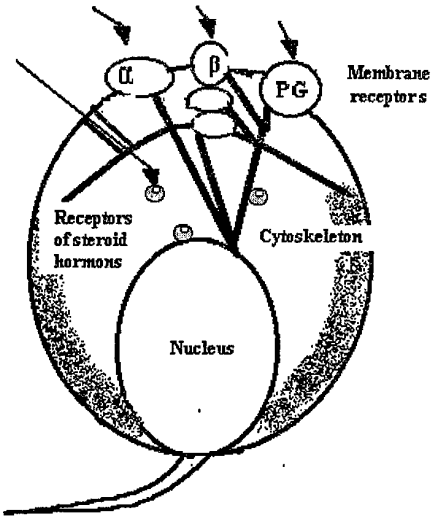


Fig.1. The bounds system of the cells components

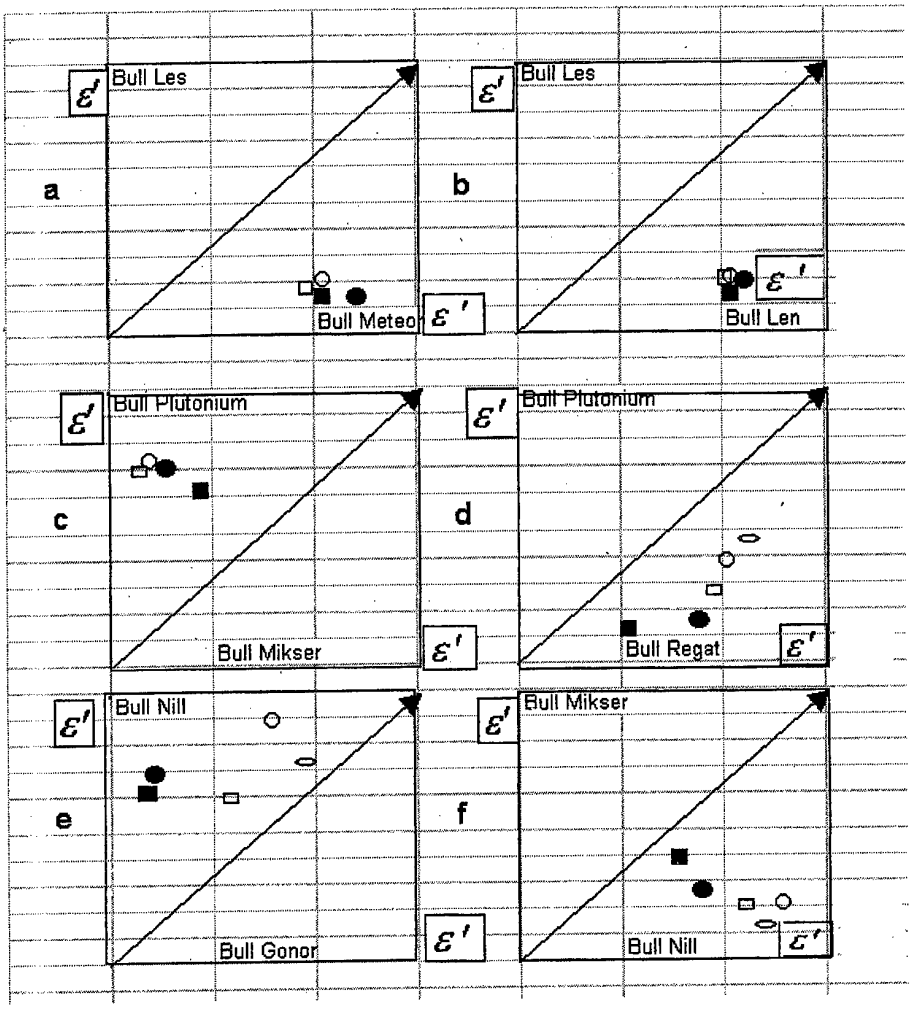


Figure.2 The individual contrast of the diviation real part of the complex dielectric constant of the cells suspension (a-c) and post hormonal action (d-f) ,the measuring time 2 -5h, the interval of the measuring time 1/2-1 hour

References

1. T.Yu. Shchegoleva. Research of biological objects in millimeter range of radiowaves, Naukova dumca, Kiev, 1996 -182.

2. T.Yu. Shchegoleva, Hydration environment and macromolecule structure. Advance of modern biology., 1996,116,6,700-714

3. M.V. Zubets, T.Yu. Shchegoleva, V.G. Kolesnikov, Application of millimeter range waves in agriculture, Agrarian science, Kiev, 1996 - 163.

4. M.V. Zubets, T.Yu. Shchegoleva, V.G. Kolesnikov,The same iIndividual, genetically determined and singularities of the cells molecular mechanisms controlling, The bulletin of an agrarian science, № 3,pp.38-42,1997.

APPLICATION OF METHOD OF EHF- DIELECTROMETRY IN ANALYSIS OF MECHANISMS, STIPULATING INDIVIDUAL LEVEL OF CORONARY RISK

Gridasova L.N., Shchegoleva T.Yu., Kolesnikov V.G., Nicolenko U.J
Institute of Radiophysics and Electronics of the National Academy of Sciences of Ukraine
12 Ac. Proskura St, Kharkov, 310085, Ukraine
The Problem Scientific-Research Laboratory of Molecular Mechanisms
4/32 Solanikovski lane, Kharkov, 310003, Ukraine
Institute of Therapy of Academy of Medical Sciences of Ukraine, Kharkov
2a Posteshev prospect, Kharkov, 310125, Ukraine
Tel.8-0572-448506,8-0572 23-04-38,Fax 8-0572 441105,E-mail tsch@ire.kharkov.ua

Investigations of molecular mechanisms of controling systems of cell open new possibilities both in study of key questions of its regulation and for analysis of mechanisms of development of pathologies of organism as a whole. This work was aimed on investigation of relation of adenylcyclase system (ACS) complex and erythrocytic cytoskeleton for analysis of its changes in different levels of coronary risk and study of stipulating it molecular mechanisms.

At present it is known a number of molecular mechanisms, stipulating development of cardiovascular pathology on differnt stages. However, construction of general picture of disturbances in development of this type of pathology is still not finished. This takes place mainly because of labour-consumption character of such investigations, complicacy of analysis of received results when comparing of data of different methods, received as a rule in destruction or modification of the cell. Method of EHF-dielectrometry gives new approach to decision of this problem as it allows to study cell's condition changes when effecting with biologically active substances in real time, in conditions of non-destructive control [Shchegoleva T.Yu,Bachova L.K,1998].. It is used widely in investigations of molecular mechanisms of controlling systems of cell and opens new possibilities for investigation of key quiestions of its regulation. In present work it is made the analysis of molecular mechanisms of cellular disturbances on the early stages of development of cardiovascular pathology on the base of data of population investigations of risk prophile of coronary risk with use of method of EHF-dielectrometry.

Methods and materials.

This work was carried out on 60 volunteers aged from 35 to 59 years (representative 10% sample of organised contingent). Investigated material was saline erythrocytic suspension. Hormones and cytostatics in standard terapeutic doses were used as effecting agents, as well as substances, modifying lipid membrane component. Measurements of complex dielectric permeance $\varepsilon^* = \varepsilon' + i\varepsilon''$ in millimetric wave length band was performed on EHF-dielectrometer (modification A-17), designed in Scientific and Research Laboratory of Molecular Mechanisms, measurement error for $\varepsilon', \varepsilon''$ was 1%, time of sample measuring 5 min., sample volume 0,005 ml. Presence or absence of cells system's response on effect on adenylcyclase complex proteins and cytoskeleton were determined by changes $\varepsilon', \varepsilon''$.

Mathimatical processing was performed on IBM 486/DX with application of methods of variation statistic and standard packets of applied programs BMDP. For estimation and prognosys of epydemiological situation in relation of coronary heart disease and risk factors of its davelopment, imitative multidimensional model was worked out on the basis of approaches, describing investigated process with appli6ation of spectral and correlation function [Nikolenko, 1996].

Results and discussions.

Aadenylcyclase system (ACS) is the universal mechanism for almost all cells of organism, so it was choosen as test system. Investigation of cell's responses on effects of biologically active substances was carried out with the use of model ACS, built on the base of data of EHF-dielectrometry. This model is well conformed to known literary data, and system of connections of functionally active elements, received in conditions of non-destructive control, essentually makes clear some key

ε'	Level of individual coronary risk		
	low n=33	middle n=15	high n=12
Dielectric permeance of cell's suspension	17.8 ± 0.1	17.8 ± 0.1	17.7 ± 0.2
Cellular response on adrenaline	20.7 ± 0.6	19.8 ± 0.7	13.2 ± 0.6
Cellular response on adrenaline+kolchicin	20.3 ± 0.6	19.5 ± 0.8	15.2 ± 0.8

Table. Changes of dielectric permeance of erythrocytic suspension on cellular response on addition of bioregulators in subjects with different individual coronary risk level.

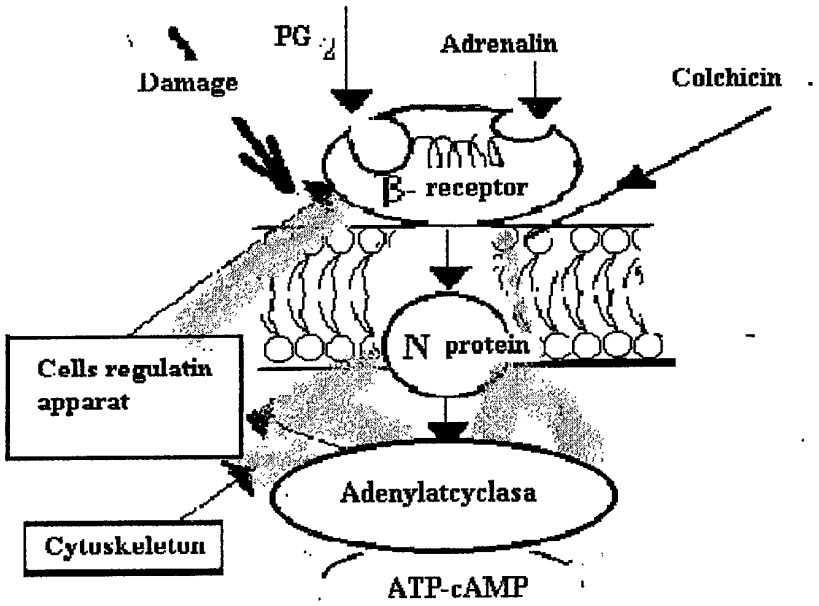


Figure. The model of damage the molecular mechanisms of transmembrane signal transmissions by of cardiovascular pathology

regulation mechanisms. Mechanisms of hormone stimulation of beta-receptor complexes with accounting of interaction with cytoskeleton as well as stability of cytoskeleton when effecting with cytostatics on it, were studied.

Erythrocyte was choosen as a model since simplicity of its organisation permits to investigate functional properties of plasma membrane without obstacles, to avoid distortions of membrane functions that can appear for a second time, for instance, in cardiomyocytes, with reinforcement of contractive activity of cells. Erythrocytic membrane reflects changes of membrane functions. That's why this comparatively simple object is the base for study of essence of this changes.

After statistical processing of findings it was revealed that cell response on addition of the used bioregulators varied by its directions in subjects with different individual level of coronary risk. Thus in case of low coronary risk all mechanism of transmembrane signal transmission is engaged:the cell actively responded to effects of hormones, modulators and their combinations. This value is reliably lower in middle individual risk level. In high level of individual coronary risk cellular response to addition of adrenaline changed direction to sharp reduction of dielectric permeance index of erythrocytic suspension. Changes in direction of cellular response on addition of cytostatic depending on coronary risk level were of similar but less pronounced character. Thus, in high individual coronary risk transformation of cellular response takes place and in comparison with clinical indices this fact should be estimated as unfavorable prognose symptom.

It is interestingly to note that dielectric permeance of erythrocytic suspension in individuals with different degree of coronary risk is almost not differ, though it is well known that in formed stages of cardiovascular pathology - bordeline hypertension, hypertensive disease, coronary heart disease - this index for platelets and erythrocytes differs reliably (Veselovsky,1982). In some papers (by Malaya L.T., Tshegoleva T.Yu., Bakchova L.K.,1992) molecular mechanism of this process was considered and it was shown that it is stipulated by different state of beta-receptor complex in healthy and sick individuals. By the way of screening we established in our study that previously revealed relation between centres of regulation of beta-receptor function with hormones and modulators depends on cytoskeleton condition. Most probably, beta-receptor is directly connected with cytoskeleton.

Differences, observed in responses of ACS on stimulation, are stipulated with different reasons - by functional system condition, genetic determination and many others. As shown in some papers (Tshegoleva, Bakchova, Vasileva, 1993), development of cardiovascular pathology results in increase of rigidity between centres of binding PGE2 and adrenaline in beta-receptor complex. Reason was unclear. Our findings suggest that, with account of effect's magnitude during cytoskeleton distruction, the initial cause of changes of this rigidity might be structural and functional changes in cytoskeleton and that this element is directly connected with beta-receptor. (Modification of membrane state with nitroglycerin is acompained with dielectric permeance changes on the bound of the error). It is known, that N-binding protein participates in this bond (Agutter G.1985). Is it realized directly or through N-protein, is a matter of future investigation. According to a whole number of indirect data, charactarising membrane disturbance, it is clear that lipid membrane component also participates in this process. Nevertheless, modification or injury of cytoskeleton and beta-receptor binding is primary and modification of lipid component is secondary. Possible, it is determined genetically.

Conclusions.

Thus, correlation between functional condition of erythrocytic membranes and direction of pathological process, reflected in integrated level of coronary risk, is revealed in population investigations. Key moment that permits to predict possibility of development of pathology on the most early stages, is found. Timely intervention will permit to prevent change of reversible injuries to irreversible.

EHF-dielectrometry permits to monitor cell dynamics by influence of endogenous and exogenous factors on molecular and cellular levels, to control effectiveness of corrective influence and to predict the development of acute coronary stroke in conditions of population. Analysis of the process by method of EHF-dielectrometry with application of specific agents of transmembrane transmission and signal blocade permits to indicate the concreet injury site in the scheme of molecular mechanism, that is one of the main in development of cardiovascular pathology.

EHF-DIELECTROMETRY METHOD IN INVESTIGATION MOLECULAR MECHANISMS OF STRESS REALIZATION

Kovaljova O., Sidorov D., Smirnova V., Shchegoleva T.Ju., V.G., Lepeeva E.F.
Institute of Radiophysics and Electronics of the National Academy of Sciences of Ukraine
12 Ac. Proskura St, Kharkov, 310085, Ukraine
The Problem Scientific-Research Laboratory of Molecular Mechanisms
4/32 Solanikovski lane, Kharkov, 310003, Ukraine
Kharkov State Medical University
Tel.8-0572-448506,8-0572 23-04-38,Fax 8-0572 441105,E-MAIL tsch@ire.kharkov.ua

Diseases are appearing in organizm when the stress adaptation in decreasing. Fundamental role in this case belong to disturbanse of neuro-endocrinical regulation. Function of molecular systems of cells' membrans upset when disease appears. It's important to study functions of system-messengers, which determinate the functional cell's response to the adrenergic influenct by the investigftion of the stress.

The dielectrometry in mm wave region give us the possibility to investigate molecular mechanisms of information to the alive cell. [1]. In case of essentional hypertention the platelet section of hemostasis disturb. [2]. The production of thromboxan and correlation thromboxan/prostacyclin increases during essentional hypertention [3]. .These disturbances appear in the begining of disease and then increase. They take leading part in the development of embolic complications in hypertensive patients. It's unknown now weather these disturbances are primary or they are the effect of disease. The influation of catheholamines is very impotant in the process of adaptation to functional load. They stimulate key enzymatical systems of the cells through -adrenoreceptors (α- β receptors') complex of system of adenylatcyclaza (ACS). But the activity of sympatoadrenal system during in case of border hypertention was still normal 33,3% . It had been checked with stress- test (ST) on cycle ergometric

To study the ACS function of platelets in patients with mid hypertention during stress. Examination included: 30 patients with mild essentional hypertention without the hypertrophia of left ventricule and 18 volunteers. The average age of patients was 20,3+2,2, the ave rage age of volunteers was 18,7+1,8. Essentional hypertention was diagnosed in clinic with dueregards for recomendations of WHO.

Methods: submaximal stress test was applicated to everybody with method of B.P.Prevarsky [4]. The function of platelet's ACS was investigate before and after ST by using EHF-dielectrometry method. Concentration of noradrenaline, adrenaline, thromboxan, correlation Tx B2/6-keto-PG F1 was measured also. Blood pressure/ heart rate were measured continuasly.The basal index in table 1. After the ST index in table 2. The concentration of N increased 1,3 time more, the concentration of A increased 2,1 time more in 20 % of patients. ε' changed the direction in 50 % of patients after ST. $\Delta\ \varepsilon'$ 'changed in 20% of patients with the middle increasing of H & A too. After ST H was 0,84+0,09 mcg/l & A was 0,27+0,08 mcg/l, Tx B2 was 0,91+0,12 mM/l, Tx B2/6-keto-PG F1 was 1,20+0,11 in volunteers (Fig).

After statistical processing of findings it was revealed that cell responce on addition of the used bioregulators varied by its directions in subjects with different state before and after stress test.. Increasing of platelet's functional activity in 20 % of patients with 1 stage of essentional hypertention wasn't caused by hyperactivity essentional hypertention but disturbanse of molecular systems functios,whicy take part in transmission of signal into cell.

The function of ACS changes in all hypertension patients. It is the correlation between functional condition of red cell membranes and direction of pathological process, reflected in stress-adaptation .Perhaps changes are primary: increasing platelet's - mesothelim -of vessels of sensytivity to cathecholamines.The ACS reflect the molecular mechanisms of stress realization.

The EHF -dielectrometry method can estimate individual ability to adaptation. It can be used for individual control in time of essentional hypertention treatment.

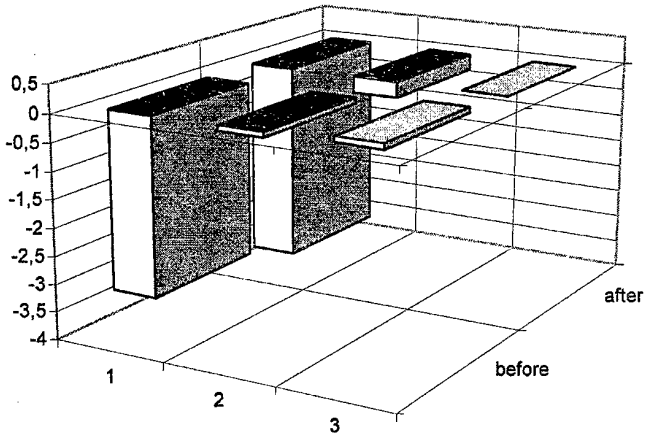
	SBP mm Hg	DBP mm Hg	N mcg/l	A mcg/l	TxB_2 mMK	TxB_2/g-keto Res F
Patients (n=30)	150, 1±5,3	92,3±3,3	0,8±0,2	0,17±0,05	1,1± 0,1	1,6± 0,2
Volunteors (n=18)	118,6±2,0	76,2±1,7	0,2±0,2	0,12±0,03	0,6± 0,03	1,2± 0,08

Table 1. Before stress-test ($p \leq 0,05$)

	SBP mm Hg	DBP mm Hg	N mcg/l	A mcg/l	TxB_2 mMK	TxB_2/g-keto Res F
Patients (n=30)	196, 6±1,3	98,3±5,2	3,8±0,3	0,28±0,04	1,2± 0,1	1,9± 0,1
Volunteors (n=18)	168,6±1,7	92±2,2	0,8±0,08	0,3±0,08	0,9± 0,1	1,2± 0,1

Table 2. After stress-test ($p \leq 0,05$)

a)



b)

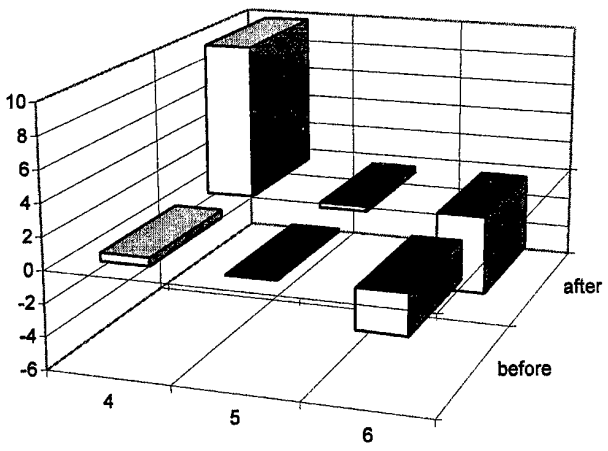


Figure. The dinamic of the change dielectric constant of suspension trombocites with mild essentional hypertention patients in results of veloergometree (a) - 1-3 - control, b) - 4-6- patients)

Reference

1.Щеголева Т.Ю. Измерение электрических параметров тонких образцов полидисперсных, жидких и твердых диэлектриков с большим поглощением в микроволновом диапазоне , Радиотехника и электроника, ,Т 26, .№1, с 2328-2333, 1981.
2.Гогин Е.Е. Гипертоническая болезнь, М., с. 76-93, 1997
3.Старченко Т.Г. Факторы эндотелиальной дисфункции гипертонической болезни., В кн.: Сб. трудов ИТАМН Украины, Х., с.57-58, 1997.
4.Преварский Б.П., Буткевич Г.А., Клиническая велоэргометрия, Киев, «Здоров'я», с. 80 ,1985

APPLICATION OF DIELECTROMETRY IN MM RANGE OF RADIOWAVES FOR RESEARCH OF MOLECULAR MECANISMS OF PHARMACOLOGICAL PREPARATIONS ACTION

Kiselova N.E., Shchegoleva T.Yu., Kolesnikov V.G.
Institute of Radiophysics and Electronics of a National Academy of Sciences of Ukraine,
12 Ac. Proskura St, Kharkiv, 310085, Ukraine
The Problem Scientific-Research Laboratory of Molecular Mechanisms
4/32 Solanikovski lane, Kharkiv, 310003, Ukraine
Tel. 8-0572-448-506,8-0572-230-438, Fax 8-0572-441-105, E-mail tsch@ire.kharkov.ua

Now days development of a science has allowed to approach to study of molecular mechanisms of operation of macromolecule cell complexes, which determine physiological and pathological processes on organisms level, and as individual person singularities. In this connection the special interest represents the study of molecular mechanisms of cell regulation processes. At a level of the whole organism operating hormon mechanisms regulatotion is one of basic. It is carried out by hormon-receptor interactions and transmembrane transmission of a signal by adenylate cyclase system (ACS) and cytoskeleton [1]. For study of these processes it is necessary to select an adequate technique permitting to carry out a researches in conditions of non-destructive control in real time [2].

The method EHF-dielectrometry in mm a range waves lengths - area of free water dispertion - allows to decide these problems. The developed methodology of the analysis of work of cell controlling complexes at the presence of the different bioregulators on a modification of hydrate environment macromolecule enables to describe molecular mechanisms of cell processes.

In the present work this method was used for study of molecular mechanisms of work ACS and cytoskeleton both erythrocytes and trombocytes of the person. It is known, that cytoskeleton of these cells is different [3]. The analysis of obtained outcomes has shown, that the key moment of regulation ÀÑS of erythrocytes and trombocytes of the person -β-receptor and cytoskeleton - are identical, but the answer of this macromolecule complex differs on intensity and directedness. Modification in answers magnitude during action on a researched complex by hormone stimulator have shown the distinctions in a response of erythrocytes and trombocytes β-receptors. And the trombocytes response was more significant. (Fig.1.)

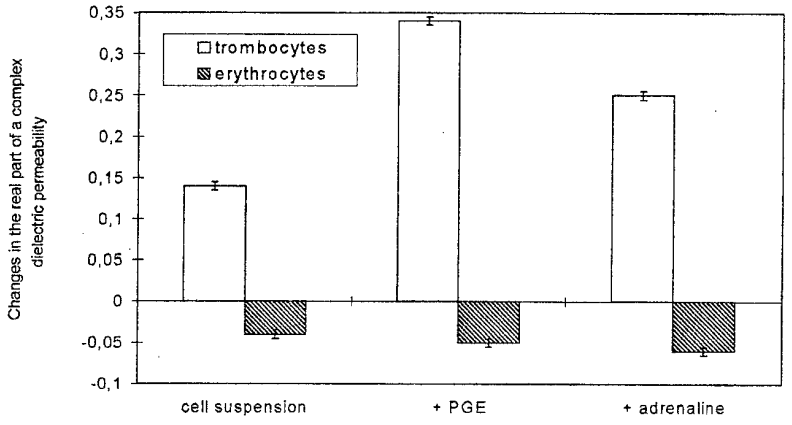


Figure 1. Cell ansver of the erythrocytes and trombocytes suspension during adrenaline and prostaglandine stimulation

In experiment the cell suspension answers on an action of the modulator and stimulator were always in different direct, that can be connected with distinctions in organization of cytoskeleton. Some singularities of a response of a researched complex reflecting individual difference were observed.

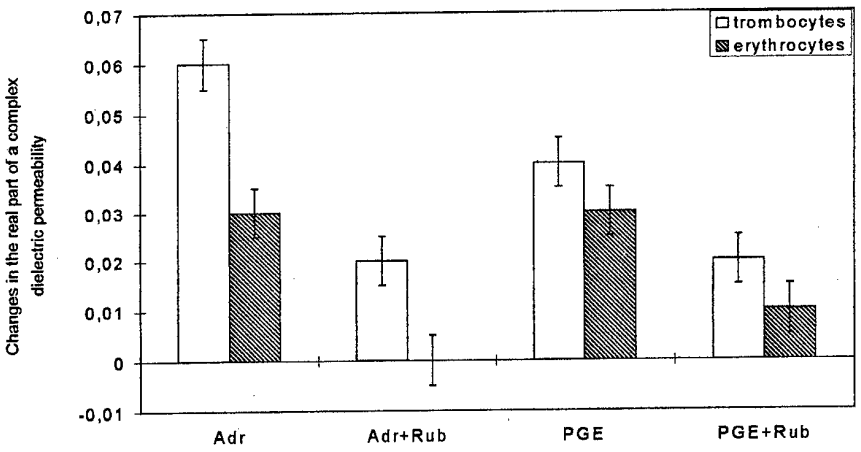


Figure 2. Cell answer of the erythrocytes and trombocytes suspension in the presence of rubomycine (Rub), (Adr - adrenaline, PGE - prostaglandine).

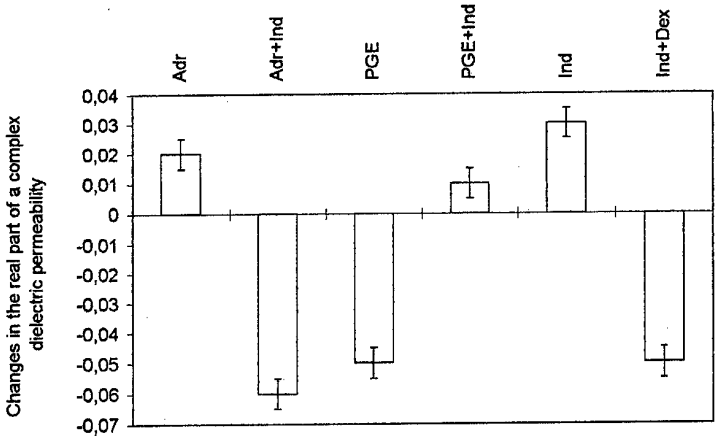


Figure 3. Cell answer of the erythrocytes suspension in the presence of indometacine (Ind) and dexamethasone (Dex). (Adr - adrenaline, PGE - prostaglandine)

The presence of rubomycine, which renders cytostatic action, oppresses an operation of adrenaline and prostaglandine, but in erythrocytes the destruction cytoskeleton reduces to full violation of transmembrane transmission of a signal, whereas in trombocytes the action of adrenaline is not removed completely. The influence of rubomycine itself so appears various, and trombocytes cytoskeleton appears more sensitive to the cytostatic influence, that also testifies to different structural organization of a cytoskeleton web. (Fig. 2).

It is known, that indometacine ingibate prostaglandine synthesis. Dring hormone stimulation by adrenaline, indometacine removed it stimulating action. The presence of this preparation hindered to the modulation by prostaglandine. Apparently, indometacine changes β-receptor, conformation as it loosens an operation both stimulator and modulator. To define is indometacine operates inside or outside of a cell, we used dexamethasone, which, as is known, penetrates inside cell and operates on the nuclear, and, on our datas, on cytoskeleton there are receptors for this steroid hormone. In all experiments the presence of dexamethasone

influences an operation of indometacine. (Fig.3.). Therefore, the intracellular correlation of these catalysts wich is observed, probably, is carried out by means of cytoskeleton. Thus, the modification of β- receptor conformation by indometacine can happen through cytoskeleton.

From obtained outcomes we can made a conclusion, that probably, it is possible to use the indometacine as substance wich chang intracellular cytoskeleton web organization, realze ACS regulation. As this drug has the known toxycal action, the obtained outcome, for example, it is possible to use for study on a model of ÀÑS the molecular mechanisms of toxycal effects and for a selection of modes of their correction.

The use of a method EHF-dielectrometry enables to realize the thin analysis of molecular mechanisms of an operation of various drugs classes, and for a directed correction of their action.

References

1. Checkman I.S., Biochemical farmacodinamic., Kiev, Zdorove, 1991.
2. T.Yu. Shchegoleva. Research of biological objects in millimeter range of radiowaves, Naukova dumca, Kiev, 1996 -182.
3. T.Yu. Shchegoleva, Functional system of communications of a erythrocytes adenylat cyclase complex, Advance of modern biology, 1997, 117, 4, 442-454

RESEARCH OF A SINGULARITIES OF DRUGS TOXYCOLOGICAL ACTION ON THE PREGNANT WOMEN BLOOD BY METHOD EHF-DIELECTROMETRY

Kiselova N.E., T.Yu. Shchegoleva, V.G.Kolesnikov, Nikitina N.S.,
Institute of Radiophysics and Electronics of a National Academy of Sciences of Ukraine,
12 Ac. Proskura St, Kharkiv, 310085, Ukraine
The Problem Scientific-Research Laboratory of Molecular Mechanisms
4/32 Solanikovski lane, Kharkiv, 310003, Ukraine
State Scientific Center of Drugs, Kharkiv, Ukraine
Tel. 8-0572-448-506,8-0572-230-438, Fax 8-0572-441-105, E-mail tsch@ire.kharkov.ua

The problems of perynatal pharmacology are little investigated and require a deep and multifold research. The drugs, used by the pregnant women, render influence not only on mother organism, but also on embrio, frequently exhibiting toxycological effects, that can reduce to violations in development of a foetus and even to loss of it at early stages of embriogenesis. The special difficulties in study of embriotoxycology and teratogene effects calls extrapolation per person the outcomes of a research on animals. [1]

Thus important task is searching adequate object and methodics, suitable for a scrining-evaluation of action of medicinal substance at pregnant. In this connection the use of EHF-dielectrometry method is represented rather perspective for a solution of these tasks.

The use of mm range of waves lengths allows to receive a unique information about state of water component of biosystems. There is a possibility to observe the modification of conformation of macromolecule structures according to modification of their water environment under influence of specific action on their various elements. It is possible to realize thin differenciation of connections of cell molecular mechanisms and diagnostics in work it's controlling complexes using the various bioregulator as the test components [2]. The specific regulators ensure interaction of agonist and receptors, modulation of transmembran transmission of a signal, and a cytoskeleton and cell components function at a molecular level. These processes are determined on a change of a complex dielectric permeability of cell suspension. The new methodological approach which allows to analyze the connections systems of cell controlling complexes is lays in a basis of work [3,4].

In the present work the circumscribed approach was applied to study of distinctions in action of adenilate cyclas system and cytoskeleton both trombocytes and erythrocytes of pregnant and non pregnant women, and so influences of drugs on molecular mechanisms of transmambrane transmission of a signal. The substances of known toxicological action - indometacine, substances of intracellular action - rubomycine, dexamethasonum, and adrenaline and prostaglandine as modulators is selected as model objects of a research for development of the methodics. The study were carried out on of trombocytes and erythrocytes suspension in three groups of the women with different term of pregnancy, the group of non pregnant healthy women we use for control.

In a comparison with erythrocytes, in trombocytes of all groups the answer on adrenaline and prostaglandine was more expressed. The response both thrombocytes and erythrocytes of the pregnant women on adrenaline is significant less, than non pregnant women. The temporal assotiation is well visible: beginning with the second half II trimester this effect is significant. In I trimester sinfase modification of the cell answers during of adrenaline stimulation was marked. Thus, the condition of blood cells of pregnant has an effect on ACS. In presence of the modulator prostaglandine different directedness of the answer of thrombocytes and erytrocytes of the pregnant women was observed. There is no any essential difference from control it was not observed, but with increasing term of pregnancy the thrombocytes answer decreased. Probably it is connected with a diminution of receptors number on a thrombocytes membrane surface, or with modifications in work of ACS and transmembrane transmission of a signal in an organism of the pregnant woman. (Fig. 1). The obtained values reflect also individual singularities of macromolecule complex action, that can be hereinafter used for an individual selection of drugs. The using of terapevtic fnd toxycal indometacine concentration (Fig. 2) as the test components has shown, that, at first, the during interaction with a membrane, substance changes β-receptor conformation, secondly, in group of the pregnant women in presence of toxical indometacine concentration, the significant on magnitude answer on hormone stimulation was observed, i.e. there is a difference in a response pregnant and non pregnant women on toxical concentration of a preparation. Rubomycine interrupts transmembrane transmission of a signal, hindering an adrenaline action and removes

doze-depended toxical effect, caused by indometacine (Fig. 3). And, as rubomycine operates inside a cell, it gives a foundation to assume, that during interaction of these drugs cytoskeleton participates, calling conformation modification in β-receptor, may be through N-protein, or may be immediately. Distinctions in work ACS of pregnant and non pregnant women in presence of rubomycine it is not revealed.

The outcomes, obtained in the given work, can be hereinafter used for development the express train-test for diagnostics of toxical effects, caused by drugs at the pregnant women and a for selection of individual therapy.

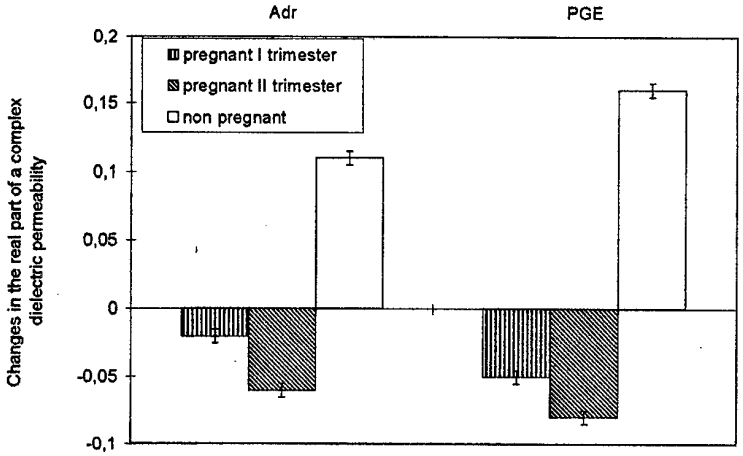


Figure 1. Changes in cells answer of pregnant and non pregnant women while adrenaline (Adr) and prostaglandine (PGE) stimulation

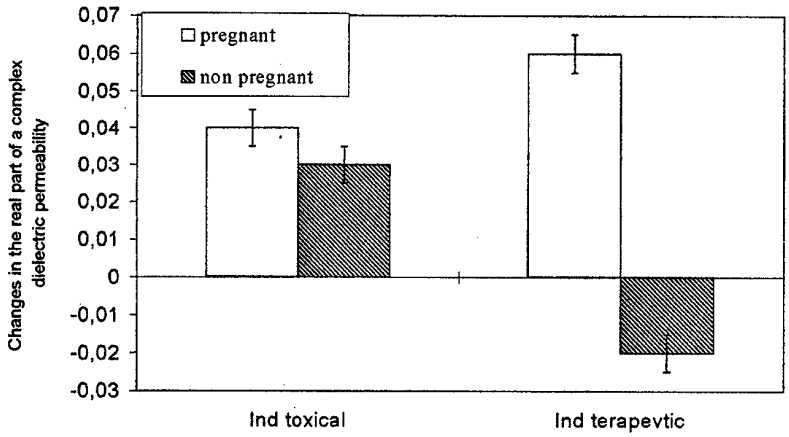


Figure 2. The influence of terapevtic fnd toxycal indometacine (Ind) concentration on erytrocytes of the pregnant and non pregnant women

The outcomes, obtained in the given work, can be hereinafter used for development the express train-test for diagnostics of toxical effects, caused by drugs at the pregnant women and a for selection of individual therapy.

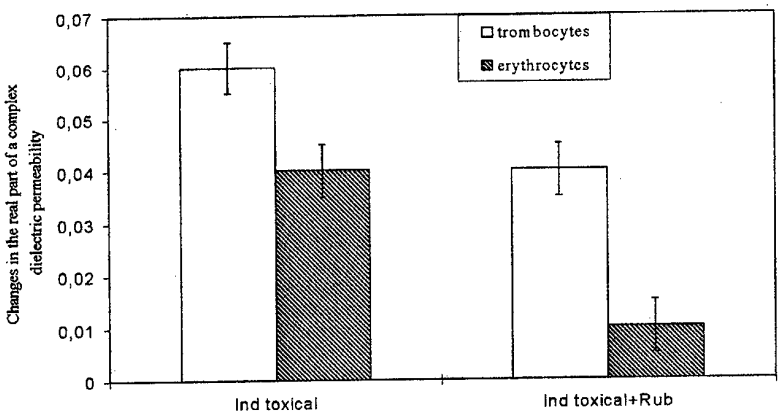


Figure 3. Cells answer while interaction of rubomycine (Rub) toxical doze of indometacine (Ind).

References

1. Kiruschenkov A.P., Tarachovsky M.L., The influence of medical drugs on embrio., M, Medicine, 1990.
2. Alberts B., at all, Molecular biology of a cell., Moscow, Mir, 1994.
3. T.Yu. Shchegoleva. Research of biological objects in millimeter range of radiowaves, Naukova dumca, Kiev, 1996 -182.
4. T.Yu. Shchegoleva, Functional system of communications of a erythrocytes adenylat cyclase complex, Advance of modern biology, 1997, 117, 4, 442-454

THE METHODOLOGY OF THE ANALISIS OF MOLECULAR MECHANISMS OF ANTROGENEOUS INFLUENCE BY METHOD OF EHF- DIELECTROMETR

Shchegoleva T.Yu., Kolesnikov V.G., Begma L.A., Begma A.A.,
Kiselova N.E.
Institute of Radiophysics and Electronics of a National Academy of Sciences of Ukraine,
12 Ac. Proskura St, Kharkiv, 310085, Ukraine
The Problem Scientific-Research Laboratory of Molecular Mechanisms
4/32 Solanikovski lane, Kharkiv, 310003, Ukraine
Institute of Cultivation and Genetics of Academy of Agrarian Sciences of Ukraine,
Tel. 8-0572-448-506,8-0572-230-438, Fax 8-0572-441-105, E-mail tsch@ire.kharkov.ua

The transmitters permitting to fix total unfavorable effect of an operation of a large gang of rather the harmless factors of action per person are necessary for a solution of a large circle of the ecological tasks. The purpose of the present work is the development of the methodology of the express-testing of combined unfavorable action on humane organism with the analysis of molecular mechanisms of damage for the express-selection of modes of a correction with use of the alive cells as transmitters. It is known, that the functional ability of the sperms hardly depends on many an exterior factors, one of which is direct or indirect antropogeneous action. The condition of cell control systems is a reliable index of a cell condition and even alive organism as a whole.

In the present work the ruling molecular mechanisms of the sperm for a choice those, which is a principal, are investigated with the purpose to use them for the analysis of a structurally functional condition of a cell during various antropogeneous action both on sperm samples, and on an organism. Now there are no reliable datas on regulation systems of these sperm cells, with the elemination of separated datas about prospective mechanisms. This is because the sperm rather fast perish if the special measures of preservation are not applied, against many other cells. Besides, as a rule, the molecular mechanisms of cells on a modern level of science development, is analyzed on yields of its modification or destruction. The method of dielectrometry in mm a range of waves lengths enables to avoid it. The choice of key moment of a cell regulation allows to fix not only fact of influence, but also to carry out the express-analysis of affected cell molecular mechanisms of a and to select correcting action in real time.

In an outcome of conducted researches the methodology which allows to approach to the thin analysis of various aspects of antropogeneous action at a molecular level, using the complex of molecular mechanisms of a cell membrane and cytoskeleton as a test-system, on the base of EHF-dielectrometry of bioobjects in conditions of non destractive monitoring is developed. The approach, which basing on of fundamental bases knowledge of molecular mechanisms operation, allows to fix the fact of antropogeneous influence in a condition the express-testing, to make inferences about molecular mechanisms of damage and enables to realize it's directed correction.

The study of molecular mechanisms transmembrane transmission of a signal with the participation of adenylate cyclase system is rather important in a research of the functional answers of a cell and organism as a whole on various actions. That will allow to expand existing representations about biology of a cell and can be used in medicine, pharmacology, agriculture, ecology. On the basis of results of this work, the series of express train-test for the analysis of the reasons of origin of various diseases and deterioration of a condition of patients, prediction of illness current, and by that diminutions of its duration, and probabilities death outcome in acute cases can be created. (Patents of Russian Academy of Sciences for prediction of complications for want of current acute myocardial infarction befor 1-2 days and individual correction of therapy hypertonic illness II level is already obtaned.)

The analysis of receptors complexes function in native cell will allow to objectivize the influence of non-drags therapy, electromagnetic radiation and many other combyned actions. The analysis of the molecular mechanisms of transmembrane transmission of a signal in sperm and blood cells of animals with the help of EHF-delectrometry enables to determine a degree of action on living steady of organism on various process engineerings of cultivation, and also some breed attributes and individual indexes, for example, stress steady. The definition of influence modifications of ecological circumstances and complicated complex of exterior actions, both in the test-system, and at a level of an organism is possible.

At the presence work the differente way of sperms use for solving number of immunocorrection problems of antropogene influence. On Figure 1. we show the concentration dependence of immunostimulator - echinaze action. It is visible, that it is possible to select optimum concentration.

At the presence work the differente way of sperms use for solving number of immunocorrection problems of antropogene influence. On Figure 1. we show the concentration dependence of immunostimulator - echinaze action. It is visible, that it is possible to select optimum concentration.

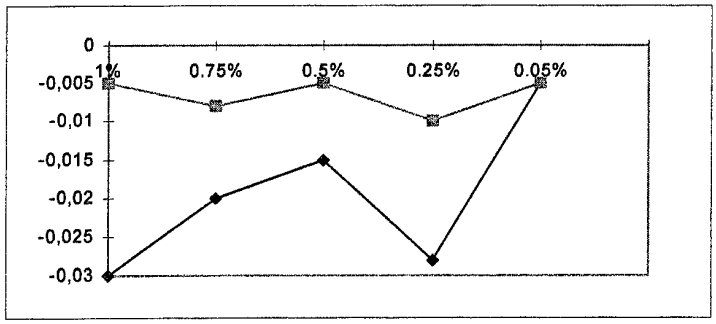


Figure 1. Concentration dependence of Echinaze action for different bulls

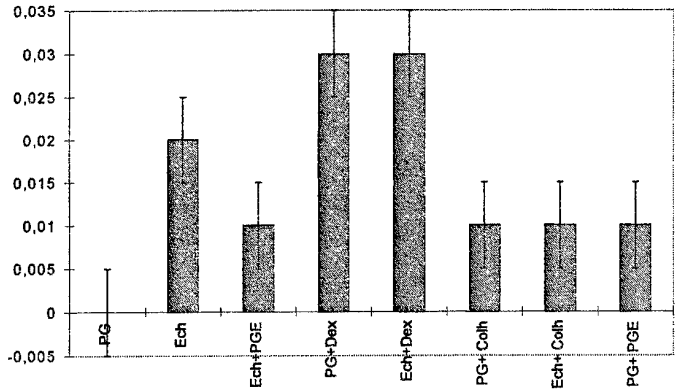


Figure 2. Comparative datas of action Echinaze (Ech) and Panax Ginseng (PG)

(Dex - dexamethasone,Colc - colchicine)

On Fig. 2. the diagram of the cell answers during action on a cell immunostimulators - Panax Ginseng and Echinaze is represented. Is shown direct antihormonal action of these preparations on a cell. The scheme of the molecular mechanism of echinaceum operation with possible ways of an individual correction of sperm immunostimulation is developed by scrining of specific binding stimulators and blockator on dielectric parameters (Fig. 3). The possibility of direct connection of systems which care for the immune answer, with adenylate cyclase system including cytoskeleton is shown. The developed methodology allows to approach to a correction of immunostimulators and immunemodulator actionat a molecular level.

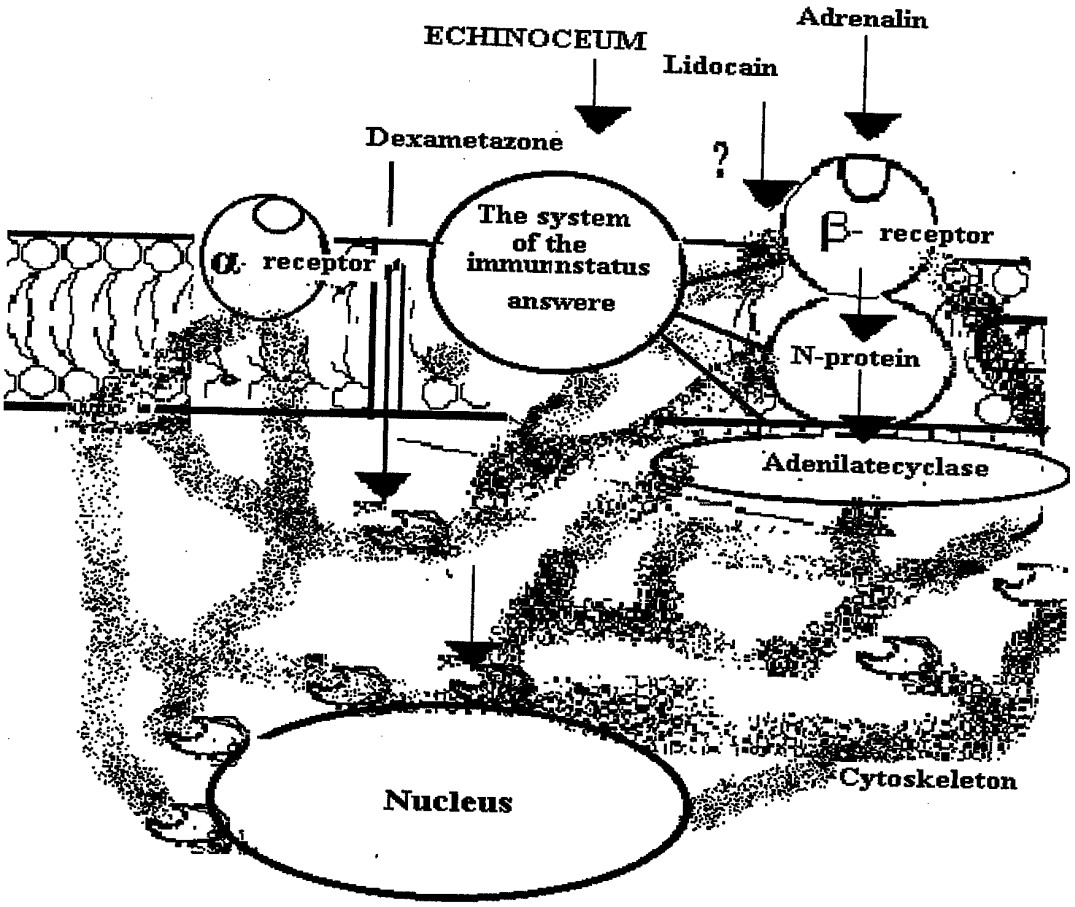


Figure 3. The molecular mechanism of echinaceum operation

Reference

1. T.Yu. Shchegoleva, «Hydration environment and macromolecule structure». Advance of modern biology., 116,6,700-714, pp 1996.
2. T. Yu. Shchegoleva, V. G. Kolesnikov, « Change in the hydrate environs of erythrocytes on hormonal stimulation», Biophysics, Vol.41, No.5, pp.1093-1097,1996.
3. T. Yu. Shchegoleva, V. G. Kolesnikov, «The adenylat cyclase system and calcium channels», Biophysics, Vol .40, No.6, pp.1301-1304, 1995.
4. T.Yu. Shchegoleva, «Functional system of communications of a erythrocytes adenylat cyclase complex», Advance of modern biology, , Vol 117, No.4, pp .442-454,1997.
5. T.Yu. Shchegoleva. «Research of biological objects in millimeter range of radiowaves», Naukova dumca, Kiev, pp. 182,1996.
6. M.V. Zubets, T.Yu. Shchegoleva, V.G. Kolesnikov, « Application of millimeter range waves in agriculture, Agrarian science», Kiev, pp.163,1996.

Authors Index

A

Abdulkadyrov V.A. C21, C22
Afonin D.G. H9
Akinshin N.S. F2, F15
Ala-Lauriaho J. INV.4
Alekseev E.A. I1
Alexeev G.A. E12, B17
Ando M. D24
Andreev M.V. I3
Andrenko A.S. D24
Antifeev V.N. F1, F2, F5, F6
Antyufeev V.I. F26
Arkusha Yu.V. A8, A15
Averkov Yu.O. C13
Ayzatskiy N.I. B1

B

Büchler J. INV.J1
Böhm H. A1
Bacherikov A.N. L11
Bakhvalov B.N. H17
Balabanov V.N. INV.11
Ballard J. INV.5
Bandopadhyaya T.K. E5
Barantsev S.A. H21
Baumgartner M.O. A3
Begma A.A. L17
Begma L.A. L17
Beletskii N.N. C13, C14
Belous O.I. A13, A17, L8
Belousov Ye.V. B5
Bereshnyj V.L. J3
Berezhinsky L.I. L3, L10
Berezhnyj L.V. J2
Bessonov V.A. H21
Betskii O.V. INV.L1
Blank A.Ya. C19
Bludov J.V. C16
Bogdashov A.A. H4
Borisenko S.A. C14
Borsov A.B. F1, F2, F5, F6
Borulko V.F. H22, H23
Botsula O.V. A9
Bratman V.L. B2
Brovenko A.V. D1, D11
Bubke K. D4
Budnikov A.T. C11
Bugaev A.S. C18
Bulgakov A.A. C15
Bulgakov B.M. A17, L8
Burov A.B. INV.10
Buts V.A. B7
Bychkov V.V. INV.I1
Bykov V.N. F26
Bykov Yu.V. INV.J2
Bystrov R.P. F1, F2, F3, F4, F5, F6

C

Chayka V.E. C7, C8
Chemerovsky V.I. F9
Chepel' L.M. L8
Cherny I.V. H12
Cherpak N.T. B24, C2, C11
Cheslavsky G.V. F23
Chigryai E.E. C9
Chizhov V.V. H15
Chornaya L.F. E1
Chovnjuk Yu.V. L7
Churyumov G.I. B18, B19
Claassen M. A1

D

Dachov N.F. B12
Dakhov V.M. H12
Dan'ko A.Ya. C11
Das N.K. H3
Demchenko M.Yu. B6, H29
Denisov G.G. H4
Derkach V.N. D11, L4, L11
Detlefsen J. INV.J1
Dikmen F. D16
Dolia A.N. F9
Dovbeshko G.I. L3, L10
Dovbnya A.N. B19
Drobakhin O.O. K9
Dryagin Yu.A. INV.10
Dubko S.D. E2
Dyubko S.F. I1
Dubovitskaya O.V. L2
Duxbury, G. INV.5
Dyadchenko A.V. A10

E

Efimov V.B. INV.11
Erckmann V. B1
Eremeev A.G. INV.J2
Eremeev D.B. B19
Eremenko Z.E. A12, H27
Ermak G.P. B6
Evtukh A.A. C7

F

Falko V.L. C4
Falkovich S.E. F19
Fedoseev L.I. F12

Fernandes H.C.C.	D6, D7, D8, D9
Filipov Yu.F.	A12, H27
Fisun A.I.	A13, A17, L5, L8
Fomin I.P.	J2, J3
Freitas E.L.	D8
Frolova T.I.	B18
Fumeaux C.	A2
Furashov N.I.	E9

G

Gaikovich K.P.	F11
Ganapolskii E.M.	INV.11, B13, H26
Garanina L.V.	C19
Garin B.M.	C9
Gayvoronskaja S.A.	F25
Goldenberg A.	INV.9
Golik A.V.	INV.11
Golubyatnikov G.Yu.	INV.I1
Gomozov A.V.	H17, H18
Goncharuk N.M.	C7, C8
Gorbach N.V.	E4, E11
Gorbunenko O.A.	F19, F20
Gorobets N.N.	H10, H11, H12
Gorobets Yu.N.	H10
Grechko L.G.	C19
Greed R.B.	INV.C1
Grichaniuk A.M.	F26
Gridasova L.N.	L13
Gridina N.Ya.	L10
Grimalsky V.V.	H5
Grishin A.M.	I4
Grom Yu.D.	B2
Gudim I.	H28
Gusev V.A.	J1
Gutnic V.G.	E11

H

Herrmann W.	A2
Herscovici N.I.	H3
Hirvonen T.	INV.4
Holoptsev V.V.	INV.J2
Holotyak, T.	F30
Homenko S.I.	F28
Hong J.-S.	INV.C1
Hornbostel A.	INV.E1

I

Ignatov M.Yu.	L4
Ilchenko M.E.	D3
Ilyushin V.V.	I1
Iounevitch E.O.	A5
Ivanchenko I.	H29
Ivanilov V.E.	H23
Ivanyuta A.N.	H16
Izhyk E.V.	C2, C11

J

Jacob A.F.	D4
Jedamzik D.	INV.C1
Judaschke R.	INV.2

K

Kalynov Yu.K.	B2
Kamenev Yu.E.	B11, B12
Karacuha E.	D16
Karyakin E.N.	INV.I1
Kashpur V.A.	L2, L9
Kasparek W.	B1
Kasyanov A.O.	D25
Khankina S.I.	C4
Kharkovsky S.N.	H27, H34
Khlopov G.I.	H33
Kholod P.V.	F24
Khomenko E.V.	L1
Khoroshun V.V.	H13, H14
Khorunzhiy M.O.	B21
Kirichenko A.Ya.	C2, C11, K10,
Kirichenko V.A.	F14, F28
Kirilenko A.A.	INV.H1, A13, D2, D3, D12,
Kiseliov V.K.	B12, H25, J5
Kiselova N.E.	L15, L16, L17
Kishenko Ya.I.	H5
Kitaj Sh.D.	F10
Kitaytsev A.A.	A14
Kiyko V.I.	H10
Kleiman A.S.	INV.K1
Klugman J.	H3
Kneubühl F.K.	A2, A3
Knyaz'kov B.N.	H24
Koberidze A.V.	K8
Kogut A.E.	H34
Koledintseva M.Yu.	A14
Kolesnikov V.G.	L6, L12, L13, L15, L16, L17
Komyak V.A.	F17, F18, H33
Konov V.I.	C9
Kopilovich L.E.	G3
Kopnin A.N.	C9, I2
Kordoš P.	INV.6
Korneenkov V.K.	H35
Korneyenkov V.	H29
Kornienko Yu.V.	G2, G5, G6
Korolyuk A.P.	INV.11
Korshunov I.P.	D19
Korshunova E.N.	D19
Korzh V.G.	B5
Koshevaya S.V.	H5
Koshparenok V.N.	B21
Kostenko A.A.	H33
Kostenko L.V.	E2, H17, H18
Kovalchuk I.K.	B7
Kovaljova O.	L14

Krakovskiy V.A. C3
Krasilnikov A.A. F12
Krasnitskaya A.A. L2
Kravchenko N.I. . D32
Kravchenko V.F. D26, D28, D29, D30, D31, D32, D33, D34, D35, F20
Krizhanovsky V.V. H30, H31, H32
Kropotkina E.P. INV.F1, J1
Krupnov A.F. INV.I1
Kudryashov V.E. L1
Kukin L.M. INV.10
Kulagin O.P. B8, B9, B22
Kulemin G.P. INV.8, F7, F8, F14, F16,
Kuleshov E.M. B12
Kuleshov Y.M. H24
Kulik D.Yu. INV.H1
Kulikov Y.Y. F12
Kuraev A.A. D29, D30
Kurekin A.A. F7, F9
Kurekin A.C. INV.11
Kushta T.M. J5
Kutuza B.G. INV.E1, E8
Kutuzov V.V. H34
Kuz'michev I.K. B15, B16, H8
Kuzmichov V.M. K2, K3, K4, K5
Kuzmichova E.V. K4

L

Lancaster M.J. INV.C1
Lapty V.K. J6, J7
Laqua T.H. B1
Lavrinovich A.A. B24
Lebedeva N.N. INV.L1
Lehto A. INV.4
Leonov I.I. INV.I1
Lepeeva E.A. L14
Levin G.Ya. B22
Lima G.A.de B. D7
Lima R.L.M. D8
Lioubtchenko V.E. A5, F22
Lipphardt B. A2.
Litovchenko V.G. C7
Litvin Yu.M. C7
Litvinenko L.N. E2
Litvinov P.V. D22
Ljashchuk O.B. K6, K7
Logvinenko S.V. J1
Logvinov Yu.F. E3
Lubyako L.V. INV.10, B1
Lukin A.N. INV.F1, J1
Lukin K.A. INV.F2, F29
Lukin V.V. F7, F8, F9
Lukovnikov D.A. H4
Lutsenko V.I. F28, H35
Luy J.-F. INV.J1

M

Makarenko B.I. E2, F26, F27, H19, K1, L1
Makarov N.M. C17, E6, E7
Makeev Yu.G. H36, H37
Maleev V.Ya. L2
Malihin A.V. L4
Malyshev V.Y. H16
Malyshkin A.K. H9
Malyshkin P.A. D18
Manuilov V.N. B2
Markov V.N. INV.I1
Marquardt J. H1
Martinenko D.V. L1
Martynuk S.P. H33
Masalov S.O. D20
Maslov V.A. H6
Mazur A.B. C9
McPhail M. INV.5
McPheat R. INV.5
Medvedev V.V. A11
Medvedev Yu.V. I4
Melkov G.A. H16
Meriakri V.V. INVI2, I2
Mikhailova D.V. F21
Militinskiy I.M. H6
Mironov D.V. C8
Miroshnichenko V.S. B14, H35
Mishnjov A.A. A10
Mogila A.A. F29
Moroz A.V. E6
Moroz I.P. H5
Mos'pan L.P. INV.H1, D12
Motornenko A.P. H37

N

Nagnibeda V.G. G1
Nagornyi D.A. B5
Naumenko V.D. INV.BI
Naumov A.P. F10
Nazarchuk Z.T. K6
Nesterenko A.V. B23
Nesterov P.K. J5
Newnham D. INV.5
Nicolaenko Yu.M. I4
Nicolenko U.J. L13
Nikiforov P.L. J1
Nikitin A.A. A6
Nikitina N.S. L16
Nikolaev V.A. F2
Nosdrachev D.A. F2, F5, F6

O

Oberschmidt G. D4
Obukhoveths V.A. D25
Ocheretenko V.L. J2, J3
Ofitserov M.M. B2

Onishchuk V.A. F20
Onufrienko V.M. D14
Orlenko A.A. F24
Osharin A.M. E10
Osharina N.N. F10

P

Panin İ.A. F2
Panin S.B. D13
Parkhomenko M.P. C9
Parshin V.V. INV.I1
Parshin Y.V. C9
Passoke J. H1
Pavlichenko O.S.
Pavlov G.L. F5
Pedchenko I.E. H14
Pedenko Yu.A. E3
Pedyash V.G. C11
Penkin Yu.M. D21
Pereira W.P. D7
Perov A.O. D17
Petrusenko I.V. D10
Pinos I.B. J2
Pogorelov S.V. K5
Pogrebnyak V.A. C6, C18
Pojedinchuk A.E. D1, D11, D13
Pokhil'ko S.N. K3
Polupanov V.N. H24
Popenko N. H28
Popov V.V. C10, H15
Prilepsky E.D. F27
Prokhorov E.D. A8, A9, A10, A11
Prudyus I. F30
Pushkaryov K.A. B4, B5
Puzanov O.O. D20

R

Räisänen A. INV.4
Radionov V.P. B12
Ralchenko V.G. C9
Razskazovsky V.B. E3
Revin I.D. B6
Rothuizen H. A2
Rozanov B.A. INV.G2, F23, G1
Rozanov S.B. INV.F1, INV.G2, J1
Ruban A.I. B3, B4
Rud' L.A. INV.H1, D2, D3
Rudenko V.N. H18
Rvachev V.A. D28
Rvachev V.L. D28, D31, D34
Ryazantseva N.V. E4
Rybakov K.I. INV.J2
Ryskin V.G. F12

S

Saarinen K.P. F7
Sagaidakova N.N. L9
Saltykov D.Yu. K9
Samsonov S.V. B2
Saxena P. E5
Schünemann K. INV.1, INV.2, INV.BI
Schitov A.M. INV.I1
Schroth A. INV.E1
Semenov M.A. L9
Semenov V.E. INV.J2
Semenuta V.Ye. INV.BI
Serebryannikov A.E. B10
Sergeev A.G. INV.11
Sergeev V.I. F25
Shablovsky Ya.O. C20
Shachbazov V.G. L8
Shahabadi M. INV.1
Shakirin A.I. D30
Shapovalov A.S. A6
Sharapov L.I. E4, E11
Shatrov A.D. D18, D19
Shchegoleva T.Ju. L6, L12, L13, L14, L15, L16, L17
Shilo S.A. F17, F18
Shokin M.G. F27
Shramkova O.V. C15
Shtanjuk A.M. INV.10, J1
Shulga V.M. INV.G1
Shvetsov A.A. F13
Siart U. INV.J1
Sidorov D. L14
Silin A.O. H20
Sinitsyn A.K. D30
Sinyavskij G.P. D23
Sirenko S.P. L8
Sivov A.N. D19
Sizova N.D. D32
Skalyga N.K. INV.10, B1
Skibenko A.I. J2, J3
Skripnik Yu.A. J4
Skrynnik B.K. B15
Slesarenko S.S. A16
Smirnova T.A. B24
Smirnova V. L14
Smith K. INV.5
Sokolnikov A.V. F19, F20
Sokolov A.V. F1, F2, F3, F4, F5, F6
Solodovnik V.A. H34
Solokha E.I. E2, H18
Solomonov S.V. INV.F1, J1
Songfa Li A4
Soroka A.S. H19, H20
Sova A.V. B10
Stephanishin Ya.I. F17
Storozhenko I.P. A7, A8
Strizhachenko A.V. H15
Stulova L.V. F21, G4
Suchkov V.B. F6
Sugak V.G. F14
Sukhinin B.V. F15
Sulima T.N. L5
Suvorov E.V. INV.10, B1

Suvorova O.A.	K10
Sverdlov B.A.	E9
Svich V.A.	H6
Syvozalizov N.A.	H14

T

Tarakanov V.V.	INV.11
Tarasov Yu.V.	E7
Tcymbal V.N.	INV.11
Tcymbalov G.M.	C10
Teperik T.V.	C10
Teryokhin S.N.	B22
Timchenko A.I.	D20
Tishkovets V.P.	D22
Titov S.V.	E1
Tkachenko V.I.	INV.H1, A13, D2, D3, H6, H20,
Tkachev G.B.	C17
Topkov A.N.	H6
Torchinov V.V.	D31, D34
Tretyakov M.Yu.	INV.I1
Troitskij A.V.	F10
Troitsky R.V.	F11
Tsakanyan I.S.	H19, H20
Tsvyk A.I.	B3, B4, B23
Tuchkin Y.A.	D16

U

Uliyanova I.I.	H21
Unger H.-G.	INV.1
Uvarov V.N.	A18
Uzlenkov A.A.	F28
Uzlenkov V.I.	H35

V

Vashenko E.V.	F1, F3, F4
Vavriv D.M.	INV.BI
Vdovenko K.V.	D23
Vekslerchik V.E.	C17
Velasco Hererra V.M.	F19, F20
Velichko A.V.	C2
Veliev E.I.	D14
Velikiy A.Yu.	K9
Velychko L.G.	D5
Vendik O.G.	INV.7
Vertij A.A.	D11
Viltchinsky A.S.	F27
Voitsenya V.S.	J3
Volkov V.A.	INV.BI
Volokhov S.A.	INV.I1
Voloshynovskiy S.	F30
Volosyuk V.K.	F19, F20,
Vorobiov S.N.	H8
Vorobjov G.S.	B3, B4, B5
Vyazmitinova S.S.	H11

W

Watanabe K.	H2
Weiss C.O.	A2
Wollitzer M.	INV.J1

Y

Yakovenko I.V.	C12
Yakovenko V.M.	INV.3, C4, C12, C13
Yanenko A.F.	J4
Yanovsky M.S.	H24
Yaremenko Yu.G.	INV.L1
Yasumoto K.	H2
Yatsik V.V.	D15
Yegorov Y.V.	H16
Yeremka V.D.	B8, B20, B21, B22
Yevdokimov A.P.	H30, H31, H32
Yurchenko L.V.	C5, H7
Yurchenko V.B.	C5, H7
Yushchenko A.G.	D3

Z

Zagorin G.K.	INV.E1, E1
Zaitsev N.M.	F22
Zakalyukin A.B.	D29
Zakutin V.V.	B19
Zamyatin A.A.	D26, D33
Zargano G.F.	D23
Zelensky A.A.	F7, F8, F9
Zharkova N.A.	G1
Zheltov V.N.	B23
Zinchenko I.I.	INV.G1
Zolotuhina L.I.	L4
Zubez M.V.	L12
Zubkov A.N.	F15
Zvyagintsev A.A.	H15